UTS UNIVERSITY OF TECHNOLOGY SYDNEY

# Characterisation of Expansive Soils Treated with Hydrated Lime, Bottom Ash and Bagasse Ash

**By Minh Thang Le**

Thesis submitted in fulfilment of the requirements for the degree of

**Doctor of Philosophy**

under the supervision of A/Prof Hadi Khabbaz and A/Prof Behzad Fatahi

University of Technology Sydney

Faculty of Engineering and Information Technology

June 2021

## CERTIFICATE OF ORIGINAL AUTHORSHIP

I, Minh Thang Le declare that this thesis, is submitted in fulfilment of the requirements for the award of Doctor of Philosophy, in the School of Civil and Environmental Engineering at the University of Technology Sydney. This thesis is wholly my own work unless otherwise referenced or acknowledge. In addition, I certify that all information sources and literature used are indicated in the thesis. This document has not been submitted for qualifications at any other academic institution. This research is supported by the Australian Government Research Training Program.

Signature: Production Note:
Signature removed prior to publication.

Date: 30/06/2021

**DEDICATION**

I would like to dedicate this Doctoral dissertation:

*To my respective mother, Nguyen Thi Ha Mat and my passed-away father, Le Mau Thao*

For their endless love, supports, inspiration and sacrifices.

*To my supportive wife, Le Diem Thu*

For her patient love, sacrifices, supports and understanding

*To my lovely sister, Le Thi Nhu Quynh*

For her encouragement and supports

## ABSTRACT

Expansive soil is regarded as a kind of problematic soil that has a low bearing capacity and excessive volume change (shrinkage or swelling) under climate change or changes of ambient moisture. These characteristics are seen as pivotal factors that pose a threat to the foundations of civil structures, such as pavements, highways, light buildings, and canal linings and beds. Hence, it has a necessity of reducing the shrinkage-swelling potential of expansive soil and enhancing its strength so that the improvement can minimise adverse impacts of soil. To stabilise expansive soil, lime treatment is a common technique to limit its shrinkage-swelling potentials because the treatment significantly alters the hydromechanical and physical features of the soil. When the treatment includes ash materials, the modification from both lime and the silicate materials in soil properties becomes stronger than each binder does.

In this study, readily available waste by-products rich in silica, including bottom ash and bagasse ash collected in Australia, were utilised to mix with hydrated lime for stabilising expansive soils. The study includes extensive programs of experiments in electrical, physical, mechanical and micro-structural properties of stabilised soils, followed by a numerical analysis on an embankment on soft soils in Australia. Particularly, electrical conductivity methods were carried out to determine the optimum ratio of ash to lime in their treatments, based on pozzolanic reactivity of ash mixtures. The methods are novel because there is a lack of studies on predicting behaviours of two-ash-lime treated soils by using electrical conductivity tests. For this purpose, modified electrical conductivity (EC) methods were proposed to estimate the changes in loss of conductivity when bottom ash and bagasse ash were added to lime-soil suspensions. Due to the testing credibility, a homogeneous expansive soil was artificially constituted from kaolinite (65%), bentonite (30%) and sand (5%). When mixing ash with soil and lime, three EC tests were suggested, namely Tests A, B and C. While Test A was used for bagasse ash in various maximum particle sizes (i.e., 75, 150 and 425 μm), Test B was designed for bottom ash excluded from the gravel size particles. When it comes to combining bottom ash and bagasse ash for soil stabilisation, Test C was employed, in which the optimal ratio of bottom ash to bagasse ash was determined in their aqueous solutions. As testing results, the findings showed that with 5% hydrated lime, the optimal content for each ash was 25% for bottom ash and 15% for bagasse ash. However, when two ashes were combined, the ratio was 17.5% for bottom ash and 7.5% for bagasse ash. The combination ratios are based on the total dry mass of dry soil and ash, resulting in 75% for soil content.

As for the characterisation of soils treated with lime, bottom ash, and bagasse ash, soil samples with 5% lime and 25% bottom ash were superior to other treated soils in most mechanical results. Bottom-ash-lime-treated soil had the lowest swelling ratio of 2.6%, the highest pre-consolidation pressure of 463 kPa, unconfined compressive strength (*UCS*) of 2.1 MPa, unsoaked California bearing ratio (*CBR*) of 84%, soaked *CBR* of 128% after 62 days of saturation, and the stable and largest small-strain shear modulus ($G_{max}$) of 653 MPa after one year curing for saturated samples. Meanwhile, the soil specimens with 5% lime, 17.5% bottom ash and 7.5% bagasse ash had the lowest linear shrinkage of 12.2 %, the highest 90-day matric suction of 298 kPa, and the largest $G_{max}$ of 675 MPa in saturated specimens after 28 days of curing. These improvements have been explained via scanning electron microscope (SEM) analysis. The analysis indicated a formation of reticular networks, where calcium silicate hydrate (CSH), ettringite and lime coexist in the interfacial transition zone between bagasse ash and bottom ash. Meanwhile, the soils stabilised with 5% lime and 15% bagasse ash still have their advantages in triaxial properties with high values of friction angle and cohesion. As a result, these beneficial properties assisted in reducing the lateral movement of a working platform on the topsoil layer under a modelled embankment in Ballina, NSW, Australia. The numerical outcomes from the PLAXIS program suggested that using both bagasse ash for lime treatment on the soil surface and bottom ash for lime-treated soil columns is the optimal solution to effectively decrease the settlement and horizontal deformation of the ground under the embankment. This study also provides a detailed discussion on the relationships of electrical conductivity results with swell-shrinkage and strength behaviours of ash-lime-treated soils and the evolution of $G_{max}$. In summary, this investigation can facilitate comprehending the complex behaviour of expansive soils treated with hydrated lime, bottom ash and bagasse ash, incorporating the electrical conductivity measurements and predicting their behaviour in the field through modelling analysis.

## ACKNOWLEDGEMENT

Foremost, I would like to express my profound gratitude to my principal supervisor, A/Prof Hadi Khabbaz, and my co-supervisor, A/Prof Behzad Fatahi, for their valuable guidance and continuous supports in my doctoral study, allowed me to be able to grow as a researcher in geotechnical engineering discipline. It would not have been possible to complete this thesis without their motivations and immense knowledge. Their valuable guidance gave me great inspiration in all time of my study, especially the precious and unforgettable period for conducting the experimental program and writing the dissertation.

I am indebted to the Vietnamese government and the University of Technology Sydney (UTS) for granting me the PhD scholarships. Without those scholarship offers, I could not have the chance to enrol the doctoral course and enhance my academic research skills and experience.

I also owe my sincere respect and earnest thankfulness to Dr Anh-Minh Tang, Dr Lam Dinh Nguyen, Mr Scott Graham, Mr Rami Haddad, Mr Antonio Reyno, Mr Herbert Yuan, Dr Mark Lockrey, Dr Thang Pham Ngoc, Mr Peter Brown, Mr Muller Hailu, Dr Johir Mohammed and other Civil Engineering laboratory staff for their assistance, supports and knowledge that they gave me. Under their guidance, my first glance of doctoral research was enlightened, which made me engaged in a relentless pursuit of geotechnical research career.

I also wish to thank my best colleagues, Dr Liet Chi Dang and Ms Reem Omar Alqaisi, who not only helped me a lot in experiments but also gave me great constructive comments and inspirations. I will not forget the time we carried out tests and the moments for stimulating our interesting discussion in the last four years.

I would like to offer my sincere gratitude to Prof David McGloin and Ms Van Le for their great advice and support. They have been really indispensable supporters for me to carry on investigations and complete the dissertation on time. I also would like to thank all my friends at the University of Technology Sydney for their consideration, sympathy and assistance in my research. They are Mohammad Adnan Farooq, Glen Burton, Tran Huyen Vu, Huu Sam Doan, Harry Nguyen, Habib Rasouli and Hossein Haddad.

Last but not least, I would like to express that I am eternally indebted to my parents and my sister. Because of them, I have had more power and passion to pursue my dream to study abroad. Finally, I would like to give my special thanks to Le Diem Thu, my beloved wife, whose patient love enabled me to complete this work.

## LIST OF PUBLICATIONS

- Le, M.T., Dang, L.C., & Khabbaz, H. (2018). Combined effects of bottom ash and lime on behaviour of expansive soil. *GeoMEast conference 2018*, Cairo, Egypt, vol. 10, pp. 28-44.
- Le, M.T., Dang, L.C., & Khabbaz, H. (2019). Strength characteristics of lime and bottom ash reinforced expansive soils. *Geo-Congress conference 2019*, Philadelphia, Pennsylvania, USA, 309, 352-362.
- Le, M.T., Fatahi B., & Khabbaz, H. (2022a). A modified electrical conductivity test to predict shrinkage-swelling behaviour of expansive soil treated with hydrated lime and bottom ash. *Géotechnique* (ready to be submitted).
- Le, M.T., Fatahi B., & Khabbaz, H. (2022b). Assessment of mechanical properties of expansive soils treated with hydrated lime, bottom ash and bagasse ash. *Géotechnique* (ready to be submitted).
- Le, M.T., Fatahi B., & Khabbaz, H. (2022c). Size effects of bagasse ash on the mechanical properties of bagasse-ash-lime-treated expansive soils. *Engineering Geology* (ready to be submitted).

## RELATED PUBLICATIONS

- Le, M.T., & Khabbaz, H. (2019). Predicting consolidation coefficient of soft clay by time-displacement-velocity methods. *16$^{th}$ Asian Regional Conference on Soil Mechanics and Geotechnical Engineering conference*, Taipei, Taiwan, TF-1, 1-4.
- Alqaisi, R., Le, M.T., & Khabbaz, H. (2019). Applications of recycled sustainable materials and by-products in soil stabilization. In *International Congress and Exhibition" Sustainable Civil Infrastructures",* 91-117, Springer, Cham.
- Alqaisi, R., Le, M.T., & Khabbaz, H. (2021). Combined effects of eggshell powder and hydrated lime on the properties of expansive soils. Australian Geomechanics Journal, *56*(1).

# Table of Contents

## LIST OF FIGURES

## LIST OF TABLES

## NOTATIONS

### Latin notations

| | |
|---|---|
| $C$ | Concentration |
| $C_c$ | Compression index |
| $C_s$ | Swelling index |
| $C_\alpha$ | Creep index |
| $c_k$ | Change in permeability |
| $e$ | Void ratio |
| $e_0$ | Initial void ratio |
| $E$ | Young's modulus |
| $EC$ | Electrical conductivity |
| $I_p$ | Plastic index |
| $G_{max}$ | Small-strain shear modulus |
| $G_s$ | Specific gravity |
| $K_0$ | At-rest earth pressure coefficient |
| $k_x$ | Vertical permeability |
| $k_y$ | Horizontal permeability |
| $LC_0$ | Initial loss in conductivity |
| $n$ | Porosity |
| pH | Potential of hydrogen |
| $PI$ | Plastic index |
| $PL$ | Plastic limit |
| $RC$ | Rate of electrical conductivity |
| $S_r$ | Degree of saturation |
| $t$ | Time |

$T$ Temperature

$T_c$ Temperature compensation coefficient

$V_s$ Shear wave velocity

$LL$ Liquid limit

**Greek notations**

γ Unit weight

κ Kappa

λ Lambda

ν Poisson's ratio

$\sigma'_v$ Effective stress

Φ' Friction angle

**Acronyms**

CBR California bearing ratio

CRS Constant rate of strain

CSH Calcium silicate hydrate

CASH Calcium aluminum silicate hydrate

BA Bagasse ash

BO Bottom ash

BB Bottom ash – bagasse ash

EDX Energy dispersive x-ray spectroscopy

*ITS* Indirect tensile strength

IL Incremental loading

KBS Kaolinite – bentonite – sand

L Lime

LVDT Linear variable differential transformer

MC Mohr Coulomb

MCC Modified cam clay

*MDD* Maximum dry density

MSH Magnesium silicate hydrate

*OCR* Over consolidation ratio

*OMC* Optimum moisture content

PVDs Prefabricated vertical drains

UCS Unconfined compressive strength

SEM Scanning Electron Microscopy

SSC Soft soil creep

XRD X-ray diffraction

# CHAPTER 1

# Introduction

## 1.1 Background

Expansive soil is a kind of any weak rock or soil that contains considerable fine clay particles with a potential to volume change when water content increases. The soil also has a low bearing capacity, swelling or shrinking under the change of ambient moisture, such as drying or wetting conditions under the changeable weather. The displacement range of changing from its swell to collapse can be considerable and expand the gaps in the unsaturated soil ground, causing the additional pressure developed in civil structures above. The phenomenon with increasing cracks becomes obvious to observe once the stresses increase to a stage greater than the strength capacity of highway subgrade or slab foundations, causing damage to superstructures, as shown in Figure 1.1.

The main goal of this study is to examine the effects of hydrated lime, bottom ash and bagasse ash on the engineering properties of expansive soil. The combination of lime and ashes can promisingly stabilise the soft soil by reducing its shrinkage-swelling behaviour and enhancing the mechanical characteristics of soil. The application of combining binders also provides a cost-effective construction material via reduction of lime dosage and extra soil reinforcement by the inclusion of lime and the two ashes. Therefore, a comprehensive study on experiments was carried

out on expansive soils with optimum hydrated lime contents and different ratios of bottom ash and bagasse ash after long-term curing.

*Figure 1.1 A damaged building in Melbourne caused by shrinkage settlement of foundation over-drying expansive soil after Considine (1984)*

Firstly, to predict the optimal ratio of bottom ash to lime, a series of electrical conductivity (EC) tests was conducted by changing ash content from 0% to 40% in suspensions of lime and soil. The initial loss in conductivity ($LC_0$) in aqueous mixtures was monitored, and the optimal ash-lime ratio was determined at the deflection of $LC_0$, which indicated an excess of lime over bottom ash. Secondly, for bagasse ash, the rates of *EC* were measured to evaluate the pozzolanic reaction of the ash in various sizes (i.e., 75, 150, 425 μm) and contents from 0% to 30%. Thirdly, for the combination of bottom ash and bagasse ash, *EC* was first used to determine the reasonable ratio of bottom ash to bagasse ash in their aqueous solution, and then $LC_0$ was employed to define their final ratios against lime. After ratios of ash to lime were estimated from EC tests, an array of experiments was performed to evaluate the characterisation of soil treated with lime, bottom ash and bagasse ash. The tests range from physical to mechanical approach, and micro-structural analysis was finally conducted to explain or validate the results of soil experiments. Finally, a

numerical analysis was also carried out to apply the experiment results to a case study of embankment on soft ground. A full-scale embankment constructed in Ballina, New South Wale, Australia, was employed to investigate the effect of chemical stabilisation on soft ground behaviour, including settlement and lateral movement. Numerically, in this 6.5-Ha embankment site, five models were proposed, including soil columns and the load transfer platform of embankment laying on the soft ground, which were created to support the embankment by providing a uniformly distributed settlement or reducing it by using the columns of treated soils. These treatments are provided and compared with behaviours of untreated ground to evaluate the proposed method.

In conclusion, through the experimental and numerical research, the study attempts to potentially contribute the knowledge of stabilisation of expansive soil by the combination of agricultural-industrial ashes (bagasse and bottom ash) with hydrated lime. The research implication indicates the importance of using the agricultural and industrial wastes to stabilise the problematic soil with lime for manual of designing light foundations or road subgrade on expansive ground.

## 1.2 Scope and objectives of research

The scope of study is to propose methods of electrical conductivity to predict the proper content of bottom ash and bagasse ash with hydrated lime to mitigate swell-shrinkage adverse effects and enhance the strength of expansive soils over curing days. Furthermore, extensive experimental methods, covering from physical to mechanical tests, were conducted to test the stabilised blends. The study results can show the geotechnical characteristics of bottom ash, bagasse ash and their compounds with expansive soil treated with hydrated lime. The goals are to produce optimum ratios of components in the mixtures to satisfy the road authorities' requirement as an engineering fill material as well as the need of reducing the energy use and conserving natural resources through economizing the conventional stabiliser like cement or lime for soil stabilisation. For this, an empirical investigation was undertaken to use the waste materials in road or light constructions on expansive ground to protect the environment from dumping ash in landfill sites. Finite element analysis of the mixtures is also performed using PLAXIS software for applying bottom-bagasse-ash-lime compounds to stabilise soft clay under embankment. Various solutions can be developed to eliminate the settlement and lateral displacement of ground beneath the embankment, which is based on a mechanical model of their blends during the long-term period. As a result, the objective of research is to achieve a comprehensive vision for the importance of recycling agro-industrial

wastes for sustainable infrastructure constructed on the expansive soft ground. Overall, the specific objectives of this study are shown as follows:

- To propose methods for electrical conductivity tests to predict the proper percentage of bottom ash and bagasse ash in ash-lime-treated soil to reduce the swell-shrinkage potential and improve the engineering characteristics of expansive soil so that the treated blends are suitable to be road subgrade materials. The relationships between electrical conductivity results and characteristics of treated soils can be established.
- To compare the effects of mixing ratios on the strength properties of soil treated with hydrated lime and bottom ash. The compared ratios include three types, which are based on the mass of: (1) dry soil; (2) dry total mixture; and (3) dry soil and ash.
- To study the effects of bagasse ash size on the characteristics of soil treated with hydrated lime and bagasse ash. The ash sizes consist of 75, 150 and 425 μm.
- To investigate the characterisation of soil treated with hydrated lime, bottom ash and bagasse ash. The investigation includes chemical, index/physical, mechanical and micro-structural analysis tests.
- To develop numerical models for predicting the settlement and deformation of Ballina road embankment constructed on treated soils in NSW, Australia using finite element method in the PLAXIS 2D program.

## 1.3 Thesis organisation

According to the research objectives of using bottom ash and bagasse ash for soil stabilisation, the study is divided into nine chapters, focusing on three main topics, namely electrical conductivity tests, characterisation of lime-ash-treated soils and numerical analysis of embankment on treated ground. These three contents are conveyed from Chapter 4 to Chapter 8, constituting the main body of the study. From Chapter 1 to Chapter 3, the necessity, literature gap and research design of the three mentioned topics are respectively addressed. The summary of this study is illustrated in Figure 1.2, presenting the structure of this dissertation. In this section, the contents of each chapter from 1 to 8 are summarised as follows:

In Chapter 1, the introduction of stabilising materials is presented in the context that expansive soil is causing gradual and extensive damages to civil constructions. In order to mitigate the relevant monetary loss, soil stabilisation is critical, and using binders for chemical treatments is highly recommended. Due to the proximity of local resources, bottom ash and bagasse ash are suggested as potentially effective binders to stabilise soil with the presence of hydrated lime.

However, there is limited research on quickly determining an optimal mixing ratio among binders to obtain the highest effectiveness of soil treatment. Furthermore, there is also a lack of study in mixing ratio and ash-size effects on strength characteristics of treated soils. The numerical design of embankment on treated soils with lime and studied ashes is also needed to support the technical and cost management of road construction projects in soft soil areas. Following this approach, the study aims to propose a rapid experimental method to roughly determine the optimal ratio of bottom ash and bagasse ash to lime for the effectiveness of soil shrinkage-swelling reduction and strength improvement. The research significance also includes the outstanding characterisation of expansive soil treated with hydrated lime, bottom ash and bagasse ash. The application of newly suggested material in the treatment design of embankment on soft soil is also depicted in numerical analysis. As a result, the study structure is proposed in Chapter 1.

Chapter 2 is allocated to a critical and comprehensive literature review on the three main research objectives. Chapter 3 discusses materials and testing methods suggested to address the proposed experimental program with the introduction of electrical conductivity tests A, B and C. Chapter 4 commences from lime-treated soil with the tests, which are later used in Chapters 5, 6 and 7 to determine the final ratio of bottom-bagasse ratio in their mix with soil and lime. In Chapter 5, three mixing ratios in bottom-ash-lime-treated soils are compared to have the suggestion of soil-ash ratio (SB ratio) for further investigations. With SB ratio, Chapter 6 compares the effects of ash size on linear shrinkage and strengths of bagasse-ash-lime treated soil and indicates that bagasse ash with 425µm gives the most effective stabilisation. The size of 425µm and SB ratio are utilised in Chapter 7 to investigate the characterisation of soils treated with hydrated lime, bottom ash and bagasse ash mixed in the ratio determined from electrical conductivity tests. Finally, four treated soils become input materials of treated soft ground under a testing embankment in Ballina Bypass in NSW, which are compared between five suggested models in Chapter 8, as shown in Figure 1.2.

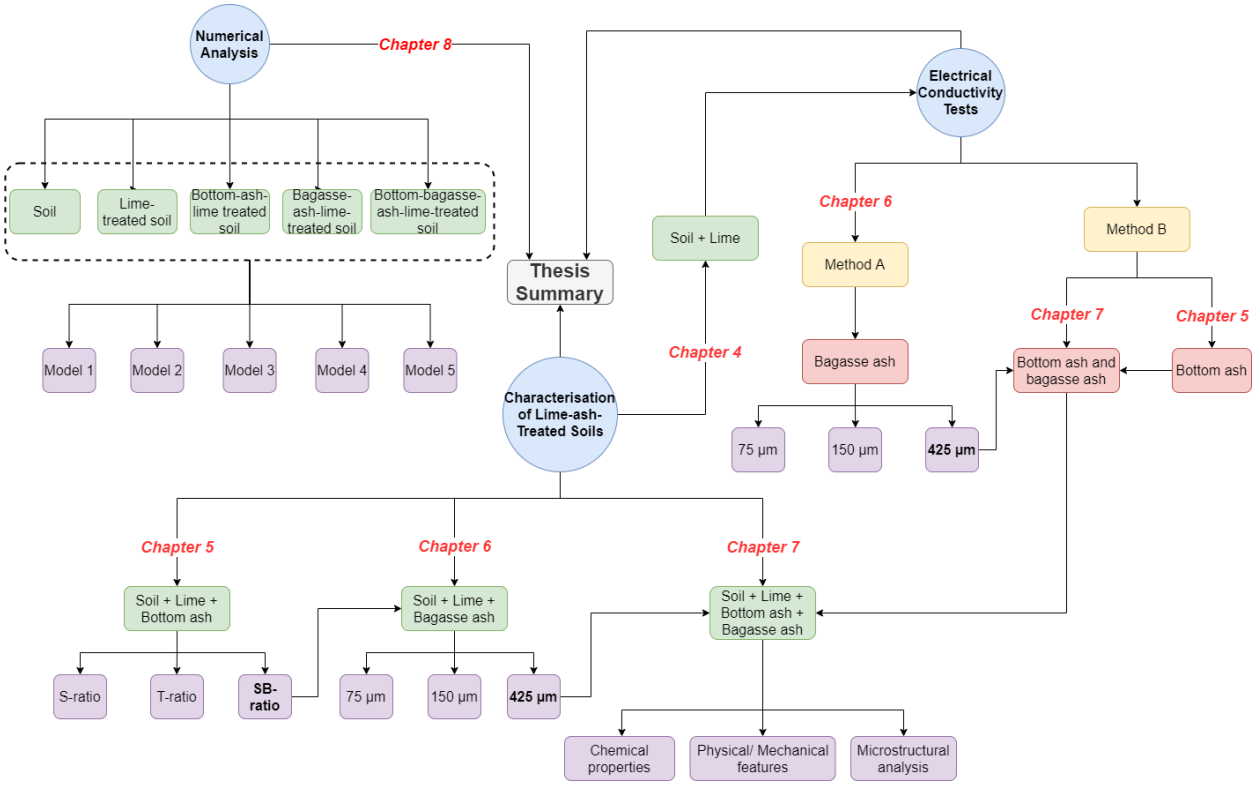


*Figure 1.2 Thesis structure from Chapter 4 to Chapter 8*

In detail, the thesis contains nine chapters as follows:

- Chapter 1 gives the introduction related to expansive soil, hydrated lime, bottom ash and bagasse ash, and methods of soil stabilisation. The chapter also indicates problem statements, describes research objectives, and outlines of thesis structure.
- Chapter 2 provides an intensive literature review on the stabilisation of expansive soil. The review goes from the global overview of using agricultural and industrial wastes in soil stabilisation to focusing on the local waste materials in Australia. The bottom ash and bagasse ash are then concentrated in investigations on characteristics of soil treated with ash and hydrated lime in various contents and curing time. The chapter aims to provide the overall view of the current studies of ash-lime-stabilised soils and emphasises their gap of research.
- Chapter 3 highlights the overview of studied materials, research methodology, including experimental methods, testing procedures and techniques of preparing samples. For materials, the chapter clarifies the components of testing samples, namely expansive soil, hydrated lime, bottom ash and bagasse ash. The combination of materials in treated soils is also described. For research methodology, an extensive testing program is provided, consisting of electrical, physical, mechanical, and micro-structural analysis tests. For

chemical tests, the chapter focuses on the electrical conductivity (EC) tests with the introduction of Tests A, B and C. For the EC procedure, the chapter also provides three testing methods, namely Test A, B and C, which are utilised in Chapters 4-7 for soils treated with lime, bottom ash and bagasse ash. The sample preparation and mixing designation are also illustrated with compaction types, moisturising and curing techniques. Finally, a numerical model is depicted to briefly demonstrate applications of treated materials to stabilising embankment on soft ground.

- Chapter 4 presents characteristics of expansive soils treated with hydrated lime. This chapter covers the experiments ranging from chemical tests to physical and mechanical ones. For electrical conductivity tests, the chapter clarifies the conductance properties of expansive soil, such as the relationship of *EC* with bentonite concentration and temperature. The temperature compensation coefficients of soil, lime and their mixture are also measured and calculated. From physical, mechanical and micro-structural analysis, engineering properties of soils treated with lime are revealed and compared with characteristics of untreated samples.
- Chapter 5 exhibits the use of electrical conductivity test (Test B) to predict the swell-shrinkage and strength characteristics of soil treated with bottom ash and hydrated lime. As a result, the optimal ratio of bottom ash to lime is also defined and discussed with the analysis from x-ray diffraction (XRD) and scanning electron microscopy (SEM). In the second part of this chapter, three types of mixing ratios are investigated and compared with the results of unconfined compressive strength (UCS), indirect tensile strength (ITS) and California bearing ration (CBR) tests. The discussion on the variation of small-strain shear modulus is also provided.
- Chapter 6 represents the utilisation of electrical conductivity test (Test A) to compare the pozzolanic activity of bagasse ash in different sizes (i.e., 75, 150, 425 μm) when the ash is mixed with soil and hydrated lime. The chapter attempts to find out which size of bagasse ash is appropriate to combine with hydrated lime to effectively stabilise expansive soil. The empirical approach includes four tests, namely linear shrinkage, UCS, bender element for $G_{max}$ and SEM tests. The chapter results also help to decide the proper bagasse-ash size to mix with bottom ash in their combination with soil and lime, which is illustrated in Chapter 7.
- Chapter 7 is the main chapter of this study, encompassing two sections, namely designation and application. In comparison, the properties of soil treated with hydrated lime and bottom

ash or bagasse are compared as an adaptation from Chapters 5 and 6. From the comparison, the evaluation on the combination of two ashes with lime in soil stabilisation is conducted, suggesting some recommendations on optimal ratios of ashes. In designation, there are two steps. In the first step, a trial process is performed, in which the optimal ratio of bottom ash to lime (found out from Chapter 5) is fixed, while the content of bagasse ash with a selected size (from the conclusion of Chapter 6) is varied. The results of the first step are references for the second step which uses Test C to design the optimal ratio of bottom ash to bagasse ash in lime-treated soils. Finally, in the application part, the found ratio is applied in testing programs to study the characterisation of bottom-bagasse-ash-lime-stabilised soils.

- Chapter 8 illustrates the numerical analysis of a Ballina embankment on soft ground in NSW, Australia, by using the PLAXIS program. Five models are suggested, including the use of studied material to treat topsoil layers and install treated soil columns in stratum to reduce settlement and deformation of the embankment. In each model, four materials, namely lime-treated soil, bottom-ash-lime-treated soil, bagasse-ash-lime-treated soil, and bottom-bagasse ash-treated soil, are assigned and compared while their input parameters are retrieved from Chapters 4, 5, 6 and 7, respectively. The chapter results in an optimal design to construct road embankment on soft ground in Ballina, NSW, Australia.
- Chapter 9 presents the summary and recommendations for future studies. The summary indicates three main conclusions related to electrical conductivity tests, characterisation of ash-lime-treated soils and numerical analysis. The chapter also suggests recommendations for future investigations.

# CHAPTER 2

# Literature Review

## 2.1 Expansive soil

Expansive soil appears mainly in decomposed soil and expands its volume under dry-wet conditions or exposure to the change of water content. To explain these expansive characteristics, clay micelle is termed to consider three main elements for expansion, including minerals, cations and associated water (Nelson et al., 2015). The clay mineral or particle and the cations with hydration and osmotic water, which is the water molecules in the location of high concentration of cations, are held around the inner core of mineral to form a clay micelle, which is shown in Figure 2.1.

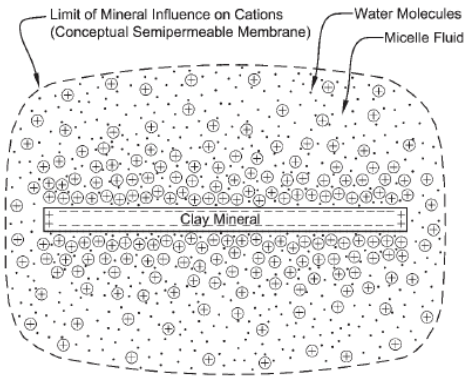


*Figure 2.1 A clay micelle (after Nelson et al. 2015)*

The aqueous solution covering a micelle unit is the micelle fluid building up the unit thickness and expanding the influence area of the clay particle by the absorbed cation and electrical charges of surface. The micelle fluid thickness is different among the clay minerals, such as 200 Angstrom for montmorillonite and 400 Angstrom for kaolinite, resulting in the size of kaolinite being 100 times thicker than that of montmorillonite (Grim, 1959; Lambe, 1958a). The swelling phenomenon of expansive soil related to the micelle fluid consists of two consecutive stages, namely crystalline phase related to cation hydration and osmotic phase involved in the attraction of osmotic water to the interparticle. The cycles of drying and wetting the expansive soil cause the addition and removal of much crystalline and osmotic water around the soil particle, resulting in a massive change of volume when the water content fluctuates. With the smaller size of particle but the larger ratio of micelle fluid to the particle in montmorillonite than in kaolinite, the former mineral has plenty of micelles more than the latter one. As a result, montmorillonite is an expansive mineral with a high liquid limit and expansive potential, while kaolinite is commonly non-expansive. Meanwhile, illite particles have the same structure as montmorillonite. However, illite is filled by potassium ions among the silica sheets building up strong bonds between the particles (Grim, 1959). Therefore, illite and kaolinite are much less expansive than montmorillonite, thus does not pose a dire problem to civil structures, such as footings, highways, earth fill constructed on expansive soft ground.

There is an urgent need to carry on the building safety related to construction and occupation of facilities and infrastructure on expansive soil. Twenty per cent of Australia continent surface is expansive soil or problematic soft soil (refer to Figure 2.2), which yields the demand to recycle this soil for civil purposes. Furthermore, due to its high swelling and shrinkage, various commercial buildings are suffering from minor damages such as cracks to serious ones like inclined façade or even collapse. Unfortunately, there are a few effective remedies to solve this issue once it occurs. In contrast, the prevention from design steps in which foundation reinforcement is produced can best help to solve the root cause of the problem. The research on this area is by far promising when it can enable the sustainable development of future infrastructure by using the recycled waste to stabilise ground; by there, a cost of approximately 100 million AUD can be economised from the damage maintenance every year. The expansive-soil stabilisation, therefore, becomes the indispensable requirement for large-scale projects of constructions on expansive foundations.

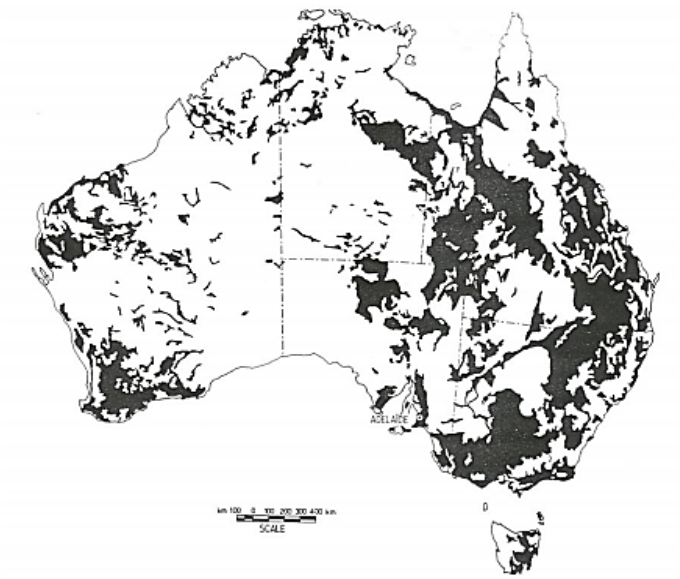


*Figure 2.2 Distribution of expansive soil in Australia (Richards et al., 1983)*

However, the degree of swelling or shrinkage of expansive soil is not consistent and varies from one region to another. Even in the same location, the presence of expansive soil makes a considerable variation of soil characterisation. This type of soil is also known as problematic soil. Nevertheless, for studying the behaviour of this soil systematically, it can be noted that some chemical compounds in this soil play a primary role in its swelling and shrinking properties. Of the chemicals considered, montmorillonite, a kind of expansive clay mineral, can speed up the swelling and shrinkage rate, whereas kaolinite is perceived as a less expansive material, which helps to reduce the swelling incidence (Das & Sobhan, 2013; Holtz et al., 1981). Likewise, sand as a coarse and non-plastic material can diminish the swelling potential of expansive soil. The right combination of three materials can produce a compacted sample that illustrates the field characteristic of expansive soil, and thus a desired constitutive sample can be formed, which facilitates research on the complex behaviour of soft soil (Le, 2015; Le et al., 2015).

## 2.2 Stabilisation methods for expansive soil

### 2.2.1 Problems from expansive soil

As mentioned above, expansive soil has a low bearing capacity, high potential of swelling and shrinkage due to changes in ambient moisture. These properties pose a threat to the foundations of civil structures, such as railway track beds, pavements, highways, light buildings and canal linings (Tang et al., 2009). The risks become visible in cracks on superstructures when the expansive ground has high swelling pressure or low bearing capacity, causing heave- or settlement-related damages, respectively (Phani Kumar & Sharma, 2004). Annual statistics of these damages

indicated that there was a loss of about 400 million pounds in the UK and over 15 billion dollars in the USA (Jones & Jefferson, 2012; Viswanadham et al., 2009). Therefore, it is crucial to evaluate and control the shrinkage-swelling potential of expansive soil to reduce the detrimental impacts.

### 2.2.2 Chemical stabilisation method

Regarding the expansive soil stabilization, this is the process in which the characteristics of soil are stabilized and improved, resulting in higher bearing capacity, shear and compressive strengths and durability under adverse weather conditions like continuous drying and wetting cycles. The existing mechanical methods to limit the problematic behaviour of expansive soil are stone columns (Fatahi et al., 2012), pile-supported and geosynthetic earth platform (Han & Gabr, 2002; Liu et al., 2007), sand cushion technique (Satyanarayana, 1966), belled piers (Chen, 2012), granular pile-anchors (Phanikumar, 1997). However, chemical soil stabilisation has recently received much more attention (Nguyen et al., 2019; Wang et al., 2020a; Wang et al., 2017b; Wang et al., 2020b; Wang et al., 2017c). This method is one of the effective solutions to enhance these properties by mixing chemical stabilizers or additives with expansive soils (Cokca, 2001; Edil et al., 2006). The chemical treatment, mixing chemical agents with soil, is also promising and received a great deal of attention through extensive studies (Bergado et al., 1996; Cokca, 2001; Edil et al., 2006; Fatahi et al., 2013; Fatahi et al., 2012; Khabbaz & Fatahi, 2012; Nguyen et al., 2014; Osinubi et al., 2009a; Phanikumar, 2009). The binders for soil chemical stabilization can be originated from a variety of sources, but simply they can be classified into two main categories, including agricultural and industrial materials. For agricultural by-products, some ashes like bagasse ash were explored to enhance the engineering properties of expansive soil (Dang et al., 2016b; Dang et al., 2015; Osinubi et al., 2009a). Other farming wastes, such as rice husk ash, coconut coir fibre or even eggshells, are utilized to enhance the soil strength and alleviate the problems related to free swelling and shrinkage of expansive soil (Anggraini et al., 2016; Basha et al., 2003; Rahman, 1986; Sivakumar Babu et al., 2008). Meanwhile, industrially originated products, such as fly ash, silica fume or cement, become common stabilizing additives in soil treatment (Bagherpour & Choobbasti, 2003; Consoli et al., 1998; Lorenzo & Bergado, 2004; Miller & Azad, 2000).

On the major demand for recycling ash wastes from agricultural and industrial activities, a great deal of by-products is becoming the chemical binders in this sort of stabilization method, such as bagasse ash (Dang et al., 2016b), rice hush ash (Kumar & Gupta, 2016), fly ash or bottom

ash (Kamei et al., 2013; Kim & Do, 2012). Generally, these waste products are the materials rich in divalent and trivalent cations, namely $Ca^{2+}$, $Fe^{3+}$ and $Al^{3+}$, which can promote the flocculation or aggregation of clay particles through the exchange of cation with reactive soil (Chen, 2012; Sharma et al., 2008). However, the combination of expansive soil and ash products does not always generate a significant improvement in soil strength. That is, only a minor increase of strength in the ash-soil samples could be observed in the high content of ash in the admixtures (Dang et al., 2016b). Even worse, increasing the content of coal ash in mixtures of soft soil had a negative impact on the stress-strain improvement (Kamei et al., 2013; Le et al., 2018). The reduction in the mixture strength can be attributed to the fact that the ash materials, considered as class F ash, has an unremarkable ability of self-cementation due to the insufficient content of calcium oxide (CaO) for activating pozzolanic reactions in the soil blend (Kamei et al., 2013; Le et al., 2018). Therefore, lime, as the great source of calcium ions ($Ca^{2+}$), can enrich this amount of divalent cations in the ash-lime-soil mixture. The combination of ash and hydrated lime, as a result, brings about their combined effect on soil strength, producing higher compressive strength and bearing capacity of expansive soil than ash or lime when each of them is used to stabilize the soil (Dang et al., 2016b; Le et al., 2018).

### 2.2.3 Lime stabilisation

Hydrated lime is an outstanding example for the treatment of expansive soil because of its impressive improvement effect on soil strength. The development of strength in lime-soil mixture can be clarified into two processes, namely, the modification and stabilization (Nguyen et al., 2014). While soil modification relates to reactions of flocculation and cation exchange between lime and clay in the short term, the next process in long terms is involved in the soil stabilisation with pozzolanic reactivity to form cementitious bonds with crystal formulation, namely compounds-calcium silicate hydrates (CSH) and calcium aluminate hydrates (CAH) in the soil blend. Further studies on the combination of lime and bagasse ash in soil admixture have proven the better enhancement in soil strength by addition of divalent and trivalent cations, such as $Ca^{2+}$, $Fe^{3+}$ and $Al^{3+}$, from ash to enhance the exchange of cation with reactive soil (Ajay Goyal et al., 2007; Chen, 2012; Ganesan et al., 2007; Manikandan & Moganraj, 2014; Osinubi et al., 2009a; Sharma et al., 2008). Bottom ash is one of such pozzolanic materials that can be utilized to improve this exchange formulation. However, there are very limited studies on the combination of bottom ash and lime for the stabilisation of expansive soil. Hence, further investigation on their combined dosage for soil treatment is necessary to provide a better understanding of the bottom ash-lime-soil behaviour.

## 2.3 Agricultural-industrial wastes for soil stabilisation

### 2.3.1 Agricultural-industrial waste materials

The enormous quantities of by-product materials have been produced by agricultural and industrial (agro-industrial) developments as well as the growth of population. The agro-industrial wastes consist of a wide variety of by-products: (1) for agricultural by-products, including ash wastes (bagasse, eggshell, rice husk, straw and wood ash), and fibres (coconut and bagasse fibre); (2) for industrial by-products, such as bottom and fly ash, silica fume, steel slag, carpet and polypropylene fibre, asphalt residue, tyre rubber, glass cullet. The escalating disposal of these waste products and shortage of natural material and landfill sites show the urgency of sustainable and reasonable usage of these waste materials (Ali et al., 2011; Disfani et al., 2011; Disfani et al., 2015). Therefore, reusing discarded materials can ease the pressure on the increasing need for virgin natural resources and recycling wastes, resulting in a minimization of waste, cutting down the energy use and lowering carbon footprints (Disfani et al., 2012; Disfani et al., 2013). As one of the solutions for waste treatment, incineration is recommended to burn the waste due to the escalating cost of removal and constraint areas for landfill sites. Ashes with unburned residues can be produced from incinerators in which the agro-industrial wastes are combustible to generate the energy of heating. With the development of agriculture and industry in many countries, more and more ash waste production is increasing in large quantity (Frías et al., 2011; Punthutaecha, 2002). According to the American Coal Ash Association (ACAA), there was 18.6 million tons of bottom ash generated from US industrial facilities in 2006 (Association, 2008). Meanwhile, there will be more than 1 trillion tons of sugarcanes produced in 2020 from farms in Brazil, which indicates the burning issues of recycling bagasse ash from combustion chambers which obviously induces pollution and harms human health (Frías et al., 2011). The utilisation of both agricultural and industrial wastes for soil stabilisation in construction projects is the multiple benefits not only for the environment but also for sustainable development of local infrastructure on the expansive ground. There are a variety of admixtures that could be used for reinforcing expansive soils, and their combination can improve some characteristics of soft soil. While each additive can harness the strength of expansive soil, the mixture can, to some extent, impact the engineering properties of soil more positively.

### 2.3.2 Classification

Waste material is generated from manufacturing and human activities, and the material is also seen as the by-product at low costs. Meanwhile, soil stabilisation methods have been existed for many years to enhance the ability of highways, railways, bridges, and runways to carry traffic by mixing

the soft soils with cement or pozzolanic wastes as raw materials like fly ash and limestone (Hejazi et al., 2012). Unlike waste, conventional materials like cement are confronting a scarcity from the gradual depletion of natural resources, whereas the amount of wastes is increasing rapidly in quantity and from various sources (Bolden IV, 2013; Correia et al., 2016). According to the 2010-2011 report from the Department of the Environment and Energy (DEE), Australia, the considerable amount of waste was from the process of construction and agriculture, occupying 26% and 24% in total proportion, respectively (Figure 2.3). The fly ash, as the light coal ash floating into the exhaust tacks of coal-fired factories, was the second-highest waste disposal in Australia, and other waste materials have marginal portions, which are shown in Figure 2.3. Therefore, the waste resource could be considered into two main categories: (1) agricultural waste and (2) industrial waste.

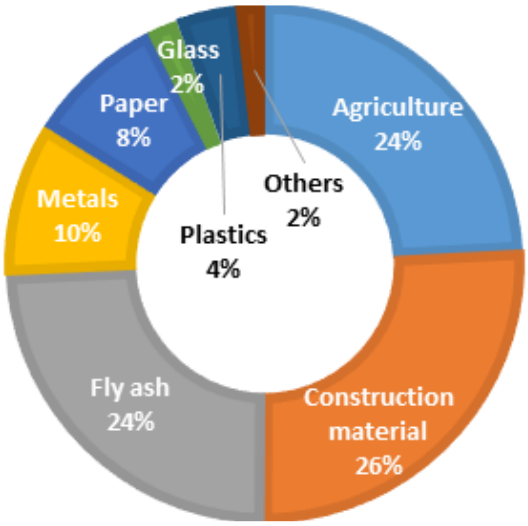


*Figure 2.3 Proportion of waste material in a total of 57.9 million tons disposed in Australia from 2006 to 2010 (DEE report 2010)*

Based on the form of the waste, the binders can be classified into two kinds: (1) waste powder and (2) waste fibre. Of more than 100 papers reviewed from 1992 to 2017, the additives in each kind are clarified in the percentage they are used for soil stabilisation, as presented in Figure 2.4. In this figure, the left pie (Figure 2.4a) compares the proportion of powder binders employed in recent publications, while the right-hand-side pie (Figure 2.4b) illustrates the proportion of fibre binders surveyed in 50 recent papers.

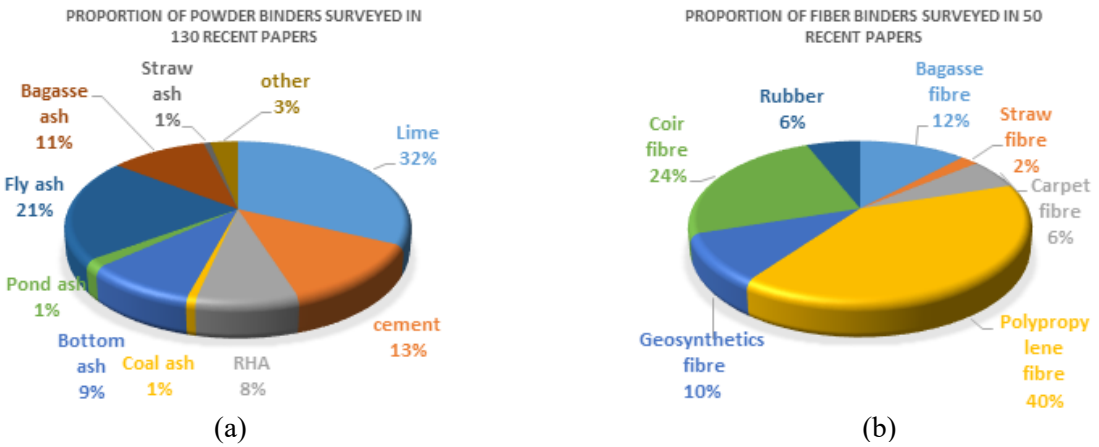


(a) (b)

*Figure 2.4 Comparison of studies on different types of binders in terms of (a) powder and (b) fibre*

Overall, as shown in Figure 2.4a, burgeoning research papers referred to lime as a pivotal role of chemical agents in the reinforced mixtures with expansive soils. Even though some new binders appear related to ash, the list of powder binders is obviously inundated with lime in most studies on chemical soil-hardening methods. Meanwhile, Figure 2.4b shows the dominant proportion of polypropylene fibre in treated soil mixtures, indicating the interest in studying this kind of domestic waste for soil stabilisation. The agricultural fibre, namely coir and bagasse fibre, is the second most common fibrous material for soil treatment research. This research mainstream is reasonable with the increasing disposal of agricultural waste with the industrialisation and globalisation in many countries, especially tropical and developing nations.

### 2.3.3 Brief history

The history of stabilising weak soils by stabilising agents has lasted for a long time since Romans used pulverised limestone or calcium to reinforce the pathways on soft soils (Ellaby, 2010). When it came to fibre reinforcement, the application of fibre to ancient civilizations experienced the utilisation of straw or hay to treat mud for building up the blocks of buildings more than 5 millennia ago (Abtahi et al., 2009). In the modern technique of soil stabilisation, Vidal (1969) introduced the principal concept of using reinforcing additives to increase the shear resistance of soil mass. So far, around 4000 constructions have been erected in about 40 countries using his concept of ground reinforcement (Azeem & Ati, 1992; Juyal et al., 1994). Consequently, it can be concluded that the principles in using the agent and fibres were started in ancient times. However, the combinations of various agro-industrial wastes for expansive soil treatment have recently received special consideration from geotechnical engineers and researchers for the second time (Hejazi et al., 2012).

## 2.4 Agricultural wastes for soil stabilisation

### 2.4.1 Bagasse ash

Bagasse ash is collected from the sugarcane fibrous by-product as a result of manufacturing in the sugar refining industry. The solid material is disposed of the extraction of sugarcane is the bagasse, which is burned to produce bagasse ash. In the sugar refining factories, this waste is incinerated at the heating temperature from 700°C to 900°C, and it turns into bagasse ash. For composition, bagasse ash primarily comprises oxides of aluminium and silicon, which can be employed to enhance the engineering properties of black cotton soil (Sabat & Pati, 2014; Srinivasan & Sathiya, 2010). The ash contains a significant amount of silica and aluminium, which can enhance the engineering characteristic of expansive soils (Sabat & Pati, 2014; Srinivasan & Sathiya, 2010) and concreate admixtures (Bahurudeen et al., 2014; Bahurudeen & Santhanam, 2014; Chusilp et al., 2009b; Cordeiro et al., 2008; Cordeiro et al., 2009b; Frías et al., 2011; Ganesan et al., 2007; Oliveira De Paula et al., 2010). Extensive studies were performed to investigate the combined effects of bagasse ash (BA) and lime on the engineering properties of various types of soil (Alavéz-Ramírez et al., 2012; Anupam & Kumar, 2013; Manikandan & Moganraj, 2014; Sujjavanidi & Duangchan, 2004). Furthermore, the combined effect of bagasse ash and lime was more effective than that of bagasse ash alone in improving the engineering characteristics (Dang et al., 2016b; Modarres & Nosoudy, 2015). It is of interest to note that intensive studies have indicated the pozzolanic reactions in bagasse ash treated soil and concluded that this ash is a promising material for improving the engineering behaviour of expansive soil (Anupam & Kumar, 2013; Manikandan & Moganraj, 2014; Sujjavanidi & Duangchan, 2004).

For compacted blocks of soils, Alavéz-Ramírez et al. (2012) referred that 10% BA with 10% lime can improve the mechanical behaviour of soil samples. For lateritic soil, (Salahudeen & Ochepo, 2015) asserted that 6% BA with 8% lime could produce the highest unconfined compressive strength (*UCS*) and California bearing ratio (*CBR*). Regarding the reinforcement of road subgrade on expansive soil, Sabat (2012c) believed that the lime-bagasse ash ratio of 1 to 4 is the optimum value for the swelling improvement. In the combination of bagasse and cement, the ratio of 8% BA to 4% cement in lateritic soil mixtures can change shear strength properties by increasing internal friction angles and decreasing the cohesion (Mu'Azu, 2007). Although some study by (Manikandan & Moganraj, 2014) concluded that using bagasse ash alone can have negative impacts on consolidation properties, Kharade et al. (2014) realised that 6% BA can increase the maximum dry density, *UCS* and *CBR* to optimum values. However, the inclusion of lime and bagasse ash can obviously give a significant improvement in the engineering characteristics of mixed expansive soil.

### 2.4.2 Eggshell ash

From the food manufacture in factories, shops and hatcheries, a large source of eggshell is dumped. This certainly impacts the environment because it contains a large content of calcium and needs to recycle properly. Due to the composition of eggshell with high calcium content, this is a promising resource for soil stability instead of lime as usual (Pliya & Cree, 2015; Rao & Chittaranjan, 2011). When the eggshell is ground, it turns into eggshell powder (ESP). The study carried out by Amu et al. (2005) discovered that the optimum ratio of lime to ESP is 3 to 4%, respectively, while Muthu Kumar and Tamilarasan (2014) found that without lime, the optimum percentage of ESP for expansive soil treatment should be 3%. However, Barazesh et al. (2012) assured the optimum content of ESP should be much than that, up to 16%. In terms of shrink-swell properties, the optimal lime-ESP ratio should be 4% to 8% in their admixtures with expansive soils (Nyankson et al., 2013). In the case of lateritic soil from the study of Olarewaju et al. (2011), cement-treated soil is compared with eggshell-treated soil, and the author claimed that 8% eggshell is equivalent to 2% cement in terms of Atterberg limits and *CBR*. In the research by Paul et al. (2014), quarry dust is combined with ESP to enhance the shearing properties and compressive behaviours. The optimum value was produced at 20% for ESP with 30% for quarry dust.

### 2.4.3 Rice husk ash

Rice husk ash (RHA) is produced through burning rice husk, which is obtained from paddies. The material has a rich source of silica which is the promising activator with pozzolanic features (Rao & Chittaranjan, 2011). Mixing with cement in soil stabilisation, RHA can be blended with lateritic soil in the content varying from 4 to 6% to replace cement partly but still improve *UCS* and *CBR* values with the small cement dosage at 6-8%. For generating a proper road subbase, the optimal cement-RHA ratio of 3 to 6% is proposed by Rahman (1987). Similarly, the residual soils need RHA and cement and RHA content, at 4% and 5%, respectively, for the highest *CBR* value of 60%. In natural clayey soils, at the lime-RHA ratio of 10% to 12.5%, most engineering properties of the mixture are improved, including plasticity index, swelling potential, *CBR* and shearing properties. The inclusion of fibre or calcium chloride in RHA-treated soils also enhance *UCS*, *CBR*, hydraulic conductivity and swelling behaviour (Sabat, 2012a; Sharma et al., 2008). However, without the third element, expansive soil treated with RHA alone could not be improved significantly in *UCS* value even the percentage of RHA from 8% to 12% added to soil blend (Alhassan, 2008).

### 2.4.4 Wood ash

Wood ash is produced from the combustion of wood branches or trunks in the fireplace or power plants. In the form of powder, the ash is rich in potassium as a good fertiliser for gardening (Demeyer et al., 2001). The wood ash also enhances the plasticity of clayey soil when 1-25% ash content can reduce the liquid limit of clay (Barazesh et al., 2012). Similarly, Bade et al. (2017) mixed wood shaving ash with black cotton soil and found the optimum ash content of 25%, reducing the plasticity index to the lowest value of 16.56. For natural sand, wood ash with a content of 10 and 20% in soils can improve the immediate bearing index fourfold compared to untreated soil (Šķēls et al., 2016). However, concerning *CBR* values, Amu et al. (2005) inferred that soil stabilisation should be carried out with lime only rather than wood ash. For maximum dry density, wood ash is preferred at the optimal percentage of 6% for wood ash and lime.

### 2.4.5 Coconut fibre

Coconut fibre or coconut coir is given from the coconut husk, consisting of 54% cellulose and 46% lignin (Anggraini et al., 2016). The fibrous material with a high lignin content could be accepted as the stabilising additive for soil (Khatri et al., 2016). With the optimum length of 1.5 cm and 5% in weight content, coir fibre could improve the *CBR* value and plays the role of coir geotextile (Abhijith, 2015). The effectiveness of placing the coir in subgrade for strength improvement is on the surface rather than the lower positions. When it comes to adding coal ash in coir-treated silty soil, the optimum ash-fibre ratio of 20% to 0.25% gave the maximum values of *CBR* and *UCS* (Singh & Palsule, 2014). It means the combination of ash and fibre with soil can greatly enhance the soil properties than ash or fibre alone for soil treatment. Furthermore, using the short length of coir fibre in the random mixing with soil can reinforce the mixture strength.

### 2.4.6 Bagasse fibre

Bagasse fibre is the by-product from the manufactory of the sugar cane industry. The fibre is obtained by crushing the sugar can for juice extraction. Alongside applications to soil stabilisation, bagasse fibre can be used for cement and composites (Bilba et al., 2003; Cao et al., 2006). For clayey and sandy soil treatments, the high content of bagasse fibre could increase the shearing parameters of mixed soils with the highest values at the optimum fibre content at 1.4% (Oderah, 2015). Where lime inclusion is concerned, the enhancement of soil properties by combining lime and fibre is more apparent. The optimum ratio of bagasse fibre to lime is obtained at 0.5 compared to 7%, respectively (Dang et al., 2016a). The longer curing time also reduced the linear shrinkage

of lime-fibre treated expansive soil while the *UCS* value increased. However, despite advantages in soil strength reinforcement, using the bagasse fibre for mixture durability should be noticed with more modifications for fibre treatment.

### 2.4.7 Summary of agricultural wastes

To have an overall look at recycling the agricultural waste material for soil stabilisation, the merits and demerits of each waste in this treatment are tabulated and compared in Table 2.1.

*Table 2.1 Comparison of agricultural wastes for soil stabilisation*

| Agricultural wastes | Origin | Merits | Demerits | References |
|---|---|---|---|---|
| Bagasse ash | Sugar cane factories | High content of silica.<br>At no cost.<br>Low $CO_2$ emission and energy consumption. | Insignificant stabilising effects on soil<br>Environmental issues related to store raw material for prolonged time. | Schettino and Holanda (2015) |
| Eggshell ash | Farming hatcheries, diary shops, factories | The natural resource of lime<br>Soil reinforcement in shearing resistance.<br>At low cost and carbon footprint. | Cations on the ash dosage in soil treatment to avoid any adverse effect. | Pliya and Cree (2015) |
| Rice husk ash | Paddy fields, rice mills | The material recycling can minimise carbon footprint and energy consumption. | Carefully control ash quality by grinding or incinerating to obtain the highest impacts on soil stabilisation.<br>Be more suitable to farming countries or local regions to meet the transport cost. | Rao and Chittaranjan (2011) |
| Wood ash | Fireplace or power plants in forests | Using ash for soil treatment reduces carbon footprint and energy consumption for forest road stabilisation.<br>The material at low cost and good fertilizers for farming.<br>Ability to absorb contaminants to filter wastewater as alkalinity. | Because of low corrosive capacity, the ash mixed material can be cracked under external impacts.<br>Cracking-prone characteristics induce the ash mixtures to have low stability and durability. | Cheah and Ramli (2011) |
| Coconut fibre | Coconut plantations | Environmentally friendly nature with fungi and rot resistance.<br>Low-cost material.<br>Good heating and sound insulation. | Chemical impacts such as permeability, penetration of saturated lime and solidum hydroxide cause the strength reduction of fibre-soil mixtures. | Ali et al. (2012) |
| Bagasse fibre | Sugar cane factories | Combustible material for energy supply.<br>Recycling fibre waste resolves the environmental issue related to disposal. | Low durability with prolonged time with fibre degradation.<br>Low resistance with moisture change<br>Fibre incompatibility.<br>The concentration of fibre defect causes the unreliable effects on soil improvement. | Ghazali et al. (2008) |

## 2.5 Industrial wastes for soil stabilisation

### 2.5.1 Bottom ash

Bottom ash is a by-product from the burning process in coal-fired power stations, which constitutes most coal ash production to produce energy. It is also known as the dry pulverized coal boiler from the combustion process in the thermoelectric plants. This product of the coal-burning furnace is the remaining 20% of non-combustible material with porous, dark grey material in size of gravel and sand (Wilcox, 1978). Although bottom ash exists at the bottom of combustion chamber, the waste material is rather lighter and brittle (Rogbeck & Knutz, 1996). Therefore, bottom ash is aggregate utilised in lightweight concrete or raw material for cement (Association, 2008; Canpolat et al., 2004; Cheriaf et al., 1999). About 45% of all bottom ash was used for transportation construction such as road subgrade or subbase and embankment fill (Association, 2008). Figure 2.5 presents the most common utilisation of bottom ash in many sectors from cement replacement to waste stabilisation.

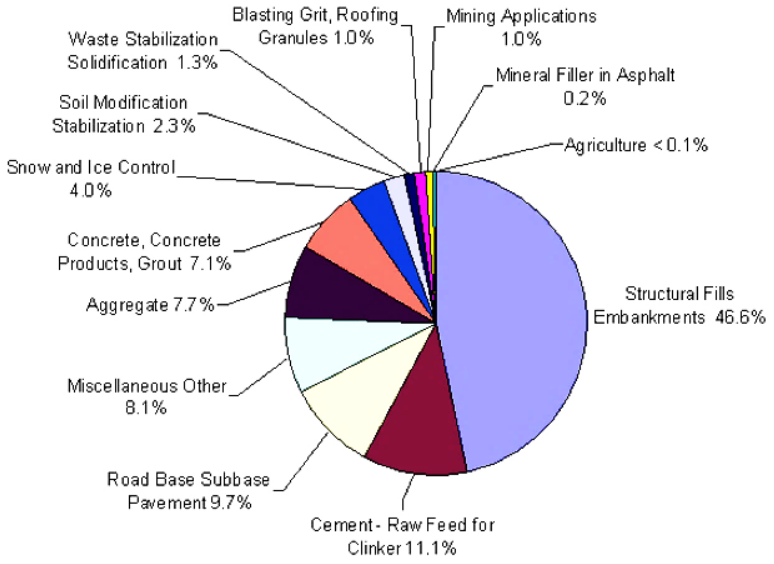


*Figure 2.5 Bottom ash utilisation in the percentage of total recycling usage (Association, 2008)*

As for embankment or backfill material, bottom ash has been used as a fill material for road embankments or retaining walls. This sand-like material suitable for construction application should be designed at the optimum moisture content and eliminate the porous particle or popcorn-like grains. Therefore, using bottom ash may require grinding or screening to dispose of the large material of about 2 cm in size. In the grain size distribution, Figure 2.6 compares the sieving analysis results from various sources of bottom ash samples in the US.

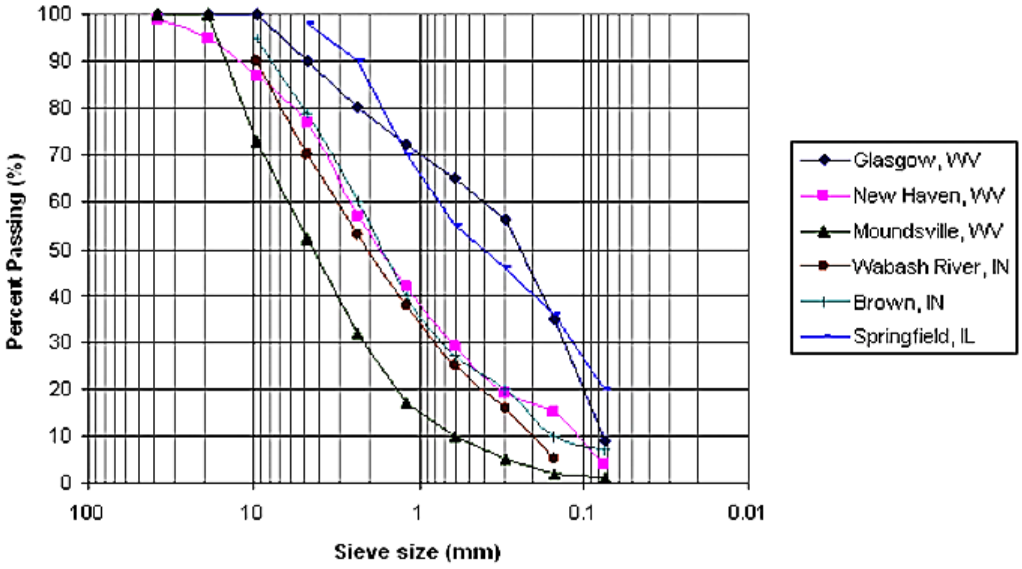


*Figure 2.6 Particle size distribution curves of several bottom ash resources (Katz & Kovler, 2004; Kim & Prezzi, 2008; Kumar & Vaddu, 2004; Moulton, 1973)*

As can be seen from this figure, bottom ash is predominated by the sand-size particles, which usually pass the sieve of 4.75 mm and 0 to 10%, passing the sieve of 0.075 mm. This material is commonly the well-graded grain particles, even though there are some variations of the grain size distribution of ash from various power plants. The physical and mechanical properties of bottom ash, therefore, have a great similarity to sand material, which are listed in Table 2.2.

*Table 2.2 Physical and mechanical properties of bottom ash (Lovell et al., 1991; Majizadeh et al., 1979; Moulton, 1973; Prakash & Sridharan, 2006; Rogbeck & Knutz, 1996; Siddiki et al., 2004; Tanyu et al., 2004)*

| Physical Properties | Values | Mechanical Properties | Values |
|---|---|---|---|
| Specific gravity | 2.1-2.7 | Maximum dry density ($Mg/m^3$) | 1.18-1.57 |
| Dry unit weight ($kN/m^3$) | 7.07-15.72 | Optimum moisture content (%) | 12-24 |
| Plasticity | None | Internal friction angle (°) | 32-45 |
| Absorption (%) | 0.8-2.0 | California Bearing Ratio (*CBR*) (%) | 21-110 |
| | | Hydraulic conductivity (cm/sec) | 1-0.001 |

In terms of chemical composition, bottom ash encompasses primarily silica ($SiO_2$) and alumina ($Al_2O_3$), and a lesser content of calcium oxide (CaO) and ferric oxide ($Fe_2O_3$) (López-López et al., 2015). Figure 2.7 shows the chemical analysis of bottom ash samples from many places in the US. The composition characteristic of bottom ash is similar to class F fly ash which has a grey colour and low calcium content (Lav & Kenny, 1996).

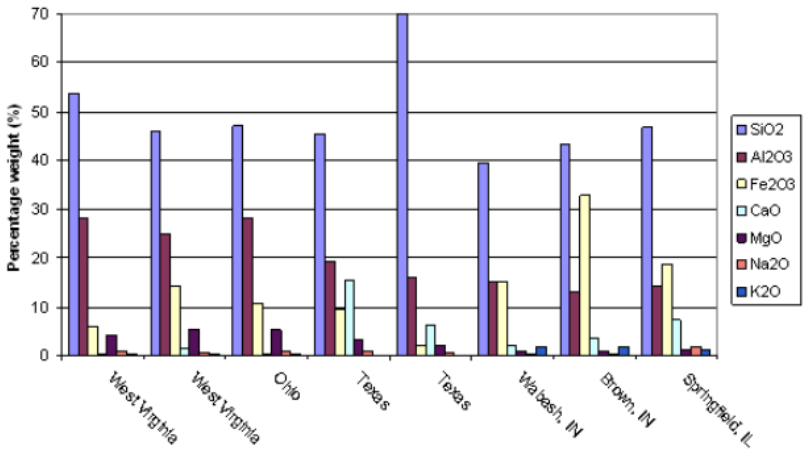


*Figure 2.7 Chemical composition of bottom ash samples from various power plants in the US (Andrade et al., 2007; Kim et al., 2005; Kumar & Vaddu, 2004; Moulton, 1973; Özkan et al., 2007)*

However, unlike fly ash with a fine structure, bottom ash is a granular and coarse material. Therefore, it is reasonable to treat fine-grained soil in applications related to geotechnical solutions for the filling materials with large volumes, such as highways, embankments, fills or backfills (Kim & Prezzi, 2008). Therefore, bottom ash can produce high-quality aggregates when it is combined with fine clay binders (Geetha & Ramamurthy, 2011). Furthermore, coal ash has an extensive record in utilization for soft soil stabilization due to its pozzolanic reactions and self-cementing properties (Kayabal & Buluş, 2000; Mackiewicz & Ferguson, 2005). The engineering performance of bottom ash as a construction material relies on various factors, such as the density, the grain size distribution, the compaction properties, the hydraulic conductivity and the shear strength parameters (Cheriaf et al., 1999; Huang & Lovell, 1990; Jorat et al., 2011; Kim et al., 2005; Kim & Do, 2012; Kim et al., 2011). From these influencing factors, recent studies on bottom ash have indicated adverse effects on soil compressive strength when only bottom ash stabilises expansive soil without combining other activators like basanite or rice husk ash (Kamei et al., 2013; Modarres & Nosoudy, 2015). In contrast, a noticeable increase in strength is observed in soil mixtures with lime/cement and bottom ash because of the cementing ability of hydrated lime/cement and pozzolanic impact of bottom ash (Geliga & Ismail, 2010; Kayabal & Buluş, 2000; Kolay et al., 2011; Mackiewicz & Ferguson, 2005).

### 2.5.2 Fly ash

Fly ash is a residual product from the combustion of coal ash in coal-fired steam or electric plants. This ash contains many oxides of aluminium, silicon, calcium, iron and unburnt carbon. There are two main types of fly ash: Class F fly ash with low calcium content, and Class C fly ash with higher calcium. However, both ashes are still pozzolanic materials with the most aluminous and

siliceous content (Cokca, 2001; Fatahi & Khabbaz, 2015). Table 2.3 compares the composition of these two kinds of fly ash. Due to the environmental impacts of fly ash, this ash is recycled by utilisation for soil stabilisation (Sabat & Pati, 2014). Adding 3% fly ash into 9% cement-treated soils can attain the highest *CBR* and shearing strength (Akinwumi & Aidomojie, 2015). However, for typical expansive soil, Zumrawi (2015)'s study on ash-cement treated soils showed that the optimum ratio should be 15% fly ash to 5% cement. At this ratio, the *CBR* value is highest with the 15% decrease in optimum moisture content and a 7% increase in maximum dry density. Furthermore, in some studies, without cement, fly ash still improves the engineering properties of expansive soil or is more pronounced in combination with lime (Bhuvaneshwari et al., 2005; Bose, 2012; Edil et al., 2006). Different additives rather than lime or cement were considered to stabilise the expansive soil, such as magnesium or aluminium chloride (Radhakrishnan et al., 2014). With the addition of these divalent cations to expansive soil, the swelling pressure and free swell ratio are reduced. The inclusion of fibre with 1% in content and 12 mm in length can also improve the swelling potential and strength of the soil (Sabat & Pradhan, 2014). Meanwhile, the optimum content of fly ash is 20% for the highest *CBR* value of black cotton soil (Pandian & Krishna, 2003). The same effect is repeated in the study of (Ramesh et al., 2011), when 20% fly ash can produce the maximum *UCS* of treated shedi soil samples. Similarly, phosphogypsum can double the *UCS* of fly-ash blended expansive soils (Krishnan et al., 2014). For organic soil, the soil type and fly ash properties influence treated soil strength (Tastan et al., 2011). When more additives like sand and tile waste are combined with fly ash for soil stabilisation, both soaked or unsoaked *CBR* of the admixture increase (Singh et al., 2014).

*Table 2.3 Comparison in chemical composition between Class F and C fly ash (Cokca, 2001; Fatahi & Khabbaz, 2013; Punthutaecha et al., 2006)*

| Chemical composition (%) | Class F fly ash | Class C fly ash |
|---|---|---|
| $SiO_2$ | 54.8-64.2 | 44.18.58.62 |
| $Al_2O_3$ | 19.70-25.50 | 19.44-22.13 |
| $Fe_2O_3$ | 3.92-5.10 | 4.85-10.18 |
| CaO | 2.27-9.80 | 2.18-18.98 |
| MgO | 0.69-1.60 | 1.01-1.66 |
| $K_2O$ | 1.24 | 1.50-1.52 |
| $TiO_2$ | 0.97 | 0.98-1.11 |
| $Na_2O$ | 0.52 | 0.19-0.45 |

### 2.5.3 Pulp paper

Pulp paper ash is produced from paper mills in which pulping wood is stretched to create products of paper (Zavatta, 1993). Instead of whitening or colouring it by bleaching chemicals, paper mill ash could be used to stabilise soils in terms of various properties, such as *CBR* or *UCS* (Byiringiro,

2014). With the optimum content of paper mill ash at 20%, the *CBR* growth is observed obviously from 2.8 to 64.4%, indicating the highest positive effect of pulp paper on soil strength reinforcement. The paper ash from multi-fuel boilers and lime mud from the pulp paper treatment is recommended for expansive soil and road stabilisation (Eroglu et al., 2006). More improvements in Atterberg limit, shearing parameters, *MDD* and *OMC,* can be obtained with the paper ash-treated soils.

### 2.5.4 Quarry dust

Quarry dust is an aggregate by-product that is collected from the crushing process of rubble. This dust material could treat soil subgrade/subbase without additional additives like lime or cement, but it still produces reasonable improvements. At the 40% quarry dust content, the *CBR* of treated samples was read at the highest value, indicating this percentage is the optimum value of material content for soil reinforcement. The dust addition also helps reduce the liquid limit, thus decreasing the plasticity index. Repeatedly, the optimal content of quarry dust at 40% was obtained for the optimum *CBR* value when the material was mixed with black cotton soil (Chansoria & Yadav, 2016). However, in the investigation by (Sabat & Bose, 2013), this percentage should be 45% to result in the highest *UCS*, *CBR* and the shearing characteristics of stabilised soils. Regarding the combination of quarry dust and lime for their effects on engineering properties of expansive soil, the optimum ratio of 40% dust is combined with the increasing content of lime from 2 to 7% make the quarry dust-treated soil more durable than admixtures without lime (Sabat, 2012b). The optimum content of lime is 5% after 28 days for curing. The author also proposed the statistical models that generate the relationship between quarry dust and lime content with *MDD, OMC* and curing duration. The model predicted the swelling pressure of treated soil after 28 days based on the pressure after 7 days.

### 2.5.5 Silica fume

Silica fume is the industrial waste from the production of ferrosilicon alloys or metals. Because of plenty of pozzolanic composition, the fume has many applications to soil stabilisation (Uzal et al., 2010). The utilisation of silica fume not only reduces swelling pressure, permeability and enhance *UCS* but also improves the durability of treated soil during the cycles of freezing and thawing (Kalkan, 2009; Kalkan & Akbulut, 2004). In connection to black cotton soil, (Negi et al., 2013) confirmed that the best percentage of silica fume should be 20% to obtain the 31 and 72% increase in *UCS* and *CBR*, respectively. For lime combination, the lime-fume ratio of 5-9 to 10% in clayey

soil stabilisation can improve *CBR*, shearing capacity and reduce the swell pressure and consolidation parameters (El-Aziz et al., 2004).

### 2.5.6 Steel slag

Steel slag is the industrial residual of the most common generation from the process of making steel and the post-combustion process. Different stages of the process could result in different slag materials, such as electric arc furnace slag (EAFS) and ladle furnace slag (LFS). However, steel-slag mixed soil might suffer a high swelling potential (Hua-dong & Liu, 2009; Maghool et al., 2017; Vaníček et al., 2016; Vaníček & Vaníček, 2013). The granulated blast furnace slag (GBFS) can present as a cementitious material due to the substantial calcium, silicon, aluminium, and magnesium content, which potentially improves the soil properties (Punthutaecha, 2002; Wild et al., 1999; Yi et al., 2014). In the case of basic oxygen steel slag fines (BOS), the content of 15-20% in BOS can enhance the durability and the strength of expansive soil (Poh et al., 2006). In comparison between BOS and GBFS, the testing finding indicated that BOS is more effective in stabilising the dispersive soils than GBFS (Goodarzi & Salimi, 2015). Smaller content of 10% in BOS is required for optimum soil stabilisation compared to 20-25% in GBFS. With respect to ladle furnace slag (LFS), the research by (Manso et al., 2013) concluded that the durability of LFS-treated soil is higher than that of lime-treated admixtures. Using electric arc furnace slag (EAFS) is also an effective measure for soil stabilisation. According to (Akinwumi, 2014), the optimum 8% content of EAFS can build up 40% increase in *CBR* while reducing all Atterberg parameters.

### 2.5.7 Carpet fibre

Carpet fibre is made from shredding carpets which can be 70 mm in length. The fibre material is suitable to reinforce the tensile strength of the blended objects. At a low cost, the fibres waste from carpets is reasonable to use for stabilising soft soils (Wang, 2006). For sandy soil, the short fibre strips for soil treatment can enhance the compressive and shearing strength of silty sand and maximise its elastic modulus and ductility (Ghiassian et al., 2004). The 3% content of 70 mm long fibre is the optimum fibre dosage in longer carpet fibre to obtain the highest triaxial compressive strength (Wang, 2006). The other optimum percentage of fibre is 1% for the peak stress of treated soil from undrained triaxial tests (Mirzababaei et al., 2009).

### 2.5.8 Tyre rubber

Every year, there is a 2% increase of tyre waste in Australia, which is being destined to landfill sites, accumulating to 20 million tyres in many types and sizes in 2010 (Mohammadi et al., 2014).

The environmental issues are challenging to recycle this waste properly while the landfills full of tyre rubber are more toxic (Kalkan, 2013; Mohammadi et al., 2014; Tafreshi & Norouzi, 2015). For civil application, much attempt was made to mix the waste tyres with asphalt paving and cement as the applications of tyre rubber in pavement construction and concrete manufacture (Bignozzi & Sandrolini, 2006; Shu & Huang, 2014). For adaptation in soft soil stabilisation, rubber material in small particles can limit the swelling potential of expansive soil (Seda et al., 2007). Furthermore, the rubber-treated soil also has lower swelling pressure and percentage than untreated soil, especially at the optimum rubber content of 20%. The combination of shredded rubber from tires with binders like cement can produce the maximum *UCS* value at the 4 to 5% cement content with the 15% randomly shredded rubber. Therefore, the recycled tyres can be potentially used for soft soil stabilisation in road reinforcement, embankment construction and retaining walls (Tafreshi & Norouzi, 2015)

### 2.5.9 Glass cullet

Glass cullet is the crushed glass raw materials, which is transparent and brittle in the form of waste ready to be remelted. With a plentiful silicon dioxide and sodium carbonate source, the glass waste can improve the physical property, crushing resistance and stiffness of the treated soil (Rao & Chittaranjan, 2011). Regarding the investigation into the combined effect of glass waste and cement for expansive soil stabilisation, the optimum glass-cement of 20% to 8% gave the highest *UCS* and *CBR* of 1.2 MPa and 53.8%, respectively after 7 days of curing (Ikara et al., 2015). For black cotton soil, 5% glass powder content produced the maximum *CBR* value while 10% glass proportion enhanced the shearing parameters highest (Olufowobi et al., 2014), which indicates that glass powder can be the suitable binder for clay stabilisation. Concerning the laterite soil, additional fly ash is added to the glass-treated soil and an optimum percentage of ash-glass combination can be found. Based on the study of (Boraste & Sharma, 2014), the ratio of 7% glass power to 20% fly ash can improve the soaked and unsoaked $CBR_s$ at their highest values. Consequently, glass wastes can be an effective soil stabiliser because of their outstanding improvement in the engineering behaviour of expansive soil.

### 2.5.10 Summary of industrial wastes

Table 2.4 shows the summary and comparison of various industrial by-products in terms of pros and cons for soil stabilisation.

*Table 2.4 Comparison of industrial wastes for soil stabilisation*

| Industrial wastes | Origin | Merits | Demerits | References |
|---|---|---|---|---|
| Bottom/Fly ash | Coal-fired power generation plants | Ash recycling reduces the carbon footprint.<br>Solve the environmental problem by using ash as fill materials in earth dams. | Leaching problems related to water contamination.<br>Literature gaps in ash usage for sensitivity to erosive risks.<br>Transporting cost for coal fly ash. | Vaníček et al. (2017) |
| Pulp paper | Paper mills and factories | Environmentally friendly natural resources.<br>Recycling paper helps decrease pollutions. | Treated chemicals cause health hazards.<br>Low durability. | Seyyedalipour et al. (2014) |
| Quarry dust | Aggregate factories | Low-cost waste.<br>Alternative to natural sand.<br>Application in soil stabilisation help reduce the great disposal in landfill sites.<br>Less dependent on the variation of water content in stabilising the expansive soil. | Struggles to determine the liquid limit tests of dust samples. | Shyam Prakash and Rao (2016) |
| Silica fume | Alloy and metal factories | High strength and durability of fume-treated mixtures.<br>High elastic modulus and toughness of blended admixtures.<br>Outstanding resistance to chemical erosion, such as acids, nitrates.<br>Solidification results in low permeability and high electrical resistance. | High costly material.<br>Risk assessment problems related to handling the material.<br>Potential of health hazards. | Khan and Siddique (2011) |
| Steel slag | Steel factories | Playing a role of protecting material for natural aggregate in their admixtures. | Negative effects on swelling.<br>Potentials to cause water pollution. | Maghool et al. (2017) |
| Carpet fibre | Carpet factories, household | Reuse of fibre can reduce landfilling and carbon footprint for energy consumption.<br>Improvement in shearing characteristics of soil. | Limited dosage of fibre can be used to enable the stabilising effectiveness with expansive soil. | Mirzababaei et al. (2009) |
| Tyre rubber | Rubber factories, household | Very low costly material with raw material in landfill sites.<br>Recycling helps reduce energy and carbon footprint. | Tyre abrasion can cause negative effects on soil stabilisation. | Presti (2013) |
| Glass cullet | Glass factories | Sand-like properties of material help improve the soil engineering properties.<br>Recycling reduces the issue of disposing of the waste. | Optimum content of the material should be controlled strictly to avoid any adverse effects on treated soil behaviour. | Ikara et al. (2015) |

## 2.6 Combinations of binders for soil stabilisation

There were many kinds of binding materials or binders used for enhancing the engineering characteristics of soft soil. It is to turn such weak soil into a fill material able to bear loads of construction adhering to the requirement of effectiveness and application. However, selecting a proper combination of additives or just each sole element in soils is not an easy task and requires intensive research in terms of their interaction behaviours. Indeed, there is a correlation between

them making an effective blend (Sarkar et al., 2016). In this review paper, the authors showed the comparison of the admixtures used to reinforce the expansive soil, which is illustrated in Table 2.5 below.

*Table 2.5 Comparisons in outcomes of binding agents (Sarkar et al., 2016)*

| Binding agents | MDD (g/cm$^3$) | OMC (%) | CBR | UCS (kPa) |
|---|---|---|---|---|
| Coir fibre (1%) | - | - | Soaked-9.22<br>Unsoaked-13.55 | 620.7 |
| Coir fibre (1%) and Fly ash (20%) | - | - | 11.6 | 669 |
| Crushed glass (5%), Fly ash (20%), and Coconut coir fibre (1%) | - | - | 5.2 | - |
| Fibres (0.6%) and Stone dust (3%) | 1.53 | 23 | Soaked-4.16 | 918 |
| Fibres (1%), stone dust (10%), and lime (6%) | 1.63 | 18 | Soaked-12<br>Unsoaked-5 | 570.75 |
| Fly Ash (6%) | 2.35 | 10.2 | 4.82 | 88.8 |
| Fly ash (20%) | 1.52 | 22.19 | Soaked-2<br>Unsoaked-13.55 | - |
| Lime (9%) and Stone dust (20%) | 1.77 | 21 | Soaked-21 | 182 |
| Lime (6%) and Sodium silicate (3%) | 1.44 | 26 | 2.01 | - |
| Lime (6%) | 1.68 | 12 | 15.2 | - |
| Moorum (20%), and RBI Grade 81 (4%) | 1.49 | 24.76 | Soaked-14.76 | - |
| Moorum (7.5%) and Fly ash (5%) | 4.92 | 16.14 | - | 26.47 |
| RBI grade 81 (6%) | 2.4 | 26.4 | 32.63 | 589.58 |
| Rice husk ash (20%) and Lime (5%) | 1.51 | 22 | 7.52 | 140.2 |
| Rice hush ash (12%) and Fly ash (25%) | 1.58 | 15 | 10 | 1250 |
| Rice husk ash (20%), Fly ash (20%), and Lime (8%) | 1.65 | 18 | 12.7 | 350.217 |
| Stone dust (15%) and rice husk ash (10%) | 1.76 | 18.1 | Soaked-5.67<br>Unsoaked-10.43 | 89.46 |
| Stone dust (30%) | 1.891 | 13.25 | Soaked-2.91 | - |
| Stone dust and Fly ash (50%) | 1.88 | 16 | 3.9 | 148 |
| Stone dust (20%) and Rice husk ash (20%) | 1.79 | 23 | - | 1581.72 |
| Quarry dust (40%) and coir fibre (2%) | 1.29 | 21 | 23.06 | - |
| Quarry dust (40%) | 1.94 | 11.8 | 4.19 | - |

(Note: *OMC*: optimum moisture content, *MDD*: Maximum dry density, *UCS*: Unconfined Compressive Strength, *CBR*: California Bearing Ratio)

It is clear from the table that many combinations of binders can be available to produce evaluated parameters, say 4 values including 2 physical indices (*MDD*, *OMC*) and 2 mechanical ones (*CBR* and *UCS*). Not stated in the table, the admixtures can also be generally classified into 2 main categories: (1) powder binders, such as lime or fly ash and (2) fibre binders like coir. This is attributed to the fact that Sarkar et al. (2016)'s paper emphasised the power mixtures rather than fibre blend with soils. Therefore, Hejazi et al. (2012) proposed another review of soils treatment

reinforced by fibres encompassing natural and synthetic origin. Although only 4 natural sorts of fibre are expressed in Table 2.6, a total number of 8 fibre types were considered in Hejazi's study. Hejazi et al. (2012) recommended using bagasse or cane fibres amongst those natural fibres in soil reinforcement since the application would be still a dearth of the research area. Meanwhile, seven kinds of artificial fibre originating in plastic material were also added in the admixture with soils as artificial components to enhance the ductile feature of the reinforced blend.

*Table 2.6 Summary of the study performed on widely-used natural and synthetic fibres to reinforce soil (Hejazi et al., 2012).*

| Fibre type | Name | D ($\mu m$) | SG (g/cm$^3$) | E (GPa) | UTS (MPa) |
|---|---|---|---|---|---|
| Natural fibre | Coir | 10-20 | 1.15-1.33 | 4-5 | 250 |
| | Sisal | 25-400 | 1.2-1.45 | 26-32 | 560 |
| | Palm | 25-60 | 1.3-1.46 | 0.55 | 21-60 |
| | Jute | 10-50 | 1.44-1.46 | 22 | 453-550 |
| Synthetic fibre | Polypropylene | 23-150 | 0.92 | 3-3.5 | 120-450 |
| | Polyester | 30-40 | 1.35 | 10-30 | 400-600 |
| | Polyethylene | 400-800 | 0.92 | 0.14-1 | 100-620 |
| | Glass | 3-19 | 2.49-2.60 | 53-95 | 1500-5000 |
| | Polyvinyl alcohol | 100 | 1.3 | 25 | 1078 |

(Note: *D*: Diameter, SG: specific gravity, UTS: ultimate tensile strength, E: Young's modulus

Furthermore, a viable combination for soil reinforcement must meet the requirements of either mechanical strength or economical budget or practical application while the solutions to have implications of research outcomes for the real world remain abandoned. Meanwhile, little is known about how both bottom ash and bagasse ash with lime can enhance the properties of expansive soil in a final mixture efficiently and effectively. In fact, some longitudinal studies have indicated that the right blend of lime and bagasse ash can enhance the physical and mechanical characteristics of expansive soils (Dang et al., 2016b; Dang et al., 2015; Hasan et al., 2016a) as well as bottom ash (Kamei et al., 2013; Kim et al., 2005; Kim & Do, 2012).

## 2.7 Expansive soils treated with hydrated lime, bagasse ash from agricultural wastes, and bottom ash from industrial wastes

To limit the problems related to the shrinkage-swelling behaviour of expansive soil, chemical stabilisation methods are usually utilised. This method is one of the most effective solutions for expansive soil treatment through mixing soil with chemical stabilizers, such as lime and pozzolans (Cokca, 2001; Edil et al., 2006; Fatahi et al., 2013; Nguyen et al., 2014; Phanikumar, 2009). In addition to lime, the pozzolans for chemical stabilisation can come from various origins, but generally, they fall into two main sectors, agriculture and industry. In the agricultural by-products

group, rice husk ash and bagasse ash are used to alleviate the swelling and shrinkage problems of expansive soils (Basha et al., 2003; Dang et al., 2016b; Osinubi et al., 2009b). Among ash binders for soil stabilisation, bagasse ash is a fine by-product from burning bagasse in cogeneration boilers of sugarcane factories. In Australia, more than 30 million tonnes of sugar cane is cultivated every year (Arif et al., 2017), dumping over 4 million tonnes of bagasse, which is then burnt to dispose of about 30 thousand tonnes of bagasse ash annually (Fairbairn et al., 2010). Although bagasse residual is an environmental constraint due to the risk of airborne particles of silica with its small respirable size (Le Blond et al., 2010), burning bagasse produces reasonable heating energy for mill factory operations and producing sugar or running electricity generators.

Meanwhile, industrial wastes, such as coal ash and silica fume, are becoming common additives in soil stabilisation (Kamei et al., 2013; Kim et al., 2005; Kim & Do, 2012). Bottom ash, the waste product of thermal processes in coal power stations, has extensive usage as fill material and soil binders, respectively, due to its coarse and pozzolanic properties (Kayabal & Buluş, 2000; Kim & Prezzi, 2008). The waste material is rich in divalent and trivalent cations, such as $Si^{2+}$ and $Al^{3+}$, which can trigger the aggregation and flocculation of clay particles and enhance the cation exchange in reactive soils (Chen, 2012; Sharma et al., 2008). However, this class-F ash lacks calcium oxide, so pozzolanic reactions cannot be completely developed in soil mixtures (Kamei et al., 2013; Le et al., 2018). Adding hydrated lime as the source of calcium ions directly solves this problem, constituting a stiffer and more ductile sample than merely-lime-treated soil (Kayabal & Buluş, 2000; Le et al., 2018; Le et al., 2019). This combination can limit linear shrinkage and cracks because cementing bonds develop between soil particles (Bell, 1996; Buhler & Cerato, 2007; Puppala et al., 2006; Sarkar et al., 2012). This also makes expansive soil coherent and solid, helping soil structure less porous and flaky (Modarres & Nosoudy, 2015). From the environmental point of view, using bottom ash for soil treatment can minimise the disposing issue of the waste destined to landfills, approximate 2.5 billion tonnes all over the world every year (Ardejani et al., 2010; Kim & Prezzi, 2008; Modarres & Nosoudy, 2015). Therefore, evaluating potentials of volume change (shrinkage or swelling) of bottom ash-lime treated expansive soils is in demand to define their best combination in stabilisation.

It is clear that binders from mineral sources can come from various industrial or agro-industrial activities and locations to stabilise expansive soils, such as rice husk ash from rice farms, bagasse ash from sugar cane factories, and fly ash from steel or thermo-electricity plants. These ashes are residual products from the relevant manufacturing process in varied conditions of collecting, burning, cooling and dumping in the field. This variation affects their physical and

chemical properties, thus influencing their stabilising capability when mixed with the soil. In physical aspects, Cordeiro et al. (2008) proclaimed that particle size, shape and texture influence packing in ash-soil mixtures. Meanwhile, chemical effects are related to the capability of producing siliceous or aluminous compounds from ash and soil to react with calcium hydroxide in the condition of moisture or saturation (Cordeiro et al., 2008). Therefore, when ash lacks calcium component but is rich in silica, the inclusion of hydrated lime is necessary to catalyse pozzolanic reactions between $SiO_2$ and free lime to form calcium silicate hydrate (CSH) (Alavéz-Ramírez et al., 2012; Ganesan et al., 2007). This cementing product is mainly generated from the combination of calcium ions with amorphous silica from ash, which is in charge of soil stabilisation (Alavéz-Ramírez et al., 2012). Therefore, to effectively stabilise soil and increase its strength in treated mixtures, raw silica ash needs to be processed to enhance its pozzolanicity by modifying the content of amorphous and crystal particles (Cordeiro et al., 2016). As a result, the combination of bottom ash as the material rich with crystalline silica and bagasse ash with amorphous particles is promising for a good pozzolan material in soil treatment with hydrated lime. Furthermore, for a better combination, the process can change the fineness and burning degree of bagasse ash so that the combined material has advantages in both physical and chemical properties to stabilise soil (Hernández et al., 1998).

## 2.8 Expansive soils treated with hydrated lime and bagasse ash in a variation of ash size and burning temperature

Using mineral admixtures to treat expansive soil become more common in road construction or the foundation of lightweight superstructures, such as pilling or sewage in municipal systems. The effective treatment involves contributions from both physical and chemical aspects, including relevant parameters from additive minerals and parent soil. In mill factories, variable burning temperatures turn bagasse into different shapes of particles, including fibre and porous ash, but possibly classified in two main types: cellular and quartz particles (Arif et al., 2017; Cordeiro et al., 2016; Le Blond et al., 2010). Studies on morphology and silica minerals of these particles provided valuable information for geotechnical engineers to environmentally-friendly use ash for civil applications, such as ground stabilisation or silica-rich filler for geo-materials (Arif et al., 2017). In these applications, the combination of various particles from different sources in bagasse ash gives it a variation of pozzolanic performance with lime or cement (Bahurudeen et al., 2015b). In raw bagasse ash, unburnt carbon amount can lower the specific gravity and fineness of ash to only 1.91 and 169 $m^2$/kg, respectively (Bahurudeen et al., 2014; Bahurudeen et al., 2015b). By sieving raw ash through a sieve of 300 μm, Bahurudeen et al. (2015b) indicated that the processed

bagasse ash has a higher specific gravity (2.1) and specific surface area (210 $m^2$/kg) than coarse bagasse one. In other words, removing large unburnt fibrous particles from bagasse ash increases fineness and reduces the particle size of the material. As a result, Cordeiro et al. (2008) and Ganesan et al. (2007) confirmed that removing a large part of bagasse ash increases its fineness with smaller particle sizes, resulting in its higher pozzolanic activity. Regarding the loss on ignition, the large particles of bagasse ash contain a large amount of unburnt carbon, increasing the ignition loss of raw ash to about 20% (Bahurudeen et al., 2015b; Chusilp et al., 2009a). Therefore, selecting bagasse ash with a smaller size (e.g., under 300 µm) reduced the loss on ignition to only 3-6%, enhancing the pozzolanic performance of ash material (Bahurudeen et al., 2015b).

Alongside the sieving approach, grinding is a preferable method to lessen particle size and minimise the negative impact of crystalline silica on the reactivity of ash (Chusilp et al., 2009a; Cordeiro et al., 2009b; Ganesan et al., 2007). Since the crystalline compound is regarded as inert silica, which generates much lower pozzolanic activity than silica in an amorphous state (Amin, 2011; Chusilp et al., 2009a; Cordeiro et al., 2016; Cordeiro et al., 2009a), a selective grinding process can enhance the pozzolanic reactivity of bagasse ash by removing the content of crystalline quartz (Cordeiro et al., 2016). In this process, tumbling ball mill and screening methods were used to partly separate quartz components from bagasse ash. The remaining ash with a majority of cellular-based particles continued to be ground in planetary ball mill to obtain a size of 20 µm. The grinding method was proved to effectively produce a fine bagasse ash product with less proportion of quartz or cristobalite, and high content of amorphous silica, helping to improve the pozzolanicity of bagasse ash (Cordeiro et al., 2016). De Souza et al. (2020) also confirm the superior of ball mill to knife mill in reducing the grain size of bagasse ash sand. Bagasse ash from ball milling has a higher intensity of quartz than from knife milling, and ball-ground ash has an ultra-fine average diameter of about 3µm and a higher surface area (60.32 $m^2$/g). The quartz mineral came from the attachment of soil sand to the sugar cane plant that was not completely removed after washing in mill factories (De Souza et al., 2020). This sand contamination can be mitigated by grinding ash in a planetary ball mill to obtain $D_{80} = 20$ µm as the 80% passing size, found out by Cordeiro et al. (2009b), confirming a linear relationship between fineness and pozzolanic activity index of bagasse ash.

The pozzolanicity of the ash relies not only on its fineness or particle size but also the controlled burning degree of sugarcane bagasse ash (Cordeiro et al., 2016; Cordeiro et al., 2009a; Cordeiro et al., 2009b; De Souza et al., 2020). Various studies indicated that firing temperature to

burn bagasse ash affects its level of pozzolanic reactivity. Payá et al. (2002) used the thermos-gravimetric method to analyse the change in lime-ash mix weight over the range of calcination temperature. They found out that the thermal zone from 520-580°C was correlated to de-hydroxylation of calcium hydroxide, resulting in a high fixed lime content as evidence of pozzolanic potential in bagasse ash mix. Cordeiro et al. (2009a) also asserted that bagasse ash obtains the highest reactivity when burnt at about 600°C, producing a maximum amount of amorphous silica, low carbon content and high specific surface area. Meanwhile, under a non-controlled burning process in boilers, the ash can be burnt at high temperatures over 800°C, turning ash into black colour due to the formation of carbon and crystalline silica (Cordeiro et al., 2009a). Consequently, bagasse ash contains silica as a form of cristobalite, which is associated with high calcination temperature and long-time burning, reducing the pozzolanicity of ash (Bahurudeen et al., 2015a; Cordeiro et al., 2009a; Cordeiro et al., 2009b). Ideally, under the controlled laboratory-scale burning condition, bagasse ash with low-quartz contamination can be produced as a cellular-rich material (Barroso, 2011; Cordeiro et al., 2016). Consequently, the calcination temperature should be kept in the range from 500°C to 600°C and not over 800°C to avoid the formation of cristobalite in bagasse ash and achieve the highest index of pozzolanic activity (Cordeiro et al., 2016; Cordeiro et al., 2008; Cordeiro & Kurtis, 2017; de Soares et al., 2016; Deepika et al., 2017; Ganesan et al., 2007).

## 2.9 Influencing factors on engineering properties of treated expansive soil by bottom ash, lime, bagasse ash or fibre

### 2.9.1 Introduction

This part investigates the engineering characteristics of expansive soil stabilised by bottom ash, bagasse ash or bagasse fibre and lime or cement. The factors of curing time and additive content that influence these properties are also reviewed and compared in various impact factors. They might be the effect of curing period or content of ash, lime and fibre on shrink-swell, stress-strain relationship, unconfined compressive strength, California bearing ratio, compressive behaviour and pH value. The investigation is to interpret the recent studies on the combined effects of the waste materials on the engineering properties of expansive soil.

### 2.9.2 Linear shrinkage (LS)

The linear shrinkage is a crucial parameter for investigating the shrinkage potential of expansive soil and evaluating its stabilisation, particularly when the soil is treated with binders. In

calculation, linear shrinkage is the relative reduction in length of soil specimen after it is dried completely, compared to the length of the moisturised sample at its liquid limit. The linear shrinkage test is usually performed in adherence to AS 1289.3.4.1 (2008).

Figures 2.8 and 2.9 show the influence of variation of lime content without or with ash on the linear shrinkage of many kinds of soils, including black cotton soil (Dang et al., 2015), artificial expansive soil (Hasan et al. 2016), highly plastic clayey soil (Buhler & Cerato, 2007) and Montmorillonitic clay soil (Bell, 1996). Overall, *LS* decreases with the increase of lime content. However, the black soil and montmorillonite soil have a more significant reduction of about 8% in *LS* at the first mixing with 2% lime content, whereas the artificial soil and CH clay only gain a slight decrease of *LS* even at the lime content higher than 6%.

When it comes to ash-treated soil samples, a much higher ash content is needed to reduce *LS*-value in their combination with expansive soil. Figure 2.10 illustrates the addition of bagasse ash or fly ash in soil mix to limit the shrinkage potential of expansive soil. As can be seen from this figure, the agricultural ash from bagasse gives the higher remarkable decrease of *LS* than industrial class C fly ash. However, when the content of ash is higher than 10%, the rate of *LS* reduction is similar between the two kinds of ashes surveyed. Furthermore, regarding the research on *LS* of lime treated soil, the combined effect of ash-lime content on shrink behaviour of natural soil is more significant than artificial soil (see Figure 2.9). In this figure, the ratio of bagasse ash to lime was fitted into 3:1 as their optimum combination. In addition, the artificial soil is less influenced by the combination of lime and ash content in terms of linear shrinkage than natural soil (refer to Figure 2.9).

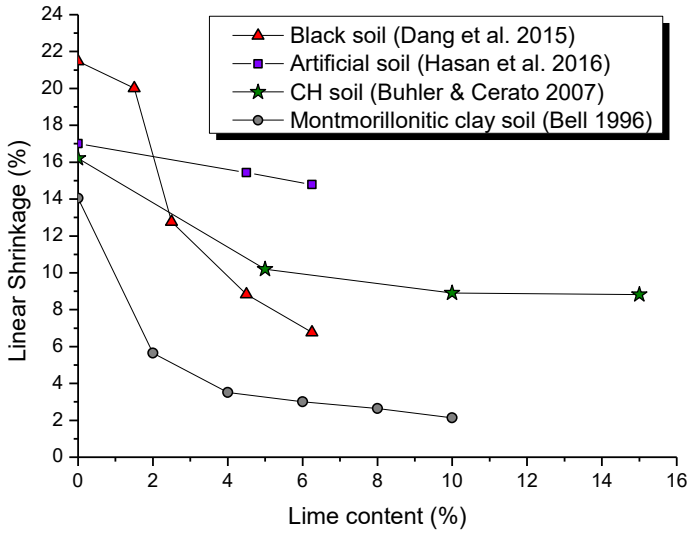


*Figure 2.8 Effect of lime content on linear shrinkage of expansive soils*

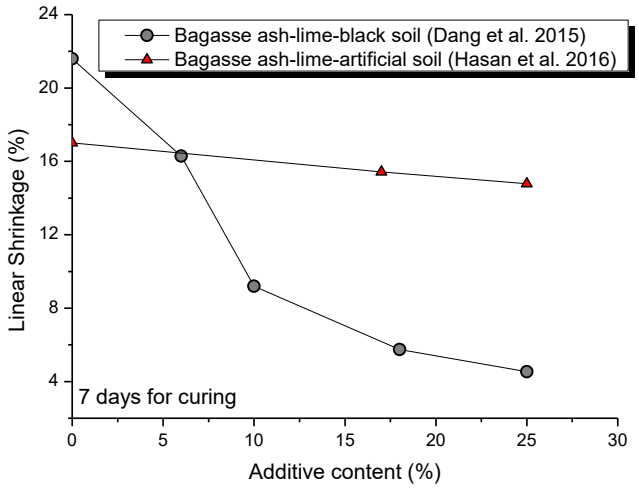


*Figure 2.9 Effect of ash-lime content on linear shrinkage of expansive soils*

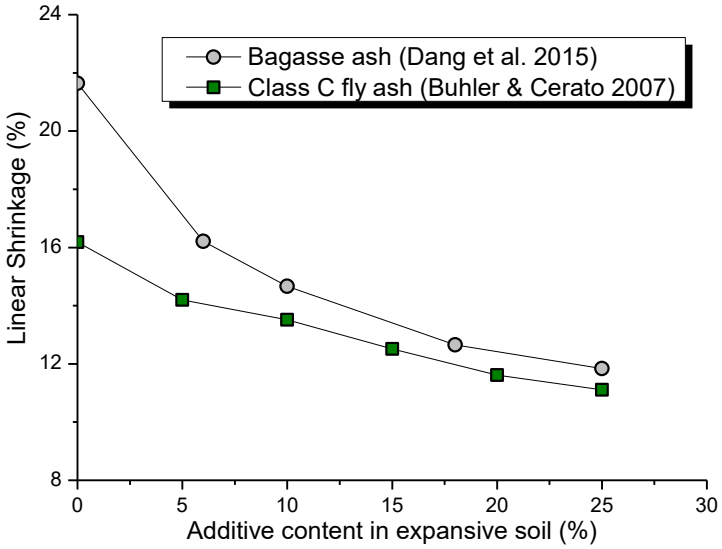


*Figure 2.10 Effect of ash content on linear shrinkage of expansive soil*

Turning to the effect of fibre waste and lime on *LS* of expansive soil, the study conducted by (Dang et al., 2016a) confirmed the effectiveness of this combination for *LS* reduction. The more content of bagasse fibre is added in lime-treated soil, the more linear shrinkage is reduced, as illustrated in Figure 2.11. The percentage of 4.5% in lime content can also be regarded as the reasonable dosage for fibre-soil treatment because higher than that *LS* decreasing rate decelerates. This is for 7-day curing. In the case of curing period effect on *LS*, more research was conducted in artificial and natural expansive soil after different days for self-hardening treatment. Figure 2.12 depicts the change of *LS* caused by the inclusion of lime and both lime and bagasse ash in the two kinds of soil. Referring to this figure, *LS* after 7-day curing is relatively constant for the ash-lime-treated natural soils, which have *LS* only decreased after 28 days, whereas *LS* of artificial soils stabilised by lime and ash is almost constant after 7 curing days.

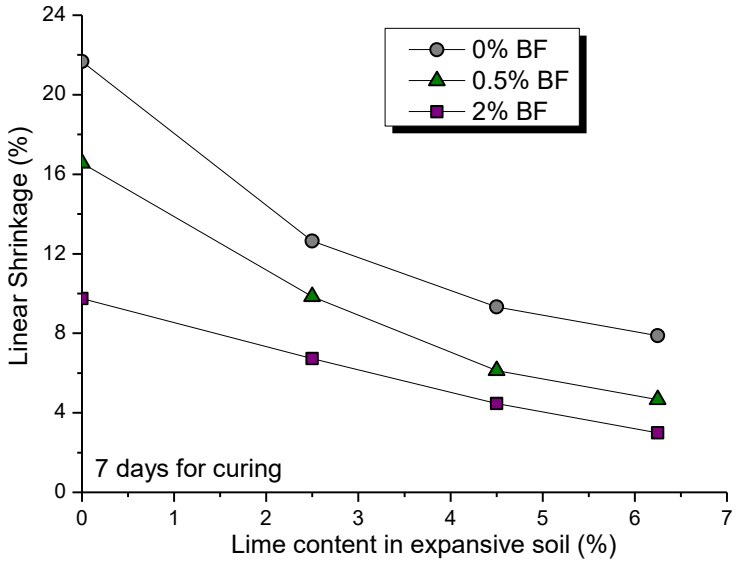


*Figure 2.11 Effect of bagasse fibre-lime content on linear shrinkage of expansive soils, BF: Bagasse fibre (Dang et al., 2016a)*

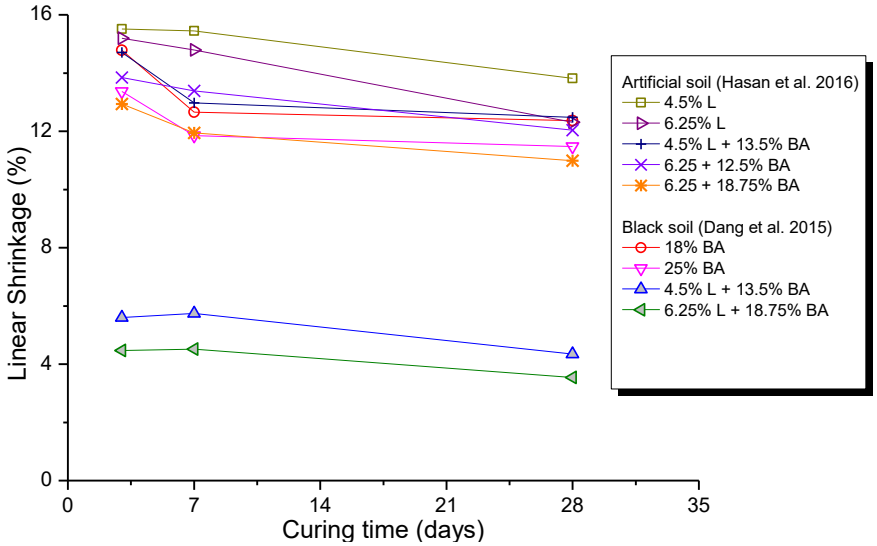


*Figure 2.12 Effect of curing time on linear shrinkage of treated expansive soils (Dang et al., 2015; Hasan et al., 2016a)*

### 2.9.3 Swelling behaviour

Swelling behaviour of expansive soil can be evaluated through swelling-related parameters, such as free swell index (FSI) or free swell ratio (FSR) in kerosene and swelling ratio from oedometer tests. FSI can be obtained by comparing changes of soil volume in water and in kerosene with that in kerosene. Meanwhile, FSR is measured as the ratio of volume of soil in water to that in kerosene, which is suggested by Prakash and Sridharan (2004). However, the swelling ratio is obtained from changes in vertical displacement of soil samples in consolidation tests, which is standardised in

ASTM D4546 (2014). The standard also shows how to measure swelling pressure as the pressure to prevent swelling in tested soils.

Figure 2.13 shows the results of a study conducted by Phanikumar et al. (2015) on the swelling behaviour of lime and cement-treated expansive soil. As illustrated in this figure, the swell potential demonstrated as the swelling ratio or swell percentage (%) deceased suddenly when the lime content reaches only 1% while cement-treated samples could not approach this level even with 15% cement. However, both lime and cement treatment gain the same swell potential of about 11% once their mixture is at 4% and 20% in content, respectively. The reduction of swell potential in these treated soil admixtures indicates the more pozzolanic effect of lime than cement in this behaviour. However, the case study by Sivapullaiah et al. (2000) presents that the overuse of lime larger than 3% could increase the free swell index. A small addition of lime quantity is related to liquid limit behaviour, but once the lime content increases more than 3%, the flocculation controls, resulting in a higher free swell index (see Figure 2.14).

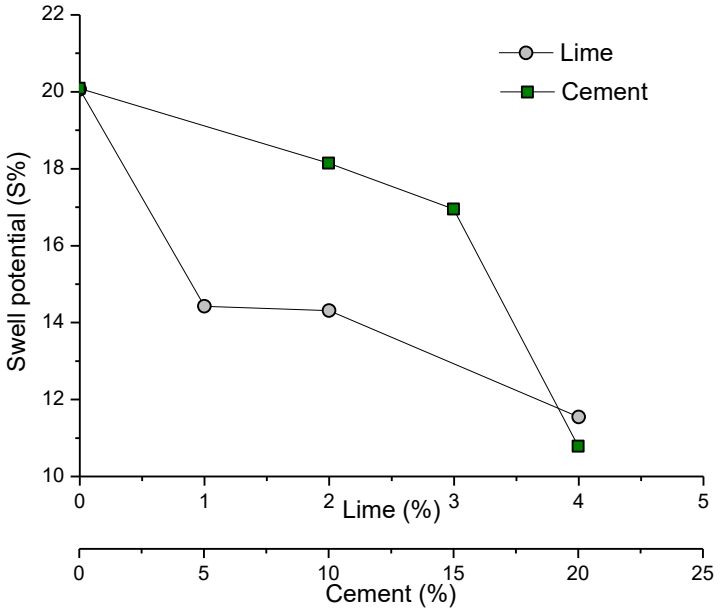


*Figure 2.13 Effect of lime and cement content on swell potential (Phanikumar et al., 2015)*

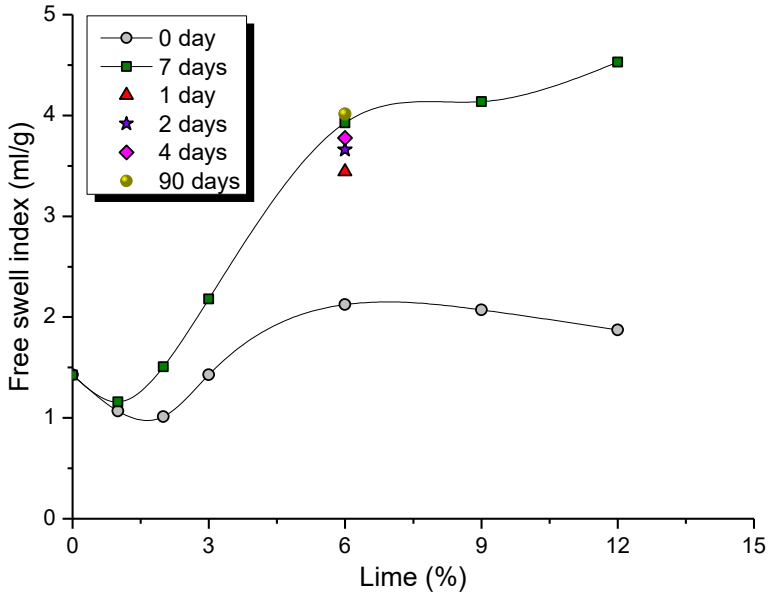


*Figure 2.14 Effect of lime content on the free swell index of black cotton soil (Sivapullaiah et al., 2000)*

When the fibre is involved in the lime-treated soil, the greater the percentage of fibre, the lower the swell percentage of fibre-lime treated soil, shown in Figure 2.15. However, the difference of swelling value is most considerable when the 2% lime content is combined with 0.25% fibre, resulting in a reduction of about 0.15% in swell percentage. Fly ash also works when it is combined with soil for swelling treatment. From the swell-consolidation tests, Phanikumar (2009) confirmed that 20% fly ash inclusion reduced the swell pressure from more than 300 kPa to only about 100 kPa. Nevertheless, the effects of minor addition of 4% on the pressure are more pronounced than that of fly ash, and when the swelling pressure is impossible to obtain in the case of 6% lime due to the hardening sample, as shown in Figure 2.16. This percentage of 6% is also the optimum fly ash content when it is mixed with lime in their admixture with expansive soil, which is indicated in Figure 2.17. The figure plots the decrease of swell pressure in the increasing content of lime and bottom ash as well as the curing time. The combination of 6% fly ash and 3% lime significantly dropped swell pressure from 250 kPa (approximately) for untreated samples to only about 50 kPa. The flocculation of soil particles explains the decrease of pressure through the cation exchanges with lime and ash. The prolonged period of curing allows more pozzolanic reactions to occur in the mixture, which means more formation of crystal CSH and CAH; thus, this enhances the stiffness of the sample and reduces the pressure necessary for swelling resistance.

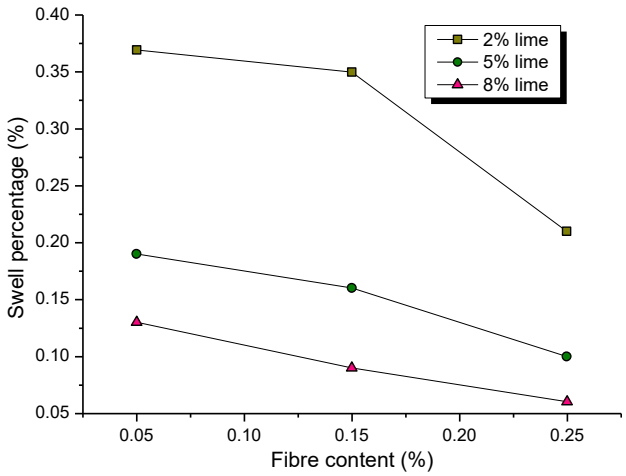


*Figure 2.15 Effect of the fibre content on the swell percentage of fibre-lime treated soil specimens after 7 days of curing (Cai et al., 2006)*

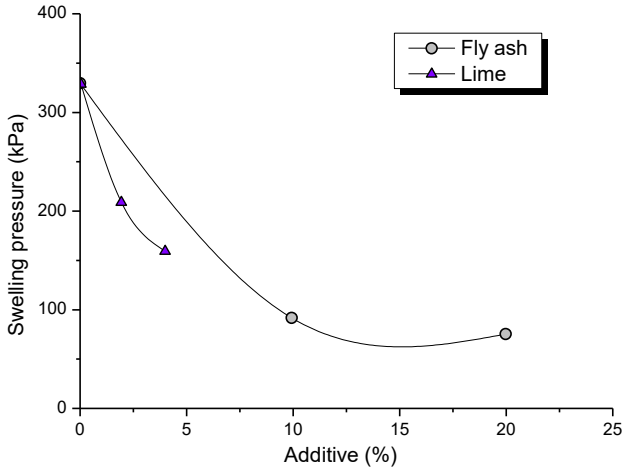


*Figure 2.16 Effect of lime and fly ash on swelling pressure (Phanikumar, 2009)*

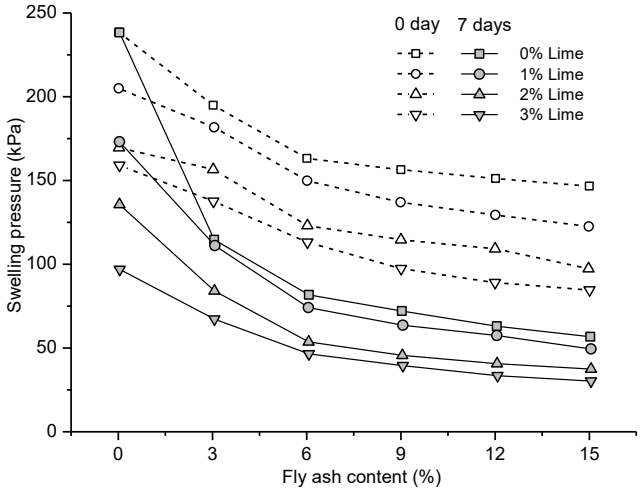


*Figure 2.17 Variation of swelling pressure of expansive soil mixed with various content of fly ash and lime without curing or with 7 days of curing (Zha et al., 2008)*

### 2.9.4 Unconfined compressive strength (*UCS*)

The unconfined compressive strength (*UCS*) is the testing result from compressing soil samples in a cylindrical form until they are destroyed without any confining pressure. The test is also known as the unconsolidated undrained test in accordance to AS 5101.4 (2008). The *UCS* values from the test indicate the failure point or the highest stress which unconfined soil samples can withstand.

Figure 2.18 compares the effects of lime content on unconfined compressive strength of treated samples in various kinds of soil. While Bell (1996) conducted the UCS tests for soils from montmorillonite and kaolinite, Ghobadi et al. (2014) utilised natural residual soil including kaolinite, illite and cholorite as the principal clay minerals. The result shown in Figure 2.18 indicates that the lime content of 4 % might be the optimum dosage for the highest *UCS* value in its treated admixture with soil. This strength was also time-dependent when it increased rapidly after more than 7 days (see Figure 2.18). This is also true for the artificial soil, which was researched by Hasan et al. (2016b). Figure 2.19 demonstrates the effects of curing time on *UCS* of lime or bagasse ash treated soil samples. This figure shows that the curing time of 28 days experienced a significant reinforcement of soil strength with lime much rather than bagasse ash treatment, even with 25% ash content compared to only 6% lime used (refer to Figure 2.19). Worse, the introduction of coal ash in cement-blended soil degrades the *UCS* of soil when ash content increase from 10% to 20%, as demonstrated in Figure 2.20. The stress-strain relationship in this figure also reveals the ductile behaviour in ash-cement treated soil.

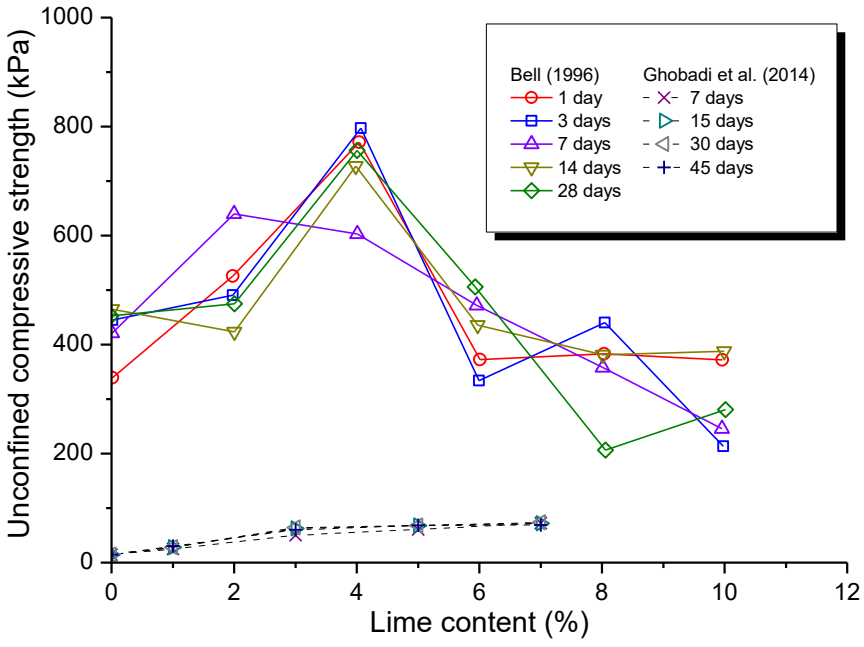


*Figure 2.18 Effect of lime content and curing time on the UCS of expansive soils (Bell, 1996; Ghobadi et al., 2014)*

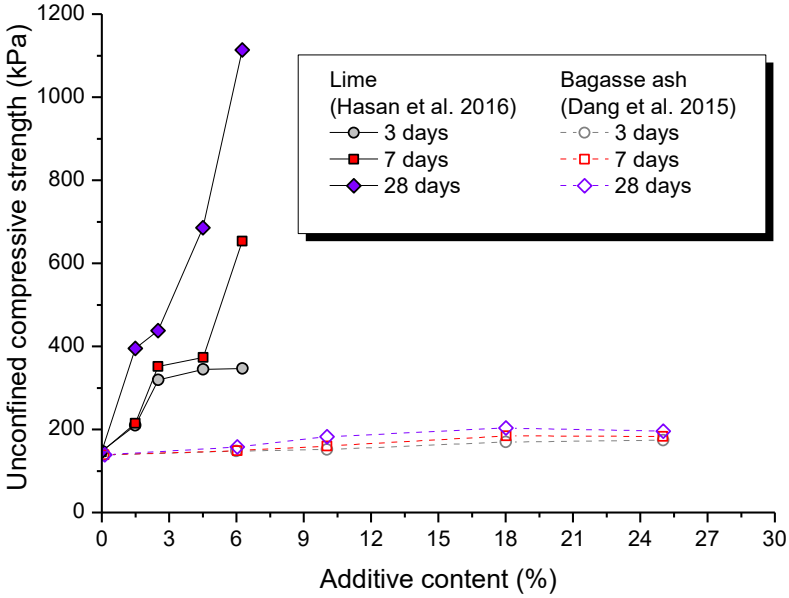


*Figure 2.19 Effect of lime, bagasse ash content and curing time on the UCS of expansive soil in Queensland, Australia (Dang et al., 2015; Hasan et al., 2016a)*

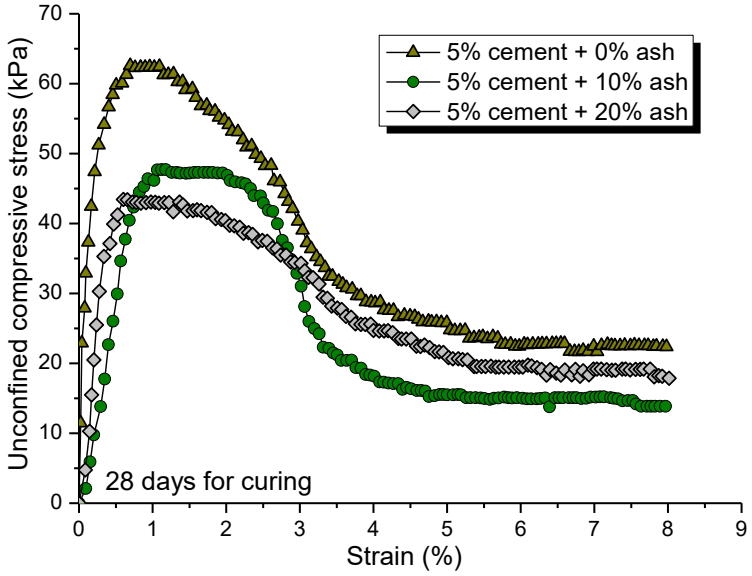


*Figure 2.20 Stress-strain relationship for samples stabilised with different contents of coal ash in 5%-cement-treated soil after 28 days of curing (Kamei et al., 2013)*

However, the soil stabilisation by ash is more promising with agricultural by-products such as rice husk ash (RHA) and bagasse ash (BA), which are shown in Figure 2.21. In both cases of ash inclusion, the ash content of about 12% generates the highest *UCS* value in expansive soil treated with about 4% content of lime. After 28 days of curing, *UCS* of RHA-treated soils is much higher than that of bagasse ash (about 1200 kPa as against roughly 700 kPa, respectively). The strength difference might be attributed to the fact that more silica content is observed in RHA than in BA, generating more pozzolanic reaction and more hardening the mix strength. The role of lime is essential for this reinforcement because its addition can result in the *UCS* of untreated soils

doubled or tripled (see Figure 2.21). The activation of lime in soil is also given in combination with bagasse fibre (BF), as presented in Figure 2.22. In this figure, while the curing time of 28 days still witnessed the increase of *UCS* in BF-lime treated samples, the same curing period did not impact the strength of soil treated with BF only. The lime content of 4.5% is optimum for *UCS* of fibre-lime treated expansive soil, which is indicated in Figure 2.22. Furthermore, according to the study of Jairaj et al. (2018), the treated coir fibre can enhance the compressive strength of treated expansive soil more than untreated fibre (refer to Figure 2.23). This is consistent to the combination with optimum lime content of 3%, shown in Figure 2.22.

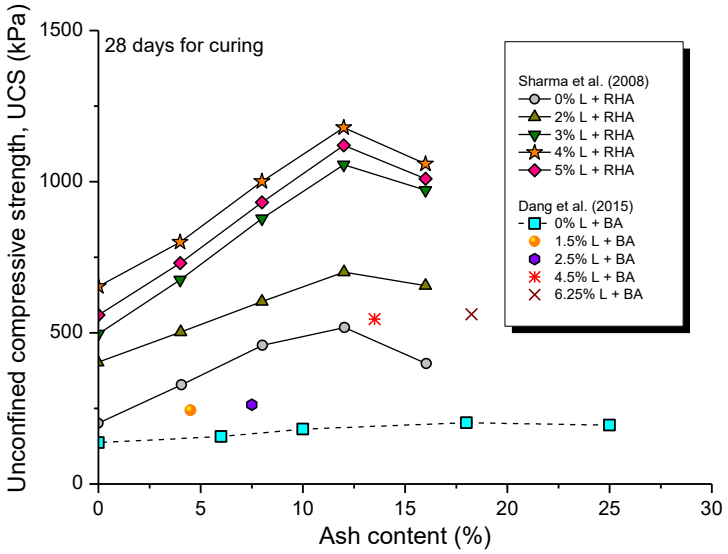


*Figure 2.21 Effect of rice husk ash (RHA) and bagasse ash (BA) contents on UCS values of lime-treated expansive soils after 28 curing days (Dang et al., 2015; Sharma et al., 2008)*

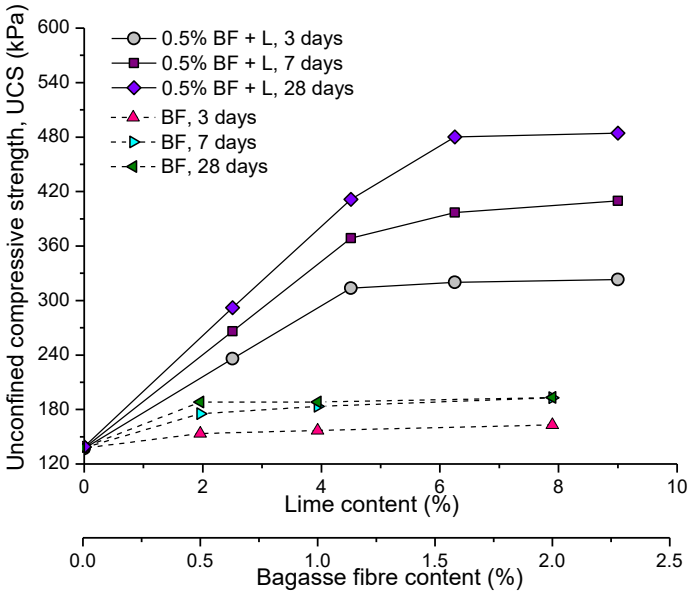


*Figure 2.22 Effect of bagasse fibre alone, bagasse fibre-lime combination and their curing time on the UCS of expansive soil in Australia (Dang et al., 2016a)*

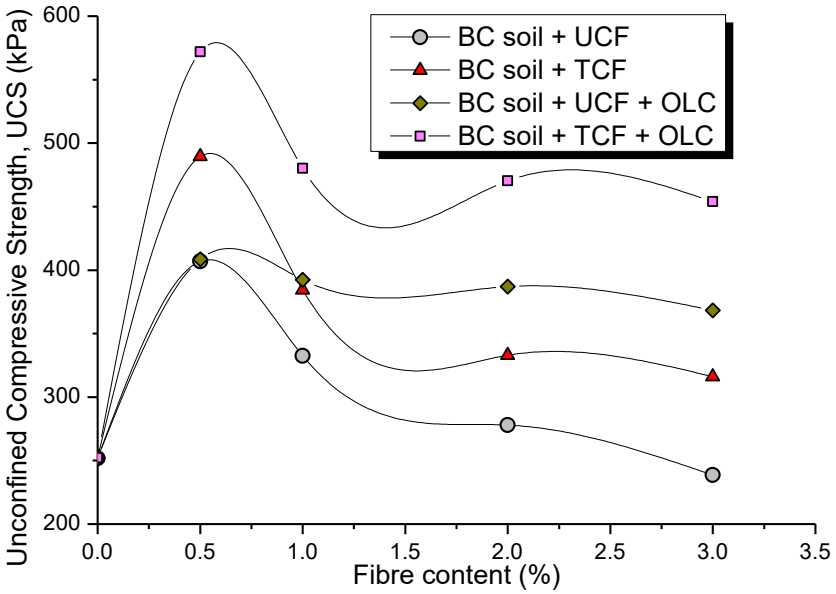


*Figure 2.23 Effect of fibre content on the UCS of untreated coir fibre (UCF) or treated coir fibre (TCF) black cotton (BC) soil with or without optimum lime content (OLC) of 3% (Jairaj et al., 2018)*

### 2.9.5 Indirect tensile strength (ITS)

The indirect or splitting tensile strength (ITS) was investigated with a variation of lime and fly ash content in the study by Kumar et al. (2007). Figure 2.24 indicates the gradual increase of tensile strength in line with higher ash content. The highest strength of about 45 kPa is observed for the optimum combined lime-ash ratio of 8% to 15%, respectively. Also, in the research project of Kumar et al. (2007), the polyester fibre with longer lengths produced the higher tensile strength of its treated soil admixtures (refer to Figure 2.25). Where the effect of curing time on tensile strength is concerned, the lime-treated soil samples have the ITS increase gradually in about 360 days while the addition of cement to lime-soil admixtures give the most of tensile strength after 90 days, which are shown in Figure 2.26.

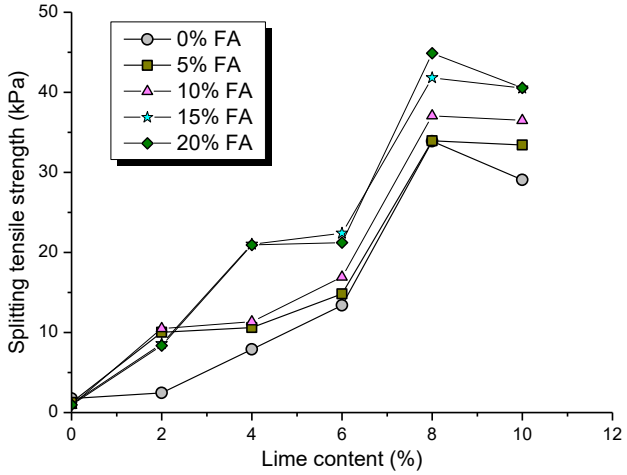


*Figure 2.24 Variation of splitting tensile strength with different contents of lime and fly ash after 28 days of curing (Kumar et al., 2007)*

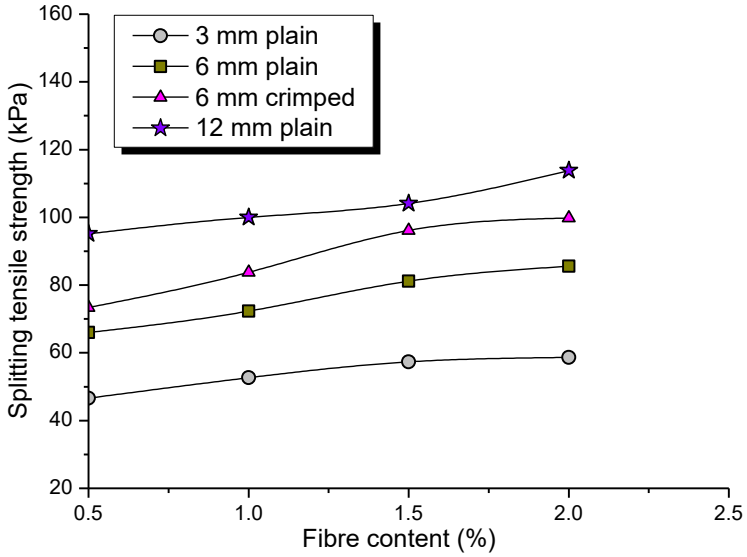


*Figure 2.25 Variation of splitting tensile strength with different content of fibres in 8%lime-15% fly ash treated soil (Kumar et al., 2007)*

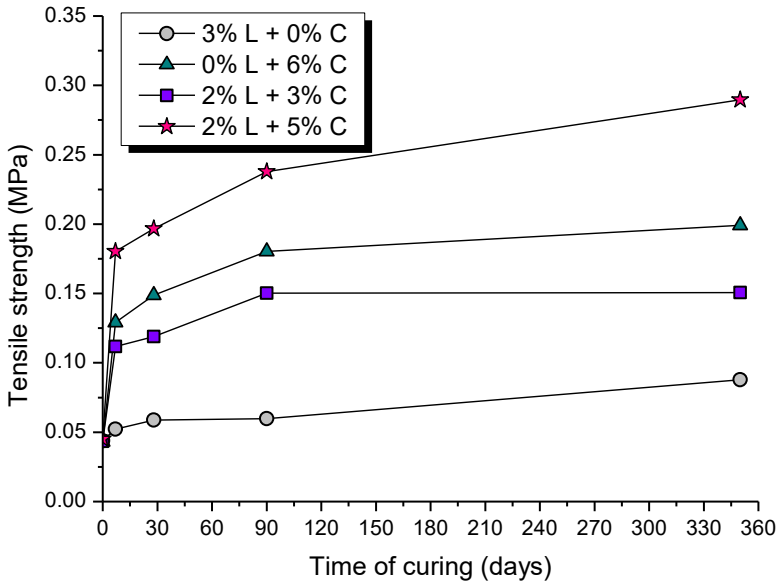


*Figure 2.26 Variation of splitting tensile strength of treated soil with different content of lime-cement and curing time (Okyay & Dias, 2010)*

### 2.9.6 California bearing ratio (*CBR*)

The California bearing ratio (*CBR*) is the ratio of measured force to a designed one when a circular plunger penetrates a compacted soil sample at the constant rate of 1 mm/minute. *CBR* is calculated in percentage for a load reading at the penetration of 2.5 mm or 5 mm, which is mentioned in AS 1289.6.1.1 (1998).

Figure 2.27 compares the California bearing ratio (*CBR*) of natural soil samples treated with lime or both lime and bagasse ash (BA) in soaked or unsoaked conditions. As can be seen in this figure, the inclusion of lime in the sample increases *CBR* significantly at the highest value of about

80% for total lime-ash content of 25%, compared to 10% in *CBR* value of samples without lime. Furthermore, although the soaked-*CBR* value of BA-treated specimens is greater than the unsoaked one, this order is inverse once the lime is added to the mixtures. This might be due to the fact that more lime is involved in the pozzolanic reaction during the soaking process (Dang et al., 2016b). However, concerning the stabilisation of artificial soil, Hasan et al. (2016b) asserted that the soaked *CBR* should be lower than the unsoaked one (see Figure 2.28). However, with the highest content of bagasse ash and lime for the longest curing time of 28 days, the two values of *CBR* are almost the same (refer to Figure 2.28). This prolonged curing time also gave the highest *CRB* value in the soil sample blended with fly ash or bagasse ash in the study of Anupam and Kumar (2013). In this study, the optimum content of fly ash for *CBR* is 20%, while this content for bagasse ash is 25%, which is demonstrated in Figure 2.29.

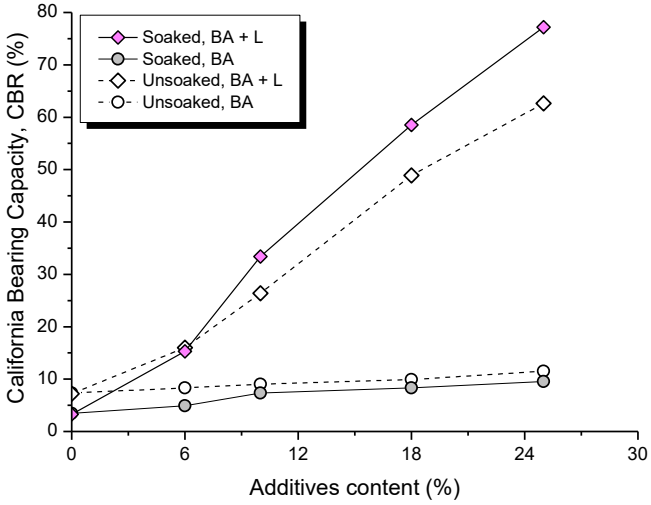


*Figure 2.27 Effects of bagasse ash (BA) and combination of hydrated lime (L) and BA with the ratio of 1 to 3 on unsoaked and soaked CBR of treated expansive soil after 7 curing days (Dang et al., 2016b)*

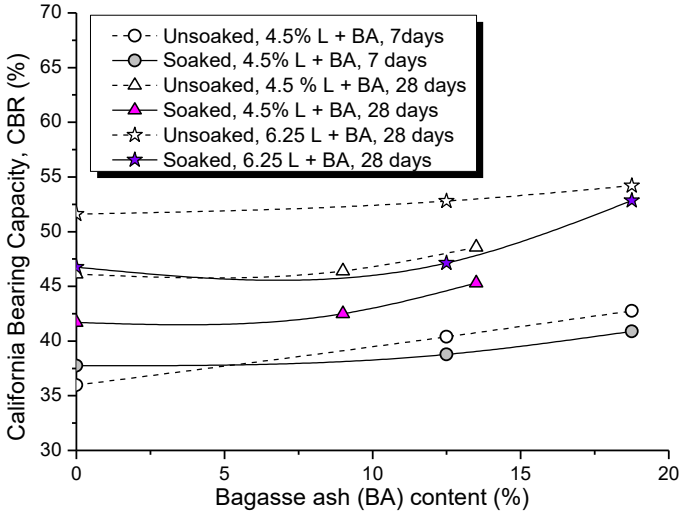


*Figure 2.28 Combined effect of bagasse ash (BA), lime (L) and curing time on CBR of treated artificial expansive soil (Hasan et al., 2016b)*

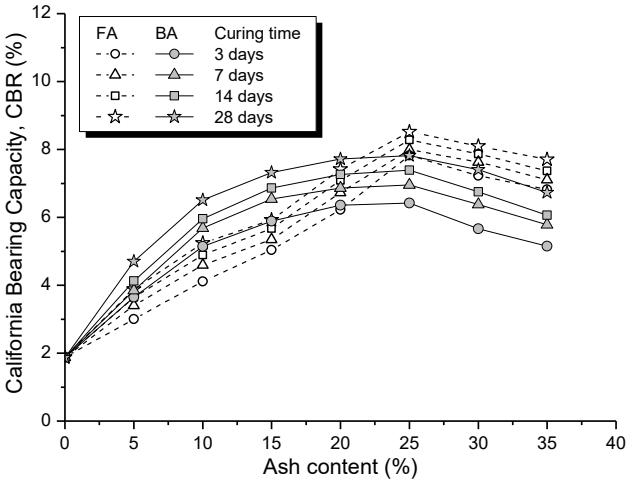


*Figure 2.29 Effect of fly ash (FA), bagasse ash (BA) and curing time on CBR of treated clayey soil (Anupam & Kumar, 2013)*

### 2.9.7 Consolidation behaviour

The consolidation behaviour of soil can be expressed in the void ratio-stress curve in the plot of $e$ versus the logarithm of $\sigma$, respectively. Through analysing the plot, several parameters can be measured, such as compression index ($C_c$), swell index ($C_s$) and pre-consolidation pressure ($\sigma'_p$). The procedure of consolidation test can follow the requirements mentioned in AS 1289.6.6.1 (1998).

Figure 2.30 represents the consolidation curves in the plot of void ratio versus the logarithm of vertical effective stress of soil samples with different content of lime after 28 days for curing. As depicted in this figure, although the initial void ratio increases with the higher content of lime in samples, the compressibility in these specimens is much less than that of parent soil (Jha & Sivapullaiah, 2015). The less swelling phenomenon is observed in lime-treated soil samples compared to the neat soil (Nalbantoglu & Tuncer, 2001). Figure 2.31 indicates this behaviour repeat with the inclusion of fly ash (FA) alone in the soil blend, but it is in the lower level of swelling than natural soil. It is worthy of note that the combination of 15% FA with 3% lime in the soil can duplicate the compressive behaviour of 7% lime treated soil sample. This shows that using fly ash with lime can economise the lime dosage for expansive soil stabilisation. Moreover, only after the curing time of 7 days, the only small addition of lime at 2% can produce the low value of compression index that is approximate to those in more prolonged curing, which is depicted in Figure 2.32. As for fibre reinforcement, the optimum dosage of lime combined with fibre for soil treatment can be shown in Figure 2.33. Regarding the study of Dang et al. (2017),

the 4% content of lime with the same 0.5% bagasse fibre minimised the compressive behaviour more than other combinations (see Figure 2.33).

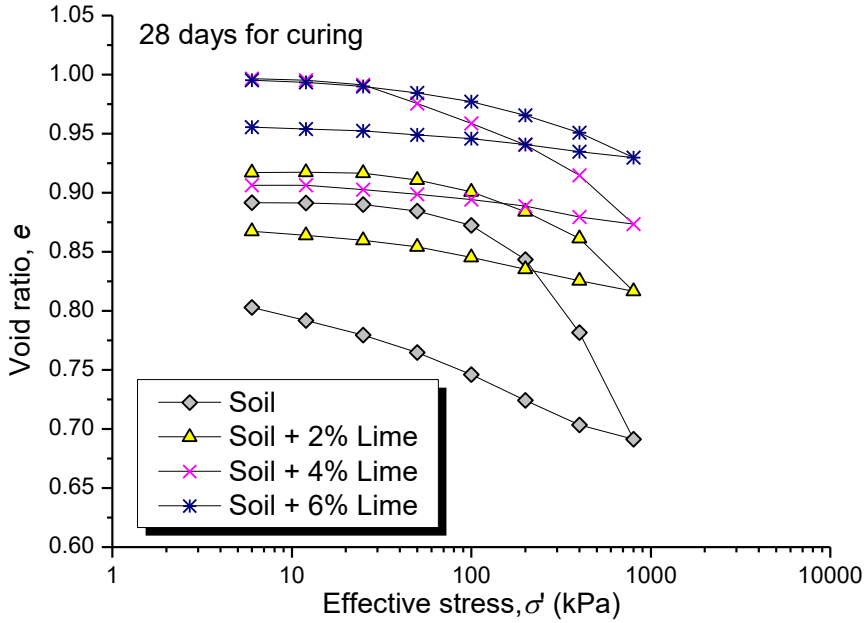


*Figure 2.30 Void ratio versus effective stress of soil treated with varying lime content after 28 days of curing (Jha & Sivapullaiah, 2015)*

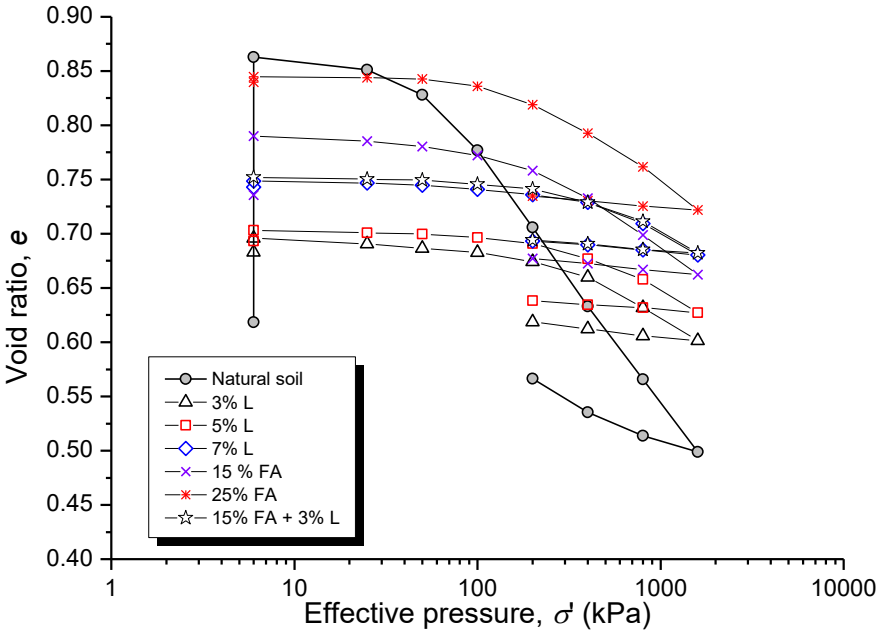


*Figure 2.31 Void ratio – pressure curves for natural soil and soil treated with lime, fly ash and fly ash-lime (Nalbantoglu & Tuncer, 2001)*

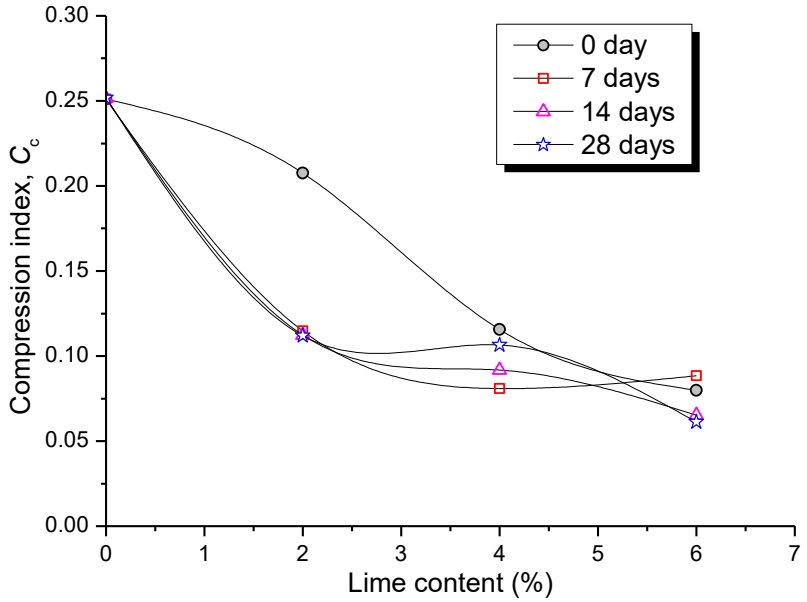


*Figure 2.32 Effect of lime and curing period on compression index $C_c$ of soil (Jha & Sivapullaiah, 2015)*

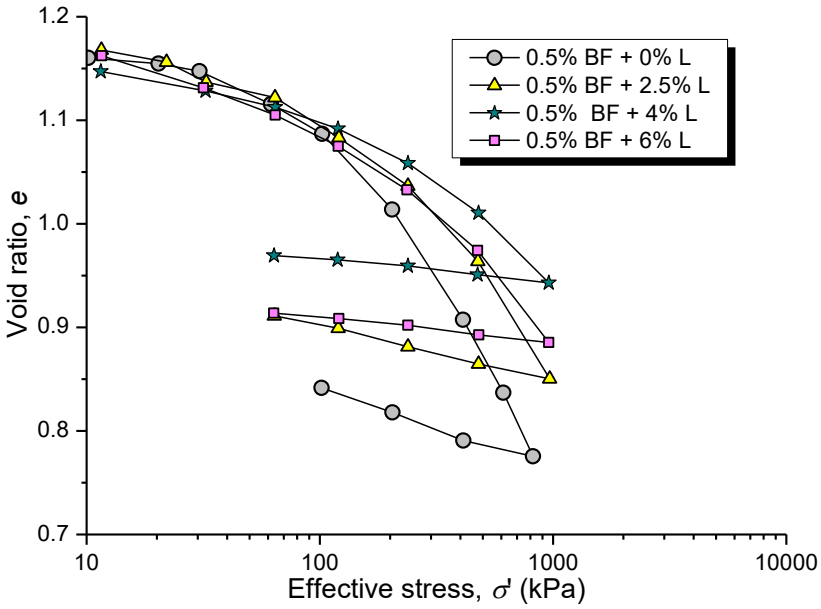


*Figure 2.33 Effective stress – void ratio curves of varying lime content in 0.5% bagasse fibre treated expansive soils (Dang et al., 2017)*

### 2.9.8 *pH* values

The influence of different contents of lime, class C fly ash and cement kiln dust on the *pH* values of treated clay samples are shown in Figure 2.34. As illustrated in this figure, the pH value increased considerably at the initial marginal content of additives. With 2% lime or 10% fly ash and cement dust generated a high pH of about 12.3 (Solanki et al., 2009). This agrees well with the studies on the environment for pozzolanic reactions when the additives with rich calcium content are concentrated on clay particles to produce cation exchange and flocculation (Bell, 1996;

Chen, 2012; Cokca, 2001; Nalbantoglu & Tuncer, 2001). This high alkaline concentration decreases with the increase of curing time in various soil combinations with lime, gypsum and incinerated sewage sludge ash and cement, as shown in Figures 2.35-37). From Figures 2.36-37, it is essential to note that the pozzolanic reaction is in line with the decrease of calcium and hydroxide, causing the significant pH-value reduction for the formulation of ettringite, a crystal formed by the reactions between natural soil and additives like lime and gypsum with high content of calcium (Aldaood et al., 2014; Chen & Lin, 2009)

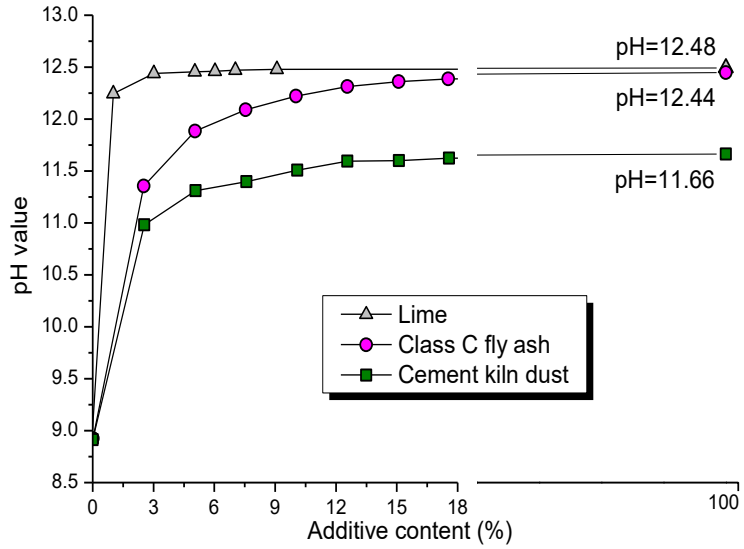


*Figure 2.34 pH values with the different content of additives in treated soils (Solanki et al., 2009)*

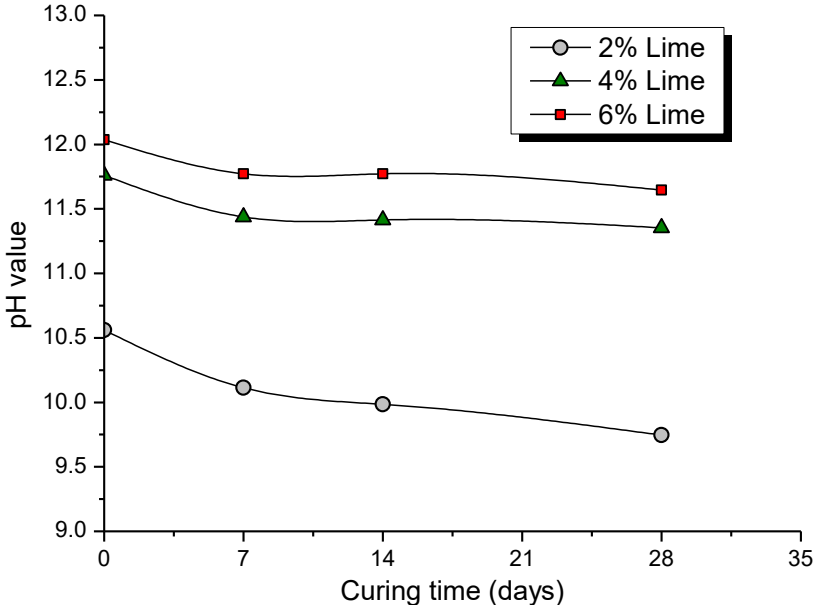


*Figure 2.35 Alkalinity of soil treated with various lime content after different periods of curing (Jha & Sivapullaiah, 2015)*

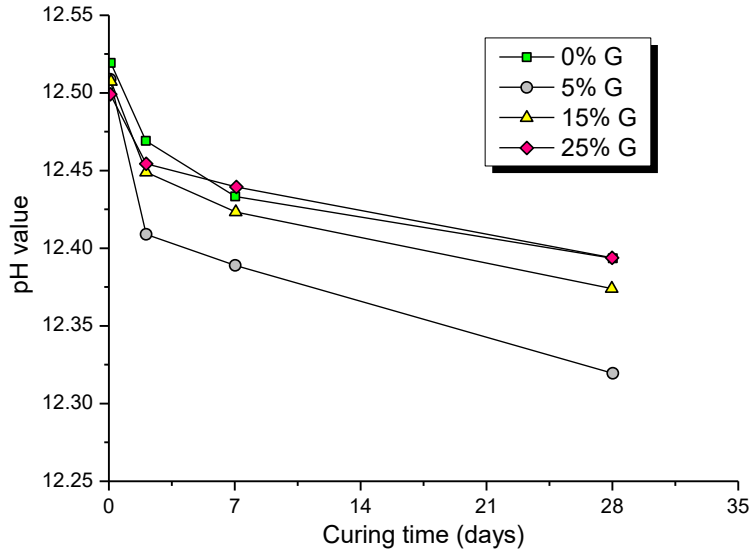


*Figure 2.36 pH values of treated soil samples with various content of gypsum (G) (Aldaood et al., 2014)*

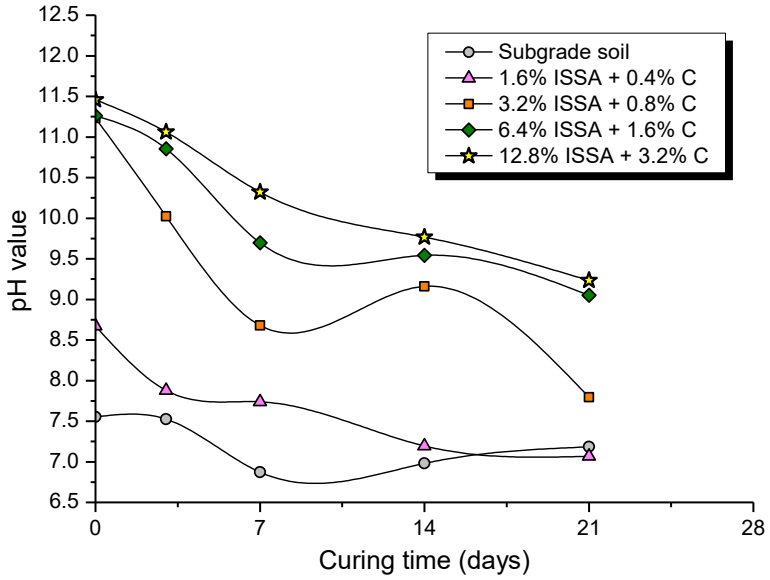


*Figure 2.37 Effect of curing time on pH value with various content of incinerated sewage sludge ash (ISSA) and cement (C) in subgrade soil (Chen & Lin, 2009)*

## 2.10 Electrical conductivity test for evaluating the pozzolanic performance of ash

To evaluate the pozzolanic performance of ash in aqueous solutions like pH test, three main standard methods were proposed, namely Frattini approach, the lime saturation method and the electrical conductivity tests (Bahurudeen et al., 2015b). Frattini method is based on the titration of ash-cement solutions to determine $Ca^{2+}$ concentration, which is then compared with saturation curve in the graph of $OH^-$ on X-axis versus $Ca^{2+}$ on Y-axis, so-called Frattini graph (CEN, 2005). If the measured concentration is lower than the curve in the graph, the studied ash is regarded as a pozzolanic material due to its consumption of calcium hydroxide [$Ca(OH)_2$]. The lime saturation

method is also based on the titration measurement similar to the Frattini method. The difference is using a saturated lime solution with a concentration of 2 g/L reacting with ash, which is then kept in an oven at 40°C for 3 and 7 days before titration test is conducted to quantify the pozzolanic reaction of ash (Donatello et al., 2010; Frı & Rodrı, 2008; Frías et al., 2005; García et al., 2008). Therefore, lime saturation test results usually agree well with Frattini tests. The main advantage of these methods is that they make it possible for ash to be mixed in saturated lime suspension so that the pozzolan can completely react with lime (Bahurudeen et al., 2015b). On the other hand, the electrical conductivity method uses the unsaturated lime solution with a concentration of 0.8 g/L (Paya et al., 2001; Tashima et al., 2014). The method generates an electrical conductivity (EC) curve, which indicates the powdered activation of ash in the unsaturation of lime suspension. The generated curve can be divided into four stages: (I) initial, (II) dormant period, (III) huge collapse region and (IV) final set stage, as shown in Figure 2.38 (McCarter & Tran, 1996). While the drop in the initial stage shows the good reactivity of cementitious ash in the first 4 hours, the dormant stage (Stage II) has a marginal change in conductivity, indicating the low reactivity of material. Stage III shows a remarkable drop in conductivity, indicating an increase in rigidity of the suspension. Finally, the last stage (Stage IV) has conductivity stabilise gradually, showing a slowing down in chemical activity of tested solution (McCarter & Tran, 1996). According to Bahurudeen et al. (2015b), it is unnecessary to have all stages observed in a material. Generally, they mentioned that coarse ashes do not have Stage IV, while Stage II disappears in fine materials.

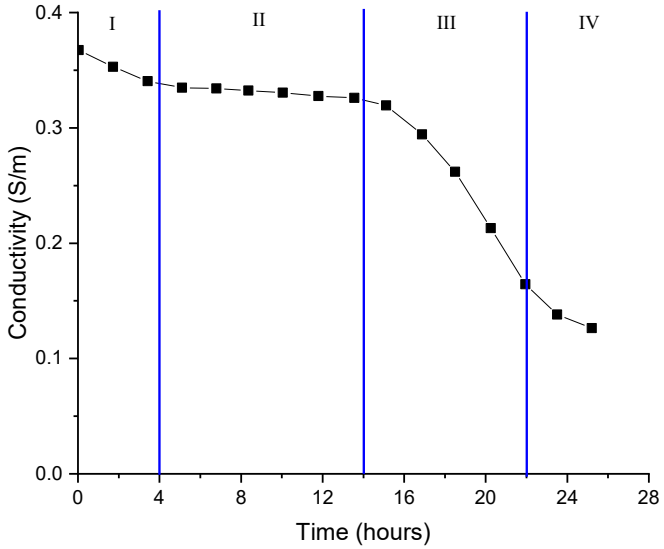


*Figure 2.38 Conductivity response using electrical conductivity method with unsaturated hydrated lime solution (McCarter & Tran, 1996)*

To define the shrinkage-swelling potentials of untreated or treated soils, several methods have been proposed (Puppala et al., 2006; Seed & Lundgren, 1962; Sridharan et al., 1986). For example,

direct methods measure parameters that represent swelling and shrinkage potentials, such as the free swelling rate or linear shrinkage (AS 1289.3.4.1, 2008; ASTM-D4546, 2014). Meanwhile, indirect methods estimate these potentials through its correlation with other soil's characteristics, such as soil plasticity with plasticity index (IP), methylene blue value (VBS), clay activity with the content of montmorillonite, and soil pH, electrical resistivity or conductivity (Chen, 2012; Chu et al., 2018; Puppala et al., 2006). With untreated soil, these characteristics are usually invariable. However, when it comes to lime-soil mix, they change with curing time, leading to the complexity of soil analysis because the timing presence of pozzolanic products from reactions between lime and soil (Villar-Cociña et al., 2003). Compared with other chemical tests, such as pH, Fantini tests, the electrical conductivity test was commonly used for lime-soil investigation because the test can show the change in data with time. Furthermore, the test is also used to define moisture and salinity of subgrade soil (Fukue et al., 1999; Yoon & Park, 2001).

It is clear that there are extensive studies on methods to evaluate the pozzolanic activity of bagasse ash, in which pozzolanic activity index and electrical conductivity are the two commonly used techniques (ABNT NBR 5752, 1992; Luxan et al., 1989). While the pozzolanic index method compares the compressive strength of cylindrical specimens (50mm × 100mm) after 28 days curing in wet mortar, Luxan et al. (1989) suggested measurement of change in electrical conductivity (*EC*) of saturated calcium hydroxide and aqueous sample. Compared to the pozzolanic index technique with 28 prolonged curing days for specimens, the method using *EC* rate is more advantageous since it only requires the variation of conductivity in testing time of 2 minutes to evaluate the pozzolanic property of materials. Table 2.7 shows the evaluation of pozzolanicity based on the change of EC in the tested solution. Generally, the more significant the change in EC of samples, the higher the pozzolanic activity of studied suspension.

*Table 2.7. Evaluation of pozzolanicity of materials (Luxan et al., 1989)*

| **Pozzolanic evaluation of material** | **$\Delta EC$ (mS/cm) in 2 minutes** |
|---|---|
| Non-pozzolanic | $\Delta EC < 0.4$ |
| Variable pozzolanicity | $0.4 < \Delta EC < 1.2$ |
| Good pozzolanicity | $\Delta EC > 1.2$ |

In a strong relationship with the chemical and mineralogical features of expansive soil, which determines its volume-change behaviour (Thomas et al., 2000), a good correlation between the electrical resistivity (or conductivity) and the free swelling rate of the soil was recently recognised (Chu et al., 2018; Lesmes & Friedman, 2005). However, the relationship between electrical conductivity and shrinkage-swelling behaviour of lime-ash treated soils has not been investigated yet. Therefore, it is necessary to investigate the correlation between the electrical conductivity,

shrinkage and swelling ratio of soil treated with hydrated lime. As a result, it is expected to propose a simple and reliable method to better predict the swell-shrinkage behaviour of treated soils by electrical conductivity test.

### 2.11 Numerical analysis in a case study of embankment on soft ground in Australia

Distributed widely in a vast area in New South Wales and Queensland, Australia, soft clayey ground causes significant settlement of embankments due to its high compressibility with time, leading to damages to roads subgrade and pavements. If the embankments are built on expansive ground, the heavy weight of earth fill is often much over the swelling pressure, but significant settlement can be observed. The settlement duration can prolong for many months or even several years before the stabilisation is achieved. Therefore, various methods were proposed to speed up the consolidation process, such as prefabricated vertical drains (PVDs) and vacuum-assisted vertical drains. However, there are also other methods to reduce the consolidation or settlement of soft soil through reinforcing foundations under embankments. They might be the installation of stone columns (Fatahi et al., 2012), or pile-supported and geosynthetic-reinforced earth platform on the ground (Han & Gabr, 2002; Liu et al., 2007). Occasionally, lightweight fill materials can be utilised to decrease the loading from the embankment weight.

To investigate the reliability of the model of soil employed for modelling, the embankment model illustrated the middle zone of the embankment or the cross-section 3 with 16 m wide, 3 m high and about 90 m long, as shown in Figures 2.39 and 2.40. The embankment and soil layers were discretised in 15-node triangular elements, using the finite element method in PLAXIS 2D version 2017. While the embankment-fill material and subsoil layers (e.g., sand, clayey sand) were subjected to the model of Mohr-Coulomb (MC), alluvial crust and estuarine silty clay (Ballina clay) are adopted with the model of modified Cam clay (MCC), and soft soil creep (SSC) model, respectively. The SSC model assumes that the plastic strains start after the primary consolidation when the pore water pressure is dissipated completely, which is consistent with conventional consolidation calculation. The model, therefore, well presented the actual behaviour of the Ballina clay layer under the initial pressure in the field because the time rate of filling the embankment was relatively low and the filling intervals for consolidation was in a few days, which could be regarded as a short-term consolidation because mainly the primary consolidation took place. Therefore, the model is adequate to validate the behaviour of embankment on soft clay. In the full-scale embankment in Ballina, Australia, the field embankment was treated with PVDs under the working platform to help fully dissipate the pore-water pressure through horizontal drainage layers (Kelly et al., 2018).

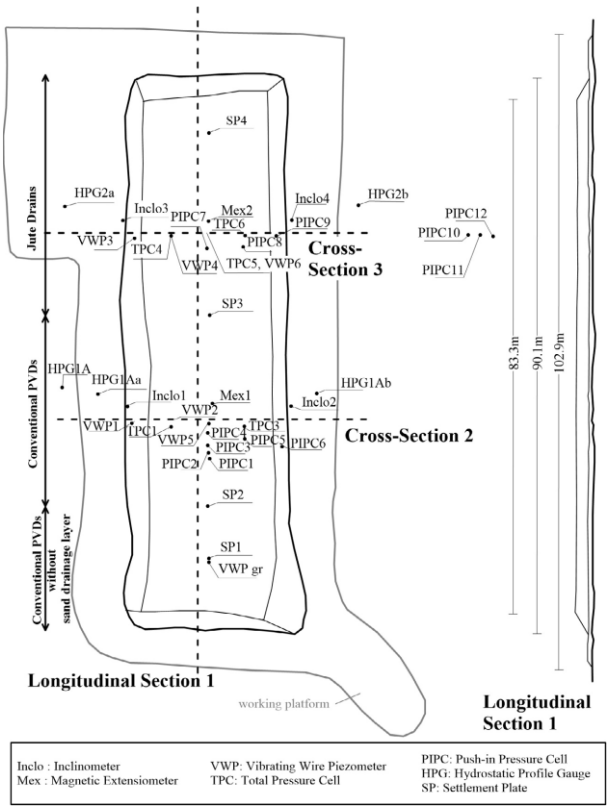


*Figure 2.39 Longitudinal section of embankment post-construction in Ballina, NSW, Australia (Kelly et al., 2018)*

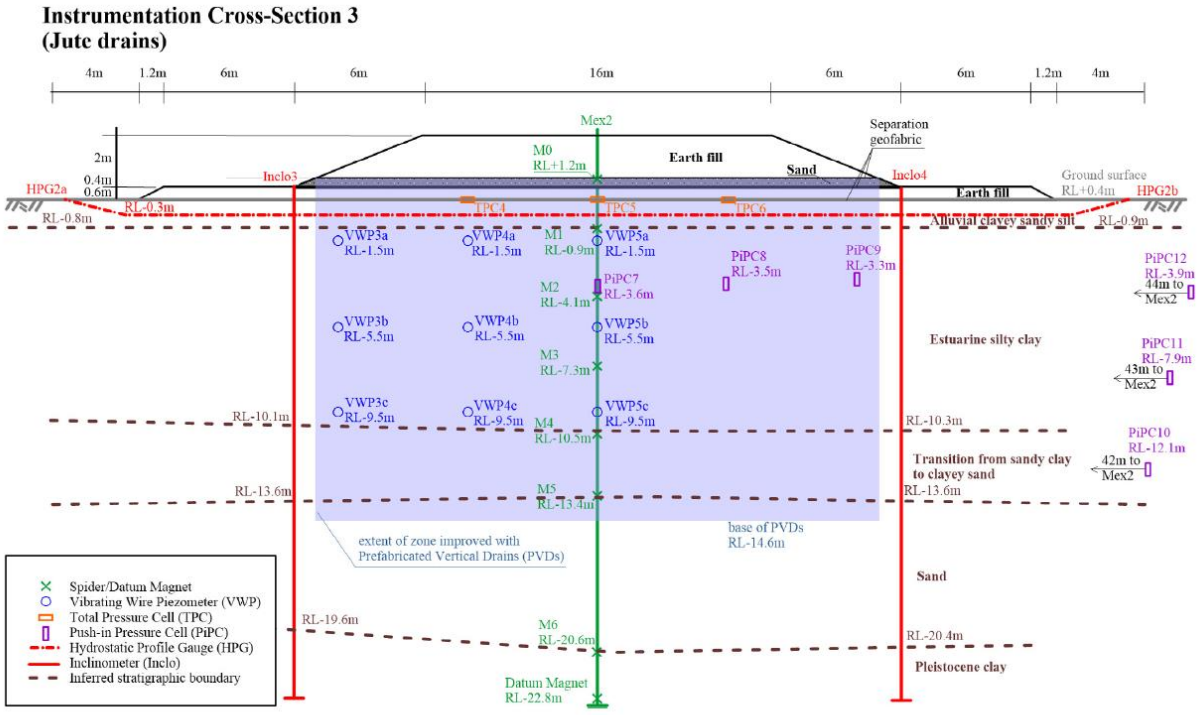


**Fig. 8.** Nominal cross sectional dimensions, locations of the instruments and interpreted stratigraphy.

*Figure 2.40 A typical cross-section of the case-study embankment on soft soil (Kelly et al., 2018)*

Referring to the study conducted by Gong and Chok (2018), the estuarine silty clay, also known as Ballina clay and distributed in the depth from 1 m to 10 m, stems for most of the ground settlement under embankment loading, which should be divided into two layers with variations of soil parameters, from unit weights to friction angles. The transformation from 1 layer into 2 layers of clay is also mentioned by Amavasai et al. (2018) as an update of "Class A" predictions of one layer to "Class C" model with upper and lower layers of estuarine clay. Class A with a single homogeneous layer was adopted in previous extensive studies, such as the Class A model conducted by Indraratna et al. (2018) or Yang and Carter (2018). However, Class C prediction separated the soft clayey soil into two parts, according to changes in their geotechnical properties. Studies on later models indicated that Class-C-based predictions resulted in a good agreement with both vertical settlement and horizontal displacement, whereas the Class A model has issues with lateral movement (Gong & Chok, 2018). Class C also predicted well the changes in pore pressure under the embankment, which could not be obtained in Class A (see Table 2.8).

In addition, there is an array of vertical drains underneath the embankment and attached to the medium sand layer, which allows dissipation of pore water pressure horizontally and speeds up the ground settlement and lateral movement (Figure 2.40). There were two kinds of drains used in the Ballina embankment project, including conventional prefabricated vertical drains (PVDs) and jute drains. While conventional drains were installed in cross-section 2, jute vertical drains were constructed in cross-section 3 and attached to the drained sand layer, as illustrated in Figure 2.40. Unlike the model with installed drains suggested by Gong and Chok (2018), Rezania et al. (2018) did not use these drains but employed the equivalent permeability parameters to generate modelling outputs with Class A and C models. Interestingly, better predictions of settlement with Class C than Class A were obtained, as shown in Figure 2.41. Therefore, it is recommended to use Class C model for numerical analysis on the ground under the Ballina embankment.

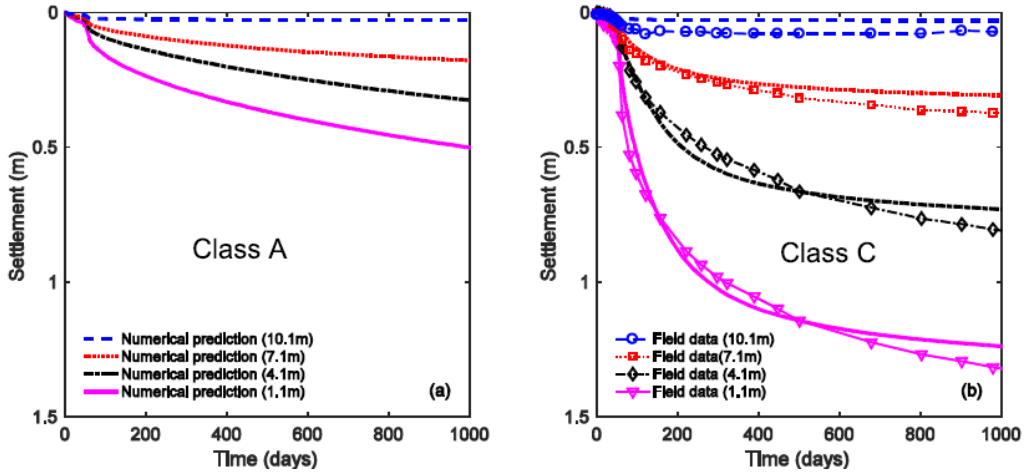


*Figure 2.41 Settlement predictions from numerical analysis conducted by Rezania et al. (2018)*

*Table 2.8 Comparison between results from Class A and C in the study done by Gong and Chok (2018)*

| Class A model | Class C model |
|---|---|
| 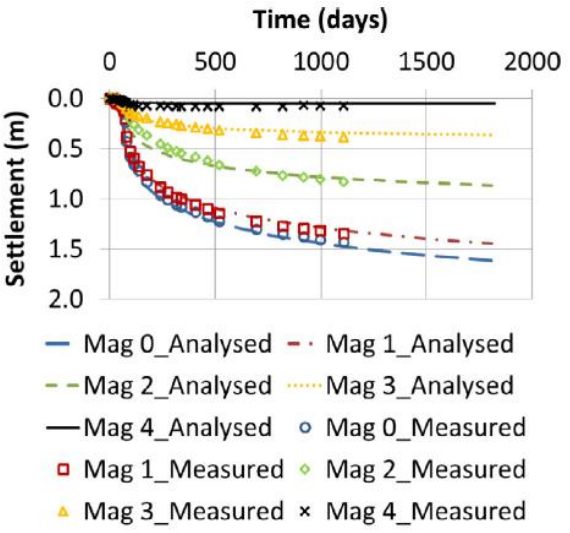 | 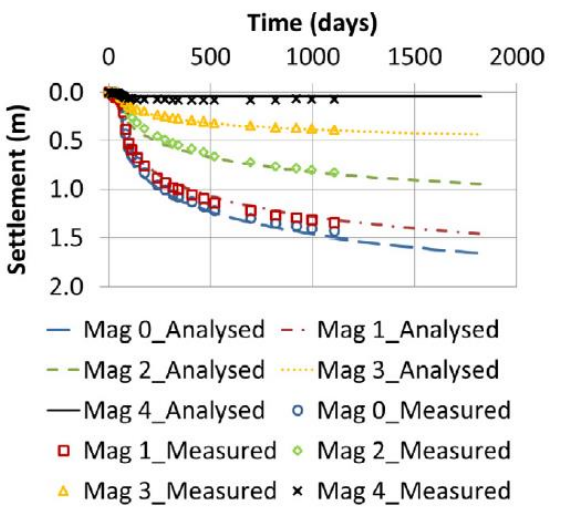 |
| 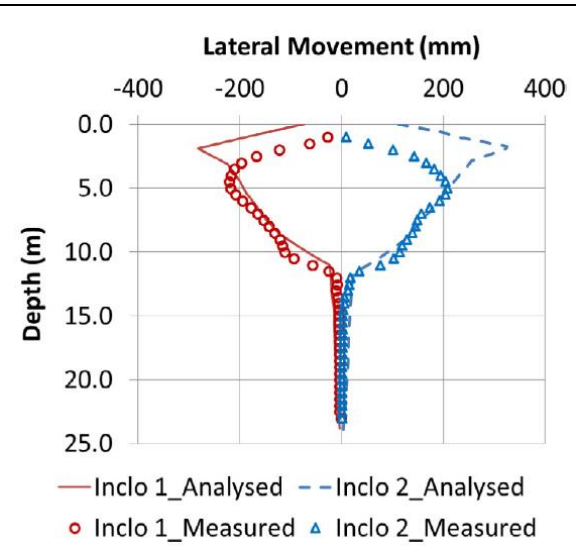 | 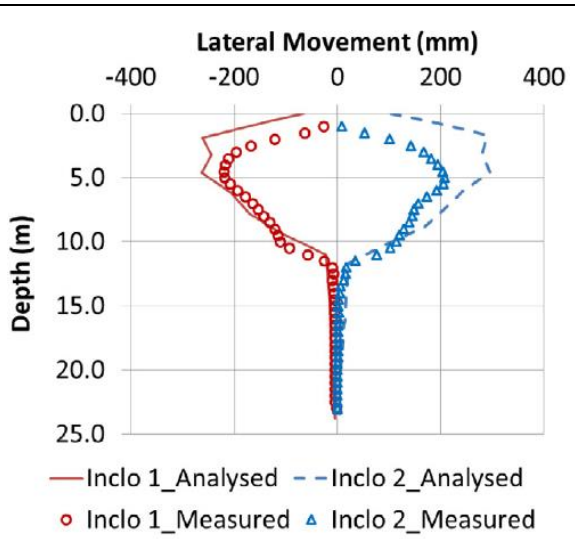 |
| 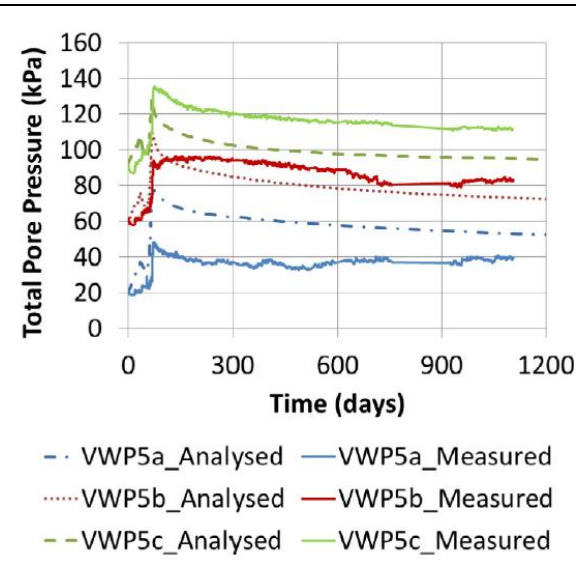 | 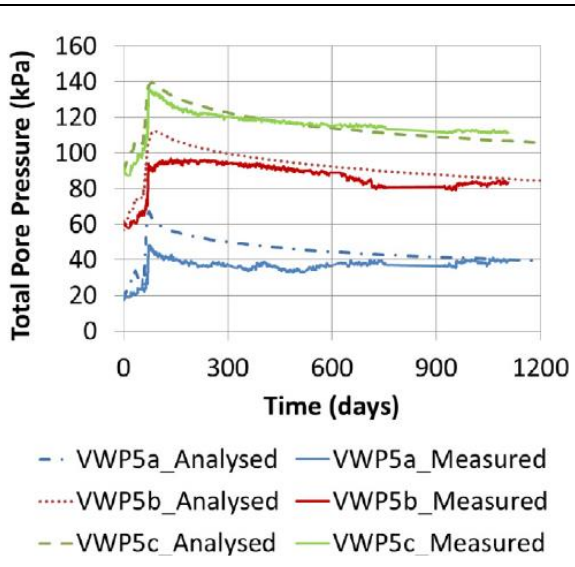 |

## 2.12 Gap identification, problem statement and hypotheses

Through literature review, the gaps are identified and related to using ash and lime for expansive soil stabilisation, including a chemical testing method to determine their optimal mixing ratio, relevant characterisation of engineering, and numerical application for embankment on treated expansive ground. Of mentioned literature gaps, the testing method for mixing designation is the most concern. Although there is a testing standard, named as a lime-demand method, to estimate the optimal ratio of hydrated lime in lime-treated soils by using pH tests, there is still a lack of research on using a similar mechanical procedure to define the proper ratio of ash to lime in their blends with expansive soils. From the literature review in concrete engineering, the electrical conductivity (EC) test is commonly used to evaluate the pozzolanicity of ash in the unsaturated solution of hydrated lime, while the electrical conductivity is also employed in the geotechnical field to estimate the bentonite content in their mixture with sand. Since the pH testing method is based on the electrical exchange of lime-soil solution, it is possible to utilise and modify the EC method to define the optimal ratio of ash to lime. The determination is based on the sufficient amount of ash that is enough to generate the lime fixation. With an excess of ash over lime, the variation of *EC*-values deflects in its relationship with ash content, as indicated in studies on the measurement of pozzolanic reactivity in lime suspensions.

The shrinkage-swelling characteristics of expansive soil are also considered as a pivotal factor that threatens foundations of civil structures such as, pavements, highways, light buildings and canals. The cracking phenomenon is caused by heave or settlement of expansive soil, which were reported in many countries (Phani Kumar & Sharma, 2004). Furthermore, the annual statistics from damage cases in the UK and USA indicated a loss of over 15 billion dollars and about 400 million pounds, respectively, caused by the impact of expansive soil (Jones & Jefferson, 2012; Viswanadham et al., 2009). The expenses spent on building maintenance caused by ground expansion or collapse is always high and requires a significant budget to repair or possibly reconstruct (Chenarboni et al., 2021; Gourley et al., 2020; Jones & Jefferson, 2012; Nelson & Miller, 1997; Puppala & Pedarla, 2017; Viswanadham et al., 2009). Therefore, it is necessary to reduce the shrinkage-swelling potential of expansive soil by enhancing its strength, and thus limiting its detrimental impacts.

As for ash materials, bottom ash and bagasse ash are amounts of waste generated extensively from human, agricultural and industrial activities in industrialised and developing countries. The economic problems from disposing of them and shortages of natural resources require effective methods to reuse the agricultural and industrial ash compound for engineering purposes such as

road construction materials. This combination is promising because both bottom ash and bagasse ash play an important role in generating pozzolanic reactions, solidifying the bagasse-bottom ash treated soil with the presence of hydrated lime. The primary research significance is to show the combined effects of bottom and bagasse ash in stabilizing expansive soils to use them as binders to stabilise the soft ground under embankments with the inclusion of lime. The problems from the combination can be outlined as follows:

- It takes excessive time and monetary consumption to perform a series of mechanical tests for ash-lime-treated soil samples with varied ratios between bottom ash and bagasse ash. If the percentage of ash changes from 0% to 40% with the span of 5%, the combination number is 81 tests required for only a kind of test and with a specific content of hydrated lime. Therefore, it is necessary to design a testing method that can quickly predict the optimal ratios of bottom ash and bagasse ash to lime to reduce the number of mechanical experiments.
- The amount of hydrated lime significantly influences the engineering characteristics of lime-treated soils. When adding hydrated lime to soil, the content of lime is based on the mass of dry soil weight. However, when mixing both hydrated lime and ash with soil, fixing the content of lime and changing the percentage of ash does not mean that the lime amount is constant in ash-lime-soil blends. This relies on whether the ratio of lime and ash is based on the mass of dry soil, total mixture or even the combined weight of dry soil and ash.
- The size of ash affects its reactivity with hydrated lime in soil blends. While bottom ash behaves as a coarse material, bagasse ash contains many fine particles that make its combination with soil and lime reliant on the size effect. However, less research was conducted to reveal how the changes in the size of bagasse ash influence the engineering properties of ash-lime-treated soils.
- Recent studies indicate a detrimental effect of hydrate products on the strength development of lime-treated soils. Therefore, it is possible to occur the same degradation of strength and strength modulus in ash-lime-treated soil. The research on this phenomenon is necessary to predict the strength development of soils stabilised with lime, bottom ash and bagasse ash in the long term.
- There are extensive studies on using bottom ash or bagasse ash for soil stabilisation in road projects of constructing embankments on soft soil. However, the applications of combining bottom ash and bagasse ash to treat ground under road embankment are still questionable.

From the five research issues mentioned above, five main hypotheses can be generated and experimented throughout this study. They are corresponding to the problem statements and shown as follow:

**H1.** *Using electrical conductivity tests helps quickly determine the optimal ratio of bottom ash and bagasse ash to lime in mixtures with expansive soil for stabilisation.*

**H2.** *The mixing content in lime-ash-treated soils based on different dry weights gives different engineering characteristics of mixed samples.*

**H3.** *Studied bagasse ash with smaller maximum diameters can enhance the engineering characteristics of lime-bagasse-ash-treated expansive soils.*

**H4.** *There is a degradation in strength modulus of expansive soils treated with hydrated lime, bottom ash and bagasse ash over a long period of time.*

**H5.** *Using both ash and lime to stabilise expansive soils can further reduce settlement and lateral displacement of embankment on soft ground.*

To test these hypotheses, there are sections in thesis chapters that address them. In detail, Hypothesis 1 will be solved in Chapters 5-7, in which electrical conductivity tests are performed for soil mixtures with hydrated lime, bottom ash and bagasse ash. Hypothesis 2 is confirmed in Section 5.3 of Chapter 5, while Hypothesis 3 is tested in Chapter 6. Lastly, Hypotheses 4 and 5 will be solved in Chapters 7 and 8, respectively. Conclusions on hypotheses are shown in Chapter 9.

## 2.13 Summary

From the comprehensive review of literature on soils treated with hydrated lime, bottom ash and bagasse ash, the salient concluding remarks and suggestions can be summarised as follows:

- Using ash for soil stabilisation is becoming a sustainable solution to reuse the waste for engineering applications. With the development of agricultural and industrial activities, agro-industrial wastes are dumped in the environment and causing severe polluting issues. Using wastes for stabilising soil is urgent to minimise the disposal and ease the pressure of exploiting natural materials in shortage.
- While agricultural by-products include ash and fibre wastes, industrial waste materials, ranging from slag, asphalt residue, silica fume, fly ash, coal bottom ash, glass cullet and fibres. In the utilisation of agricultural waste for soil stabilisation, there are both merits and disadvantages when combining agricultural ash and fibres with soil. Notably, bagasse ash

in Australia becomes a promising candidate that provides overwhelming advantages of stabilising expansive soil due to its high content of silica and low cost. Likely, industrial waste has bottom or fly ash as an excellent material to combine with soil for stabilisation because of its richness of amorphous silica and availability.

- Studies on combinations of ash or fibre with lime indicate the improvement of treated soil in unconfined compressive strength (*UCS*), Young's modulus (*E*) and California bearing ratio (*CBR*). The soil reinforcement is also observed in linear shrinkage and swelling potential. The extensive research indicates that the optimal content of lime is 4%, based on the mass of dry soil, resulting in a much lower linear shrinkage and free swelling ratio than soil treated with ash or fibre without lime. The same results are confirmed in UCS, ITS and CBR experiments. Some studies also indicate the adverse effects of soil mixed with coal and bagasse ash if hydrated lime is not included. However, once both lime and ash are present in soil, the stabilising enhancement is much higher than soil treated with lime, which is called combining effects of ash and lime in soil stabilisation.
- With the local availability, measures to deal with climate changes and high demand for developing road infrastructure in regional areas of Australia, it is essential to reuse bottom ash and bagasse ash for soil stabilisation with hydrated lime in projects to construct road embankments on soft grounds. The previous studies indicated that combining bottom ash with hydrated lime produces an excellent improvement not only in reduction of swell-shrinkage potentials but also in the enhancement of soil strength. The relationship between the enhanced properties of treated soil with electrical features was also revealed, opening a possibility of using electrical conductivity to predict the engineering behaviour of bottom-ash-lime-treated soils. Meanwhile, established studies on bagasse ash in various particle sizes demonstrated a close correlation between the size of bagasse ash with its reactivity with soil and lime. Therefore, the electrical conductivity test can also be used to evaluate the pozzolanic reaction of bagasse ash in different ash sizes in the solution of soil and lime.
- From the literature review, the gap of literature is identified into three subjects: (1) a quick testing method to deal with an excessive number of combining soil, lime, bottom ash and bagasse ash; (2) characterisation of expansive soil treated with hydrated lime, bottom ash and bagasse ash; and (3) numerical analysis of road embankment on the soft ground treated with lime, bottom ash and bagasse ash. These gaps form three main research objectives,

including electrical conductivity tests, characterisation of ash-lime-treated soils, and numerical analysis of road embankment on the treated ground.

- From gap identification, five research problems followed by five main hypotheses are identified. They are related to electrical conductivity test, mixing ratio, size of bagasse ash, strength degradation and embankment on soft soils. Thesis chapters from 5 to 8 will address these five hypotheses.

# CHAPTER 3

# Materials and Methods

## 3.1 Introduction

This chapter presents the details of materials and relevant methods, including tests and experimental analysis. Firstly, the materials are introduced to demonstrate their physical, mechanical and micro-structural properties before conducting the proposed tests. Following the selection of the testing program, test methods are expressed along with the corresponding standards. Any modifications and upgrades in the methods are also emphasised in this chapter. Furthermore, testing interpretation and analysis are illustrated. These steps are essential in converting raw testing data into meaningful results.

## 3.2 Materials

In the perspective of materials, there are four main elements, namely expansive soil, hydrated lime, bottom ash and bagasse ash. For soil, since the studied material is an artificial compound of three components, including kaolinite, bentonite, and fine sand, properties of each sub-components should be delved before mixing them to constitute the proposed soil. Meanwhile, hydrated lime is made of calcium hydroxide, adhering to the standards from manufacturers; hence, main characteristics of lime are investigated. On the other hand, bottom ash and bagasse ash are field materials, including various chemicals, and generally, they are not homogeneous. This requires

thorough physical and chemical research on the materials to understand the effects of their properties on soil treatment. Accordingly, effective ways to attain relevant results can be suggested to stabilise expansive soil with ash. In summary, there are five main combinations for treated soils, resulting in six objective materials: (1) soil, (2) lime-treated soil, (3) bottom-ash-lime treated soil, (4) bagasse ash-lime treated soil, and (5) bottom ash-bagasse ash-lime treated soil, shown as treated soil samples in Figure 3.1.

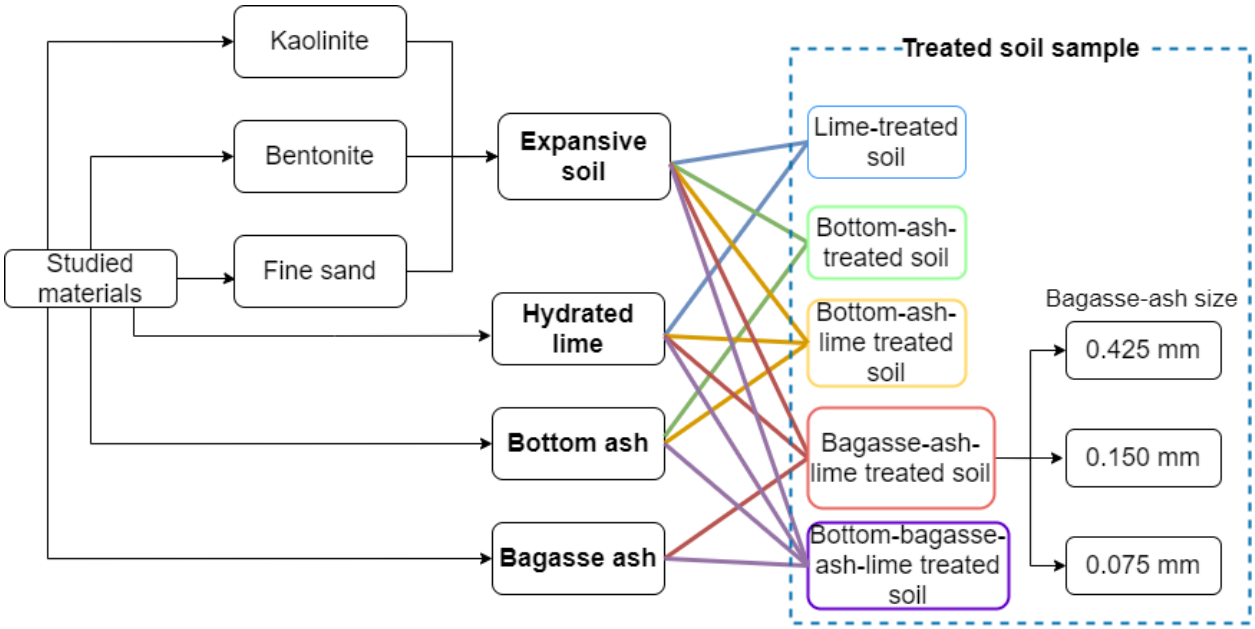


*Figure 3.1 Flowchart for studied materials*

### 3.2.1 Expansive soil

Expansive soil in this study contains three components, bentonite Active Bond 35, Kaolinite Q38 and Sydney fine sand. The soil is also called an artificial material, which has the advantage that each element can be controlled in the right ratio so that every constituted soil sample is homogeneous and has the same composition. This is especially important in this study with electrical conductivity tests because the tests require precise amounts of components mixed in the solutions for acceptable credibility of results. In the detail of soil elements, Figure 3.2 shows the images on their appearance in colour. While Kaolinite has a white cream colour, illustrated in Figure 3.2a, bentonite is dark grey in finer particles than kaolinite (refer to Figure 3.2b). Sydney fine sand appears in many yellow colours and in granular shapes (see Figure 3.2c).


(a) (b) (c)

*Figure 3.2 Microscopic images of (a) kaolinite, (b) bentonite and (c) Sydney fine sand*

Composition analyses from x-ray diffraction (XRD) tests show all components contain quartz, especially Sydney fine sand. In addition, bentonite presents a large content of montmorillonite, while kaolinite, as its name, has a majority of kaolinite mineral and small amounts of muscovite, which are depicted in Figure 3.3.

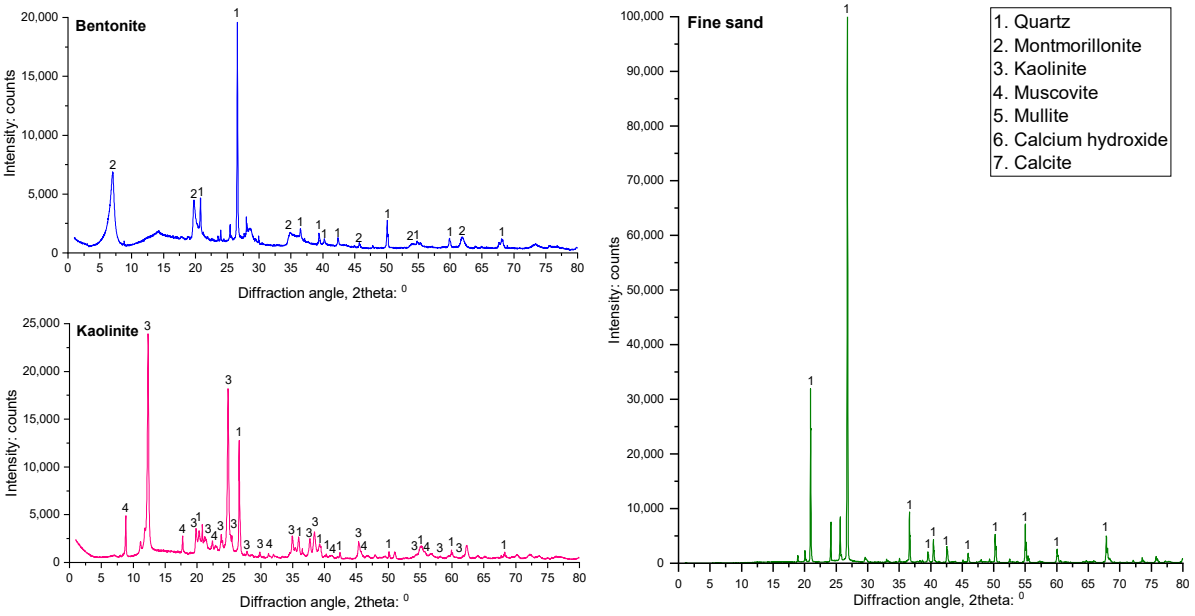


*Figure 3.3 XRD analysis on components of studied soil*

The white Q38 kaolinite has a lower liquid limit (*LL*) and linear shrinkage (*LS*) than the dark grey bentonite (50.5% as against to 340% in *LL*, and 9% compared to 35% in *LS*, respectively). Fine sand has grain diameters from 0.075 to 1.18 mm, which has the 60% passing grain diameter ($D_{60}$) of 0.35 mm, $D_{30}$ of 0.24 mm, and $D_{10}$ of 0.17 mm (see Figure 3.4). The sand is named as poorly graded sand (SP) with $C_u$=2.05 and $C_c$=0.96. The grain size distribution curves of the studied soil and fine sand are shown in Figure 3.4.

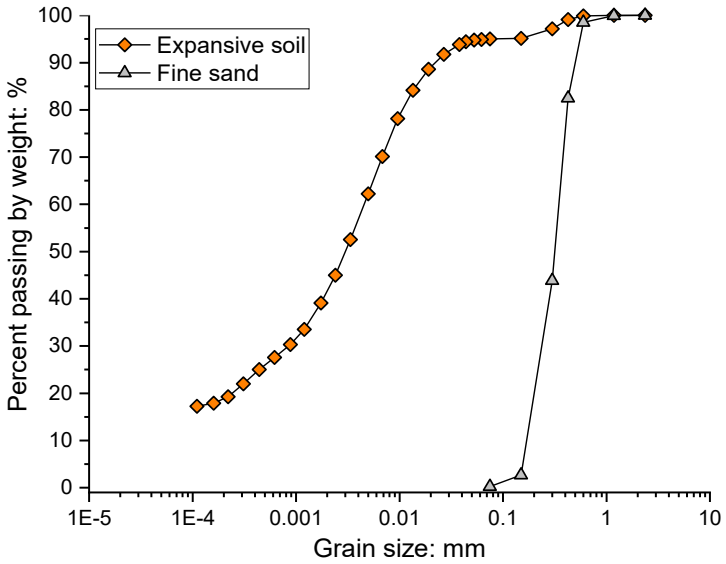


*Figure 3.4 Particle distribution curve of studied soil and fine sand*

When combing all three components, preliminary linear shrinkage tests were performed with bentonite content varying from 0% to 40%, replaced by the kaolinite content while sand content is kept constant at 5% in total dry mass. The tests were conducted using three shrinkage moulds at each percentage, adhering to AS standard (AS 1289.3.4.1, 2008). As shown in Figure 3.5, over 30% in bentonite content, *LS* of soil levelled off around 21% while *LL* increased linearly with bentonite percentage. In this study, soil with bentonite of 30% was used while sand content was 5%, resulting in 65% in kaolinite amount by the total dry mass.

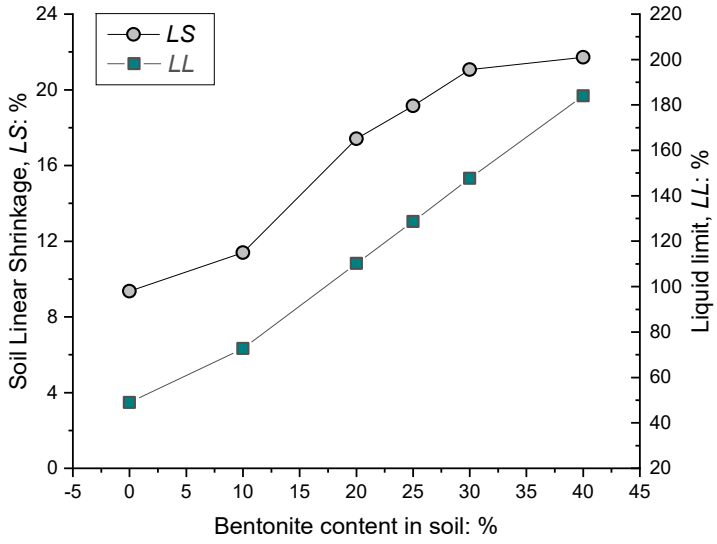


*Figure 3.5 Linear shrinkage of studied soil with 5% sand and various bentonite-kaolinite content*

### 3.2.2 Hydrated lime (L)

Hydrated lime used in this study is a commercial product, manufactured and supplied by Cement Australia, Adelaide, Australia, with a specific gravity ($G_s$) of 2.5. The lime contains 75-80% calcium hydroxide or $Ca(OH)_2$ and 7% silica $SiO_2$ in terms of dry weight. The XRD analysis shows that hydrated lime mainly contains calcium hydroxide with an amount of calcite or calcium carbonate with the formula of $CaCO_3$ (see Figure 3.6). The chemical composition of employed lime, shown in Table 3.1, is provided by the manufacturer. The lime powder was kept in tight bags to avoid its contact with ambient humidity.

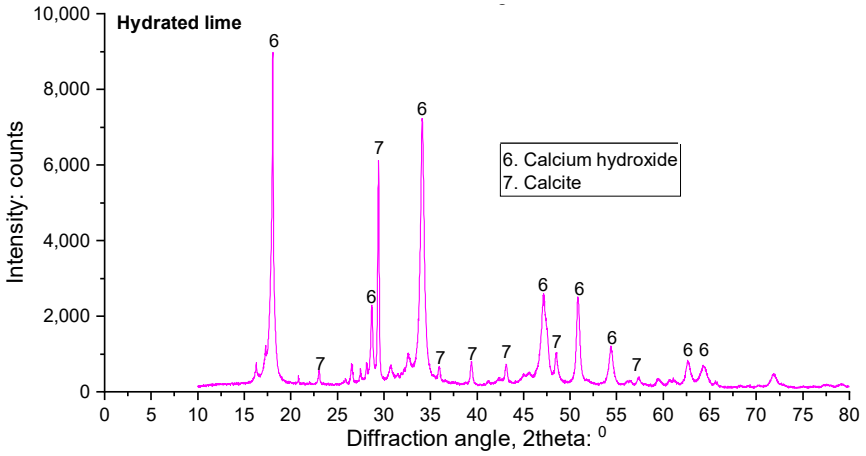


*Figure 3.6 XRD analysis on studied hydrated lime*

*Table 3.1 Chemical composition of hydrated lime (Adelaide Brighton Cement Ltd)*

| Composition of Oxide | Proportion (%) |
|---|---|
| CaO | 72 |
| SiO2 | 1.8 |
| MgO | 1 |
| $Fe_2O_3$ | 0.6 |
| $Al_2O_3$ | 0.5 |
| $CO_2$ | 2.5 |
| Loss in Ignition | 24 |

### 3.2.3 Bottom ash (BA)

Bottom ash behaves as a coarse material with zero shrinkage. Bottom ash in this study was collected from Eraring Power Station, New South Wales, Australia. The ash is the class-F fly ash, which has a grey colour and low content of calcium oxide. When collected from the station, the natural moisture content of ash has been 25% with a specific gravity ($G_s$) of 2.0. Through sieving analysis, the ash is classified as poorly graded sand (SP) with $C_u$=24 and $C_c$=0.38. However, the bottom ash was firstly air-dried for sample preparation, followed by drying in the oven at 105 $^{\circ}$C, and then the dry ash was sieved on 2.36 mm. The grain size distribution of the bottom ash used in this study is shown in Figure 3.7, compared to expansive soil. With this selection, the ash is

classified as well-graded sand ($C_u$=6 and $C_c$=1). Composition analyses from the X-ray diffraction (XRD) test show that the ash mainly contains amorphous silicate and minor calcium-related compounds, which is the reason why this ash is classified as class-F fly ash, as specified in Figure 3.8.

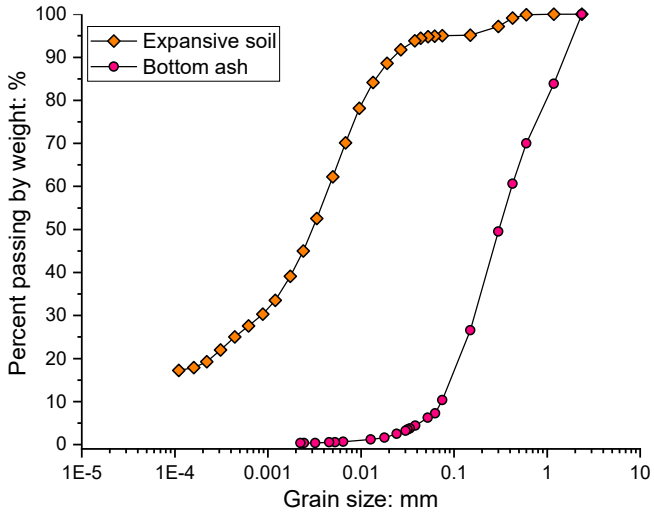


*Figure 3.7. Particle distribution of studied soil and bottom ash*

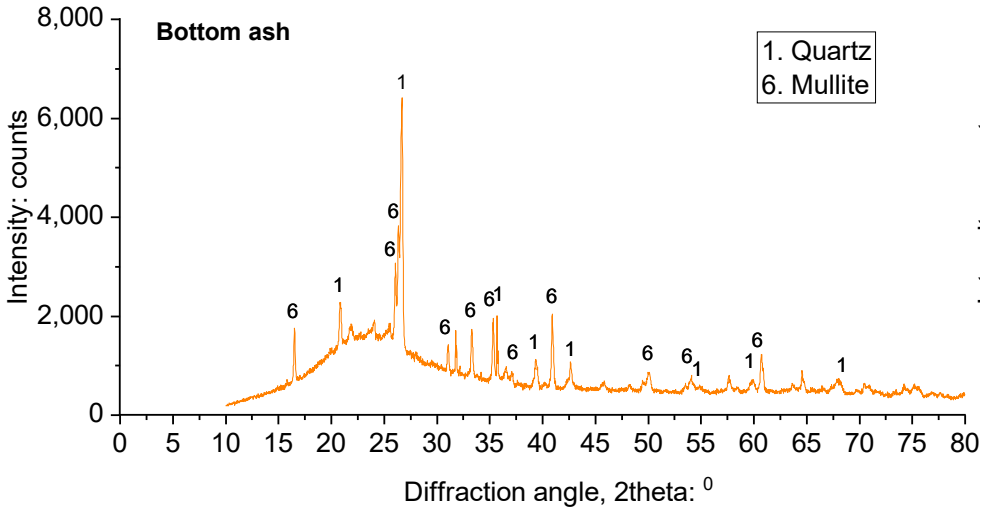


*Figure 3.8 XRD analysis on bottom ash*

Figure 3.9 presents some photos obtained by microscopic imaging and Scanning Electron Microscopy (SEM). In this figure, mullite mineral mainly distributes on thin-shell-structured spheres (Figure 3.9a-d), with a few holes on the surface and cheese-like sections (Figure 3.9d). This indicates the micro-porous structure of bottom ash, contributing to the extreme porosity of the ash material. Meanwhile, amorphous silica presents in the form of porous granular, referred by red asterisks. Both kinds of particles show the micro-porous structure of bottom ash, contributing to its high porosity (see Figure 3.9c-d).

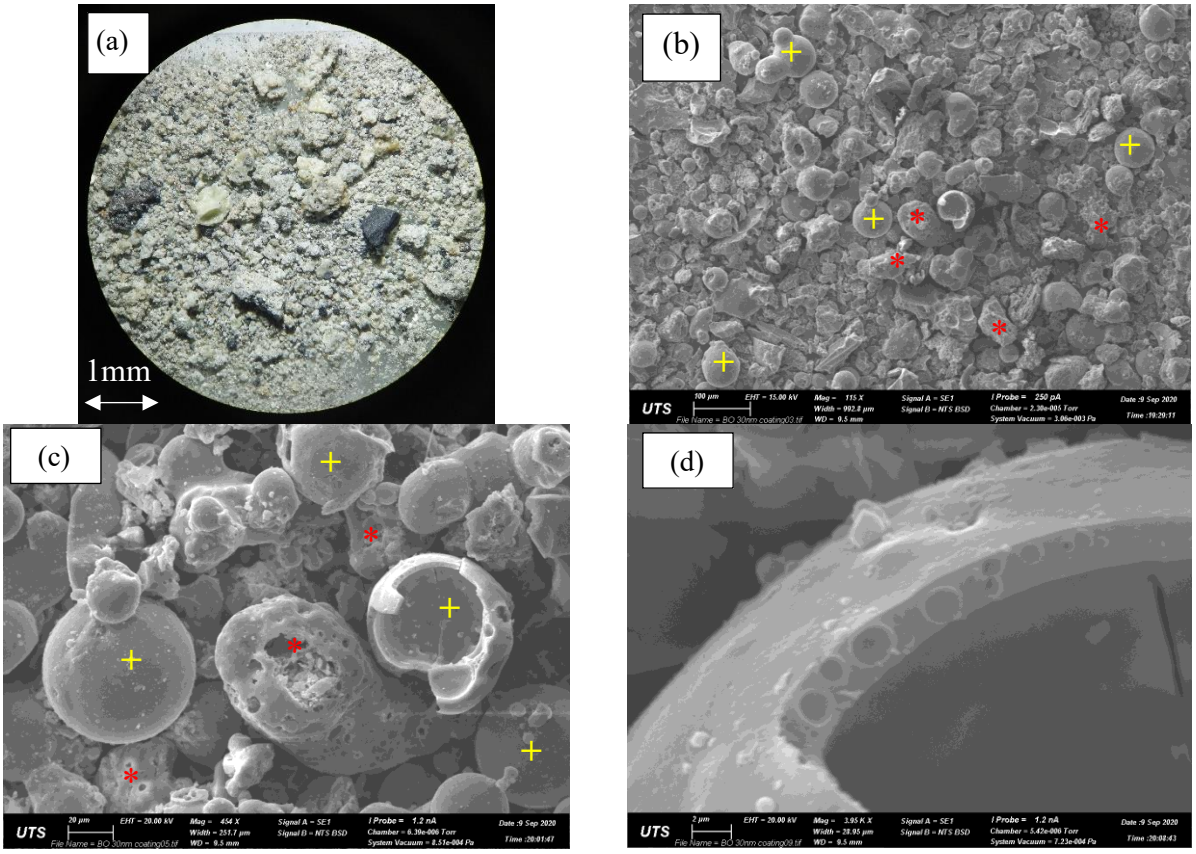


*Figure 3.9 images of bottom ash in: (a) a microscopic colour image, (b) the width of 993 µm, (c) the width of 252 µm (granular and spherical particles are marked by red asterisks and yellow crosses, respectively), and (d) a width of 29 µm to a broken bottom ash*

### 3.2.4 Bagasse ash (BA)

Bagasse ash is a silicate material, which was collected from ISIS Central Sugar Mill in the Bundaberg, Queensland, Australia. The material is usually in the form of black powder and a by-product from the burning process of sugarcane bagasse in the furnaces of boilers to generate steam for electricity production in sugarcane mill factories located in the regions of Australia. Collected from field site, the ash was air-dried in an oven at 110°C before sieving on 3 sizes of 425, 150 and 75 µm. According to the sieving analysis, the employed natural bagasse ash had 47.6% clay content (see Figure 3.10). Furthermore, sieving ash under the size of 425 µm does not change its distribution curve significantly, compared to curves of 150 µm and 75 µm. In all particle size distribution curves of ash, the proportion of ultra-fine ash (10 µm) occupies a small amount (about 3% passing), indicating the small fineness of three studied ashes.

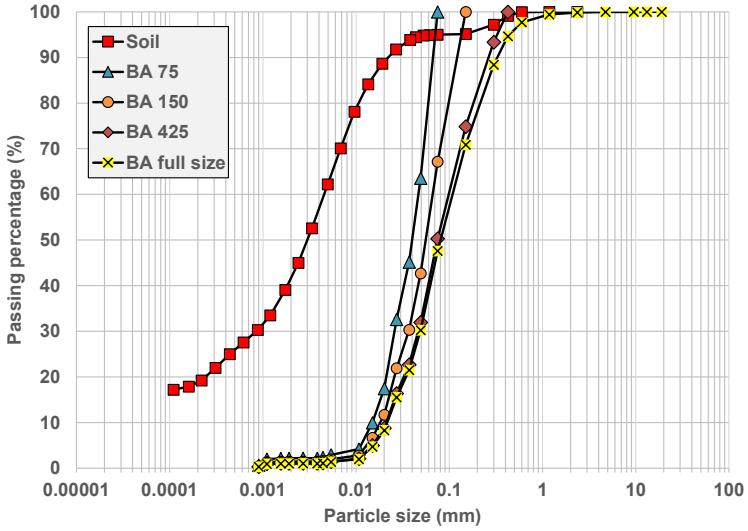


*Figure 3.10 Particle size distribution curves of soil and bagasse ash in different sizes (75, 150, 425 µm and full size)*

When physical property based on fineness among ashes is approximate, chemical analysis becomes crucial to evaluate their influence on pozzolanic interaction with soil and lime. Microscopical images of bagasse ash in three different sizes are shown in Figure 3.11. As can be seen in this figure, in the maximum size of 425 µm, bagasse ash partly contains large white granular particles of fine sand, indicating the contamination of white quartz. Being smaller in diameter, the ash becomes darker with a few big white dots. Figure 3.12 presents the images of bagasse ash generated from the Scanning Electron Microscopic (SEM) tests. As can be observed in Figure 3.12, the shape of bagasse ash varies from fibrous to porous debris, but mainly bagasse fibre-shaped ash can be observed on any occasion. This indicates the presence of fibrous or cellular over the granular or coarse grains. The dominance of cellular particles indicates the darker colour of finer bagasse ashes (i.e., 150 and 75 µm), as shown in Figure 3.11. The presence of cellular particles is also associated with the same intensity of amorphous silica in bagasse ash under the diameter of 150 and 75 µm from XRD results (see Figure 3.13).

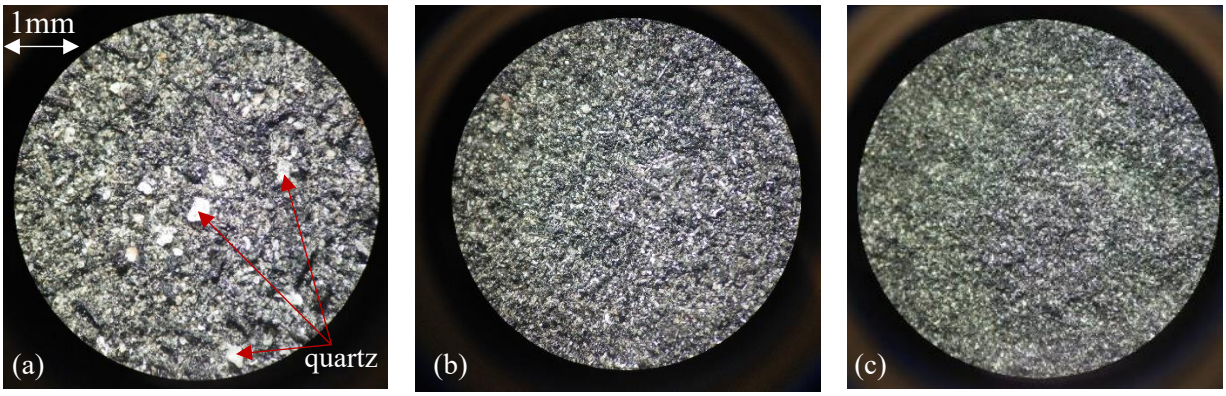


*Figure 3.11 Colour microscopic images of bagasse ash with the maximum size of (a) 425 µm, (b) 150 µm, and (c) 75 µm*

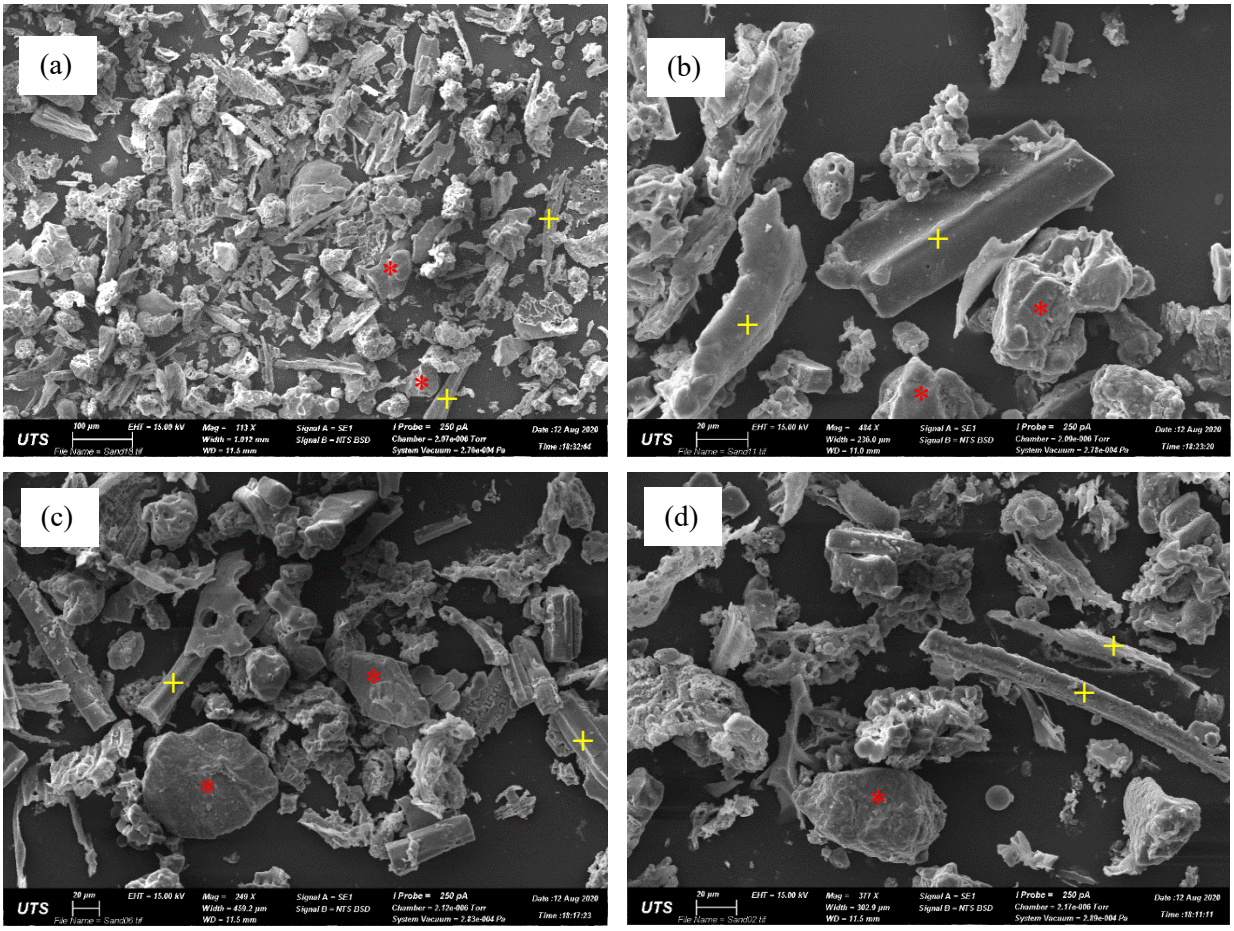


*Figure 3.12 SEM images on 425-µm bagasse ash in magnification of (a) 113x, (b) 484x; and bagasse ash in the size of (c) 150 µm and (d) 75 µm (Quartz and cellular particles are marked by red asterisks and yellow crosses, respectively)*

The studied bagasse ash has contamination of sand or soil from sugarcane root, causing a high concentration of quartz. The analysis from the XRD test confirms this notion. As shown in Figure 3.13, the intensity of quartz in bagasse ash in 425 µm obtains a peak of 70,000 counts, indicating a majority of quartz minerals as silicate oxide in the material. Figure 3.13 also shows the difference in intensity of amorphous and crystalline silica between studied ashes. Generally, X-ray diffraction (XRD) results illustrate that ash composition contains plenty of quartz. Not observing critobalite was an indication that the raw bagasse ash was burnt at the medium temperature under 800°C. In comparison between bagasse ash over and under 425 µm, the larger ash consists of a significant content of graphite or carbon while the smaller one has a small amount of unburnt carbon particles (refer to Figure 6.2). This indicates that sieving bagasse ash through the size of 425 µm effectively removes a majority of carbon contamination. However, the highest intensity of quartz in bagasse ash 425 µm (about 70,000 counts) indicates high contamination of crystalline sand in comparison to others with smaller sizes (i.e., 150 µm and 75 µm). Sieving also increases the content of amorphous silica in these fine bagasse ashes with higher humps of intensity from 20° to 30° in

diffraction angle (see bottom plot in Figure 3.13). This mineral also determines the black colour of studied ash as shown in Figure 3.11.

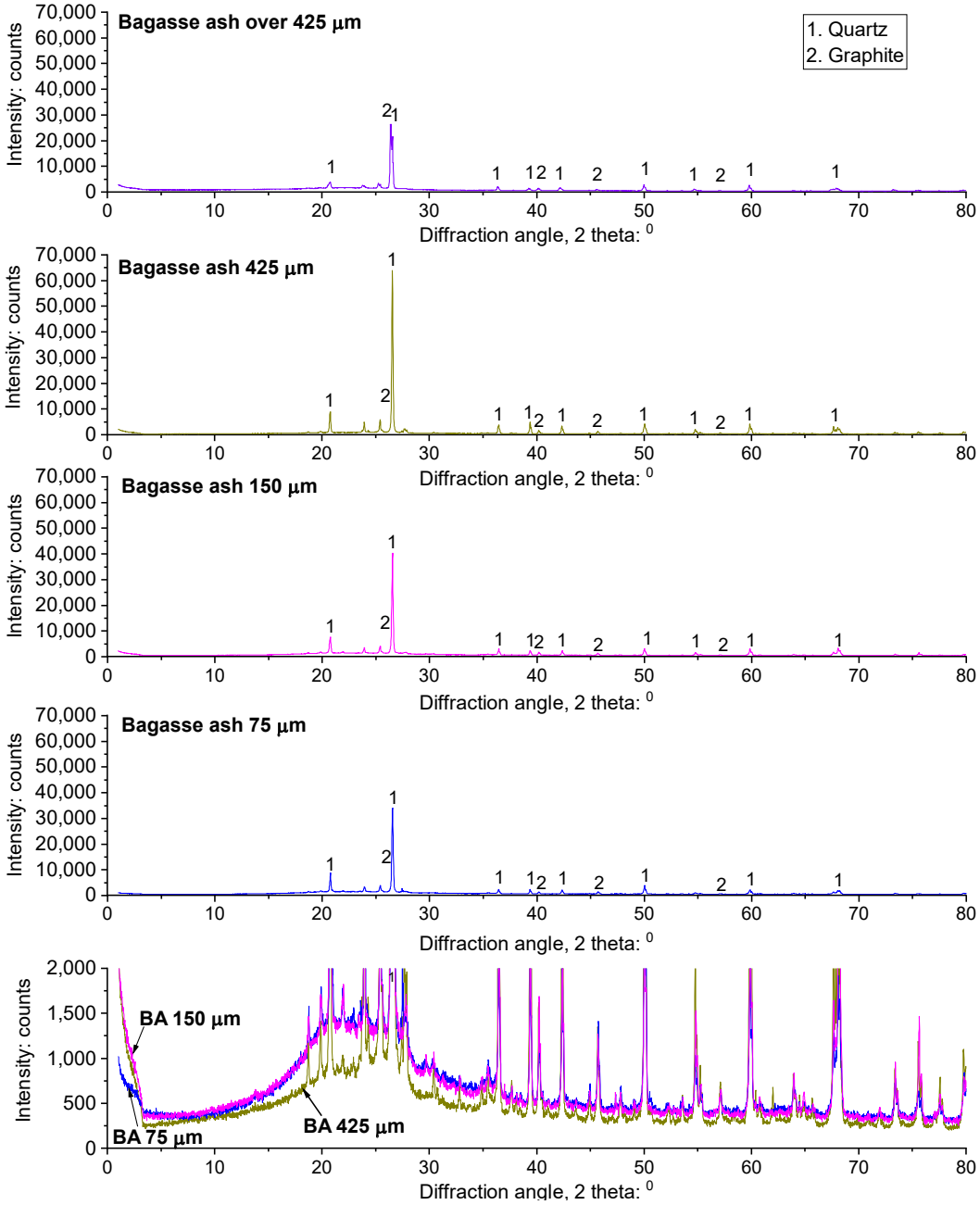


*Figure 3.13 X-ray diffraction results on bagasse ash in the size of 425, 150 and 75 µm*

### 3.2.5 Comparison between bottom ash and bagasse ash for their combination in soils

#### *3.2.5.1 Density and particle distribution*

When combining bottom ash and bagasse ash, there are changes in their characteristics. In terms of index properties, the specific gravity and distribution curve are first considered. While specific gravity ($G_s$) of bottom ash is close to 2.0, that of bagasse ash is about 2.3. Since $G_s$ of soil is about

2.7, the mix of bottom ash and bagasse ash has a bulk weight much smaller than ash-treated soil. Due to the high porosity of bottom ash, the unit weight of the bottom-bagasse ash mix is only about 0.90 Mg/m$^3$, whereas the ash-treated soil is about 1.25 Mg/m$^3$. This is a reduction of 28% in unit weight. The percentage is even higher when the ash mix is compared with earth or sand fill, 0.90 Mg/m$^3$ against roughly 2.00 Mg/m$^3$, equivalent to 55% in reducing unit weight. Low weight means the combined ashes are useful as lightweight fill materials for embankments and pavement on soft ground. Hence, the settlement of construction is reasonably reduced since the applied load of fill material is minimised. However, the combined materials of the two ashes have limitations in strength because of the porous structure of bottom ash and the uneven fibrous shape of bagasse ash.

Adding bagasse ash into bottom ash can alter their distribution of ash size in various ratios of mixing. Since the bottom ash is classified as poorly graded sand, the small bagasse ash added to this ash can improve the bottom distribution curve and turn it into a well-graded one. In detail, the bottom ash passing the sieve of 2.36 mm has $C_u$=5.67 and $C_c$=0.91. According to USCS classification of soil, bottom ash is poorly graded sand with 10% clay. Bagasse ash, on the other hand, is the silty clayey sand with the clay content of 47.6%, as indicated in Figure 3.14.

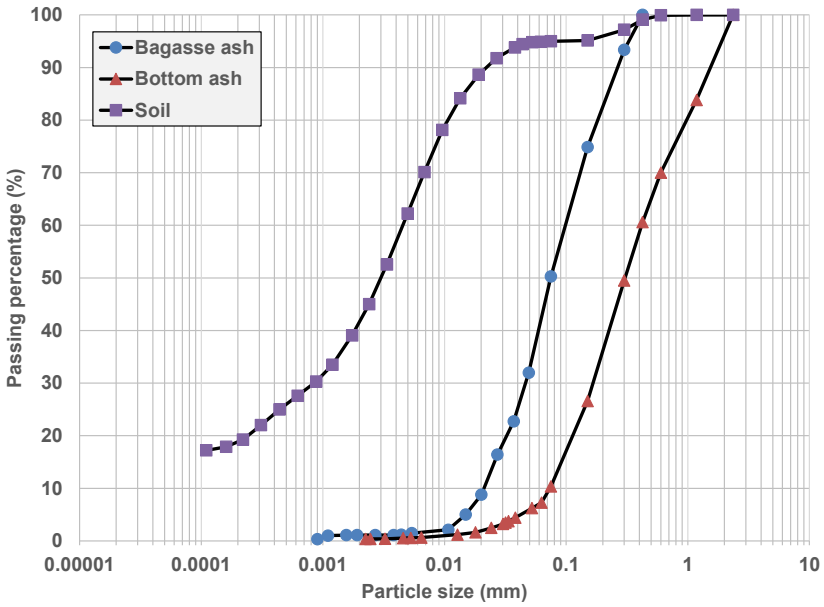


*Figure 3.14 Particle distribution curve of soil, bottom ash and 425-µm-sized bagasse ash*

Due to the lack of clay-sized particles in the distribution curve of bottom ash, the inclusion of bagasse ash will contribute to this range of grain, shifting the curve to the left to become a well-

graded one. From the previous chapter, the study on bagasse ash separates its property into three passing sizes, namely 425, 150 and 75 µm. As illustrated in Figure 3.14, the bottom ash in 425 µm occupies 60% passing while the 150-µm grain accounts for 26%, and 10% for 75 mm. Since $C_u$ and $C_c$ of bottom ash is on the boundary of poorly and well-graded sand, 6 and 1, respectively, the contribution of bagasse ash from 60% passing (equivalent to 425 µm) will probably turn the curve into the zone of well-graded grain. The bagasse ash passing of 425 µm is preferably to be utilised in combination with bottom ash because of a large range of effect on distribution curve, compared to other ash with small grain size. In the comparison of $D_{50}$, the bagasse ash with $D_{max}$ of 425 µm has $D_{50}$ of 75 µm, referring to its balance of clay- and fine-sand-sized ash in particle distribution. Meanwhile, the bagasse ashes with smaller particle sizes (i.e., 150 and 75 µm) result in $D_{50}$ less than 75 µm, indicating a majority of clay particles in the ashes (refer to Figure 3.14). Consequently, the inclusion of these clayey ashes to bottom ash will tend to turn their mix with bottom ash into clay's properties, such as higher liquid limit and more compressibility. To keep coarse-to-fine parts from bagasse ash, including its sand properties, it is recommended to use the bagasse ash with the size of 425 µm when combining it with bottom ash.

#### *3.2.5.2 Micro-structural comparison between bottom and bagasse ash*

For micro-structural analysis, Scanning Electron Microscopy (SEM) and X-ray Diffraction tests were conducted on bottom ash and bagasse ash. While SEM results show images of ashes in appearance from few micro- to nanometre, X-ray diffraction gives their composition of chemicals. Figures 3.8 and 3.13 illustrate the X-ray diffraction results of the two ashes. By using the software Profex, composition in multiple phases was analysed to reveal the proportions of chemicals or crystals in studied materials.

It is clear from Figures 3.8 and 3.13 that both ashes contain quartz with the chemical formula of $SiO_2$. However, bottom ash has a second majority of mullite as a silicate mineral of $Al_2O_3$ and $SiO_2$, whereas bagasse ash has quartz as its main chemical. Due to the colour of these minerals, bottom ash has a dark grey appearance, while bagasse ash is black from silica-rich compounds with marginal carbon contamination in its composition (refer to Figures 3.10a and 3.12).

In the colourful microscopic image of bottom and bagasse ash, the fine bottom ash appears in black dots while the bigger bottom ashes have a grey colour (see Figure 3.9a). However, bagasse ash appears in black colour with a majority of fibrous grains as graphite particles, as shown in Figure 3.11. There are also bright white grains in bagasse ash, indicating the presence of crystalline silica or fine sand in this ash (see Figure 3.11a). Due to the supplementation of silica, the

combination of bottom ash and bagasse ash will increase reasonably the amount of quartz for soil stabilisation. Especially, mullite from bottom ash plays an important role in catalyse pozzolanic reactions with hydrated lime if the binder is added in ash-treated soil blends.

SEM images also show the shapes of bottom and bagasse ash in Figures 3.9 and 3.12. While the bottom ash is in the form of spheres, bagasse ash is in variable forms, including fibrous debris and tiny fragments. When the size of bottom ash is less than 75 µm, the ash appears in a shape of sphere dominantly, indicating the existence of fly ash in bottom ash. Energy Dispersive X-ray Spectroscopy (EDX) analysis on the surface of the ash sphere reveals the presence of mullite ($Al_2O_3$ and $SiO_2$) with the mild veins, as an initial form of Calcium Silicate Aluminium Hydrate (CASH) with low calcium, expressed in Figure 3.15a. Meanwhile, bagasse ash is a silica-related material containing a majority of $SiO_2$, indicated in Figure 3.15b. The fibrous ash also contains a small amount of calcium and sulphate, predicting the potential of ettringite production when the ash contacts calcium hydroxide from hydrated lime.

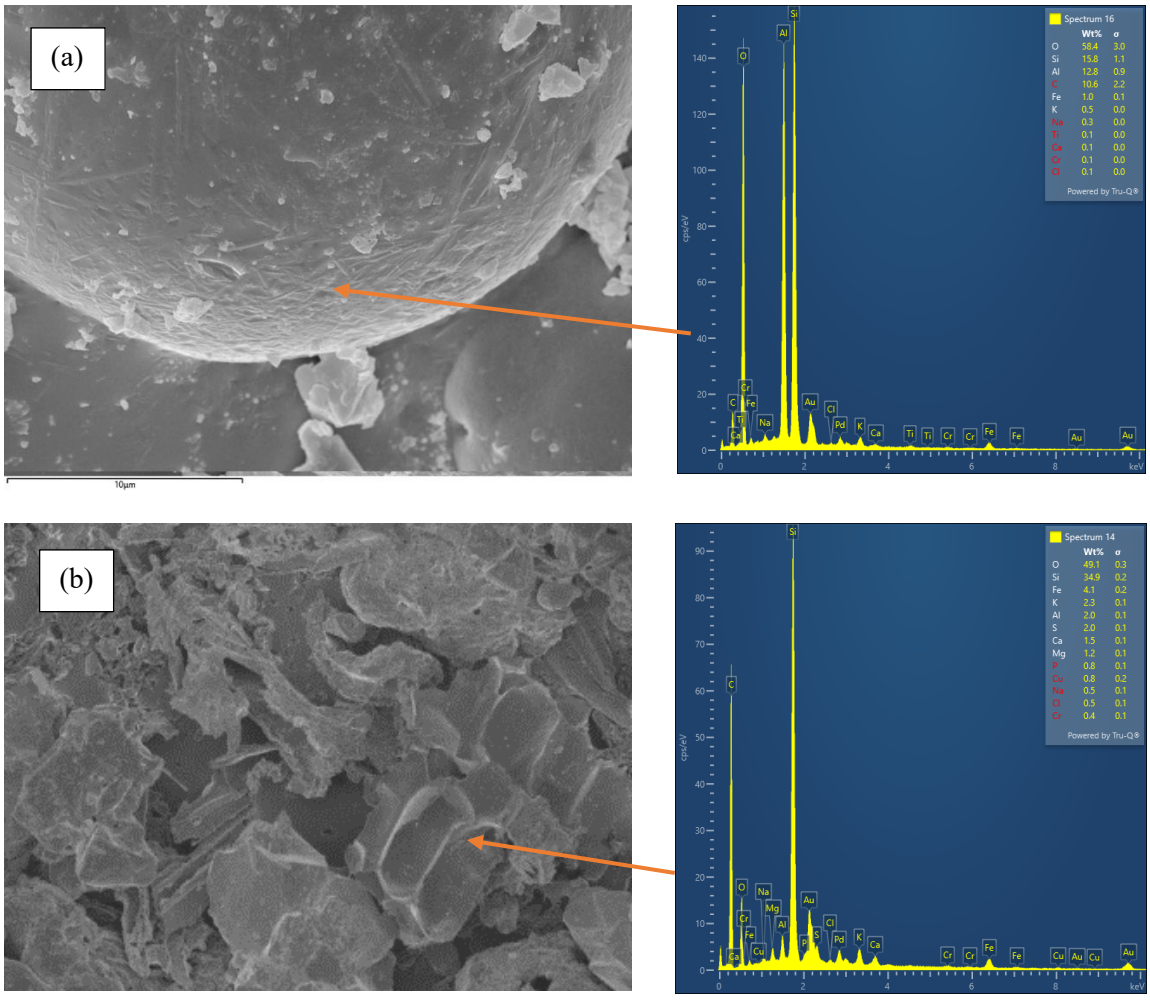


*Figure 3.15 EDX analysis on (a) bottom ash and (b) bagasse ash*

### 3.2.6 Summary

Table 3.2 summarises the main geotechnical characteristics of soil components and target ashes, including bottom ash and bagasse ash. The table includes moisture, Atterberg limits, linear shrinkage, free swelling ratio, specific gravity, compaction parameters and USCS classification. For the free swelling ratio, oedometer rings were used to confine samples in a diameter of 50 mm and a height of 15 mm. A seating pressure of 6 kPa was applied, and the swelling rate was monitored throughout days until the displacement plateaued.

*Table 3.2. Geotechnical properties of the studied expansive soil, bottom ash and bagasse ash*

| Properties | Kaolinite | Bentonite | Sand | Soil (KBS) | Bottom ash | Bagasse ash |
|---|---|---|---|---|---|---|
| Ambient moisture: % | 2 | 11 | 0.1 | 4 | - | - |
| Liquid limit, *LL*: % | 50.5 | 340 | - | 155 | - | - |
| Plastic limit, *PL*: % | 29 | 50 | - | 31 | - | - |
| Plasticity index, $I_p$: % | 21.5 | 290 | - | 124 | - | - |
| Linear shrinkage, *LS*: % | 9 | 35 | 0 | 21.23 | 0 | 0 |
| Free swelling ratio: % | - | - | 0 | 60 | 0 | 0 |
| Specific gravity, $G_S$ | 2.64 | 2.70 | 2.65 | 2.69 | 2.0 | 2.5 |
| Optimum moisture content, *OMC*: % | - | - | - | 28.80 | 17.00 | - |
| Maximum dry density, *MDD*: Mg/m$^3$ | - | - | - | 1.32 | 0.95 | - |
| Soil classification (USCS symbol) | CL | CH | SP | CH | SW | SC |

## 3.3 Sample preparation and mixing designations

### 3.3.1 Introduction

Sample preparation is a critical task in experimental investigations since it significantly affects the validity of test results and the consistency of findings. One of the main factors, which influence the quality of mixed samples, is the maximum diameter of particles. This is due to the fact that the coarser and finer particle diameters cause smaller and larger specific surface areas, respectively. In pozzolanic reactions of binders and soils, this surface parameter determines the probability of contact between them, thus directly impacting the bonding effects from the reactivity. In this study, the maximum size of materials decreases from soil to bottom ash and bagasse ash, which is depicted in Figure 3.16.

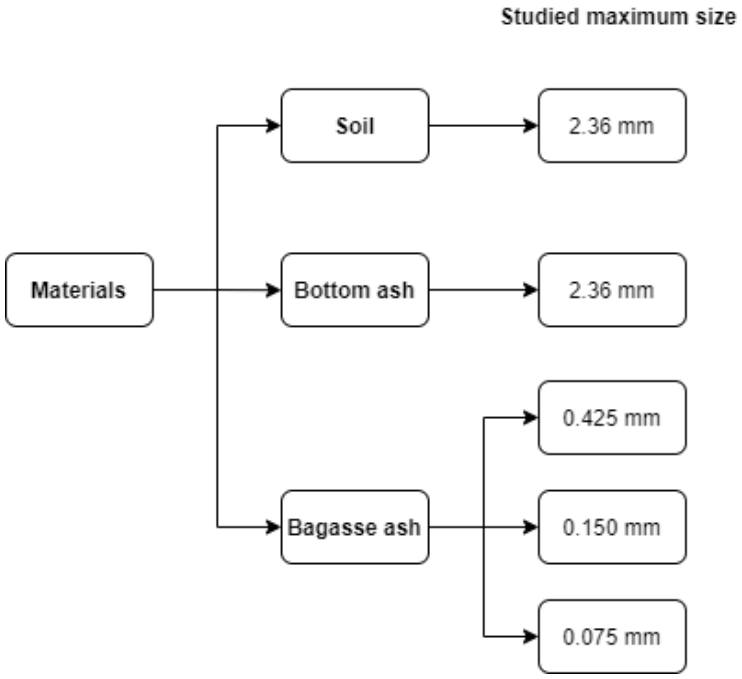


*Figure 3.16 Maximum sizes of studied materials*

### 3.3.2 Materials and soil sample preparation

#### *3.3.2.1 Artificial soils (KBS)*

The expansive soil in this study was made with the combination of kaolinite, bentonite and fine sand in the ratio of 65%, 30% and 5% based on dry mass, respectively. When mixing the dry components at these percentages, the ambient moisture content of the soil is around 4%. The soil was then spread in each layer interleaved with each layer of water, as illustrated in Figure 3.17. A tank of pressurised water was prepared with pre-determined volume to obtain the final water content of soil being around 20%. The soil container was then wrapped in 3 days for moisture homogenisation before the soil was sieved through diameters of 2.36 mm and finally stored in suction bags to prevent water loss (see Figure 3.18).

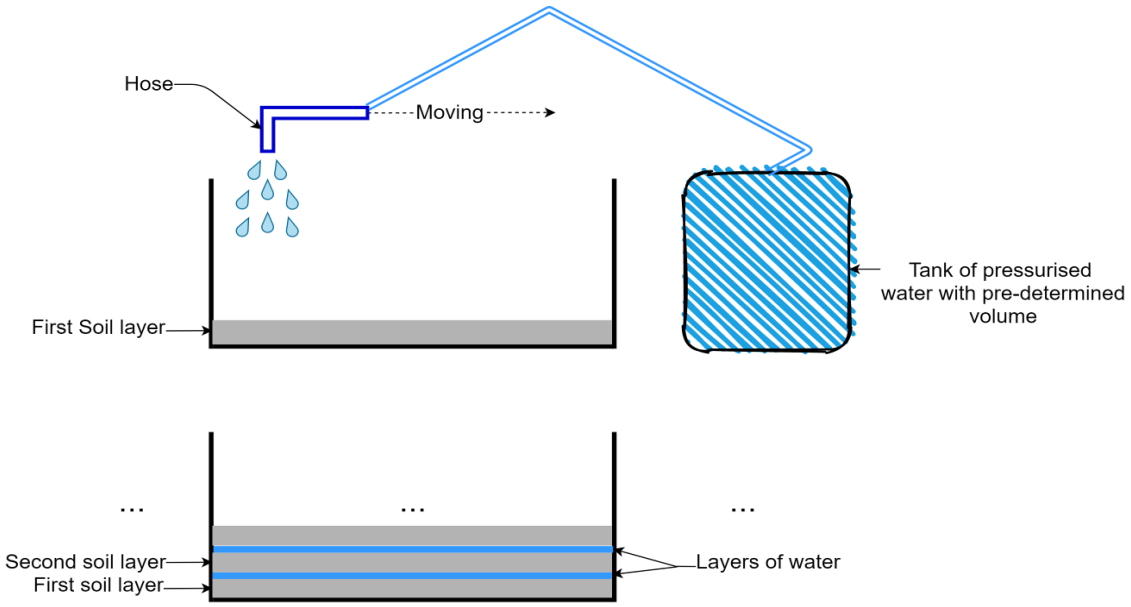


*Figure 3.17 Schematic diagram for soil preparation*

*Figure 3.18 Soil sample preparation*

### *3.3.2.2 Bottom ash and bagasse ash*

Bottom ash in the study was first dried in an oven at 105°C, then spread on the floor to select the representative samples, presented in Figure 3.19. The quartering method was adopted in the selection, adhering to (ASTM-C702, 2018). Selective bottom ash was then sieved through the diameter of 2.36 mm for required tests, such as UCS or CBR experiments. For specific tests (e.g., Atterberg limits or linear shrinkage tests), bottom ash was passed through the sieve of 0.425 mm. For bagasse ash, the sample was sieved through the diameter of 0.425 mm and wrapped in a tray to avoid moisture absorption of fine ash, as demonstrated in Figure 3.20.

*Figure 3.19 Quartering method for selecting representative samples of bottom ash*

*Figure 3.20 Sample preparation for bagasse ash*

### *3.3.2.3 Sample preparation*

**Dynamically compacted samples (for UCS and CBR tests)**

Sample preparation for UCS tests was conducted following the Australian standard AS 5101.4 (2008). The UCS samples were dynamically compacted in three layers in a cylindrical mould, with a height of 100 mm and a diameter of 50 mm. Figure 3.21 shows the equipment needed for constituting UCS samples. In the process, the energy hammer hit a piston to compact soil particles in a mould with a proper settlement, which could be checked by a settlement stick to achieve the desired density and moisture content. A scratching tool was used to scratch the surfaces between two consecutive layers. For the last layer, a connecting ring connected the bottom mould to the top one, and a 100 mm × 50 mm piston was assembled to the top mould to finalise the compaction of the last layer. A rectifying hammer was used lastly to flat the surface of the sample at both sides of the mould. Samples were cured for a few hours before extruding from the mould by an extruder. Similar procedures were applied for the preparation of CBR samples, but the main difference was

related to the compaction of soil in five layers in the CBR mould. It can be noted that spacers replaced settlement stick with a pre-determined thickness (refer to Figure 3.22).

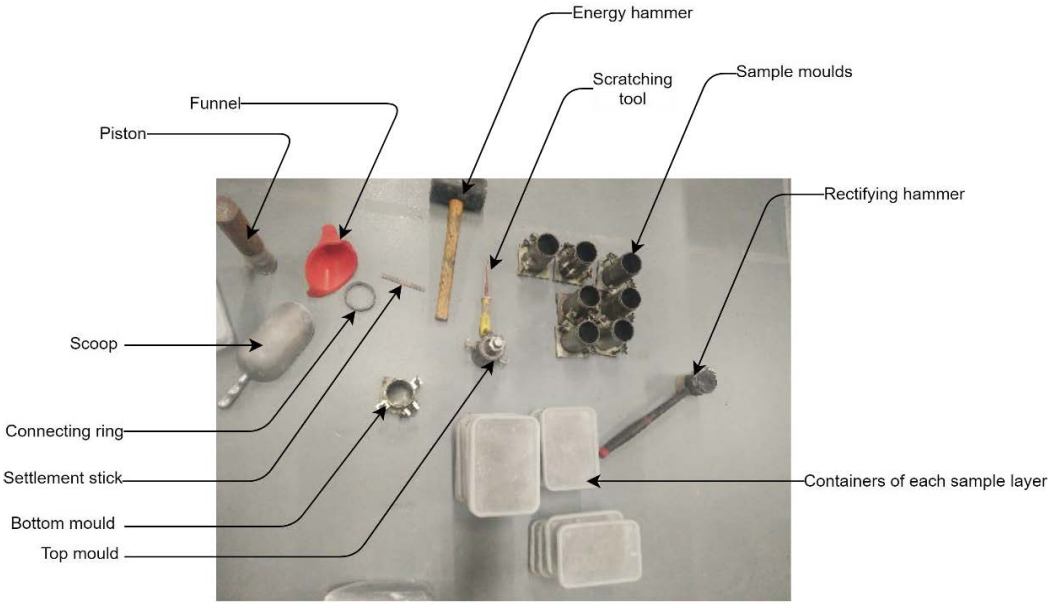


*Figure 3.21 Preparation for making UCS samples*

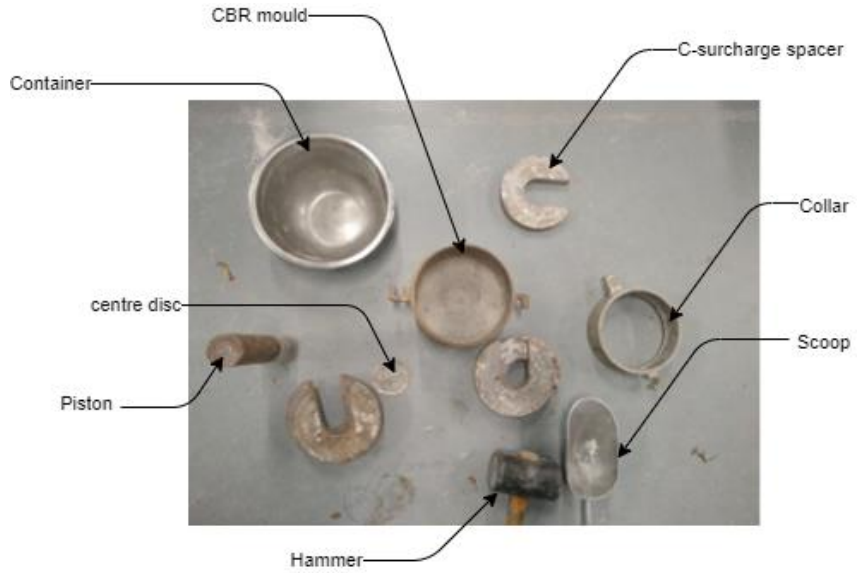


*Figure 3.22 Preparation for making CBR samples*

## Statically compacted samples

A statically compacted method is specially designed for high-quality samples that require accurate test measurements, such as swell-consolidation, bender element, suction and triaxial tests. In the static compaction method, samples were compacted in each layer not larger than 20mm. Two odometer rings were assembled together by a steel hose clamp for swelling-consolidation samples, as shown in Figure 3.23a. While the bottom ring was the one put in the oedometer cell, the top ring was used to guild a piston penetrating into the bottom ring. The right penetration was

controlled by a loading machine (i.e., Tritech 50 kN) with an automatic stopping control once a designed settlement was obtained. The velocity of static compaction was selected at 1 mm/min, resulting from trials with different rates of penetration for the same soil samples, as depicted in Figure 3.23b.

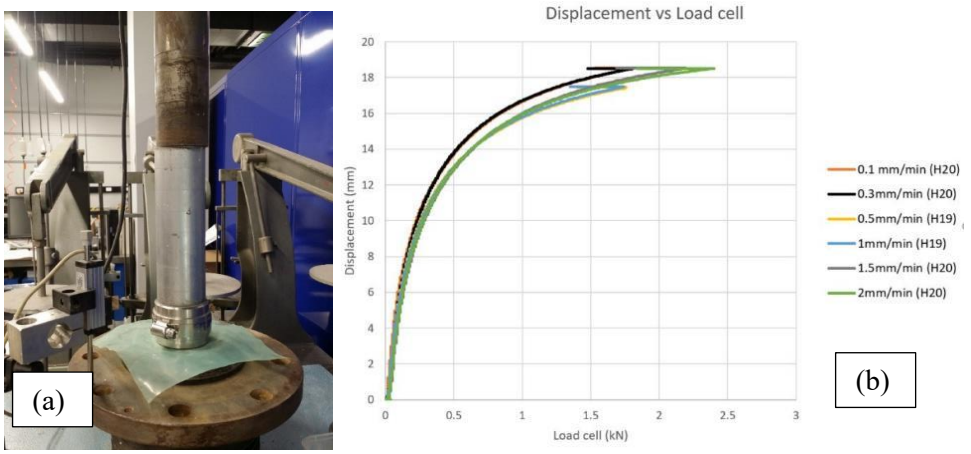


*Figure 3.23 (a) Static compaction for swelling-consolidation samples and (b) determination of static compaction velocity*

As for bender element and triaxial samples, they were compacted in the same mould of UCS samples (100 mm × 50 mm). However, in static compaction, there were five layers with a thickness of 20 mm for each layer. For the top or fifth layer, the double oedometer rings (see Figure 3.23) were assembled to the mould by a connecting ring (refer to Figure 3.21) to leave room for loose particles before compacted, as indicated in Figure 3.24. At the end of each-layer compaction, the load cell was allowed to go down and level off before the next sample layer was poured into the mould. Notably, the samples for triaxial shearing tests were compacted at the maximum dry density (*MDD*), but a determined amount of water was added to the mould to increase moisture higher than optimal moisture content (*OMC*). By following this approach, the high saturation level (*S*r) of compacted triaxial samples was obtained at about 0.9.


*Figure 3.24 Snapshots of sample preparation for suction, bender element and triaxial tests*

### *3.3.2.4 Preparation of treated samples*

**Moisturising treated samples**

The treated soil samples, including hydrated lime or ash, were humidified to the target water content in the same way for constituted soil samples (refer to Figure 3.25). However, the moisturising process was conducted after thoroughly mixing the binders and soil samples in the desirable maximum diameter (e.g., 2.36 mm). The wet samples were kept in at least 1 hour for mellowing (see Figure 3.25).

*Figure 3.25 Moisturisation for treated soil samples*

**Covering samples by paraffin**

According to Germaine and Germaine (2009), when it comes to samples required for strictly avoiding water loss (e.g., field samples or bender element specimens), the waxing method is often employed. In this method, paraffin liquid was used to cover soil samples with a thin waxing layer directly. Under the heating temperature of 60°C, the soy paraffin was smelt, and it was quickly solidified when cooling down. The cover material should be plastic so that the covering layer did not crack during cooling. For smoothing, vaseline cream, also known as petroleum jelly, was added to paraffin. By trials and errors, the optimum ratio of paraffin to vaseline was found to be 9 to 1 to produce plastic paraffin for covering samples. It is also noted that if some bubbles started to pop up on the cover, a brush could be used to fill the holes by aqueous paraffin (refer to Figure 3.26).

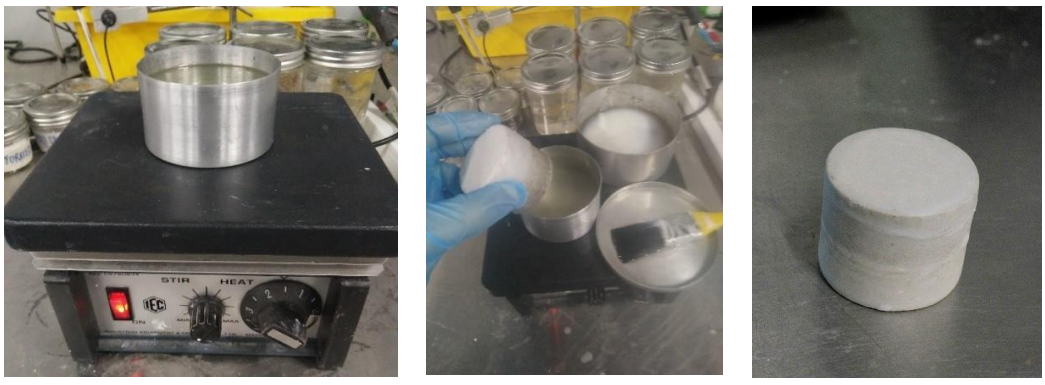


*Figure 3.26 Snapshots of waxing preparation for bender element samples*

The waxing procedure has a few modifications, if a larger sample is utilised for waxing, such as CBR one. The first step is to ensure no cover around the sample since the CBR mould surrounds its outside perimeter. Secondly, a brush was be used to spread the paraffin liquid on both ends of CBR sample. Care on the boundary between sample and steel mould should be paid to make sure no gap exists, as presented in Figure 3.27.

*Figure 3.27 Snapshots of waxing preparation for CBR samples*

**Freeze-drying preparation for SEM samples**

SEM sample preparation is generally based on the freeze-drying method, suggested by Shi et al. (1999). Recently, the method also has been also mentioned by Trzciński (2004) and Di Remigio et al. (2021). Regarding samples required for pore measurements, this method is better than the air-dried technique since the latter can cause additional cracks from shrinkage of samples in the oven. The freezing method was conducted by cooling a small soil specimen in nitrogen liquid to slow down the sample temperature to -198°C, resulting in icing all water liquid in soil voids. After freezing, the sample was put in a suction chamber to directly turn the ice into gas, known as sublimation, and without crossing the vaporisation line, as plotted in Figure 3.28. After the freezing-drying process, the sample was mounted on a disc to be prepared for sputtering with a gold-palladium layer, as shown in Figure 3.29. Coating the sample with a thin layer with a thickness of 30 nm increased the electrical conductivity of the soil surface, resulting in a high resolution of SEM images.

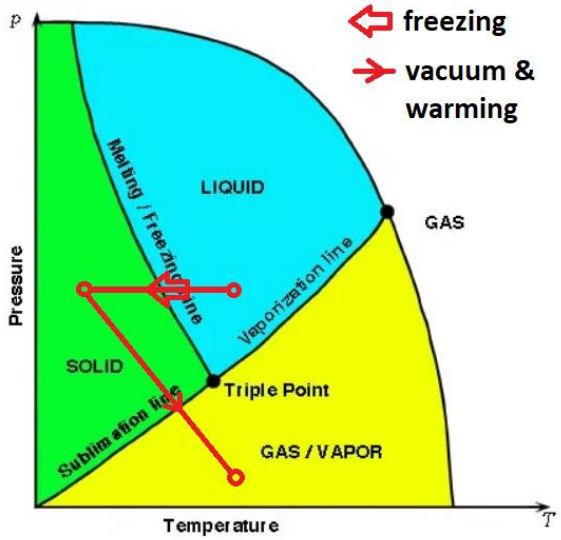


*Figure 3.28 Freezing-and-drying line on the pressure-temperature plot*

*Figure 3.29 Snapshots of SEM sample preparation*

## Storing samples

For samplers cured for a period of time, containers with water at the bottom were used to prevent samples from losing their moisture content. This created an environment of 100% humidity surrounding samples, thereby eliminating the water evaporation from samples. To check any change of water content, the weight of samples was determined before and after a period of time for storing in containers or desiccants (see Figure 3.30).


*Figure 3.30 Snapshots of storing samples in humidity containers*

### 3.4 Experimental program for testing categories

The experimental program of this study can be categorised into three main parts, electrical, physical & mechanical and micro-structural analysis test, as illustrated in Figure 3.31. Part I is allocated to electrical tests with two representatives, pH and electrical conductivity tests. After that, Part II addresses physical, index and mechanical tests. Physical tests include the specific gravity, the particle size distribution (sieving and hydrometer analysis), the Atterberg limits and compaction tests. Meanwhile, mechanical tests in this study comprise linear shrinkage, free-swelling consolidation tests, unconfined compressive strength (UCS), indirect shear strength (IDS), California bearing ratio (CBR), consolidation undrained (CU) shear triaxial, bender element, and suction tests using filter paper method. Finally, Part III covers the micro-structural analysis on samples from Part I and II, consisting of four experiments: X-ray Diffraction, microscopic imaging and Scanning Electron Microscopy (SEM) tests followed by Energy Dispersive X-ray spectroscopy (EDX) analysis.

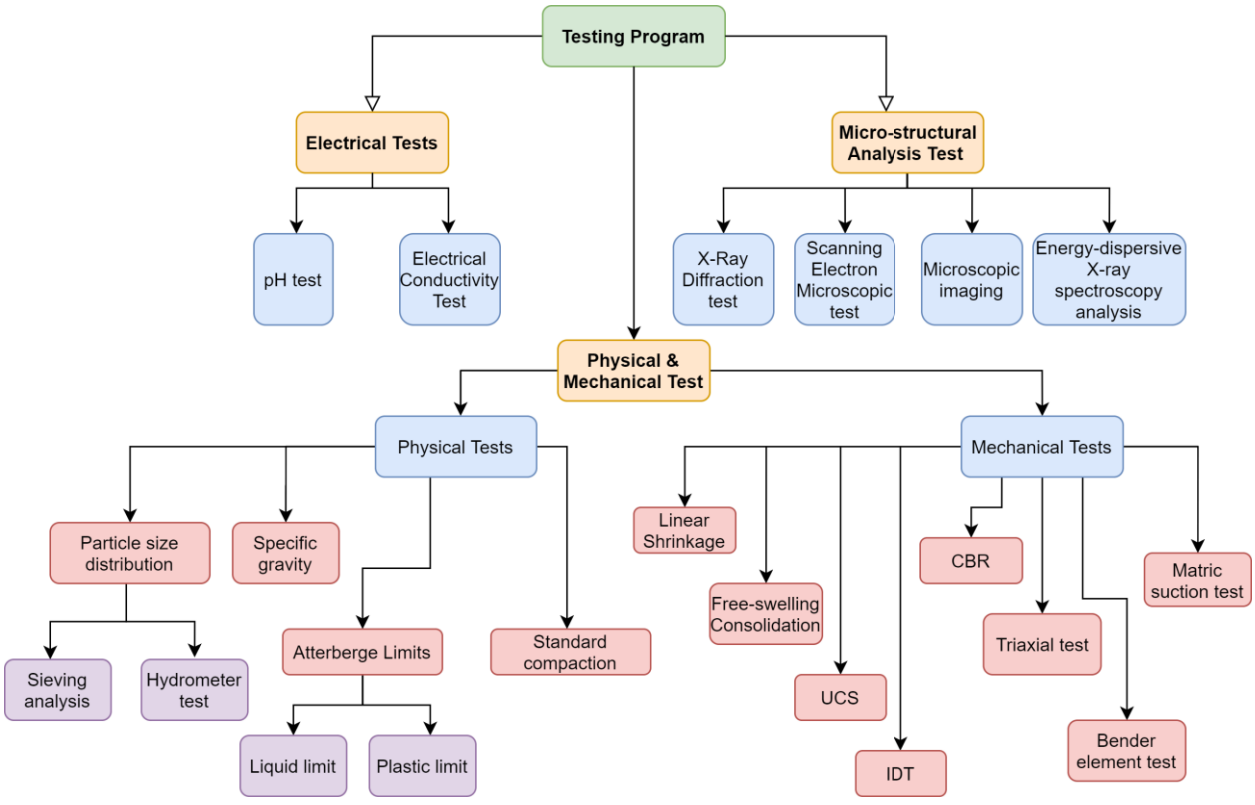


*Figure 3.31 Experimental program in the study*

In total, approximately 1,350 tests (excluding preliminary tests) were performed in this study, across 19 test types incorporating chemical, physical, mechanical and micro-structural aspects of treated and untreated materials. The number of these tests are tabulated in Table 3.3. The unconfined compressive strength tests were the type of experiments conducted with the highest

frequency (388 tests), followed by the electrical conductivity tests with 202 tests. Linear shrinkage and bender element tests also occupy a large proportion with 139 and 123 tests, respectively. The details of the experimental program in each test are shown in the next sections.

*Table 3.3. Quantity of conducted tests*

| No. | Test name | Number of tests |
|---|---|---|
| Electrical test | | |
| 1 | pH | 38 |
| 2 | Electrical conductivity | 202 |
| Physical test | | |
| 3 | Sieving | 3 |
| 4 | Hydrometer | 4 |
| 5 | Specific gravity | 4 |
| 6 | Atterberg limits | 40 |
| 7 | Standard compaction | 52 |
| Mechanical test | | |
| 8 | Linear shrinkage | 139 |
| 9 | Swelling-consolidation | 45 |
| 10 | Unconfined compressive strength | 388 |
| 11 | Indirect tensile strength | 102 |
| 12 | California bearing ratio | 57 |
| 13 | Consolidation undrained triaxial | 16 |
| 14 | Bender element | 123 |
| 15 | Filter paper | 48 |
| Micro-structural analysis test | | |
| 16 | X-ray Diffraction | 27 |
| 17 | Microscopic imaging | 7 |
| 18 | Scanning electron microscopic | 40 |
| 19 | Energy dispersive X-ray spectroscopy | 10 |
| **TOTAL** | | **1,345** |

### 3.4.1 Electrical tests

#### *3.4.1.1 pH test*

The soil pH tests were carried out in this study following the ASTM standards (ASTM-D4972, 2019). For the specific purpose to determine the soil-lime ratio for soil stabilisation, another ASTM standard for this aim has been utilised (ASTM D6276 (2019). In addition to these standards, requirements from Australian authorities for this lime demand test were also considered, namely Test method T144 introduced by the New South Wales Government (NSW Government, 2012). The pH test equipment is shown in Figure 3.32. In adaptions from all standards, lime content was varied from 2% to 7% in this study, while the applied curing time was up to 28 days, in observing the development of pozzolanic reactions (see Table 3.4).

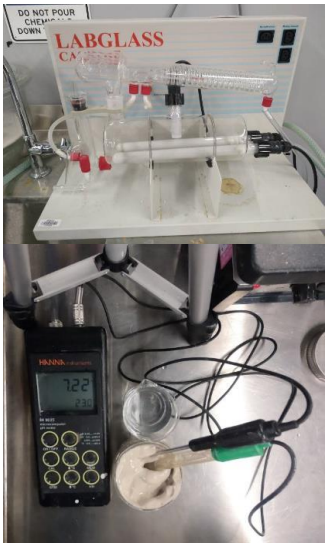



*Figure 3.32 Photographs of the equipment for pH tests*

*Table 3.4 Testing program for pH tests*

| Soil: % | Lime: % | Bottom ash: % | Bagasse ash: % | Curing time (hour/day) | Number of tests |
|---|---|---|---|---|---|
| 100 | 0 | 0 | 0 | 1h | 2 |
| 100 | 2, 3, 4, 5, 6, 7 | 0 | 0 | 1h, 7d, 14d, 28d | 6 |
| 100 | 4, 5, 6 | 5, 10, 15, 20, 25, 30 | 0 | 1h, 7d, 14d, 21d | 18 |
| 95, 90, 85, 80, 75, 70 | 4, 5 | 5, 10, 15, 20, 25, 30 | 0 | 1h, 2h, 12h, 24h, 4d, 7d | 12 |
| **Total** | | | | | **38** |

### *3.4.1.2 Electrical conductivity tests*

The schematical diagram of the electrical conductivity (EC) test setup used in this study is presented in Figure 3.33. In this diagram, the EC probe was placed at the centre of a 400-mL vessel, which was heated by an AREC.X ceramic digital heating magnetic stirrer. During the EC test, the temperature was controlled at 25 or 40°C, and stirring velocity was set at 800 rounds per minute (rpm). A convex glass was placed at the bottom of vessel in order to avoid grinding ash from stirring of a bar. The stirring rotation of 800 rpm was fast enough to keep the bar balanced on the top of the glass and to stir the solution evenly. Therefore, the experimental setup was designed to preserve the original form of coarse bottom ash so that the test could reveal its true electrical behaviour. The test could last for 2 hours, and the value of electrical conductivity then displayed on the screen of a conductimeter, which was a shot by a fixed camera in a time-lapse manner, which is presented in Figure 3.33.

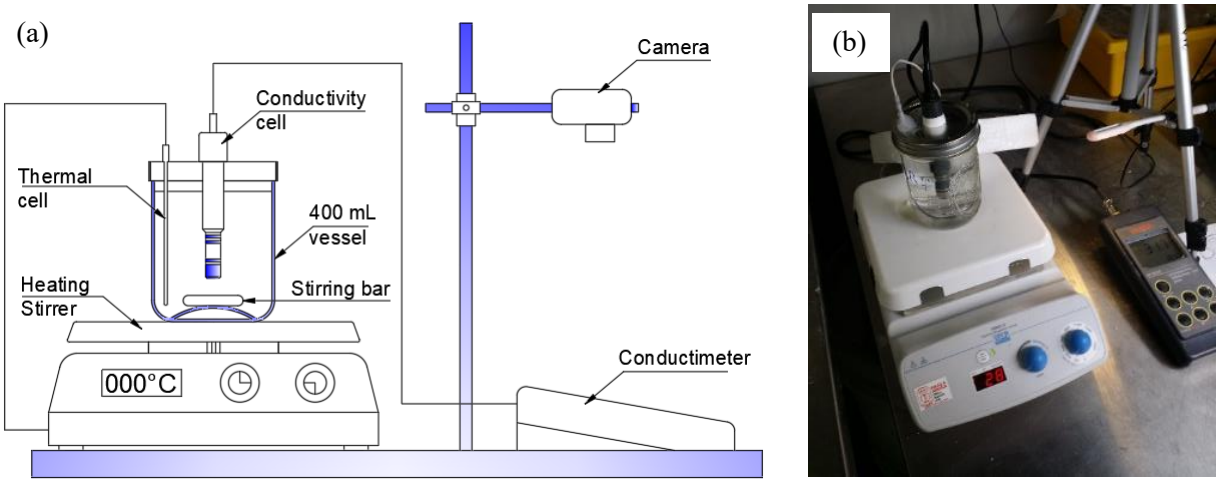


*Figure 3.33 (a) Schematic diagram of the experimental setup and (b) photo of equipment for electrical conductivity test*

To evaluate the reaction of soil/ash with hydrated lime, a Hana HI 9835 conductimeter was used with EC probe out-puts in the electrical conductivity test (see Figure 3.34). The EC probe was calibrated with the proper solution of pure seawater (100% NaCl) at 25°C to obtain the standard *EC* value of 5.00mS for 1-point calibration, based on the Hanna HI 9835 manual. Four annular platinum rings or electrodes were assembled on an ebonite probe in a diameter of 11 mm, at a spacing of 2 mm between ring 1 and 2, 3 and 4, and 12 mm between ring 2 and 3. The two outer rings (1 & 4) were electrodes with a direct current (voltage equals 0.2 mV), while the inner electrodes (2 & 3) were designed for measuring the voltage, which was converted to *EC* values of tested solutions. Furthermore, the temperature of solution was measured by a built-in temperature sensor which was fabricated as a thermistor in ring 4. There was also a sleeve assembled in the cell to cover four rings with a gap of 3 mm (refer to Figure 3.34). This small gap produced the cell constant of 1, giving a measured conductivity equal to the electrical conductivity of a tested solution (Sensorex, 2021). If the test does not use the sleeve, the measured *EC* data must be divided by a constant area coefficient (denoted as *a*) to gain standard *EC* values, equivalent to the value from the test with sleeve. For converting *EC*, if the distance of area surrounding the probe is larger than 25 mm, the coefficient is constant at 9.4. As for the studied vessel of 400 mL, it has an inner diameter of about 80 mm, leaving a gap around the probe within about 35 mm [= (80-11)/2], larger than 25 mm; hence, the coefficient *a* of 9.4 can be used to correct the *EC* value if the test does not include the sleeve.

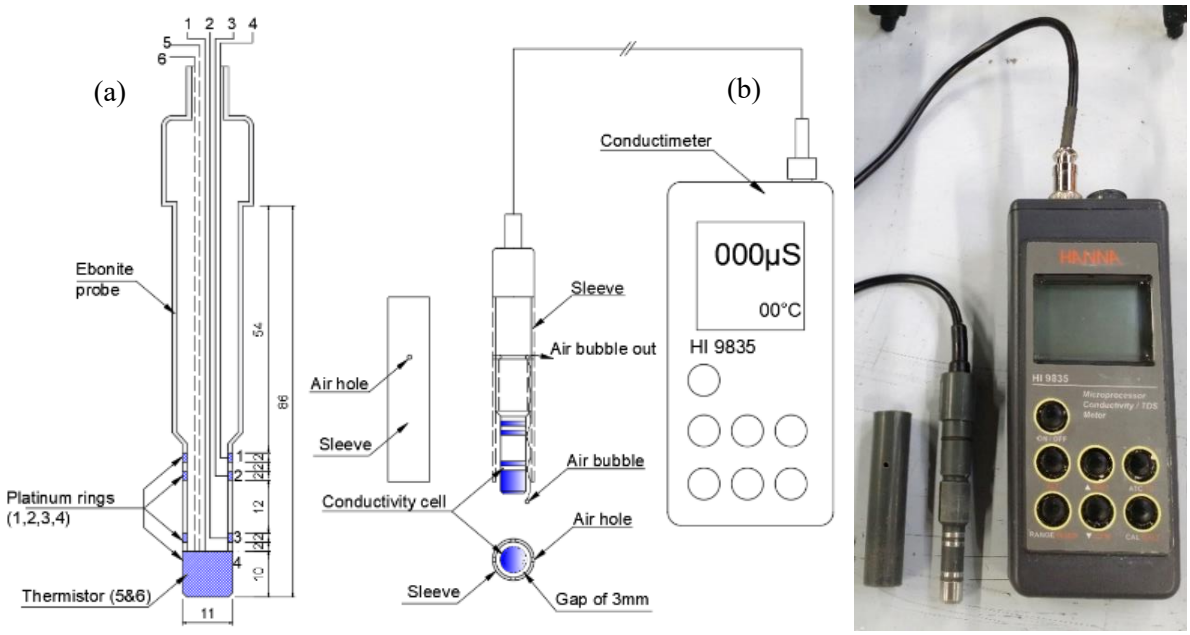


*Figure 3.34 Details of (a) conductivity cell and (b) conductimeter*

**Testing procedure and interpretation**

For electrical conductivity tests for lime-soil or ash-lime-soil suspension, three methods are suggested for mixing the soil sample in lime solution with or without ash, namely Test A, B and C. The main difference between these three methods is that in Test A, dry soil powder with or without ash was directly be poured into the lime aqueous solution, while in Test B and C, soil slurry was prepared by mixing soil powder with water before pouring with or without ash into the lime solution. Test C is an upgraded experiment of Test B, in which two ashes (i.e., bottom ash and bagasse ash) were first mixed with water in varied ash content to determine their proper ratio from the changes in their *EC* values. Once the ash ratio is determined, the following procedure of Test C is totally similar to Test B.

The second difference between Test A and B or C is related to temperature. In Test A, the testing temperature was kept at 40°C, while the thermal condition in Test B and C was 25°C. The temperature in Test A was higher than in Tests B and C to ensure the soil powder in Test A could quickly dissolve in water without significant clay clouds in the solution. Test B and C, on the other hand, did not need to be tested with hydrated lime at this high temperature since the soil power was mixed well with water beforehand. Regarding the volume of suspension, since the total volume of EC test solution was 400 mL, in Test B, 200 mL soil slurry was poured in 200 mL lime solution. Unlike Test B, in Test A, dry soil powder would directly be poured into the 400 mL solution of hydrated lime.

***Test-A procedure and interpretation (Subtests A1 and A2)***

Test A was used to evaluate the reactions between studied materials and hydrated lime suspension at 40°C, so all *EC*-values were modified by the temperature compensation coefficient ($T_c$). Test A consists of two subtests, namely Subtest A1 and Subtest A2 as follows:

**Subtest A1**: Mixing dry soil powder with or without ash into 400mL hydrated lime at 40ºC.

**Subtest A2:** Mixing soil/ash into 400mL water at 40ºC.

For Subtest A1, an unsaturated lime solution was prepared following the conductivity test, which was proposed by Payá et al. (1995). This was then utilised in various studies investigating pozzolanicity (Frías et al., 2005; Tashima et al., 2014; Velázquez et al., 2014; Villar-Cociña et al., 2003). In this test, to obtain the concentration of lime in its unsaturated solution (0.8 g/L), 0.32 g of hydrated lime powder was added to 400 ml of deionised/de-aired water, and the vessel was sealed. To increase the dissolution rate, only lime powder passing the 75µm sieve was used in the test. After about 30 minutes of stirring at 800 rpm and 40°C, *EC* of lime solution was finally obtained, denoted as $EC_0$. Following this procedure, the unsaturated lime solution could be gained quickly (see Figure 3.35a). When the lime solution was prepared, soil and ash in powder at their determined ratios were poured into the hydrated lime suspension. At this stage, the conductivity test started, and *EC* values were recorded to the camera with time, forming a curve of data points $EC_i$ with time, starting from $EC_0$ (see Figure 3.36). After 4 hours, the tests were stopped, and the solution was dried in an oven to check the solution concentration. The testing results are shown as "raw results", indicated in Figure 3.36.

However, when soil and ash were added to the solution (see Figure 3.35b), $EC_i$-values from Subtest A1 were influenced by two simultaneous processes: process (1) - a marginal increase by the dissolution of ions from chemicals of sand/ash into the water, and process (2) - a large decrease by the lime fixation caused by pozzolanic reactions between hydrated lime and pozzolans from soil and ash (Paya et al., 2001). Consequently, $EC_i$-value decreased significantly in the early duration but then reduced steadily over 120 minutes (see the raw curve in Figure 3.36). However, to determine the EC curve produced from only lime fixation (process 2), the raw curve from Subtest A1 should be corrected by being subtracted at every reading point with the *EC* values caused by soil/ash mixture in water (process 1), shown in Figure 3.36. Therefore, Subtest A2, corresponding to process 1 was performed by mixing soil/ash into 400mL water at 40°C, resulting in the curve "results on soil/ash mixture" in Figure 3.36. The "corrected results" curve was generated by the subtraction of the curve "raw results" to the curve "results on soil/ash mixture",

as shown in Figure 3.36. This generated the corrected curve, which reflected the decrease in pozzolanic reactions between lime and soil/ash, causing lime fixation (Frías et al., 2005; Paya et al., 2001; Tashima et al., 2014; Velázquez et al., 2014; Villar-Cociña et al., 2003).

As shown from Figure 3.36, the corrected results show $EC_{cor,i}$-values decrease suddenly from the initial value ($EC_0$) during the first minutes and decrease gradually and linearly with elapsed time during the last hour (from $t$ = 60 min). This corresponds to stage II of the electrical conductivity test, where the pozzolanic reaction decelerated, mentioned by Bahurudeen et al. (2015b) and McCarter and Tran (1996). The line, obtained from the linear relationship of the corrected results of $EC$ with elapsed time from $t$ = 60 – 120 min, determines $EC_{cor,0}$ as the intercept of the line to the vertical axis (refer to Figure 3.36). The value of $EC_{cor,0}$ is used to determine the initial loss in conductivity ($LC_0$) as follows:

$$LC_0 = \frac{EC_0 - (\frac{EC_{cor,0}}{a})}{EC_0} \times 100 \quad (3.1)$$

where, $LC_0$ (%): loss in conductivity of soil-ash-lime mixture at $t$=0

$EC_0$ (S/m): Electrical conductivity of soil-ash-lime mixture at $t$=0

$EC_{cor,0}$ (S/m): Corrected electrical conductivity of soil-ash-lime mixture at $t$=0, the intercept of line fitting to the corrected points $EC_i$, which are shown as corrected results in Figure 3.36.

$a$: the area coefficient, which depends on whether using the sleeve in the EC test

($a$=1 if the sleeve is used, and $a$=9.4 if the sleeve is not used)

Since the sleeve is not used in the main EC subtests, including Subtests A1, B1 and C2 (see Figures 3.35c, 3.38c and 3.39d), from Equation 3.1, it can obtain:

$$LC_0 = (1 - \frac{EC_{cor,0}}{9.4EC_0}) \times 100 \quad (3.2)$$

The initial loss in conductivity ($LC_0$) is expressed as a ratio in percentage rather than an absolute value. When the $EC$ of lime solution is different from each preparation, $LC_0$ in percent facilitates disqualifying the error in measurement and emphasising the relative changes in EC. In addition to $LC_0$, the raw results shown in Figure 3.36 can also be used to calculate the rate of $EC$ (denoted as $RC$). To determine conductivity rate, only $EC$ evolution from minute 2 to minute 20 was considered, which is corresponding to Stage 1 of electrical conductivity test, as shown in Figure 3.37. In this duration, the slope of this curve in a log-scaled plot of $EC$ versus time was

determined as the rate of electrical conductivity of mixing ash-soil materials with lime solution (see Figure 3.37). Since the test aims to determine the rate of *EC* change with time, no temperature compensation coefficient was applied in *EC*-values, and the area coefficient of 9.4 was also not used.

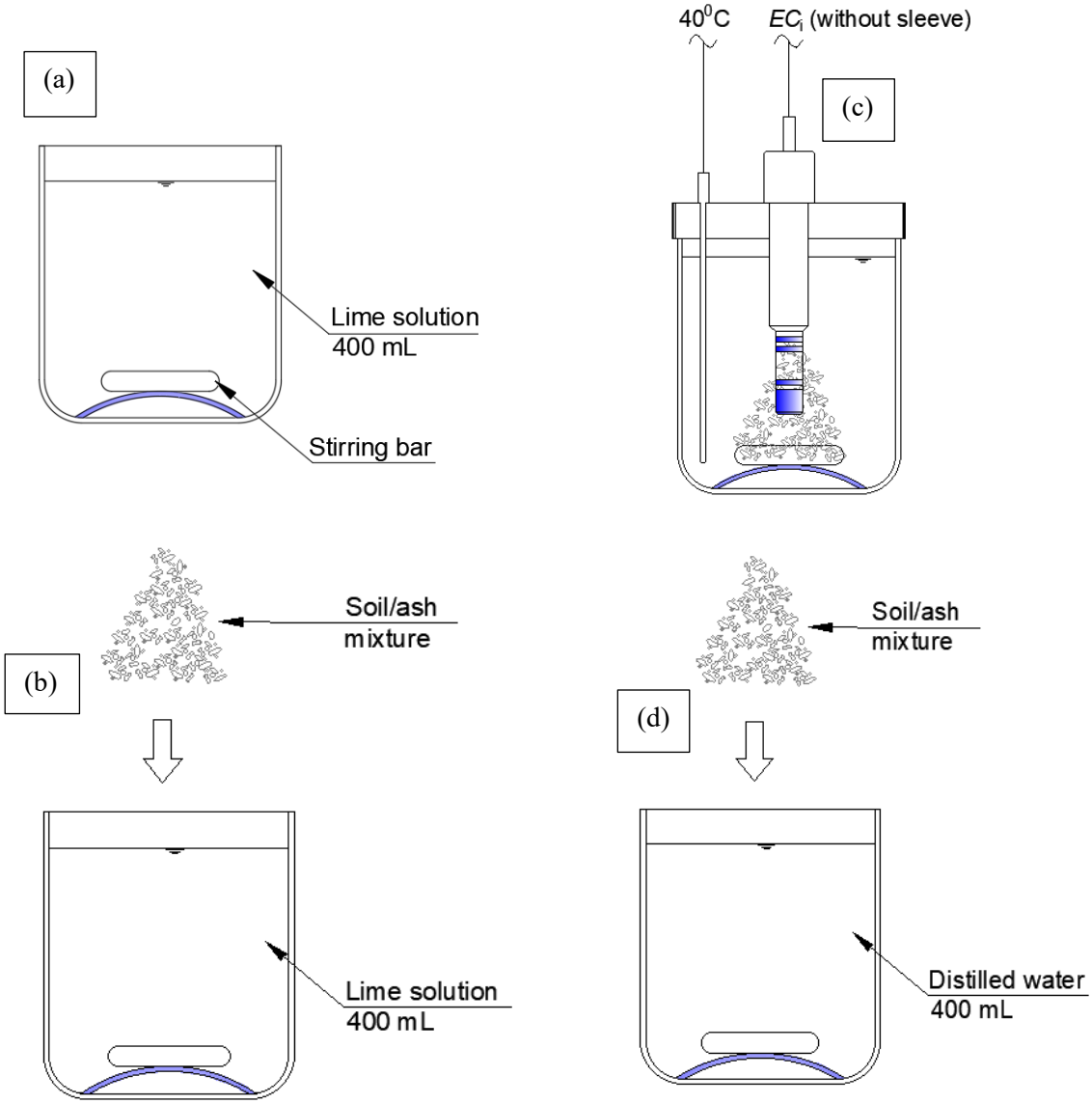


*Figure 3.35 Test-A procedure of mixing solutions for the vessel of 400mL: Subtest A1-(a) Preparation and EC measurement of 400mL lime solution, (b) Mixing soil-ash mixture into 400mL lime solution, (c) Measurement of EC at 40˚C; Subtest A2- (d) Mixing soil/ash mixture into 400mL distilled water and measuring EC at 40˚C*

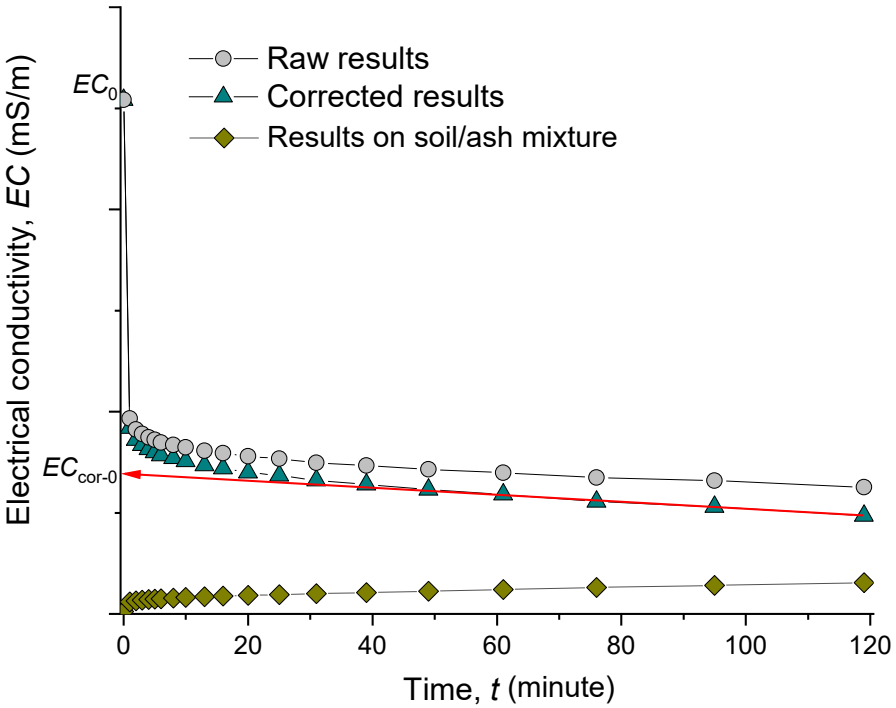


*Figure 3.36 Results from the electrical conductivity test for determining initial loss in conductivity ($LC_0$)*

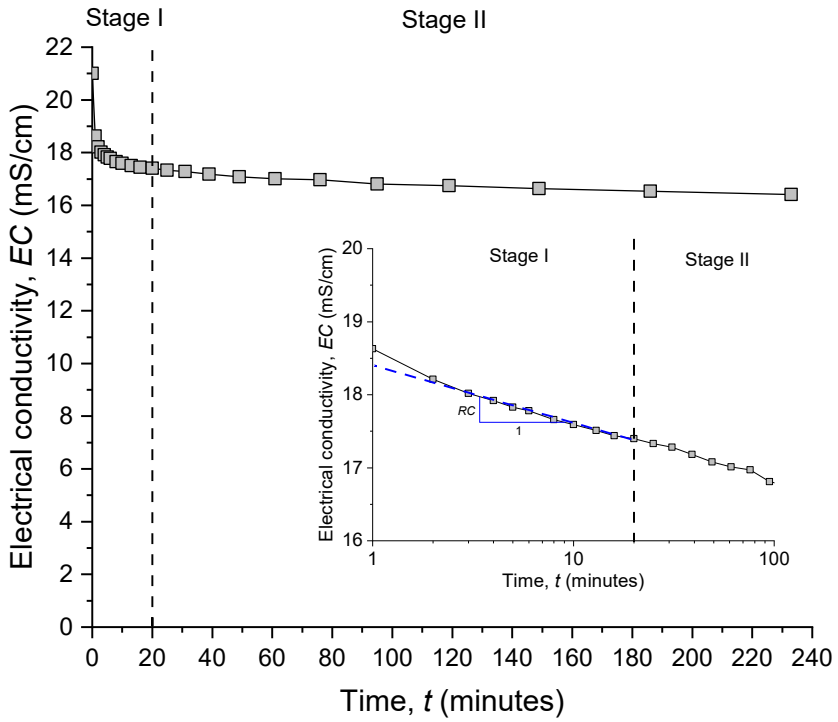


*Figure 3.37 Determination of the rate of electrical conductivity (RC)*

***Test-B procedure and results (Subtests B1 and B2)***

Test B was used to monitor the reactions between soil and ash with the solution of hydrated lime at the room temperature of 25°C, so no temperature compensation coefficient ($T_c$) is used to modify *EC*-values. Test B comprises of two subtests, namely Subtest B1 and Subtest B2 as shown below:

**Subtest B1**: Mixing 200 mL clay slurry with 200 mL hydrated lime at 25°C with or without ash.

**Subtest B2**: Mixing sand/ash into 400mL water at 25°C.

Since the temperature of Test B is at a lower value than Test A, it is recommended to mix clay components of expansive soil (i.e., bentonite and kaolinite) with water prior to EC test to avoid clayey clods (Abu-Hassanein et al., 1996). Therefore, in Subtest B1, two vessels of 200 mL were utilised to prepare a homogeneous lime solution and clay suspension separately (see Figure 3.38). To obtain the 200 mL final lime solution, it took 30 minutes using the magnetic stirrer, while clay suspension needed approximate 1 hour to obtain an aqueous blend without any clod. Constant electrical conductivities of these two solutions were then measured, with the inclusion of sleeve, denoted as $EC_L$ for lime and $EC_{BK}$ for Bentonite-Kaolinite compound, which is indicated in Figure 3.38a. After that, they were poured simultaneously into the vessel of 400 mL for EC tests (see Figure 3.38b). Right after both lime and clay liquids were combined and stirred together, sand or/and bottom ash were added in the vessel, as indicated in Figure 3.38b, then the lid, which was attached with conductivity cell without the sleeve, closed the vessel on the top to start the EC test, producing $EC_{mix,i}$ with time, as shown the raw results in Figure 3.36. At the end of the test, the solution was oven-dried to check its concentration and then collected for X-ray diffraction analysis.

For determining $LC_0$, the calculation in Test B is the same as to Test A. However, because of the change in sample preparation between the two tests, the value of $EC_0$ does not equal to $EC_L$ as indicated in Test A. Different to 400mL solution of unsaturated lime in Test A, combining 200 mL lime solution and 200 mL clay slurry in Test B dilutes their concentration in the new total volume of 400 mL. Therefore, the $EC$ value at time $t$=0 (denoted as $EC_0$) is the sum of $EC$ from each component in 400 mL minus that of distilled water ($EC_w$) as the following equation:

$$EC_0 = EC_L + EC_{BK} - EC_w \quad (3.3)$$

Where, $EC_L$ (S/m): electrical conductivity of 200mL hydrated lime solution.

$EC_{BK}$ (S/m): electrical conductivity of 200mL solution of bentonite and kaolinite.

$EC_w$ (S/m): electrical conductivity of water used in the test.

Besides, unlike Subtest A2, Subtest B2 in Test B is the mixture of sand and ash into 400mL water at 25°C. Therefore, for Test B, the curve of "results on soil/ash mixture" in Figure 3.36 turns

in to the curve of "results on sand/ash mixture" because the raw results from Subtest B1 are affected by the dilution of sand and ash into the solution.

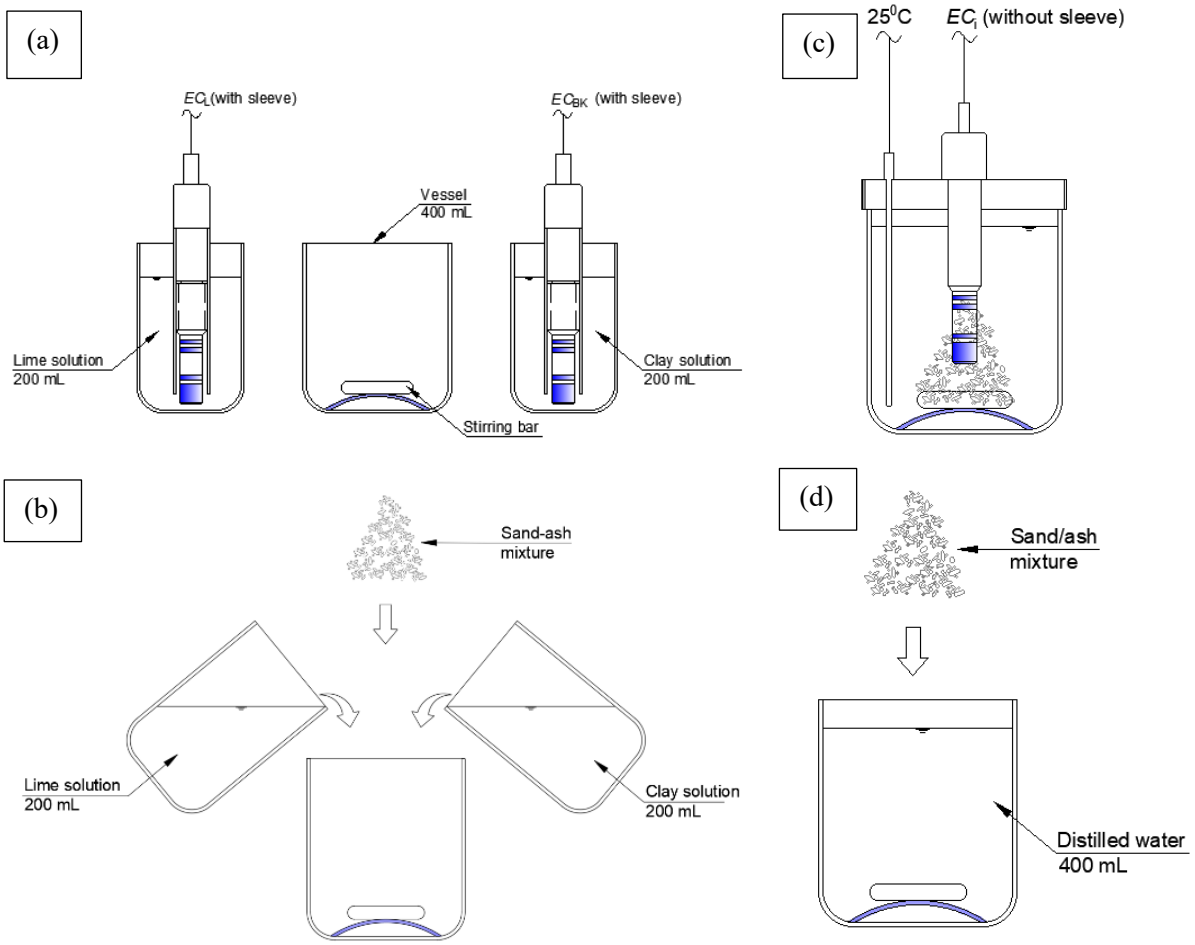


*Figure 3.38 Test-B procedure of mixing solutions for the vessel of 400mL: Subtest B1-(a) Preparation and EC measurement of 200 mL lime and 200mL clay solutions, (b) Combination of two solutions and sand/ash mixture, (c) Measurement of EC at 25˚C; Subtest B2-(d) Mixing sand/ash mixture into 400mL distilled water and measuring EC at 25˚C*

***Test-C procedure (Subtests C1, C2 and C3)***

Test C was designed to evaluate the pozzolanic performance of the mix of two ashes in the ash-lime soil solution. Test C includes three subtests, namely Subtests C1, C2 and C3, as follows:

**Subtest C1**: Mixing two ashes in 400mL water at 25ºC.

**Subtest C2**: Mixing 200 mL clay slurry with 200 mL hydrated lime at 25ºC and two ashes.

**Subtest C3**: Mixing sand/two ashes with 400mL water at 25ºC.

While Subtests C2, and C3 are similar to Subtests B1 and B2, respectively. Subtest C1 is the test performed by mixing two studied ashes (i.e., bottom ash and bagasse ash) in 400mL water at 25°C. In this notion, Subtests C1 and C3 have many points of similarity, including mixing two

ashes in the same amount of 400mL water at the similar temperature of 25ºC. However, these two tests are different from the purpose and ash proportion. Subtest C1 was conducted by varying the proportion of two ashes in a total content of 100% to determine their constant ratio, which was used for Subtest C2. Meanwhile, Subtest C3 results in the sand-two-ashes results for calculating $LC_0$ from the relationship of raw and corrected curves (see Figure 3.36).

Performing Subtest C1 is also based on the relationship between raw and sand/ash mixture results, as shown in Figure 3.36. The $EC_{cor,i}$-values are measured by subtracting *EC* of ash-lime-soil suspension to that of ash solution at every reading. If the ash solution has a high increasing rate of *EC*, the loss in conductivity is high and vice versa. Based on this correlation, if the bottom-bagasse ash solution has a high increase in values of *EC*, the reactivity of combined ash is also high due to the huge loss in conductivity. Therefore, it is possible to mix bottom ash and bagasse ash at various contents with water solution to quickly find out which ratio gives the reasonably high increase of *EC* (see the curve of ash mixture in Figure 3.36). For ratio determination, the plot of *EC* versus the logarithm of time can be drawn, as shown in Figure 3.37, but for the results of ash mixture indicated in Figure 3.36. The intercepts of curves on the *EC* line at the minute of 1 (not at 0 because of logarithm scale) can be determined and compared to evaluate the conductivity of each combination of two ashes. The optimal ratio of ash is equivalent to the high value of *EC* with the balance in combining two ashes in their solution for a well-graded particle distribution. Once the ash ratio is determined, the next procedures of Subtest C2 and C3 can be performed and correspond to Figure 3.39b-d, which are similar to Subtest B1 and B2, respectively, as shown in Figures 3.38a-c. The calculation of $LC_0$ in Test C is the same as that in Test B.

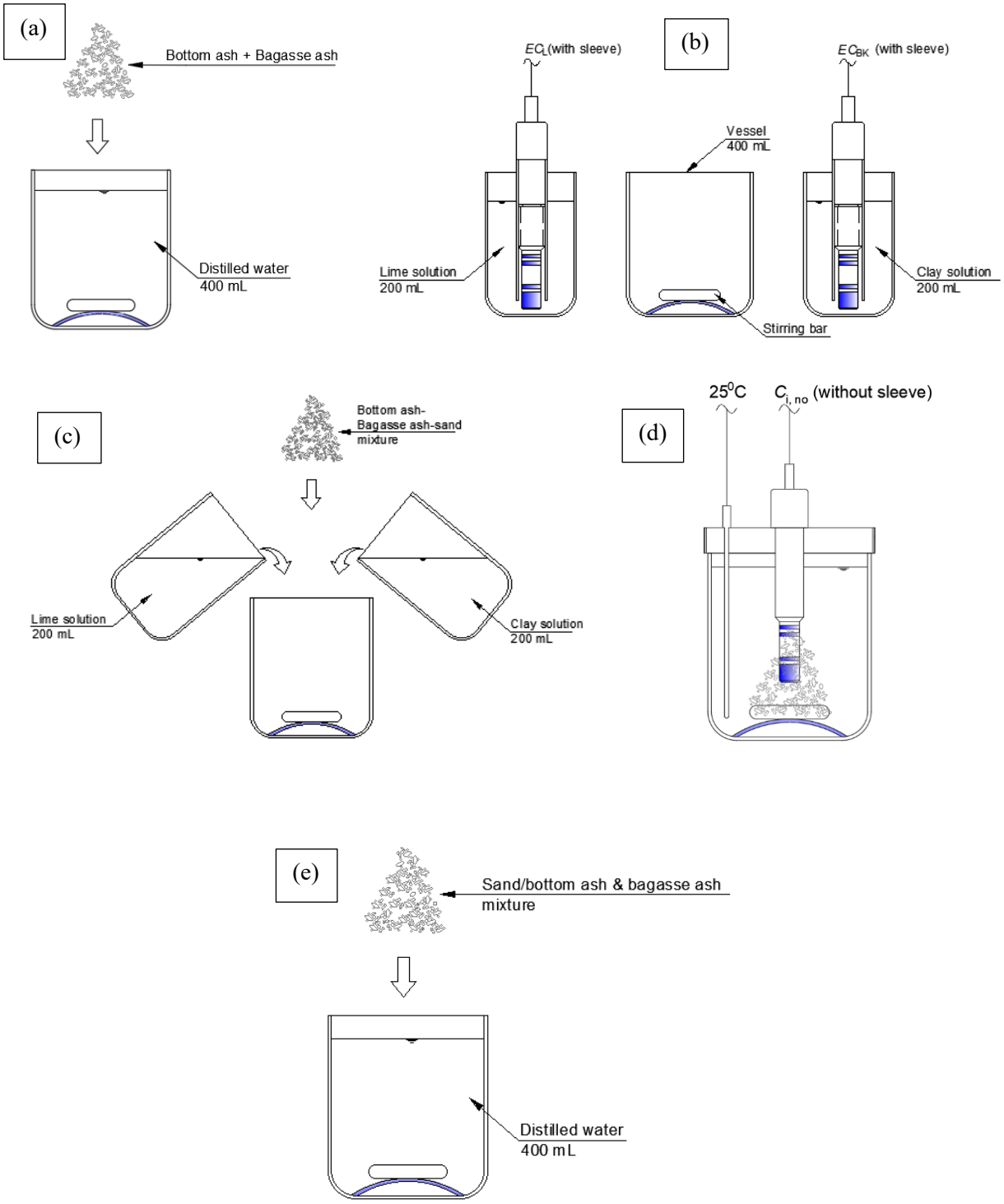


*Figure 3.39 Test-C1 procedure of mixing solutions for the vessel of 400mL: Subtest C1-(a) Mixing and measuring EC of two ashes into 400mL water at 25˚C; Subtest C2- (b) Preparation and EC measurement of 200 mL lime and 200mL clay solutions; (c) Combination of two solutions and sand-two-ashes mixture, (d) Measurement of EC at 25˚C; Subtest C3-(e) Mixing and measuring EC of sand/two ashes mixture at 25˚C*

## Testing program

In the testing program of EC, temperature and measured parameters are based on the involvement of ash used in treated material to get acceptable credibility of results. For lime-soil material with only bagasse ash with a majority of fine components in clayey size, the rate of electrical conductivity and temperature of 40°C, whereas the samples with the introduction of bottom ash in sandy sizes have their tests at 25°C and initial loss in conductivity ($LC_0$) for evaluation. Table 3.5 illustrates the specific tests employed for a specific material with temperature and obtained results. The studies on particular materials are also located in relevant chapters (see Table 3.5). Furthermore, the programs of electrical conductivity tests can be categorised with curing time (Table 3.6) and temperature (Table 3.7).

*Table 3.5 Tests A, B and C of electrical conductivity for studied materials*

| No. | Material | Test | Temperature (°C) | Testing results | Chapter |
|---|---|---|---|---|---|
| 1 | Soil | A2 & B2 | 25-40 | $EC_i$ | 4 |
| 2 | Soil + hydrated lime | A & B | 25-40 | $LC_0$ | 4 |
| 3 | Soil + hydrated lime + bottom ash | B | 25 | $LC_0$ | 5 |
| 4 | Soil + hydrated lime + bagasse ash | A | 40 | *EC* rate (*RC*) | 6 |
| 5 | Soil + hydrated lime + bottom ash + bagasse ash | C | 25 | $LC_0$ | 7 |

*Table 3.6 Testing program of electrical conductivity with various curing time*

| Soil: % (*g/mL*)* | Lime: % | Bottom ash: % (*g/mL*) | Bagasse ash: % | Curing time (hour/day) | Number of tests |
|---|---|---|---|---|---|
| Bentonite (*0.060, 0.063, 0.066, 0.068, 0.07, 0.073*) | 0 | 0 | 0 | 1h, 2h, 4h, 8h, 1, 2d, 4d, 7d | 6 |
| 0 | 0 | (*0.052, 0.042, 0.033, 0.024, 0.016, 0.008*) | | 1h, 1d | 6 |
| 100 | 0 | 0 | 0 | 1h | 6 |
| 100 | 4, 5, 6, 7 | 0 | 0 | 21d, 28d | 4 |
| 100 | 4, 5, 6, 7 | 5, 10, 15, 20, 25, 30 | 0 | 14d, 21d, 28d | 24 |
| 95, 90, 85, 80, 75, 70, 65 | 4, 5 | 5, 10, 15, 20, 25, 30 | 0 | 1h, 2h, 12h, 24h, 4d, 7d, 14d, 21d, 28d | 12 |
| **Total** | | | | | **58** |

Note: (*): concentration of material in gram per mL of water

*Table 3.7 Testing program of electrical conductivity with various temperatures*

| Soil: % | Lime: % | Bottom ash: % | Bagasse ash: % (mm) | *T* (°C) | Number of tests |
|---|---|---|---|---|---|
| 100 | 0 | 0 | 0 | 40 | 2 |
| 100 | 5 | 0 | 0 | 40 | 2 |
| 95, 90, 85, 80, 77.5, 75, 72.5, 70, 67.5, 65, 60 | 5 | 5, 10, 15, 20, 22.5, 25, 27.5, 30, 32.5, 35, 40 | 0 | 40 | 32 |
| 95, 90, 85, 80, 77.5, 75, 72.5, 70, 67.5, 65, 60 | 0 | 5, 10, 15, 20, 22.5, 25, 27.5, 30, 32.5, 35, 40 | 0 | 40 | 24 |
| 95, 90, 85, 80, 75, 70 | 5 | 0 | 5, 10, 15, 20, 25, 30 (0.425) | 40 | 6 |
| 95, 90, 85, 80, 75, 70 | 0 | 0 | 5, 10, 15, 20, 25, 30 (0.425) | 40 | 6 |
| 95, 90, 85, 80, 75, 70 | 5 | 0 | 5, 10, 15, 20, 25, 30 (0.150) | 40 | 6 |
| 95, 90, 85, 80, 75, 70 | 0 | 0 | 5, 10, 15, 20, 25, 30 (0.150) | 40 | 6 |
| 95, 90, 85, 80, 75, 70 | 5 | 0 | 5, 10, 15, 20, 25, 30 (0.075) | 40 | 6 |
| 95, 90, 85, 80, 75, 70 | 0 | 0 | 5, 10, 15, 20, 25, 30 (0.075) | 40 | 6 |
| 95, 90, 85, 80, 75, 70, 65, 60 | 5 | 5, 10, 15, 20, 25, 30, 35, 40 | 0 | 25 | 17 |
| Fine sand | 0 | 5, 10, 15, 20, 25, 30, 35, 40 | 0 | 25 | 8 |
| 0 | 0 | 100, 90, 80, 70, 60, 50, 30, 40, 20, 10, 0 | 0, 10, 20, 30, 40, 50, 60, 70, 80, 90, 100 (0.425) | 25 | 11 |
| 95, 90, 85, 80, 75, 70, 65, 60, 55, 50, 45, 40 | 5 | 3.5, 7, 10.5, 14, 17.5, 21, 24.5, 28, 31.5, 35, 38.5, 42 | 1.5, 3, 4.5, 6, 7.5, 9, 10.5, 12, 13.5, 15, 16.5, 18 | 25 | 12 |
| **Total** | | | | | **144** |

### 3.4.2 Physical tests

#### *3.4.2.1 Particle size distribution*

Particle size distribution determination includes sieving analysis and hydrometer test for studied materials. For the sieving analysis, soil materials were dried in the oven at the 105°C before passing through a pack of sieves in different sizes. The testing procedure in this study is clearly explained in the Australian Standard AS 1289.3.6.1 (2009). For particles with sizes less than 0.075 mm, hydrometer tests were performed. In this method, about 30 grams of soil power is mixed thoroughly with 40 grams sodium hexa-meta-phosphate [$(NaPO_3)_6$] in a 1L sedimentation cylinder

of distilled water, following the Australian Standard AS 1289.3.6.3 (2003). The hydrometer tests were applied to bentonite, kaolinite, bottom ash and bagasse ash samples.

### *3.4.2.2 Specific gravity*

The specific gravity ($G_s$) test is utilised to determine the ratio of soil particle density to density of water. For each employed material, three pycnometers have been used to obtain the average value of $G_s$, as shown in Figure 3.40. The specific gravities of expansive soil, hydrated lime, bottom ash and bagasse ash were measured, following the vacuum method, elucidated in AS 1289.3.5.1 (2006).

*Figure 3.40 Three pycnometers for specific gravity tests*

### *3.4.2.3 Atterberg limits*

The Atterberg limits, including plastic limit and liquid limits, are essential quantities to classify the fine-grained soils and assess their behaviours. While rolling soil samples was the common method for determining the plastic limit, illustrated in Figure 3.41, the fall cone penetrometer was used to define the liquid limit, as shown in Figure 3.42. Both experiments have been conducted according to the Australian standards, AS 1289.3.2.1 (2009) and AS 1289.3.9.1 (2015). It is worth mentioning that three values were collected to get the average value for each test. The testing programs for plastic limit and liquid limit tests are illustrated in Tables 3.8 and 3.9, respectively.

*Figure 3.41 Plastic limit tests*

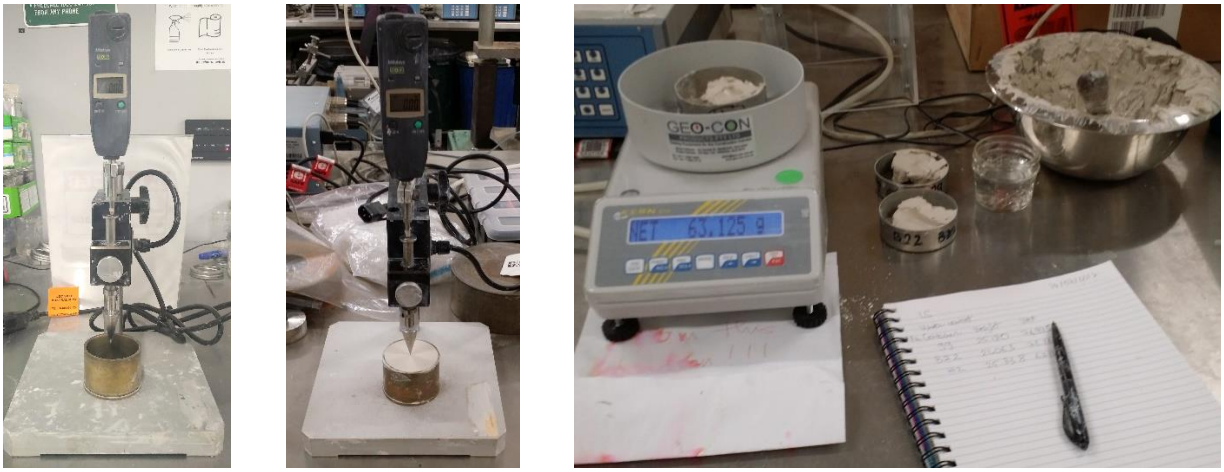


*Figure 3.42 Liquid limit tests*

*Table 3.8 Testing program for plastic limit*

| **Soil: % (*mm*)*** | **Lime: %** | **Bottom ash: % (*mm*)** | **Bagasse ash: % (*mm*)** | **Curing time (days)** | **Number of tests** |
|---|---|---|---|---|---|
| 100 | 0 | 0 | 0 | 1 | 2 |
| 100 | 5 | 0 | 0 | 1 | 2 |
| 85 | 5 | 0 | 15 | 1 | 2 |
| 75 | 5 | 25 | 0 | 1 | 2 |
| 75 | 5 | 17.5 | 7.5 | 1 | 2 |
| Total | | | | | 10 |

*Table 3.9 Testing program for liquid limit*

| **Soil: % (*mm*)*** | **Lime: %** | **Bottom ash: % (*mm*)** | **Bagasse ash: % (*mm*)** | **Curing time (days)** | **Number of tests** |
|---|---|---|---|---|---|
| 0, 10, 20, 25, 30, 40 in % Bentonite | 0 | 0 | 0 | 1 | 6 |
| 100 (*0.425*) | 0 | 0 | 0 | 1 | 1 |
| 100 (*0.425*) | 5 | 0 | 0 | 1 | 5 |
| 100 (*0.425*) | 0 | 5, 10, 20, 30 (*0.425*) | 0 | 1 | 4 |
| 95, 90, 85, 80, 75, 70, 65, 60 (*2.36*)* | 5 | 5, 10, 15, 20, 25, 30, 35, 40 (*2.36*)* | 0 | 1 | 8 |
| 85 (*2.36*)* | 5 | 0 | 15 (*0.425*) | 1 | 1 |
| 85 (*2.36*)* | 5 | 0 | 15 (*0.150*) | 1 | 1 |
| 85 (*2.36*)* | 5 | 0 | 15 (*0.075*) | 1 | 1 |
| 85 (*2.36*)* with 20% Bentonite | 5 | 0 | 15 (*0.075*) | 1 | 1 |
| 85 (*2.36*)* with 10% Bentonite | 5 | 0 | 15 (*0.075*) | 1 | 1 |
| 75 (*2.36*)* | 5 | 17.5 (*2.36*)* | 7.5 (*0.425*) | 1 | 1 |
| **Total** | | | | | **30** |

Note: (*) Ratios based on the size of 2.36 mm, after sieving through the sieve of 0.425 mm, the ratio based on 0.425 mm may change

### *3.4.2.4 Standard compaction*

The maximum dry density (*MDD*) and the optimal moisture content (*OMC*) were determined from compaction tests, as presented in Figure 3.43. This is a standard proctor compaction test conforming to the Australian Standard, AS 1289.5.1.1 (2017). At least five compaction points were tested to draw compaction curves for determining *MDD* and *OMC*. The testing program for compaction tests is tabulated in Table 3.10.

*Figure 3.43 Compaction tests*

*Table 3.10 Testing program for compaction tests*

| Soil: % | Lime: % | Bottom ash: % (*mm*) | Bagasse ash: % (*mm*) | Curing time (hour) | Number of tests |
|---|---|---|---|---|---|
| 100 | 0 | 0 | 0 | 1 | 6 |
| 100 | 5 | 0 | 0 | 1 | 6 |
| 100 | 0 | 5, 10, 20, 30 | 0 | 1 | 8 |
| 100 | 5 | 5, 15, 25, 30 | 0 | 1 | 8 |
| 65, 60, 55, 50, 45, 40 | 5 | 25 | 5, 10, 15, 20, 25, 30 | 1 | 6 |
| 75 | 5 | 25 | 0 | 1 | 7 |
| 85 | 5 | 0 | 15 | 1 | 6 |
| 75 | 5 | 17.5 | 7.5 | 1 | 5 |
| **Total** | | | | | **52** |

## 3.4.3 Mechanical tests

### *3.4.3.1 Linear shrinkage (LS)*

Liquid limit values obtained from the fall cone test in Table 3.10 were used to prepare soil samples for the linear shrinkage test (see Figure 3.44). The experiment was conducted according to the Australian standards, AS 1289.3.4.1 (2008). Each linear shrinkage value is the average obtained from three samples tested and cured after 7 days. The LS testing program is summarised in Table 3.11.

*Table 3.11 Testing program for linear shrinkage tests*

| Soil: % (*mm*)* | Lime: % | Bottom ash: % (*mm*) | Bagasse ash: % (*mm*) | Curing time (days) | Number of tests |
|---|---|---|---|---|---|
| 0, 10, 20, 25, 30, 40 in % Bentonite | 0 | 0 | 0 | 3 | 19 |
| 100 (*0.425*) | 0 | 0 | 0 | 3 | 7 |
| 100 (*0.425*) | 5 | 0 | 0 | 7 | 5 |
| 100 (*0.425*) | 0 | 5, 10, 20, 30 (*0.425*) | 0 | 7, 14 | 33 |
| 100 (*0.425*) | 5 | 5, 10, 20, 30 (*0.425*) | 0 | 7 | 12 |
| 95, 90, 85, 80, 75, 70, 65, 60 (*2.36*)* | 5 | 5, 10, 15, 20, 25, 30, 35, 40 (*2.36*)* | 0 | 7, 28 | 44 |
| 85 (*2.36*)* | 5 | 0 | 15 (*0.425*) | 7, 14, 28 | 9 |
| 85 (*2.36*)* | 5 | 0 | 15 (*0.150*) | 7 | 3 |
| 85 (*2.36*)* | 5 | 0 | 15 (*0.075*) | 7 | 3 |
| 75 (*2.36*)* | 5 | 17.5 (*2.36*)* | 7.5 (*0.425*) | 7, 28 | 4 |
| **Total** | | | | | **139** |

Note: (*) Ratios based on the size of 2.36 mm, after sieving through the sieve of 0.425 mm, the ratio based on 0.425 mm may change.

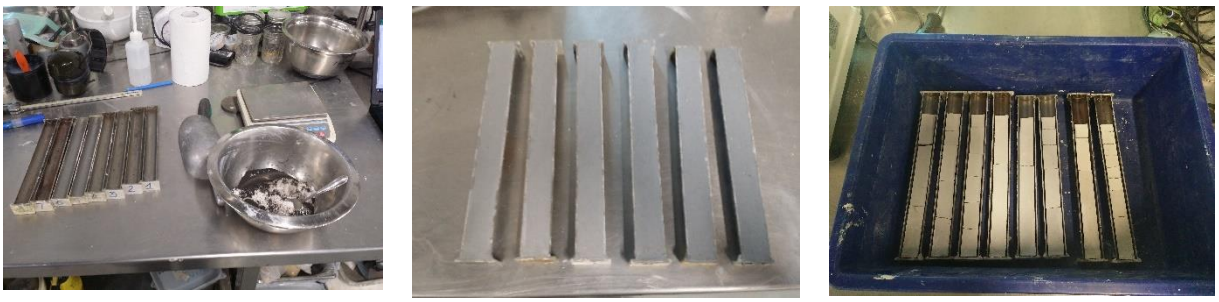

*Figure 3.44 Linear Shrinkage tests*

### *3.4.3.2 Unconfined compressive strength (UCS) tests*

Unconfined compressive strength tests were carried out according to the Australian standard, AS 5101.4 (2008). In this test, soil samples were compressed into three layers evenly in moulds with dimensions of 100 mm × 50 mm, as demonstrated in Figure 3.45. Then, soil samples were wrapped and cured in desiccators for 7, 28, 56 or 90 days. The sample mass was checked before and after curing to ensure that there is no water loss. After 7 or 28 days, the samples were compressed in a loading frame to find the *UCS* values. It can be noted that each point is the average value of three UCS tests on identical samples. The UCS testing program is shown in Table 3.12.

*Table 3.12 Testing program for UCS tests*

| Soil: % | Lime: % | Bottom ash: % (*mm*) | Bagasse ash: % (*mm*) | Curing time (days) | Number of tests |
|---|---|---|---|---|---|
| 100 | 0 | 0 | 0 | 3 | 6 |
| 100 | 3, 5, 7, 9 | 0 | 0 | 7, 28 | 55 |
| 100 | 0 | 5, 10, 20, 30 (*2.36*) | 0 | 7, 28, 56 | 56 |
| 100 | 0 | 5, 10 (*0.075*) | 0 | 28, 56 | 14 |
| 100 | 5 | 5, 10, 20, 30 (*2.36*) | 0 | 7, 28, 56, 90 | 56 |
| 90, 85, 75, 70, 65 | 5 | 5, 10, 20, 25, 30 (*2.36*) | 0 | 7, 28, 56 | 27 |
| 65, 60, 55, 50 | 5 | 25 (*2.36*) | 5, 10, 15, 20 (*0.425*) | 28, 56 | 22 |
| 100 | 0 | 0 | 0 | 3 | 2 |
| 100 | 5 | 0 | 0 | 7, 28, 56 | 9 |
| 95, 90, 80, 75, 70 | 5 | 5, 10, 15, 20, 25, 30, 40 (*2.36*) | 0 | 28, 56 | 48 |
| 85 | 5 | 0 | 15 (*0.425*) | 7, 28, | 9 |
| 85 | 5 | 0 | 15 (*0.150*) | 7, 28 | 9 |
| 85 | 5 | 0 | 15 (*0.075*) | 7, 28 | 9 |
| 75 | 5 | 17.5 (*2.36*) | 7.5 (*0.425*) | 7, 28 | 9 |
| 0 | 0 | 100 (*2.36*) | 0 | 3 | 3 |
| 0 | 3, 5, 7, 9 | 100 (*2.36*) | 0 | 14, 28, 56 | 46 |
| 0 | 5 | 70 (*2.36*) | 30 (*0.425*) | 7, 28 | 8 |
| **Total** | | | | | **388** |

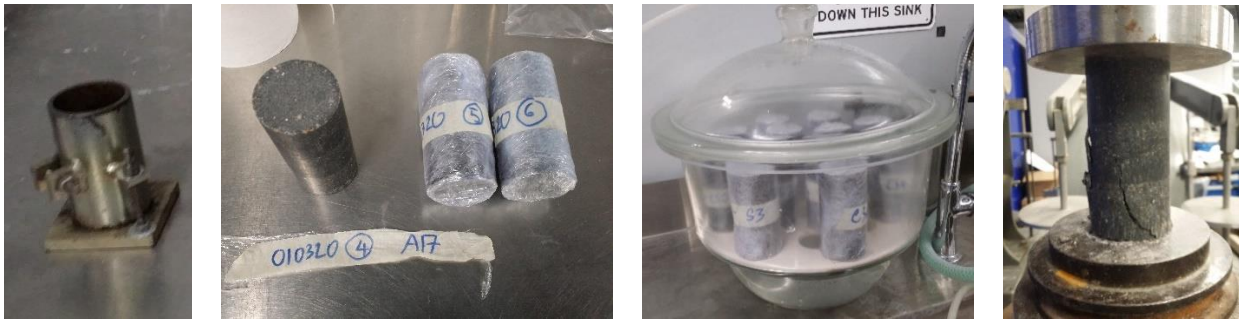


*Figure 3.45 Unconfined compressive strength tests*

### *3.4.3.3 Indirect tensile strength (ITS) tests*

The sample preparation for ITS sample is similar to that explained in UCS specimen preparation. The only difference is laying down the sample on the loading plate when applying pressure on the soil cylinder (see Figure 3.46). Following AS 1012.10-2000, the ITS from Brazilian tests were performed on specimens of treated expansive soils with different ratios of bottom ash and lime for two curing periods of 7 and 28 days. Like the UCS sample, soil mixtures are compacted into 50 mm × 100 mm steel moulds in three equal layers to obtain maximum dry density (*MDD*). Afterwards, the samples are extruded, sealed in plastic wrap, cured at room temperature and at the relative humidity of 80% before testing. In the ITS tests, the samples are weighed, and their

dimensions were measured to quantify the dry density before the tests. The loading frame Tritech with the capacity of 50 kN was utilized in these tests, including a linear variable differential transformer (LVDT) and a S-shaped load cell. They were connected to a computer via a data logger and displayed the dial data via the Datacomm program. The samples were horizontally placed on the base of loading frame, and a strain rate of 1 mm per minute was applied. The ITS of the soil sample can be calculated using Equation 3.4:

$$\sigma_T = y\frac{2P}{\pi DL} \tag{3.4}$$

Where, $\sigma_T$ is the indirect tensile strength (kPa), $P$ is the maximum load (kN), $D$ is the diameter of the soil sample (m), $L$ denotes the sample height (m), and $y$ is the correction coefficient for the effect of sample size on ITS values (Yu et al. 2006). The coefficient has a linear relationship with $k$, the ratio of height to diameter ($k$=$L$/$D$), given that $y$=0.262$k$+1 (Yu et al. 2006). The testing program is described in Table 3.13.

*Figure 3.46 Indirect tensile strength test*

*Table 3.13 Testing program for ITS tests*

| **Soil: %** | **Lime: %** | **Bottom ash: % (*mm*)** | **Bagasse ash: % (*mm*)** | **Curing time (days)** | **Number of tests** |
|---|---|---|---|---|---|
| 100 | 0 | 0 | 0 | 3 | 3 |
| 100 | 0 | 5, 10, 20, 30 (*2.36*) | 0 | 7, 28, 56 | 21 |
| 100 | 5 | 5, 10, 20, 30 (*2.36*) | 0 | 7, 28, 56, 90 | 38 |
| 90, 85, 75, 70, 65, 55 | 5 | 5, 10, 20, 25, 30, 40 (*2.36*) | 0 | 56 | 23 |
| 55 | 5 | 25 (*2.36*) | 15 (*0.425*) | 28 | 3 |
| 0 | 0 | 100 (*2.36*) | 0 | 3 | 3 |
| 0 | 5 | 100 (*2.36*) | 0 | 28 | 3 |
| 0 | 5 | 70 (*2.36*) | 30 (*0.425*) | 7, 28 | 8 |
| **Total** | | | | | **102** |

### *3.4.3.4 California bearing ratio (CBR) tests*

The soaked CBR tests have been conducted in accordance with the Australian standard, AS 1289.6.1.1 (2014) to investigate the load-bearing performance of the soil samples. Like the ITS sample preparation, CBR samples were constituted from filling and shaping the soil mixtures into cylindrical moulds but with a bigger size (152 mm × 178 mm), and five equal layers were tamped separately for the uniformity of compacted samples at *OMC* and *MDD*. The samples were then wrapped in plastic covers in order to prevent moisture loss during curing. After a given curing period, the samples with a surcharge of 4.5 kg, placed on the top, are soaked in tanks of water in 7 days for soaked CBR tests. The same loading equipment as for ITS test was employed in the CBR test; however, the load cell with a penetration piston of 50 mm in diameter was employed, as illustrated in Figure 3.47. *CBR* values were calculated and selected from the higher ratio of applied force to 13.2 kN and 19.8 kN at the penetration of 2.5 mm and 5 mm, respectively. For each sample, *CBR* is the average value from two repetitive tests. The CBR testing program is presented in Table 3.14.

*Figure 3.47 California bearing ratio test*

*Table 3.14 Testing program for CBR tests*

| Soil: % | Lime: % | Bottom ash: % (*mm*) | Bagasse ash: % (*mm*) | Curing time (days) | Number of tests |
|---|---|---|---|---|---|
| 100 | 0 | 0 | 0 | 3 | 2 |
| 100 | 5 | 0 | 0 | 28 | 2 |
| 100 | 0 | 5, 10, 20, 30 (*2.36*) | 0 | 28 | 8 |
| 100 | 5 | 5, 10, 20, 30 (*2.36*) | 0 | 28 | 8 |
| 90, 85, 75, 70, 65 | 5 | 5, 10, 20, 25, 30, 40 (*2.36*) | 0 | 28 | 11 |
| 55 | 5 | 25 (*2.36*) | 15 (*0.425*) | 28 | 2 |
| 100 | 0 | 0 | 0 | 3 | 2 |
| 100 | 5 | 0 | 0 | 28 | 4 |
| 95, 90, 80, 75, 70, 60 | 5 | 5, 10, 20, 25, 30, 40 (*2.36*) | 0 | 28 | 14 |
| 85 | 5 | 0 | 15 (*0.425*) | 28 | 2 |
| 75 | 5 | 17.5 (*2.36*) | 7.5 (*0.425*) | 28 | 2 |
| **Total** | | | | | **57** |

### *3.4.3.5 Swelling-consolidation tests*

The swelling-consolidation tests were conducted on samples cured for 3, 7 or 28 days, following the Australian Standard AS 1289.6.6.1 (1998) procedure. In addition to this standard, other standards from ASTM were mobilised to perform advanced consolidation tests, such as rapid consolidation and constant rate of strain (CRS) tests (see Figure 3.48). For the rapid consolidation test (ILeop), the experiment followed method B mentioned in ASTM D2435 (2020). Meanwhile, CRS test was performed using the hydraulic Rowe cell in accordance with ASTM D4186 (2020). CRS test was also used for conventional oedometer cell and CBR mould in zero-volume-swelling tests. The detail of testing program is presented in Table 3.15.

(a) (b) (c) (d)

*Figure 3.48 Snapshots of swelling-consolidation tests: (a) conventional cell in oedometer systems, (b) conventional cell in the loading frame, (c) CBR mould in the loading frame and (d) hydraulic Rowe cell*

*Table 3.15 Testing program for swelling-consolidation tests*

| Soil: % | L: % | BO: % (*mm*) | BA: % (*mm*) | Curing time (days) | Test type | Cell | Number of tests |
|---|---|---|---|---|---|---|---|
| 100 | 0 | 0 | 0 | 3 | Preloading swelling-ILeop | Oed. | 5 |
| 100 | 0 | 0 | 0 | 3 | Free-swelling ILeop | Oed. | 4 |
| 100 | 0 | 0 | 0 | 3 | Zero-volume- CRS test | Oed. | 7 |
| 100 | 0 | 0 | 0 | 3 | Swelling-CRS | Rowe | 2 |
| 100 | 0 | 10, 20, 25, 30, 40 (*2.36*) | 0 | 3 | Swelling-CRS | CBR | 5 |
| 100 | 5 | 0 | 0 | 1, 7 | Free-swelling ILeop | Oed. | 2 |
| 100 | 5 | 0 | 0 | 7 | Swelling-CRS | Rowe | 1 |
| 95, 90, 85, 80, 75, 70, 60 | 5 | 5, 10, 15, 20, 25, 30, 40 (*2.36*) | 0 | 1 | Free-swelling ILeop | Oed. | 15 |
| 85 | 5 | 0 | 15 (0.425) | 1 | Free-swelling ILeop | Oed. | 1 |
| 85 | 5 | 17.5 (2.36) | 7.5 (0.425) | 1 | Free-swelling ILeop | Oed. | 1 |
| 0 | 5 | 70 | 30 | 7, 28 | Swelling-CRS | Rowe | 2 |
| **Total** | | | | | | | **45** |

Note: (*) Ode. = Oedometer cell

### *3.4.3.6 Triaxial shearing tests*

In triaxial tests, soil samples with a diameter of 50 mm and a height of 100 mm were compacted at the wet side of optimal moisture content for fully saturated state, targeting 90% of saturation level. For treated soil samples, the specimens were cured for 28 days prior to the test. The sample weight and dimensions were measured to quantify any volume changes during the curing process, which were also used for parameters in the shear test. The test procedure follows Australian Standard for consolidated-undrained (CU) test, referred in AS 1289.6.4.2 (2016) and shown in Figure 3.49. To satisfy the Skempton's B value of 0.95 as indicator of checking the fully-saturated level of sample, ramping back-pressure from 0 to 600 kPa over 3 days was conducted, obeying the recommendation in AS 1289.6.4.2 (2016). Furthermore, abiding by the associated standards, the recommended shear rate of 1%/hour was employed in the tests since the end of primary consolidation was not obviously determined from the back volume during the stage of consolidation. The confined pressures of 50, 100 and 200 kPa were utilised in the tests to reach a linear relationship between these effective pressures and shear strength, resulting in frictional angles and cohesions. The main testing program features are indicated in Table 3.16.

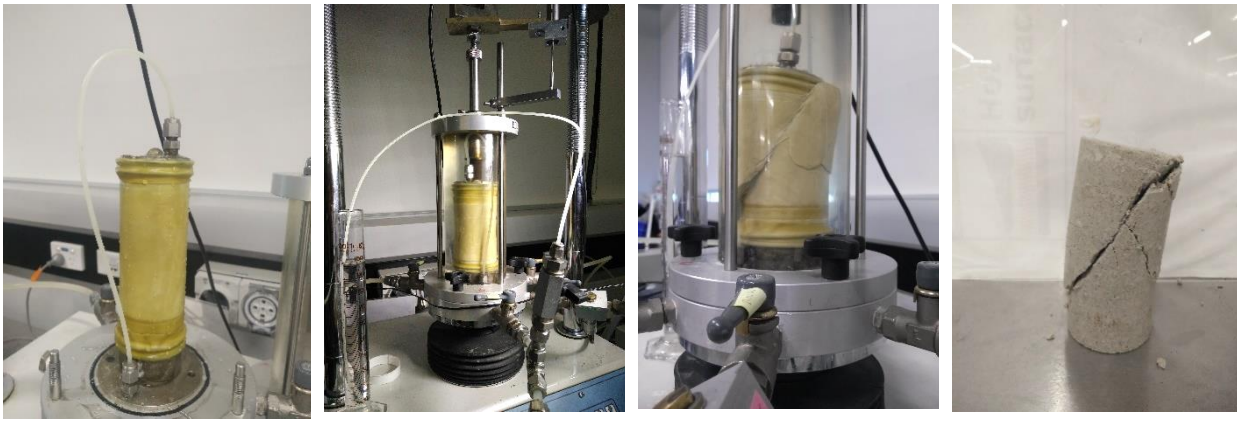

*Figure 3.49 Triaxial shear test*

*Table 3.16 Testing program for triaxial test*

| Soil: % | Lime: % | Bottom ash: % | Bagasse ash: % (*mm*) | Curing time (days) | Number of tests |
|---|---|---|---|---|---|
| 100 | 0 | 0 | 0 | 28 | 4 |
| 100 | 5 | 0 | 0 | 28 | 3 |
| 100 | 5 | 25 | 0 | 28 | 3 |
| 100 | 5 | 0 | 15 | 28 | 3 |
| 100 | 5 | 17.5 | 7.5 | 28 | 3 |
| **Total** | | | | | **16** |

### *3.4.3.7 Bender element tests*

Most of the samples for bender element tests were compacted statically, except for specimens from UCS and CBR tests. Paper frames are specially designed for samples with various sizes to precisely mark and scratch cavities at both ends of samples (see Figures 3.50 and 3.51). The S+P wave method was used to determine the travelling time through studied samples. The method was based on the arrival time of P wave, which is coincidental with arrival time of S wave (Wang et al., 2017a). Following this method, the time period of 0.05 millisecond, equivalent to 20 kHz, was selected when measuring velocity and calculating for small-strain shear modulus ($G_{max}$). The testing program is listed in Table 3.17.

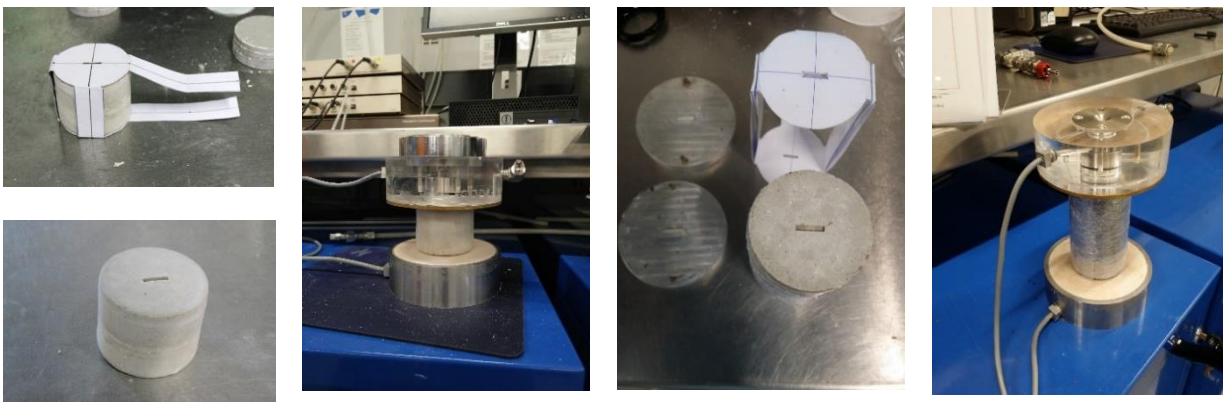

*Figure 3.50 Bender element test for samples in the diameter of 50 mm*

*Figure 3.51 Bender element test for CBR sample*

*Table 3.17 Testing program for bender element tests*

| Soil: % | Lime: % | Bottom ash: % | Bagasse ash: % (*mm*) | Sample height (mm) | Curing time (days) | Number of tests |
|---|---|---|---|---|---|---|
| 100 | 0 | 0 | 0 | 40 | 0 - 240 | 3 |
| 100 | 5 | 0 | 0 | 40 | 0 - 240 | 3 |
| 75 | 5 | 25 | 0 | 40 | 0 - 240 | 3 |
| 75 | 5 | 25 | 0 | 40 | 0 – 240 (wet side) | 1 |
| 85 | 5 | 0 | 15 (*0.425*) | 40 | 0 - 190 | 3 |
| 85 | 5 | 0 | 15 (*0.075*) | 40 | 0 - 190 | 3 |
| 75 | 5 | 17.5 | 7.5 (*0.425*) | 40 | 0 - 120 | 3 |
| 75 | 5 | 17.5 | 7.5 (*0.425*) | 40 | 0 – 120 (dry side) | 3 |
| 75 | 5 | 17.5 | 7.5 (*0.425*) | 40 | 0 – 120 (wet side) | 3 |
| 100 | 0 | 0 | 0 | 100 | 3 | 2 |
| 100 | 5 | 0 | 0 | 100 | 28 (wet side) | 2 |
| 75 | 5 | 25 | 0 | 100 | 28 (wet side) | 3 |
| 85 | 5 | 0 | 15 (*0.425*) | 100 | 28 (wet side) | 3 |
| 75 | 5 | 17.5 | 7.5 (*0.425*) | 100 | 28 (wet side) | 3 |
| 100 | 0 | 0 | 0 | 117 | 0 – 28 | 2 |
| 100 | 5 | 0 | 0 | 117 | 0 - 28 | 2 |
| 75 | 5 | 25 | 0 | 117 | 0 - 28 | 2 |
| 85 | 5 | 0 | 15 | 117 | 0 - 28 | 2 |
| 75 | 5 | 17.5 | 7.5 | 117 | 0 - 28 | 2 |
| 100 | 5 | 0 | 0 | 100 | 7, 28, 56 | 9 |
| 95, 90, 85, 80, 75, 70, 60 | 5 | 5, 10, 15, 20, 25, 30, 40 | 0 | 100 | 7, 28, 56 | 45 |
| 85 | 5 | 0 | 15 (*0.425*) | 100 | 7, 28, 56 | 9 |
| 85 | 5 | 0 | 15 (*0.075*) | 100 | 28 | 3 |
| 75 | 5 | 17.5 | 7.5 | 100 | 7, 28, 56 | 9 |
| **Total** | | | | | | **123** |

#### *3.4.3.8 Filter paper method for matric suction tests*

To determine the change of matric suction versus moisture content for the studied soil sample during curing, the filter paper method was employed, based on ASTM D5298 (2016). For this test, the soil sample was statically compacted to form a specimen with 50 mm in diameter and 20 mm in height at *MDD* and *OMC*. The mixed samples and curing durations are shown in Table 3.18. The water contents of filter paper were measured to calculate the equivalent soil matric suction via their relationship shown in the calibration curve of Whatman No. 42 filter paper (ASTM D5298, 2016). The accuracy of weight measurement is 4 decimals using an automated accurate scale, as shown in Figure 3.52.

*Figure 3.52 Filter paper tests*

*Table 3.18 Testing program for filter paper (suction) tests*

| Soil: % | Lime: % | Bottom ash: % | Bagasse ash: % | Curing time (day) | Number of tests |
|---|---|---|---|---|---|
| 100 | 0 | 0 | 0 | 11, 77, 90 | 6 |
| 100 | 5 | 0 | 0 | 14, 29, 63, 91 | 10 |
| 75 | 5 | 25 | 0 | 15, 28, 57, 90 | 12 |
| 85 | 5 | 0 | 15 | 7, 28, 56, 90 | 11 |
| 75 | 5 | 17.5 | 7.5 | 7, 28, 56, 90 | 9 |
| **Total** | | | | | **48** |

### 3.4.4 Micro-structural tests

#### *3.4.4.1 X-ray diffraction tests*

X-ray diffraction tests were used to define compounds in a studied material based on fitting the peaks of intensity varying on diffraction angles with original peaks of a specific chemical's spectrum, shown as an example in Figure 3.53. For soil materials, samples were dried and ground to be finer than 100 μm. The range of diffraction angle changes from 0° to 80°, taking approximately 30 minutes for testing each sample. Bruker D8 Discovery XRD was used for the test, and its testing configuration was added to Profex software for analysis after testing (see Figure

3.53). Intensity peaks of a compound can be selected from the crystallography open database (crystallography.net), which is emerged in the software through the import-structure-file function. A few coding lines in structure files can be modified for optimising the process of fitting data in XRD analysis, as shown in Figure 3.33 (Doebelin & Kleeberg, 2015). Details of the testing program for XRD analysis is summarised in Table 3.19.

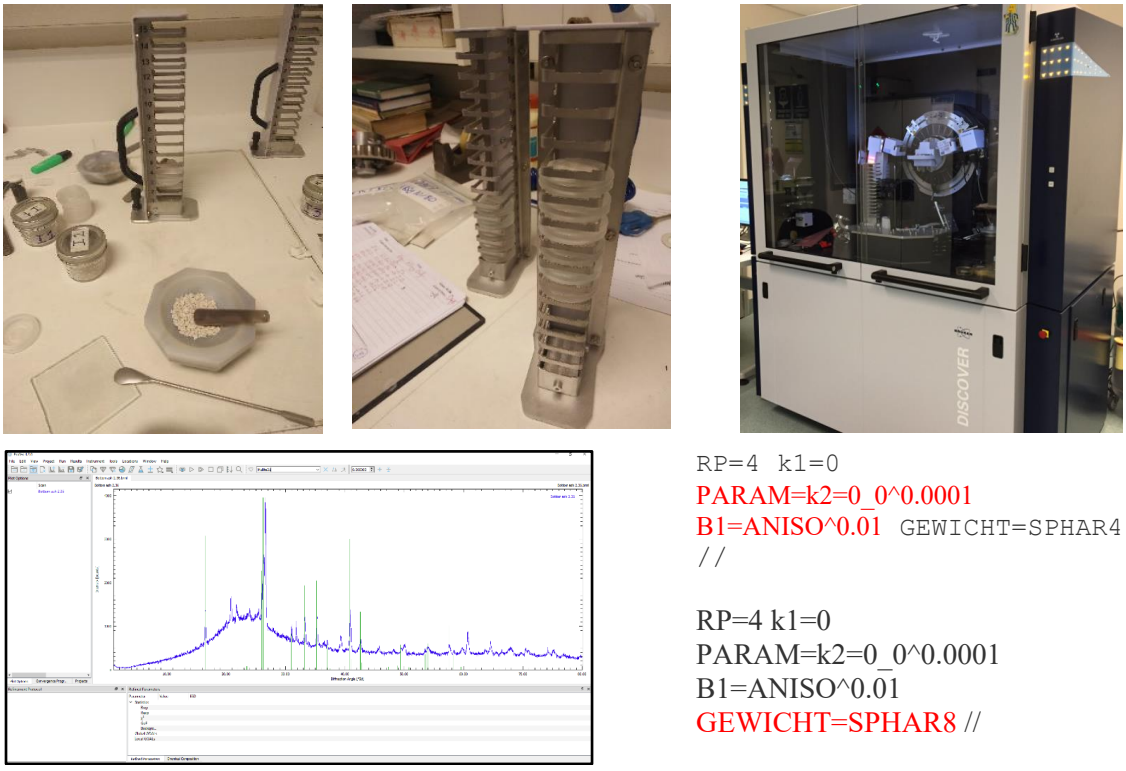


*Figure 3.53 Equipment and analysis codes in software for X-ray diffraction test*

*Table 3.19 Testing program for X-ray diffraction tests*

| Soil: % | Lime: % | Bottom ash: % | Bagasse ash: % (*mm*) | Curing time (days) | Number of tests |
|---|---|---|---|---|---|
| 100 | 0 | 0 | 0 | 0 | 3 |
| 0 | 5 | 0 | 0 | 0 | 1 |
| 0 | 0 | 100 | 0 | 0 | 1 |
| 0 | 0 | 0 | 100 (*0.425, 0.150, 0.075*) | 0 | 4 |
| 100 | 5 | 0 | 0 | 7 | 2 |
| 95, 90, 85, 80, 75, 70, 65, 60 | 5 | 5, 10, 15, 20, 25, 30, 35, 40 | 0 | 7 | 16 |
| **Total** | | | | | **27** |

### *3.4.4.2 Microscopic imaging*

Microscopic imaging can be employed to take proper and colourful photographs of a sample with a medium magnification (e.g., 30 times). The test requires a digital single-lens reflex camera (Canon D70) to capture the picture in a close focus. In addition, a tripod stabilises the camera to gain a clear and super-high resolution of sample images, as shown in Figure 3.54.

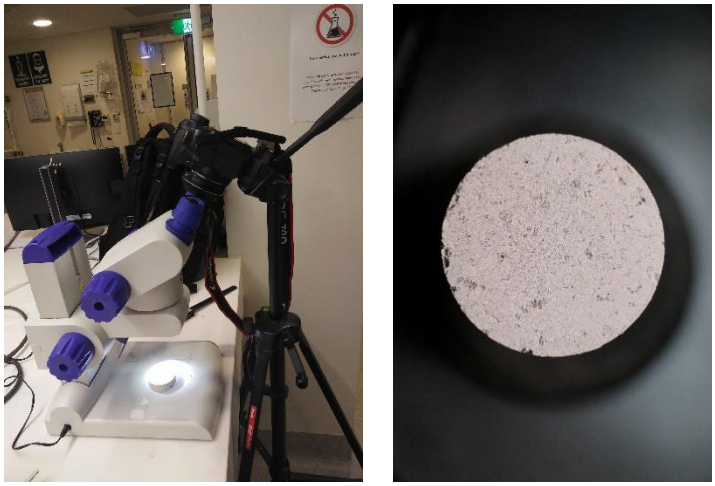

*Figure 3.54 Microscopic imaging test device*

### *3.4.4.3 Scanning electron microscope (SEM) and Energy dispersive X-ray spectroscopy (EDX) analysis*

The SEM and EDX procedure followed the instruction from Myscope, Microscopy training (Microscopy Australia, 2020), as the recommendation of the Micro-structural Analysis Unit at University of Technology Sydney, Australia. The tests were performed on samples coated with an Au-Pd layer to increase the image resolution. The working distances for Zeiss EVO and Supra are 10 and 5mm respectively. While Zeiss EVO has an advantage of overall EDX analysis on sample, Supra one assists to focus on EDX spectrum on a specific location or interest site (Figure 3.55). For super-high resolution (up to 100,000-time magnification), EVO Supra was used most of the time, more preferable than Zeiss EVO because the latter limited the acceptable image resolution within only 2000-time zooming. When Zeiss EVO EDX is conducted, the gun voltage increases to 15 kV, the fine function was enabled, and I Probe decreases to 250 nA. In EVO Supra, the site interest was selected by clicking on its location in a few nanometres and EDX analysis time for approximately 90 seconds. There were also multiple selections available in the program. Finally, in data analysis, the recognition of Au and Pd was disregarded from the EDX spectrum to reveal other elements existing on the sample image (see Figure 3.55).

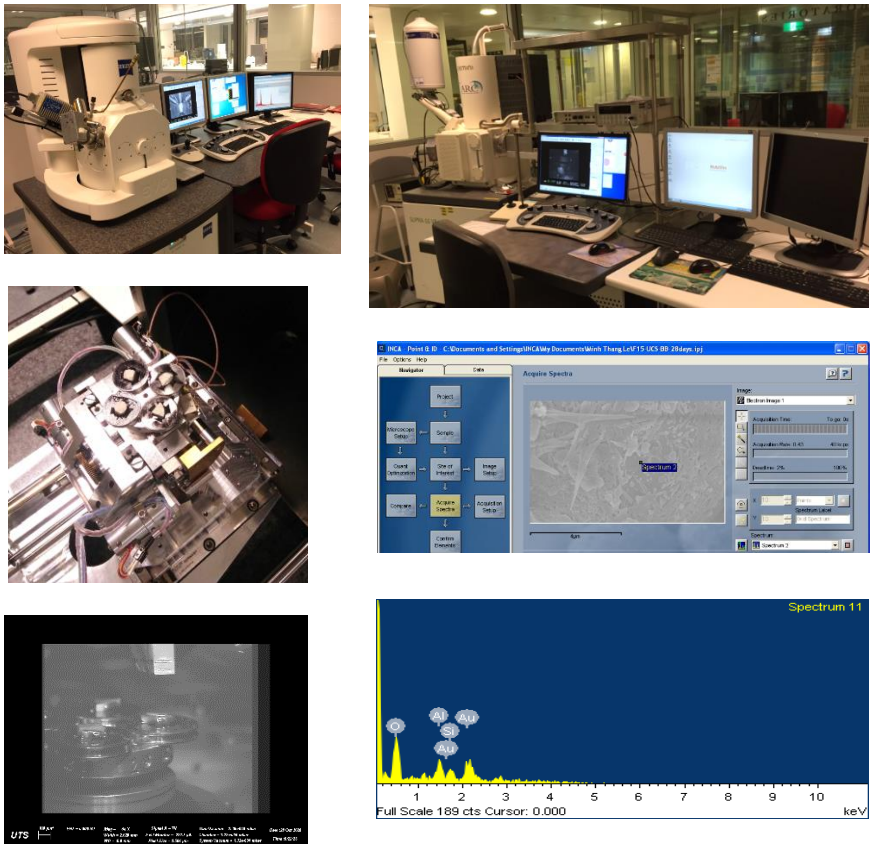


*Figure 3.55 SEM and EDX tests on Zeiss EVO LS15 SEM (LHS) and Zeiss Supra 55VVP SEM (RHS)*

## 3.5 Experimental program for various types of mixing ratios

### 3.5.1 Introduction

This section has three subsections, including strength tests for soil samples with various ratios of mixing. Firstly, the unconfined compressive strength tests were performed for soil treated with bottom ash varied in content from 5 to 30% and 5% lime, which was based on the dry weight of soil (100%), named as S-ratio. In the second subsection, indirect tensile strength tests were conducted for two ratios: (1) 5% lime and bottom ash contents based on the dry mass of soil (S-ratio), and (2) 5% lime and bottom ash contents based on the total dry weight of treated soil (T-ratio). Finally, in the last subsection, UCS, California Bearing Ratio (CBR) and bender element tests were done with both soils treated by mixing in two kinds of ratios: (1) 5% lime and bottom ash based on the total dry weight of treated soil (T-ratio), and (2) 5% lime and bottom ash based on the total dry weight of soil and bottom ash (SB-ratio). The flow chart of testing structure is shown in Figure 3.56, indicating that the bender element and matric suction test were performed for treated soil with SB-ratio. SEM tests were also utilized to explain the strength behaviour of

treated soil and its correlations with electrical conductivity results. The testing results are shown in Section 5.2 of Chapter 5.

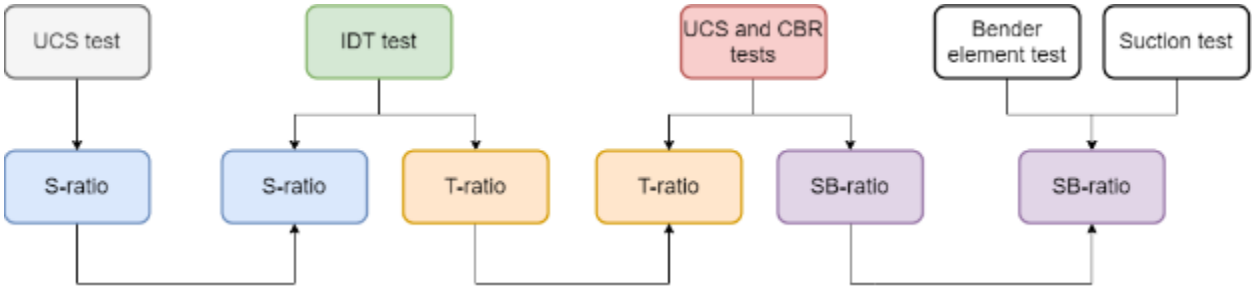


*Figure 3.56. A flow chart to present the testing structure and ratios for comparison*

### 3.5.2 Mixing ratio based on dry mass of soil (S-ratio in UCS tests)

In this investigation, the additive contents in the admixture were attained by the ratio of their dry weight to the dry weight of soil for UCS tests, herein denoted as S-ratio. Artificial expansive soil with particles smaller than 2.36 mm was prepared to be mixed with bottom ash or hydrated lime in the percentage by the dry weight of soil, as shown in Table 3.20. The density of S-ratio samples is similar to that of T-ratio samples.

*Table 3.20 UCS mixture ratios based on dry mass of soil (S-ratio)*

| Mix No. | Bottom ash (%) | Hydrated lime (%) | Soil (%) |
|---|---|---|---|
| S0x | 0 | 0 | 100 |
| S5x | 5 | 0 | 100 |
| S10x | 10 | 0 | 100 |
| S20x | 20 | 0 | 100 |
| S30x | 30 | 0 | 100 |
| S0 | 0 | 5 | 100 |
| S5 | 5 | 5 | 100 |
| S10 | 10 | 5 | 100 |
| S20 | 20 | 5 | 100 |
| S30 | 30 | 5 | 100 |

### 3.5.3 Mixing ratio based on total dry weight (T-ratio in ITS tests)

In ITS samples, the additive contents in each admixture were determined by the ratio of their dry weight to either the dry weight of only soil (S-ratio) or the total dry weight of entire mixture (T-ratio). To eliminate the unburnt and coarse-sized particles, the bottom ash smaller than sand size (2.36 mm) was gathered to mix with hydrated lime and artificial expansive soil in the two kinds of ratios shown in Table 3.21.

*Table 3.21 Mixture ratios for ITS tests*

| S-ratio | | | | T-ratio | | | |
|---|---|---|---|---|---|---|---|
| **Mix No.** | **BA (%)** | **L (%)** | **Soil (%)** | **Mix No.** | **BA (%)** | **L (%)** | **Soil (%)** |
| S0 | 0 | 5 | 100 | T0 | 0 | 5 | 95 |
| S5 | 5 | 5 | 100 | T5 | 5 | 5 | 90 |
| S10 | 10 | 5 | 100 | T10 | 10 | 5 | 85 |
| S20 | 20 | 5 | 100 | T20 | 20 | 5 | 75 |
| S30 | 30 | 5 | 100 | T30 | 30 | 5 | 65 |

*Note: S-ratio: ratio based on dry weight of soil, T-ratio: ratio based on total dry weight of mixture*

### 3.5.4 Mixing ratio based on dry weight of soil and bottom ash (SB-ratio in UCS and CBR tests)

In this section, the mechanical tests include unconfined compressive strength (UCS), California bearing ratio (CBR), bender element (BE) and matric suction tests. For testing samples, the ratios of components were determined based on the dry weight of soil and ash (denoted SB ratio). The details of tests with SB-ratio in comparison with T-ratio are shown in Table 3.22.

*Table 3.22 SB ratios for mechanical tests*

| Total ratio (T-ratio) | | | | Soil-bottom-ash ratio (SB-ratio) | | | |
|---|---|---|---|---|---|---|---|
| UCS, CBR test | | | | UCS, CBR, BE and Suction test* | | | |
| **Sample** | **Bottom ash (%)** | **Lime (%)** | **Soil (%)** | **Sample** | **Bottom ash (%)** | **Lime (%)** | **Soil (%)** |
| T0 | 0 | 5 | 95 | S0 | 0 | 5 | 100 |
| T5 | 5 | 5 | 90 | SB5 | 5 | 5 | 95 |
| T10 | 10 | 5 | 85 | SB10 | 10 | 5 | 90 |
| T20 | 20 | 5 | 75 | SB15 | 15 | 5 | 85 |
| T25 | 25 | 5 | 70 | SB20 | 20 | 5 | 80 |
| T30 | 30 | 5 | 65 | SB25 | 25 | 5 | 75 |
| T40 | 40 | 5 | 55 | SB30 | 30 | 5 | 70 |
| - | - | - | - | SB40 | 40 | 5 | 60 |

(*): Only SB0 and SB25 are used for BE and suction tests

For mechanical experiments, two methods of sample compaction (i.e., dynamic and static compaction) were utilised to investigate their impacts on the optimal content of bottom ash. In UCS and CBR samples, dynamic compaction was applied while bender element and suction samples were compacted in a static way. In studied tests, samples with the maximum soil aggregate size of 2.36 mm were experimented. Figure 3.57 shows the flow chart of the mechanical tests with total and soil-ash mixing ratios.

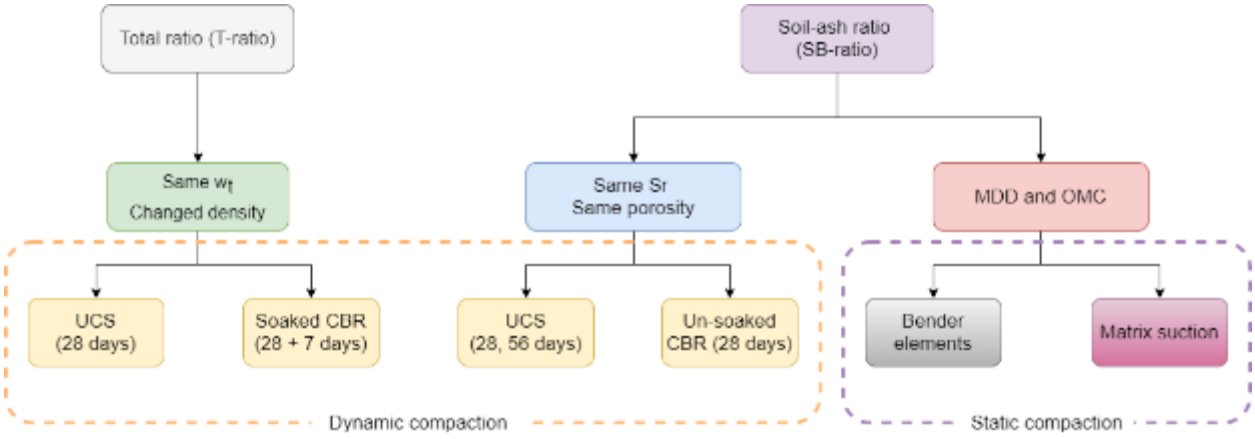


*Figure 3.57 Flowchart for ratio designation*

In this testing program, the authors aim to compare the effects of two mixing ratios on soil strength, including total ratio and soil-ash ratio, denoted as T-ratio and SB-ratio, respectively. Compared to T-ratio, SB-ratio reflects the same mixing ratio in conductivity tests (see Table 3.22). However, mixing density and moisture is different between the ratios. While the optimum moisture content of lime-treated soil (i.e., 28.5%) was used for samples with T-ratio, various moistures were applied in UCS and CBR tests for specimens with SB-ratio (refer to Figure 3.58). The moisture variation for SB-ratio samples was calculated from the assumption that they have the same value of saturation level ($S_r$) and porosity ($n$), which are equal to $S_r$ and $n$ of lime-treated soil at its optimal compaction, accounting for 0.73% and 0.51, respectively (refer to Figure 3.59). For bender element and matric suction tests, only S0 and SB25 samples were tested, producing their small-strain shear modulus ($G_{max}$) and matric suction. For these tests, the samples were compacted at their optimal moisture content (*OMC*) and maximum dry density (*MDD*), as shown in Figure 3.59. In addition to sample SB25 compacted at *MDD* and *OMC*, an additional sample was also constituted at *MDD* but with moisture higher than *OMC* to gain a high saturation level ($S_r = 0.95$). In other words, the sample was compacted at its wet side of *OMC*. This wet-side static compaction was employed to investigate the effect of saturation condition on the changes of $G_{max}$ in the sample SB25.

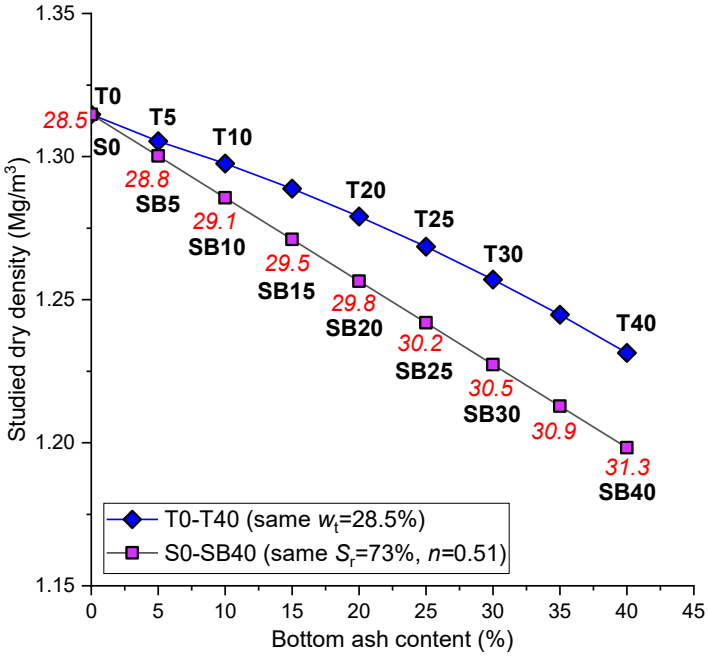


*Figure 3.58. Dry density and moisture content of samples with T-ratio and SB-ratio (the corresponding water contents in red numbers given for samples S0-SB40)*

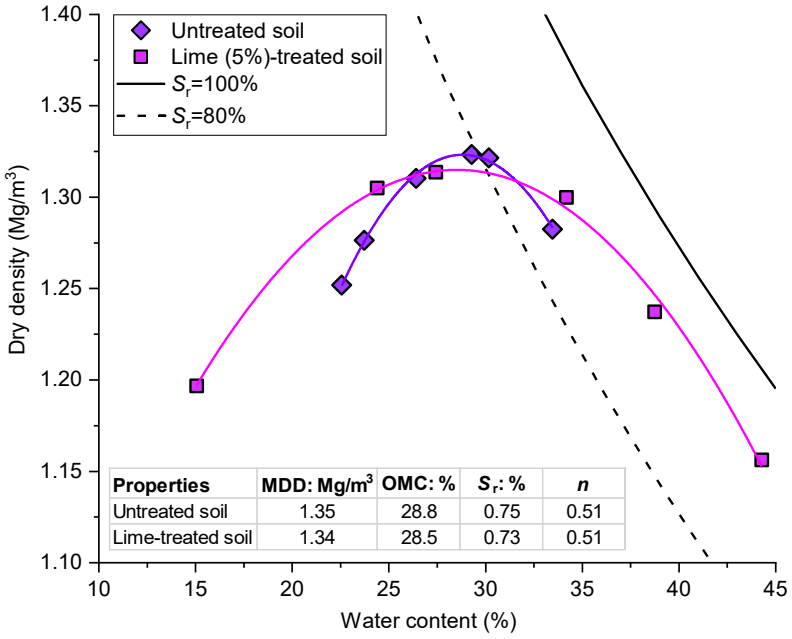


*Figure 3.59. Standard Proctor compaction curves for soil and lime-treated soil*

### 3.5.5 Experimental program for shrinkage-swelling behaviour of bottom-ash-lime-treated soils in relationship with electrical conductivity

This program aims to propose a testing method and analysis to establish a correlation between the shrinkage-swelling rate of lime-ash treated expansive soils and their electrical conductivities. To make the test analysis simple, curing time effects on results are limited. Hence, the time for

incubation of samples was restricted from 1 hour to 7 days. The tests were conducted on a mixture of bentonite, kaolinite and sand, having a high potential of shrinkage and swelling to mimic the behaviour of expansive soils. The studied soil was then treated with hydrated lime (5%) and bottom ash in a variable content from 5% to 40% in three experiments, namely electrical conductivity, linear shrinkage and free swelling test. The relationships between shrinkage/swelling deformation and the initial loss of electrical conductivity were proposed based on the procedure suggested by Paya et al. (2001) for lime-ash mixtures. X-ray diffraction (XRD) tests and Scanning Electron Microscopy (SEM) were used to analyse the chemical and microstructure changes in specimens. Discussion on the results is also provided in Chapter 5.

The test program comprises of two main tests: electrical conductivity (EC) test and shrinkage-swelling tests. For all tests, lime content was fixed at 5%. Bottom ash content in dry mass was chosen at 0, 5, 10, 15, 20, 25, 30, 35, and 40%. In EC tests, Test B with Subtests B1 and B2 was performed for each content. Each soil-ash mix test is completed with one sand-ash mix test (Subtest B2) for correction (see Figure 3.36). Shrinkage-swelling tests consist of two tests: linear shrinkage (LS) test and free-swelling consolidation test. For the linear shrinkage test, an amount of soil sample (250 g) mixed with bottom ash and lime was sieved at 425 µm at dry state prior to being mixed with water to obtain slurry having water content equal to the liquid limit. The sample preparation follows the AS standards 1289 for liquid limit and linear shrinkage test (AS 1289.3.4.1, 2008; AS 1289.3.9.1, 2015). Liquid limits were determined for soils treated by hydrated lime and bottom ash, so the fall cone method was utilised to define the liquid limits at the penetration of 20 mm. Mixed samples were prepared at these limits in plastic bags for at least 24 h for moisture homogenisation. They were then mixed, overfilled in LS mould, tapped and levelled off the excess material. The LS samples were cured for 7 days before air-dried at room temperature of 25°C for 1 day, and oven-dried at 105°C for the next days. Finally, the shrinking length of the dry specimens was measured, and soil samples were used for XRD and SEM analysis.

For swelling consolidation tests, the apparatus is the same as the conventional oedometer with a fixed ring, 20 mm in height and 50 mm in diameter. The initial height of the sample was equal to 15 mm. All specimens were statically compacted to the same degree of saturation ($S_r$ =0.73) and porosity ($n$ =0.51) to those of lime-treated soil sample (without bottom ash) at its maximum dry density and optimum moisture content (see Figure 3.59). The corresponding dry density and water content, depending on the bottom ash content, are shown in Table 3.23, similar to those of samples S0-SB40 indicated in Figure 3.58. One hour after static compaction, samples were inserted inside the oedometer cell. For free swelling test, only a seating load of 6 kPa was required. Swelling

displacement was allowed for 24 hours. After swelling tests were completed, the sample was dismounted to check final displacements, and then put in the oven to measure moisture content. Finally, the dry swell specimens were collected for XRD or SEM analysis.

*Table 3.23 Swelling-consolidation testing program*

| Sample | Swelling-consolidation tests | | | |
|---|---|---|---|---|
| | Soil content: % | Bottom ash content: % | Density: Mg/m$^3$ | Water content: % |
| BO0 | 100 | 0 | 1.32 | 28.5 |
| BO5 | 95 | 5 | 1.30 | 28.8 |
| BO10 | 90 | 10 | 1.29 | 29.1 |
| BO15 | 85 | 15 | 1.27 | 29.5 |
| BO20 | 80 | 20 | 1.26 | 29.8 |
| BO25 | 75 | 25 | 1.24 | 30.2 |
| BO30 | 70 | 30 | 1.23 | 30.5 |
| BO35 | 65 | 35 | 1.21 | 30.9 |
| BO40 | 60 | 40 | 1.20 | 31.3 |

### 3.5.6 Experimental program for behaviour of bagasse-ash-lime-treated soils in relationship with electrical conductivity

There are two types of tests in the testing program: (1) electrical conductivity test and (2) mechanical experiments, namely linear shrinkage, unconfined compressive strength (UCS) and bender element (BE) test. In EC tests, the total dry weight of bagasse ash and expansive soil is 6.4 g while lime weight is 0.32 g, indicating the ratio of a total ash-soil mix (100%) to lime (5%). The bagasse ash content was varied from 5% to 30%, equivalent to 95% down to 70% in soil content. The detailed conductivity test program is shown in Table 3.24.

*Table 3.24 Electrical conductivity testing program*

| Sample | Lime (%) | Soil (%) | Bagasse ash 425, 150, 75 µm: % |
|---|---|---|---|
| BA0 | 5 | 100 | 0 |
| BA5 | 5 | 95 | 5 |
| BA10 | 5 | 90 | 10 |
| BA15 | 5 | 85 | 15 |
| BA20 | 5 | 80 | 20 |
| BA25 | 5 | 75 | 25 |
| BA30 | 5 | 70 | 30 |

For mechanical experiments, three standard tests to measure soil strength were performed, namely linear shrinkage (LS), unconfined compressive strength (UCS), and bender element (BE) test. Prior to the linear shrinkage test, about 250 g of soil was mixed with lime and bagasse ash in different ash sizes, which were then sieved under the sieve of 425 µm at dry state for liquid limit determination. Adhering to Australian Standards for liquid limit and linear shrinkage test (AS 1289.3.4.1, 2008; AS 1289.3.9.1, 2015), the fall cone test was employed to find the water content

at the cone penetration of 20 mm into a cup. Tested samples at the determined limits were cured in plastic bags for moisture homogeneity in 24 hours. After that, they were mixed thoroughly, overfilled in long mounds of LS tests, tapped to remove air voids and levelled off the excess slurry. The mould samples were wrapped with plastic covering and cured for 7 days before dried in room (25°C and 50% in humidity) for 1 day and then oven-dried at 105°C next day. The test was triplicated in three samples, which were measured to generate the average *LS* value.

For UCS tests, soil samples were compacted dynamically in three layers at *MDD* and *OMC*. These compaction properties of ash-lime treated soils were defined at 15% bagasse ash against 5% hydrated lime. The ash-lime ratio of 3 to 1 is based on previous studies proving that this optimal proportion can help achieve the highest strength of expansive soil treated with hydrated lime and bagasse ash (Dang, 2018; Hasan, 2019). However, unlike UCS samples, all bender element samples were compacted statically at the strain rate of 1%/min. They were also covered by paraffin layers to prevent water loss whenever BE tests were executed at a certain point of time during long-term curing duration. The S+P method was utilised to find out the travelling time through studied samples. The method relies on the arrival time of P wave, corresponding to the arrival time of S wave (Wang et al., 2017a). Following this method, the period of 0.05 millisecond, equivalent to 20 kHz, was chosen to measure velocity and finally the small-strain shear modulus ($G_{max}$). The testing program of mechanical tests for bagasse-ash-lime-treated soils is described in Table 3.25.

*Table 3.25 Mechanical testing program*

| **Linear shrinkage** | | **Unconfined compressive test** | | **Bender element test** | |
|---|---|---|---|---|---|
| **Sample** | **Curing time: day** | **Sample** | **Curing time: day** | **Sample** | **Curing time: days** |
| Soil | 3 | Soil | 3 | Soil | 0-120 |
| SL | 7 | SL | 7, 28, 56 | SL | 0-120 |
| BA425 | 7 | BA425 | 7, 28, 56 | BA425 | 0-120 |
| BA150 | 7 | BA150 | 7, 28, 56 | BA150 | 0-120 |
| BA75 | 7 | BA75 | 7, 28, 56 | BA75 | 0-120 |

## 3.6 Summary

This chapter provides an overview of materials, testing procedures, techniques for sample preparation, and experimental methods. For studied materials, there are four main elements researched, namely artificial soil, hydrated lime, bottom ash and bagasse ash. For the studied soil, it is the combination of kaolinite, bentonite and fine sand. Each basic material was investigated in terms of physical and geotechnical properties for their combination. When the elements are combined, it produces five kinds of treated soil sample, including lime-treated soil, bottom-ash-treated soil, bottom-ash-lime-treated soil, bagasse-ash-lime-treated soil, and bottom-bagasse ash-lime treated soil. Therefore, a comprehensive testing program was built to study these materials.

Based on the research objectives, the experimental program was developed into three mains categories, namely electrical, physical & mechanical and micro-structural analysis test. Particularly, the electrical conductivity test in the electrical group is further developed with three kinds of test (Test A, B and C), corresponding to each combination of soil and lime with bottom ash and bagasse ash. The tests of electrical conductivity assist in determining the optimal ratios of combining chemical agents. They were supported by a systematic structure of investigating tests with mixing designation, starting from treating soil with various contents of lime, then combining them with bottom ash and bagasse ash in various sizes. Therefore, the study program is expected to reveal complex characteristics of expansive soil treated by hydrated lime, bottom ash and bagasse ash.

# CHAPTER 4

# Characterisation of Expansive Soils Treated with Hydrated Lime

## 4.1 Introduction

Expansive soil in this study is a constitutive sample, including Q38 kaolinite, Active Bond 23 bentonite and Sydney fine sand. Before studying the change of its characterisation when treated with hydrated lime, bottom ash and bagasse ash, a thorough investigation of its own characteristics is important to clarify its electrical, physical, mechanical and micro-structural behaviours. Following the materials and methods explained in Chapter 3, this chapter firstly presents the tests capturing the chemical aspects of soil samples, such as *pH*, electrical conductivity and X-ray diffraction, to find out the *pH* level, the conductivity parameter and the composition of studied soil, respectively. Each component, namely kaolinite, bentonite and sand, are researched in terms of electrical conductivity, including its relationship with the concentration, the thermoelectric coefficient, and the loss in conductivity. The composition of soil material was finally revealed through the X-ray diffraction test, in which minerals of soil components could be found out to explain the outcomes from the electrical conductivity and pH tests. After demonstrating the electrical experimental results, the physical and mechanical test results of untreated soil are provided to study the geotechnical characteristics of soils. The significant improvement in relevant

features of soil treated with hydrated lime is also emphasized to bring further evidence regarding the effectiveness of binder in the stabilisation of expansive soil. Many test results on untreated and lime treated soils, including micro-structural analysis, are also presented in this chapter.

## 4.2 Chemical properties of soil materials untreated and treated with hydrated lime

### 4.2.1 pH tests of soil and lime

Figure 4.1 shows the change in *pH* level of soil samples treated with various content of hydrated lime from 0% to 7%. As can be seen in this figure, the studied soil has a high *pH* value of around 10. This is attributed to the fact that the soil contains Na-bentonite, which increases the soil pH up to 10 (Kaufhold et al., 2008). In the employed bentonite, montmorillonite is the major mineral contributing to this value because of sodium and calcium ions. Referring to clay mineral chemistry, the formula of montmorillonite mineral is $(Na, Ca)_{0.3}(Al, Mg)_2Si_4O_{10}(OH)_2 \cdot nH_2O$ (Mineral Data Publishing, 2001). When added with an increasing content of hydrated lime [$Ca(OH)_2$], hydrate ion $(OH)^-$ gradually increases the pH in the soil-lime mixture, while a majority of calcium ion takes part in chemical reactions with soil minerals. The *pH* value in lime-soil suspension stabilizes around 13 at 4% and 5% in lime content but increases slightly over 13 when lime percentage goes up to 6% and 7%. These *pH* value are higher than one in a saturated lime solution, which is 12.3 at 8% hydrated lime or 2 g in 100 mL solution (ASTM D6276, 2019). According to this standard, the percentage of lime should be selected where the average pH change for three successive test samples is not more than 0.04. Therefore, the lime content of 5% was chosen. Furthermore, at this content, the range of pH change with curing time is small, compared to that at 4% hydrated lime. One hour is also a sufficient curing time for studied mixtures to obtain the final pH values.

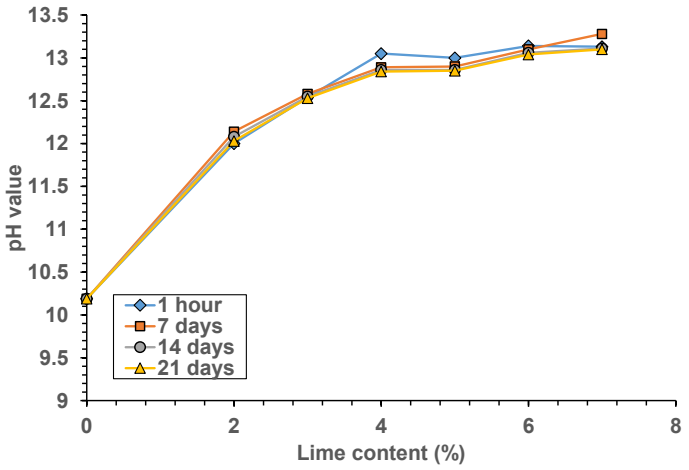


*Figure 4.1. Change in pH of soils treated with lime in various contents and curing days*

### 4.2.2 Electrical conductivity of bentonite solution

In addition to pH tests to estimate the lime-soil proportion requirement for soil stabilisation, it is feasible to use the electrical conductivity method to evaluate this ratio. The method was suggested by Abu-Hassanein et al. (1996), initially developed for bentonite solution, to determine the concentration of bentonite in its blend with sand. Later on, Castelbaum et al. (2010) adapted this method to propose an advanced procedure to prepare slurry mixed soils. Both changes in electrical conductivity (*EC*) with bentonite concentration from these two studies were compared with the studied bentonite, which are shown in Figure 4.2. Referring to this figure, it is clear that the studied bentonite Active Bond 35 has *EC* evolution similar to that in the study conducted by Castelbaum et al. (2010) on two kinds of natural bentonite samples. This indicates that the *EC* property of bentonite used in this study is close to that of natural soil, which is more electrically conducting than the material used by Abu-Hassanein et al. (1996).

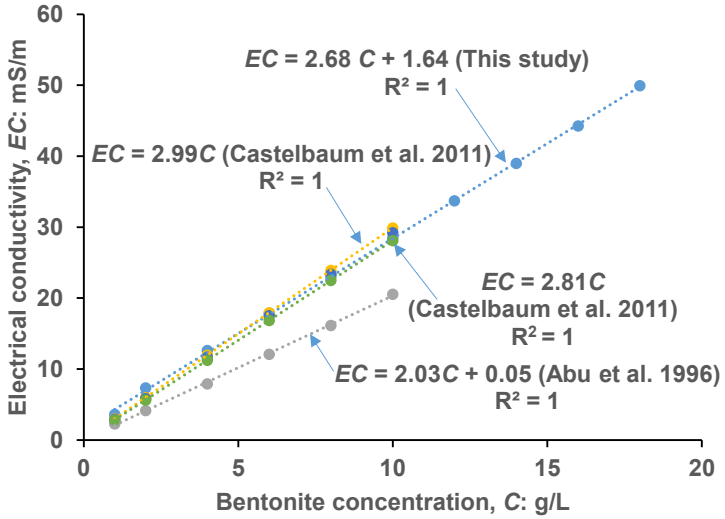


*Figure 4.2. Change of electrical conductivity with bentonite concentration (Note: intercept of EC in the study conducted by Castelbaum et al. (2010) was modified to zero)*

### 4.2.3 Electrical conductivity of bentonite-kaolinite mixtures

The inclusion of kaolinite to bentonite slurry changes the electrical conductivity property. Figure 4.3 shows the comparison of *EC* between bentonite-kaolinite suspension and pure bentonite solution. It is noted that the addition of kaolinite to aqueous bentonite solution increased the *EC* of the mixture because kaolinite contains a proportion of $OH^-$ ions on the basal surfaces of the mineral (Ma & Eggleton, 1999). However, the increase in *EC* caused by kaolinite is smaller than that produced by only bentonite. Although the proportion of kaolinite is higher than bentonite in the mixture, 65% compared to 30%, as shown in Figure 4.3. This can be attributed to the fact that the surface charge of kaolinite in aqueous suspension is lower than that of montmorillonite in

bentonite (Tombácz & Szekeres, 2006). This difference reduces the capacity of increasing *EC* when more kaolinite replaces bentonite in their blend. As a result, the mixture of bentonite and kaolinite has an *EC* increase of only 31% [= (3.51-2.68)/2.68 × 100], while adding bentonite to gain the same bentonite concentration increases *EC* by 117% [= (65/30 × 2.68 – 2.68)/2.68 × 100]. This means that kaolinite inclusion limits the *EC* increase due to bentonite by 86% (=117% - 31%) or decreases the bentonite solution conductance by about one-fourth (31%/117% × 100 = 26%).

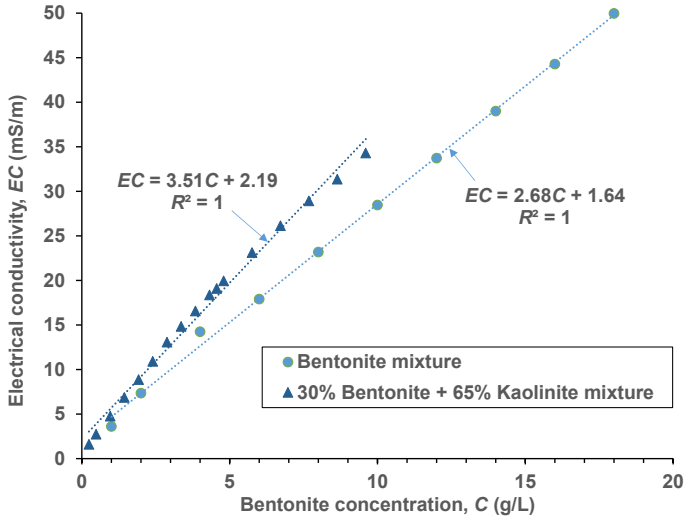


*Figure 4.3. EC change of bentonite-kaolinite mixture with various content of bentonite*

### 4.2.4 Electrical conductivity of KBS soil (bentonite – kaolinite – sand mixture)

As a final jigsaw piece for the studied KBS soil, fine sand is added to the kaolinite-bentonite suspension to investigate the *EC* change of the mixture. As can be seen in Figure 4.4, the *EC* value is expressed in a linear relationship with temperature when it increases from 25°C to about 45°C. It is obvious that the inclusion of 5% sand to bentonite-kaolinite slurry did not change the final *EC* even when the solution temperature alters in the wide range from 25°C to over 40°C. The results are in good agreement with the study conducted by Abu-Hassanein et al. (1996). It is worth mentioning that sand is made of quartz as a crystalline silicate mineral, which is known as an inert material. Sand inclusion in soil suspension, therefore, did not significantly contribute to *EC* increase. However, increasing temperature may build up *EC* marginally due to the minimal dissipation of soluble salts on sand caused by heat (Paya et al., 2001). As a result, the slope of KBS soil is slightly higher than that of bentonite-kaolinite slurry (i.e., 0.05 as against 0.04).

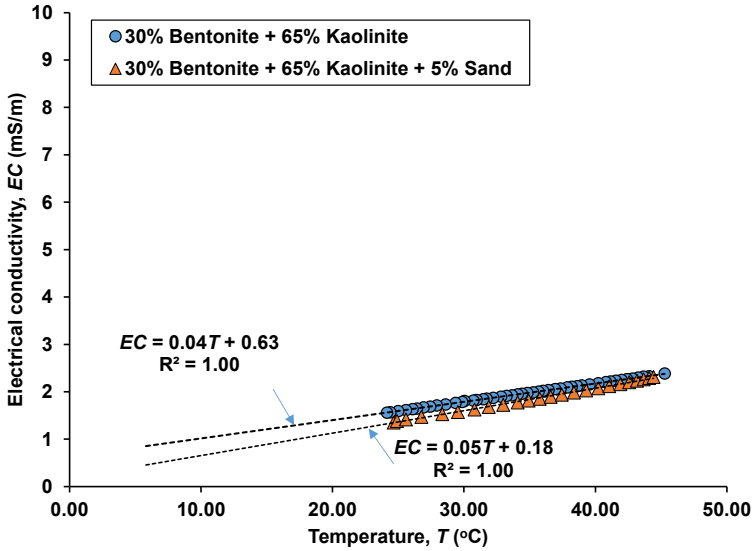


*Figure 4.4 Change of EC with temperature of bentonite-kaolinite and soil mixtures (KBS) at bentonite concentration of 0.24 g/L*

### 4.2.5 Change in thermoelectric coefficient of studied soil components

Due to the major dependence of *EC* to testing temperature, it is necessary to research changes in *EC* with thermal parameters for the studied soil solutions. Similar to the EC procedure, many tests were conducted on soil elements made of bentonite, bentonite-kaolinite and bentonite-kaolinite-sand mixtures. The thermal coefficient determination can be performed on these combinations in this order to find the relationship between the thermoelectric coefficient and *EC*.

Bentonite suspension

Figure 4.5 illustrates the temperature trend of *EC* with different concentrations of bentonite. It is apparent that increasing bentonite content can increase the growth rate of *EC* with temperature. For example, when the concentration of bentonite went up from 1 g/L to 4 g/L, the *EC* rate with temperature (thermoelectric coefficient) put up from 0.12 to 0.51, an increase by 4.25 times, as illustrated in Figure 4.5. Further increase in bentonite amount from 4 g/L to 18 g/L changed the rate from 0.51 to 1.24, which is only an over-double growth. However, to express the change in *EC* with temperature and concentration, a temperature compensation coefficient ($T_c$) was used. The coefficient was calculated by dividing the thermoelectric coefficient (indicated as slopes in Figure 4. 5) to the *EC* value at 25°C of the sample with a corresponding concentration (Abu-Hassanein et al., 1996). In other words, this coefficient is used to covert *EC* at a temperature that is different from 25°C into its value at room temperature. In most cases, the coefficient is a constant with the variation of material concentration. For the studied bentonite Active Bond 35, this coefficient is about 2.96, as the average value shown in Figure 4.6.

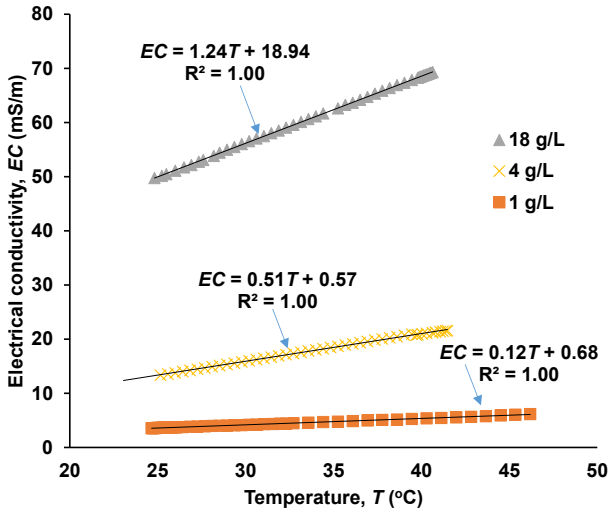


*Figure 4.5. EC change with temperature in bentonite suspension with various bentonite concentrations from 1 to 18 g/L*

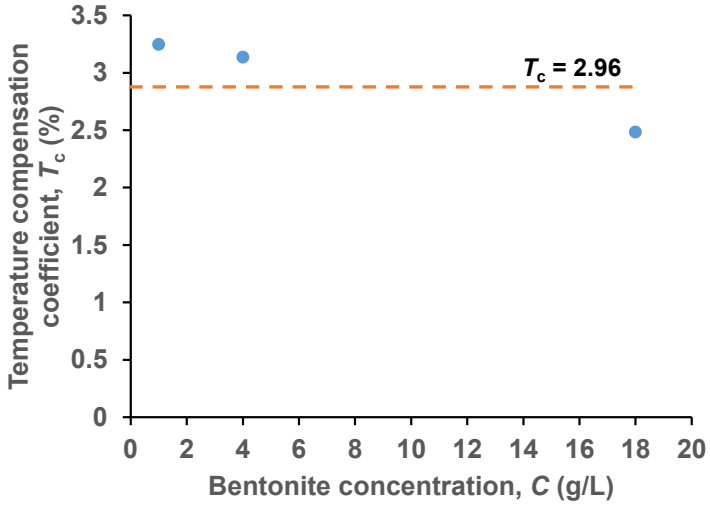


*Figure 4.6. Change of temperature compensation coefficient with concentrations of studied bentonite*

Bentonite – kaolinite suspension

Figure 4.7 depicts the change in *EC* with the various contents of bentonite in its mixture with kaolinite. When the bentonite concentration increased from 0.24 g/L to 9.6 g/L, the thermoelectric coefficient went up from 0.04 to 0.85 mS/m.°C. Compared to bentonite suspension in Figure 4.5, the coefficient in bentonite-kaolinite suspension was decelerated. This can be observed by looking at the bentonite concentration of 4.8 g/L in Figure 4.7, which has a thermoelectric coefficient of 0.51, equalling to that obtained in bentonite slurry in Figure 4.5 but with a lower concentration (4 g/L). Consequently, the temperature compensation coefficient, $T_c$, of bentonite-kaolinite suspension reduced to 2.54%, as shown in Figure 4.8. The reduction of thermoelectric and temperature compensation coefficient due to the inclusion of kaolinite to bentonite slurry can be

explained by surface charge heterogeneity of kaolinite compared to montmorillonite in its aqueous suspension (Tombácz & Szekeres, 2006).

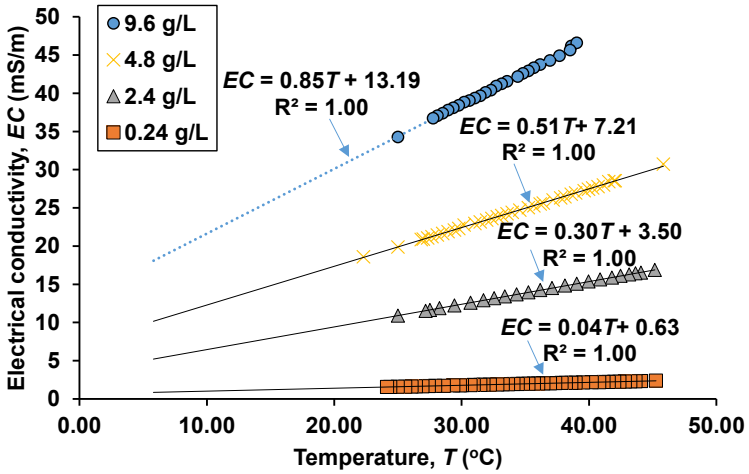


*Figure 4.7. EC change with temperature in the solution of 30% bentonite and 65% kaolinite with various bentonite concentrations from 0.24 g/L to 9.6 g/L*

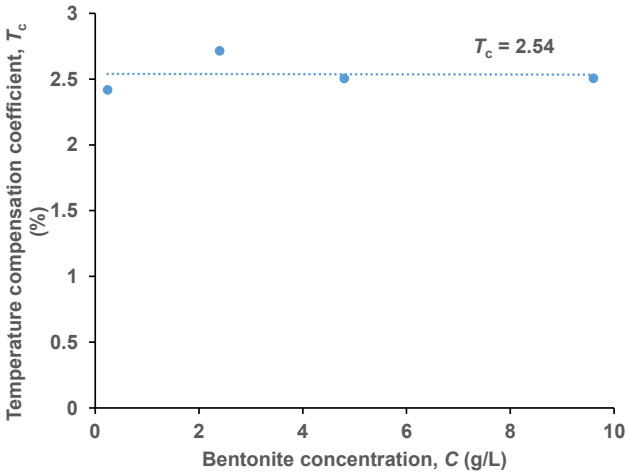


*Figure 4.8. Change of temperature compensation coefficient with concentration of 30% bentonite – 65% kaolinite in bentonite concentrations from 0.24 g/L to 9.6 g/L*

Bentonite – kaolinite –sand suspension

When sand with the content of 5% did not significantly change the *EC* property of its compound with 30% bentonite and 65% kaolinite (see Figure 4.9), lower proportions of bentonite, reducing the value of *EC*, can allow a more significant influence on *EC* from adding 5% sand to aqueous soil suspension. Figures 4.9 and 4.10 demonstrate the change in *EC*, caused by adding various contents of sand from 5% to 15% to bentonite-kaolinite slurry with only 2% and 4% bentonite. Referring to these figures, 5% sand still does not alter the *EC* of the clay slurry obviously, whereas sand content of 10% to 15% pushed the *EC* value up by about 2 (mS/m). As a result, adding 5% sand to the clay compound with a low or high bentonite content had no significant effect on *EC* of

soil. Likely, the temperature compensation coefficient $T_c$ of KBS soil is equal to that of 65%-kaolinite-30%-bentonite suspension, suggested by Abu-Hassanein et al. (1996). As a result, $T_c$ of KBS soil slurry is 2.54% (refer to Figure 4.8).

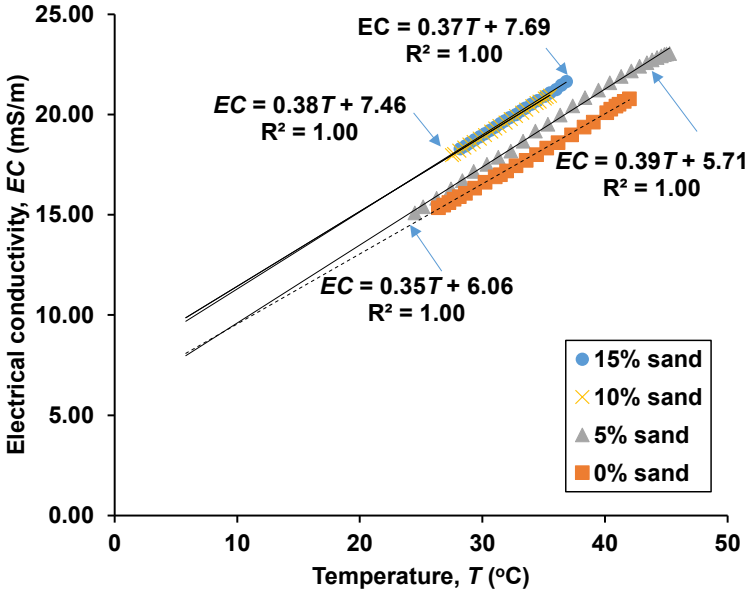


*Figure 4.9 Change of EC with temperature in 4% bentonite – 96% kaolinite with various sand contents from 0% to 15%*

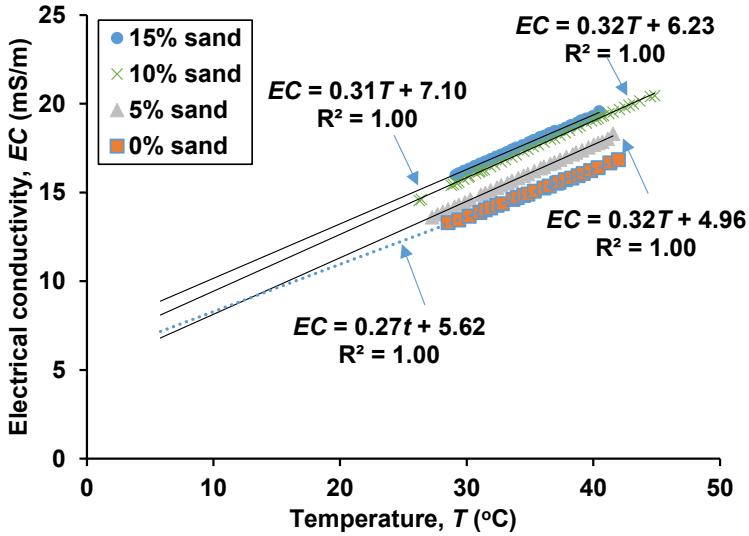


*Figure 4.10 Change of EC with temperature in 2% bentonite - 98% kaolinite with various sand content from 0% to 15%*

### 4.2.6 Electrical conductivity of lime solution

It is important to study the *EC* property of hydrated lime before combining soil suspension with the lime solution to understand their *EC*-related reactions. Figure 4.11 depicts the increase of *EC* in hydrated lime suspension when lime concentration gradually increases from 0 to 10 g/L. Compared to *EC* of hydrated lime suggested by Villar-Cociña et al. (2003), the studied lime

solution has a lower rate of *EC* with the concentration of lime. The *EC*-concentration rate is less than one-third of that in the study conducted by Villar-Cociña et al. (2003), 232.35 compared to 639.28 (mS.L/m.g), respectively. Remarkably, over 3 g/L hydrated lime, *EC* tends to increase steadily; even at 10 g/L lime, *EC* of around 800 mS/m is still lower than the maximum *EC* of around 1,000 mS/m at lower lime concentration of around 1.5 g/L from the previous study. The explanation comes from the impurity of the studied lime powder since the material contains an amount of calcite or calcium carbonate due to the reaction between hydrated lime and carbon dioxide. Considering the degradation effect of hydrated lime on soil stabilization, a lower range of *EC* under 600 mS/m corresponding to lime concentration from 0 to 2 g/L was investigated.

Figure 4.12 shows the upward trend of *EC* with temperature in various concentrations of hydrated lime from 0.1 g/L to 10 g/L. It is clear that the thermoelectric coefficient increases with the higher lime concentration. Over 1.6 g/L, the coefficient did not significantly increase even though the concentration surged to 8 g/L or 10 g/L. With high thermoelectric coefficient and *EC* values, the temperature compensation coefficient ($T_c$) is only around 1.68% (refer to Figure 4.13), which is much lower than that in soil solution at 2.54%, as shown in Figure 4.8.

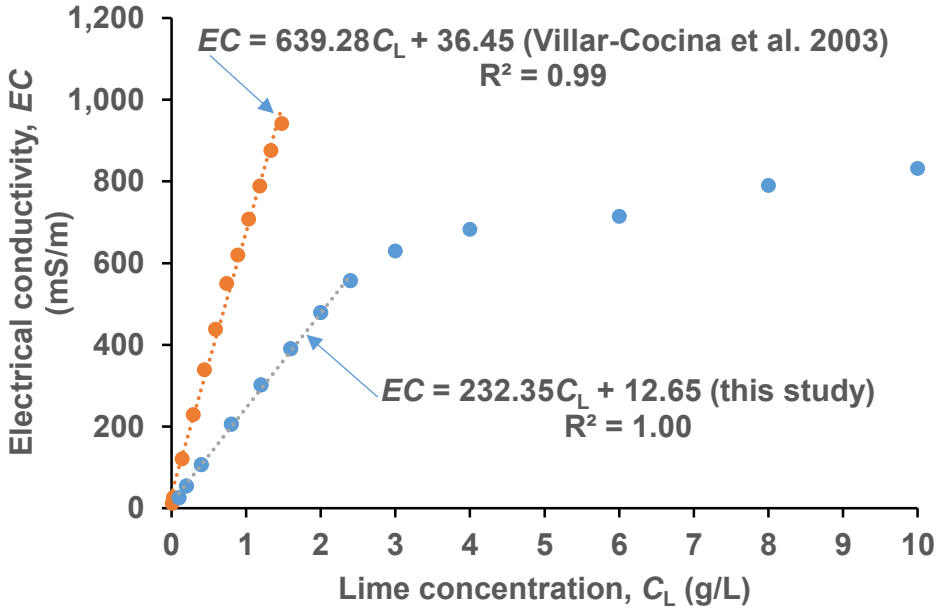


*Figure 4.11 Change in EC of lime solution with lime concentration*

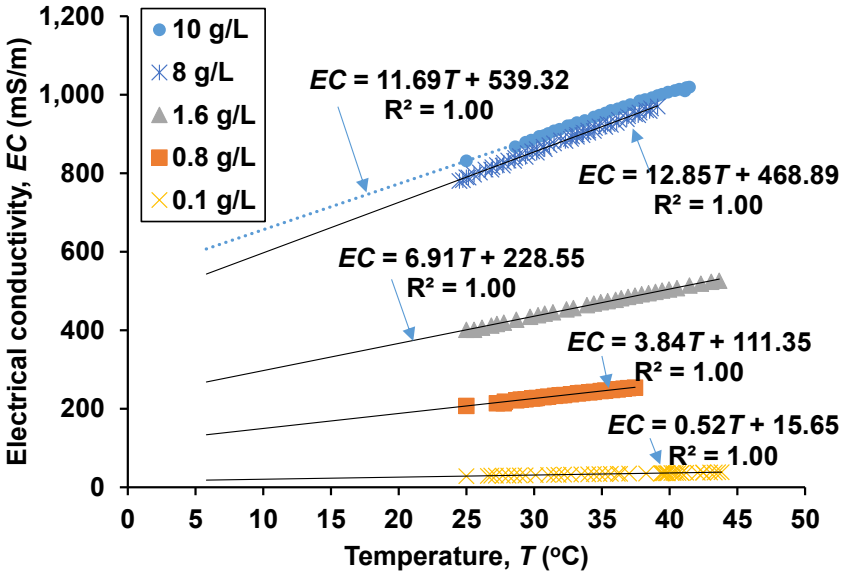


*Figure 4.12 Change of EC with temperature with various concentrations of lime solution from 0.1 g/L to 10 g/L*

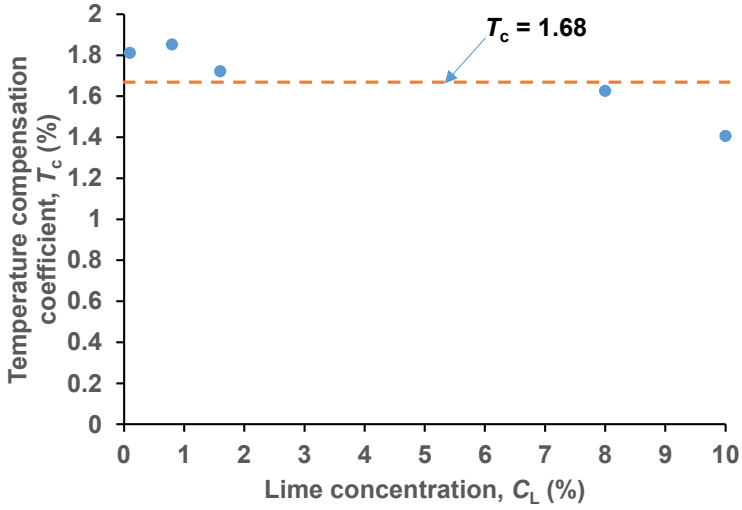


*Figure 4.13 Variation of temperature compensation coefficient $T_c$ with lime concentration $C_L$*

### 4.2.7 Electrical conductivity tests of soil in lime solution

Subtest A1 (mixing dry soil powder with 400mL hydrated lime at 40°C)

Figure 4.14 illustrates the change in electrical conductivity when soil powder (soil-to-lime dry mass ratio of 100% to 5%) is poured in lime solution with the concentration of 0.8 g/L. Two duplicate tests were performed to check the repeatability of method. As can be seen in Figure 4.14, there is a slight discrepancy between two curves within only about 2 mS/m after around 30 minutes. Starting at the same *EC* of aqueous lime solution (about 205 mS/m), *EC* goes down to about 155 mS/m after 1000 minutes. This *EC* reduction can be expressed in the difference between

205 mS/m and the intercept value of the line fitting on the curves from 200 minutes onwards. This reduction is regarded as the initial loss in conductivity ($LC_0$) of soil in an absolute value for Subtest A1 without a modification with results from Subtest A2. Diving $LC_0$ with the initial $EC$ value of lime suspension in per cent can obtain $LC_0$ (%). From Figure 4.14, the initial loss in conductivity $LC_0$ can be calculated as follows:

**Test 1:** $LC_0 = (205.86 - 162.60)/205.86 \times 100 = 21\%$

**Test 2:** $LC_0 = (205.86 - 160.22)/205.86 \times 100 = 22\%$

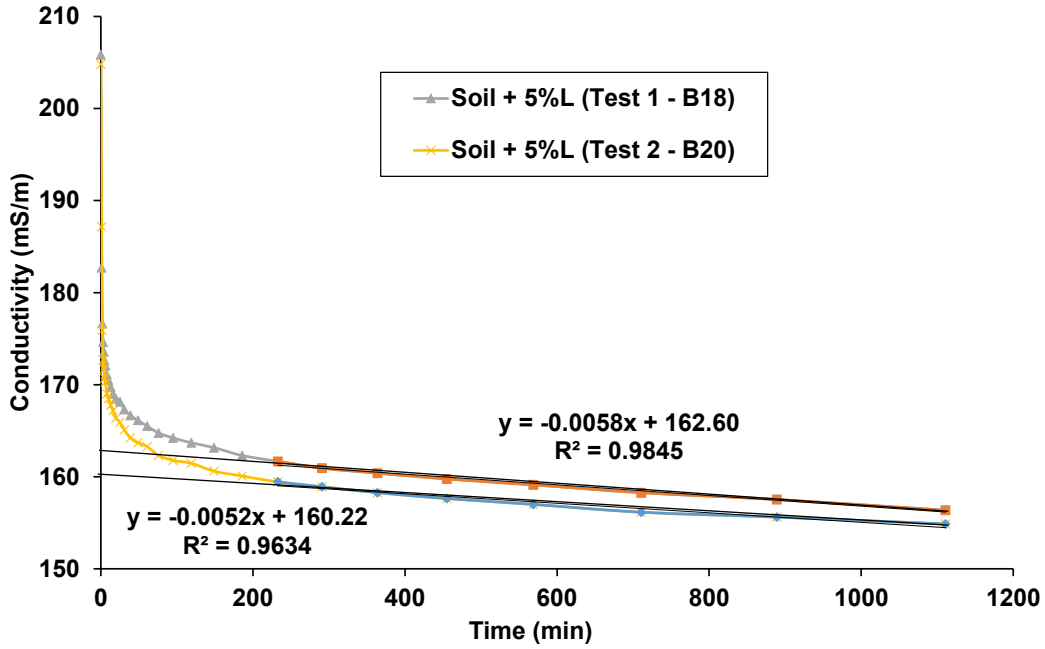


*Figure 4.14. Changes of electrical conductivity with time in 5%-lime-soil solution at 40 ℃ (compensated to 25 ℃ with Tc=1.9%)*

It can be observed that there is only 1% difference in $LC_0$ between Test 1 and Test 2. This is due to the fact that the initial loss in conductivity mainly occurs in the first minutes, which illustrates the soil capacity in its immediate reaction with hydrated lime. According to Paya et al. (2001), this initial loss in conductivity indicates a huge lime fixation caused by quick pozzolanic activities of soil and lime. Furthermore, $LC_0$ also depends on a long-term reaction between soil and lime, since the value was extracted on the curve ranging from 200 minutes to 1000 minutes, which is shown in Figure 4.14. However, testing in a few days can make the test prone to the variation of ambient temperature, influencing the accuracy of $EC$ value. In particular, the temperature compensation coefficient $T_c$ (1.9% as a value in device setting default) used in Subtest A1 might not be correct at a certain concentration of studied material (see Figures 4.6 and 4.13). Furthermore, micro-sized clayey clouds may exist during mixing soil powder with lime solution,

potentially increasing the *EC* value when these clods were dissipated completely. Consequently, the final $LC_0$ can be higher than 22% because of a possibly lower *EC* intercept value, as depicted in Figure 4.14.

Subtest B1 (mixing 200 mL clay slurry with 200 mL hydrated lime) at 25ºC, and then temperature increased to 40ºC

In Subtest B1, 200 mL homogeneous clay suspension was mixed with 200 mL lime solution and a corresponding amount of fine sand. After 2,000 minutes with 25°C, the *EC* levelled off at around 140 mS/m, which is shown in Figure 4.15. At this value, the soil suspension was quickly heated up to 40°C, producing the temperature compensation coefficient ($T_c$) is around 1.9% (Figure 4.16). At 40°C, the test was kept running over 8,000 minutes (about 6 days), revealing the smaller *EC* plateau at around 100 mS/m. It is noted that *T* value at 1.9% was used to compensate *EC* value at 40°C in assuming that the rapid increase of temperature at the minute of around 2,000 did not alter *EC* significantly (see Figure 4.16). Although increasing temperature differed the levelling-off value, the *EC* evolution rate at 25°C and 40°C is on the same line, which is indicated in Figure 4.15, resulting in the same *EC* intercept value at around 160 mS/m. To obtain this value, the duration of 900 minutes is sufficient to make a line and intersect the *EC* axis at 160 mS/m, which is illustrated in Figure 4.17. This value is close to that in Subtest A1 (162.60 mS/m for Test 1 and 160.22 mS/m for Test 2), suggesting that both Subtest A1 and Subtest B1 can give the same intercept value of *EC* regardless of temperature and procedure. However, unlike Subtest A1, Subtest B1 has a higher initial *EC* value than the first one (230 mS/m compared to 205.86 mS/m). This is due to that more than 20 mS/m in *EC* from soil slurry was added to that from lime solution (see *EC* value at 25°C for the concentration of 4.8 g/L in Figure 4.7). As a result, the initial loss in conductivity $LC_0$ is 30%, which is much higher than that in Test A1 (around 21%). This reveals that Subtest B1 gives a higher $LC_0$ but in a same surveyed time of around 1,000 minutes, compared to Subtest A1. In other words, Test B procedure can create a higher rate of *EC* reduction by mixing two materials (soil and lime), all in aqueous forms, thus accelerating the pozzolanic reaction between soil and lime, and causing a higher loss value in *EC*. In an attempt to reduce the testing time of electrical conductivity tests, particularly in a large amount of time when a series of tests is performed, the test duration was capped under 240 minutes, as illustrated in Figure 4.18. As a result, only a 1% reduction in $LC_0$ from 30% down to 29%, as illustrated in Figures 4.18-19. Therefore, a time slot of approximately 4 hours is recommended for Test B to obtain the initial loss in the conductivity value ($LC_0$).

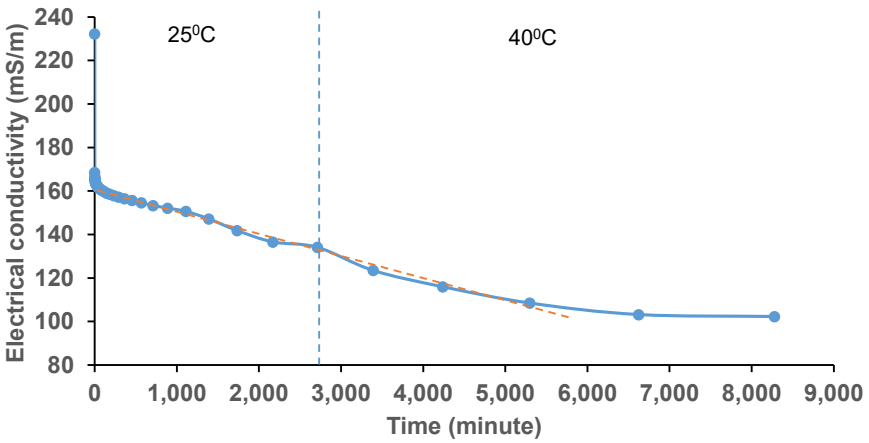


*Figure 4.15. EC evolution in soil-lime solution in different temperatures* (temperature-compensated at 25°C with $T_c$=1.89%)

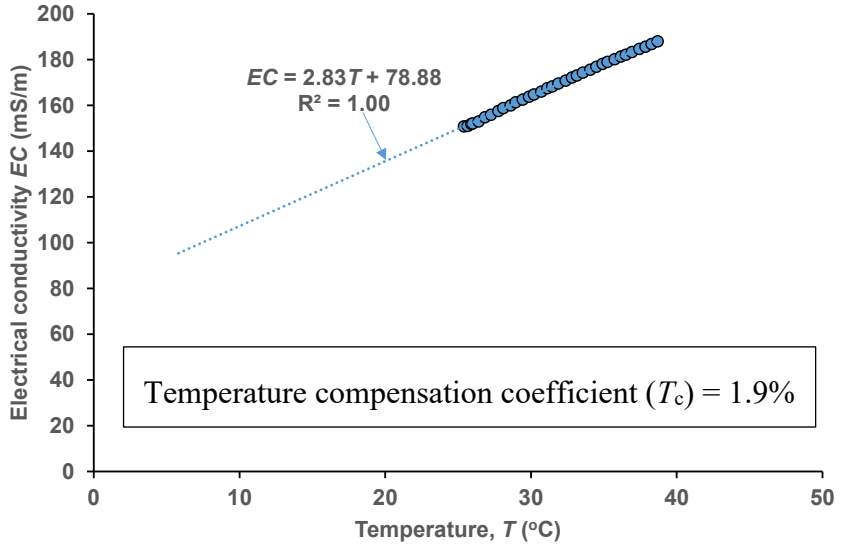


*Figure 4.16. Change in EC with the temperature of lime-soil solution with lime concentration of 0.8 g/L equivalent to the lime content of 5%*

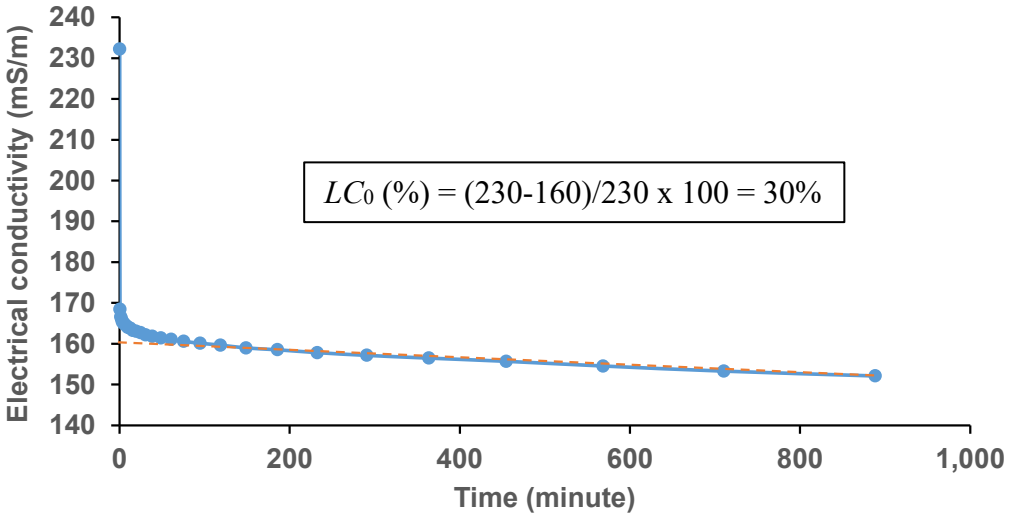


*Figure 4.17 Loss in conductivity ($LC_0$) in lime-soil solution from 0 to 1,000 minutes*

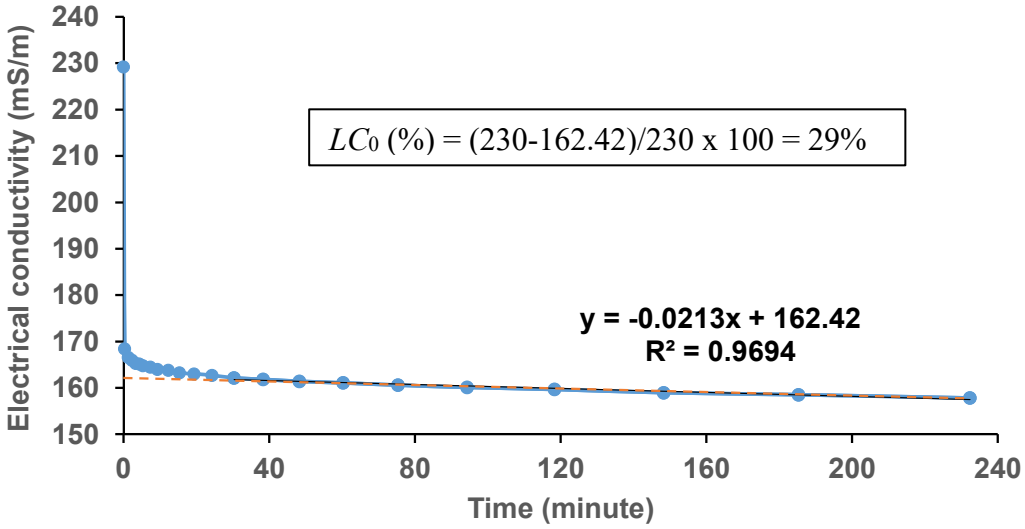


*Figure 4.18 Loss in conductivity ($LC_0$) in lime-soil solution from 0 to 240 minutes*

## 4.3 Physical and mechanical properties of soil untreated or treated with hydrated lime

### 4.3.1 Atterberg limits

There is a linear relationship between the liquid limit of the studied soil and the bentonite content, as shown in Figure 4.19. Without bentonite, the liquid limit of soil containing kaolinite (95%) and sand (5%) is about 50%. Replacing kaolinite by a proportion of bentonite increased the liquid limit of the mixed soil by about 3.4% when 1% bentonite content was added. Particularly, at 30% bentonite, the liquid limit of studied soil was obtained at about 155%, but also gained a high plastic limit at about 31%, resulting in 124% in the plastic index. According to ASTM Standard (2007), the studied soil was classified as fat clay (CH). The introduction of 5% lime significantly changed the state of expansive soil from fat clay to elastic silt (MH) since the higher reduction in the plastic index than in liquid limit, which is demonstrated in Table 4.1.

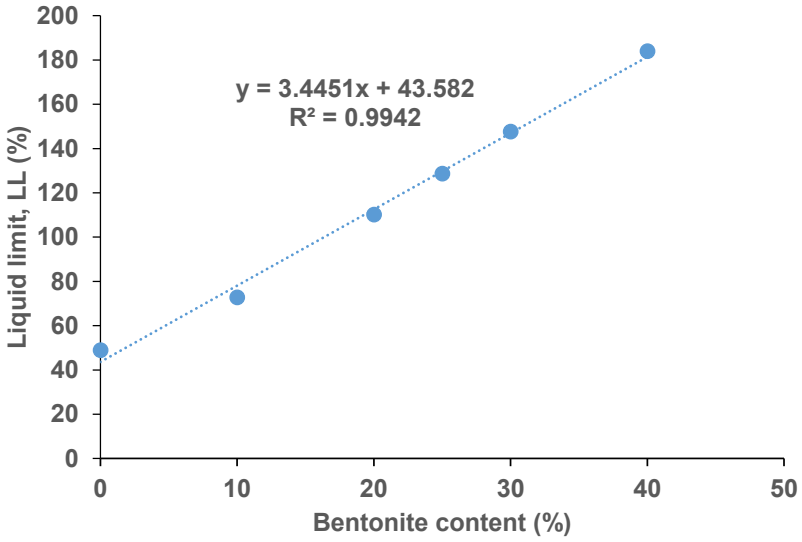


*Figure 4.19 Liquid limit of studied soil with various content of bentonite*

*Table 4.1 Atterberg limits of studied materials*

| Materials | Plastic limit, *PL* (%) | Liquid limit, *LL* (%) | Plastic index, *PI* (%) | USCS classification |
|---|---|---|---|---|
| Soil (30% Bentonite) | 30.92 | 154.95 | 124.03 | CH |
| Soil + L (5%) | 46.87 | 132.74 | 68.00 | MH |

### 4.3.2 Linear shrinkage

With the various liquid limits of expansive soil when bentonite content is altered, a series of linear shrinkage tests at these liquid limits was performed. Figure 4.20 shows the linear shrinkage at different contents of bentonite in expansive soils and various curing time. Inevitably, increasing bentonite content in the soil caused a larger soil shrinkage, but the linear shrinkage seemed to level off at around 21% when the bentonite content is over 30% (see Figure 4.20a). Less than 30% bentonite, expansive soil had linear shrinkage decreasing linearly with the reduction of bentonite content, going down to a low of 9.36% in soil without bentonite (95% kaolinite and 5% fine sand). To study the shrinkage-swelling behaviour of expansive soil, bentonite content of 30% was selected to sufficiently obtain a linear shrinkage of soil at around 21%, which was also the shrinkage of natural black cotton soil in the studies conducted by Hasan (2019) and Dang (2018). The results of linear shrinkage of soil, treated with 5% hydrated lime, is also shown in Figure 4.20b. It is worthy to note that the inclusion of 5% lime in expansive soil helped to reduce the soil shrinkage by 22% from 21.23% to 16.56%. This reduction in linear shrinkage occurred after 7 days. However, further curing until 28 days did not enhance the shrinkage decrease of lime in the soil, indicating that seven days were enough to conduct the shrinkage test on the treated soil samples. This result is associated with studies conducted by Hasan et al. (2016b) and Dang et al. (2016a).

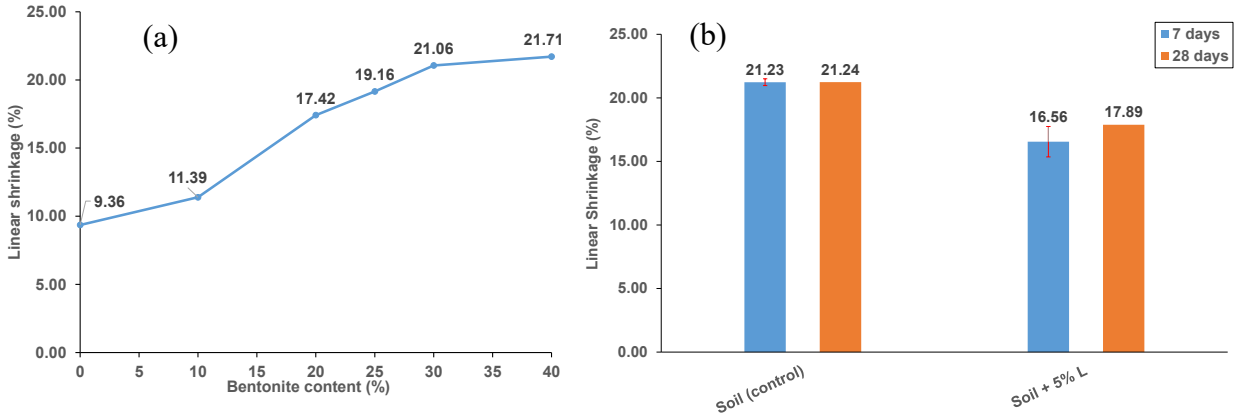


*Figure 4.20 Change in linear shrinkage of the studied soil with (a) various contents of bentonite; (b) 7 and 28 curing days with or without 5% hydrated lime.*

### 4.3.3 Standard compaction

Figure 4.21 illustrates the change of dry density with various water contents in soil samples untreated and treated with hydrated lime. The change is expressed in compaction curves, in which soil reaches the maximum dry density (*MDD*) at around 1.32 Mg/m$^3$ at the corresponding optimal moisture content (*OMC*) at 28.8%. When treated with hydrated lime, the soil sample has a lower *MDD* at around 1.32 Mg/m$^3$ while the *OMC* is the same at around 28%. This is understandable because only 5% hydrated lime was added into the soil while there is not only from a minor difference in specific gravity ($G_s$) between soil and hydrated lime (2.69 compared to 2.5, respectively), but also the small reaction between lime and clayey materials. This results in small changes in the zero-air-void curve between soil and soil treated with 5% lime. Based on this curve equivalent to 100% saturation, the saturation level of soil ($S_r$) at its optimal compaction parameters (*MDD* and *OMC*) is 0.75, while that of lime treated soil is 0.73.

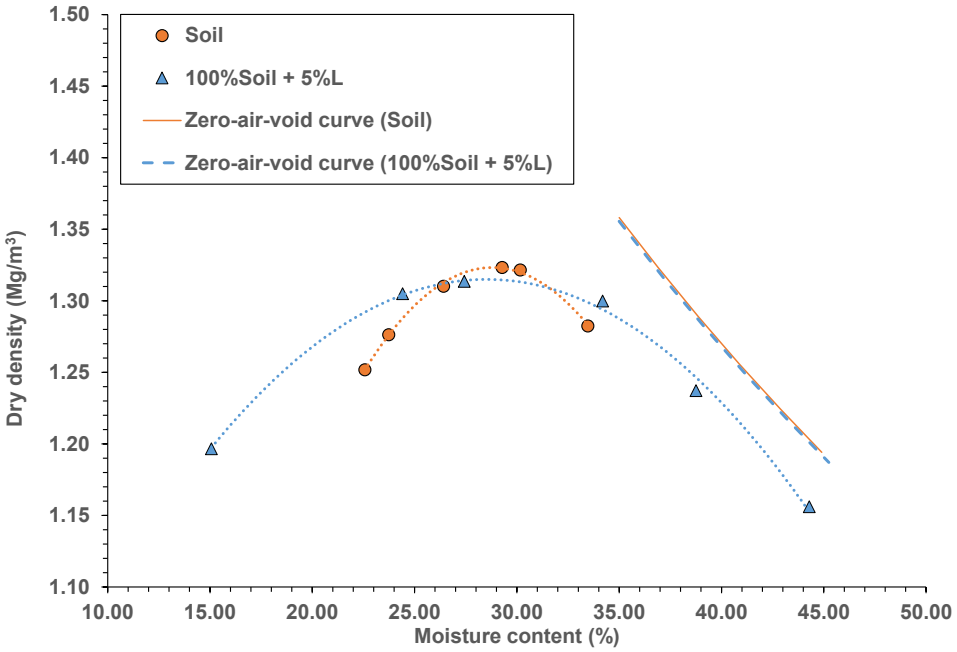


*Figure 4.21 Compaction of the test results established for untreated soil and soil treated with hydrated lime*

### 4.3.4 Swelling-consolidation tests

Studied soil

As shown in Figure 4.22, it can be calculated that the moisture content of 37% is the value to fully saturate the optimal compacted soil at *MDD* (1.32 Mg/m$^3$) and *OMC* (28.8%), turning the saturation level from 0.75 to approximate 1. Therefore, to estimate whether submerging soil samples in water for the free swelling tests makes soil fully saturated, two soil samples were

compacted at the same density of 1.32 Mg/m$^3$, but at the moisture content of 28.8% and 37%, equivalent to $S_r$=0.75 and $S_r$=0.95. Figure 4.23 illustrates the change in swelling ratio of soil samples curing in 1 hour with different $S_r$ values (0.75 and 0.95). It can be observed that both samples gave the same free swelling ratio of 60% after 3,000 minutes, indicating that the test fully saturated the unsaturated compacted soil ($S$r=0.75). The swelling rate is quicker for fully-saturated soil than in unsaturated soil since the soil with $S_r$=0.95 could obtain a 60% swelling ratio after around 1,000 minutes. This is due to the fact that there had been already more water in fully-saturated soil than unsaturated soil, accelerating the swelling process, so obtaining the final free swelling value earlier than the soil with a lower $S_r$ value.

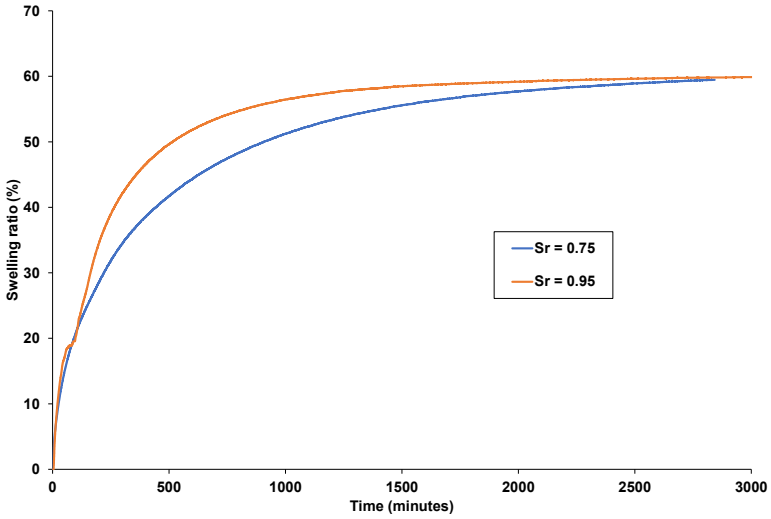


*Figure 4.22 Free swelling ratio of the studied soil (pre-loading pressure=0 and seating loading=6 kPa) with different degrees of saturation ($S_r$)*

Figure 4.23 illustrates consolidation curves of soil samples with different loads, resulting in different swell or collapse deformations, using the conventional oedometer cells. While the swelling-consolidation tests were conducted following the Australian Standard AS 1289.6.6.1 (1998) procedure, which is corresponding to ASTM D4546 (2014), the consolidation part in these tests were based on the test method B mentioned in ASTM D2435 (2020). According to this method, various preloading weights were applied on samples to describe the different fill depths, and a line connecting the starting points of swell or collapse strain on the logarithm curve intersects the stress axis at the swelling pressure corresponding to zero strain (see Figure 4.23). From this figure, it can obtain the value of swelling pressure at about 72 (kPa).

It is also noted that the consolidation curves tend to unite in the stress range from 200 to 400 kPa but deflect when the applied stress is over 400 kPa (refer to Figure 4.23). Over 400 kPa, soil samples with low seating loads would be more compressible than those with high seating pressure.

This is simply because the soils with high swelling strain, equivalent to the top expansive ground, are more porous with high void ratios than dense soils with collapse strain, corresponding to deeper depths. Under the high pressures, the consolidation settlement of the top loose soil layer is more significant than sense clay layers beneath. The results correctly reflect what were observed on the natural soil samples taken from the field, mentioned in previous studies on undisturbed soil (Chung et al., 2012).

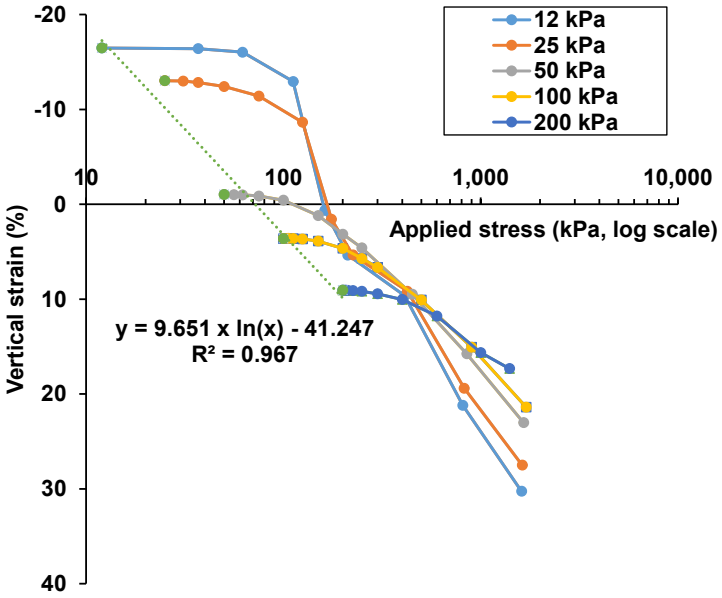


*Figure 4.23 Swelling-consolidation curves of expansive soils with various pre-loading pressures from 12 kPa to 200 kPa*

Figure 4.24 compares the consolidation results from oedometer cell and hydraulic Rowe cell. Interestingly, the constrain-rate-of-strain consolidation curve of Rowe sample united the Incremental loading (IL) curve of the oedometer cell in the pressure range from 150 to 200 kPa, intersecting the zero strain at around 170 kPa. However, consolidation curves of Rowe soil samples are more compressible than that of traditional oedometer ones.

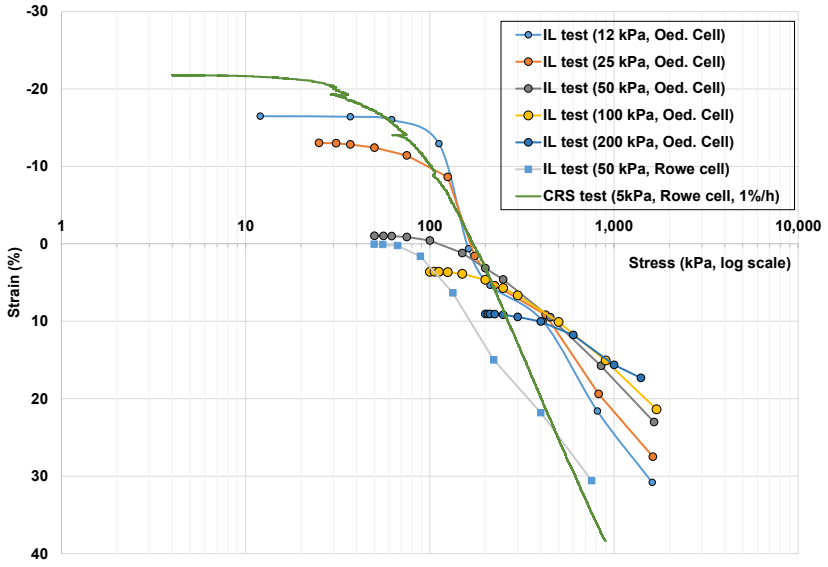


*Figure 4.24 Swelling-consolidation curves of studied soil samples with various seating pressures, methods (CRS and IL) and cells (oedometer and hydraulic Rowe cell)*

Apart from the swell-consolidation test with free swelling allowance, there is a consolidation test without allowing displacement from soil swelling, known as the zero-volume change consolidation test. Figure 4.25 illustrates the growth of pressure when soil is constrained in cells without any swelling displacement when water was poured into the cells. Two different diameters were used, namely cell of oedometer ($D$ = 50 mm) and CBR ($D$=152 mm). It is obvious from Figure 4.25 that the sample with the larger cell has a higher swelling pressure than soil in cells with the smaller size, 69 kPa as against 60 kPa. However, both pressures are smaller than the value was calculated previously (72 kPa) from IL tests. The explanation is that the condition of no volume change in relevant tests limited the water infiltration in the sample (see kinks in Figure 4.25), reducing its swelling pressure, compared to IL tests with the allowable displacement of tested samples. The kinks are also observed in the study conducted by Wang et al. (2012).

In the comparison of consolidation curves in different test methods, the constrain rate of strain consolidation (CRS) curves are in an average range between IL curves. Particularly, while IL curves change with various cells and diameters, the CRS test generates consolidation curves in a small variation that is less reliant on the cell size. With the biggest size ($D$=152 mm), CBR mould gave a good average consolidation curve with an identical consolidation curve from two repeatable tests at the strain rate of 1%/h, as presented in Figure 4.26.

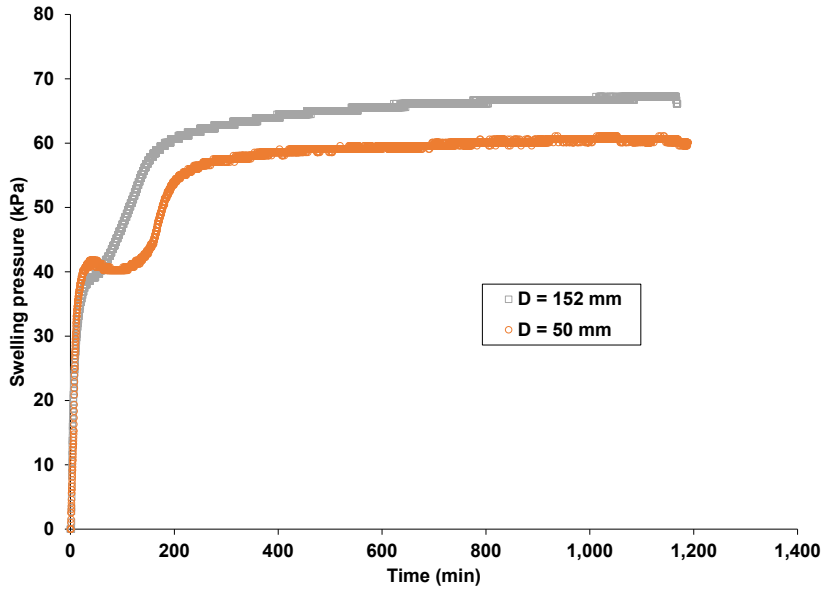


*Figure 4.25 Swelling pressure with zero volume change (no displacement allowed) with different cell diameters (D = 50 mm and 152 mm)*

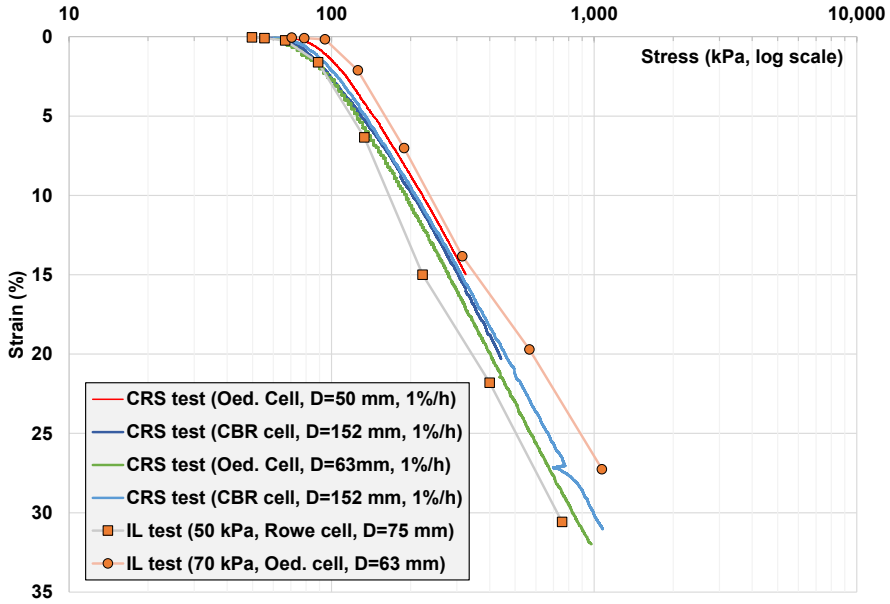


*Figure 4.26 Zero-swelling consolidation tests of studied soil with various testing methods (CRS and IL), cell types (oedometer, CBR and hydraulic Rowe) and diameters (D=50, 63, 75, 152 mm)*

Soil treated with 5% hydrated lime

The lime-treated soil samples for swelling tests were compacted at different water contents, resulting in various corresponding dry densities on the compaction curve, which is displayed in Figure 4.27. When soil is treated with 5% hydrated lime, the free swelling ratio decreased significantly to only about 12%, as indicated in Figure 4.27. It is noticeable that this free swelling ratio depends on curing time and moisture content. With longer curing time, the swelling ratio decreased remarkably, and it can deplete to about zero when the sample was incubated after 28

days (see samples with w=25% in Figure 4.27). Furthermore, the lime-treated soil samples with a lower water content had smaller free swelling ratios. For example, with the same curing time of 1 hour, lime-treated soil at the water content of 29% had the swelling ratio of about 12% but decreases significantly to around 2% with the moisture content of 25% and peters out to only 0.5% if the content is 15 % (see Figure 4.27). The swelling reduction came from the decrease of compacted density when drier soil samples were constituted. This is different from soil samples with various saturation levels but at the same density, shown in Figure 4.22. On the other hand, when lime-treated soil specimen was compacted at moisture different from the *OMC* of 29% (e.g., 15% and 25%, as shown in Figure 4.27), the sample with the lower moisture had a density lower than its counterpart (see the compaction curve in Figure 4.21). As a result, with the lower density but the same content of 5% lime in samples to ensure optimal pozzolanic reaction between hydrated lime and soil, the sample with 15% moisture had the swelling ratio significantly lower than the specimen with 25% water content, as indicated in Figure 4.27.

However, when swell samples were subject to incremental loading, the lime-treated soil compacted at optimal moisture content obtains the highest pre-consolidation pressure, compared to samples moulded at smaller water contents (refer to Figure 4.28). This is attributive to the fact that the sample compacted at *MDD* and *OMC* has the highest density with the highest amount of hydrated lime in the soil, enhancing the reinforcement from the pozzolanic reaction in treated samples.

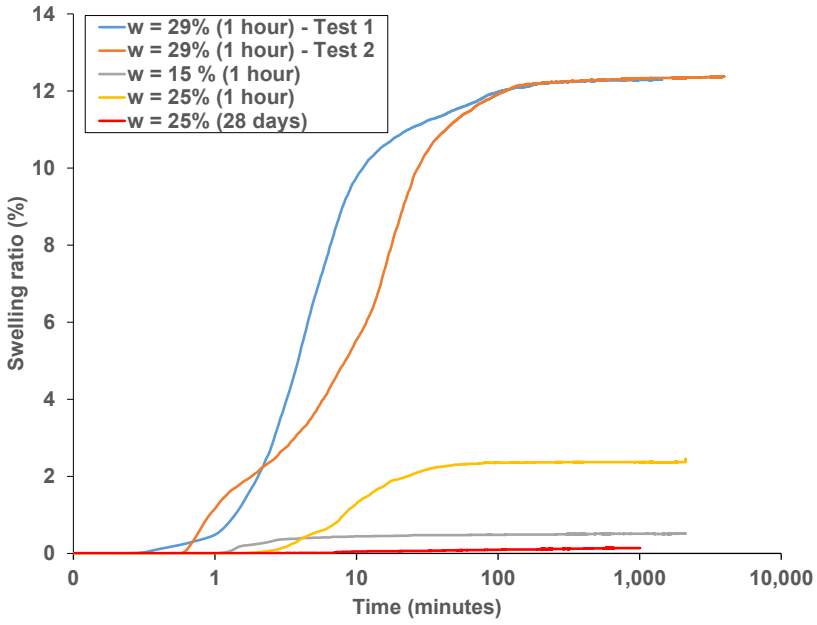


*Figure 4.27 Swelling ratio of soil treated with 5% lime with various moisture content (w) and curing time (1 hour and 28 days)*

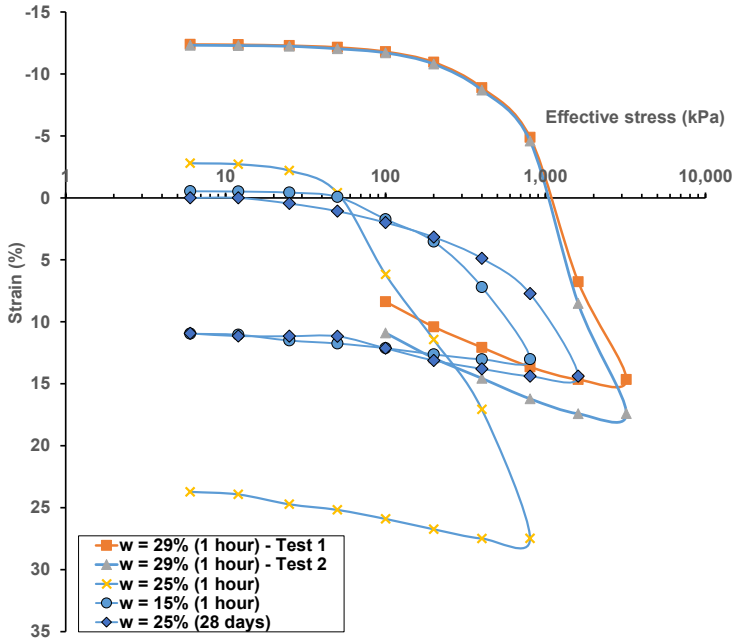


*Figure 4.28 Consolidation curves of soil treated with 5% hydrated lime with various water content and curing time*

### 4.3.5 Unconfined compressive strength test

Expansive soil treated with hydrated lime not only has higher pre-consolidation stress in confined consolidation test, but also have a higher compressive strength in the unconfined compressive experiment. Figure 4.29 illustrates the development of soil blended with various contents of hydrated lime. Overall, more lime added to the soil sample improved the UCS of treated soil, even with the content as high as 9%. In terms of curing time, longer incubation up to 28 days did not give significant strength value to samples, compared to that after 7 days. This indicates that lime-treated soil developed most of its compressive strength after 7 curing days.

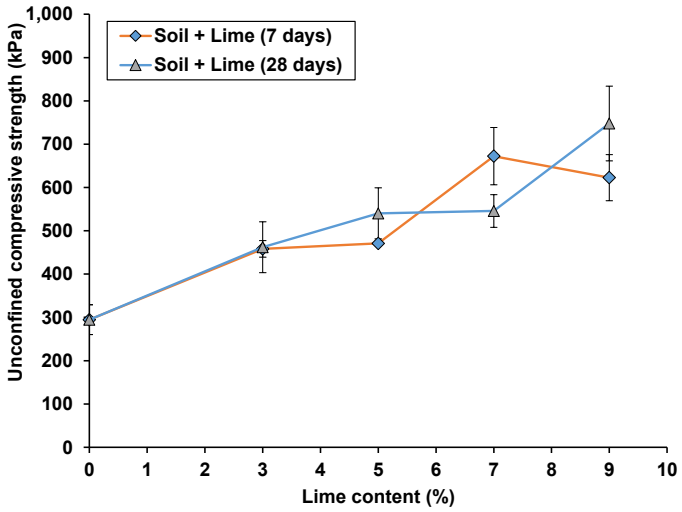


*Figure 4.29 Unconfined compressive strength of soil treated with hydrated lime with various content and curing time*

### 4.3.6 Indirect tensile strength tests

Alongside UCS, tensile pressure from the indirect tensile strength test is also a good indicator for investigating the change in the reinforcement of soil treated with different contents of hydrated lime. As shown in Figure 4.30, the lime content of 7% produced the highest tensile stress of around 150 kPa after 7 days for curing. This percentage is also observed in the samples tested in unconfined compressive strength test, presented in Figure 4.29. While the curing time after 7 days did not affect the strength evolution of lime-treated soil, the soil sample cured with 5% hydrated lime was tested in the indirect tensile strength test after 28 days. It can be seen that the tensile strength of the sample treated with 5% lime increased to the high of over 150 kPa, surpassing the strength at 7% lime content. The tensile development of soil sample with 5% lime is in a good agreement with a compressive improvement of the same sample shown in Figure 4.29. In light of the result from pH test shown in Figure 4.1, 5% lime content is selected to gain the optimal strength reinforcement in treated expansive soil.

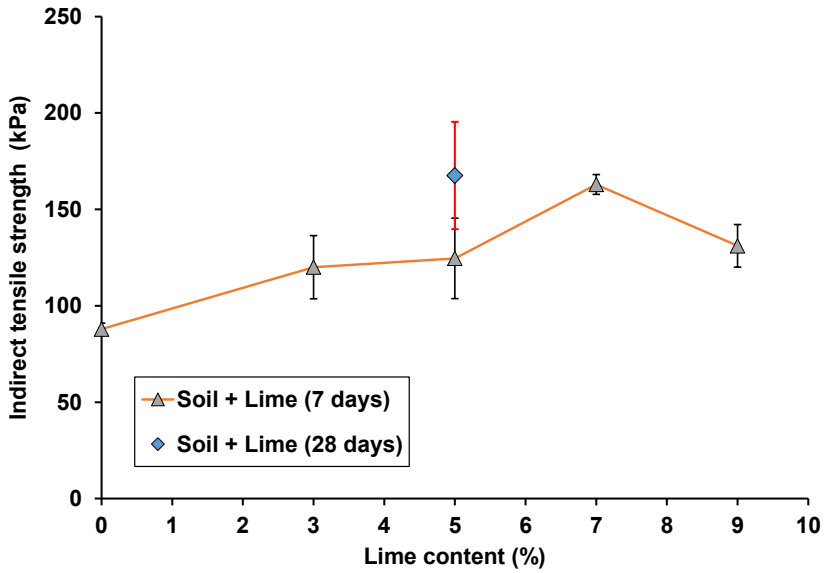


*Figure 4.30 Indirect tensile strength of soil treated with hydrated lime with various contents at different curing times*

### 4.3.7 California bearing ratio tests

When mentioning tests to evaluate the strength of soil for road material, California bearing ratio (CBR) test was utilised besides the unconfined compressive strength test. In CBR tests, there are two kinds of test, namely soaked or unsoaked CBR test, equivalent to the test with or without submerging in water for saturation, respectively. Figure 4.31 illustrates the change in soil treated with hydrated lime and in soaked and unsoaked conditions. It can be seen that soaking sample in water deteriorates soil bearing strength from 18.69% to only 0.96%, a decrease of 17.73%. The

same detrimental effect from soaking can be observed in soil treated with 5% lime, showing a decrease of 24.21% (see Figure 4.31). However, lime treatment helped increase the bearing ratio of soil by 53.2% and 46.72% in unsoaked and soaked conditions, respectively. While the improvement from lime addition to soil can be explained by the pozzolanic reaction between lime and soil, the downgrade of bearing strength caused by soaking is from a full saturation in soil matrix. The water absorption in untreated soil made the sample swell, increasing void ratio and weakening soil strength. Meanwhile, the soil treated with hydrated lime has strength reduced by soaking due to the decrease in sample suction when water occupies in voids of lime-treated soil, causing a lower strength in the soaked soil with hydrated lime compared to dry sample (Wang et al., 2019). However, when water was filled all voids in the soaked CBR samples, soaking the samples in water for a longer duration further deteriorated *CBR*. Figure 4.31 also indicates the change in *CBR* of samples soaked in water 7 days and 62 days, compared to unsoaked mould. It is obvious that longer saturated sample reduced *CBR* of sample after 7 days for 47.68% to only 22.59% after 62 days. To investigate whether the *CBR* decrease comes from the difference in saturation level between samples soaked after 7 days and 62 days, Figure 4.32 was drawn to show the variation of water content of *CBR* samples at the top, bottom and middle parts. It can be seen from this figure, a full saturation was obtained after 7 days with the water content of three soil layers at about 40%, which is due to the fact that further soaking samples until 62 days did not change the moisture. In summary, the test results from Figures 4.31-32 indicate that soaked *CBR* is lower when more time for soaking is allowed. However, after 7 soaking days, the *CBR* reduction may be due to the degradation of cementitious bonds, but not from the suction decrease because the CBR samples have been fully saturated (Wang et al., 2019).

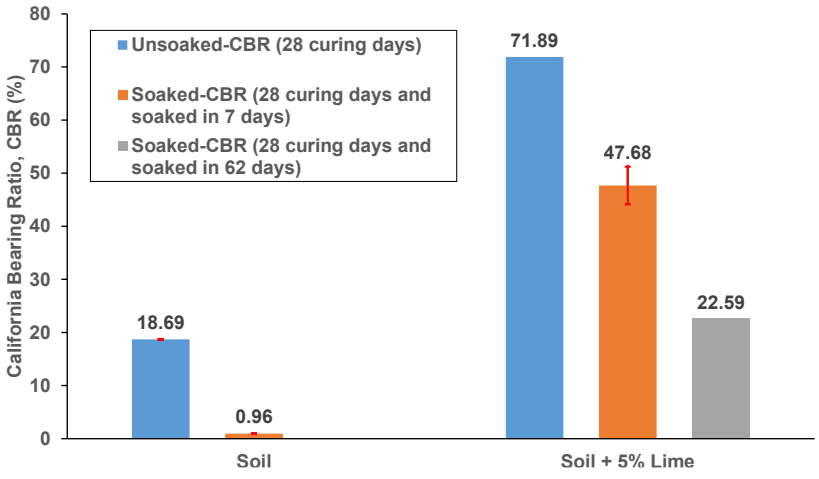


*Figure 4.31 Unsoaked and soaked CBR of untreated soil and soil treated with 5% lime*

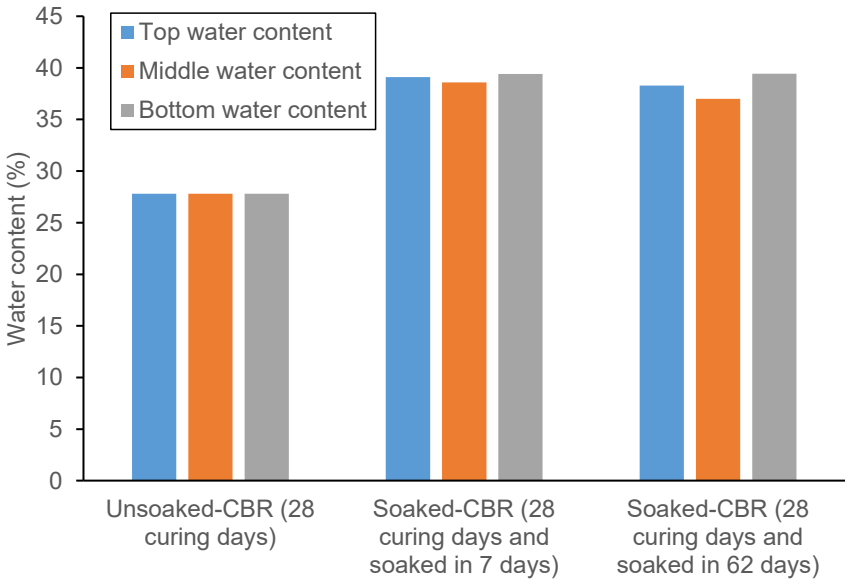


*Figure 4.32 Water contents of lime-treated soil CBR samples at top, middle and bottom sample layers.*

### 4.3.8 Triaxial shearing test

Triaxial shearing test is the experiment to evaluate the shearing behaviour of soil samples under the different confined pressures; thereby, the shearing parameters can be determined through the stress failure envelope of studied soil. For lime-treated soil, the triaxial samples were compacted in a highly saturated condition ($Sr$=0.9) but at *MDD* of the sample (see Section 3.3.2.3 for triaxial sample preparation). The test procedure followed the consolidated undrained (CU) triaxial shearing tests with the B-check at around 0.95 after saturation process, followed by the complete consolidation with the check of back volume. In this section, the test results start from the stress-strain behaviour illustrating the change in deviatoric stress with axial strain in three values of confined pressure, namely 50, 100 and 200 kPa. After that, the plot of excess pore water pressure versus strain rate is displayed in the same order of confined pressure. Finally, the effective stress failure envelope of soil untreated and treated with hydrated lime is described to reveal the internal friction angle and cohesion of studied soils.

#### *4.3.8.1 Stress strain behaviour*

Figure 4.33 compares the development of deviatoric stress ($q$) with the change in axial strain under various confined pressures of 50, 100 and 200 kPa. It is apparent that lime-treated soil developed its shear stress as a dense material, rocketing to a peak at a failure strain of about 1%, then going down and levelling off at residual strength around or under 600 kPa for all surveyed confined stresses. On the other hand, the stress-strain relationship of soil reflects a loose sample since the curve goes up to a residual stress and plateaus around or under the deviatoric stress value of 200

kPa. Furthermore, the lime-treated soil has a brittle behaviour since there was an abrupt increase of shearing stress in a few strain, say around 1%, following a sudden drop in strength. Notably, the collapse is larger when the confined pressure is higher, indicating the brittleness of lime-treated soil samples (see Figure 4.33).

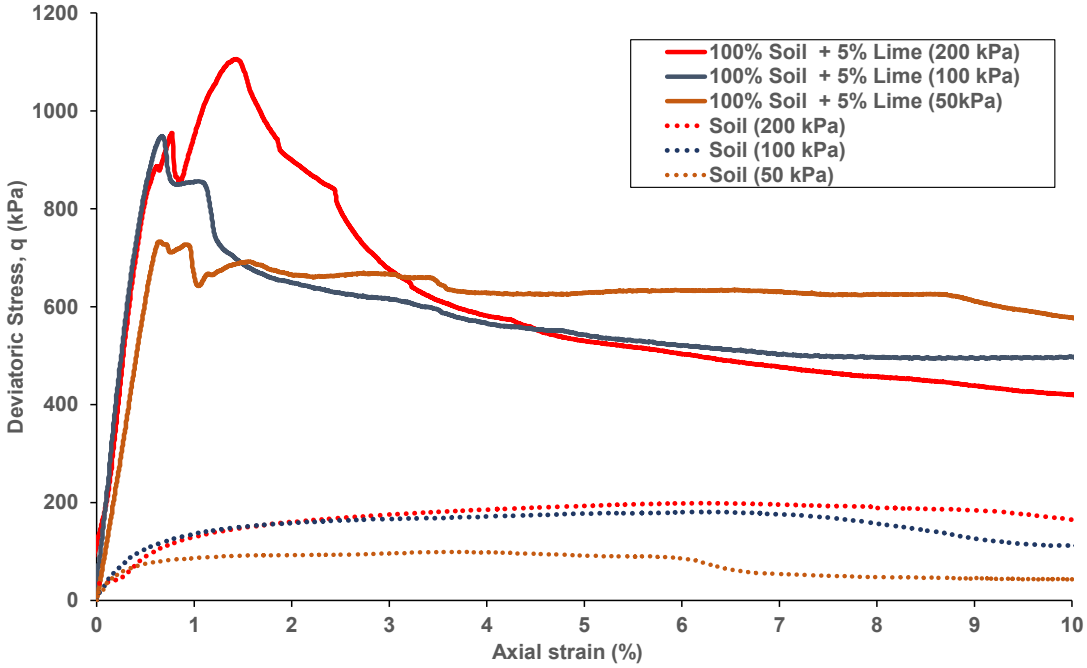


*Figure 4.33 Shearing stress-strain relationship of untreated soil and soil treated with 5% hydrated lime under the confined pressure of 50, 100 and 200 kPa*

### *4.3.8.2 Excess pore water pressure*

The variation of excess pore water pressure (PWP) versus axial strain rate can express the dilation behaviour of treated soil. In Figures 4.34, the increase of excess PWP in the first axial strain can be observed, followed by a collapse of pressure to negative values from the axial strain of 1%. With higher confining pressure, the axial strain turning PWP from positive to negative values was larger, increasing 1% to 2.2% when consolidation pressure goes up from 50 kPa to 200 kPa, respectively. However, the decrease in PWP from the peak to residual value was almost the same for three samples in different confining pressure, a collapse of approximately 300 kPa. Furthermore, three studied samples obtained the PWP equalling to their corresponding confining pressure within the first axial strain of 0.5%. This suggests that treated samples were completely saturated and consolidated; hence, they could quickly gain the same confining pressure under the undrained condition. In addition, the PWP response was rapid to the applied shear stress, building up the immediate peak of deviatoric stress but nosediving to the low level within 4% in strain,

which confirms the brittleness of treated material. Unlike lime-treated soil, the studied soil did not have an abrupt up-and-down in PWP. Instead, its PWP gradually increased and tended to keep the pore water pressure constantly over the increasing axial strain (Figures 4.34).

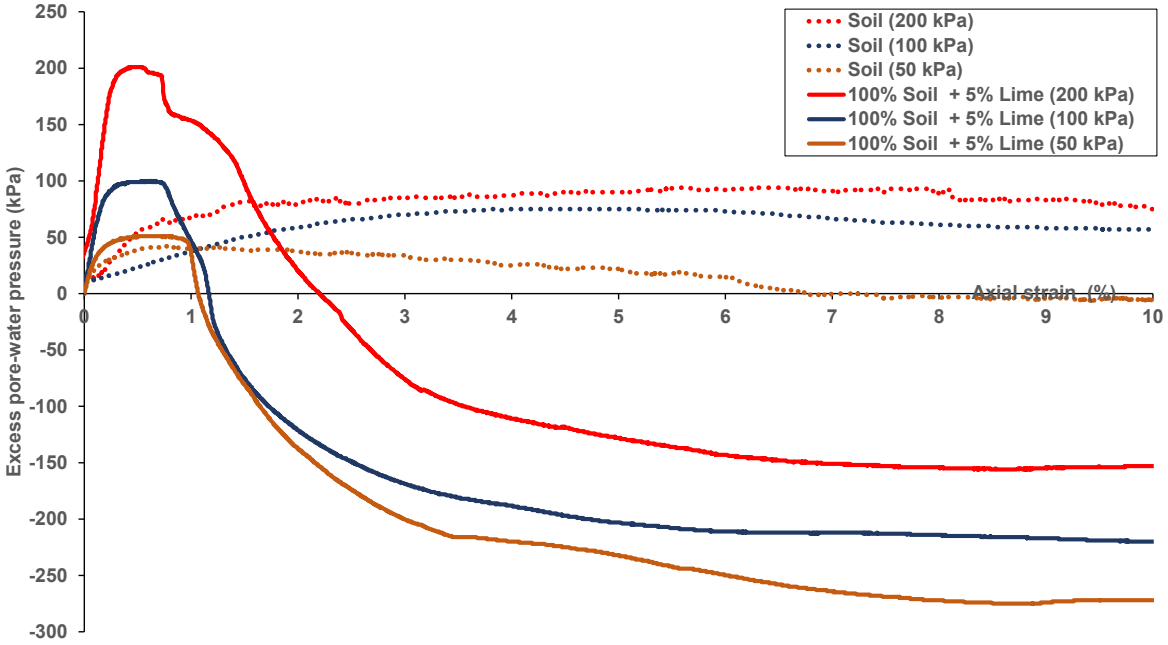


*Figure 4.34 Pore-water-pressure-strain relationship of soil untreated and treated with 5% hydrated lime under the confined pressure of 50, 100 and 200 kPa*

### *4.3.8.3 Effective stress failure envelope, frictional angle and cohesion*

Once the total pressure and excess pore water pressure at failure are defined, the effective stress failure envelope can be drawn. Figure 4.35 compares the envelope at failure occurring in soil untreated and treated with hydrated lime. It can be seen that the lime-included sample has a larger envelope than soil, at the highest of 600 kPa in both effective normal stress and shear stress, compared to only about 200 kPa for untreated soil. With greater failure envelope, shear-effective-normal-stress curve gains a higher intercept in lime-treated soil than in soil only. The slope of this curve is also significantly larger in the lime-soil sample, doubling the slope of soil specimen, 0.6882 as against to 0.3689. As a result, the internal friction angle and cohesion of soil were significantly improved when hydrated lime was added as a soil binder. In detail, the internal friction angle increased from 20° to 35°, a growth of 71%, while cohesion has a leapfrogging increase from 24 kPa to 127 kPa (refer to Figure 4.36). The improvement in both friction angle and cohesion of lime-treated soils stemmed from producing gluing hydrate products from the pozzolanic reaction between soil and hydrated lime. After a long-term incubation (i.e., 28 curing days), calcium hydroxide in lime reacted with silicate and aluminium oxide in the soil to form calcium aluminium silicate hydrate (CASH) in morphology for sheets or fibrous formation. These

gels glued soil particles together, enhancing the cohesion of soil mix and increasing friction between soil grains.

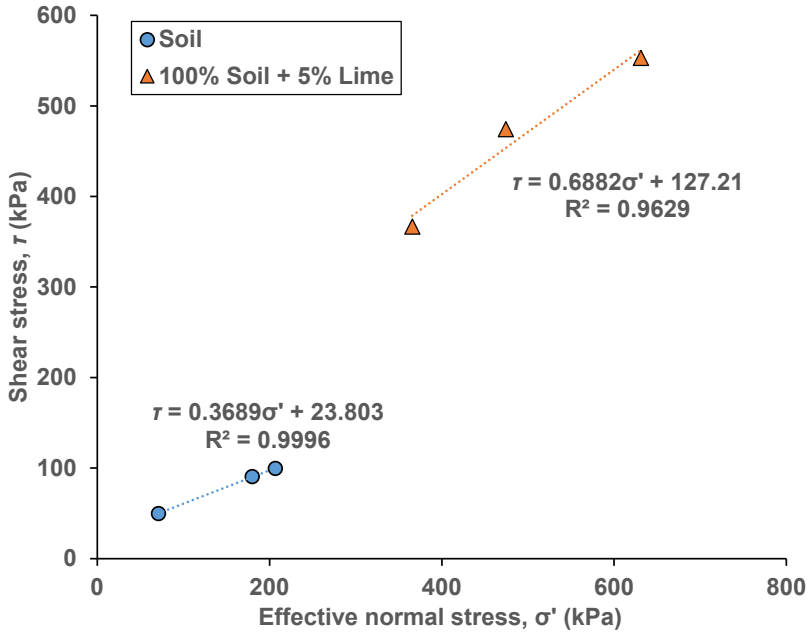


*Figure 4.35 Effective stress failure envelope of soil untreated and treated with 5% hydrated lime*

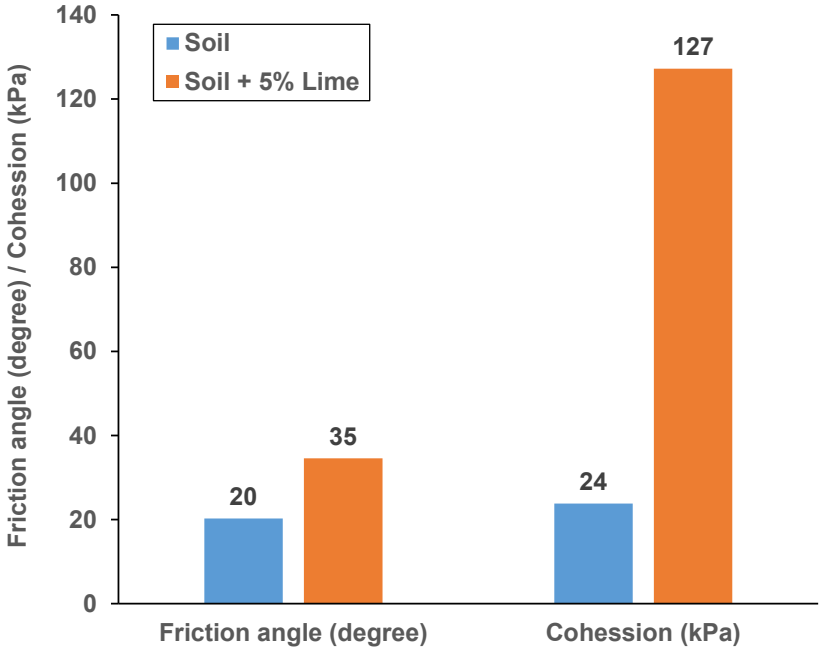


*Figure 4.36 Internal friction angle and cohesion of untreated soil and soil treated with 5% hydrated lime*

### 4.3.9 Bender element tests

From the UCS, CBR and triaxial test results, it is clear that lime inclusion to expansive soil improved its strength after long incubation, usually 28 days. However, to thoroughly investigate the strength development of studied soil all over the curing time from the beginning (compaction) to a few months (e.g., 90 days), the bender element test can be utilised to reveal the long-term development of small-strain shear modulus ($G_{max}$) in studied soils. Figure 4.37 illustrates the upward trend of $G_{max}$ in both soil untreated and treated with lime. Nevertheless, the increase of $G_{max}$ in untreated soil was marginal and gradual under 100 MPa, which was much lower than that in lime-treated soil, significant soaring to about 200 MPa after 1 day curing. The $G_{max}$ of lime-treated soil gained the highest of about 350 MPa after 28-day incubation, levelling off at this high from 28 to 56 days before sloping steeply down to about 250 MPa after 200 days. The $G_{max}$ degradation in lime-treated soil is attributable to the fact that more precipitated calcium-silicate-hydrate (CSH) produced after a long curing period, holding water with its affinity capacity, which deterred the hydration of stabilised soil layers, thus deteriorating their strength properties (Chakraborty & Nair, 2020).

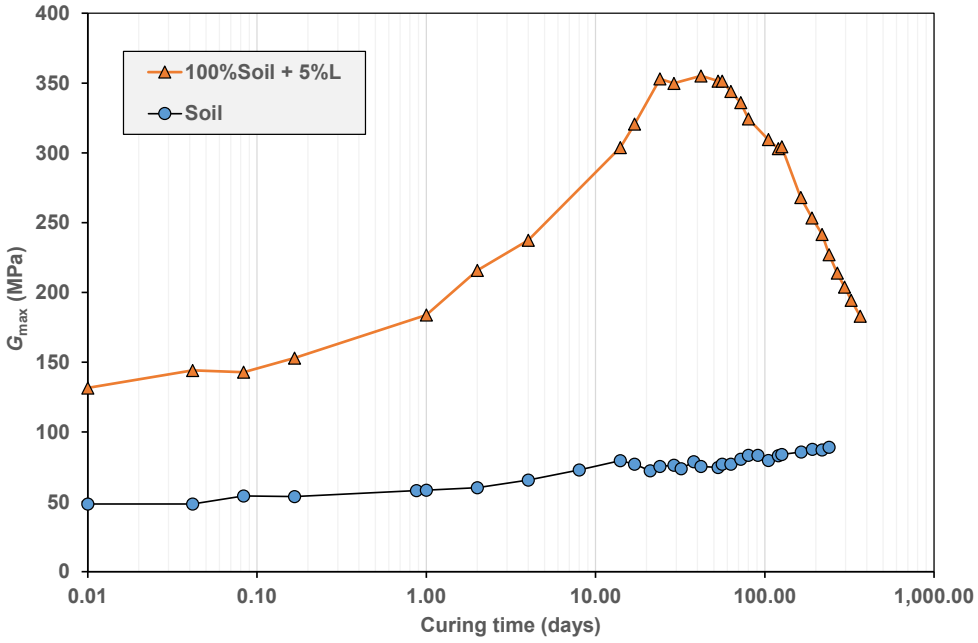


*Figure 4.37 Change in $G_{max}$ of soil sample untreated and treated with 5% hydrated lime with curing time*

### 4.3.10 Matric suction tests

The evolution of $G_{max}$ in soil untreated and treated with hydrated lime may have a relationship with the change in suction of the samples with time. Figure 4.38 illustrates the increase of matrix

suction with time for soil and lime-treated soil. It is clear that the suction of lime-soil sample is higher than that of soil, but not significant, 125 kPa compared to 75 kPa in the first 10 days. The matrix suction increased gradually but at different levels. While soil suction increased marginally around 100 kPa, lime-soil mix suction soared from around 150 kPa after 63 days to over 200 kPa after 90 days. This significant increase of matrix suction may be associated with the formation of calcium-aluminium-silicate-hydrate (CASH) product as the cementitious compound by pozzolanic reactions (Wang et al., 2019). As a result, the existence of the fibrous and linear product can redistribute the pore size in the soil since the porous feature of the hydrate compound leads to the increase of suction in the lime-treated soil sample, as shown in Figure 4.38.

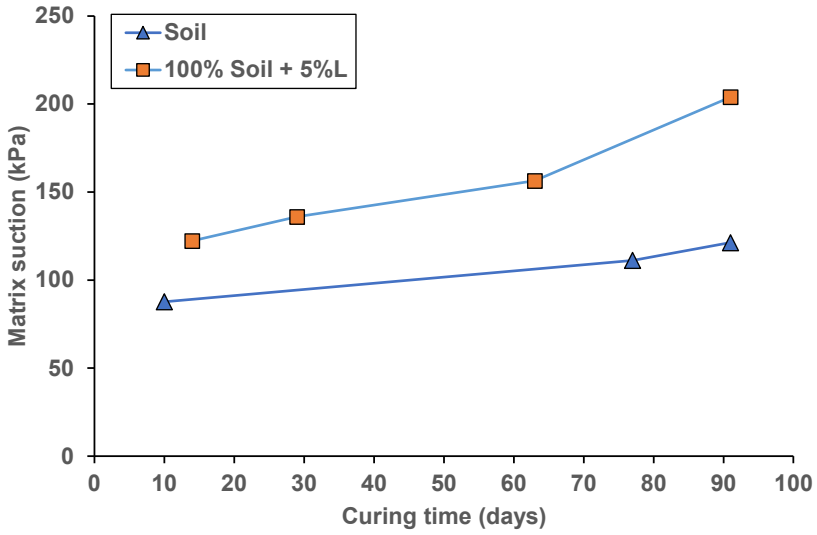


*Figure 4.38 Change in matrix suction of soil samples untreated and treated with 5% hydrated lime with curing time*

### 4.4 Micro-structural analysis on soil treated with hydrated lime

Micro-structural analysis on studied samples can illustrate by imaging the formation of products from mixing hydrated lime and soil. Furthermore, the combination of Scanning Electron Microscopy (SEM) and Energy-dispersive x-ray spectroscopy (EDS) can assist in analysing the chemical composition of a point on the images. In the scope of the study on lime-treated soil, a question was raised whether a particular hydrate was produced in lime-treated soil after a long-term curing period, which may reduce the shear modulus of treated sample, as shown in Figure 4.39. Apparently, shown in Figure 4.39, while soil particles mainly contain Silica Oxide and aluminium oxide, the introduction of hydrated lime to soil formed a hydrate product (CASH) in the shape of fibres and bars intertwining in the soil matrix after 56 curing days. The detrimental effect of the product is that more precipitated hydrate product holds more water with its affinity

capacity, so deterring the hydration of stabilised soil and reducing its strength properties (Chakraborty & Nair, 2020).

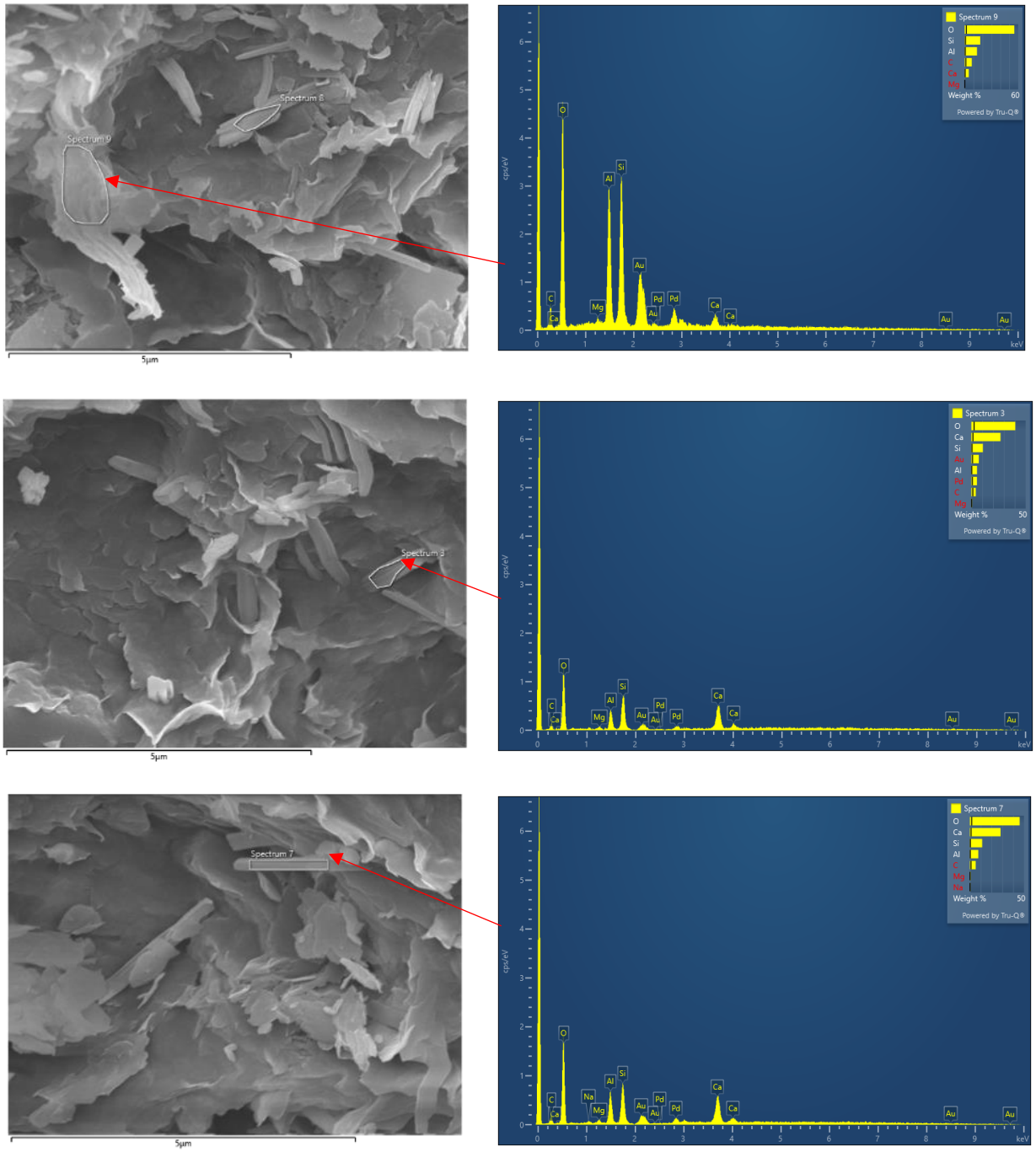


*Figure 4.39 SEM and EDS on soil samples treated with 5% hydrated lime after 56 days of curing*

## 4.5 Summary

Through experimental tests on untreated soil and soil treated with hydrated lime and analysis of results to determine the electrical, physical. mechanical and micro-structural characterisation of

samples, some remarkable conclusions can be drawn. The improvements of soil properties when lime is applied to stabilise expanse soil are also highlighted in this summary.

Chemical properties improvements:

- Soil treated with 5% hydrated lime has a high pH value of around 13%, which is contributed by the high pH of the studied soil, because the soil contains sodium bentonite, which has a pH value of up to 10. The content of 5% lime is also the average percentage to obtain a constant pH value for lime-treated soil mixture.
- Regarding electrical conductivity results of studied soil, consisting of kaolinite, bentonite and fine sand, bentonite has the highest electrical conductivity value, compared to kaolinite in the same concentration, whereas fine sand is the lowest as an inert material. When combining three components together in order, the bentonite solution has the highest temperature compensation coefficient (3%), decreasing to 2.5% when kaolinite (65%) is mixed with 30% bentonite. The compound of 65% kaolinite, 30% bentonite and 5% sand has the same temperature compensation coefficient of 2.5%. Meanwhile, the thermal compensation coefficient of the hydrated lime solution is lowest, at 1.7%, due to the fact that the electrical conductivity value of lime aqueous suspension is highest, up to about 200 mS/m with the concentration of 0.8 g/L.
- To investigate changes in electrical conductivity (*EC*) when lime was added to soil solution, Subtests A1 and B1 were used related to whether the soil was dry powder or slurry solution when mixed with lime aqueous suspension. The findings indicated that the method of mixing soil slurry with lime solution (Subtest B1) helped obtain the reliable value of initial loss in conductivity ($LC_0$) when *EC* decreased with time. The study also showed that EC testing time could last in only 240 minutes but still produce an acceptable value of $LC_0$, which solves the problem related to time consumption when a series of tests were conducted. Finally, the temperature compensation coefficient of lime-soil solution with 5% hydrated lime is 1.9%, which can be used when the testing temperature is different from 25°C.

Mechanical properties improvements:

- Bentonite is the main component in soil, changing its liquid limit and linear shrinkage. While the liquid limit increases linearly with bentonite content, the linear shrinkage obtains a constant value of about 21% when the content of bentonite is over 30%.

- Adding hydrated lime with 5% to expansive soil decreased both the liquid limit and plastic limit of the soil, turning the soil as fat clay (CH) into elastic silt (MH) because of the high reduction in plastic index and liquid limit.
- Lime inclusion in the soil also facilitates reducing soil linear shrinkage from 21% to around 16.5%. The reduction was obtained after 7 days of curing and had no significant change after 28 days.
- Compaction tests were performed in sample preparation for free swelling tests, revealing a minor change in the maximum dry density (*MDD*) and the optimal moisture content (*OMC*) when 5% lime is added to expansive soil. The *MDD* is around 1.32 $Mg/m^3$, while *OMC* is about 29%.
- The free swelling ratio of studied soil is around 60%, regardless of soil saturation level, while the free swelling ratio of lime-treated soil relies on its saturation level and curing time. At *OMC* of 29% and 1 hour of curing, the swelling ratio of lime-treated soil is roughly 12%. However, it decreases to 2% or 0.5% if the moisture content is 25% or 15% at the same curing time, respectively. The free swelling ratio is almost zero after 28 days of curing.
- Swelling tests applying various methods, including swell-consolidation and zero-volume consolidation tests, confirms the same swelling pressure of soil at around 70 kPa. The consolidation behaviour of soil relies on the swelling displacement, the cell type and the sample size. The zero-volume constant-rate-of-strain consolidation tests using CBR mould generate the most reliable consolidation curve of studied soil.
- The compressive and tensile strength tests indicated a gradual increase of strength in soil when the lime content was added to soil from 3% to 9%. The strength increase was not significant when the curing time lasted to 28 days, compared to that after 7 days, suggesting lime-treated soil gained the most strength after 7 days.
- California bearing ratio tests also confirmed the strength improvement of soil mixed with hydrated lime due to a remarkable increase of *CBR* from 18.7% to 71.9%. However, both untreated and treated soils suffered a significant decrease in *CBR* values when soaked in water after 7 days. These curing days were proven to be sufficient to fully saturate the CBR samples, causing swelling in samples of untreated soil, hence reducing their *CBR* to roughly zero. For lime-treated soil, further soaking sample in more than 7 days reduced the bearing ratio to only 22.6% after 62 days of soaking. This strength reduction was in good agreement with the degradation of small-strain shear modulus ($G_{max}$) of lime-treated soil

after 56 days of curing. The decrease was related to the formation of calcium aluminium silicate and hydrate (CASH) in the forms of fibres and bars rather than gluing gels, reducing the bonding effect among soil particles. The existence of hydrate product was confirmed by the micro-structural analysis from the scanning electron microscopy (SEM) and energy-dispersive x-ray spectroscopy (EDS) test results.

- The study on the effective stress failure envelope of untreated soil and soil treated with 5% hydrated lime revealed that a remarkable improvement in both the internal friction angle and the cohesion could be achieved when lime was employed to stabilise the soil. The enhancement could be referred to the gluing effect of hydrate gels in soil matrix from pozzolanic between soil and lime after 28 days of curing. The presence of hydrate product is also the cause of the increase in matric suction of lime-treated soil after compaction, which is higher than soil suction by a half, around 150 kPa compared to roughly 100 kPa.

# CHAPTER 5

# Electrical Conductivity Tests for Expansive Soils Treated with Hydrated Lime and Bottom Ash

## 5.1 Introduction

In this chapter, the mechanical behaviour of expansive soil is investigated with the relationship with the results from electrical conductivity tests. The tests were used to investigate the pozzolanic reactivity of bottom ash, which were mixed with hydrated lime to stabilise expansive soils. The stages of conductivity curves from test results were analysed to clarify the reactive level of ash in different ratios to lime in studied soils. An analysis method to determine the initial loss in conductivity ($LC_0$) was also suggested to compare its changes in different contents of ash to hydrated lime. This parameter was then expressed in its correlation with swell-shrinkage and strength properties of soil. Therefore, this chapter is divided into two parts: (1) studies on mechanical behaviour of ash-lime-treated soil with various types of mixing ratio, followed by shrinkage-swelling investigation with the determined ratio of mixing; and (2) research on the relationship between $LC_0$ and mechanical properties of soil, particularly linear shrinkage and free swelling ratio. For strength properties, to establish their correlation with $LC_0$, three standard soil

tests were performed, namely UCS, CBR and bender element tests. Scanning Electron Microscopy (SEM) was also conducted for micro-structural analysis on tested samples.

## 5.2 Mechanical behaviour of ash-lime-treated soils with various mixing-ratio types

### 5.2.1 UCS tests with S-ratio

Figure 5.1 illustrates the effect of bottom ash content on unconfined compressive strength of treated expansive soil after 7 days of curing. An amount of 5% hydrated lime was also added to the ash-soil sample to examine the impacts of lime-ash combination on soil strength. As can be observed in Figure 5.1, *UCS* of ash-treated soil without lime fluctuated around 250 kPa, which was about 35 kPa lower than that of untreated soil. This implies that the addition of bottom ash into soils, after 7 curing days, slightly reduced the soil strength by 12.3% as the ash content increased from 5% to 30%. However, when 5% lime content was added into the ash-soil mixtures, the strength increased considerably to 553 kPa for soil treated with 5% bottom ash, which helped enhance the strength of ash-soil mixture by 326 kPa (approximately 143.5%). Therefore, it can be noted that bottom ash has an adverse effect on the soil strength for expansive soil modification if it is merely added to the soil without supplementary reagents like lime or cement. This finding is in good agreement with previous studies on this kind of ash (Kamei et al. 2013; Lu et al. 2014; Modarres and Nosoudy 2015; Seco et al. 2011).

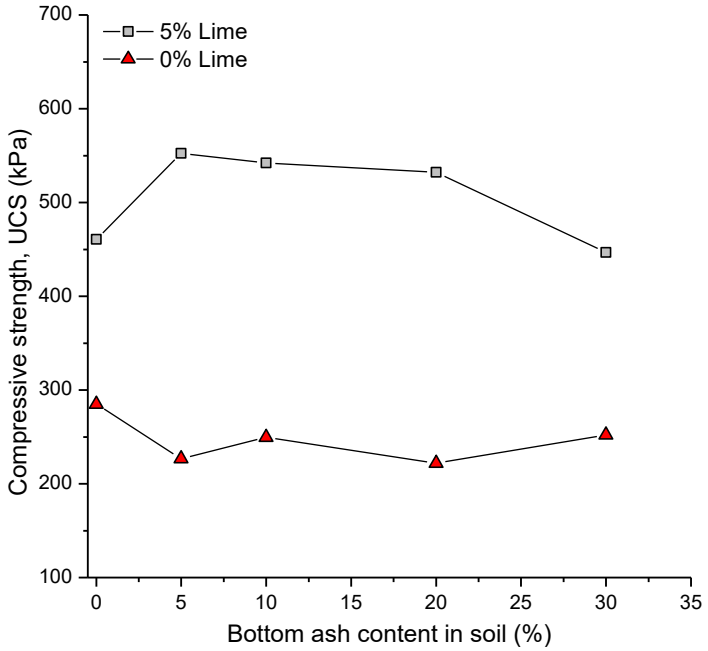


*Figure 5.1 Effect of bottom ash and hydrated lime on UCS of expansive soil samples after 7 days of curing (S-ratio)*

As can be seen in Figure 5.1, the 7-day-curing *UCS* values of lime-ash-treated soil showed a negligible decrease when the ash content approached 20%. Nevertheless, the strength still maintained a relatively same level at about 540 kPa before abruptly dropping to 447 kPa at the highest ash content (30%). This highlights the optimum combination content of lime and bottom ash for expansive soil stabilisation, ranging from 5% to 20%. The optimum combination content is defined as the highest combined additive content to achieve the highest compressive strength value (about 500 kPa), while the use of bottom ash can be maximized in an effective way.

It is also worthwhile to note that the combined effect of hydrated lime and bottom ash proves their merit in the strength improvement of expansive soil. This enhancement could stem from pozzolanic reactions brought by the combination of lime and silica from bottom ash. Consequently, cementitious bonds between clay particles developing in the moisturized lime-ash-soil mixtures harden their structural strength. Their *UCS*, therefore, are higher than that of lime-treated soil. However, once the content of bottom ash is greater than a certain level (e.g., 30%) that ash particles are abundant and left from their pozzolanic reactions with lime, these free grains of bottom ash could weaken the bonds between clay elements. Hence, the reduction of compressive strength would be a consequence as what occurs when an excessive content of bottom ash is used (see Figure 5.1). The interpretation of this investigation is consistent with previous research conducted on the lime-ash combination to stabilise expansive soil (Gullu 2014; Ranga 2016).

Regarding the curing effect on the *UCS* values, a series of UCS tests was prepared and conducted after 7 and 28 days of curing. Figure 5.2 depicts the variation of compressive strength values for ash treated soil samples with or without lime combination obtained after curing for up to 28 days. It is clear from the figure that the higher *UCS* is proportional to the longer curing time for lime-ash-soil mixtures, but the strength remains stable in the case of soil-ash samples. For instance, when curing time increased from 7 days to 28 days, there was about 32% increase in the *UCS* for lime-ash treated soil samples as ash content increasing from 0% to 10%. However, an insignificant *UCS* increase is observed for soil-ash specimens. The strength of soil treated with only ash after 28 days of curing even indicated a mild decrease when the ash content increased from 5% to 30%. By way of illustration, the 28-day *UCS* value of soil stabilised with 30% bottom ash was lower than the corresponding 7-day one (237 kPa compared to 252 kPa, respectively). By contrast, even though lime-ash-soil *UCS* after curing for 28 days declined markedly when ash content increased from 20% to 30%, the 28-day soil strength at 30% bottom ash-lime combination was still higher than that of 7-day cured samples, showing a growth of 40% from 447 kPa to 626 kPa, respectively. This increase was double when compared with the approximately 20%

improvement in *UCS* of the only lime-soil mixture as curing time extended from 7 to 28 days. Significantly, with 20% content of combined bottom ash-lime treated soil, the 28 days compressive strength leapt to 821 kPa, corresponding to a 54% improvement of *UCS* compared to the strength of soil treated with only lime at the same curing time. In order words, the strength improvement at 20% combined ash-lime content was more than 1.5 times, compared to the lime-soil *UCS*, and nearly triple of the ash-soil *UCS*. Such high increase in the strength with prolonged curing time is probably attributed to the reaction between lime and soil, leading to the more cementitious linkage formed in soil aggregates. The strength in soil-ash blends, on the other hand, is not reinforced by this chemical reaction, and thus it does not show any improvement in *UCS*.

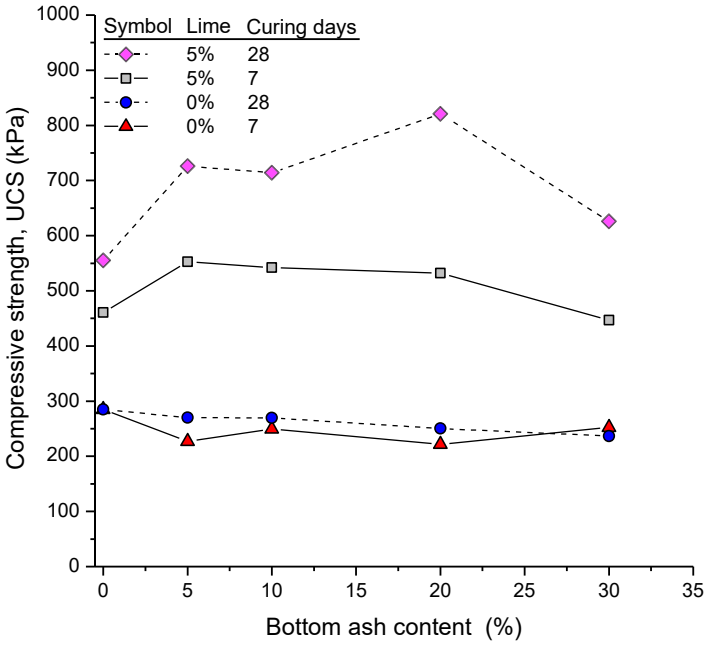


*Figure 5.2 Effect of bottom ash and lime on UCS of treated expansive soil at 7 days and 28 days of curing (S-ratio)*

When it comes to longer curing days, the same pattern is repeated. Figures 5.3 and 5.4 illustrate the impact of longer curing time on *UCS* of bottom-ash- and hydrated-lime-bottom-ash-stabilized expansive soil, respectively. Overall, the *UCS* of soil-ash admixtures increased gradually with the longer curing time from 7 days to 56 days (refer to Figure 5.3). However, this modest growth could not recover the initial *UCS* of parent soil samples which constitutes 285 kPa. The addition of 5% bottom ash into soil mixtures seemed to gain the same strength of untreated soil after curing for 56 days; meanwhile, the lower *UCS* value of about 260 kPa was observed for soils treated with higher bottom ash content at the same-curing-day, downgrading the original soil strength by 8.8%. Furthermore, whereas most specimens had an upward trend of *UCS* after 28 days, the sample with 10% ash had a slight drop from the day of 28 to 56. Interestingly, as shown

in Figure 5.4, the similar phenomenon can be observed for soils treated with the lime-ash combination. After 28 days of curing, the compressive strength of 10% combined ash-lime treated soil suddenly went down to become the weakest sample at the 56 days of curing. This low strength might be due to the binder dosage of bottom ash and its moisture content, which have a marked effect on the internal reaction of the admixture (Geetha and Ramamurthy 2011; Gullu 2014). Other reasons for this downward trend could be the physical properties of bottom ash related to particle size, surface properties, morphology and content of amorphous phases (Jaturapitakkul and Cheerarot 2003).

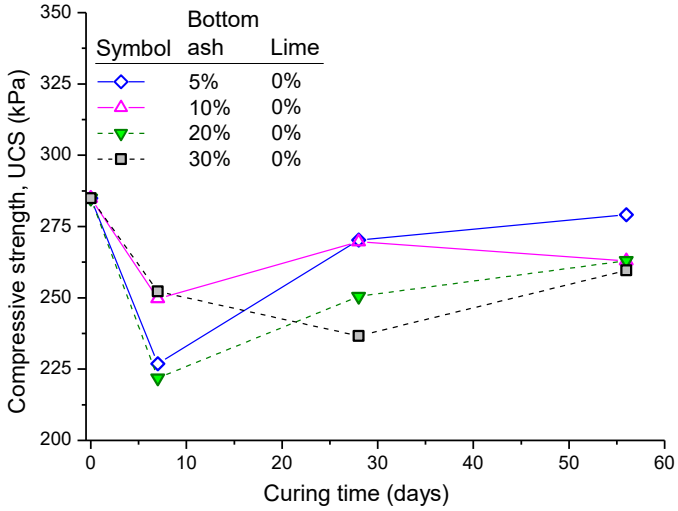


*Figure 5.3 Effect of curing time on UCS of expansive soil stabilised with different contents of bottom ash (0% Lime with S-ratio)*

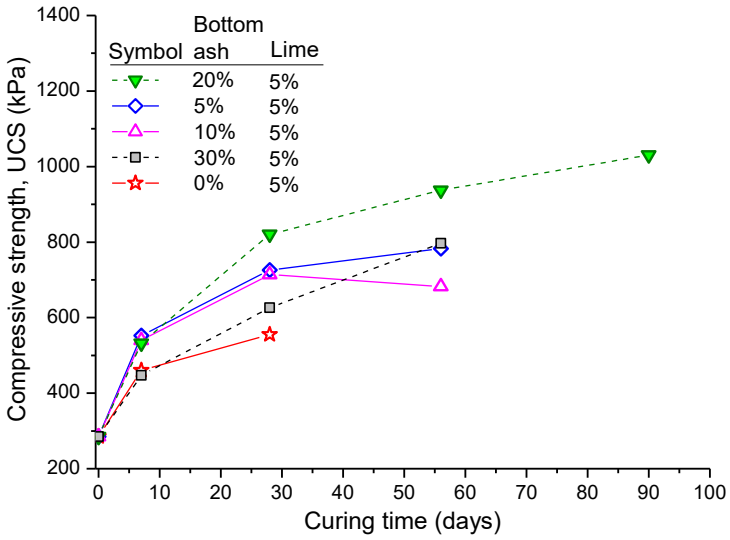


*Figure 5.4 Effect of curing time on UCS of 5% lime treated expansive soil with different contents of bottom ash (S-ratio)*

In stark contrast, Figure 5.4 also shows the significant increase in *UCS* of treated expansive soil with the ash-lime combination. It is also observed in all testing mixtures that after a curing period of more than 7 days, this *UCS* increase is set to accelerate at a slower pace than that from the beginning. This could be because the hardening process of soil stabilization in a few days after mixing creates cementitious bonds which burgeon and cover around soil particles. Such covering is a hindrance for allowing more lime to penetrate and be embedded in the soil aggregates. Consequently, the speed of forming the bonds decelerates, and the strength development goes steadily. Moreover, the smaller increment of *UCS* strength after 7 days of curing may be the result of crystal development in the mixtures (Boardman et al. 2001).

In comparison with the strength of untreated expansive soil as presented in Figure 5.4, the *UCS* increase of soil treated with 20% ash combined with 5% lime approximately doubled after 7 days, over tripled after 56 days and roughly quadrupled after 90 days of curing, becoming the highest strength sample all over the investigated curing days, and reaching the highest strength of 1 MPa. This indicates that the ratio of 20% bottom ash to 5% lime could be the optimum combination ratio of 1:4 for soil stabilisation. In addition, when compared with only lime treated soil, this combination ratio improved the strength of ash-lime-soil admixture by 15% after 7 days and 48% after 28 days of curing (see Figure 5.4). This finding indicates the combined effects of bottom ash and hydrated lime on expansive soil treatment. The combination yields the higher strength and the lower linear shrinkage than lime or bottom ash alone to stabilise the soil. It is also noted that the utilization of bottom ash-hydrated lime combination for expansive soil treatment feasibly minimizes the adverse impact of the bottom ash (waste) on the environment. The application also provides cost-effective construction material via reduction of lime dosage and extra soil reinforcement by the combination of lime and bottom ash.

### 5.2.2 ITS tests with S-ratio and T-ratio

The ITS test results are shown in Figures 5.5 and 5.6 with plots of tensile strength versus strain and photos which were taken on the broken half pieces of sample after the tests. Figure 5.5 illustrates the results of samples mixed with additive contents based on the soil dry weight (S-ratio), whereas Figure 5.6 depicts the experimental results for soils treated with additives, calculated by the total-dry-weight based ratio (T-ratio).

As can be seen from Figure 5.5, treated samples with 5% and 20% ash had higher tensile strength and corresponding axial strain than samples without ash treatment (over 200 kPa at about 0.6% compared to 188 kPa at 0.56%). The drop of peak stress was observed for samples with 10%

and 30% bottom ash content; meanwhile, their lower corresponding strains were about 0.5% (see Figure 5.5). From the visual observation of the cutting section of post-testing samples in Figure 5.5b, some lime particles could clearly be identified in specimens with 5% and 30% BA content, and more white dots observed in the 10% BA sample were indicated inside the white circles (Figure 5.5b). Regardless of the sampling technique because all samples had the same mixing quality, the phenomenon of lime remaining in the samples after 28 days proves that the level of consumed lime varied considerably among the testing mixtures. The remarkable decrease in the tensile strength as bottom ash content increased from 5% to 10% can be explained by the 5% additional increase of bottom ash that individually reduces the strength of its soil mixture without lime (Le et al. 2018, Ranga 2016). The abundant bottom ash in the 10% ash sample might lubricate the soil particles and push lime out the soil texture. Furthermore, in this sample, lime content of 5% based on the dry weight of soil can be turned out to be 4.35% of the total dry weight of the entire mixture, which could be not the optimal dosage of lime in the mixture. This is consistent with the previous findings of the adverse impacts on the strength of lime-treated soil with lime content over 4% (Sharma et al. 2008). However, when it comes to the sample with 20% bottom ash, the totally converted lime content decreased to 4% and the failure ITS and corresponding strain were found to reach their maximum values at 236 kPa and 0.6%, respectively, indicating a considerable increase of 50% in stress and 15.4% in strain when compared with the corresponding values of the lime-soil sample treated with 10% bottom ash. No lime dots can be seen in the longitudinal section of the 20% bottom ash-lime soil sample (Figure 5.5b), which confirms that the hydrated lime was almost consumed in the 1:4 ratio of lime to bottom ash. The surge in the failure tensile strength of samples with 30% bottom ash approaching the ITS level of 10% bottom ash also indicates that the ratio of 1 to 4 can be the optimum ratio of bottom ash to lime for tensile strength improvement of expansive soil. The higher ratio in the 30% ash sample produced greyer and darker traces of bottom ash (see the black ellipse in Figure 5.5b), proving the abundance of bottom ash in the mixture which caused the reduction of tensile strength. Furthermore, the relatively low content of lime could be the factor of the strength reduction because only 3.70% lime is used in terms of the total dry weight if converted from 5% lime on the soil dry weight basis. Interestingly, although both samples with 10% and 30% bottom ash had a lower tensile strength ($\sigma_T$) than that of the specimen without ash, their plateau strength in post-cracking behaviour is higher than that of 0% BA sample. This can be attributable to the column effect produced on the cracked cylindrical specimens under the diametric compression after cracking (Carmona & Aguado 2012). The existence of bottom ash in halves of samples at 10% and 30% improved the

plateau post-peak tensile strength by more than 40% $\sigma_T$ compared to the 0% ash specimen (Figure 5.5a).

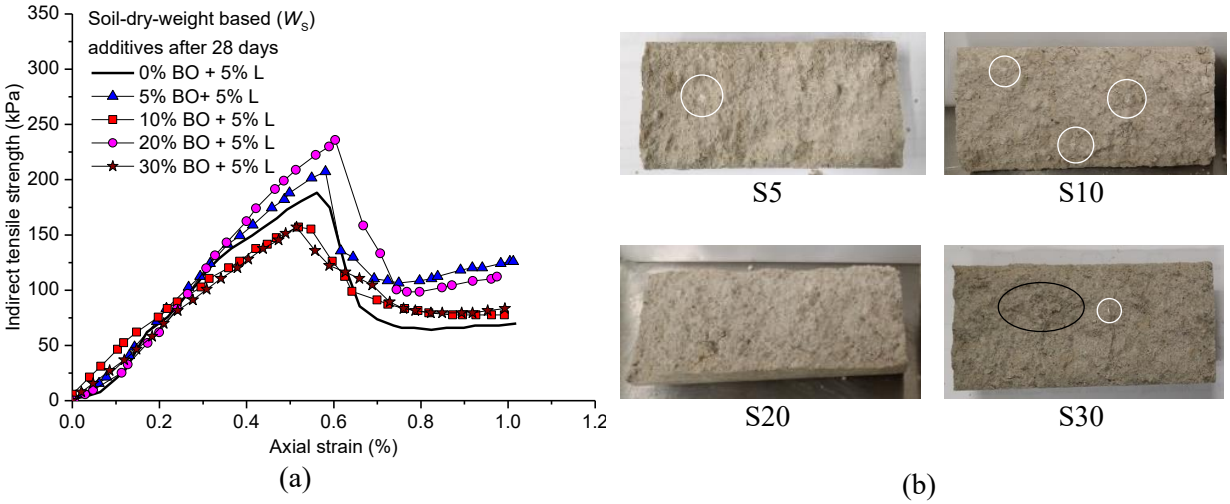


*Figure 5.5 Indirect tensile strength of bottom ash-lime-soil mixtures based on S-ratio after 28 days: (a) stress-strain relationships, (b) halves of samples after tests*

In the comparison with samples mixed by S-ratio, the samples mixed by T-ratio revealed the higher peak tensile strength and axial strain, as shown in Figure 5.6a. The soil sample mixed 20% BA by T-ratio was found to have the tensile strength of 314 kPa and the corresponding strain of about 0.73%, bringing about 33% increase in the tensile strength and 22% increase in the axial strain as compared to the corresponding values of sample mixed by S-ratio (see Figure 5.6b). It is worthy of note that as the BA content increased from 20% to 30%, there was an insignificant reduction of the tensile strength occurring in the sample with 30% bottom ash calculated based on the total-dry-weight (refer to Figure 5.6a), compared to its counterpart in Figure 5.6a. This might cause a confusing selection of the ultimate ratio of lime to bottom ash in their mixtures with expansive soil. While from the tests of samples with S-ratio, the ratio of 1 to 4 could be obtained (shown in Figure 5.5a), the ratio larger than 1:4 for the sample with T-ratio might be better since more bottom ash content (up to 30%) could be utilized but still producing a high strength sample (see Figure 5.6a). The tensile strength discrepancy between soil mixed with additive by S-ratio and T-ratio might be owing to the significant difference of the lime dosage between samples with 30% bottom ash by the soil dry weight and by the dry weight of total sample. In the samples with the highest ash content of 30%, a higher dosage of lime was used in treated samples with 5% lime by T-ratio than the corresponding mixture with 5% lime by S-ratio. The actual lime content for the sample calculated by S-ratio turns into 3.7% in the total dry-weight basis (T-ratio), which is much lower than the dosage of 5% lime in this total weight mixture. However, although more lime was used in the T-ratio-based samples than in the S-ratio-based samples, little trace of lime could be

found on the surfaces of all cracking halves from T-ratio-related samples (indicated in Figure 5.6b). This might be from the greater content of bottom ash in the T-ratio-based samples than in the S-ratio-based ones, which reacted effectively and sufficiently with most of hydrated lime in pozzolanic reactions and cementation. This enhanced their stress-strain response to the higher applied loads. Furthermore, darker spotted sections in Figure 5.6b as compared to those corresponding in Figure 5.5b indicate that more bottom ash, which is seen as the frictional and coarse material, penetrates and totally encloses the lime-soil texture in the T-ratio samples to develop the agglomeration. This effect changes the soil mixture from fine to coarse material, resulting in an increase of internal friction angle as well as the magnitude of interlocking (Gullu 2014; Kim & Do 2012). The higher degree of interlocking greatly enhances the peak failure stress as well as the plateau stress of the samples with the higher content of bottom ash.

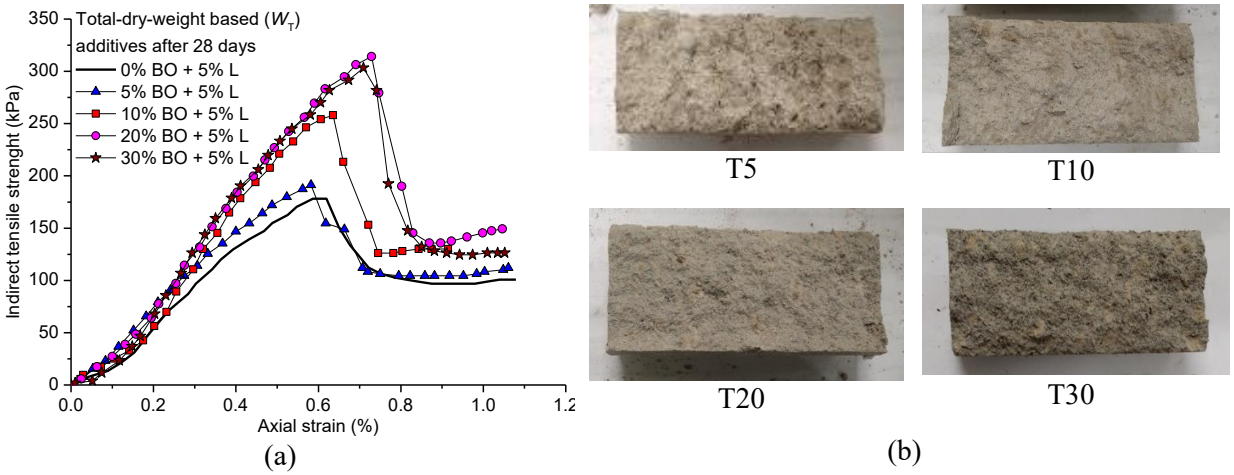


*Figure 5.6 Indirect tensile strength of bottom ash-lime-soil mixtures based on the total dry weight (T-ratio) after 28 days: (a) stress-strain relationships, (b) halves of samples after tests*

The variation of the average indirect tensile strength with ash content using the two dry-weight-based ratios and the curing time is shown in Figure 5.7. As expected, there was not a considerable improvement in the ITS for samples mixed with 5% bottom ash by S-ratio and T-ratio due to the insignificant difference in the mixing content between them. However, an equal increase of about 45% of the initial 7-day ITS was observed for the T-ratio-based samples compared to that of the S-ratio-based ones when the bottom ash content increased from 10% to 30% after 7 days of curing (see Figure 5.7). This equal gap points out the effect of lime dosage reduction on initial pozzolanic reactions in the S-ratio samples. In these samples, as the addition of BA into soils mixed with 5% lime by S-ratio increased from 10% to 30%, this 5% lime content if calculated by T-ratio in the BA-lime-soil mixture would reduce from 4.35% to 3.70%. This minor fluctuation of lime content around 4% may slightly reduce ITS of the S-ratio samples

compared to T-ratio specimens after 7 days. Overall, the 7-day soil-weight-based sample strength reached a peak at 5% content of bottom ash followed by a slight decrease, while the S-ratio tensile strength after 28 days obtained the highest value at 20% ash content, as shown in Figure 5.7. However, the T-ratio-related strength was higher than this S-ratio-counterpart by a great increase of about 53% compared to the initial 28-day ITS. This indicates that the higher ITS development with longer curing time was observed for the T-ratio samples as compared with the S-ratio samples. Moreover, the T-ratio sample with 30% ash content reached the highest ITS of 333 kPa, resulting in the largest gap between the T-ratio sample and its counterparts at this content. The highest strength of the sample at 30% BA content agrees well with the study on bottom ash conducted by Gullu (2014).

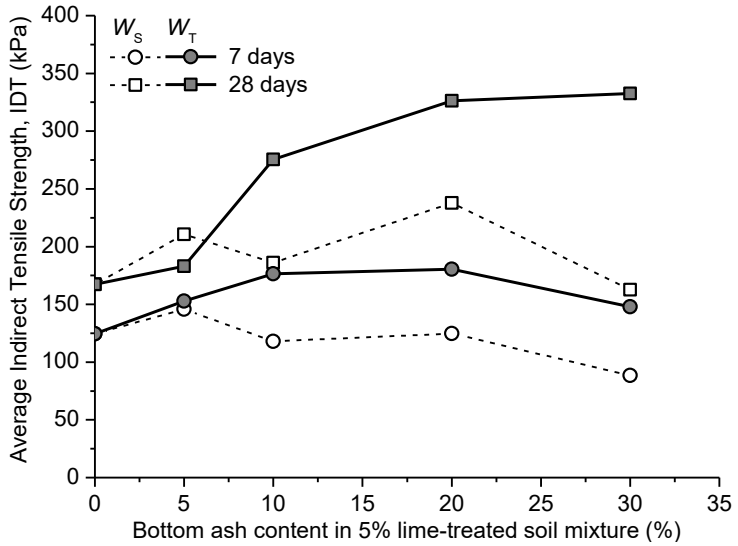


*Figure 5.7 Indirect tensile strength of bottom ash-5% lime-soil samples by soil weight $W_S$ (S-ratio) and total weight $W_T$ (T-ratio) after 7 and 28 days*

### 5.2.3 UCS and CBR tests with T-ratio and SB-ratio

Unconfined compressive and California Bearing tests were carried out for 5%-lime treated soils in various bottom contents from 0% to 40%, as presented in Figure 5.8. Two different ratios, namely total ratio (T-ratio) and soil-bottom-ash ratio (SB-ratio), are also shown in this figure. While T-ratio is depicted in Figures 5.8a and 5.8c, SB-ratio is shown in Figure 5.8b and 5.8d. Although mixing ratios are different, the highest values in *UCS* and *CBR* seem to be at 25% in bottom ash content (see Figure 5.8). However, their values are different between two different ratios. After 28 days for curing, all *UCS* values for samples with SB-ratio are higher than those with T-ratio. Unlike T-ratio-samples, only after 56 days, treated soils with SB-ratio revealed the peak of *UCS* at 25% in ash content, as illustrated in Figure 5.8b. A similar pattern was repeated in *CBR* results. *CBR* values of samples with SB-ratio are higher than those with T-ratio in bottom ash

content from 5 to 15 %. With higher ash content from 20 to 30%, soaked *CBR* significantly jumped to about 90%, much higher than unsoaked *CBR*. However, saturated *CBR* collapsed at 40% in ash content, which is much smaller than un-saturated *CBR* of larger-soil-sized samples (see Figure 5.8c-d). In short, some phenomena were observed from destructive tests as follows:

(1) The optimal ratio of bottom ash is 25%, shown in both *UCS* and *CBR* results;
(2) Higher *UCS* of samples with SB-ratio than T-ratio;
(3) Higher soaked *CBR* of samples with T-ratio than unsoaked *CBR* of SB-ratio-based specimens at around the optimal ash ratio of 25%.

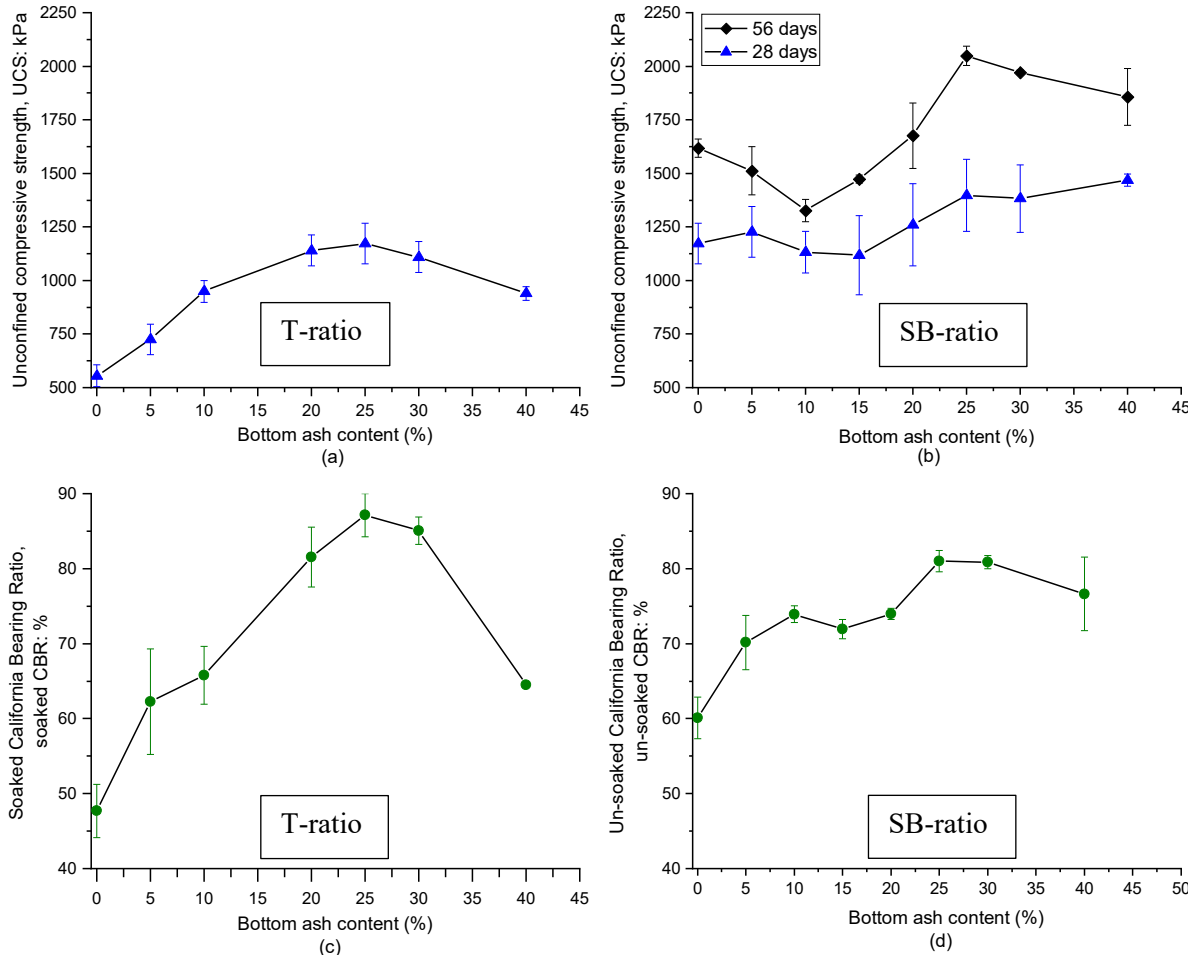


*Figure 5.8 Unconfined compressive strength and California bearing ratio after compaction: (a) UCS test with T-ratio; (b) UCS test with SB-ratio; (c) soaked CBR test with T-ratio; (d) unsoaked CBR test with SB-ratio.*

### 5.2.4 Bender element and matric suction tests with SB ratio

From the analysis on electrical conductivity, UCS and CBR test results, the ash-lime ratio of 25% to 5% was selected to constitute samples for bender element and matric suction tests (i.e., sample SB25). While the aim of bender element tests is to investigate the changes in small-strain shear

modulus (denoted as $G_{max}$) of treated soils, the matric suction test is used to find out the changes of suction in treated samples. For bender elements tests, the change of $G_{max}$ after compaction can be investigated. Particularly, in this study, the $G_{max}$ of SB25 (soil treated with 5% lime and 25% bottom ash in soil-ash ratio) is compared between compaction at *OMC* and one at the saturated side of *OMC*.

The variations of $G_{max}$ of treated and untreated soil samples are shown in Figure 5.9. Although $G_{max}$ of the parent soil levelled off around 50 MPa, $G_{max}$ of samples treated with lime and bottom ash went up from roughly 120 MPa to around 200 MPa after 1 day of curing. However, the effect of time on $G_{max}$ evolution varied between samples with or without bottom ash. It is clear that the soil sample treated with lime only had a gradual growth of strength to the peak of 353 MPa over 21curing days, whereas samples with both lime and ash had $G_{max}$ start rocketing to 500 MPa after 7 days (see Figure 5.9). However, after 14 days, the growth of $G_{max}$ in sample SB25 decelerated and gained the highest value at 581 MPa after 56 days. After a 56-day period, all treated samples suffered the degradation of $G_{max}$ at the same rate, whereas parent soil still had the strength increasing slowly with marginal values.

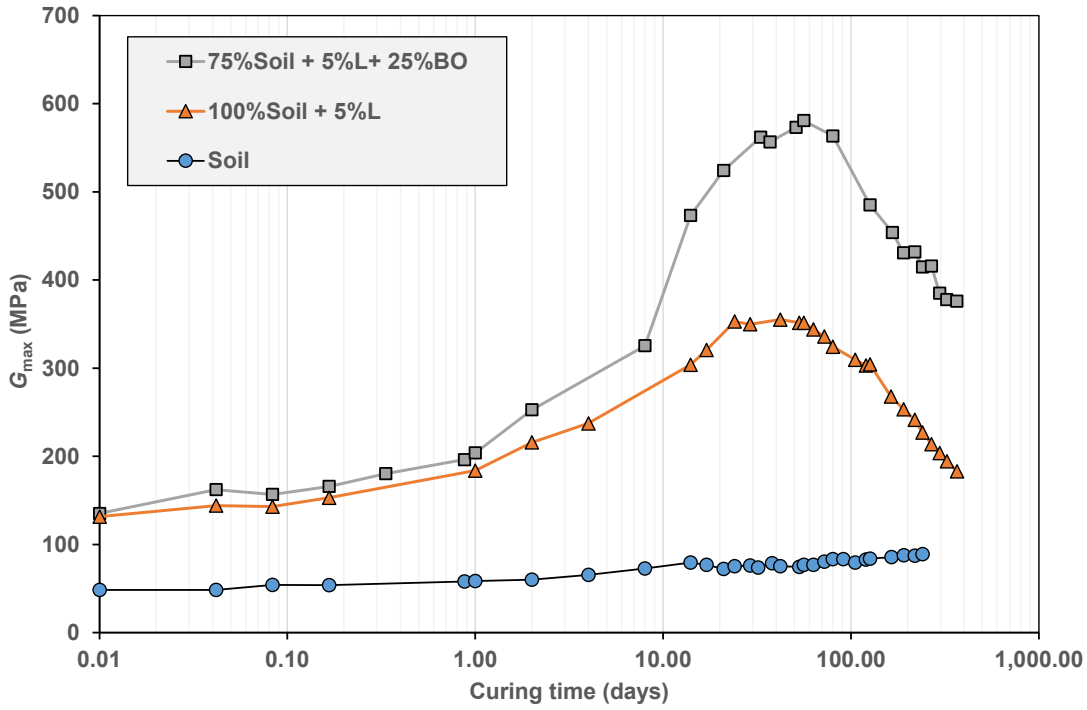


*Figure 5.9 Variation of $G_{max}$ with curing time for untreated soil and soil treated with hydrated lime and bottom ash*

Conversely, Figure 5.10 shows that the saturated sample, treated with 25% bottom ash and 5% lime, indicates no degradation of $G_{max}$ in the long term, and its value is levelled off at 653 MPa,

which is the highest shear modulus among all samples considered. Like the sample compacted at *OMC*, the $G_{max}$ of wet bottom-ash-lime treated soil started initially with a low value approximately 100 MPa after compaction. However, $G_{max}$ of the wet sample accelerated quickly from the first day to obtain the same modulus value of the optimal-moisture-content sample after 8 days (see the identical points of two curves shown in Figure 5.10). Over 14 days, the $G_{max}$ continuously grew and obtained the high of 653 MPa and still kept this value over 200 days. The constant value of $G_{max}$ at the wet side after 90 days is associated with cementitious compounds created in soil, bonding particles together (Wang et al., 2019). These compounds contain calcium silicate hydrate (CSH) products in the form of gels that glue soil aggregates and keep soil strength stable. However, in drier conditions, these products are precipitated in the sheet-like structure with intertwining gaps in soil, reducing the shear strength of soil (Chakraborty & Nair, 2020). It can also be suggested that if more water is provided during the curing period, CSH is distributed in a reticular network on surface layer with the interior in the shape of fibre bundles, which reinforces the strength of treated soil (Zhang et al., 2018).

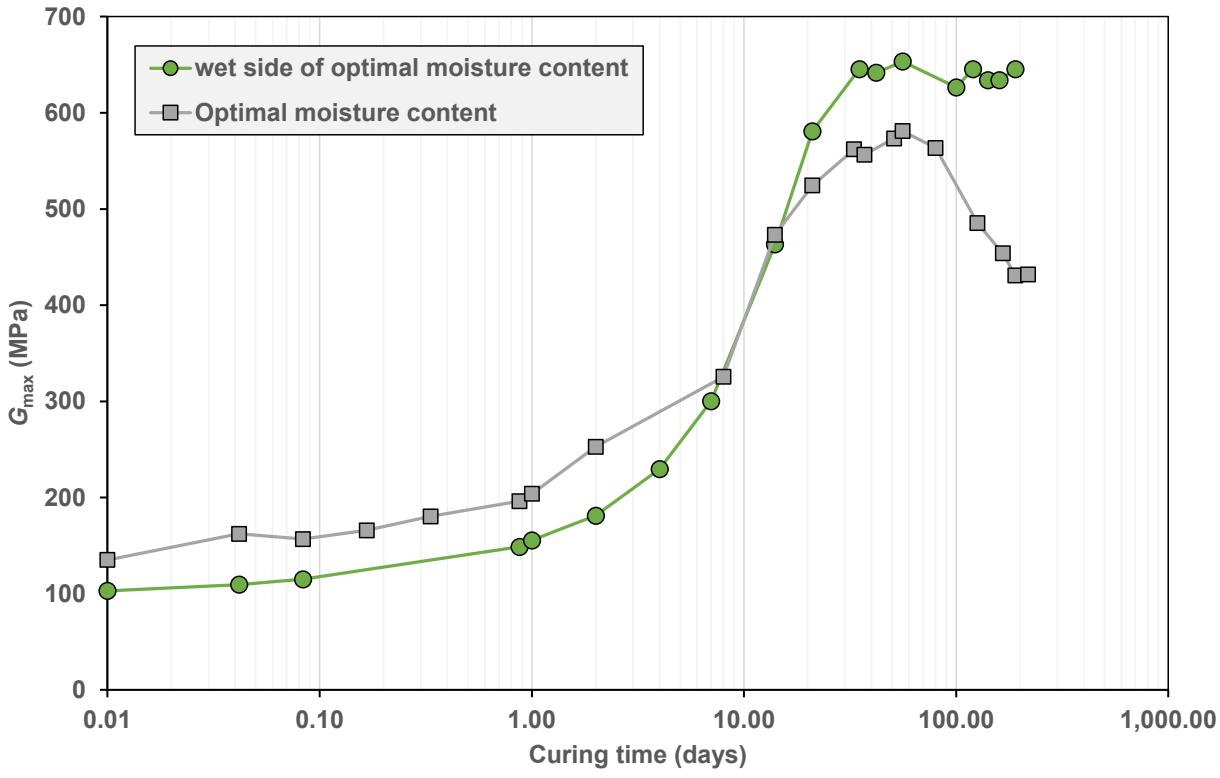


*Figure 5.10. Change in $G_{max}$ of soil treated with 5% hydrated lime and 25% bottom ash (compacted at the wet side of the optimal moisture content)*

Figure 5.11 demonstrates the change in matric suction of soil specimens treated by lime, and bottom ash. It is worthy to note that the samples are constituted by the static compaction method

at their maximum dry density and optimal moisture content. After compaction, the samples were kept in jars with the attachment of three tacked filter papers between two specimens. On the date equivalent to a curing time, the jars were opened to measure the moisture of middle paper so that the matric suction could be found. In each soil material, there would be 4 points collected in the duration from 10 days to 90 days to monitor the change of suction with time, resulting in the plot shown in Figure 5.11. Each point has at least 2 reading data to compare and obtain the average value of suction. It is obvious that the matric suction of soil with 5% lime was highest over time, increasing steadily from 170 kPa after 7 curing days to the high of 196 kPa on the day of 90. Meanwhile, the bottom-ash sample had the lowest matric suction which decreased gradually from 73 kPa to only 54 kPa after 90 curing days. This suction decrease of soil with bottom-ash is attributable to the fact that spaces inside bottom ash spheres were opened, and hydrate products (Calcium Silicate Hydrate and Calcium Aluminium Silicate Hydrate) were formed on internal ash surfaces.

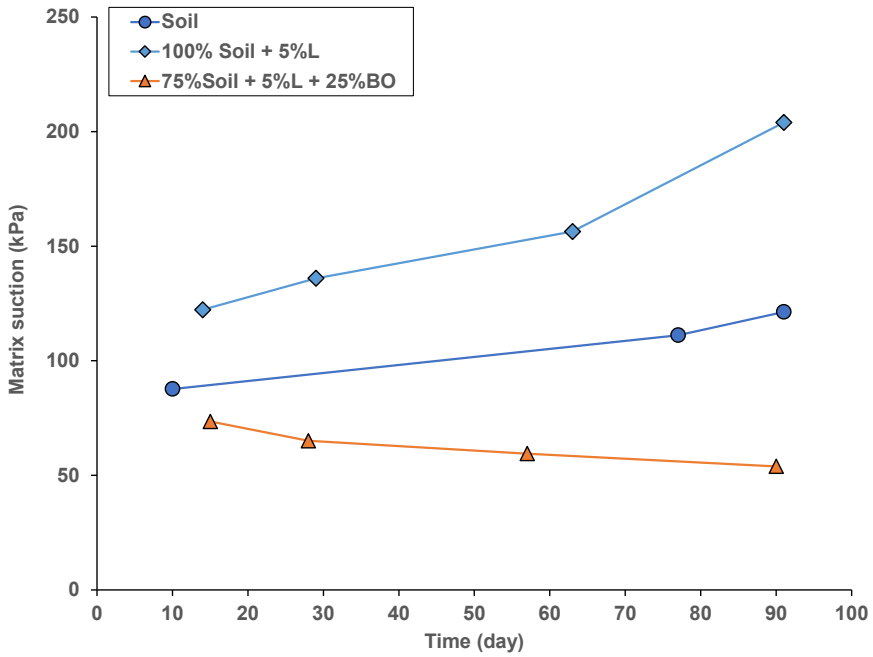


*Figure 5.11 Matric suction of soil samples treated by hydrated lime and bottom ash*

### 5.3 Shrinkage-swelling results

This section assesses shrinkage-swelling behaviour of bottom-ash-lime treated soils to investigate its relationship with the initial loss in electrical conductivity ($LC_0$) from electrical conductivity test. In linear shrinkage and free swelling tests, the ratio of bottom ash – soil – lime is based on the total dry weight of soil and ash as 100%, compared to lime with 5%.

### 5.3.1 Linear Shrinkage

Figure 5.12 shows pictures time-lapsed during the linear shrinkage test. As can be seen in these photos, the shrinkage soon developed at the first hour of drying. The total width of final cracks ($L_{shrinkage}$) was measured to determine the linear shrinkage ($LS$ (%) = $L_{shrinkage}/L_m \times 100$, where $L_m$ is the length of mould).

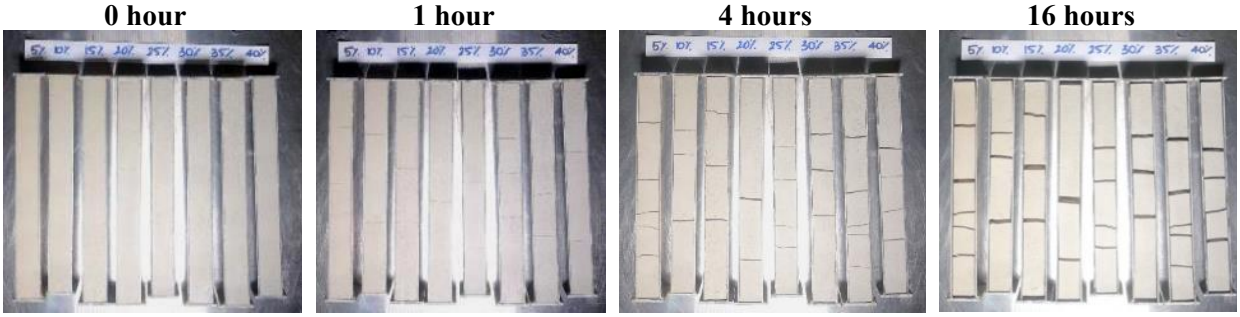


*Figure 5.12 Photographs of the samples during linear shrinkage tests*

Figure 5.13 illustrates the liquid limit and linear shrinkage versus the content of bottom ash from 0 to 40%. It can be seen that $LL$ was lower at higher contents of bottom ash ($N_{BO}$). However, $LS$ decreased when $N_{BO}$ increased from 0 to 15% and from 25% to 40%, but $LS$ levelled off at around 14% in the range of $N_{BO}$ from 15% to 25%.

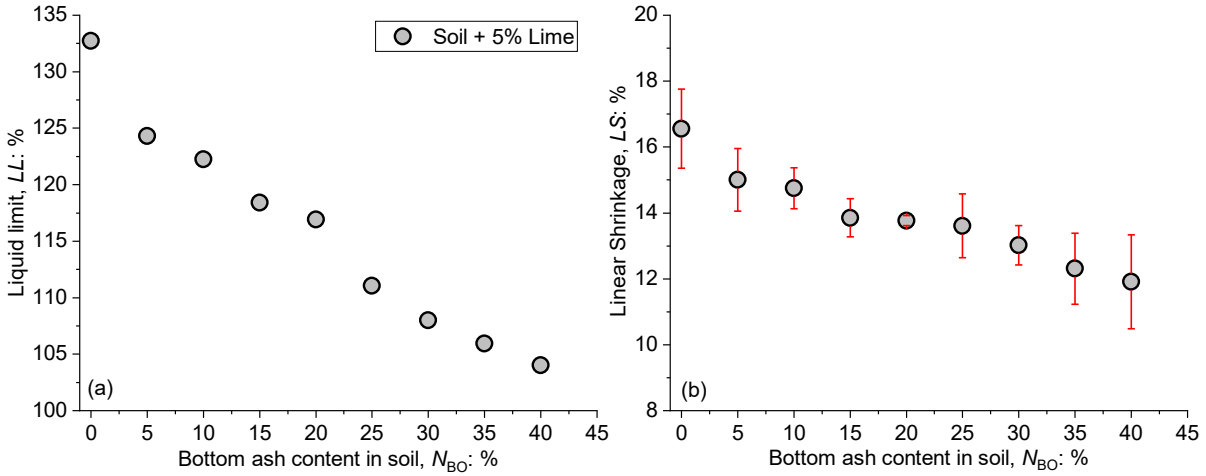


*Figure 5.13 (a) Liquid Limit (LL) and (b) Linear shrinkage (LS) with various bottom ash contents $N_{BO}$.*

### 5.3.2 Free swelling ratio

Swelling deformation versus elapsed time is shown in Figure 5.14a. All the curves show a stabilisation after 100 min, and the final results, taken at 1440 min, which are plotted versus bottom ash content in Figure 5.14a. This figure shows lower swelling ratios at higher ash contents. In addition, the relation between these two parameters can be correlated with two slopes separated by the bottom ash content of 15% (see Figure 5.14b).

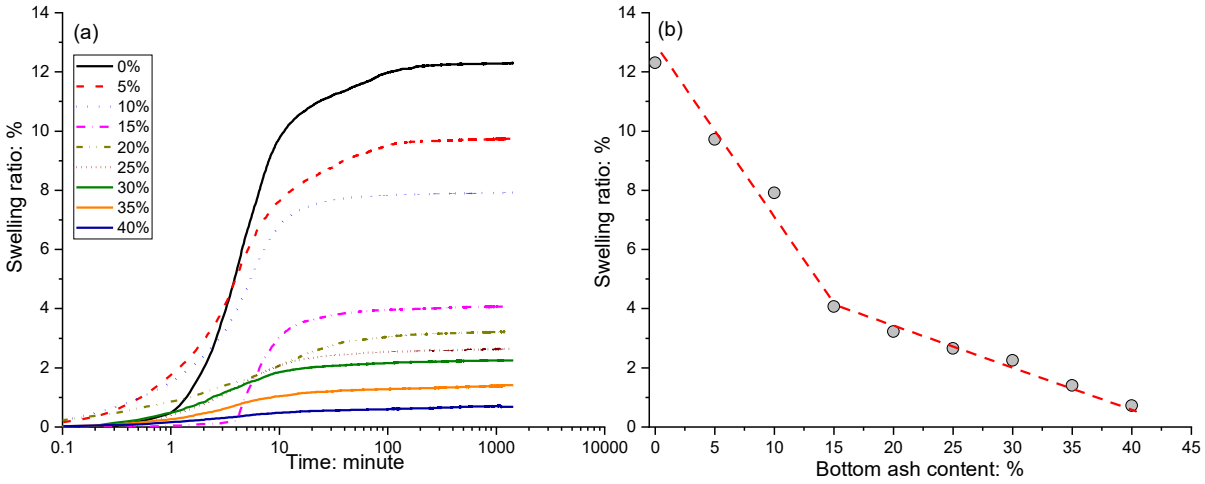


*Figure 5.14 Swelling ratio versus (a) elapsed time and (b) bottom ash content*

### 5.4 Electrical conductivity tests

The portions of components in electrical conductivity tests were based on total dry mass of soil and ash, equalling to 100% in comparison to 5% in lime content (SB-ratio). Figure 5.15 shows $LC_0$ for various bottom ash contents and the change in intensity of montmorillonite from XRD analysis. The results show that $LC_0$ of the lime-soil mixture was equal to 28%, but it reduced quickly when small content of bottom ash was added. For bottom ash content higher than 15%, $LC_0$ decreased gradually, which was similar to montmorillonite intensity but different from the mullite trend.

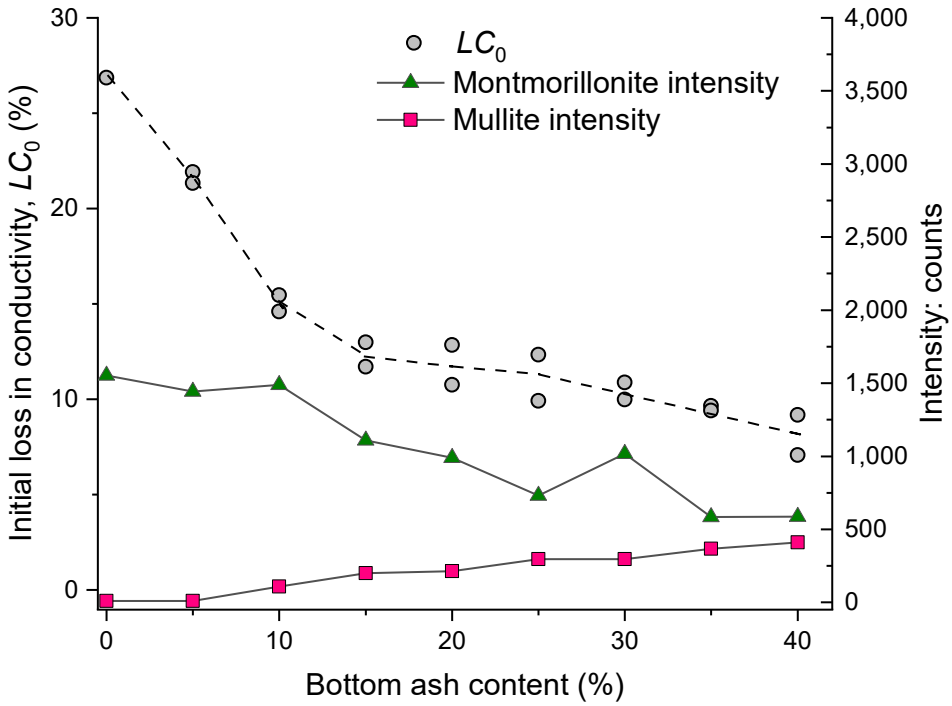


*Figure 5.15 Change of $LC_0$ with various bottom ash contents*

### 5.5 Comparison of $LC_0$, linear shrinkage and free swelling ratio with bottom ash content

Figure 5.16 summarises the relationship between initial loss in conductivity, linear shrinkage, and swelling ratio with bottom ash content. It is obvious that shrinkage, swelling and conductivity parameters decreased significantly when bottom ash content from 0% to 15% was added to the soil. From 15% to 40% in ash content, the decreasing rate is smaller in conductivity and shrinkage-swelling potential. However, while both $LC_0$ and free swelling ratio reduce gradually from 15% to 40% in bottom ash content, linear shrinkage goes down from over 25% ash at the same pace with that in ash content from 0% to 15%. It is clear that the change in the initial loss in conductivity reflected well the swelling behaviour, particularly in the bottom content from 15% to 40%, while linear shrinkage does not quite follow the same pattern in ash content from 15% to 25% with the existence of plateau. Nevertheless, it can be seen that 15% is the content of ash starting to change the characteristics of studied soil mixes to limit the reduction of conductivity loss, shrinkage and swelling ratio. Further analysis on XRD and SEM results of testing samples at the ash content from 15% to 20% may explain the phenomenon.

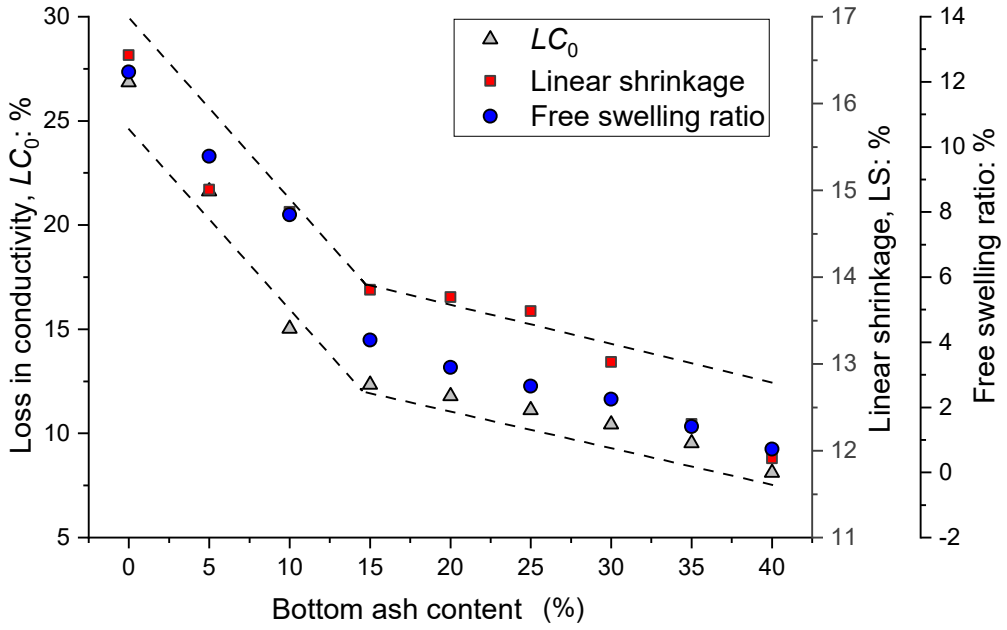


*Figure 5.16 Summary of studied parameters in relationship with bottom ash contents*

### 5.6 Micro-structural analysis

#### 5.6.1 XRD analysis

Figure 5.17 demonstrates the XRD results of EC samples with various bottom ash contents. The Montmorillonite intensity values (the peak intensity at the diffraction angle of 5.887), determined

from Figure 5.17, were plotted in Figure 5.16 versus bottom ash content. These values are high at bottom ash content equal to 0% – 10% and decrease progressively with higher bottom ash content.

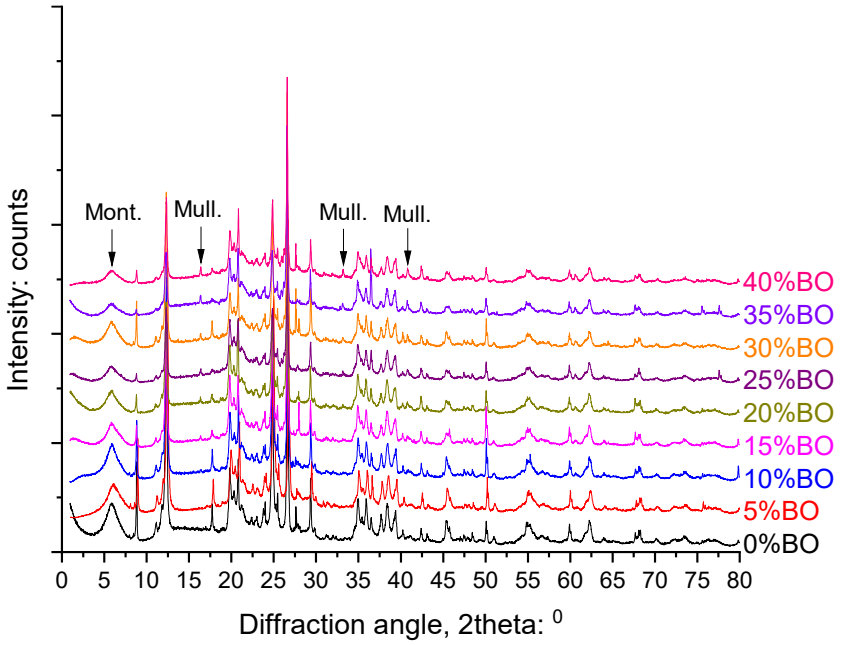


*Figure 5.17 Variation of XRD results from EC samples with various contents of bottom ash (Note: Mont.=Montmorillonite, Mull.=Mullite)*

### 5.6.2 SEM analysis

Given in Figure 5.18 are SEM images of bottom ash from LS samples at low bottom ash content (5% - 20%). At 5%, bottom ash surface is relatively smooth (see the sample with 5% bottom ash in Figure 5.18). However, from 10%, a rough area is gradually developed and obviously appeared at the ash content of 15% and 20% (refer to Figure 5.18 from 10% to 20% bottom ash). Similarly, the bottom ash spheres are rough, but in a gel form for the ash content from 25% to 40%, shown in Figure 5.19.

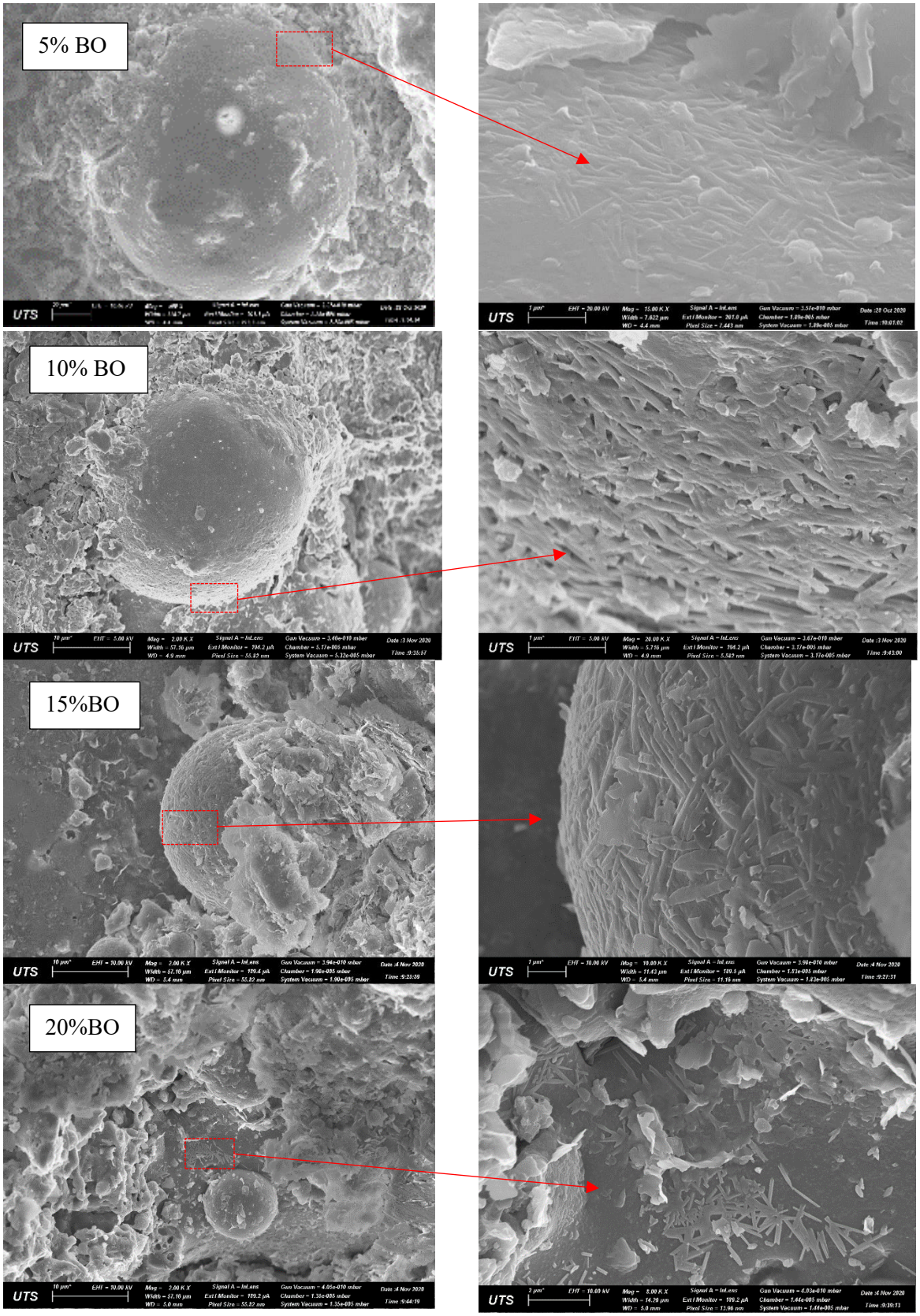


*Figure 5.18 SEM photos on samples at low bottom ash contents (5% – 20%)*

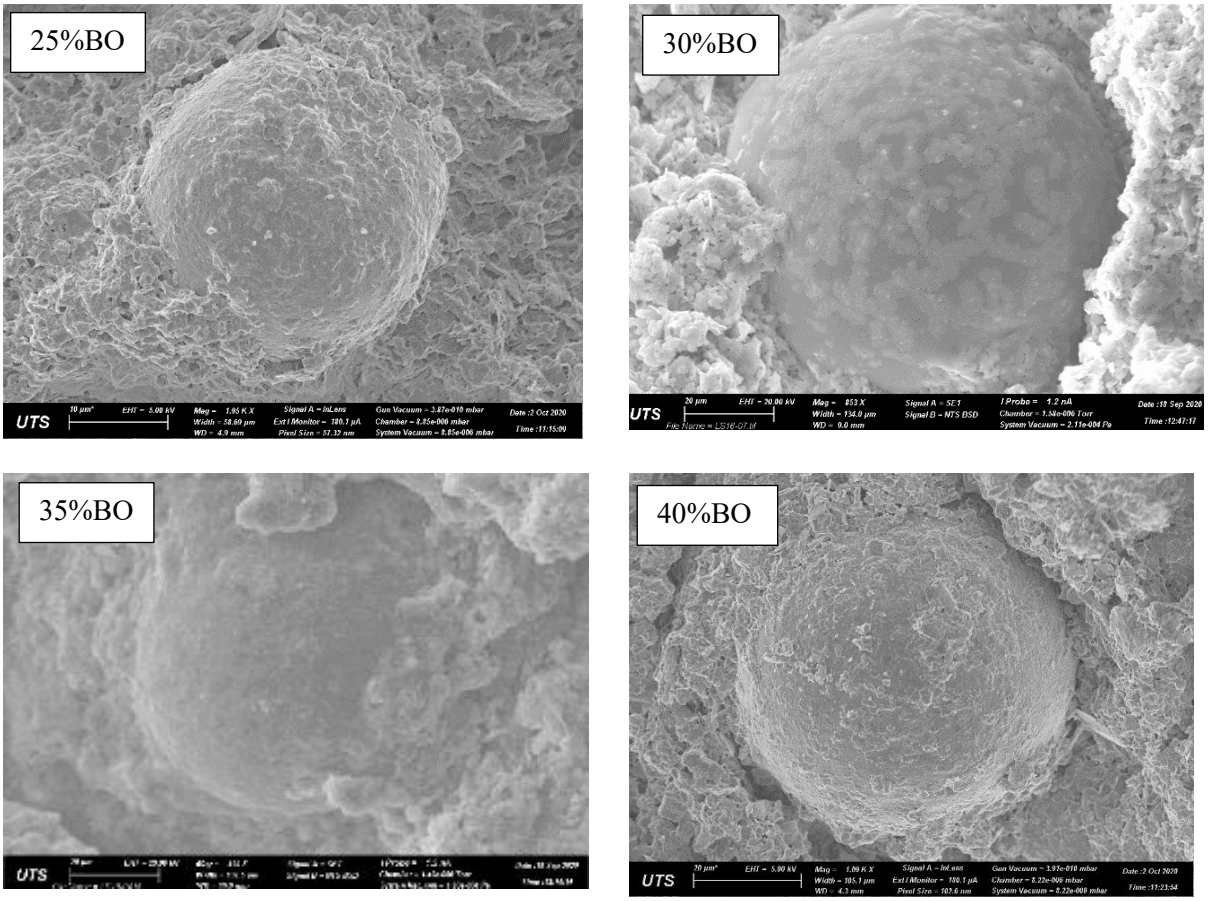


*Figure 5.19 SEM photos on at high bottom ash contents (25% – 40%)*

Micro-structural analysis on UCS, CBR samples using SEM tests can provide images of ash in its contact with soil and hydrated lime. Figure 5.20 illustrates that the bottom ash particles embraced in soil matric and hydrated lime for SB25 samples after 28 days of curing in UCS and CBR tests. It is clear that both samples have needle crystals appearing on the surface of bottom ash. Furthermore, the needles are embraced by cementitious gel compounds. Both crystals and gels grow towards the directions along the surface of bottom ash, which is near the contact between ash and soil. Few hydrated lime laminar crystals were observed in these areas of studied samples.

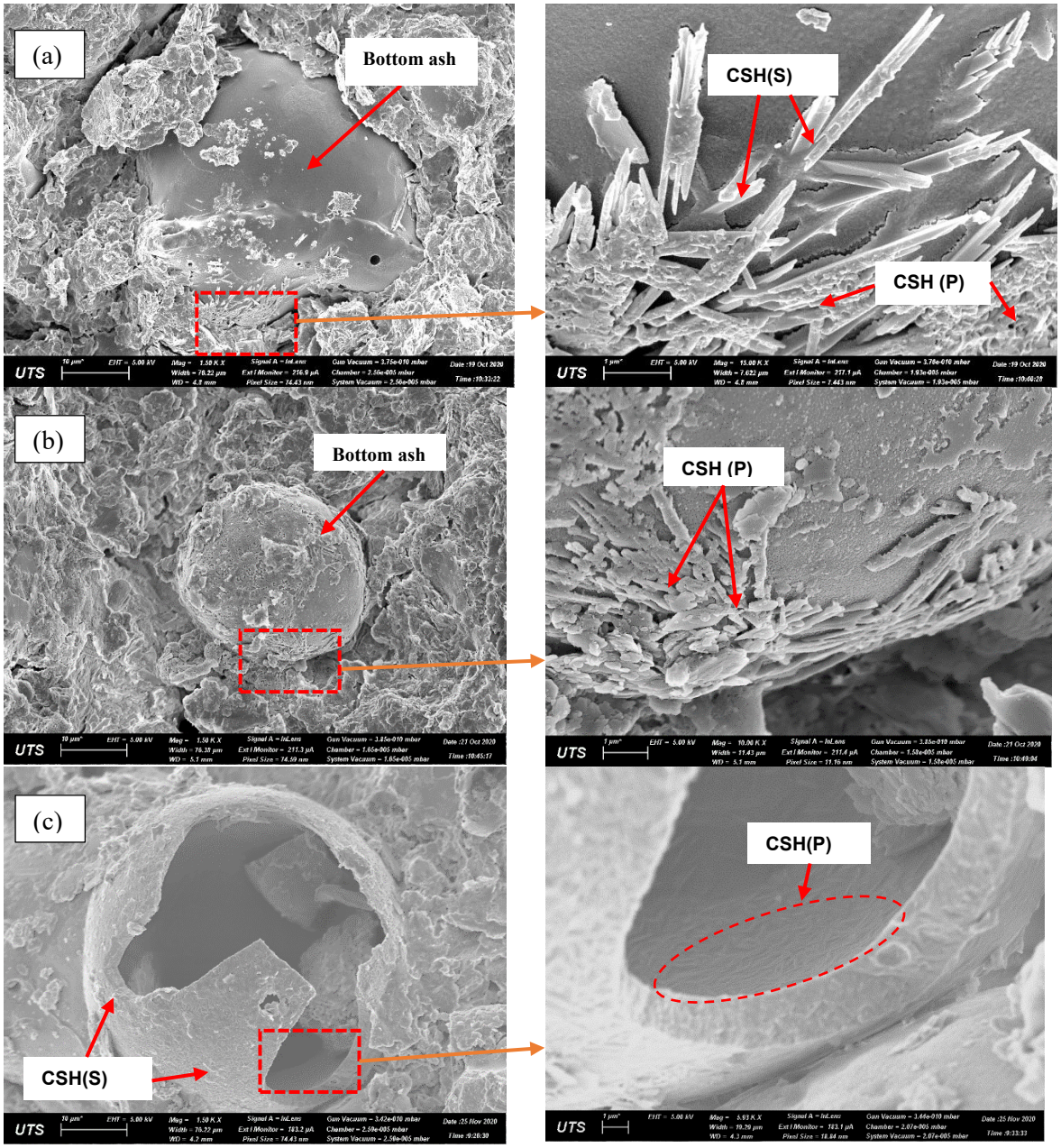


*Figure 5.20. SEM analysis on soil samples treated with hydrated lime and bottom ash after 28 days on (a) UCS samples, (b) on CBR samples indicating CSH (P), and (c) on CBR samples indicating CSH(P)*

As shown in Figure 5.20, the strength development in treated soils is correlated to the formation of hydrated gels, namely Calcium-Silicate-Hydrate (CSH). In a fibrous structure, the primary CSH or CSH(P) with Ca/Si ratio >1.5 appeared on ash surface to glue ash to soil aggregate in the interfacial transition zone (ITZ), as observed by other authors (He et al., 2011; Jha & Sivapullaiah, 2017). After 28 days for curing, the hydrated gels CSH(P) gradually turn into the sheet-like form, which is identified as the secondary CSH (S) with Ca/Si ratio < 1.5 (He et al., 2011), shown in Figure 5.20a. With the existence of CSH (S), the formation of floccules was triggered (Figure 5.20a). The phenomenon was also observed by Ríos-Parada et al. (2017). As a

result, both CSH (S) and flower-like CSH (P) densified ITZ (Ríos-Parada et al., 2017; Zhang et al., 2018). This results in less porous voids, which plays a notable role in efficient load transferring between soil particles and bottom ash to increase the compressive strength of treated soil (Ríos-Parada et al., 2017). Consequently, just after 1 day, $G_{max}$ of sample SB25 increased remarkably to overtake the strength of specimen S0 (lime-treated soil). After 28 days, the needle hydrate CSH(S) grew in ITZ of sample SB25, which made their $G_{max}$ escalate to about 580 MPa after 56 days, doubling that of S0 sample after the same curing time (refer to Figure 5.9).

However, after 56 days of curing, all samples had a considerable drop in $G_{max}$, which significantly decreased to 400 MPa for BO25 samples and about 200 MPa for the SL specimen after 210 days. This is due to the fact that, after a long curing period, more precipitated CSH was produced, holding water with its affinity capacity, which deterred the hydration of stabilised soil layers, thus deteriorating their strength properties (Chakraborty & Nair, 2020). Regarding Figure 5.20c, under dynamic compaction loading, fragile bottom ash particles in diameters of around 2 mm could easily be broken and randomly distributed in soil matric, and breaking even occurred in ash with smaller sizes, less than 75 μm. More broken ash debris significantly contributed to pozzolanic reaction of ash with lime and opened inside surfaces of bottom ash where more CSH(P) were nucleated (see Figure 5.20c). The puncture and breaking of bottom ash, as shown in Figure 5.20, also confirm the increase of micro-void in soil structure, which reduces the matric suction of lime-ash treated soil with time (refer to Figure 5.11).

## 5.7 Discussion on electrical conductivity results

### 5.7.1 Correlations between electrical conductivity and shrinkage-swelling results

The electrical conductivity method is often utilised to determine the pozzolanic performance between ash as a pozzolan material and hydrated lime (Paya et al., 2001; Tashima et al., 2014; Velázquez et al., 2014). Since mixing ash in water needs a long time due to its porous structure with soluble salts, the conductivity procedure was separated into two mixes with water, one for ash-lime combination and one for ash only (Paya et al., 2001). However, when it comes to soil-ash samples because clay is absorbing and more soluble than coarse ash or sand, clay clods appears in many forms during the initial stage of mixing with water (Abu-Hassanein et al., 1996). This may disturb the *EC* evolution of coarse material like bottom ash if soil and ash are mixed all together in water. This is also the reason why in pH tests for lime-ash mixture, only fine particles under the sieve of 425 μm are used (ASTM D6276, 2019). To avoid clay clod and include coarse materials, such as ash and sand, EC test procedure followed Test B of electrical conductivity.

Within this procedure, clay components (i.e., bentonite and kaolinite) were well mixed with water before the test was conducted in Subtest B1. The initial loss in conductivity ($LC_0$) was calculated in percentage as a relative value, making this value less dependent on absolute *EC* values (Frías et al., 2005; Paya et al., 2001; Tashima et al., 2014; Velázquez et al., 2014; Villar-Cociña et al., 2003). Furthermore, in order to estimate the test reliability, two samples were repeated for each $LC_0$ with the inclusion of bottom ash. The conductivity results indicated a good repeatability in $LC_0$ values as shown in Figure 5.15.

The proposed EC test was used to measure the change of initial loss in conductivity ($LC_0$) when more ash replaces expansive soil in their mixtures. For bottom ash content higher than 15%, a plateau of $LC_0$ with the increase of ash content was observed (see Figure 5.15), indicating that from this percentage, there was an overdosage of pozzolan from ash-soil mix, compared to hydrated lime (Paya et al., 2001). In chemical analysis, this indicates the starting dominance of mullite over montmorillonite when the bottom ash content of 15% was added (refer to Figure 5.15), causing the reduction of the expansive mineral from this percentage of ash. The ash percentage of 15% to lime (5%) as the optimal ratio of 3 to 1 was also found in previous studies on lime-ash treatment for reducing shrinkage-swelling potential of expansive soils (Dang, 2018; Hasan, 2019).

Similarly, the relationship between linear shrinkage (*LS*) and $LC_0$ can be separated into two stages: (1) slight decrease in LS in the range of $LC_0$ from 28% to 11%, and (2) large reduction of *LS* when $LC_0$ is smaller than 11% (see Figure 5.15). In the ash content from 5% to 25%, the slight reduction in *LS* even with a large change in $LC_0$ indicates that products generated from the pozzolanic reaction in ash-treated samples did not play an important role in reducing *LS*. As shown in Figure 5.18, these products are intertwined crystals, which are an early form of calcium silicate hydrate, existing in the lime treated soil with fly ash (Jha & Sivapullaiah, 2017; Sivapullaiah & Jha, 2014). It is noted that bottom ash has a majority of mullite (see Figure 3.15a in Chapter 3). This gives a condition to form another hydrate product, calcium aluminium silicate hydrate (CASH), which is the crystal created by the reaction of calcium from lime, aluminium in ash, and silica in soil (Puppala et al., 2005). In the content of ash from 5 to 25%, the hydrate product becomes obvious and occupies most ash surface at 15% (see Figure 5.18). The hydrates do not eliminate shrinkage potential since they do not have bonding effects. Even worse, large hydrate needles may develop beyond the boundary of initial void, disturbing clay matric and reducing in the ability of cementation (Sivapullaiah & Jha, 2014). Instead, the reduction of *LS* was caused by a small decrease of bentonite content from the replacement of ash in soil, which corresponds to a

slight decline in LS with bentonite content going down from 30% to 20%, shown in Figure 3.5 in Chapter 3.

In ash-lime treated soils, the dominance of CASH product appears in low contents of bottom ash with mullite in short curing time, whereas the higher amount of ash causes the reduction of crystal, which was found by Jha and Sivapullaiah (2017). They also mentioned that lime-treated soils with high content of ash generate a cementitious gel of hydrate product that binds particles in a cemented matric, which replaces fibre-shaped hydrates. As can be observed in Figure 5.19, from 25% to 40% in ash content, the fibrous product seems to be replaced by the gel ones (see Figures 5.18-19). The cementitious gels on the ash surface are calcium aluminium silicate hydrate (CASH) with Ca/Si <1.5, glued and attached a majority of soil particles to bottom ash (Jha & Sivapullaiah, 2017). With this bonding effect, the soil was cemented effectively, helping prevent internal tension during excessive drying in linear shrinkage tests. As a result, the shrinkage rate decreased significantly from 25% to 40% in ash content, as shown in Figure 5.13b.

As far as the bonding effect may be concerned, the free swelling rate was smaller when more than 15% content of ash was mixed in soil, as seen in Figure 5.14b. Beyond the bonding effect, the slow swelling rate at high ash contents could be attributed to the small surface conductivity of samples (Chu et al., 2018). In clayey soils, the matric surface conductivity is regarded as the depolarization parameter of dispersed particles where the pore water conductivity involves in swelling tests (Bussian, 1983; Feng & Sen, 1985; Niwas et al., 2007). This surface conductance closely relates to specific surface area, which strongly influences electrical conductivity (Abu-Hassanein, 1994; Abu-Hassanein et al., 1996; Sadek, 1993; Yoo et al., 2009). That is, as can be seen in Figure 5.15, the gradual decrease of $LC_0$ after 15% ash content reflects fittingly the slow pace of swelling reduction from the same content. The results from liquid limit also showed a decrease of *LL* at 15% in ash content, compared to *LL* at 10% (refer to Figure 5.13a). This is attributable to the fact that lower liquid limit means smaller specific surface area, equivalent to low clay activity and cation exchange capacity, so reducing mineralogical properties, such as the free swelling rate (Mitchell & Soga, 2005; Spagnoli & Shimobe, 2019). The relationships between electrical conductivity, specific surface area, liquid limit, saturation level and pore percentage were also mentioned by Kibria and Hossain (2012). They stated that the degree of saturation seemed to be the most crucial factor that influences the electrical conductivity of compacted clays. In this study, the swelling samples were compacted statically to obtain the same saturation level and porosity (i.e., $S_r$=0.73 and $n$=0.51) to set a relatively similar electrical condition for swelling samples. Assuming all samples have the same saturation level and porosity before swelling test, if

the studied specimens at a moisture content of around 30% and dry density from 12 to 13 Mg/m$^3$, they may have a similar resistivity at about 4 Ohm-m (Kibria & Hossain, 2012). In swelling tests, samples immersed into water might have the degree of saturation gradually increasing to around 90%, and their resistivity could be reduced to 3.2 Ohm-m. When the saturation degree was high, clods of clay were changed, eliminating inter-clod macro-voids (Lambe, 1958b). However, the decrease of bentonite fraction, which was replaced by bottom ash, induced the decrease in the area of special surface and bound water, making inter-clod micro-voids (Erzin & Gunes, 2013; Kolay & Ramesh, 2016; Santamarina et al., 2001; Wang et al., 2013). The micro-porous structure of bottom ash (see Figure 3.9 in Chapter 3) also contributed to these voids by increasing samples' micro voids. As a result, the pore water conductivity prevailed the surface conductance of the sample (Chu et al., 2018). In this study, bottom ash content of 15% was threshold where water conductivity in voids of bottom ash dominated conductance of bentonite in soil; hence, swelling rate decreased in a small range from 15% to 40% ash content due to small surface conductance of ash.

The relationship depicted in Figure 5.16, also reflects the shift of soil shrinkage-swelling behaviour with electrical conductivity. Referring to Figure 5.16, this behaviour of ash-lime treated soil can be classified into two levels: (1) high shrinkage-swelling ratios in a large range of $LC_0$ over 11%, and (2) low shrinkage-swelling ratio in a small range of $LC_0$ less than 11%. In the first level, the behaviour of treated soil is manipulated by bentonite and crystal, whereas soil in the second level is influenced by the dominance of bottom ash and bonding gels. In Level 1, the decrease in bentonite content and a little lime consumption for hydrate crystals in swelling and shrinkage samples are closely related to significant decline in $LC_0$ of aqueous solutions, swelling ratio and linear shrinkage. Level 2, on the other hand, expresses the role of bottom ash and CASH gels in consuming a majority of hydrated lime and contributing to a decrease in shrinkage-swelling ratios and $LC_0$. Compared to linear shrinkage, the swelling ratio is better correlated with $LC_0$, whereas shrinkage ratio levels off from 15 to 25% in bottom ash content, followed by a sharp decline (see Figure 5.16). In conclusion, the two-level behaviour indicates the existence of boundary, which separates low and high trends of shrinkage-swelling potential of soil treated with hydrated lime and bottom ash. This boundary is determined at 15% bottom ash content, which is in light with micro-structural studies confirming the change of bonding effects in lime-treated soils when ash content is higher than a proportion in treated soil (Jha & Sivapullaiah, 2017).

### 5.7.2 Correlations between electrical conductivity and strength results

For establishing a correlation of electrical conductivity results with strength outcomes, the change in $LC_0$ from Figure 5.15 can be generally categorised into three stages: (1) a significant downward trend of $LC_0$ from 0% to 15% in ash content; and (2) levelling off in $LC_0$ with content of ash from 15% to 25% and (3) the gradual decrease of $LC_0$ with the ash content over 25%. In Stage 1, the significant reduction in $LC_0$, equivalent to a small ash content added to the solution, is attributed to the fact that the active component of clay amount (i.e., bentonite and kaolinite) is reduced in soil proportion. Compared to the soil without ash, this led to a lower fixation of hydrated lime, causing a high $EC$ value (high $EC_{cor,0}$), resulting in a low value of $LC_0$ (see Equation 3.2 and Figure 3.36). However, in Stage 2, when a reasonable amount of ash increases, silicate from ash was released remarkably to react with hydrated lime, so $EC_{cor,0}$ is low due to a high lime fixation. However, the reduction of $EC_{cor\text{-}0}$ is compensated by the decrease of $C_0$ due to the loss of bentonite and kaolinite when soil is replaced by ash (Paya et al., 2001; Tashima et al., 2014). Consequently, the initial loss in conductivity, calculated from Equation 3.2, approaches the balanced value of around 11% in ash content from 15% to 25%. Over 25% in Stage 3, pozzolan of ash exceeded the soil in lime fixation, which reduced $EC_{cor,0}$ value in a rate lower than $C_0$ reduction (Paya et al., 2001). In other words, $EC_{cor,0}$ is high while $EC_0$ is still low, resulting in a gradual reduction in $LC_0$, which can be derived from Equation 3.2. This indicates that in Stage 3, bottom ash dominated over soil in reaction with lime and further reduced $LC_0$ due to their inert properties compared to soil.

The findings from UCS and CBR tests confirmed the significant influence of pozzolanic reactivity of ashes on lime-treated expansive soil. In Figures 5.8b and 5.8d, *UCS* and *CBR* values fluctuated from 0% to 15% of the bottom ash content, which can be attributed to the changes of compacted density and moisture content in the samples (see Figure 3.58). However, at this stage, since a portion of clayey soil is gradually replaced by sandy ash, the treated soil became coarser as a fill material, which contributed to the increase of *CBR* from 60% to about 75% in ash content from 0% to 10%, respectively, as shown in Figure 5.8d. Furthermore, the pozzolanic reaction could be dominated by soil replacement in the UCS and CBR samples with low content of bottom ash. Meanwhile, as shown in Figure 5.15, $LC_0$ significantly reduced from 0% to 15% in ash content, which is mainly determined by the reduction of clay amount in suspension, prevailing the small reactivity of bottom ash with hydrated lime. The initial decrease in *UCS*, shown in Figure 5.8b, was mainly caused by this reduction when fine clayey soil was taken by porous ash, and the ash-lime reaction was not significant (Kamei et al., 2013; Le et al., 2018). However, from 15% to 25% ash content, $LC_0$ did not change significantly and decreased modestly (see Figure 5.15), referring

to the starting presence of ash in lime reaction, which compensates the *UCS* decrease caused by the soil reduction. The domination was expressed by an increase in *UCS* and *CBR* from 15% to 25% ash content, as illustrated in Figures 5.8b and 5.8d.

Referring to Figure 5.15, from 25% or higher contents of bottom ash, $LC_0$ decreased gradually, indicating the existence of an excess of pozzolan respect to lime (Paya et al., 2001). This reactive excess of bottom ash to lime reflected a slight decrease or plateau in both *UCS* and *CBR* after 28 days in bottom ash content from 25% to 30% (refer to Figures 5.8b and 5.8d). The downhill in *UCS* at 56 curing days and *CBR* at 28 curing days at the ash content of 40% is due to the abundance of bottom ash over hydrated lime and soil component. The excessive amount of ash, gradually replacing soil particles, caused a *UCS* 56-day deduction, repeating the phenomenon of the initial decrease in *UCS* with low ash content from 0% to 15%. This correlated well with a decrease in $LC_0$ from 30% to 40% in bottom ash content, as depicted in Figure 5.15. This determined the optimal ratio of ash to lime is 5 to 1. This optimal ratio is in good agreement with previous studies (Dahale et al., 2017; Krishna Reddy, 2009).

## 5.8 Summary

In this chapter, an electrical conductivity test is developed to predict the behaviour of expansive soil treated with hydrated lime and bottom ash. The predicted behaviours include the shrinkage-swelling potential and the strength properties of treated soils. The prediction is based on the correlations between the initial loss in conductivity ($LC_0$) with linear shrinkage (*LS*) and the free swelling ratio for the shrinkage-swelling behaviour, as well as with unconfined compressive strength (*UCS*) and California bearing ratio (*CBR*) for the strength characteristics. The strength investigation evaluated three mixing ratios based on different dry weights to study their effects on soil reinforcement with various ash contents and 5% hydrated lime. The ratios include S-ratio (based on the dry weight of soil), T-ratio (based on the total dry weight of mixture) and SB-ratio (based on the dry weight of soil and ash). A series of mechanical tests, including UCS, CBR, indirect tensile strength (ITS), bender element, and matric suction tests was performed for samples mixed with the three mentioned ratios. X-ray diffraction (XRD) and scanning electron microscopy (SEM) analyses were also conducted to explain the correlations between the electrical conductivity and behaviour of shrinkage-swelling and strength in treated soils. This summary highlights the following conclusions from the findings for each behaviour of treated soil.

**Shrinkage-swelling behaviour**

- In electrical conductivity tests, the inclusion of bottom ash reduces $LC_0$ of lime-treated soil solution significantly, but the reduction rate drops when ash content is higher than 15%.
- Referring to linear shrinkage tests, the values decreased from 0% to 15% and from 25% to 40% of the bottom ash contents. Though, from 15% to 25% of bottom ash content, the linear shrinkage of lime-ash treated soil was constant at about 14%.
- The swelling ratio considerably decreased with an increase in the percentage of bottom ash. However, the pace was slower when the ash content was more than 15%. This can be attributed to the fact that the swelling ratio with more than 15% of bottom ash is mainly dependent to the electrical conductance of pore water rather the surface conductance of bentonite in soil. At the high contents of bottom ash, the bonding effect from the formation of hydrated products also facilitates reducing the swelling rate.
- The correlations between the linear shrinkage, the swelling ratio and the initial loss in electrical conductivity ($LC_0$) build up a two-stage routine for the shrinkage-swelling behaviour of expansive soil, treated with hydrated lime and bottom ash. The behaviour includes a transition point, which represents the transition between high shrinkage-swelling and low shrinkage-swelling reduction in treated expansive soils. From mineral and morphological analysis, the first-stage behaviour is associated with the reduction of bentonite in treated soil without forming primary calcium silicate hydrate or CSH (P). Meanwhile, the second-stage behaviour is dependent on the presence of CSH gels and pore-water conductance in mixtures voids. These two stages are separated at $LC_0$ of about 11%, indicating the transition from a high rate to a low rate in reducing swelling and shrinkage potential of expansive soil treated with hydrated lime and bottom ash. For other ash materials and different expansive soils, the transitional point may alter. Therefore, future research on other soils can show a variation of $LC_0$ at the transition of shrinkage-swelling behaviours in ash-lime treated expansive soils.

**Mechanical behaviour**

S-ratio with UCS tests

- The unconfined compressive strength of treated soil surged into the leap with the increase in the combined bottom ash and hydrated lime dosages. The increase in strength was apparently higher for combining bottom ash and lime to treat soils than using bottom ash or hydrated lime alone. With the addition of bottom ash and lime combination, *UCS* values levelled off or climbed up with the bottom ash content up to 20%, followed by a fall in

strength to 30%. This observation indicated that applying 20% bottom ash might be the optimum content in the combination with 5% lime for expansive soil stabilisation.

- The strength development of hydrated lime and bottom ash stabilised expansive soil is also proportional to the curing time increased. However, the rate of the strength development decelerated after 7 days of curing, which might be resulted from the first reactions of pozzolan between lime and soil, forming cementitious links that hinder more lime reacting with clay particles. Furthermore, the strengths of 10% bottom ash treated soils without or with lime inclusion decreased when the curing time extended from 28 days to 56 days. The possible reason for this phenomenon might be due to the change in the moisture content, the binder dosage and the physical property of bottom ash.
- The measured results of this experimental study demonstrated that the combined bottom ash and lime utilisation could be a promising solution for the treatment of problematic soil because it can promote higher strength and lower linear shrinkage than only bottom ash or lime mixed with soil. Furthermore, utilisation of bottom ash to stabilise expansive soil helps to reduce the negative environmental impact that the ash waste deposit can cause. Bottom ash is a cost-effective construction material which is another benefit when a certain dosage of lime for soil stabilisation can be reduced. This is because 5% lime combined with bottom ash in treatment of expansive soil can produce a material with a higher compressive strength compared to the soil treated with 5% lime only.

T-ratio with ITS tests

- The peak failure tensile strength and axial strain of mixture by T-ratio were higher than that by S-ratio in most ash contents and by a larger margin with the more prolonged curing times. The reduction of lime dosage in S-ratio-based admixture is the reason for strength loss in the samples treated with 30% of bottom ash content.
- Although less lime was used in the soil-dry-weight based samples, more lime trace could be observed in the broken halves than in the T-ratio-based specimens. The exception was the S-ratio-based sample with 20% bottom ash and 5% lime, which suggests that the ultimate lime-ash ratio should be 1 to 4 for the mixtures on the soil-dry-weight basis. However, this ratio should be larger than that in the case of total-weight-based mixtures because their strength continued increasing at the ash content of 30%.

SB-ratio with UCS and CBR tests

- There was a good correlation between the initial loss in conductivity ($LC_0$) from aqueous soil samples with the mechanical properties of compacted soils, indicating a significant influence of ash reactivity on its reinforcing performance with lime in moulded soil samples. Results revealed that the optimal ratio of 25% ash to 5% lime was sufficient to obtain the highest *UCS* and *CBR* values, while over this ratio, the strength was not improved further or even decreased.
- Expansive soil treated by both lime and bottom ash has an increase of small-strain shear modulus ($G_{max}$) right after compaction. However, $G_{max}$ of the lime treated sample started to increase after the first day of curing and accelerated until day 21, whereas shear modulus of bottom-ash-related specimen speeded up only after 7 days, but after 56 days all treated soils experienced a considerable loss of $G_{max}$. Morphology analysis indicated that the strength of bottom-ash-lime treated soils is mainly contributed by the formation of fibrillary Calcium Aluminate Silicate Hydrate (CASH) and primary Calcium Silicate Hydrate (CSH), denoted as CSH (P), in the high progress of $G_{max}$. This is also the reason for $G_{max}$ collapse of the samples after 56 days due to excessive occupation of secondary CSH(S) developing from CSH (P) in interfacial transition zones. However, in the saturating condition, $G_{max}$ of ash-lime treated soil is stable and at a high value over a long time after 56 days. This is due to the fact that with more hydration, CSH in bottom-ash-lime-soil mixtures is distributed in a reticular network, which reinforces the shear strength and modulus of treated soil.
- The compaction method also significantly influenced the $G_{max}$ values. When CBR sample preparation requires dynamic compaction, gaining $G_{max}$ higher than the waxed samples compacted statistically. This can be attributed to the fact that under high damping energy from the dynamic method, bottom ash is easily broken in debris and fragments, which assisted CSH to propagate in bottom-ash-lime treated samples. As a result, the $G_{max}$ magnitude of CBR samples treated with bottom ash increased after 1 day. The same results for matric suction of soil treated with hydrated lime and bottom ash. The suction decreased with time due to an increase of micro-voids in bottom ash particles, contrary to untreated and lime-treated soil.

# CHAPTER 6

# Electrical Conductivity Tests for Expansive Soils Treated with Hydrated Lime and Bagasse Ash

## 6.1 Introduction

In this chapter, the electrical conductivity method (Test A) was used to evaluate the pozzolanicity of bagasse ash in three different sizes, consisting of 75, 150 and 425 μm when mixed with expansive soil. The test was adhering to the procedure suggested by Luxan et al. (1989), including the preparation of saturated solution of hydrated lime, constant agitation at 40°C and monitoring for over 20 minutes. The rate of electrical conductivity (*RC*) was used to estimate the pozzolanic performance of ash-lime-treated soils with various sizes of bagasse ash. In the validation of the EC results for mechanical prediction of studied materials, three geotechnical experiments were employed to compare the strength of expansive soil samples treated with hydrated lime and bagasse ash in different sizes. They include linear shrinkage, unconfined compressive strength (UCS) and bender element tests. These experiments were used to provide a comparison of strength improvement between soil samples treated with lime and bagasse ash with various sieved sizes. A morphological analysis on treated UCS samples after 56 days of curing was conducted to have a closer look at the formation of hydrated products from the difference in proposed sizes of bagasse

ash. Discussion on the selection of bagasse ash size for pozzolanic enhancement in lime-treated expansive soil is also provided.

## 6.2 Experimental results

### 6.2.1 Electrical conductivity tests

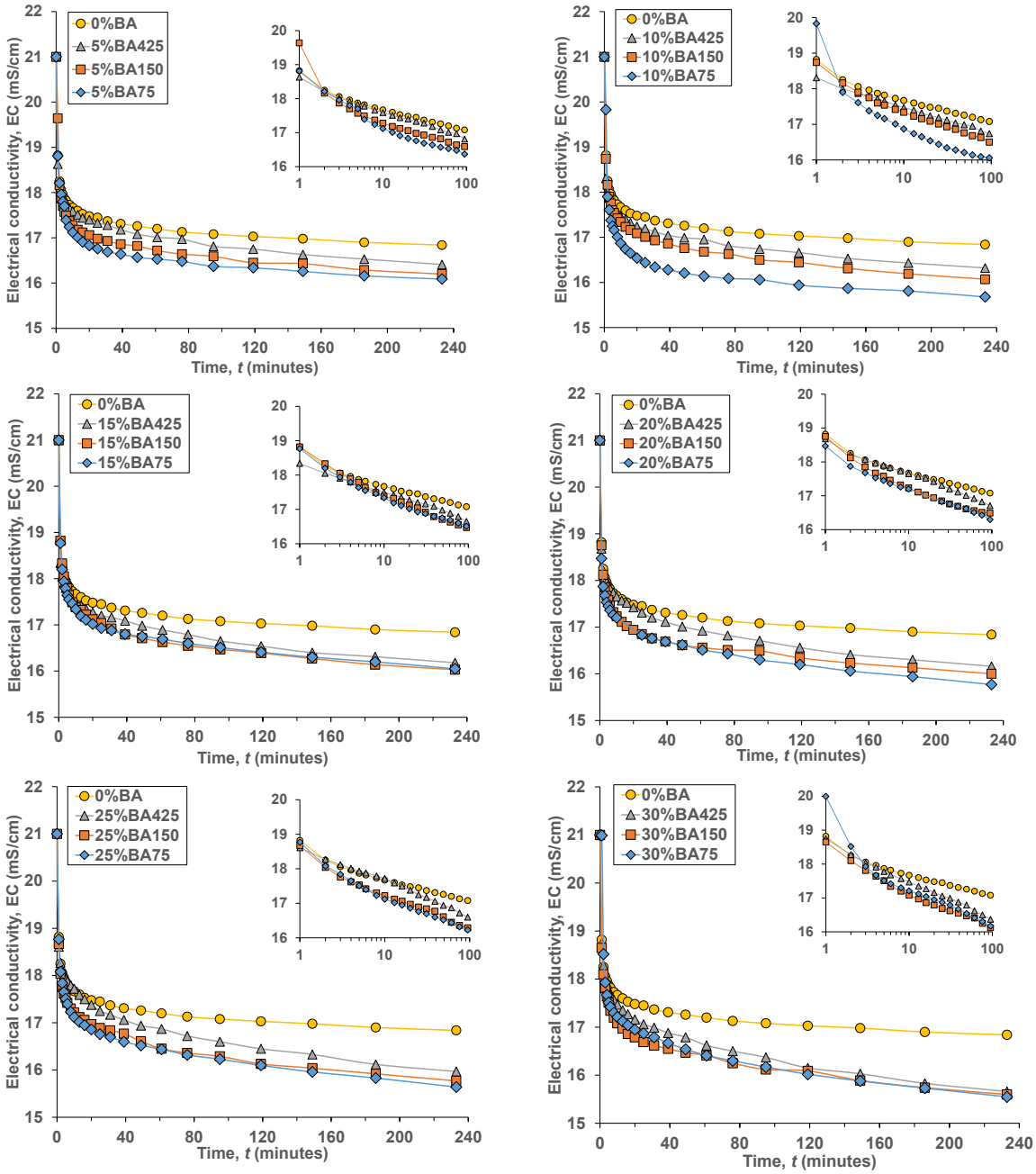


*Figure 6.1 Electrical conductivity evolution of soil solution with 5% hydrated lime and bagasse ash in various content and size*

Figure 6.1 shows the change in electrical conductivity of expansive soil solution with hydrated lime and bagasse ash in various sizes (75, 150 and 425 μm) and the content from 0% to 30%. It can be seen from Figure 6.1, adding bagasse ash to the solution decreased the conductivity, and

the more ash included, the more electrical conductivity reduced. In other words, ash inclusion helped increase the loss in conductivity of the mixed solution. In comparison between studied sizes of ash, bagasse ash with 75 µm had the largest reduction of *EC*, followed by the size of 150 µm, and 425 µm ash has the smallest decrease of *EC* among surveyed ashes. However, from the content of 15% and higher, electrical conductivity of ash in the size of 75 and 150 µm tended to unite for 240 minutes. In the first 100 minutes, the unification is repeated for the two ashes, while *EC*-value of solution with ash 425 µm is always higher than them. Confirming this finding, Figure 6.2 shows analysis on the rate of electrical conductivity in the log-scaled plots shown in Figure 6.1, revealing a linear *EC* evolution from the minute of 2 to 20 in testing time. In Figure 6.2, it is clear that all *RC* of solutions with BA in 150 µm and 75 µm is higher than 0.4 mS/cm.min, whereas most the rate for BA 425 µm is lower than this value. Particularly, at 15% in ash content, the change in EC of BA 75 and 150 µm is approximate, and from over 25% ash, the result shows an obvious increase in *RC* for all studied ash samples.

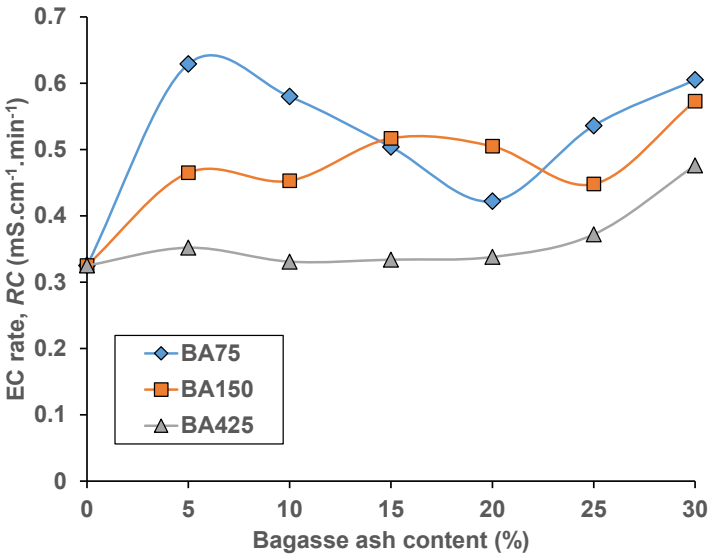


*Figure 6.2 Change in electrical conductivity per minute of soil solution with 5% lime and bagasse ash in various content and sizes (75, 150 and 425 µm)*

### 6.2.2 Linear shrinkage tests

The shrinkage potential is an important parameter of expansive soil to evaluate the effectiveness of soil stabilisation when the soil is treated with binders. In this study, bagasse ash in variable sizes from 75 µm to 450 µm was mixed with lime-treated soil in the ash-to-lime ratio of 15% to 5%, respectively. Figure 6.3 shows the linear shrinkage of soil samples treated with or without hydrated lime and bagasse ash after 7 curing days. It can be observed in this figure that the addition of fine bagasse ash (150 and 75 µm in diameter) to lime-treated soil did not change the linear shrinkage,

which is around 16.5%. When ash in large size with 425 µm was used, the linear shrinkage decreased significantly to only 13.62%. The reduction was about 36% from the linear shrinkage of parent soil, compared to 22% for the soil sample treated with 5% lime only.

In comparison with bottom ash, lime treatment with 15% bagasse ash produced a low liquid limit of about 105% for the ash size of 425 µm, whereas the liquid limit of 15% bottom ash with the same size (equivalent to 25% bottom ash in 2.36 mm size) was about 110% (refer to Figure 5.13a). This indicates that the addition of bagasse ash helped reduce the liquid limit of soil slightly better than bottom ash. The explanation is from the extremely porous structure of bottom ash that may absorb much water to form a liquid state, while bagasse ash has its own moisture, reducing the bibulous ability when mixing with wet soil. Therefore, the combination of the two ashes is predicted to produce the same liquid limit of soil mixtures, which is around 100%, if the ash proportion is from 15% to 25%.

Although lime-treated soils with bottom ash have liquid limit higher than those with bagasse ash, linear shrinkage of samples with bottom ash inclusion results in the similar value of about 14% (see Figure 5.13b), compared to that of bagasse ash with the size of 450 µm, as shown in Figure 6.3b. Particularly, with only 5% inclusion of bottom ash, soil linear shrinkage is equal to those treated with 15% bagasse ash in small sizes (i.e., 150 µm and 75 µm), 15.85% against to about 16.5% (refer to Figures 5.13b and 6.3b). Therefore, it is reasonable to combine bottom ash with the 425-µm-sized bagasse ash to significantly reduce soil shrinkage.

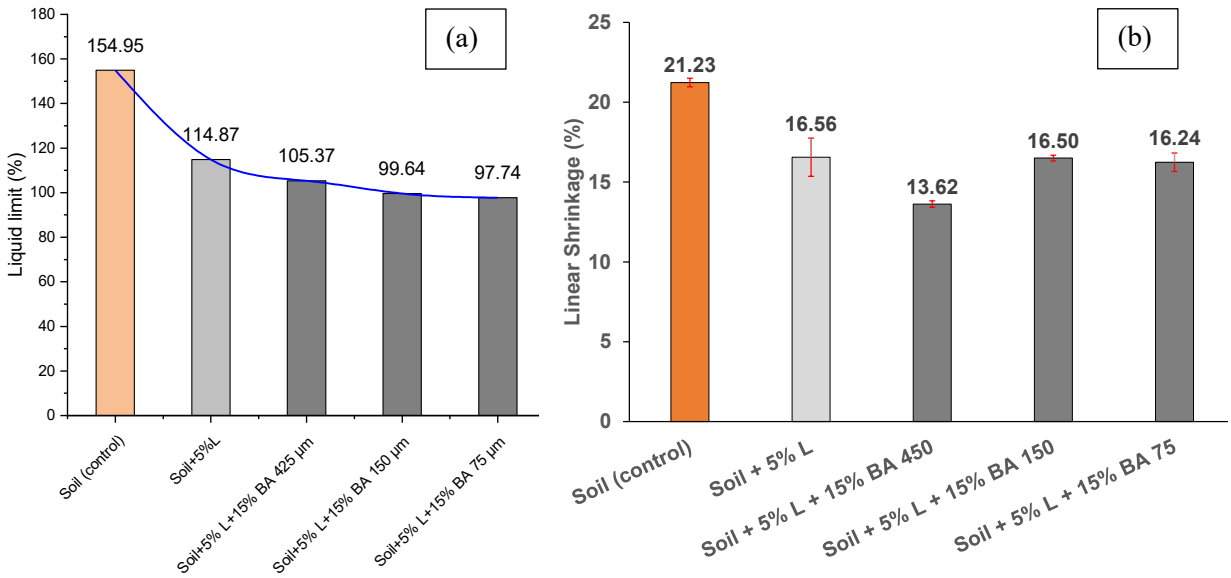


*Figure 6.3 (a) Liquid limit and (b) linear shrinkage of soil treated with 5% lime and 15% bagasse ash in various sizes after 7 days*

### 6.2.3 Unconfined compressive strength tests

While the linear shrinkage parameter shows the potential of shrinkage of expansive soil when it is under extensive drying, the unconfined compressive strength (*UCS*) can show the ability of material withstanding pressure applied on its compacted form. Figure 6.4 illustrates the *UCS* improvement of soil samples treated with hydrated lime and bagasse ash in various curing periods. It is apparent that adding bagasse ash to lime-treated soil did enhance the soil strength; however, the enhancement level is different between samples with various sizes of bagasse ash and curing time. After 7 days, *UCS* of specimens with 425 µm bagasse ash gained the highest value of 1.3 MPa, while those with 150 and 75-µm-sized ash obtained a similar strength of about 1 MPa, which is approximate to *UCS* of lime-treated soil at about 0.9 MPa. However, when the curing time approached 28 days, the strength of 150-µm-ash samples was highest at about 2 MPa, which the 450-ash soil only gained after 56 days. Meanwhile, the smallest ash did not significantly improve the *UCS* of treated soil after 28 days, which accounted for 1.4 MPa. After the same curing duration, the sample treated with the largest ash (425 µm) achieved a medium strength of about 1.64 MPa, which is also the *UCS* that the lime-treated soil only had after 56 days. Besides, after this curing time, soil treated with lime and bagasse ash with 425-µm size gained the highest *UCS* of about 2 MPa, whereas other treated soils have *UCS* at around 1.6 MPa. In particular, *UCS* of soil samples with 150-µm-sized bagasse ash suffered a huge loss by about 0.5 MPa after 56 curing days, decreasing from 1.94 MPa to only 1.41 MPa. The value of 1.41 MPa is even lower than *UCS* with the smallest ash size, which is about 1.51 MPa.

In comparison with bottom ash, the strength of bagasse-ash-treated soils was higher than samples treated with bottom ash after 28 and 56 curing days (see Figures 5.8b and 6.4). After 28 days, the average *UCS* of 15%-bagasse-ash-treated specimens reached 1.6 MPa, whereas bottom ash could only improve the soil strength up to about 1.4 MPa, even the ash content increased to 40% shown in Figure 6.4. Furthermore, the *UCS* results of soils treated with various content of bottom ash indicate that the inclusion of 25% ash to soil gives the highest strength among other ratios after 56 days. The increasing rate from 28 to 56 days at this ratio was also the highest, by about 100% from 1.3 MPa to over 2.0 MPa, as indicated in Figure 6.4. On the other hand, bagasse ash experienced degradation of *UCS* when ash with smaller sizes (i.e., 75µm and 150µm) is mixed with soil, resulting in smaller strengths than lime-treated soil after 56 days. Therefore, it confirms the use of bagasse ash with the size of 425 µm in its combination with bottom ash to enhance the compressive strength of soil. Furthermore, 150-µm bagasse ash can be considered for this

combination since the significant improvement of *UCS* after 28 days of curing, expressed in Figure 6.4.

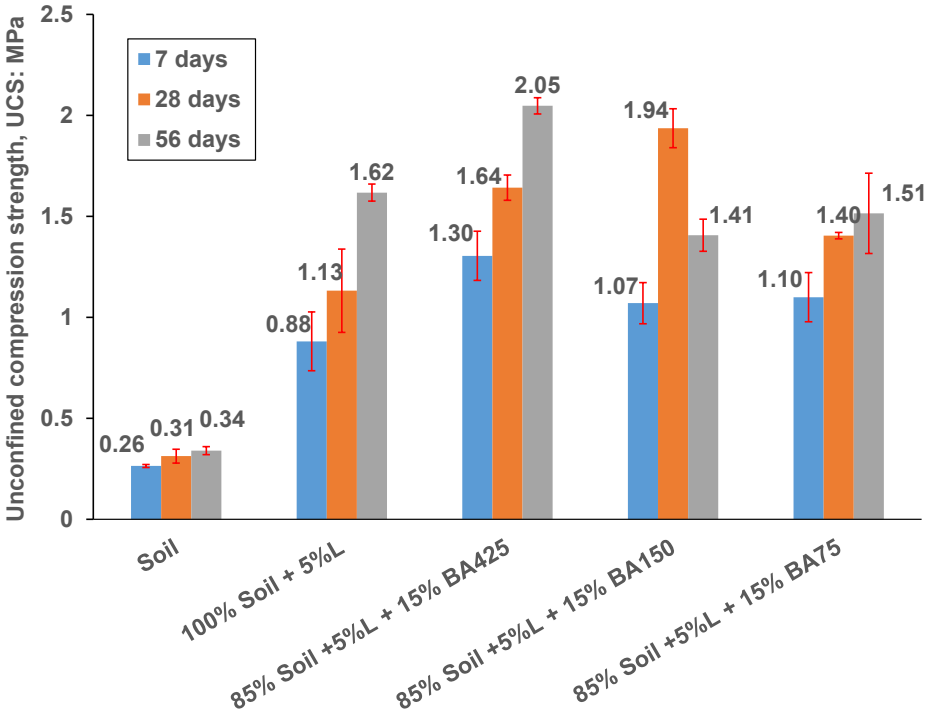


*Figure 6.4 Unconfined compressive strength of soil samples treated with bagasse ash in different sizes and various curing times*

### 6.2.4 Small-strain shear modulus ($G_{max}$)

To effectively monitor the shear development of treated samples during a long curing process, measuring small-strain shear modulus from bender element tests with time is recommended. Up to about 200 curing days, Figure 6.5 shows the revolution of shear modulus development and degradation of soil samples treated with hydrated lime and bottom ash or bagasse ash in three studied sizes, 75, 150 and 425 µm.

It can be seen in Figure 6.5, the similarity of $G_{max}$ value was observed in all treated samples in the first day after compaction, which accounted for around 120 MPa, roughly doubling that of untreated soils. However, the developing rate of $G_{max}$ in samples containing bottom ash and bagasse ash increased significantly from the second day of curing at the same pace, whereas the $G_{max}$ of lime-treated soil climbed up gradually. After 1 week, the shear modulus of bottom-ash-lime treated soil surged to a new high of 500 MPa and became the sample with the highest shear modulus, increasing the discrepancy in $G_{max}$ with bagasse-ash samples until the day of 28. At this time, all lime-treated samples have a plateau of $G_{max}$ at 353 MPa for lime-treated soil, 464 MPa for bagasse ash sample, and around 560 MPa for bottom ash specimen. However, after 56 days of

curing, all treated samples started to suffer a loss in strength. While the loss rate of bottom-ash-lime-treated soil is similar to that of the lime-soil mix, the decreasing rate of strength in the bagasse-ash-lime-soil sample is slower, resulting in an equal value of $G_{max}$ stabilising at 375 MPa in ash-lime-treated specimens after 270 days. The explanation for high rates of increase and decrease in $G_{max}$ of bottom-ash-treated samples may come from the formation of Calcium Silicate Hydrate (CSH), while the lower rate of $G_{max}$ degradation in bagasse-ash-treated specimens stems from the strength compensation of ettringite. Therefore, when combining bottom ash and bagasse ash in the lime-soil blend, it is estimated that there can be a high value of $G_{max}$ and a lower rate of its degradation.

Regarding the effects of bagasse ash size, the inclusion of all bagasse ashes to the samples immediately improved their strength modulus (about 130 MPa), equalling approximately tripled $G_{max}$ of untreated soil (roughly 120 MPa) and also tripled shear modulus of parent soil (48 MPa). After compaction, the developing trend of $G_{max}$ in treated soil specimens, including bagasse ash in the size of 450 and 150 µm, was parallel and gradually on the first day of curing. $G_{max}$ of lime-treated soil without and with 75 µm-sized bagasse ash was identical and lower than other samples. However, after 0.1 day (about 3 hours), the soil sample with the smallest ash accelerated in $G_{max}$ to gain the highest modulus of 248 MPa after 1 curing day. The sample kept this $G_{max}$ growth and obtained the highest of 522 MPa on the day of 21, levelling off at this value in the next 7 days before collapsing to the low of 480 MPa after 42 curing days. At this point, both soils treated with bagasse ash in 425 and 75 µm size had identical values and a decrease of $G_{max}$. The shear modulus of soil treated with 150 µm ash also had the same decreasing rate of $G_{max}$ after 43 days. However, because the sample had the lower peak of $G_{max}$ than other samples, 392 MPa compared to 464 MPa in 425- µm sample, and to 522 MPa in 75-µm specimen, $G_{max}$ of 150-µm-ash-lime treated soil was identical to that of soil treated with lime at 351 MPa after 53 days of curing. It is also worthwhile mentioning that after roughly 56 days, all treated samples suffered a steadily decrease in $G_{max}$ while the parent soil had no such decline observed. However, the soil with smallest ash size had $G_{max}$ degradation earlier than others, resulting in a sharp peak of $G_{max}$, compared to those of others with the plateau of $G_{max}$ during the period from the day of 21 to around 40.

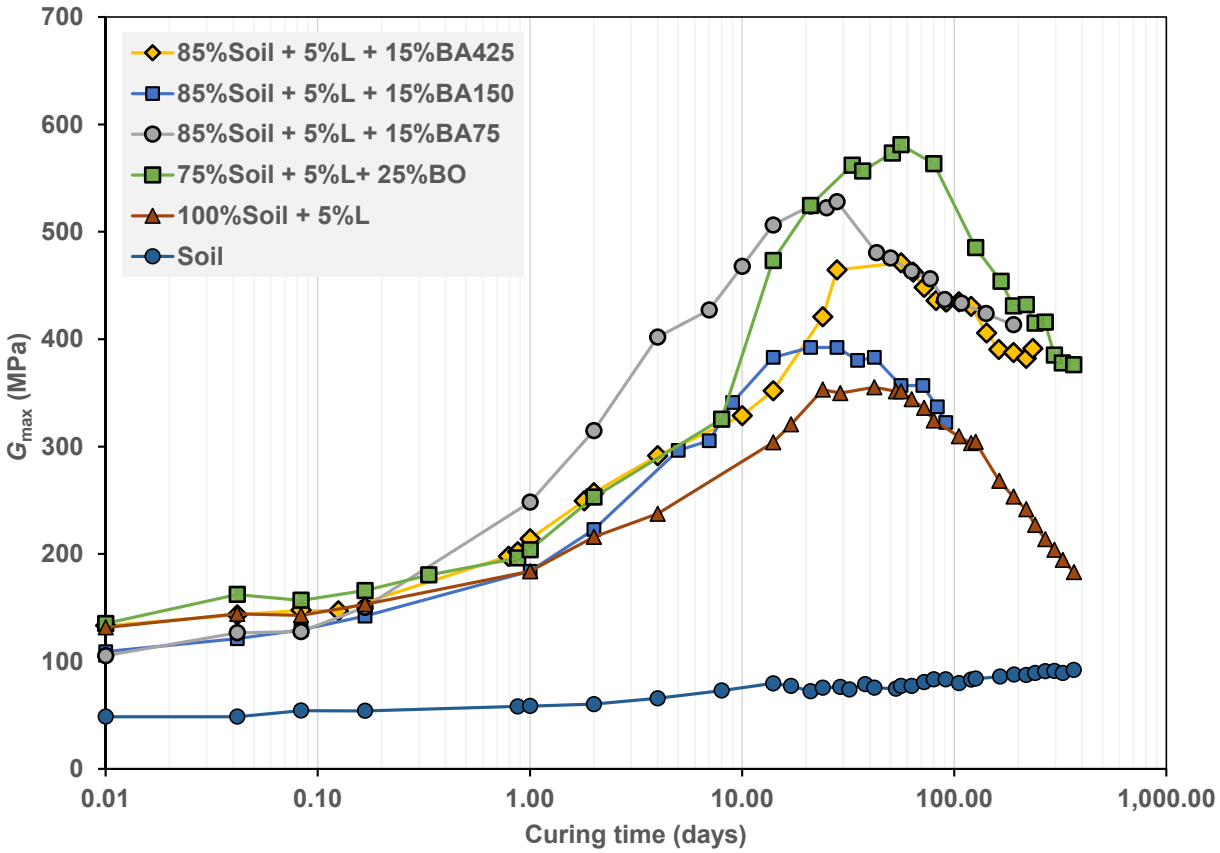


*Figure 6.5 Changes in shear modulus $G_{max}$ of soil treated with lime and bottom ash or bagasse ash with various sizes over curing time*

### 6.2.5 Scanning Electron Microscopy (SEM) tests

The highest values of $G_{max}$ in treated soil samples after 28 curing days can be further explained from the SEM analysis on their microstructure images. Figure 6.6 depicts the SEM image capturing the interaction between ash particles with soil grains with the presence of hydrated lime. It can be seen that while the samples with 425 and 150 µm mainly contain the gel formation attached on edges of cellular ash, in the specimens with the smallest ash (i.e., 75 µm), there was an existence of fibrillary structure gluing on the surface of fibrous ash (see the BA75 sample in Figure 6.6). This structure of floccules developed on the sheet gluing compounds which attach to the surface of 75-µm ash.

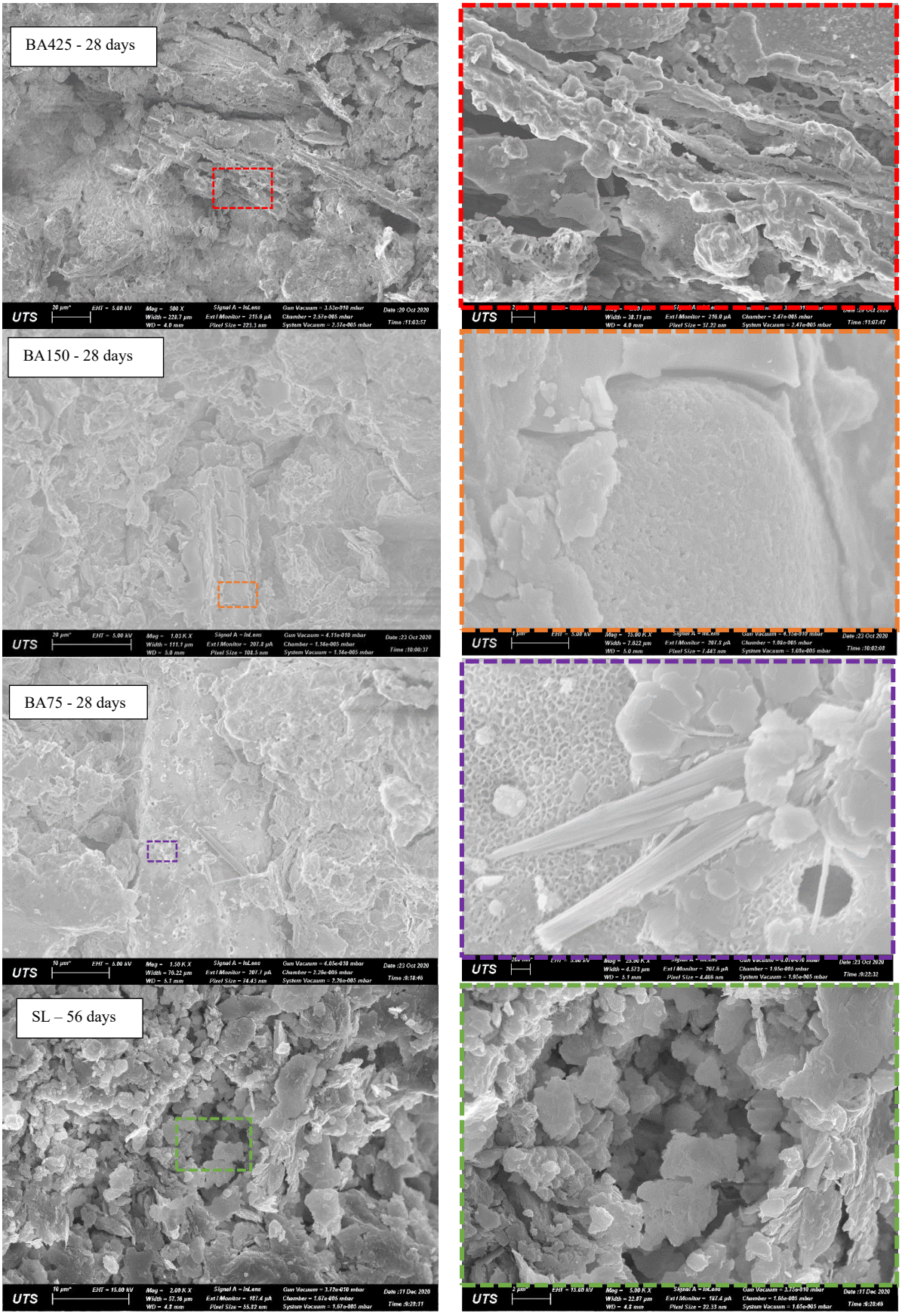


*Figure 6.6 SEM analysis on UCS soil samples treated with 5% hydrated lime and 15% bottom ash in the size of 425, 150 and 75 µm after 28 days, and lime-treated soil after 56 days*

### 6.3 Discussion

Bagasse ash in various sizes has different effects on physical and electrical properties of ash-lime treated soils, which then influences on the mechanical feature of the samples. While the physical properties rely on the fineness of bagasse ash, correlated to the packing of ash in soil structure, electrical one is relevant to the pozzolanic potential of ash in an interaction with soil and hydrated lime. Three sizes of bagasse ash, namely 75, 150 and 425 µm were utilised to investigate the change in physical, electrical, and mechanical characteristics of soil treated with lime and ash. Since no grinding was applied to raw bagasse ash, three studied ashes have an approximate and marginal amount of ultra-fine particles (around 20 µm), only accounting for around 10% passing (refer to Figure 3.10), while this ash size should be up to 80% passing for optimum fineness (Cordeiro et al., 2009b). Therefore, the electrical side of the three ash sizes were focused to clarify any change in their composition and pozzolanicity.

In this study, before electrical conductivity tests were employed to analyse the electrical properties of ash, X-ray diffraction analysis can be done to have the initial investigation on bagasse ash. XRD results showed that although the 425-µm ash has a minimum amount of unburnt carbon particles (see Figure 3.13). However, Figure 3.11 revealed that it still contains crystalline sand as ground contamination of bagasse (Barroso, 2011; Cordeiro et al., 2016). Meanwhile, bagasse ash in the size of 75 µm and 150 µm has the same amorphous amount (see hump areas shown in Figure 3.13), which is higher than that of 425-µm ash, proving that the sieving process effectively increased the amorphous silica in sieved fine bagasse ash. Particularly, while 150-µm and 75-µm ash has the same amount of this silica, the former has a higher amount of crystalline quartz than the latter (50,000 compared to 40,000 counts in intensity, respectively), illustrated in Figure 3.13. The higher amount of quartz in 150-µm particles than 75-µm ones was confirmed by Figure 3.12 because SEM images in this figure showed a dominance of cellular particles as representative of amorphous silica over the granular one. This result is in good agreement with other studies related to sieving effects on the proportion of crystalline and amorphous silica amount in bagasse ash (Chusilp et al., 2009a; Cordeiro et al., 2009b; Ganesan et al., 2007).

When it comes to electrical conductivity tests, the significant change in *EC* value is associated with the amount of amorphous silica (de Soares et al., 2016). From the ash content of 15%, *EC*-values after 240 minutes of testing were unified as the lowest conductivity in samples with 75-and-150-µm-in-diameter bagasse ash. This is attributed to the fact that the amount of amorphous silica from 15% ash content was sufficient to react with hydrated lime and soil chemicals in their solution. A further amount of ash with 75-µm and 150-µm size added to the suspension moved

down their *EC* revolution curves in the same range, caused by the same excessive ash amount dissolving in solution after enough 15% ash was used for lime fixation. As the results, the change in *EC* with time of sample for 75 and 150-µm ash was mostly identical in the content from 15 to 30%, as shown Figure 6.1. Bagasse ash with 425-µm size, on the other hand, had the highest conductivity among studied ashes and in all content surveyed. This is attributable to the smallest amount of amorphous silica in the 425-µm ash, but this minimal content of $SiO_2$ was sufficient to keep its *EC*-value lower than lime-soil solution without any ash inclusion, as shown in Figure 6.1. Particularly, when 30% bagasse ash was involved in electrical conductivity tests, ash with 425-µm size obtained the *EC* reduction as the same as two remaining ash samples. This is due to the fact that doubling content from 15% to 30% in 425-µm ash ensured the same amount of amorphous silica in 75 and 150-µm particles at 15% content, which was sufficient for total lime fixation from the pozzolanic reaction. The analysis from the *EC* rate (*RC*) indicated in Figure 6.2 is in association with this finding since from 30% content, BA425 gains the highest rate, about 0.45 (mS/cm.min), which BA75 and 150 obtained in lower ash contents. The rate fluctuation of these two ashes indicates the variable pozzolanicity, influenced by their varied reactive ability of amorphous silica with lime and soil compounds. Although there was an erratic change in *RC* of the two ashes, approximate rates are observed at the content of 15% and 30% (see Figure 6.2). The BA425 sample, however, showed a constant low rate of about 0.3 (mS/cm.min) from 0% to 25% of ash content, indicating an inert property of crystalline sand in this ash to react with lime-soil suspension (Amin, 2011; Chusilp et al., 2009a; Cordeiro et al., 2016; Cordeiro et al., 2009a).

Contributing to shrinkage and compressive behaviour of compacted soil treated with hydrated lime and bagasse ash, contamination of crystalline sand helps BA425 samples perform more outstanding soil stabilisation than other ashes after 7 curing days. In linear shrinkage tests, *LS* of samples treated with ash in 425-µm diameter was lowest at 13.62%, while those treated with 150 and 75-µm ash had no impacts on lime-treated specimens. The liquid limit results can give some hints for an explanation. The marginal reduction in liquid limit of studied ash, shown in Figure 6.3a, indicates the minimal effect of fineness or specific surface area change of ash on this water content. Indeed, three ashes have an approximate fineness since no grinding was utilised. Consequently, amorphous silica in 75 and 150-µm ash did not promote all its beneficial effects of reacting with lime to form gluing gels and withstanding shrinkage, such as calcium silicate hydrate (CSH). Meanwhile, massive granular silica in bagasse ash 425-µm occupied a larger space in soil mixture than cellular fine particles in smaller-sized bagasse ash. As a result, more volume of soil component was replaced by crystalline sand in BA425 than in BA150 and BA75, resulting in less

proportion of expansive element (i.e., bentonite) present in soil treated with 425-µm bagasse ash. As an obvious outcome, *LS* of soil treated with lime and the largest-sized bagasse ash obtained the lowest shrinkage at 13.62%, compared to samples with smaller sizes. This decrease in *LS*-value is corresponding to the shrinkage reduction with decreasing amounts of bentonite in expansive soil, reported by (Le et al., 2021).

UCS results also illustrated the superiority of granular silica over cellular one in enhancing the soil strength in the early days of curing. Containing a large amount of crystalline quartz, BA425 improved the *UCS* of treated samples after 7 days, while the bagasse ash with smaller sizes had a modest strength reinforcement (around 1.1 MPa), compared to that of lime-treated soil at 0.88 MPa (refer to Figure 6.4). The explanation is from the strength of silica composition in studied ashes, particularly when the bonding effect is not significant due to less hydrated products in early 7 curing days. Under compressive pressure, the strength of granular quartz particles is much higher than cellular ones, fundamentally contributing to the compressive strength of compacted samples (Cordeiro et al., 2016). Furthermore, in the same curing days of 7, *UCS* and *LS* values had a linear relationship due to the influence of crystalline silica on shrinkage and strength potential of ash-lime-treated soil, as shown in Figure 6.7. This result is consistent with the study conducted by Hasan (2019) when he mixed lime and bagasse ash into the kaolinite-bentonite soil mixtures for compacted samples after 7 curing days.

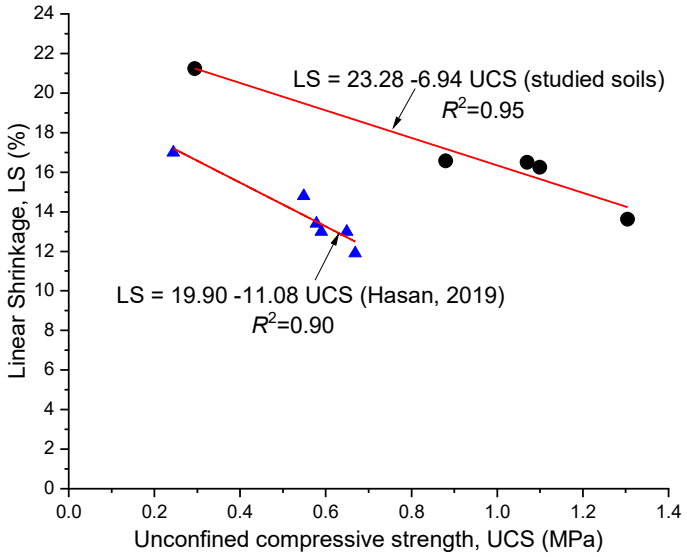


*Figure 6.7. Relationship between LS and UCS of studied samples after 7 days of curing*

However, after 28 days of curing, *UCS* of samples with ash in 150-µm size increased to become the highest value of 1.94 MPa, massively surpassing those with larger and smaller ash sizes. This is attributed to the fact that the pozzolanic reaction, enhanced by amorphous silica in

ash, became dominant and developed completely after 28 days, forming appreciable CSH products that glued and attached ash and soil grains together. At this stage, the compressive failure of long-term cured samples relies on the weakest strength of cellular particle itself. Therefore, with the same intensity of amorphous compounds, but a higher amount of crystalline quartz than 75-µm particles, bagasse ash at the size of 150 µm not only has sufficient amorphous silica, which forms bonding strength from hydrated gels, but also has enough crystalline sand content to withstand the compressive pressure in UCS tests. Sample with 75-µm ash did not have this crystalline reinforcement, thus only slightly increasing in *UCS* to 1.4 MPa after 28 days. It is also worthy to note that in 75-µm-ash samples, there was an existence of the fibre bundles, identified as ettringite crystals from the base of primary hydrates or CSH(P) with the Ca/Si ratio > 1.5, shown in Figure 6.6 (Zhang et al., 2018). These fibrillary CSH compounds indicate immature formulation of hydrated products from pozzolanic reactions, resulting in less production of secondary CSH, which is crucial gluing gels for bonding effects in samples (Chakraborty & Nair, 2020). Similarly, to produce sufficient secondary CSH products [CSH (S)] and enhance *UCS*, samples with bagasse ash in the size of 425 µm needs to be cured until 56 days to gain the same strength of about 2 MPa as that of 150-µm-sized ash (see Figure 6.11). However, after 56 days, 150-µm-related samples had a decrease of *UCS* from 1.94 MPa to only 1.41 MPa. In the same vein, the CSH(P) started to appear in BA150 samples as what happened in BA75 specimens deteriorated the sample reinforcement and reduced *UCS* values.

Although fibrillary CSH formulation had a negative impact on *UCS* of soil samples treated with hydrated lime and bagasse ash, the ettringite crystal in bender element specimens with 75-µm-sized bagasse ash has a positive influence on changes in small-strain shear modulus ($G_{max}$). The sample had an enhancement of $G_{max}$ starting after the day 1 and until the day 21 in curing time, resulting in $G_{max}$ larger than specimens with ash in the 425-µm diameter. This improvement is due to the over-abundance of ettringite than sheet-like CSH (S), producing in interfacial transition zone (ITZ) between ash and soil particles. This occupancy helped reduce the massive porosity of the sample by transforming macro-sized voids into micro-sized ones, enhancing the travelling velocity, so improving $G_{max}$ (Ríos-Parada et al., 2017; Zhang et al., 2018). However, after a long curing process, more precipitated secondary CSH is generated in gel forms, which held water due to its affinity capacity and limited the hydration of stabilised layer of soil particle, finally reducing the soil strength (Chakraborty & Nair, 2020). This detrimental effect appeared in $G_{max}$ of all treated soil from around the day of 28 onwards, even for the lime-treated sample without ash (see Figure 6.5), which is understandable because the studied soil still contains silica.

However, no *UCS* reduction is observed for soil samples treated with hydrated lime and bagasse ash in the size of 425 and 75 µm after 56 days, as expressed in Figure 6.4. The difference comes from the determining factors for *UCS* and $G_{max}$. While *UCS* mainly relies on the strength of particles and bonding compounds, small-strain modulus $G_{max}$ has a close correlation with density and porosity. The secondary CSH products play an important role of boding the particles in UCS samples, so the more production of this hydrate compound, the higher *UCS*. $G_{max}$, on the other hand, was reduced because the CSH (S) expanded the porosity of samples by its sheet-like structure, shown in Figure 6.6.

### 6.4 Summary

The findings of this chapter clarify the differences in mechanical properties of expansive soil treated with hydrated lime and bagasse ash in various sizes, including 75, 150 and 425 µm in diameter. Before performing the mechanical tests, namely linear shrinkage, unconfined compressive strength and bender elements tests, the physical and chemical properties of the employed bagasse ash was investigated. Therefore, sieving and X-ray diffraction analyses were conducted while electrical conductivity tests were utilised to evaluate the pozzolanicity of ash-lime soil suspension. Morphology investigation was also executed on the UCS samples through Scanning Electron Microscopy (SEM) tests to explain the micro-structural change of studied soils with bagasse ash in different particle sizes. The following conclusions can be shown from this empirical study:

- Inclusion of bagasse ash in lime-treated soil increases its pozzolanic reaction, in which bagasse ash with smaller particle sizes (i.e., 75 µm and 150 µm) had higher pozzolanicity than that with larger particle size (i.e., 425 µm). Although an insignificant content of unburnt carbon exists in 425-µm ash, the ash still has a low pozzolanic reactivity due to the contamination of crystalline quartz and low amorphous silica content. The 75-µm and 150-µm ashes have the same intensity of amorphous compound, but the 150-µm one has a slightly higher amount of quartz than the 75-µm bagasse ash.
- Regarding the ash contents of 15% or above in the ash-lime soil mixtures, the pozzolanic reactivity of samples including 75-µm and 150-µm ashes was identical, suggesting that 15% bagasse ash provides sufficient amorphous silica for lime fixation. Meanwhile, the suspension with 425-µm ash needs the content of 30% to obtain an identification of electrical conductivity to others. The percentage of 30% was also the necessary content of the larger size ash to obtain its highest rate of electrical conductivity was 30%, which

equals the average rate of solutions compared to the samples with smaller-bagasse ash particles.

- Mechanical analysis on soil samples treated with lime and bagasse ash revealed the reliance of sample shrinkage and strength on crystalline silica for the early curing times. For the shrinkage potential after 7 days, bagasse ash with larger sizes (i.e., 425 µm) had the lowest linear shrinkage (*LS*) due to the crystalline quartz contamination. The smaller size ashes (75 µm and 150 µm) had no effect on reducing *LS* of lime-treated soil, and they also had no significant reduction in the liquid limit of treated samples. The same results were observed for unconfined compressive strength after 7 days for curing, in which 425-µm-ash related samples had the highest *UCS* among the studied ash samples due to the higher strength of granular quartz than cellular particles, existing in ash size of 75 µm and 150 µm.
- For a long-term of incubation, the amorphous silica exhibited its superior stabilisation potential by producing the calcium silicate hydrate (CSH) in the form of gels bonding ash and soil particles together. However, the bonding effect only effectively enhanced soil compressive strength when the ash contained a sufficient amount of granular particles as stiff aggregates in its bonding matrix. Ash, with the size of 425 µm, having a balanced amount of crystalline and amorphous silica, attained the highest *UCS* in its soil compacted samples after 56 days. Meanwhile, the smallest-sized ash (75 µm) had a modest improvement in *UCS* due to its excessive amount of weak cellular particles.
- Although having the lowest *UCS* compared to others, lime-soil mixture with ash in the size of 75 µm had the fastest improvement in small-strain shear modulus ($G_{max}$), compared to samples with 150-µm and 425-µm bagasse ash sizes. The quick enhancement of $G_{max}$ could come from the development of ettringite and CSH floccules in the interfacial transition zone between ash and soil particles, reducing macro voids and the travel time of shear waves. However, after 56 days, the primary CSH products became sheet-like, further gluing the soil and ash particles. This was beneficial for *UCS* improvement in the short-term curing process within approximately 56 days, but it had a negative effect on $G_{max}$ since the sheet-shaped structures of primary CSH increased the porosity and the dehydration of soil layers. Consequently, $G_{max}$ of all lime soil samples treated with bagasse ash or without bagasse ash decreased significantly after 56 days of curing.

# CHAPTER 7

# Characterisation of Expansive Soils Treated with Hydrated Lime, Bottom Ash and Bagasse Ash

## 7.1 Introduction

As mentioned in previous chapters, bottom ash is rich in Mullite ($Al_2O_3.SiO_2$), which reacts with lime to generate the CSH crystal needles. The sword-like structure of the crystal occupies the void in soil and interlocks with its matrix, transforming the macro voids into micro-voids. The treated soil becomes dense; hence, it can harden the soil compressive and shear strengths. However, it takes time to form a sufficient amount of crystal for such strength enhancement. It can be up to 28 days under the condition of not losing the water content. Therefore, it is required to speed up the process or shorten the duration to generate an interlocking phenomenon. Adding the second ash binder, such as bagasse ash, maybe a proper and straightforward way to build up the hardening structure in soil. Bagasse ash in the fibre-like shape can initially penetrate the soil matrix as soon as this ash is included in the mixture of lime, bottom ash and soil. This combination of two ashes in lime-treated soil can have two effects. The first effect is the immediate reduction of porosity caused by the occupation of bagasse ash into the voids of soil. The second is the time-hardening impact on soil fragments from pozzolanic reactions between the ashes and hydrated lime. The

reaction is enhanced by the addition of silicate from bagasse ash to the soil mixture. Consequently, the combined effects of hydrated lime and bottom ash on soil reinforcement can be observed, resulting in an optimal shrinkage-swelling potential reduction and maximum strength improvement.

In this chapter, the effects of hydrated lime combined with two ashes, namely bottom ash and bagasse ash, are disuses on expansive soil stabilisation. This chapter comprises two sections, including determining the ash-lime ratio and then characterising bottom-bagasse-ash-lime treated soils (see Figure 7.1). Two sections illustrate relevant results, analyses, and discussion in each one.

Firstly, the ratio determination includes trial experiments and electrical conductivity to define the optimal ratio of ash-lime in treated soils. In the first part of this section, the trial tests were conducted by adding bagasse ash to lime-bottom-ash-treated soil in its optimal combination (5% lime and 25% bottom ash), which was found in Chapter 5. Unconfined compressive tests were utilised to compare soil samples treated with 5% lime, 25% bottom ash and bagasse ash in various content from 0% to 20%. Meanwhile, the electrical conductivity (EC) test was employed to find out the optimal ratio of bagasse ash to bottom ash in their mixture with lime, as against to trial results. The EC testing procedure for two-ash combination in lime-soil solution followed Test C of conductivity test, including Subtests C1, C2 and C3. In Subtest C1, bottom ash and bagasse ash were mixed in different ratios and then tested with distilled water to determine which ratio gave the highest *EC*-value of their aqueous suspensions. Later, Subtests C2 and C3 were involved in mixing two ashes with their optimal ratio, which had been found from Subtest C1, into lime-soil blend and water, respectively, to measure the initial loss in conductivity ($LC_0$). As a result, the final ratio of bagasse ash to bottom ash in soil treated with 5% hydrated lime was proposed.

The second section of the chapter shows the characterisation of soils treated with all three binders, namely lime, bottom ash and bagasse ash in their final ratio, which was revealed from the first section. The characteristics include geotechnical and micro-structural properties, which were compared between three-binder-treated soil and two-binder ones, including lime-bottom-ash-soil and lime-bagasse-ash-soil mixtures. For geotechnical features, the comparison covers particle distribution analysis to mechanical assessment, such as linear shrinkage and compressive strengths, as shown in Figure 7.1. Particularly, the small-strain shear modulus ($G_{max}$) is investigated in various soil samples compacted at different water contents. The micro-structural analysis would be conducted to explain the change in soil strength with time. The detailed structure of the chapter is illustrated in Figure 7.1.

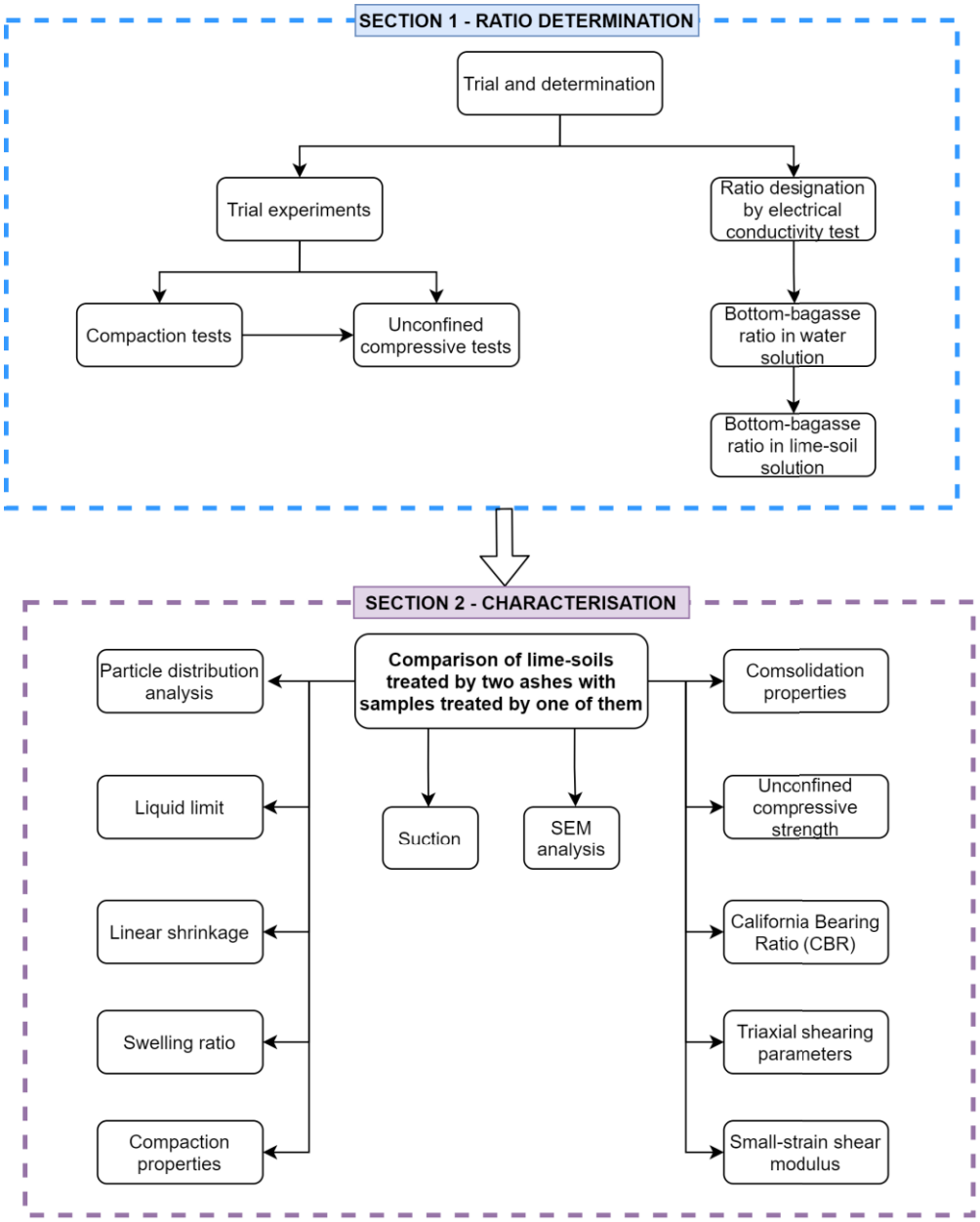


*Figure 7.1 The structure of Chapter 7*

## 7.2 Combination of bottom ash and bagasse ash in lime-treated soils

### 7.2.1 Introduction

In this first section, bottom ash and bagasse were combined to treat expansive soil with hydrated lime. The research approach is deductive from the best ratio of bottom ash versus lime to design the optimal bottom-bagasse ratio. This approach is regarded as a trial experiment since the ratio of bagasse ash would be varied with the same proportion of bottom ash and lime to find the best combination. The criteria to determine the optimal ratio is based on strength, so the unconfined compressive strength (UCS) test is preferable. Therefore, the compaction tests were conducted to

define *MDD* and *OMC* of UCS samples. In the meantime, electrical conductivity tests were also performed with two stages. Firstly, bottom and bagasse ashes will be mixed in varied proportions with distilled water to measure their electrical conductivity. The proper bottom-bagasse ratio is determined at the level where the largest proportion of bagasse ash can obtain with the highest electrical conductivity. After that, the optimal ratio of bottom ash to bagasse ash was fixed and tested with the solution of soil and hydrated lime. Consequently, the final ratio of bottom and bagasse ash versus 5% hydrated lime would be found and compared with results from trial experiments to conclude the outcome.

### 7.2.2 Compaction characteristics

From Chapter 5, the optimal ratio of bottom ash to lime in soil stabilisation is 25% against 5%. When bagasse ash is added to the bottom-ash-lime-soil mix, the percentage of bottom ash and lime was kept at 25% and 5%, respectively, which is shown in Figure 7.2. Therefore, any content of bagasse ash added will replace the soil in the same amount, which is similar to samples added with variable content of bottom ash. Figure 7.2 clearly shows the decrease in density when ash is added to lime-treated soils. In comparison between the two ashes, the rate of decrease in dry density caused by bagasse ash is more significant than that by bottom ash, 0.08 compared to 0.03. Interestingly, although the specific gravity of bagasse ash is higher than that of bottom ash, 2.3 as opposed to 2.0, adding more bagasse ash to bottom-ash-lime soil mix reduces the density significantly from about 1.25 (Mg/m$^3$) to about 1.02 (Mg/m$^3$) with 30% bagasse ash. This may be because bagasse ash in its tiny fibrous particles pushed a majority of soil and bottom ash out of the mould. Consequently, the weight reduced significantly, and density went down steeply.

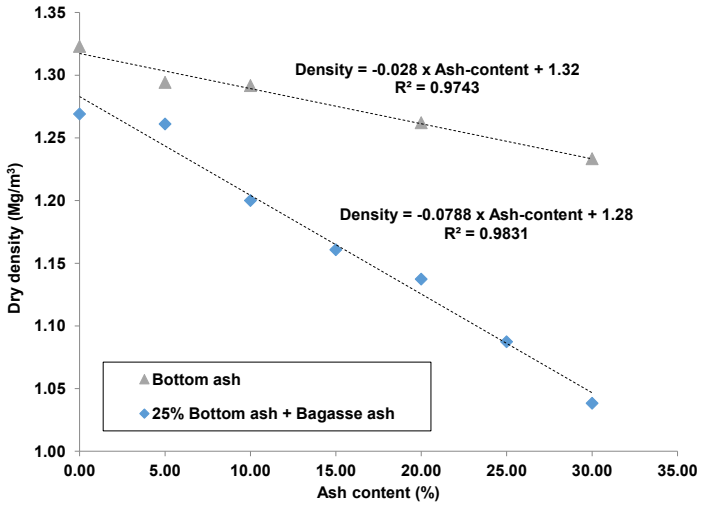


*Figure 7.2 Changes in density of soil samples treated with 5% lime, bottom ash and bagasse ash in various contents*

### 7.2.3 Unconfined compressive strength tests

Figure 7.3 illustrates the trend of *UCS* of soil treated with 25% bottom ash, 5% lime and variable content of bagasse ash from 0 to 20% after 28 and 56 curing days. It can be seen that the inclusion of bagasse ash in the ash-lime-soil mix does not finally increase the strength. Further addition of more than 5% bagasse ash content made the strength fall to the value of about 1.3 MPa at the ash dosage of 20% after 28 and 56 days. This is approximate to the strength of soil treated with lime and bottom ash without bagasse ash, which accounted for 1.2 MPa (see Figure 7.3). Mainly, after 56 days, adding bagasse ash had no effect on strength improvement; even worse, at 20% ash content, the strength degradation occurred. The results reveal that adding bagasse ash to soil treated with 5% lime and 25% bottom ash did not improve strength, suggesting the maximum ash content of 25% that soil with 5% lime can consume to generate the highest strength.

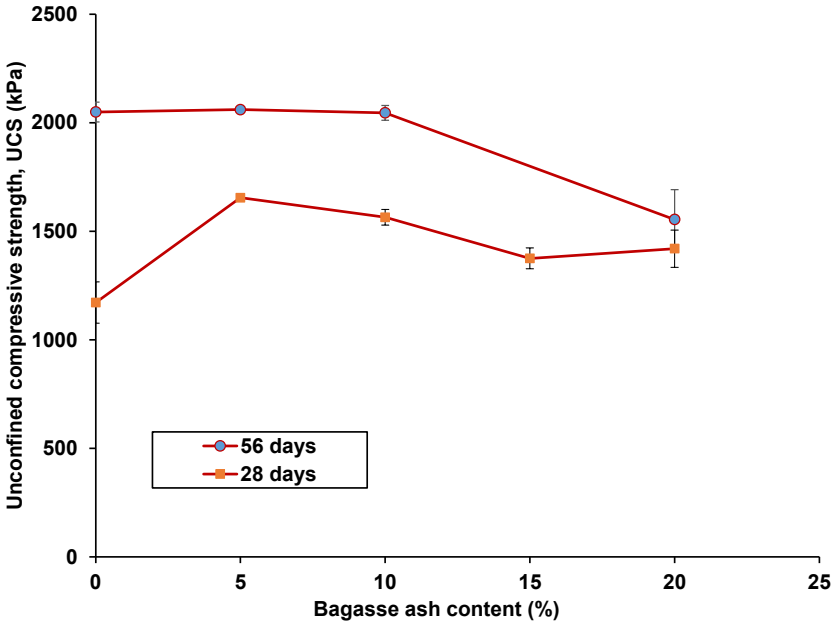


*Figure 7.3 Unconfined compressive strength of 25%-bottom-ash-5%-lime treated soils with various contents of bagasse ash*

### 7.2.4 Electrical conductivity in the combination of bottom and bagasse ash

#### *7.2.4.1 Electrical conductivity of bottom-bagasse-ash mix in Test C*

The electrical conductivity test for the ash-lime solution is utilized to evaluate the pozzolanic performance of their mix, following Test C mentioned in Chapter 3. With Subtest C1 of this test, Figure 7.4 shows the results of Subtest C1 with the different proportions of bottom and bagasse ash from 0% to 100%. Bottom ash with a maximum size of 2.36 mm and bagasse ash with

maximum size of 425 µm in diameter were tested. Figure 7.4 also shows that *EC* increased significantly from 0 to the range from 600 to 750 µS/cm after 10 minutes. The increasing trend then decelerated in a logarithm function; thus, a plot in the logarithm scale of time is drawn in Figure 7.5. It is apparent in this figure that all lines have the same slope of about 52 µS/cm per 1 minute. However, they shift down when the bagasse ash increases in its content. To evaluate this movement, intercepts of lines at the time of 1 minute were measured and depicted in Figure 7.6.

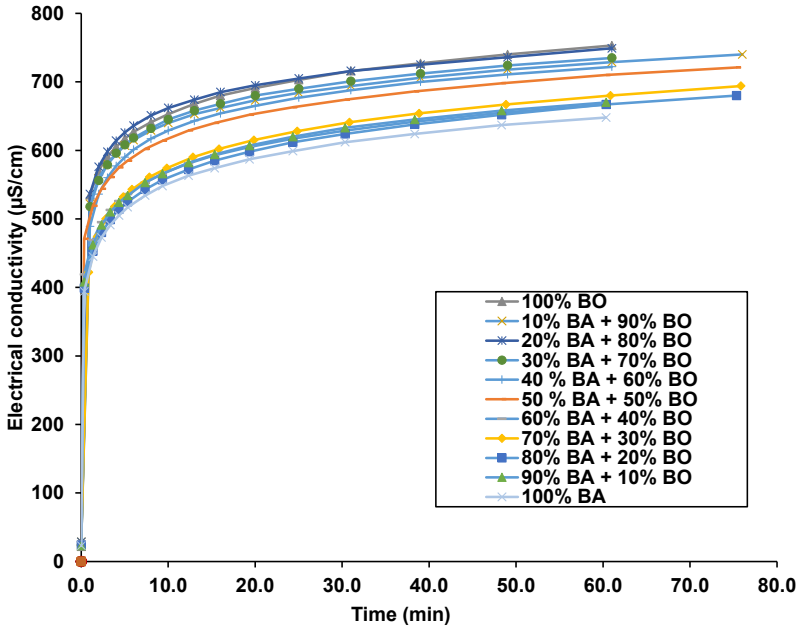


*Figure 7.4 Revolution of electrical conductivity of bottom ash*

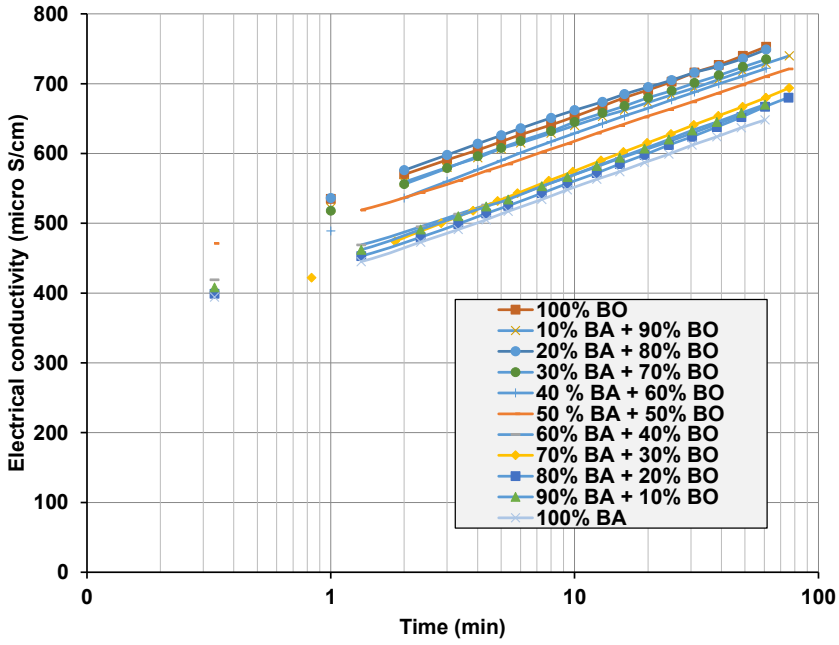


*Figure 7.5 Evolution of electrical conductivity of bottom-bagasse ash solution*

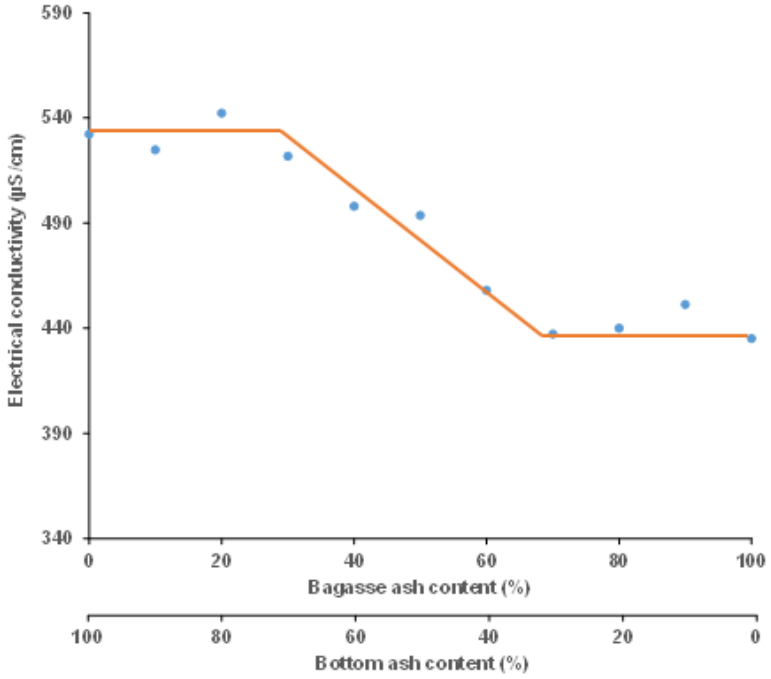


*Figure 7.6 Electrical conductivity of bottom-bagasse ash mix with different contents of ash*

Referring to Figure 7.6, the pattern of *EC* change in bottom-bagasse ash mixes can be categorised into three stages. In the first stage, *EC* value was constant at about 530 µS/cm from 0 to 30% bagasse ash. After that, *EC* reduced gradually when bagasse ash was added from 30% to 70%. Following the second stage is the constant trend of *EC* at about 440 µS/cm from 70% to 100% in bagasse ash content. The result indicates that bagasse ash reduced the electrical conductivity of ash mixes, and at the percentages less than 30%, the reduction effect was insignificant. To keep *EC* of ash at a high value to gain a maximum loss in conductivity with the hydrated lime solution but still have a reasonable portion of bagasse ash in the soil mix, the ratio of 30% bagasse ash to 70% bottom ash was selected and used for the Subtests C2 and C3.

### *7.2.4.2 Electrical conductivity of bottom-bagasse-ash-lime treated soil solutions in Test C*

The electrical conductivity tests were performed for soil treated with three admixtures, hydrated lime, bottom ash and bagasse ash. The experiments follow the procedure of Subtest C2 and C3, which was mentioned in Chapter 3. In these tests, the content of hydrated lime was kept at 5%, while soil and ash shared the proportion of 100%. The ash content was altered from 0% to 60%, leading to the equivalent decrease of soil from 100% to 40%. In the total ash percentage from 0% to 60%, bottom ash occupied 70% while bagasse ash had 30%. The results of initial loss in

conductivity ($LC_0$) of the 4-component mixtures (i.e., soil, lime, bottom ash and bagasse ash) are shown in Figure 7.27.

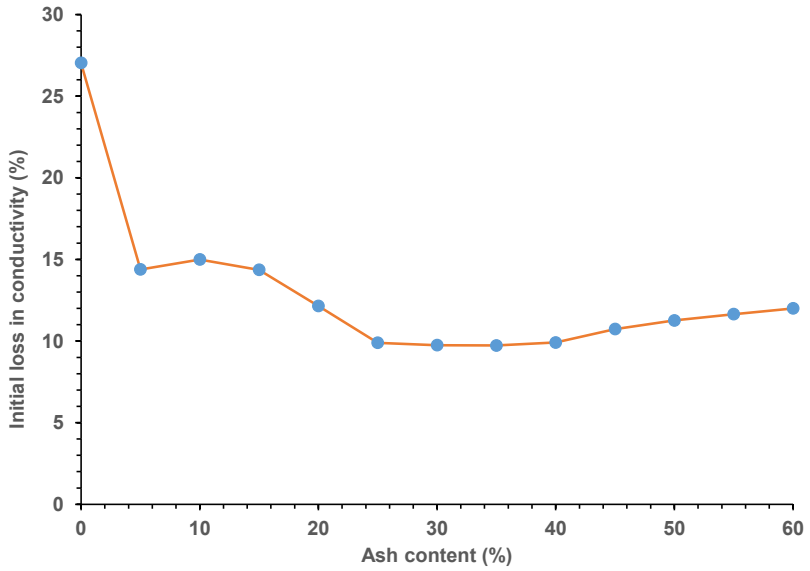


*Figure 7.7 Evolution of initial loss in conductivity of soil treated with lime, bottom ash and bagasse ash in various content of ash*

Figure 7.7 clearly illustrates a significant drop in $LC_0$ when only 5% ash content was added to the mixture. The drop is about a half from about 27% to only 14%. $LC_0$ was constant at around 15% in ash content from 5% to 15%, but it went down at 20% ash and levelled off from 25% to 35% ash content. Since 35% ash, $LC_0$ increased gradually to around 12% at the ash dosage of 60%. From Figure 7.7, the balance in electrical conductivity at the ash content of 25% indicates the infection point where ash begins to dominate soil in reactivity (Paya et al., 2001). Over this percentage, the conductivity is mainly contributed by ash with a slight increase in $LC_0$ from 40% in ash content.

According to findings on strength assessment of the bottom-ash-lime-treated soils in Chapter 5, the drop and plateau of $LC_0$ at 25% indicates a balance of soil and ash amount in their reaction with hydrated lime at this percentage. Over 25%, ash inclusion can compensate with $LC_0$ reduction caused by decreasing the amount of soil, resulting in a levelling-off in $LC_0$ at around 10%. This is also in line with results from trial experiments in the previous section. Therefore, to count for the least ash amount in a sufficient reaction with soil, 25% ash content is selected for further investigations in compaction, strength and suction. This suggests the selected optimal ratio of component content in bottom-bagasse-ash-lime-treated soil is 17.5% bottom ash, 7.5% bagasse ash, 5% hydrated lime and 75% soil in dry mass. These percentages were employed and tested to characterise the soils treated with hydrated lime and the two ashes in the second section.

## 7.3 Characterisation of bottom-bagasse-ash-lime treated soils and discussion

### 7.3.1 Particle size distribution curves

Figure 7.8 shows the changes in particle size distribution curves when 30% bagasse ash is included in bottom ash. Without bagasse ash addition, the clay component of bottom ash was about 10%, classifying the bottom ash as sand. However, when 30% bagasse ash was involved, the combined material had clay particles occupying 22% (larger than 12%) to become clayey sand-like bagasse ash. Therefore, the inclusion of 30% bagasse ash content changes the bottom ash from poorly graded sand to clayey sand.

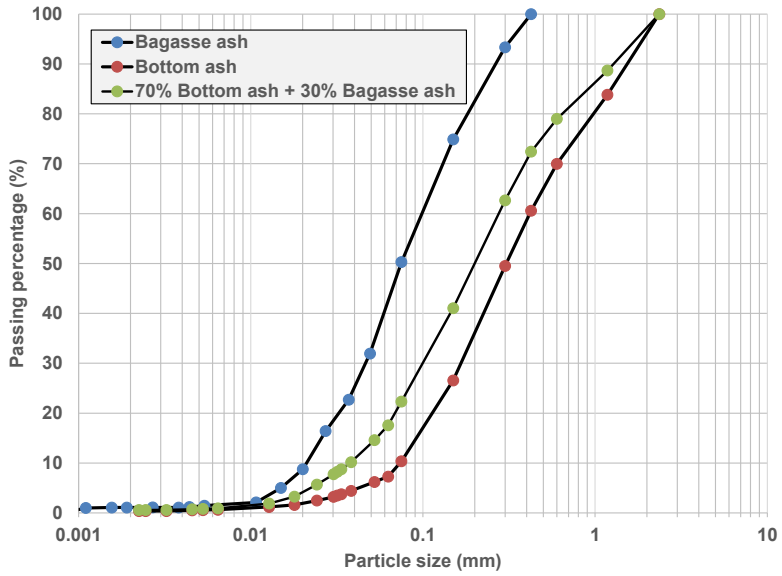


*Figure 7.8 Particle size distribution curve of bottom ash, bagasse ash and their combination*

### 7.3.2 Liquid limit

Liquid limit (*LL*) is an important parameter to evaluate the electrical reactivity of soil. Figure 7.9 shows *LL* of studied soils treated with hydrated lime, bottom ash and bagasse ash. It is obvious that the addition of binders, such as lime and ash, reduced *LL* significantly. In comparison between bottom ash and bagasse ash, bagasse ash produced a lower liquid limit with a smaller content, 105.40% in *LL* with 15% content. Bottom ash with 25% content in lime-treated soil gave higher liquid limit of 111%. With the selected bottom-bagasse-ash ratio of 17.5% to 7.5%, which means replacing only 7.5% bottom ash in its 25% by bagasse ash, the liquid limit was approximate to the mix with 15% bagasse ash, at about 105%. This indicates that in the two last samples shown in Figure 7.9 (i.e., 85% Soil + 5% L + 15% BA and 75% Soil + 5% L + 17.5% BO + 7.5% BA), 17.5% bottom ash was equivalent to 7.5% bagasse ash to produce the same *LL* as that of soil

sample treated with 5% lime and 15% bagasse ash. The equality in *LL* was associated with the same level of reactivity, and the electrical conductivity test results from Figure 7.7 predicted well this behaviour, resulting in the bottom-bagasse-ash ratio of 7 to 3. Figure 7.10 also confirms this equivalency in the ratio of 70% bottom ash to 30% bagasse because *LL* of soils treated with 35% bottom ash is approximate to that treated with 15% bagasse ash, equivalent to the bottom-bagasse ratio of 7 to 3), and the reduction of soil content in these samples (i.e., 85, 75, 65%) did not affect the mixes' liquid limit.

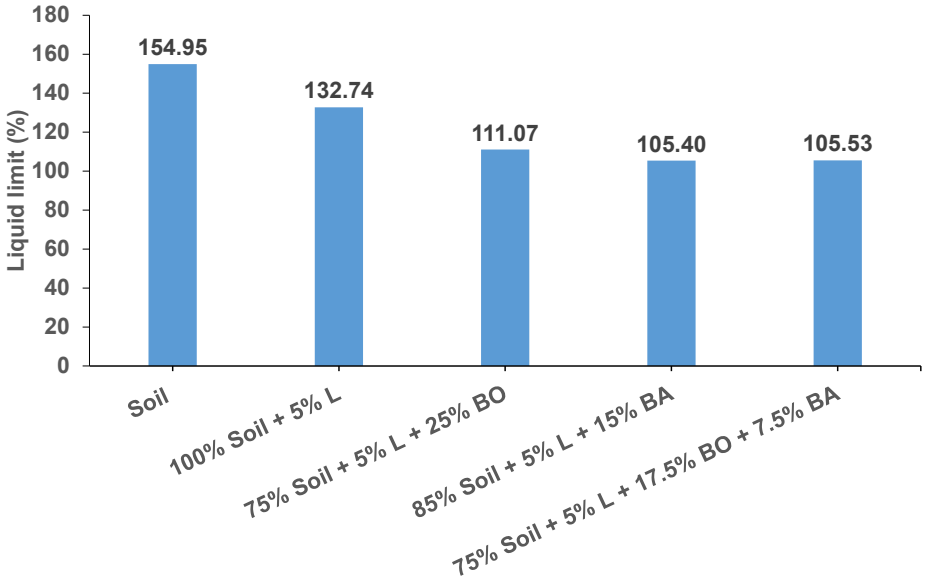


*Figure 7.9 Comparison of liquid limits of untreated soil and soil treated with lime, bottom ash and bagasse ash.*

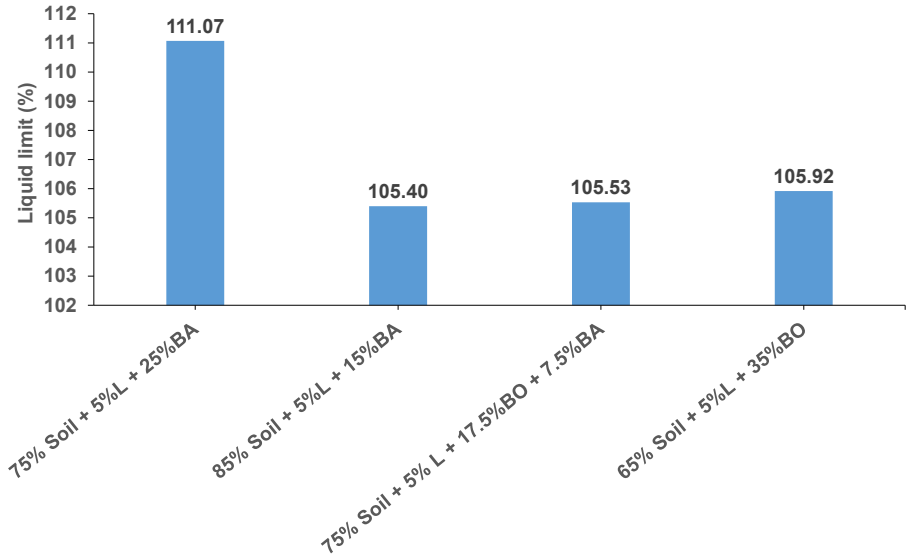


*Figure 7.10 Liquid limits of soils treated with hydrated lime, bottom ash and bagasse ash*

### 7.3.3 Linear shrinkage

The studied soil was prepared at liquid limits to perform in linear shrinkage (*LS*) test. The test result indicates the shrinkage potential of materials after extensive drying conditions. Figure 7.11 depicts the changes in *LS* for soil untreated or treated with hydrated lime, bottom ash and bagasse ash. It is apparent that linear shrinkages of samples treated with lime, bottom ash and bagasse ash were approximate at around 12%, indicating the same ash effect on the shrinkage ratio of their mixes with soils.

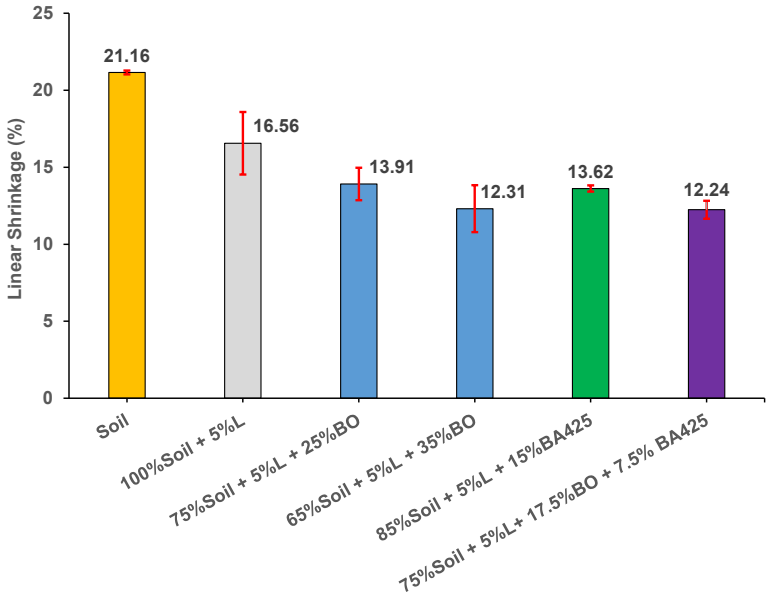


*Figure 7.11 Linear shrinkage of untreated soil and soil treated with lime, bottom ash and bagasse ash*

### 7.3.4 Compaction properties

A compaction curve of material provides its maximum dry density (*MDD*) and optimum moisture content (*OMC*) at the highest point of parabola curve. In comparison between bottom ash and bagasse ash, bagasse-ash-treated soil has *MDD* larger but *OMC* smaller than bottom-ash-treated one, as depicted in Figure 7.12. While bagasse ash has *MDD* of 1.29 Mg/m$^3$ and *OMC* of 26.24 %, bottom ash has 1.27 Mg/m$^3$ for density and 27.30 % for moisture. In addition, the shape of compaction curve is also different between them. The curve of bottom-ash-treated soil has a gentle slope and align with the lime-treated soil curve. Meanwhile, bagasse ash shows a steep slope of distribution curve, which is similar to the parent soil's curve. The difference of compaction curve between bottom ash and bagasse ash with soil and lime may be attributed to the clay content existing in ash. While bottom ash has a majority of coarse particles, bagasse ash dominates with clay-sized grains. The porous grains in bottom ash reduced the density of soil blend significantly,

so the bottom ash turns soil into a coarser material that absorbs less water than clay, resulting in a smaller value of *OMC* (about 27%). Similarly, bagasse ash also reduced the *OMC* value since the ash still contains a proportion of crystalline sand, but it has higher *MDD* than bottom ash because bagasse ash is less porous than its counterpart. In the soil treated with both ashes, its *OMC* is predicted to be lower than 26% because of the dominance of fine sand in soil added from them. The *MDD* may also be lower than 1.30 Mg/m$^3$ due to the high porosity of bottom ash, which increases soil volume and reduces its density.

Figure 7.12 also compares the compaction curve of combined-ash-lime treated soil with others, including untreated soil, soil treated with hydrated lime and bottom ash or bagasse ash. It can be seen that the addition of bottom ash to soil mixtures reduced the maximum dry density remarkably, whereas the inclusion of lime and bagasse ash to soil only made their mixture's density decrease by about 0.5 Mg/m$^3$, from roughly 1.32 Mg/m$^3$ to just below 1.30 Mg/m$^3$ with involvement of 15% bagasse ash (see Figure 7.13). However, the optimum moisture content of bagasse-ash-treated soil decreased to only 26% from 29% in soil. When it comes to 25% bottom ash, *OMC* was at the high of 27.3%, but *MDD* was low at only 1.27 Mg/m$^3$. Interestingly, replacing 7.5% bottom ash by bagasse ash did not increase *MDD* in proximity to the 15%-bagasse-ash-treated sample. Instead, *MDD* had no change, at approximately 1.25 Mg/m$^3$, while *OMC* decreased significantly to 24%, as shown in Figure 7.14.

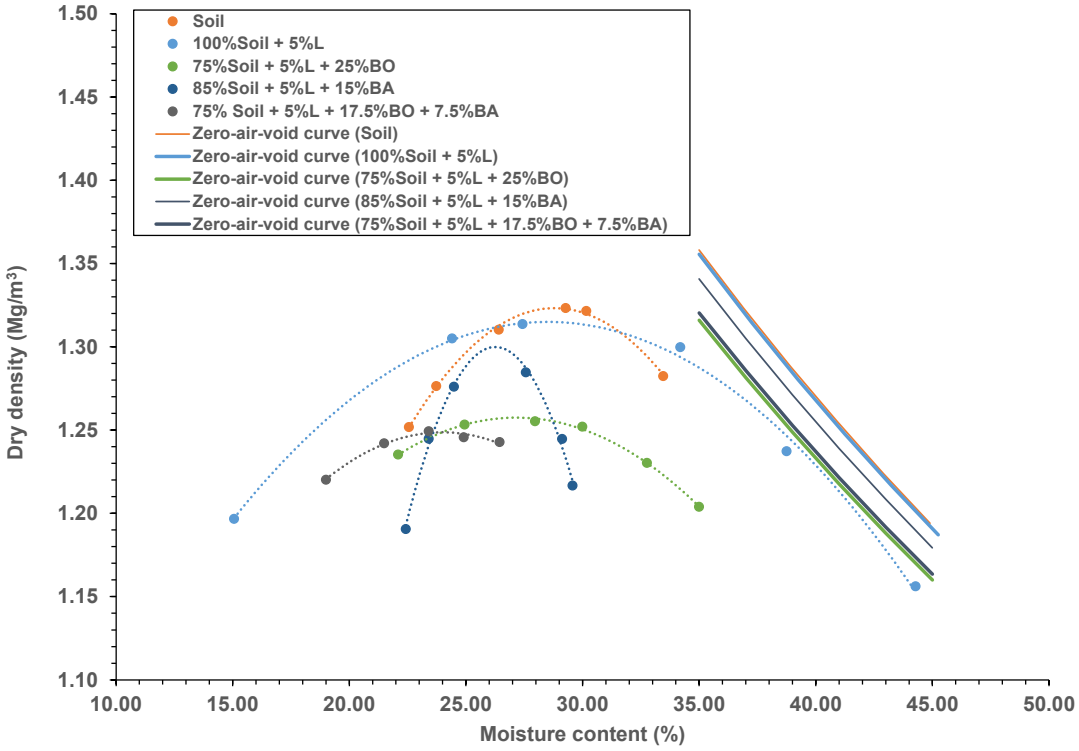


*Figure 7.12 Compaction curves of studied soils untreated and treated with lime, bottom ash and bagasse ash*

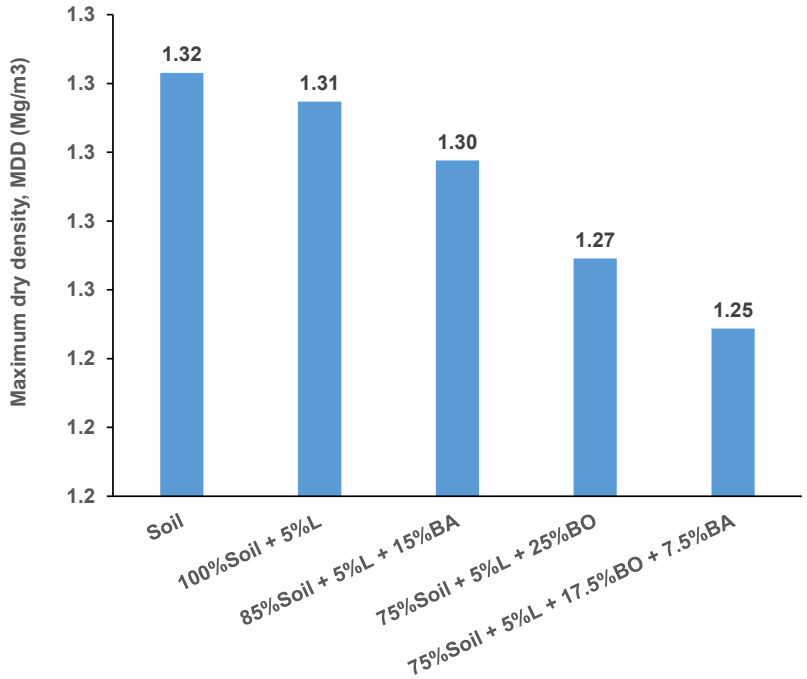


*Figure 7.13 Maximum dry density of untreated soil and soil treated with lime, bottom ash and bagasse ash*

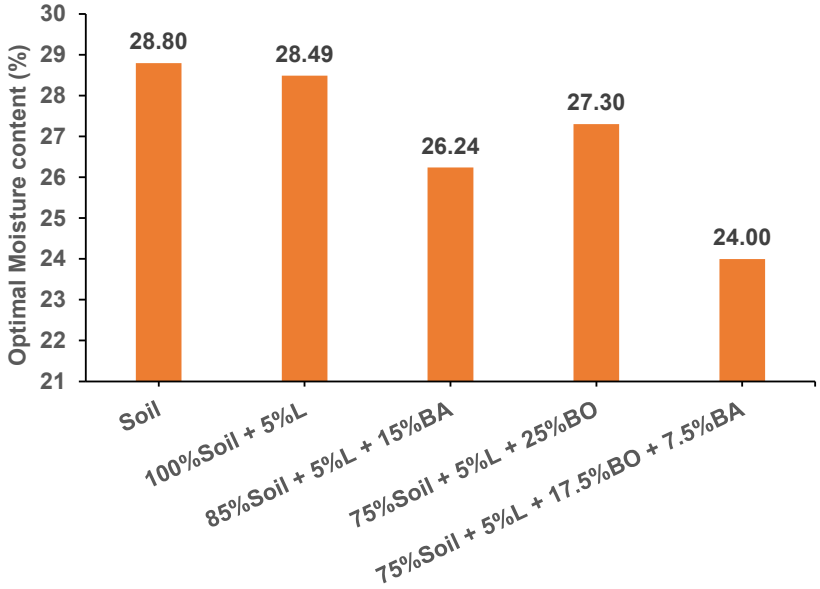


*Figure 7.14 Optimum moisture content of soil untreated or treated with lime, bottom ash and bagasse ash*

### 7.3.5 Free swelling ratio

Free swelling test on statically compacted samples was used to investigate the swelling potential of soil treated with hydrated lime, bottom ash or bagasse ash. In comparison between bottom ash and bagasse ash, the inclusion of bagasse ash reduced the swelling potential of soil by a range that is smaller than bottom ash with the same content of 15%, from 12.2% to roughly 6% in swelling

ratio for bagasse ash, compared to only 4% with bottom ash (refer to Figure 7.15a). This indicates that the swelling limitation of bottom ash in the soil is better than bagasse ash in a short curing time (i.e., 1 day). With the content higher than 15%, the addition of bottom ash to soil decreased its swelling ratio gradually, compared to those with ash proportion lower than 15%. Therefore, if there is a combination of bottom ash and bagasse ash in the soil mixture, the recommended ratio of bottom ash in their blend is equal to or larger than 15% to reduce the swelling potential effectively.

Figure 7.15b shows the change of swelling ratio with time in soil samples treated with hydrated lime, bottom ash and bagasse ash. It is worthy to note that a small amount of hydrated lime (5%) in soil helped remarkably reduce swelling potential, from under 70% swelling ratio in parent soil to only about 12% in lime-treated soil, referred to Figure 7.15b. This indicates an immediate effect of hydrated lime in eliminating the swelling problem of expansive soil. Including 15% bagasse ash in lime-treated soil continued reducing the swelling ratio down to just over 6%, and with 25% bottom ash to only 2.55% in swelling potential. Combining bottom ash and bagasse ash in the same total amount of 25% ash only slightly reduced the swelling amount to 5.5%, indicating a mild combined effect of two ashes in mitigating the swelling behaviour of expansive soil (see Figure 7.16). Soil treated with 5% lime and 25% bottom ash resulted in the lowest swelling ratio, which was about 2%. This is attributable to the fact that the inclusion of bottom ash as a coarse material reduced clay reactivity in expansive soil, whereas that of bagasse ash, regarded as clayey binder, increased the clay content in soil mixtures, causing a higher swelling ratio than soil treated with lime and 25% bottom ash (refer to Figure 7.16).

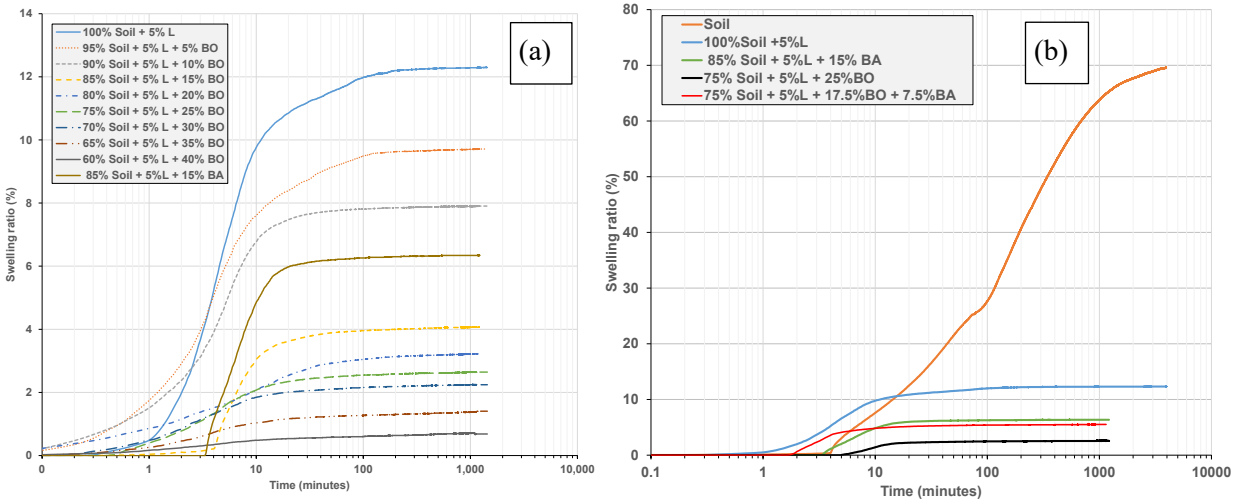


*Figure 7.15 Swelling ratio of (a) lime-treated soils with a variety of bottom ash content with 15% bagasse ash (after 1 day for curing) and (b) soils untreated and treated with hydrated lime, bottom ash and bagasse ash, and cured for 1 day.*

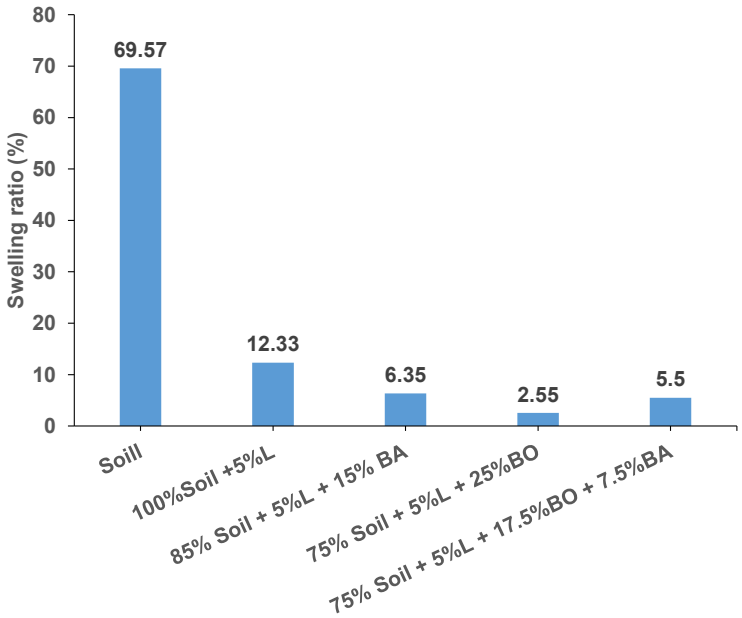


*Figure 7.16 Swelling ratio of untreated soil and soil treated with hydrated lime and bottom ash and bagasse ash*

### 7.3.6 Consolidation behaviour

Consolidation behaviour is measured by various parameters to evaluate the compressibility of soil under the application of incremental loads, which is conducted through consolidation tests. For expansive soil, this test is performed after a free-swelling experiment, which allows the sample to freely swell under a seating load, equivalent to the pressure of 6 kPa. In this study, five studied samples were tested, namely untreated soil, soil treated with lime, with lime and bottom ash/bagasse ash, and finally, with all three mentioned binders. Three consolidation features are mentioned, including consolidation curves, pre-consolidation pressure and compression index.

Figure 7.17 illustrates the variation of void ratio with the effective stress in consolidation tests, and five representative samples of studied materials were monitored. As can be seen, soil treated with both bottom ash and bagasse ash had the same void ratio to untreated soil at pressures over 1MPa, whereas lime-treated samples with bottom ash or bagasse ash had the same void ratio at the pressure of 1.6 MPa. However, compared to the change of void ratio, soil treated with lime and bottom ash had the lowest settlement among other treated soils, which was only about 0.2 from the initial ratio of 1.02 down to 0.72 at the pressure of 3,200 kPa. The low compressibility of bottom-ash-lime-treated soil is also reflected in pre-consolidation pressure and compression index, which are shown in Figures 7.18 and 7.19, respectively. As can be seen in these figures, although soil treatment with both lime and ash had the yield stress increase (see Figure 7.18), the compression indices of soil samples treated with bagasse ash were larger than that of lime-treated

soil, indicating the inclusion of bagasse ash tends to make the soil more compressible (refer to Figure 7.19). The combination of bottom ash and bagasse ash resulted in the highest index of compression among treated soils, which accounted for 0.46, as shown in Figure 7.19. This is due to the fact that bagasse ash had a higher proportion of weak cellular particles than bottom ash, which increased the compressive behaviour of treated soil (Cordeiro et al., 2016). On the other hand, bottom ash contained a majority of granular quartz which had particle strength ten times higher than cellular one, leading to the lowest compressive index of its mixture with soil.

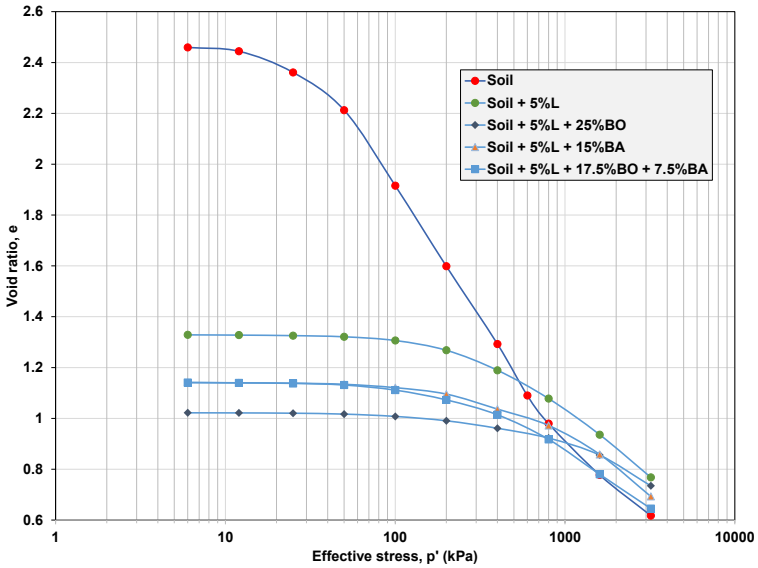


*Figure 7.17 Consolidation curves of soils treated with hydrated lime, bottom ash and bagasse ash*

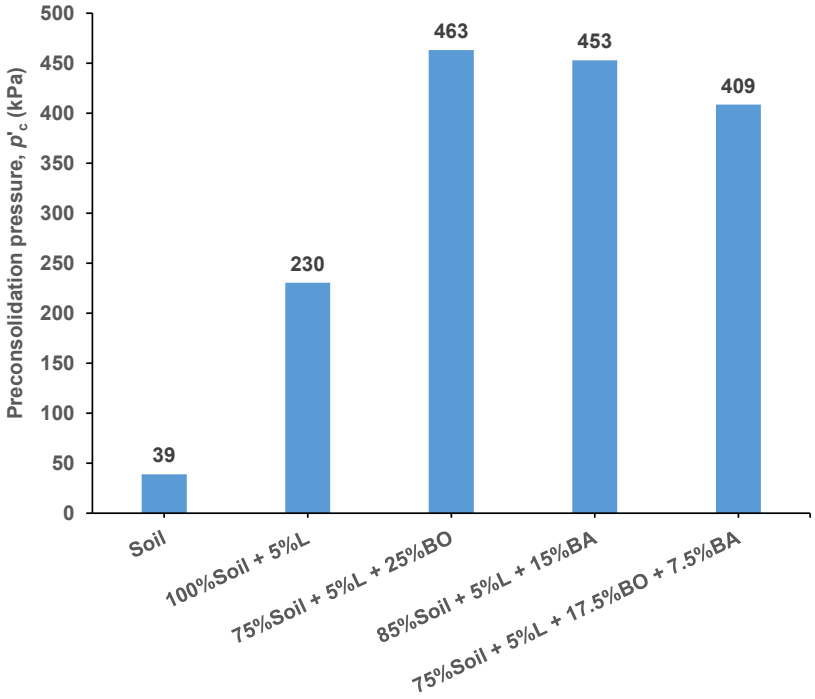


*Figure 7.18 Pre-consolidation pressure of soil treated with hydrated lime, bottom ash and bagasse ash*

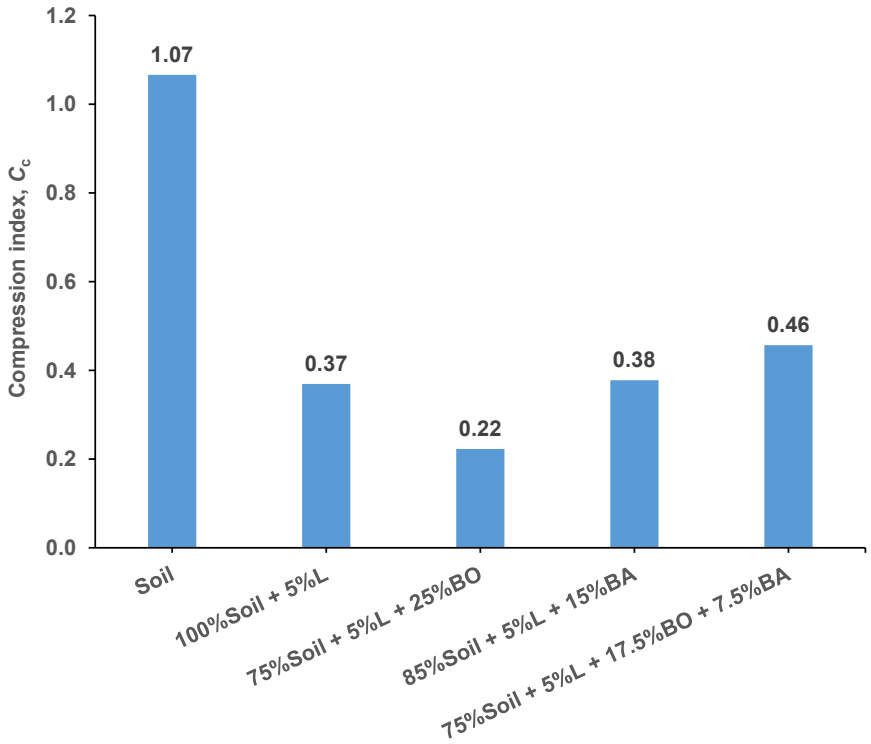


*Figure 7.19 Compression indices of soil treated with hydrated lime, bottom ash and bagasse ash*

### 7.3.7 Unconfined compressive strength (*UCS*)

Unconfined compressive strength (*UCS*) can be used to evaluate the suitability of studied soils for road construction material. Figure 7.20 shows the results of UCS tests for soil treated with hydrated lime, bottom ash and bagasse ash. It can obtain that soil stabilised with lime and bottom ash or bagasse ash can be used for road subgrade since the magnitude of *UCS* obtained about 2MPa after 56 curing days. However, using both bottom ash and bagasse ash reduced this strength to only about 1.75 MPa (see Figure 7.20). This low value was approximate to *UCS* of soil treated with lime at 1.62 MPa, indicating that the inclusion of both bottom ash and bagasse ash did not significantly improve the strength of lime-treated soil.

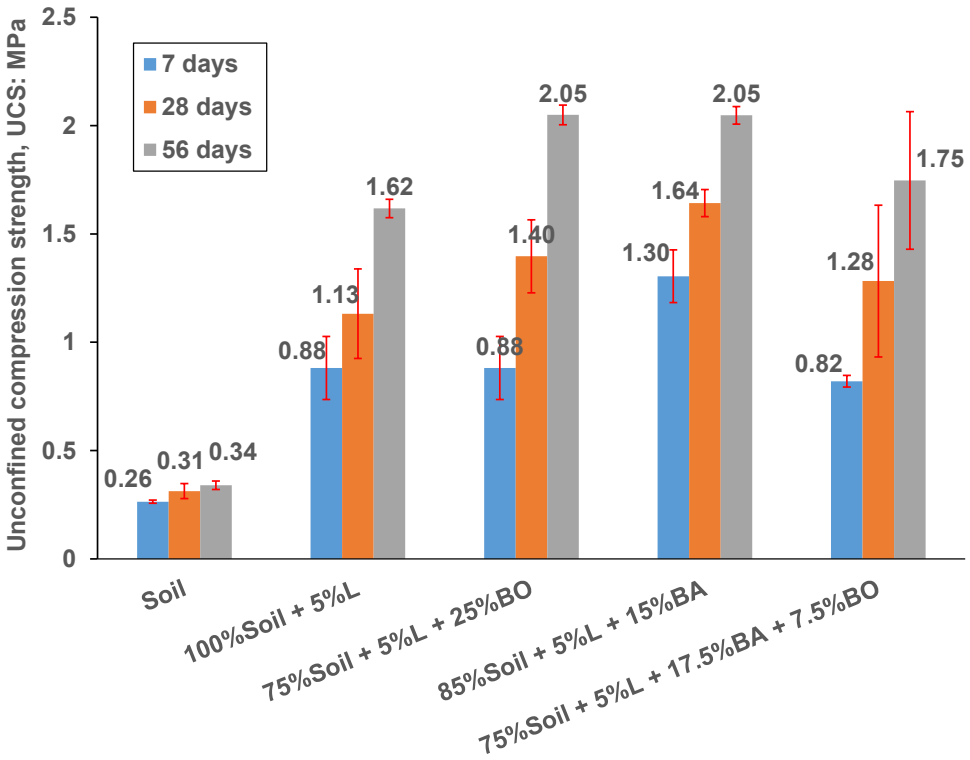


*Figure 7.20 Unconfined compressive strength of soil treated with hydrated lime, bottom ash and bagasse ash*

### 7.3.8 California bearing ratio (*CBR*)

Compared to *UCS*, California bearing ratio (*CBR*) is a good parameter to test the bearing capacity of soil materials under the pressures on the ground surface. Figure 7.12 illustrates the changes in California Bearing Ratio (*CBR*) of soil treated with 5% hydrated lime and bagasse ash or bottom ash in various content. The value of *CBR* was measured for samples compacted at *MDD* and *OMC* and cured for 28 days. Referring to Figure 7.21, the inclusion of ash in the lime-soil mixture improved the bearing capacity of soil. With the same content of 15%, both bottom ash and bagasse ash result in the same *CBR* at about 72%, indicating the reliance of *CBR* value on ash content rather than the kind of ash. From Figure 7.12, it is obvious that 25% bottom ash produced the highest *CBR* of 81%, suggesting the ash percentage of 25% is optimal for soil bearing capacity. Therefore, the combination of bottom ash and bagasse ash may be limited within a total of 25% content to result in a high value of *CBR*. Therefore, the results from electrical conductivity confirmed this total ratio of 25% ash to 5% lime in content (see Figure 7.7).

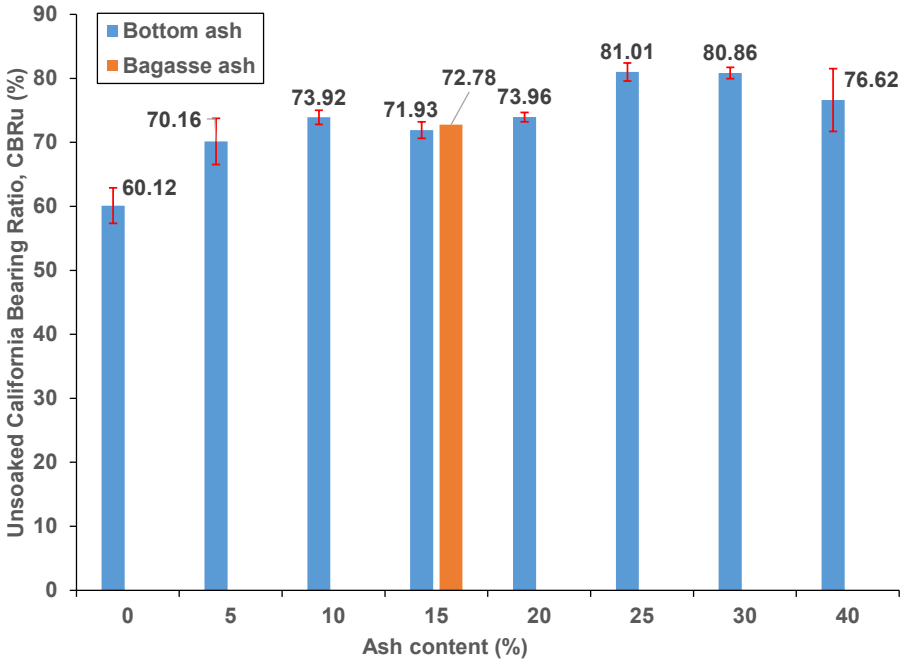


*Figure 7.21 Unsoaked California bearing ratio of soils treated with hydrated lime and bottom ash or bagasse ash*

In addition, there are two *CBR* values tested in this test, namely unsoaked *CBR* (denoted as $CBR_u$) and soaked *CBR* ($CBR_s$). While unsoaked *CBR* values involved the test performed in the dry condition, $CBR_s$ values were measured from samples soaked in water for saturation. Four treated soil materials were tested with soaked and unsoaked CBR test, including lime-, bottom-ash-lime-, bagasse-ash-lime-, and bottom-bagasse-ash-lime treated soils. For both unsoaked and tests, all CBR moulds were cured in airtight containers for 28 days. However, the soaked CBR samples were soaked in tanks of water for the next 62 days to have the samples fully saturated., Furthermore, small-strain shear modulus ($G_{max}$) was measured during the curing and saturation time using bender element equipment. The weight of samples was also monitored for the calculation of $G_{max}$. The results of shear modulus are shown in later experiments. In this test, the $CBR_u$ and $CBR_s$ with stress-displacement curves are revealed to compare the bearing capacity of treated soils.

Figure 7.22 demonstrates the unsoaked *CBR* values for studied soil materials and their stress-displacement curves. It is clear that 25% bottom ash gives the highest $CBR_u$ at 83.85%, followed by 15% bagasse ash added to soil with 5% lime. The sample treated with both bottom ash and bagasse ash is lowest, only about 52%, as shown in Figure 7.22a. However, its stress-deformation curve shows a ductile behaviour of the bottom-bagasse-ash-lime-soil sample, indicated by a

gradual increase of stress without collapse. Meanwhile, other specimens were broken down to suffer lower stresses, indicating their brittleness, as presented in Figure 7.22b.

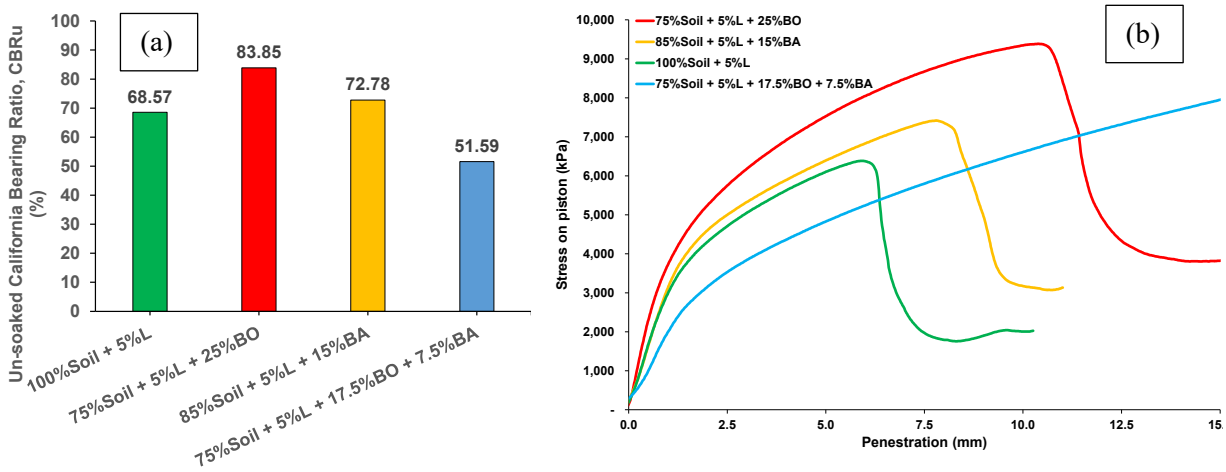


*Figure 7.22 Unsoaked California bearing ratio ($CBR_u$) of soil treated with hydrated lime, bottom ash and bagasse ash after 28 days for curing: (a) CBR values and (b) stress-displacement curves*

However, after 62 days submerged in water, all tested samples had a brittle behaviour in CBR results, shown by collapses of stress in Figure 7.23b. However, all ash-treated specimens had $CBR_s$ jumped to a premium high of the ratio over 100%, showing the highest of 127.84% in the sample treated with 25% bottom ash and 5% lime. In particular, the sample containing both bottom ash and bagasse ash had a significant growth of *CBR* and surpassed the ratio of bagasse-ash-lime-treated soil, 111.23% as against 106.80% (see Figure 7.23). However, the lime-treated soil sample suffered a loss in *CBR* by 15%, going down from 68.57% to 53.73% when the CBR mould was soaked in water. The opposite trend of *CBR* between lime-treated soil and the sample treated with all three binders can be explained by pozzolanic reactions occurring in ash-lime-treated samples. The samples treated with ash have a large inclusion of amorphous silica into soil matrix, which contributes significantly to the process that forms cementitious compounds or gels, enhancing the bonding effects and *CBR*. However, in the sample without ash, hydrated lime in soil merely generated hydrate products in sheet-like structures, which are proven in Chapter 4. These structures became weaker when water penetrates their gaps during soaking, reducing the bearing capacity of sample. In ash-lime treated soils, water, on the other hand, catalysed the reticular network of ettringite and hydrate products, reinforcing the strength of treated samples (Zhang et al., 2018). In bottom-bagasse-ash-lime soil, the inclusion of bagasse ash also increased brittleness of sample due to the fibrous shape of ash (see Figure 7.23b).

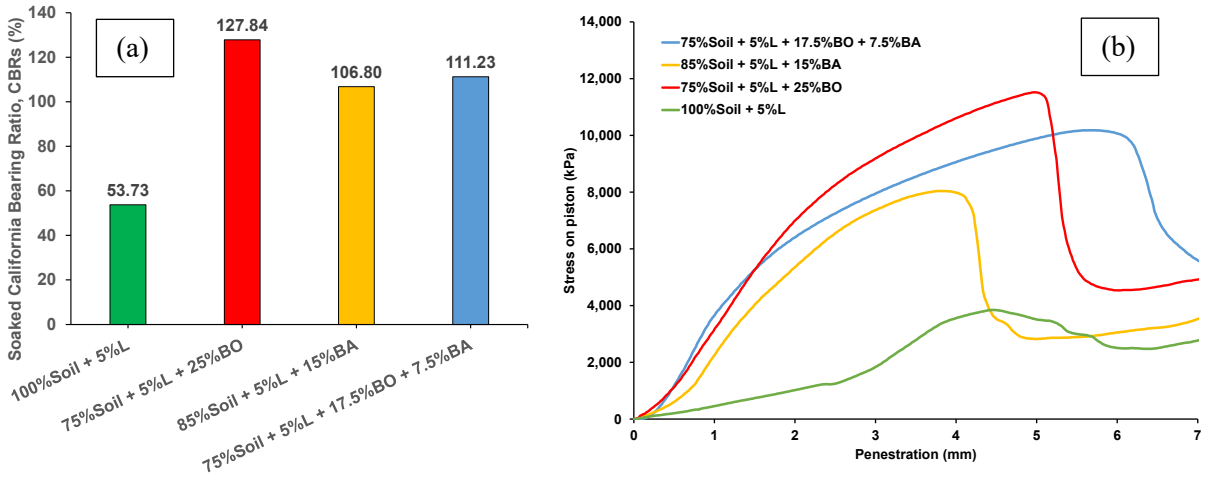


*Figure 7.23 Soaked California Bearing Ratio ($CBR_s$) of soil treated with hydrated lime, bottom ash and bagasse ash after 28 days for curing and 62 days for saturation: (a) CBR values and (b) stress-displacement curve*

### 7.3.9 Shear strength properties using triaxial tests

Shearing behaviour in triaxial tests is an important part of the study on the strength of soil under confined and measured pore water pressure conditions, which mimic soil situations at variable depths in the field. This research shows stress strain behaviour with excess pore water pressure with three confined stresses at 50 kPa, 100 kPa and 200 kPa. The effective stress failure envelope is then constructed to reveal internal friction angle and cohesion. Five soil samples were tested in triaxial shear experiments, including soil and treated soils with hydrated lime, bottom ash and bagasse ash. The samples were statically compacted at *MDD* and high moisture content for full-saturated conditions, and then they were cured for 28 days before putting in the triaxial cell for consolidated undrained (CU) tests.

#### *7.3.9.1 Stress strain behaviour and excess pore water pressure*

Figure 7.24 indicates changes in deviatoric and excess pore-water stress with axial strain in three confined compresses at 50, 100 and 200 kPa. The plots compare five soil specimens untreated and treated with hydrated lime, bottom ash and bagasse ash. It is obvious from Figure 7.24 that untreated soil expresses a behaviour of loose material with deviatoric and pore pressure increasing gradually. Meanwhile, treated soils had characteristics of dense particles, indicated by a steep increase of shear stress, followed by a collapse and then a residual value at large axial strain. The collapse was equivalent to a plunge of excess pore water pressure, illustrating the expansion of over-consolidated soil (Budhu, 2008). Among treated soils, the sample with 25% bottom ash had the least expansion due to its smallest pore pressure on the negative side. Meanwhile, lime-treated

soil and specimens with bagasse ash had greater expansion with residual excess pore water pressure at around -200 kPa. The highest peak shear stress and smallest negative pore pressure over three studied confined pressures of 25%-bottom-ash sample indicated its granular property compared to other specimens (Araei et al., 2012). Combining bottom ash and bagasse ash reduced this coarse feature with lower peak deviatoric stress and a larger range of negative pore water pressure (see Figure 7.24).

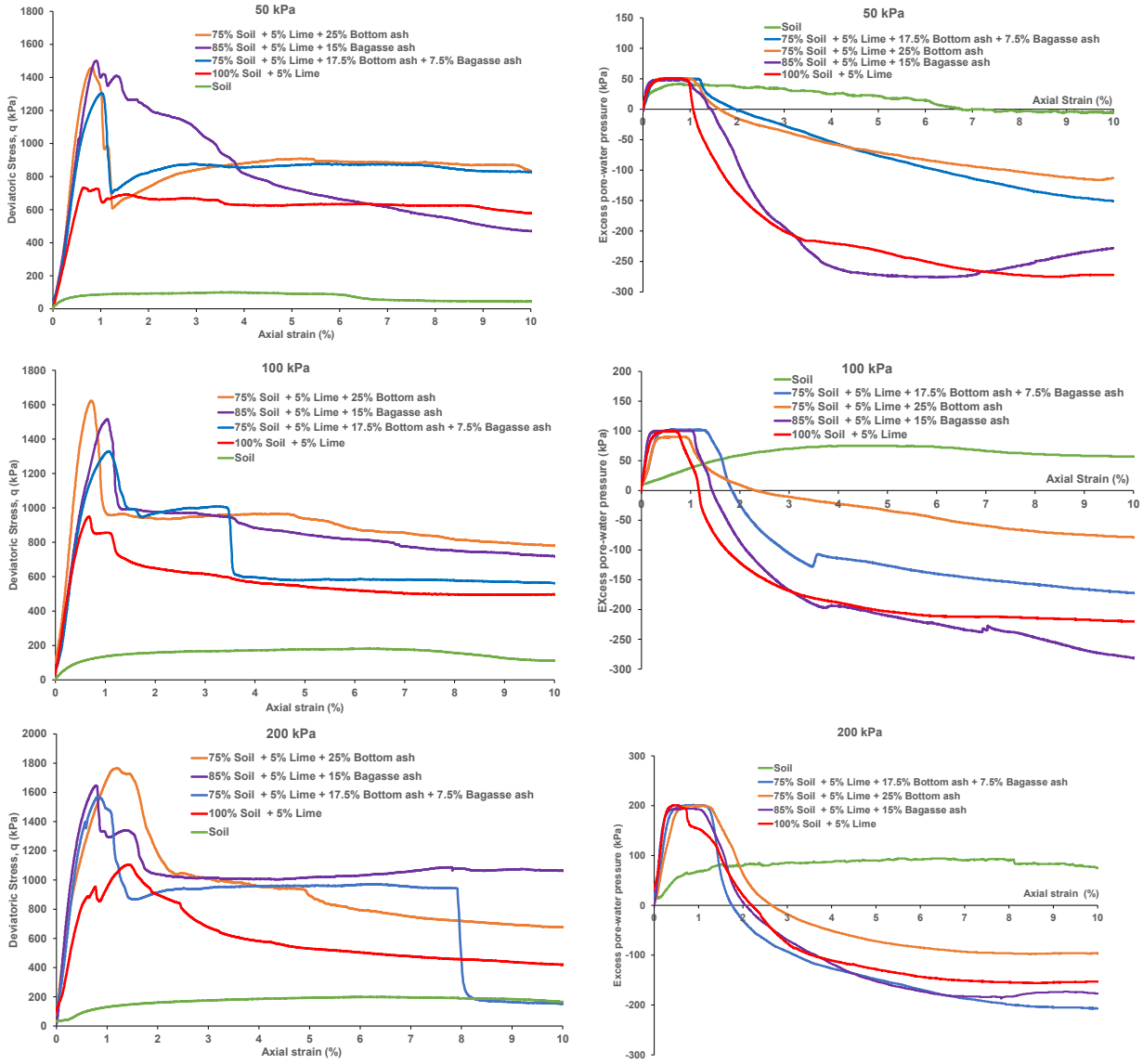


*Figure 7.24 Shearing stress-strain and pore-water-pressure-strain relationships of untreated soil and soil treated with hydrated lime, bottom ash and bagasse ash*

### *7.3.9.2 Effective stress failure envelope, friction angle and cohesion*

Shearing parameters from triaxial tests are important factors to use studied materials for earth fill construction because it relates to soil failure under an increase of loads. Figure 7.25 compares the development of an effective stress failure envelope of soil treated with lime and bottom ash or

bagasse ash. As can be seen in this figure, soil treated with lime and ash had the approximate envelope with the highest shear stress and effective normal stress in the range from 700 to 900 kPa. They also had the steepest slopes, which are about 1, compared to soil and lime-treated sample. However, the ash-treated soils also had lower intercepts than soil treated with lime. Consequently, the cohesions of ash-included specimens were much lower than that of lime-treated soil, 48 kPa for bagasse ash compared to 127 kPa for lime, which is shown in Figure 7.26. Bottom-ash-treated samples had the highest internal friction angle at 45° but also had no cohesion. Meanwhile, bagasse-ash-lime-treated soil had an angle of 43° but still has a value of 48 kPa in cohesion. The combination of bottom ash and bagasse ash in soil with lime gave the same friction angle around 45° and zero cohesion. The elimination of cohesion caused by the inclusion of bottom ash is attributed to the fact that this ash played a role of coarse material, which became dominating over clayey particles in soil, including bagasse ash, turning the soil into granular material like sand without cohesion (refer to Figure 7.26).

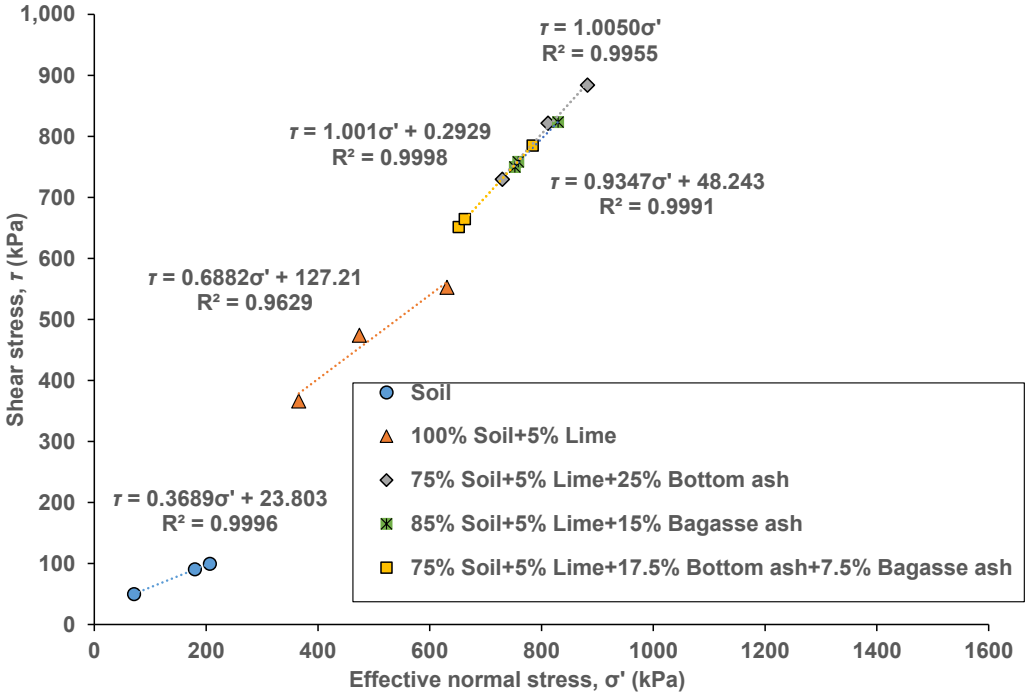


*Figure 7.25 Effective stress failure envelope of untreated soil and soil treated with hydrated lime, bottom ash and bagasse ash*

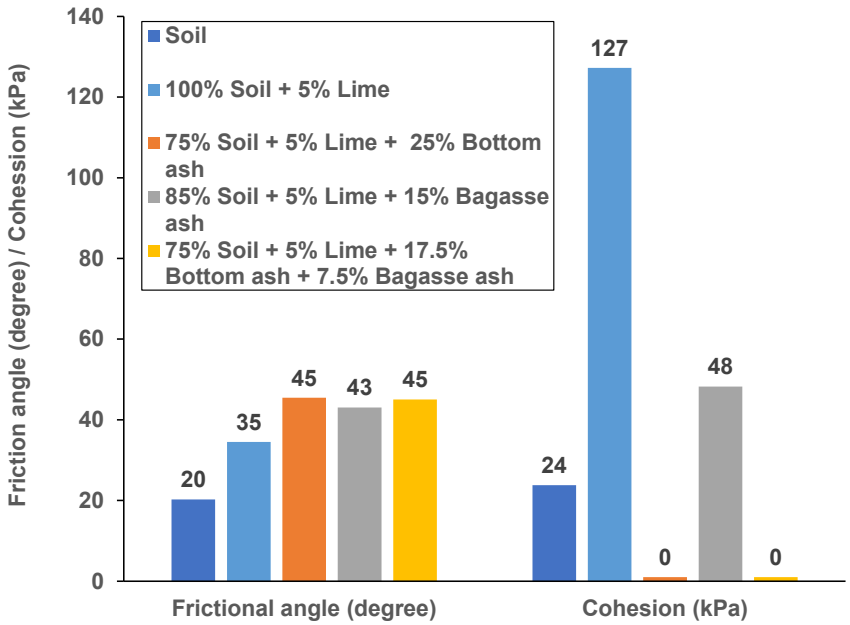


*Figure 7.26 Internal friction angle and cohesion of soil treated with hydrated lime, bottom ash and bagasse ash.*

### 7.3.10 Small-strain shear modulus ($G_{max}$)

In addition to investigation on shear stress through triaxial tests, bender element tests also provide an important parameter to study on soil strength, namely small-strain shear modulus ($G_{max}$). Due to the small strain measure, the shear modulus has a higher value than the ones calculated from triaxial shear tests with longer strains surveyed. However, unlike triaxial test, bender element test offers a premium approach to monitor the strength development with time since the experiment does not destruct soil structure while measuring its strength. In this study, there are three heights of samples used for bender elements tests, namely 100 mm from triaxial tests, 117 mm from CBR tests, and 40 mm for waxed samples. For triaxial tests, samples were measured for $G_{max}$ after 28 days, while others were monitored continuously after compaction to over 90 days.

#### *7.3.10.1 Triaxial (CU) samples (H=100 mm)*

Figure 7.27 compares small-strain shear modulus of samples treated with hydrated lime, bottom ash and bagasse ash. It is apparent that the sample treated with both bottom ash and bagasse ash obtained the highest modulus at 675 MPa, followed by soil treated with 25% bottom ash and 5% lime at 596 MPa, which is shown in Figure 7.27. Soil treated with 5% lime had the lowest shear modulus at about 500 MPa. The lowest modulus of lime-treated soil is in good agreement with triaxial shearing test results, indicated by its lowest initial slope of the stress-strain curve, which is shown in Figure 7.24. Meanwhile, in this figure, the shear modulus of soils treated with ash and

lime was higher that of lime-soil sample in a small discrepancy, which is also associated with bender element results illustrated in Figure 7.27.

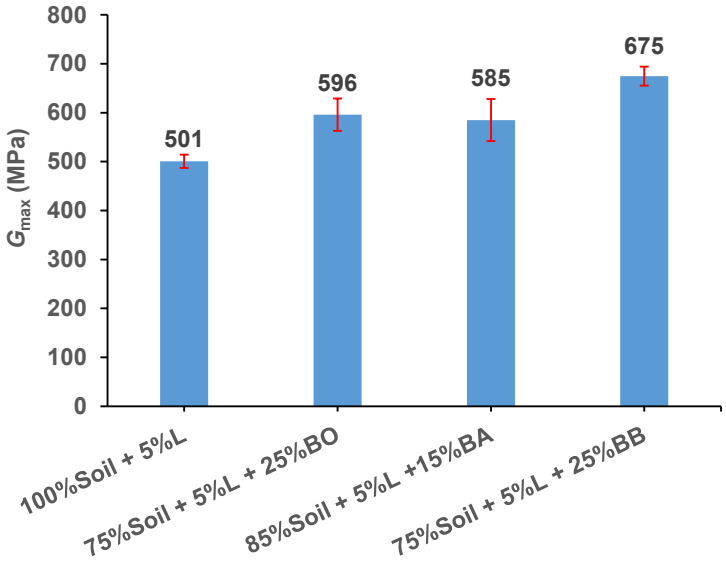


*Figure 7.27 Small-strain shear modulus ($G_{max}$) of soil treated with hydrated lime, bottom ash and bagasse ash (fully saturated and cured for 28 days), Note: BO = Bottom ash, BA = Bagasse ash, and BB = bottom ash and bagasse ash*

### *7.3.10.2 Unsoaked and soaked CBR samples (H=117 mm)*

As mentioned in Figures 7.22 and 7.23, CBR samples were measured in small-strain shear modulus using bender elements to monitor the changes of $G_{max}$ over 28 days of curing in the unsoaked condition and then next 62 days for soaking in saturating process. Figure 7.28 shows these changes for four treated samples in a logarithm of curing time. It can be seen that all ash-treated samples started from the same value of $G_{max}$ at about 200 MPa after compaction, but their modulus polarised after 1 day of curing. The soil sample treated with 5% lime and 25% bottom ash obtained the highest increasing rate of $G_{max}$ to become the sample with the highest shear modulus after 28 days, accounting for about 1,000 MPa (see Figure 7.28). Samples treated with bagasse ash had the same tendency of $G_{max}$ over 90 curing days, while lime-treated soil experienced a lowest rate and value of modulus before and after soaking process. It is also worthy to mention that all studied sample suffered a loss in shear modulus right after soaked in water for saturation. However, after 1 day for soaking, $G_{max}$ of treated samples gradually increased. The 25%-bottom-ash sample gained the highest rate, overtook its 28-day $G_{max}$ to reach the high of 1171 MPa after 90 days for curing. On the other hand, samples with bagasse ash had a lower rate of soaked $G_{max}$, so they only obtained a slightly higher modulus value of 844 MPa after 90 days than that after 28 days (810 MPa), as shown in Figure 7.28. Lime-treated soil had the largest drop of

$G_{max}$ after soaking by 124 MPa and the lowest rate of modulus recovery, resulting in a lower value of $G_{max}$ at 90 days than that at 28 days, 568 MPa compared to 600 MPa, respectively. The strength degradation of lime-treated soil and the strength improvement in lime-ash-treated samples after the soaking process are in line with *CBR* results, shown in Figures 7.22 and 7.23. This confirms that soil treated with 25% bottom ash and 5% hydrated lime was more durable than lime-treated soil. Compared to the bagasse-ash-treated sample, the only inclusion of bottom ash to soil improved the strength with time regardless of wet condition. The addition or combination with bagasse ash reduced this ability of reinforcement, causing the lower rate of shear modulus development with time and soon obtaining levelling-off values after 90 days (refer to Figure 7.28). Over the period observing the increase of $G_{max}$, the reinforcement during the soaking period was much related to the formation of hydrated products in the wet condition. However, to investigate the change of soil strength over the long-term period in samples with the optimum moisture content, a series of specific samples with the height of 40 mm can be tested, which are shown in the next tests.

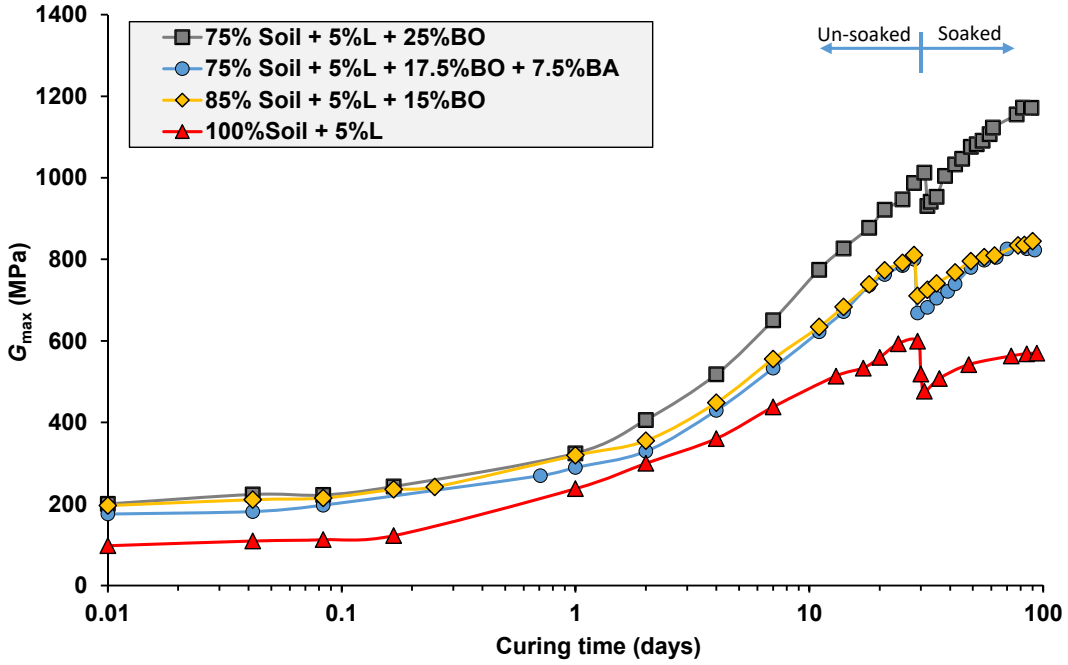


*Figure 7.28 Variation of small-strain shear modulus ($G_{max}$) of soil treated with hydrated lime, bottom ash and bagasse ash (CBR samples unsoaked in 28 days and then soaked in 62 days)*

### *7.3.10.3 Long-term curing samples (H=40 mm)*

For bender element tests over a long-term curing time, waxed samples were statically compacted at *MDD* and *OMC*, as obtained from Figure 7.12. Studied soil samples in the height of 40 mm were monitored in their changes of $G_{max}$ with time over about 1 year to oversee shear modulus

evolution. It can be seen from Figure 7.29, soil treated with all three binders had a high rate of $G_{max}$ after the first day of curing to be the sample with the highest shear modulus after 4 days, accounting for 309 MPa. However, all treated samples had $G_{max}$ levelling off after 28 days, with the highest of 595 MPa for the sample treated with lime, bottom ash and bagasse ash, as illustrated in Figure 7.29. Although 17.5%-bottom-ash-7.5%-bagasse-ash sample obtained $G_{max}$ slightly higher than the 25%-bottom-ash sample from Day 4 to Day 56, after 56 curing days, both samples have the same $G_{max}$ at about 580 MPa. This is also the point of time where all samples experience a downward trend of $G_{max}$. However, the $G_{max}$ degradation of bottom-ash-related samples is much quicker than bagasse-ash-lime-treated soil, resulting in their same modulus value of 396 MPa after 270 curing days. This degradation is similar to the lime-treated soil, suggesting that they may be impacted by the detrimental effects of excess calcium silicate hydrate formulation in sheet-like structures. Furthermore, bagasse ash played a role in accelerating $G_{max}$ of bottom-bagasse-ash-lime-treated soil after 4 curing days, but it did not prevail over bottom ash to reduce the $G_{max}$-decreasing rate after 56 days (refer to Figure 7.29). In comparison between Figures 7.28 and 7.29, the $G_{max}$ degradation might be related to moisture condition, since no decrease in $G_{max}$ was observed in saturated samples after 90 days (see Figure 7.28), whereas these can be seen obviously in Figure 7.29, which has drier samples tested. The dependence of strength on moisture content in lime-treated soils is in good agreement with the study conducted by Chakraborty and Nair (2020). The two authors mentioned that there are possibly moisture-induced damages caused by hydrate products, reducing soil strength because precipitated CSH held water with its affinity capacity, which deterred the hydration of stabilised soil layers.

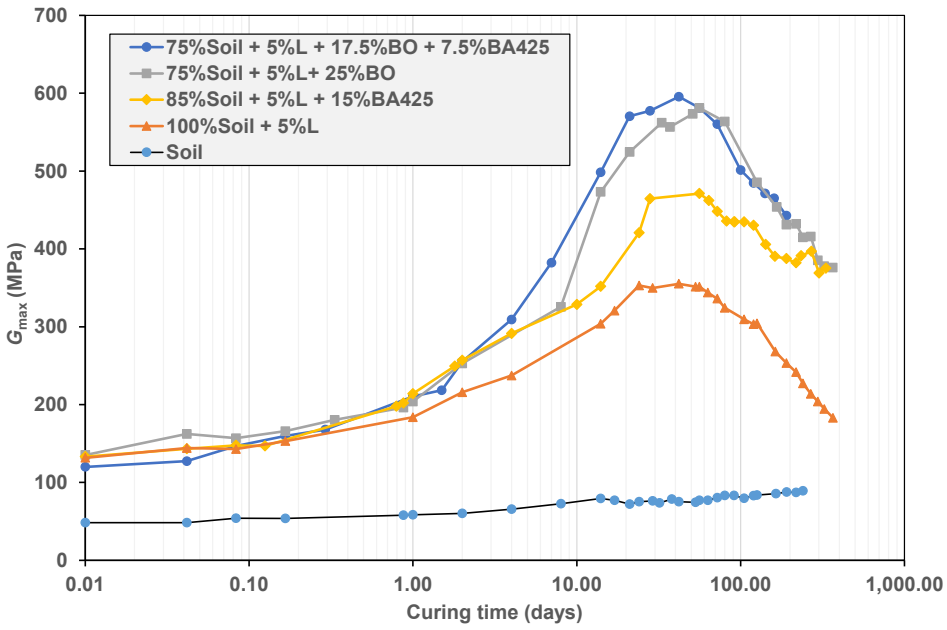


*Figure 7.29 Change in small-strain shear modulus $G_{max}$ of soil treated with hydrated lime, bottom ash and bagasse ash (compacted at optimum moisture content) with time*

Compared to bender element tests for CBR samples, all $G_{max}$ values waxed specimens ($H$ = 40 mm) is much lower (see Figures 7.28 and 7.29). This is attributed to the difference in the compaction methods; the dynamic compaction method was used for CBR samples, whereas the static method was applied on waxed specimens (Kawajiri et al., 2017). When compacting samples dynamically, soil particles are in a random structure, whereas statically compacted samples have a structure in orientation (Yong & Warkentin, 1966).

To investigate the effects of moisture on $G_{max}$ evolution, soils treated with both bottom ash and bagasse ash were compacted at both the dry side and wet side of *OMC* and measured the changes in shearing modulus, as shown in Figure 7.30. It can be obtained that bottom-bagasse-ash-lime treated samples showed different changes in $G_{max}$. Starting with the highest $G_{max}$ at around 150 MPa after compaction, the dry-compacted sample had the steadiest growth of strength among others to suffer the lowest $G_{max}$ after 14 curing days. On the other hand, the wet-side sample, albeit having the lowest $G_{max}$ for the first day, was stiffer and stiffer in the following days to surpass the dry-side sample after 14 days and optimal-content one after 24 days. It is worthy to note that $G_{max}$ of the wet-prepared sample was still going down under 600 MPa after 56 days but in a lower rate, whereas the two remaining samples experienced a significant downhill in shear modulus after 42 days for *OMC* specimens and 56 days for dry ones.

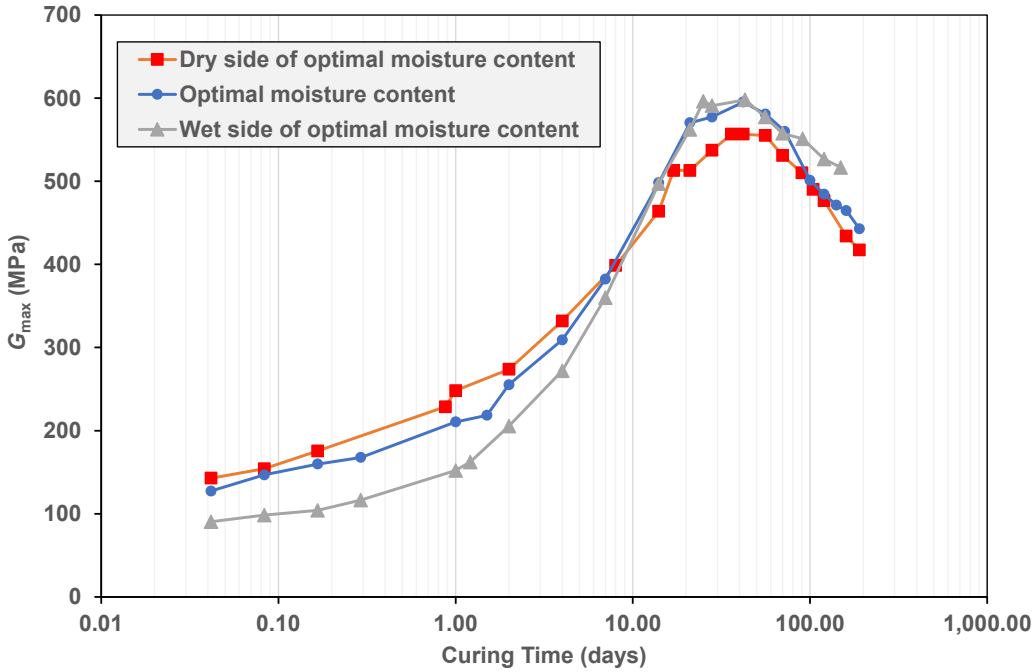


*Figure 7.30 Change in small-strain shear modulus $G_{max}$ of soil treated with 5% hydrated lime, 17.5% bottom ash and 7.5% bagasse ash (compacted at different water contents) with time*

When moisturisation did not affect the change in $G_{max}$ of soil sample treated with lime, bottom ash, and bagasse ash, this mixture with bagasse ash in particle sizes smaller than 425µm may enhance shear modulus. However, it is not the case, since there is a further degradation of $G_{max}$ if smaller bagasse ash is added into bottom-ash-lime treated soils, which is shown in Figure 7.31. Although after compaction, all samples started at the same modulus of just over 100 MPa, samples with 425µm had $G_{max}$ growing quickly after 7 days, gained and kept shear modulus at the highest value of 580 MPa for 51 days from the day of 21 to 72. The samples with smaller bagasse ash shortened this duration, down to 28 days for 150 µm, and 7 days for 75 µm. The shortening effects on high $G_{max}$ are also observed in bagasse-ash-lime-treated soils, as shown in Figure 7.32. It can be observed that samples with finer bagasse ash tend to form a peak of $G_{max}$ as indicated in Figure 7.32c. It can be attributed to the fact that fine bagasse ash absorbs more water than the coarser one, causing dehydration of stabilised soil layers, reducing the shear modulus quickly. This is in light of the study of moisture effect on soil strength in lime-treated soil, which was observed by Chakraborty and Nair (2020).

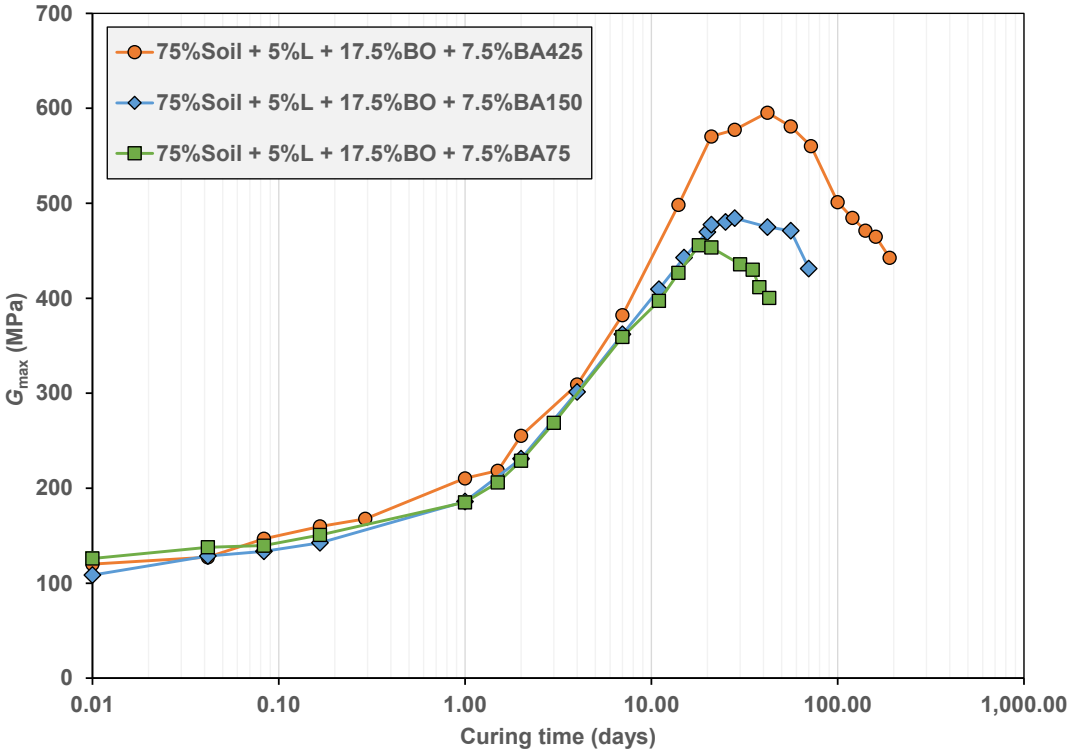


*Figure 7.31 Variation of $G_{max}$ of soil treated with 5% hydrated lime, 17.5% bottom ash and 7.5% bagasse ash with various sizes of bagasse ash (425, 150 and 75 µm)*

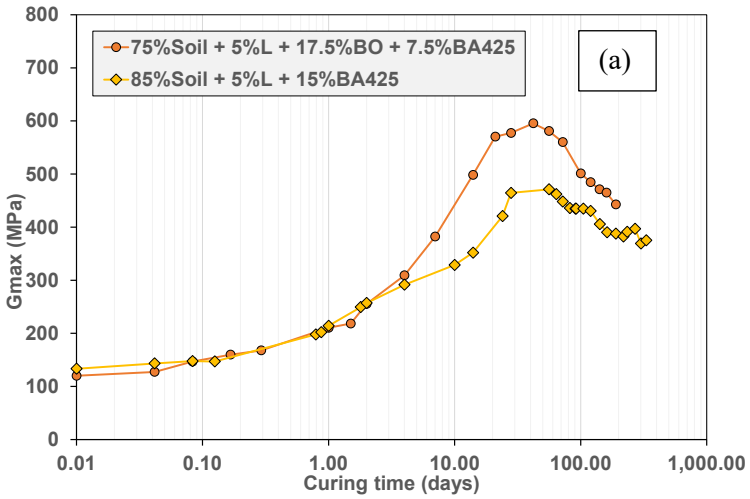

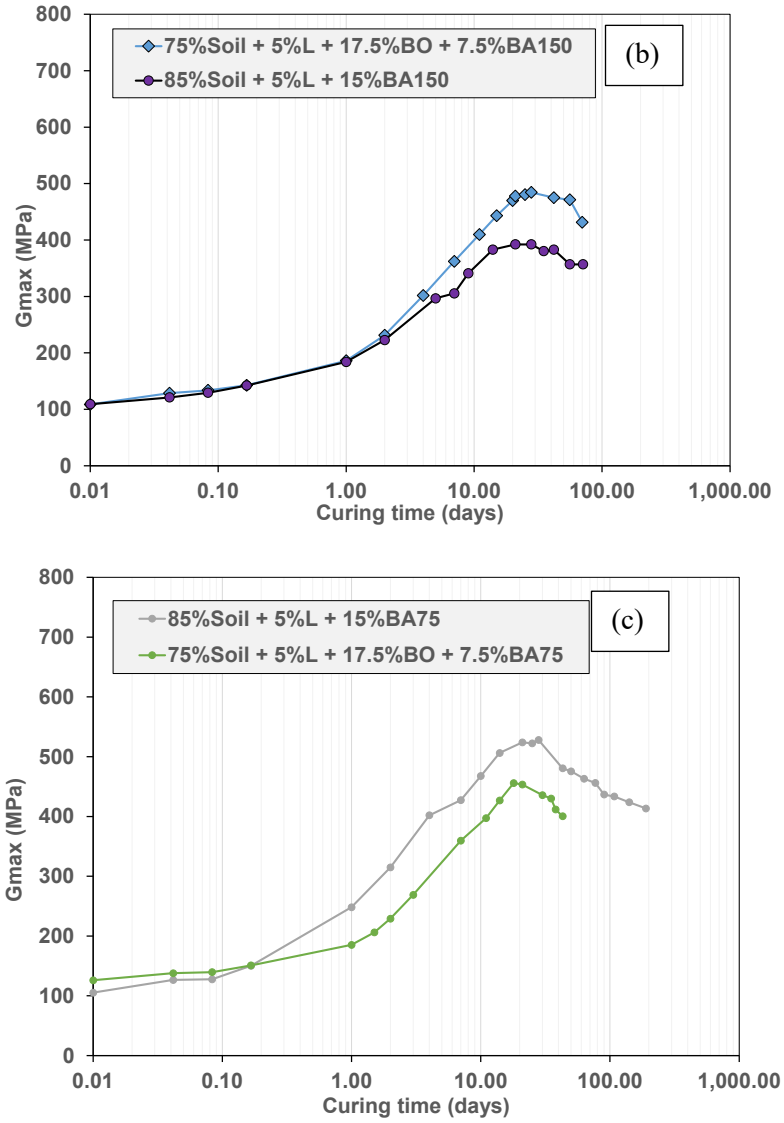


*Figure 7.32 Variation of $G_{max}$ of soil treated with hydrated lime, bottom ash and bagasse ash with various sizes of bagasse ash (in comparison with lime-bagasse-ash-treated soils): (a) 425 µm, (b) 150 µm, and (c) 75 µm*

### 7.3.11 Matric suction

In this study, matric suction or soil suction is measured by the filter paper method. Unlike small-strain shear modulus, matric suction of soil treated with bottom ash and bagasse ash with lime significant increased suction over 90 days, as illustrated in Figure 7.33. As can be seen in this figure, the soil containing all binders started the suction equalling to 25%-bottom-ash-lime sample, at around 70 kPa. However, the suction increased significantly to be equivalent to the 15%-bagasse-ash-lime soil after 28 curing days, which is 177 kPa. Turning to the sample with 56 days, the three-binder-treated soil gained the highest suction of 289 kPa and kept increasing to about 300 kPa after 90 days of curing. This suction was more than 6 times as large as that of the 25%-

bottom-ash sample. The significantly high suction value in bottom-bagasse-ash-lime treated soil was related to the formation of reticular network between bottom ash and bagasse ash, which increased nano-sized voids in treated soil, increasing its suction (Zhang et al., 2018).

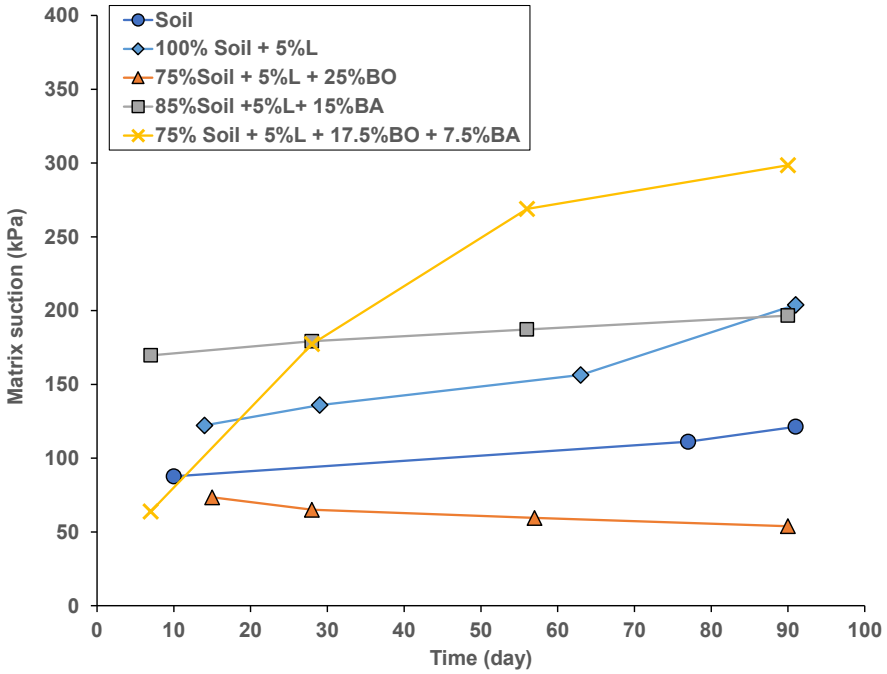


*Figure 7.33 Matric suction of untreated soil and soil treated with hydrated lime, bottom ash and bagasse ash over 90 days*

### 7.4 Micro-structural analysis on soil treated with lime, bottom ash and bagasse ash

The study on small-strain shear modulus of treated soil reveals five (5) typical stages of strength development in ash-lime treated samples. Illustrated in Figure 7.29, Stage 1 is equivalent to the gradual increase of $G_{max}$ after compaction. This stage may last from 1 day to a few days, depending on type and particle size of ash used. For example, bottom-ash-lime-treated soil has 7 days for Stage 1, whereas bagasse-ash-treated one extends to 10 days with the ash size of 425 µm (refer to Figure 7.29). After Stage 1, the shear modulus goes up significantly until the day of 28 for Stage 2. Stage 2 is then followed by a plateau of modulus, indicating Stage 3 of the process. After about 56 days, Stage 4 is signified by a downward trend of shear modulus until the levelling-off level of $G_{max}$ obtained, indicating Stage 5 in the evolution of shear modulus. Since the five stages are expressed with curing time, these stages are closely related to the formation of products from pozzolanic reactions occurring in treated soils. In this section, Scanning Electron Microscopy (SEM) analysis was conducted to explain the five-stage development of shear modulus in bottom-bagasse-ash-lime-treated soil using images captured for hydrate products. The analysis is also taken to reveal the reason why the three-binder treated soil compacted at the wet side of optimum

moisture content can keep high shear modulus over a long time in Stage 3, omitting Stage 4 and 5. A schematic diagram depicting the reticular connection between bottom ash and bagasse ash in treated soil is also provided to support the notion.

### 7.4.1 Bottom-bagasse-ash-lime-treated soil samples compacted at *OMC*

Figures 7.34-7.38 show SEM images on soil samples treated with 5% hydrated lime, 17.5% bottom ash and 7.5% bagasse ash, which were compacted at the optimum moisture content and cured after 7, 21, 28, 63 and 90 days. As shown in Figure 7.34, there was the presence of calcium silicate hydrate (CSH) around bottom ash and bagasse ash. The hydrate products play the role of gels with the ratio of Ca/Si <1.5, indicating the existence of secondary CSH (He et al., 2011). Over 21 days, magnesium silicate hydrates (MSH) appeared in treated soil, which combined with calcium silicate hydrates to coexist in a web system, as shown in Figure 7.35 (Bernard et al., 2018). The web form may be the combination of multilayer disk-like globule of CSH and a spherical one of MSH as gels that glue soil particles together (Chiang et al., 2014). The formation of MSH and CSH gels explained the significant growth of $G_{max}$ in Stage 2. However, after 28 days, ettringite crystals appeared dominantly with a few CSH in sheet-like structures, which sandwiched between soil particles and the needle crystals, as shown in Figure 7.36. While the ettringite improves soil strength, sheet-like CSH deteriorated the strength due to its affinity capacity (Chakraborty & Nair, 2020). This resulted in a plateau of $G_{max}$ in Stage 3. Over a long period of time, ettringite crystals decreased in their density while primary CSH in sheet-shaped structures lubricated ettringite and dominated over this crystal, as shown in Figures 7.37 and 7.38, respectively. This dominance led to degradation of $G_{max}$ in Stage 4 after 63 curing days. Once the amount of primary CSH formed was stable over a long period of time, $G_{max}$ attained its stabilisation, indicating Stage 5 is obtained.

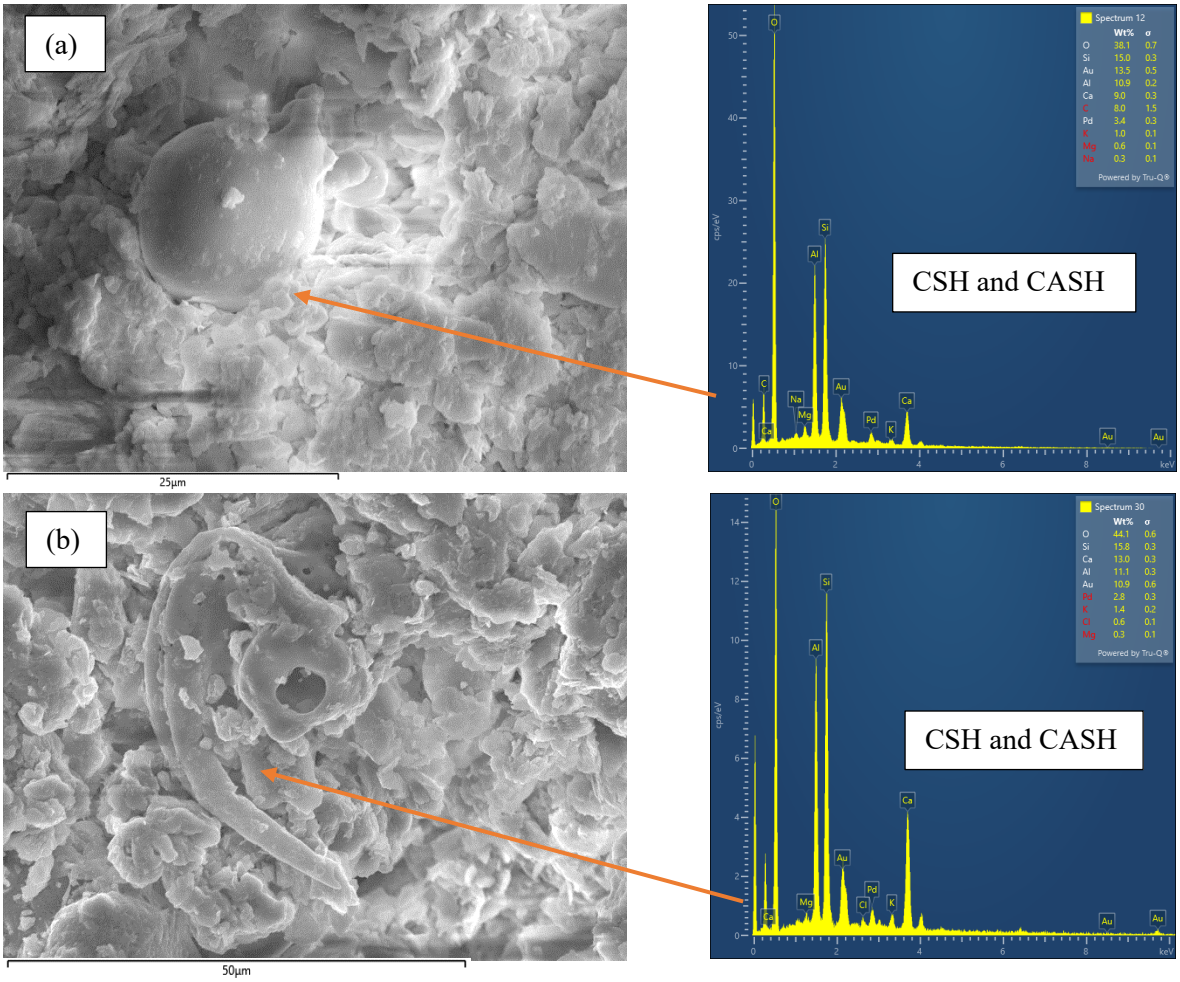


*Figure 7.34 SEM and EDS results on soil sample treated with 5% lime, 17.5% bottom ash and 7.5% bagasse ash after 7 curing days, with a photo at (a) bottom ash and (b) bagasse ash*

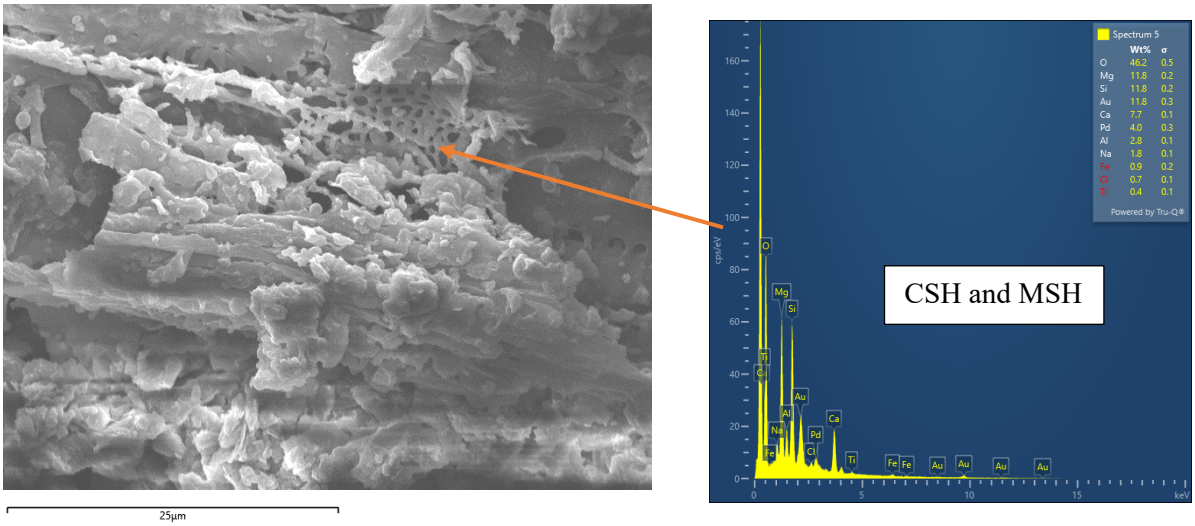


*Figure 7.35 SEM and EDS results on soil sample treated with 5% lime, 17.5% bottom ash and 7.5% bagasse ash after 21 curing days, with a photo captured at a bagasse ash*

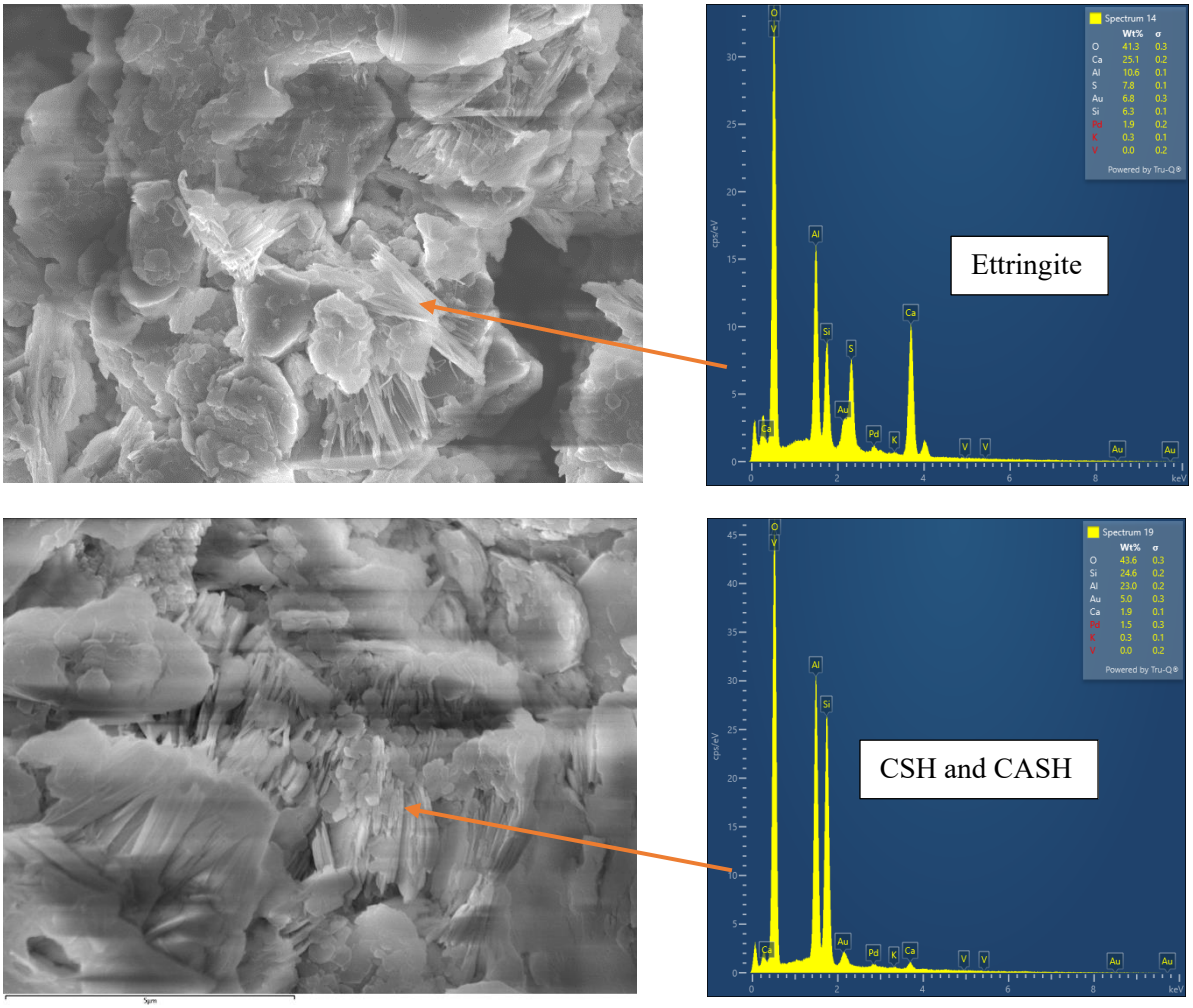


*Figure 7.36 SEM and EDS results on soil sample treated with 5% lime, 17.5% bottom ash and 7.5% bagasse ash after 28 curing days*

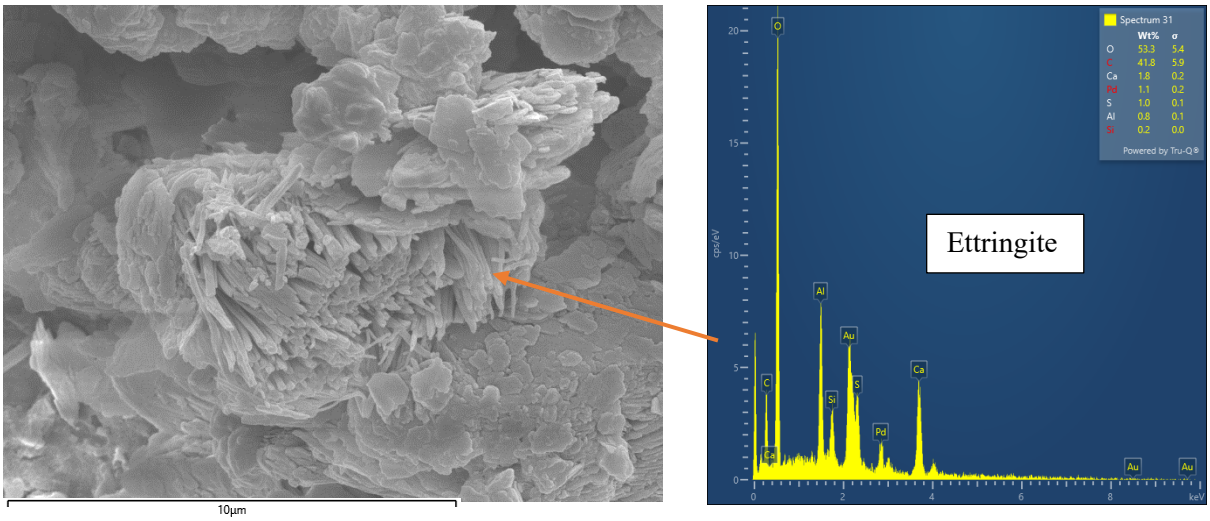


*Figure 7.37 SEM and EDS results on soil sample treated with 5% lime, 17.5% bottom ash and 7.5% bagasse ash after 63 curing days*

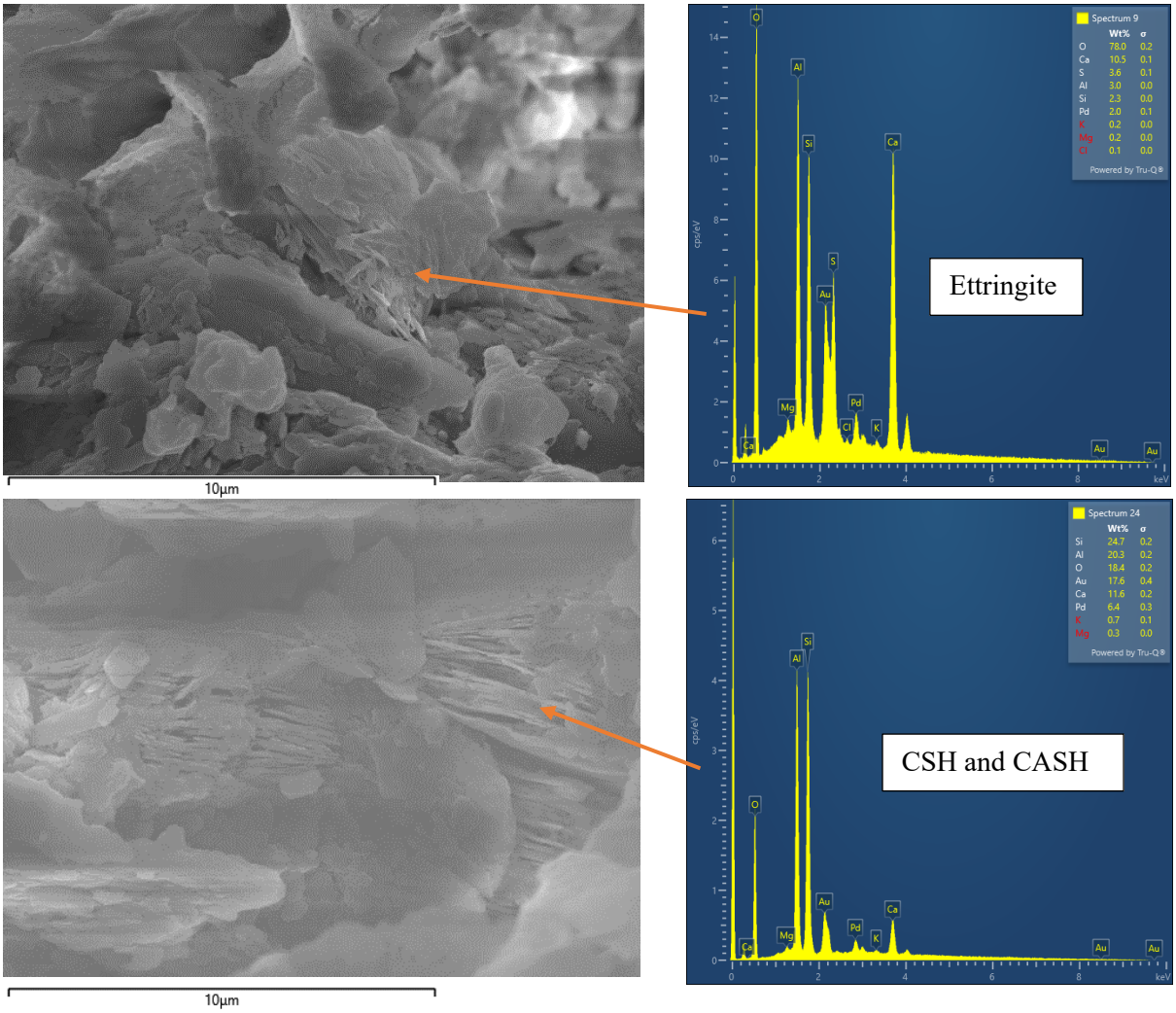


*Figure 7.38 SEM and EDS results on soil sample treated with 5% lime, 17.5% bottom ash and 7.5% bagasse ash after 90 curing days*

### 7.4.2 Bottom-bagasse-ash-lime-treated soil samples compacted at the wet side of *OMC*

SEM results on wet-compacted soil samples treated with hydrated lime, bottom ash and bagasse ash is also worth mentioning. Figure 7.39 illustrates the images captured on a hole left by the bottom ash sphere, which was pulled out of soil matrix. The hole is valuable to display the holistic close-contacting surface between two ashes. It can be seen in the in-zoomed image of the hole, fibrous crystals developed massively in a spoke-like system, which were mixed with gels in a web- or beehive-like shape. Referring to Figure 7.39, there were also large particles of hydrated lime in polygon shapes, scattering on the soil matrix.

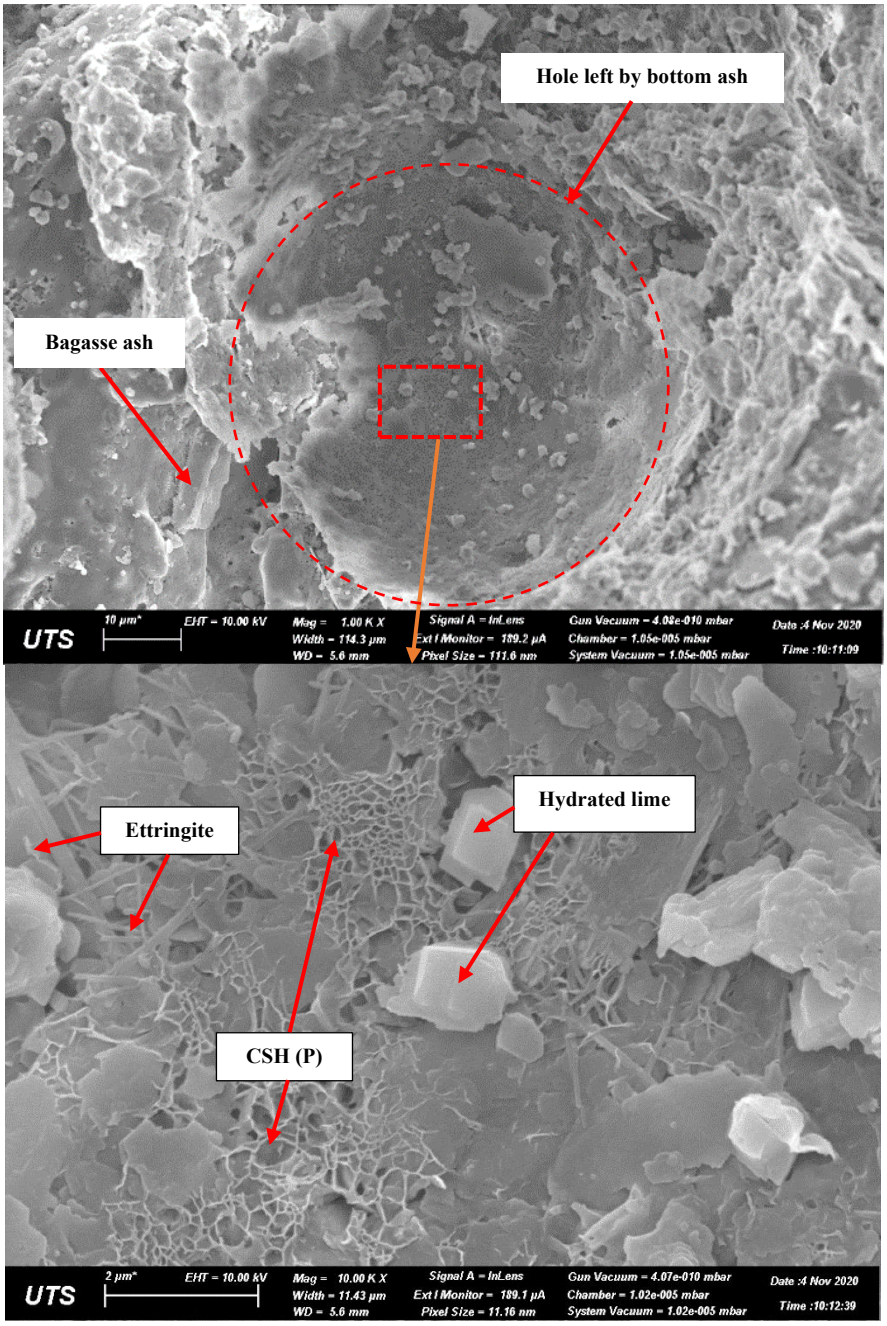


*Figure 7.39 SEM analysis on soil samples treated with hydrated lime, bottom ash and bagasse ash compacted at wet side after 28 curing days*

As can be seen in Figures 7.29 and 7.39, the early increase of $G_{max}$ caused by CSH (S) also led to a decrease in $G_{max}$ due to the excessive generation of CSH floccules which were nucleated on CSH (S) phase (Ríos-Parada et al., 2017). To evaluate the detrimental effects of CSH (S) on soil strength, study on wet-dry sides of bottom-bagasse-ash-lime-treated (BB) samples were investigated in CBR and bender element tests, as shown in Figure 7.28 and 7.30, respectively. It is suggested that if more water is provided during curing period, CSH will distribute in a reticular network on surface layers with the interior in the shape of fibre bundles (Zhang et al., 2018). This

CSH is the primary one with the Ca/Si ratio > 1.5, in which ettringite rod is embedded (see Figure 7.39). Compared to the BB sample at *OMC*, the BB sample on the wet side developed a mature 'sintered' structure of the CSH (P) reticular network interleaved with ettringite crystal in ITZ between bottom ash and bagasse ash, which is shown in Figure 7.40. The BB specimen at *OMC*, on the other hand, contains both CSH (P) and (S), which distributes discretely with little ettringite observed (see Figures 7.36-38). The ITZ in the wet-side BB sample becomes denser than that in optimum or dry-side ones, improving $G_{max}$ significantly 1 day after compaction, and the strength went up and surpassed $G_{max}$ of OMC sample after 28 days (refer to Figure 7.30). However, over the period of 56 days, $G_{max}$ of the wet BB sample went down and equalled to that of BB specimen at optimum moisture. This is because of the over-abundance of ettringite than CSH in ITZ of both samples (Figures 7.37-38), weakening the transition of pressure and deteriorating further development of strength in treated samples (Chakraborty et al., 2020; Sivapullaiah & Jha, 2014).

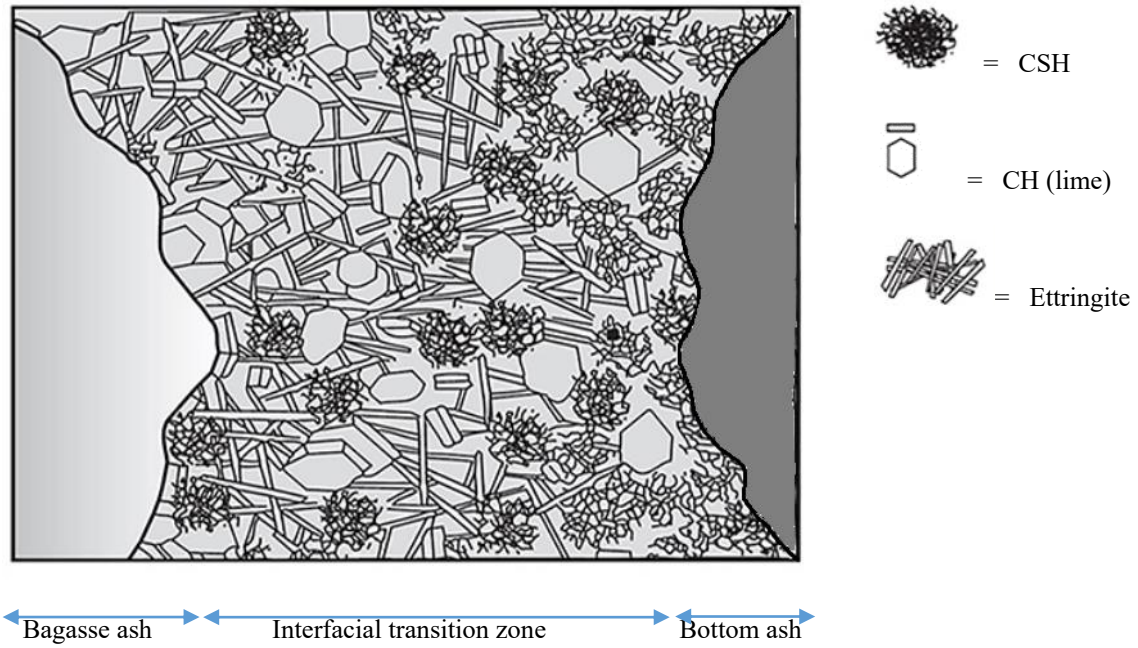


*Figure 7.40 Schematic diagram of Interfacial transition zone in expansive soil treated with hydrated lime, bottom ash and bagasse ash compacted at the wet side of optimum moisture (after Hilal (2016)).*

### 7.5 Summary

In this chapter, the characterisation of soil treated with hydrated lime, bottom ash and bagasse is clarified into two sections, namely ratio designation and application. Firstly, a designation of bottom-bagasse ratio is proposed using the electrical conductivity test C. Secondly, characterisation of bottom-bagasse-ash-lime treated soils with the bottom-bagasse ratio is illustrated in the ranges of experiments from particle distribution to SEM analysis. In summary, the chapter findings can be outlined as follows:

Designation of the ratio between bottom ash and bagasse ash in soil treatment with lime:

- The trial UCS experiment results indicate that the inclusion of bagasse ash into soil treated with 5% hydrated lime and 25% bottom ash does not improve the compressive strength of treated soils. This shows that 25% may be a threshold of ash content with 5% lime in the soil to produce the highest *UCS* value.
- Results from electrical conductivity tests also confirm that the percentage of 25% is the level where ash starts to dominate soil in reactions with lime to reduce the electrical conductivity of suspension. In this percentage, 70% bottom ash and 30% bagasse ash is their optimal combination, giving the highest conductivity value with the largest proportion of bagasse ash in aqueous solutions. As a result, the optimum bottom-to-bagasse ratio of 17.5% to 7.5% is proposed for soil treatment with 5% lime, based on soil-ash ratio or SB ratio (refer to Chapter 5).

Applications of the suggested bottom-bagasse ratio to the characterisation of ash-lime-treated soils:

- The ratio of 7 to 3 in the combination of bottom ash to bagasse ash, respectively, turns the property of bottom ash as poorly graded sand into clayey sand. As a result, the liquid limit of bottom-bagasse-lime-treated soil is approximate to the bagasse-ash-lime soil sample (about 105%).
- The linear shrinkage of samples including the two ashes is lowest among lime-soils treated with bottom ash or bagasse ash, 12.2% compared to 14% for bottom ash and to 13.6% for bagasse ash. However, the swelling ratio of two-ash-lime treated soil is higher than the bottom-ash-included sample (5.5% as against 2.6%) but slightly lower than bagasse-ash-lime-treated soil (6.4%).
- For compaction parameters, soil treated with 5% lime, 17.5% bottom ash and 7.5% bagasse ash has an approximate *MDD* value of 25%-bottom-ash-5%lime soil (1.25 $Mg/m^3$) but a much low *OMC* value of 24%, indicating the sandy or coarse property of the new ash-combined material.
- In consolidation behaviour, the two-ash-combined sample has either pre-consolidation pressure lower than or compression index higher than soils containing bottom ash or bagasse ash. This means that replacing 7.5% of bottom ash with bagasse ash slightly reduces the yield stress and makes the treated soil more compressible in a small margin.

- The same pattern is repeated in unconfined compressive strength (UCS) tests. The combined-ash-lime-treated soil has a lower *UCS* than samples with bottom or bagasse ash and approximate to *UCS* of lime-treated soil. However, in terms of bearing capacity, *CBR* of two-ash sample is higher than bagasse-ash-included one after 90 curing days, including 62 days for soaking in waters, even though the results of unsoaked *CBR* reverse this position. Furthermore, although 25%-bottom-ash-5%lime-treated soil is the sample with the highest *CBR* at any conditions, but the bottom-bagasse-included specimen has the largest failure penetration, indicating the ductile behaviour of the new ash-combined soil material.
- In triaxial test to determine shear strength properties, the new ash-combined material had the same internal friction angle and cohesion of soil treated with 5% lime and 25% bottom ash, indicating 17.5% bottom ash in two-ash-lime treated soil was sufficient to turn the soil into a coarse material.
- In small-strain shear modulus ($G_{max}$), the newly suggested treated soil has the highest $G_{max}$ among other ash-treated samples if the soil is statically compacted, at 675 MPa for the fully saturated triaxial sample with the height of 100 mm, and at about 600 MPa for the wet-compacted waxed specimen with the height of 40 mm. However, in the case of dynamically compacted samples in CBR tests, the new ash-combined sample has $G_{max}$ identical to the shear modulus of bagasse-ash-lime-treated soils, even after saturation. Their values of $G_{max}$ are lower than CBR sample with 25% bottom ash, which is associated with its high *CBR* values, indicating bottom ash is preferable for material of road subgrade material rather than bagasse ash.
- The $G_{max}$ evolution of studied material can be classified into five stages: (1) a gradual increase in the first day after compaction, (2) a significant growth from the second day or later to the day of 28, (3) a plateau from the day 28 to the day 56, (4) a remarkable collapse after 56 days, lasting up to 1 year, (5) a final plateau after about 1 year of curing.
- It can be noted that the above combination uses the bagasse ash with the size of 425µ rather than 150 µm or 75 µm, since the inclusion of small ash reduces the $G_{max}$ of bottom-bagasse-ash-combined material. The addition of finer bagasse ash in the material also depletes the duration of $G_{max}$ peak after about 28 days (Stage 3), and then quickly reduces the $G_{max}$ in Stage 4 after 28 days.
- Matric suction of the bottom-bagasse-ash-lime treated soil is equal to only-bottom-ash-included sample (about 50 kPa) after 7 days, and to the only-bagasse-ash-included

specimen (roughly 180 kPa) after 28 days. However, the matric suction of the newly suggested material keeps going after 56 days for curing to become the highest pressure of over 300 kPa after 90 days of curing.

- SEM analysis on the new ash-combined soil material clarifies that Stage 1 is associated with the formation of calcium silicate hydrate (CSH) and calcium aluminium silicate hydrate (CASH), Stage 2 with CSH and magnesium silicate hydrate (MSH), Stage 3 with a small amount of ettringite, CSH and CASH, and Stage 4 with a large amount of ettringite, CSH and CASH. The saturated or wet condition plays an important role in creating a reticular network of ettringite and primary CSH in treated soils, which densifies the interfacial transition zone between ash particles and reduces the $G_{max}$ degradation in Stage 4. As a result, the bottom-bagasse-ash-lime treated soil compacted at the wet side of optimum moisture content has a decreasing rate of $G_{max}$ in Stage 4 lower than other drier samples.

# CHAPTER 8

# Numerical Analysis of a Road Embankment on Soft Soils Treated with Hydrated Lime, Bottom Ash and Bagasse Ash

## 8.1 Five treated-soil models

In this study, the reinforcement method is applied to a case study of a road embankment on soft soil in Ballina Bypass, part of Pacific Highway upgrade in New South Wales, Australia. Following this approach, hydrated lime, bottom ash and bagasse ash are used to stabilise the soft soil under the embankment. The stabilisation may be applied to the topsoil layer under a working platform, and columns of treated soil going through the soil profile. This soil stabilisation is in design to withstand the loading from the embankment or transfer this pressure to deeper dense soil layers underneath the embankment. Hence, the settlement of soft ground under embankment can be minimised. Furthermore, in this numerical study, PVDs were not activated in PLAXIS, but the permeability of soil profile was altered as long as the equivalent seepage flows are allowed as if PVDs were used. By using this mimicry, the soil treatment through various soil layers (e.g., installation of soil columns) is not affected by installed PVDs while the permeability is equivalent

to properly comparing treated model with untreated one. In comparison, the soil is treated with studied binders in the assessment of settlement and lateral movement. The stabilisation of soft soil under the road embankment in Ballina is modelled by PLAXIS software. In this study, cross section 3 was utilised for modelling because of its relatively symmetrical soil profile, enabling using only a half of embankment to model (Rezania et al., 2018). This is different from the study mentioned by Gong and Chok (2018) because they modelled full size of embankment at cross section 2 with asymmetrical layers under estuarine silty clay.

Regarding materials and methods for modelling analysis, five models (cases) are proposed to be applied on the Ballina embankment to reduce its settlement with time. Each case is corresponding to changes of adding soil treatment on alluvium layer or installing soil columns or both (see Figure 8.1). In each model, materials of treatment are altered for studied treated soils, including the combination of lime-soil, lime-bottom-ash-soil, lime-bagasse-ash-soil, and lime-bottom-bagasse-ash-soil samples. Finally, operational load with pavement installation on earth fill is applied on the model to define the bearing capacity of treated ground under road embankment. The ash fill can also be considered to replace the earth fill so that the settlement and vertical displacement of ground can be reduced further, which is mentioned in recommendations for future research. Model and material selection is based on the magnitude of displacement and settlement elimination.

To minimise the deformation of embankment both in vertical and horizontal directions, the soil reinforcement can be applied. The reinforcement may include soil chemical treatments or mechanical improvements to enhance the ground properties, such as reducing compressibility and increasing bearing capacity. From-top-to-bottom direction, the method of soil settlement reduction without a long-waiting period can be listed as follows:

- Embankment: replace earth fill and sand fill by lightweight materials. In this study, bottom ash and bagasse ash can be combined to form a fill material for embankment. However, in the scope of study, researching on bottom-bagasse-ash fill is saved for future applicable approach.
- Working platform: Reinforcing earth fill platform by installing geosynthetic-reinforced grids or mixing soil with binders, such as hydrated lime, bottom ash and bagasse ash. In this study, the earth-fill working platform was not reinforced to keep the same loading applied on ground under embankment. The comparison, therefore, is eligible between models with untreated and treated soil.

- Soil profile: The soil replacement and treatment can go from the top layer (alluvium) to the lower soil stratum (transition layer) in order to enhance the bearing capacity of soil. In the case of replacement, a massive excavation can be executed to remove weak soil layers and replace them by coarse and dense backfill soils, such as fine sand. In another case for soil treatment, soil surface layers can be excavated to mix with binders, such as hydrated lime, bottom ash and bagasse ash, to enhance their strength withstanding pressure from the embankment right above. Going deeper, the treatment can be expanded with the depth in the form of soil columns, which are distributed in a matrix under the embankment. Both surface or subgrade treatment and column installation can be combined to ultimately eliminate embankment settlement. By following this approach, this study suggests five models, equivalent to 3 design modes, namely single, combining and mixing mode, which is illustrated in Figure 8.1.

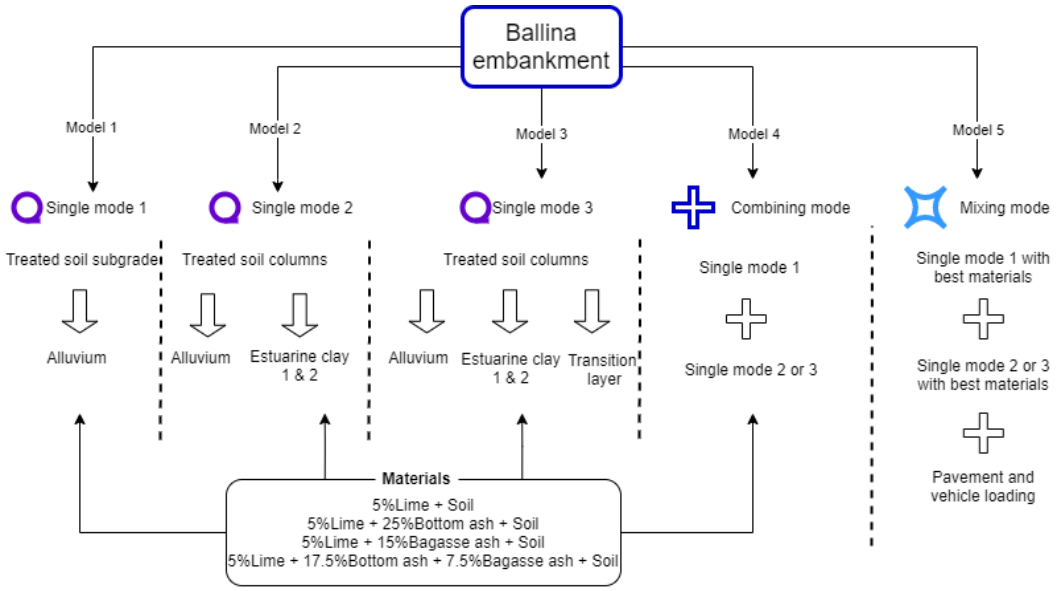


*Figure 8.1 Diagram of the proposed models for numerical simulations*

Given in Figure 8.1 is the developing process of model design from Model 1 to 5 in the increasing order of complexity. While Model 1 to 3 are relevant to the single mode, in which only one location of treatment is applied, such as a treated soil layer or columns, in Model 4, there is a combination of subgrade and column construction (refer to Figure 8.1). From Model 1 to 4, four treated-soil materials are assigned in each model to compare the material effects on results of ground behaviour. Particularly, while Model 1 regards the use of treated soil subgrade for the alluvium layer, single Model 2 and Model 3 indicate employing columns reaching to estuarine clay 2 and transition layer, respectively (see Figure 8.1). In Model 4, both treated soil surface and

columns are used with the same material located at these treated soil locations. After investigating four models, the best materials for each single mode in their combining mode will be selected to mix in the mixing mode for Model 5. The criteria of selection are based on the effectiveness of materials in reducing settlement and horizontal displacement in single modes. In Model 5, loads from pavement installation and working operation of vehicles are applied to test the long-term performance of embankment with the ultimate solution of treated soil.

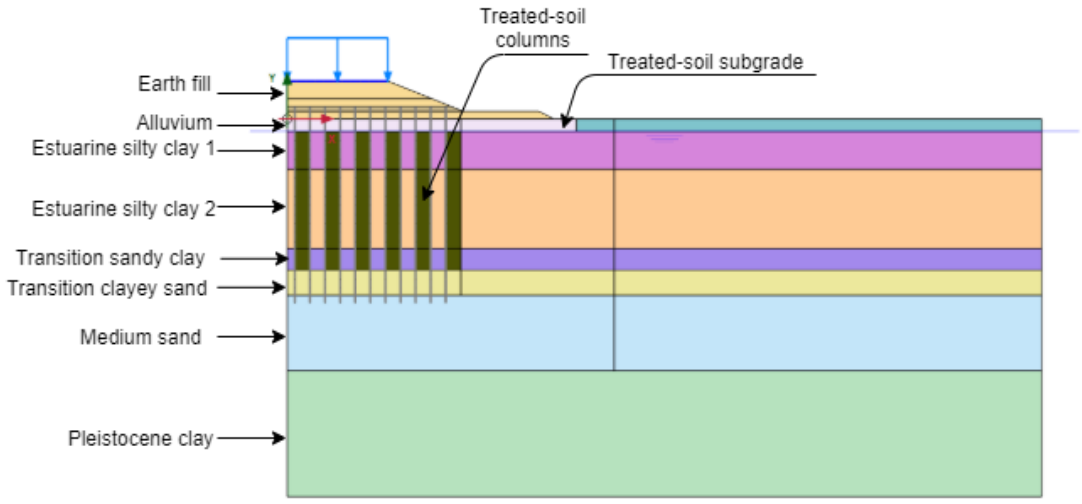


*Figure 8.2 PLAXIS models for treated soil columns and subgrade.*

In the above-mentioned models, the treated soil subgrade replaces the alluvium with the thickness of 1 m while the column installation includes six columns in the area under the embankment, as shown in Figure 8.2. The cross-section of treated soil surface layer is extended to 23 m from the embankment centre, with an offset of 2 m from the toe of the working platform. The diameter of column is 1.2 m with the centre-to-centre distance between columns of 2.4 m, leaving a gap of 1.2 m between the treated soil columns. The column length varies from Model 2 to 4. While both Model 2 and 3 has column tops starting right beneath the working platform, Model 2 has column foot stopping at the boundary between estuarine silty clay 2 and transition sandy clay, and Model 3 has columns lengthen to the middle of transition layer as indicated in Figure 8.2. In Models 4 and 5, with the presence of top treated soil layer, column heads are below the added subgrade layer, while column bottoms are selected from Model 2 or 3, depending on its modelling results. Furthermore, the meshing area below the embankment is generated with a coarseness factor of 0.2 to refine the finite elements of subgrade, columns and surrounding soils, improving the modelling accuracy. For stage construction, the two first stages will be added to the process before filling embankment materials, namely column installation and subgrade treatment. In Models 4 and 5, both stages are activated, while one of them is allowed in phase explorer for

Models 1 to 3. The time interval for constructing treated soil columns is 7 days and 3 days for subgrade. After that, there are 28 days waiting for curing incubation of treated soils, then the embankment construction stages are conducted as normal. Since the untreated soil model works well with the prediction of vertical and horizontal movements, only numerical results of these displacements are shown and compared for treated soil models.

## 8.2 Validation of numerical model of soil layers under the Ballina embankment

It is necessary to build a reliable soil model under the studied embankment with behaviour simulating the field conditions. Hence, understanding the difference of soil characteristics in every ground profile is important to have a proper investigation of their behaviour under loading of earth fill. In this study, class C suggested by Gong and Chok (2018) was implemented in PLAXIS models to reflect the soil behaviour under embankment through monitoring settlement, lateral displacement and excess pore water pressure over the surveyed period, up to 1,200 days. The model is expected to convey reliable results of ground movement as to what natural ground behaved under the construction of earthy embankment above. In addition, the values of permeability suggested by Rezania et al. (2018) are utilised in this chapter to mimic the drain effects on treated ground behaviour under Ballina embankment. Therefore, unlike Gong and Chok (2018), the author does not activate the drains in the drainage model. Instead, the effect of jute drain on soil drainage is displayed by modifying the permeability of entire soil layers as if the drains were installed in these layers. The equivalent modification by removing the physical presence of drains but keeping their effects aims to avoid any possible interaction between vertical drains and installed soil columns in the PLAXIS model, which may cause inaccuracy of settlement and displacement results in this study. The representative soil model without drain existence has already been adopted in the study conducted by Rezania et al. (2018), in which the equivalent vertical and horizontal permeabilities were calculated and employed to produce the drainage of soil without drains equivalent to that with drains. In addition, it might not be obvious in dividing estuarine silty clay into two layers for modelling, but it is clear to see a gradual difference of soil in the transition layer with an increase of sand content with depth. Hence, there is a necessity to make this layer separate into parts. However, to make it simple, the author will divide the transition layer into two distinct layers, sandy clay above and clayey sand underneath (see Figure 8.2). The depth of sandy clay layer is down to 12 m deep, based on the profile of material parameters provided by Pineda et al. (2016). The details of soil profile and selection of input parameters for modelling the studied ground is discussed in the next section.

### 8.2.1 Selection of input parameters for modelling soil profile under studied embankment

Based on the half divisions in soil layers of estuarine clay and transition layer, it results in ten soil materials that need to be assigned in the model. Considering the symmetrical distribution of soil layers in cross-section 3 (refer to Figure 8.2), the depths of layers are fixed in approximate values. In particular, estuarine clay has an upper layer from 1 m to 4 m deep, while the transition layer comprises sandy clay and clayey sand, from 10.3 m to 12 m, and from 12 m to 14 m in depth, respectively, as summarised in Table 8.1.

Regarding the soil model for subsoil layers, there are two main groups from studied materials, including sand and clay. For coarse materials like sandy soil, Mohr-Coulomb (MC) model was utilised for earth fill, sand fill, and sand layers, including medium and transition clayey sand (see Table 8.1). The MC model was also applied to the bottom clay layer (Pleistocene clay), where the soil becomes dense and has a low initial void ratio. This bottom clay is assigned as undrained, which is also set for clay-related layers, consisting of alluvium, estuarine silty clay and transition layer. Other materials with most components as coarse grains or sand are modelled as drained in PLAXIS, namely earth fill, sand fill and medium sand, as presented in Table 8.1.

Of the soil layers, the profile in the depth from 1 m to 10.3 m, accounting for estuarine silty clay, is estimated to cause most ground settlement under embankment; thus, a proper soil model for this layer is needed for modelling validation. In the study conducted by Rezania et al. (2018), a number of soil models was applied to the estuarine layer, ranging from MC to modified cam clay (MCC), which was also utilised for the alluvium top layer. Rezania et al. (2018) also developed a new model titled EVP-SANICLAY to improve PLAXIS prediction of vertical settlement with time, compared to other conventional models. However, the new model was not successful in forecasting lateral deformation and excess pore water pressure variations. To better predict the behaviour of Ballina embankment, Gong and Chok (2018) used Soft Soil Creep (SSC) model for estuarine silty clay in two clayey layers, resulting in a good prediction in settlement, lateral displacement and pore pressures. However, the model was employed only for the asymmetric PLAXIS model of Ballina embankment (cross section 2) and with the presence of PVDs system. No half-analysed model from a symmetric soil profile under the embankment (cross section 3) has been established with the SSC model and without considering the PVDs installation in the soil stratum. Therefore, this study uses SSC model for two estuarine clays without activation of drains. For input parameters in the model, the author investigates lab test data for the clays collected from the research conducted by Kelly et al. (2018), as shown in Figure 8.3.

As can be seen in Figure 8.3, the compression ($C_c$), the recompression ($C_s$) and the creep ($C_\alpha$) indices vary with depth. Both $C_c$ and $C_\alpha$-values depend on the stress level and gain a peak after the pre-consolidation pressure is obtained. Lower and upper bounds for $C_c$ and $C_\alpha$ are depicted in Figure 8.3. In comparison between these two indices, peak values of $C_c$ are much scattering than that $C_\alpha$ in the depth from 4 m to 10 m, so $C_c$ at this depth is not selected at its highest value. Instead, the interpreted value of $C_c$ in the lower layer of estuarine clay is calculated based on the increase of $C_c$ from upper to lower clay profile at pressure larger than yield stress 5 times, which is about 0.2. Since interpreted $C_c$-value from 1 m to 4 m deep is 1.3, based on peak values and consideration of disturbance effects on laboratory samples, $C_c$ index at the depth from 4 m to 10 m is 1.5. Finally, the compression index at 10-12 m deep is 0.9, reliant on the lower bound at the depth of 10 m because increasing sand content in this layer makes clay less compressible.

According to results established by Gong and Chok (2018), secondary consolidation or creep contributes a significant proportion to the overall settlement of embankment. Therefore, in this study, the author selects peak values of $C_\alpha$ for modelling. The creep index at the transition layer is 0.028, as the average of $C_\alpha$ values at the depth of 10 m. Similarly, the recompression index at the layer from 1 m to 4 m is 0.04, an average of $C_s$ at 1 m and 3 m deep. The $C_s$ values at deeper soil profile are selected at the lowest levels because of disturbance effects, increasing this value in laboratory consolidation tests.

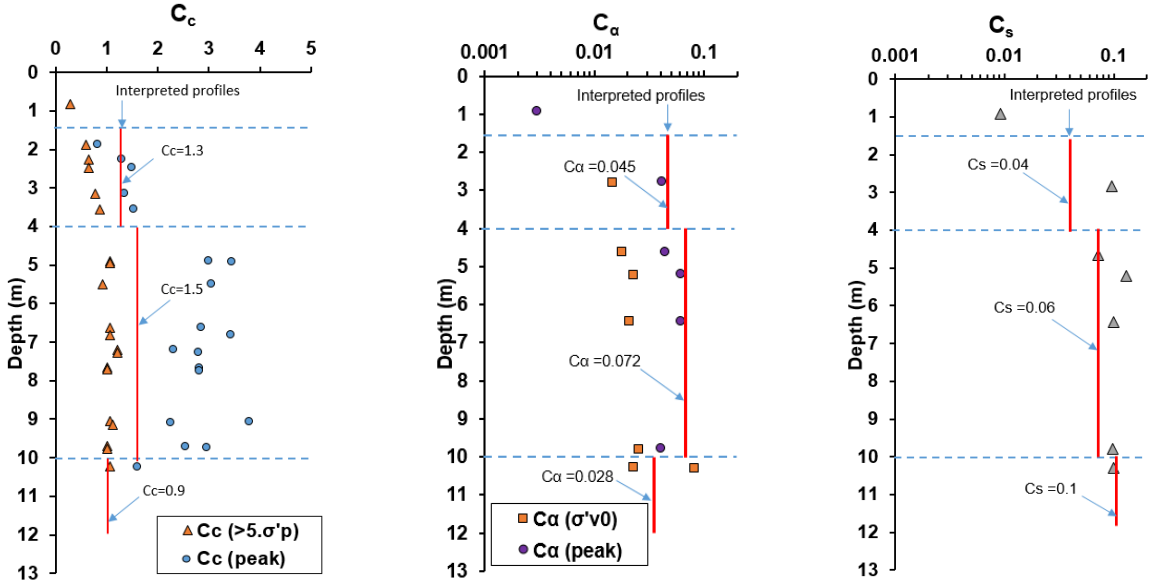


*Figure 8.3 Profiles of compression ($C_c$), recompression ($C_s$) and creep ($C_\alpha$) indices with selected values in the selected case study (after Pineda et al. (2016))*

Table 8.1 summarises the input parameters for the studied soil profile under Ballina embankment. In this table, most values are collected from previous studies on this embankment,

such as unit weight, friction angle, Young's modulus ($E$) from the study by Gong and Chok (2018) or void ratio, cohesion obtained by Rezania et al. (2018). Particularly, the initial void ratio was modified from values suggested by Rezania et al. (2018) in the decreasing order from upper estuarine clay with depth, reflecting the intact soil state becomes denser in deeper layers. The top layer, alluvium soil, is also assigned with a modified Cam clay model from their study with relevant main parameters, including $\kappa$, $\lambda$ and $M$. The material properties of the embankment and the soil profile are summarised in Table 8.1.

*Table 8.1 Material properties of embankment and soil profile*

| Parameters | Earth fill | Sand fill | Alluvium soil | Estuarine silty clay (upper) | Estuarine silty clay (lower) | Transition sandy clay | Transition clayey sand | Medium sand | Pleistocene clay |
|---|---|---|---|---|---|---|---|---|---|
| Model | Mohr-Coulomb | Mohr-Coulomb | Modified Cam-clay | Soft soil creep | Soft soil creep | Soft soil creep | Mohr-Coulomb | Mohr-Coulomb | Mohr-Coulomb |
| Drainage type | Drained | Drained | Undrained | Undrained | Undrained | Undrained | Undrained | Drained | Undrained |
| Depth (m) | | | 0-1.0 | 1.0 – 4.0 | 4.0-10.3 | 10.3-12 | 12-14.0 | 14.0-20.0 | 20-30 |
| Unsaturated unit weight, $\gamma$ (kN/m$^3$) | 21 | 21 | 16 | 12.5 | 12.5 | 16 | 16 | 16 | 16 |
| Saturated unit weight, $\gamma_{sat}$ (kN/m$^3$) | 25 | 25 | 18 | 14.5 | 14.5 | 18 | 18 | 18 | 18 |
| Initial void ratio, $e_0$ | 1 | 0.5 | 1 | 3 | 2.85 | 1.65 | 1 | 1 | 1 |
| Yong Modulus, $E$ (MPa) | 20 | 10 | - | - | - | - | 10 | 20 | 15 |
| Poisson's ratio, | 0.3 | 0.3 | 0.3 | 0.3 | 0.3 | 0.3 | 0.3 | 0.3 | 0.3 |
| Cohesion, $c$' (kPa) | 4 | 1 | - | 2 | 2 | 2 | 2 | 1 | 4 |
| Friction angle, $\Phi$' ($^0$) | 28 | 30 | - | 24 | 24 | 26 | 26 | 34 | 28 |
| Dilation angle ($^0$) | 0 | 0 | - | 0 | 0 | 0 | 0 | 0 | 0 |
| Lambda ($\lambda$) | - | - | 0.13 | - | - | - | - | - | - |
| Kappa ($\kappa$) | - | - | 0.007 | - | - | - | - | - | - |
| $M$ | - | - | 1.033 | - | - | - | | - | - |
| Compression index, $Cc$ | - | - | - | 1.3 | 1.5 | 0.9 | - | - | - |
| Swelling index, $C_s$ | - | - | - | 0.04 | 0.06 | 0.1 | - | - | - |
| Creep index, $C_\alpha$ | - | - | - | 0.05 | 0.072 | 0.028 | - | - | - |
| OCR | - | - | - | 2.3 | 1.65 | 1 | - | | |
| $K_0$ | - | - | 0.5 | 0.5 | 0.5 | 0.5 | - | - | - |

Permeability parameters define the settlement and displacement of ground under embankment, closely related to clayey layers, including alluvium, estuarine silty clay and transition sandy clay. The parameters are critical when the Soft Soil Creep model is used for estuarine silty and transitional sandy clay because of a close association between creep index and permeability (Gong & Chok, 2018). Selecting proper permeability values is critical and challenging to predict settlement. In this study, the Van Genuchten's model with soil type was applied to the corresponding soil profile, which is demonstrated in Table 8.2. To model the permeable behaviour of soil without drains but with the same drainage effect of soil with drains, the equivalent permeability was mobilised in Table 8.2, including vertical and horizontal values. The equivalent values were collected from the study of Rezania et al. (2018), based on modification for plane strain simulations, which Yildiz et al. (2009) suggested. Furthermore,

Rezania et al. (2018) only applied the modification for soil clusters surrounding drains while soil part from the embankment toe zone or over still has permeability from tests. However, unlike Rezania et al. (2018), this study applied the permeability adjustment for the whole soil layer since the smear zone may expand over the drain installation zone, particularly when a large deformation occurs. Simply, the author will assign entire soil layers with new permeability since the problem of determining the exact impact zone of drains on soil permeability when the soil settles down becomes too complicated.

*Table 8.2 Permeability parameters for soil profile*

| Parameters | Earth fill | Sand fill | Alluvium soil | Estuarine silty clay (upper) | Estuarine silty clay (lower) | Transition sandy clay | Transition clayey sand | Medium sand | Pleistocene clay |
|---|---|---|---|---|---|---|---|---|---|
| Data set | USDA | USDA | USDA | USDA | USDA | USDA | USDA | USDA | USDA |
| Model | Van Genuchten | Van Genuchten | Van Genuchten | Van Genuchten | Van Genuchten | Van Genuchten | Van Genuchten | Van Genuchten | Van Genuchten |
| Soil type | Loamy sand | Sand | Clay | Silty clay | Silty clay | Sandy clay | Sandy clay loam | Sand | Clay |
| $k_x$ (m/day) | 0.1 | 1 | $0.116\times10^{-3}$ | $8.78\times10^{-6}$ | $8.78\times10^{-6}$ | $8.61\times10^{-4}$ | 0.05 | 1 | 0.005 |
| $k_y$ (m/day) | 0.1 | 1 | $16.30\times10^{-3}$ | $3.78\times10^{-3}$ | $3.78\times10^{-3}$ | $5.84\times10^{-2}$ | 0.05 | 1 | 0.005 |
| Change in permeability, $c_k$ | $1\times10^{15}$ | $1\times10^{15}$ | 0.1660 | 0.766 | 0.766 | 0.1660 | 0.05 | $1\times10^{15}$ | 1 |
| $K_0$ | - | - | 0.5 | 0.5 | 0.5 | 0.5 | - | - | - |

### 8.2.2 Stages of embankment construction on soft soil

Loading stages from filling embankment increase the overburden pressure on soft ground and impacts the settlement rate of clay layers. Therefore, the timing rate of filling and fill thickness must be considered properly to ensure a reasonable prediction of settlement can be attained. Table 8.3 shows the dates and activities of filling materials for embankment construction, based on the filling report for SP3 and SP4 in the study by Kelly et al. (2018). It is noticeable that the construction process lasted for about 2 months, which was intertwined with consolidation stages having durations varied from a few days to about 3 weeks (22 days). In the case study, this is long enough for drain installation on the sand fill layer, but in this study, the duration is literally for consolidation only. The filling stage of earth material lasted in many timing steps in the field. However, to simply put, there were only two main stages for this activity, 0.6-m-high earth fill is for the first stage in 2 days, followed by 3-day consolidation, and 1.4-m-high fill is for the second one extending for 8 days. After 60-day for fill works, the embankment was let to settle down and monitored its consolidation behaviour. For this, datum magnets were installed at 7 reduced levels (M0 to M6) to measure centre settlement, whereas two inclinometers located at toes of

embankment to obtain the lateral deformation from surface to the depth of 20 m in the layer of medium sand, indicated in Figure 8.2 and Table 8.1. At the centre line of embankment, three vibrating wire piezometers (VWPs) were installed at 1.5, 5.5 and 9.5 m in depth to monitor the changes in pore pressure. Contributing to total pore water pressure, groundwater was considered at 1m below the ground surface, based on MEX01 borehole (Kelly et al., 2018). Furthermore, due to the loading process and settlement, a part of alluvium and embankment fill is under the groundwater level. Therefore, the function of updated water pressure and updated mesh is activated in PLAXIS phase explorer for the final stage of long-term consolidation.

*Table 8.3. Stages of filling embankment (Kelly et al., 2018)*

| No. | Dates | Activities | Fill thickness (m) | Embankment height | Duration (days) | Accumulative duration (days) |
|---|---|---|---|---|---|---|
| 1 | 2/08/2013 - 8/8/2013 | Working platform construction | 0.6 | 0.6 | 6 | 6 |
| 2 | 8/08/2013 - 19/8/2013 | Consolidation | - | 0.6 | 11 | 17 |
| 3 | 19/8/2013 - 27/08/2013 | Sand fill construction | 0.4 | 1 | 8 | 25 |
| 4 | 27/08/2013 - 18/09/2013 | Consolidation | - | 1 | 22 | 47 |
| 5 | 18/09/2013 - 20/09/2013 | Earth fill construction | 0.6 | 1.6 | 2 | 49 |
| 6 | 20/09/2013 - 23/09/2013 | Consolidation | - | 1.6 | 3 | 52 |
| 7 | 23/09/2013 - 1/10/2013 | Earth fill construction | 1.4 | 3.0 | 8 | 60 |
| 8 | 1/10/2013 - 17/7/2016 | Consolidation | - | 3.0 | 1020 | 1080 |

### 8.2.3 Results and discussion

Figure 8.4 shows the settlement and lateral deformation of embankment over about 1,200 days. For settlement evolution, only results at $M_0$ and $M_1$ are compared, corresponding to movement at a point in embankment (RL+1.2) and another in soil just below ground surface (RL-1.0), respectively. Two investigated points are on the embankment centre. Meanwhile, there is only one lateral displacement on the right-hand side of embankment. The calculation is along the vertical line from the toe of embankment to the depth of 20 m (refer to Figure 8.4). As can be seen from this figure, numerical prediction is in good agreement with measured data. In detail, predicted settlement at the embankment centre $M_o$ has fitted well with monitoring data over 400 days. However, the final analysed settlement after 1,100 days is slightly smaller than the measured value, 1.40 m compared to 1.51 m. Meanwhile, the vertical movement of point below embankment $M_1$ reasonably agrees with monitoring data after 800 days, with approximately 1.27 m (see Figure 8.4). Horizontal deformation prediction reflects a good alignment with measured points, especially at the depth of 5 and 10 m. Compared to other previous studies (Gong & Chok, 2018; Rezania et al., 2018), this prediction result is a good accomplishment, since there was no calculated lateral deformation with accuracy at these levels mentioned in their papers. Therefore, the soil model in this study is in an acceptable validation in terms of deformation parameters.

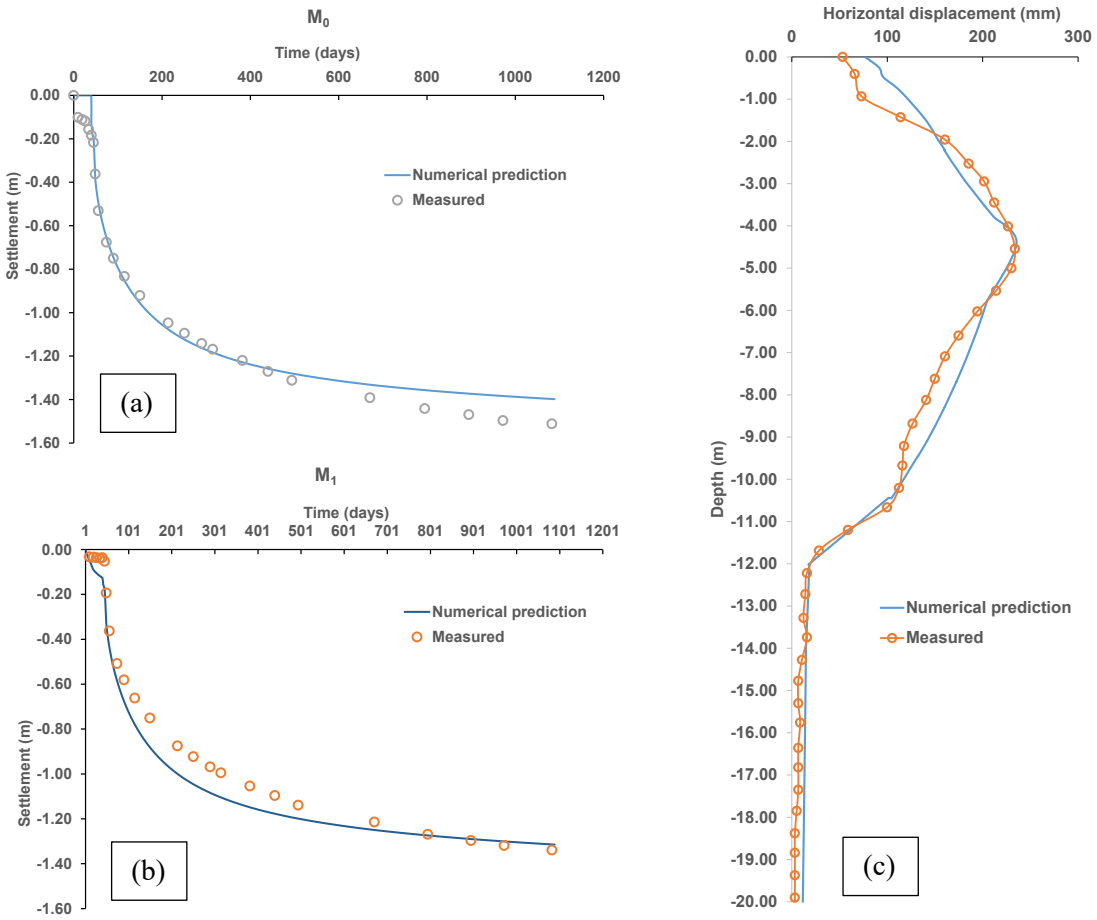


*Figure 8.4 Vertical settlement and horizontal displacement of embankment on soft soils: (a) settlement of $M_0$ point in embankment at the centre with time, (b) settlement of $M_1$ point under embankment at the centre with time, (c) lateral displacement of embankment toes with depth after 1200 days*

In pore pressure investigation, the pressure of pore water at three depths arrayed on the embankment centre was estimated under the embankment model. Figure 8.5 illustrates the change in total pore water pressure at three positions over the survey period of time. It is obvious that all the analysed curves are lower than monitored ones by a larger and larger gap with the depth. However, the predicted peaks of pore water pressure (PWP) quite match with measured values, particularly at 1.5 m and 5.5 m in the depth, accounting for 45 kPa and 93 kPa, respectively, as plotted in Figure 8.5. However, the peak value at the deepest position from modelling is much lower than the field pressure, 119 kPa as against 134 kPa. The difference between prediction and measurement of PWP is always challenging due to discrepancies between the two variables, and probably from the intrinsic limitation of suggested model (Rezania et al., 2018). In addition, the high-rate dissipation of pore pressure in numerical results compared with what was observed can be caused by over-valued equivalent permeability, which is actually lower in real soil and the drain

system. Hence, the model with modified permeability may not reflect the actual behaviour of soil layers in terms of pore pressure dissipation (Chai et al., 2001).

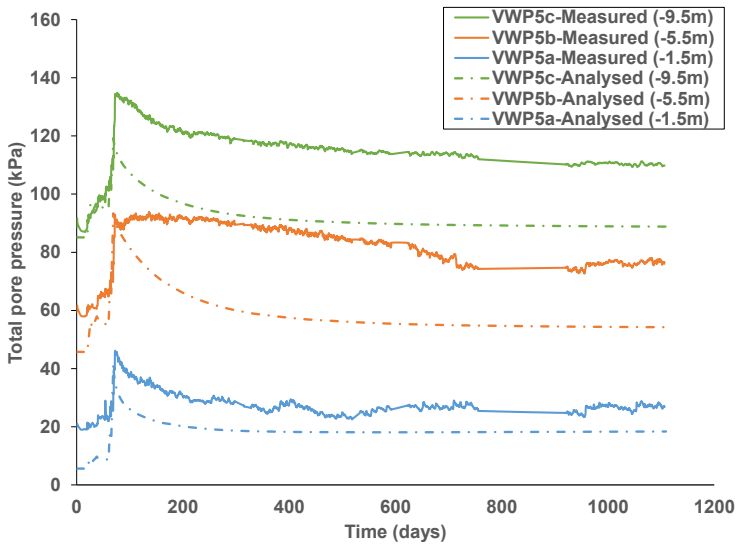


*Figure 8.5 Total pore water pressure prediction and measurements*

## 8.3 Implementation of five treated-soil models to the case of Ballina embankment

### 8.3.1 Input parameters of materials for suggested models

Based on research findings attained from previous chapters, the properties of assigned materials for the suggested models are tabulated in Table 8.4. It is clear that soil treated with binders becomes coarser and enhances compressive stiffness and shearing strength. Therefore, the Mohr-Coulomb (MC) model is chosen for all treated soils with undrained type A for treated surface and undrained type B for treated columns, as tabulated in Table 8.4. While undrained type A allows an input of cohesion and friction angle, undrained type B replaces these by undrained shear strength, which is evaluated from unconfined compressive strength modified with the effect of fully saturated condition. The cohesion and the friction angle, on the other hand, are measured from triaxial shearing test and derived from the intercept and the slope of the effective stress failure envelope as shown in Figure 8.6. The Young's modulus E of treated materials is measured from the average slope of the stress-strain curves as the results of the unconfined compressive tests. The permeability of treated soils was set at the value of 0.05 (m/day), which is equal to that of the clayey sand layer because of their similar characteristics (see Table 8.2). Regarding the unit weight, the lime-treated soil has the highest value among other soil materials, 1.33 $Mg/m^3$ compared to 1.23 $Mg/m^3$ for soils treated with lime and ash. However, the initial void ratio is assumed to be 1.0 for the studied soils due to the rough calculations of their specific gravity, density and water content after compaction.

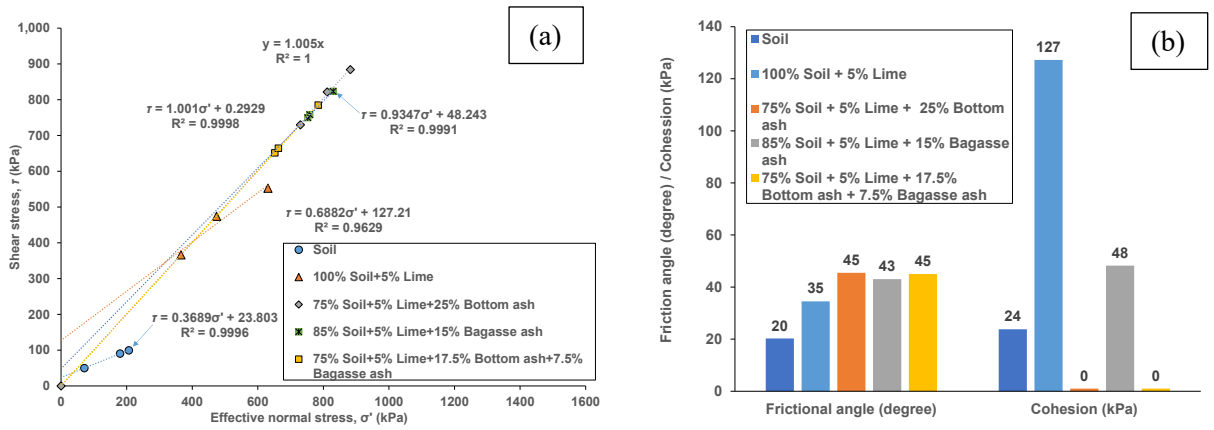


*Figure 8.6 (a) Effective stress failure envelope and (b) internal friction angle and cohesion of soil untreated and treated with binders*

*Table 8.4. Material properties of treated soils*

| Parameters | Surface treated soil layer (Model 1, 4, 5) | | | | Treated soil columns (Model 2, 3, 4, 5) | | | |
|---|---|---|---|---|---|---|---|---|
| | Lime-treated soil | Lime-bottom-ash treated soil | Lime-bagasse-ash treated soil | Lime-bottom-bagasse-ash treated soil | Lime-treated soil | Lime-bottom-ash-soil | Lime-bagasse-ash-soil | Lime-bottom-bagasse-ash soil |
| Model | MC | MC | MC | MC | MC | MC | MC | MC |
| Drainage type | Undrained A | Undrained A | Undrained A | Undrained A | Undrained B | Undrained B | Undrained B | Undrained B |
| Depth (m) | 0-1.0 | 0-1.0 | 0-1.0 | 0-1.0 | 0-10 (0-12) | 0-10 (0-12) | 0-10 (0-12) | 0-10 (0-12) |
| Unsaturated unit weight, γ (kN/m$^3$) | 13.3 | 12.3 | 12.3 | 12.3 | 13.3 | 12.3 | 12.3 | 12.3 |
| Saturated unit weight, γ (kN/m$^3$) | 15.3 | 14.3 | 14.3 | 14.3 | 15.3 | 14.3 | 14.3 | 14.3 |
| Initial void ratio, $e_o$ | 1 | 1 | 1 | 1 | 1 | 1 | 1 | 1 |
| Young's Modulus, E (MPa) | 80 | 125 | 180 | 105 | 80 | 125 | 180 | 105 |
| Poisson's ratio, | 0.3 | 0.3 | 0.3 | 0.3 | 0.3 | 0.3 | 0.3 | 0.3 |
| Cohesion, c' (kPa) | 127 | 1 | 48 | 10 | $s_u$ = 270 | $s_u$ = 450 | $s_u$ =400 | $s_u$ = 430 |
| Friction angle, ϕ′ (°) | 35 | 45 | 43 | 45 | 0 | 0 | 0 | 0 |
| Dilation angle (°) | 0 | 0 | 0 | 0 | 0 | 0 | 0 | 0 |
| Permeability, k (m/day) | - | - | - | - | - | - | - | - |
| Soil type | Coarse | Coarse | Coarse | Coarse | Coarse | Coarse | Coarse | Coarse |
| $k_x$ (m/day) | - | - | - | - | 0.05 | 0.05 | 0.05 | 0.05 |
| $k_y$ (m/day) | - | - | - | - | 0.05 | 0.05 | 0.05 | 0.05 |

## 8.4 Results and discussion on five models of embankment on treated ground

### 8.4.1 Model 1 - Top soil layer treated with hydrated lime, bottom ash and bagasse ash

Figure 8.7 compares the settlements and lateral deformation of ground, which is treated with lime, bottom ash and bagasse ash under the embankment. The vertical settlements were shown at two points on embankment centre, $M_0$ point at 1m above soil surface, and $M_1$ at the bottom of treated

soil subgrade. It can be seen that the inclusion of treating alluvium layer by binder helped to reduce the embankment settlement. With untreated alluvium soil, the final settlement after about 1,200 days is around 1.4 m, but with the introduction of 5% lime, the downward movement is only 1.09 m, a reduction of 22% in vertical settlement. Meanwhile, horizontal deformation also shifted from the peak of 236 mm down to only 162 mm at the depth of 4 m when the lime binder is mixed with surface soil, showing a 31% decrease in this movement. When 15% bagasse ash is combined with hydrated lime to treat the alluvium layer, no significant improvement is observed in settlement and lateral displacement (refer to Figure 8.7). However, including bottom ash or both bottom ash and bagasse ash in lime-treated soils increased the deformation at embankment toe. When both bottom ash and bagasse ash are combined with lime in soil surface, the lateral movement of embankment toe is largest, extending to 216 mm, which is 92 mm larger than the top displacement of lime-bottom-ash treated soil (124 mm). This detrimental effect may come from the low magnitude of elastic modulus and cohesion of three-binder treated soil. These marginal values are compensated by the highest friction angle of $45^0$, resulting in a limitation in vertical settlement. This positive effect of high friction angle on ground surface deformation was also proven in the study conducted by Gong and Chok (2018). At this notion, since the vertical deformation mainly relies on friction angle, the embankment settlement is identical in lime-bottom-ash treated soil with and without bagasse ash, which has the same internal friction angle of $45^0$. However, this moving-down improvement is only about 50% of what soil subgrade treated with lime with or without bagasse ash can obtain, 0.18 compared to about 0.35 for $M_0$, and 0.12 as against around 0.26 for $M_1$. In short, treating surface soil with lime and bagasse ash significantly reduces both settlement and lateral displacement, whereas the involvement of bottom ash reduced these enhancements and even increased the horizontal movement.

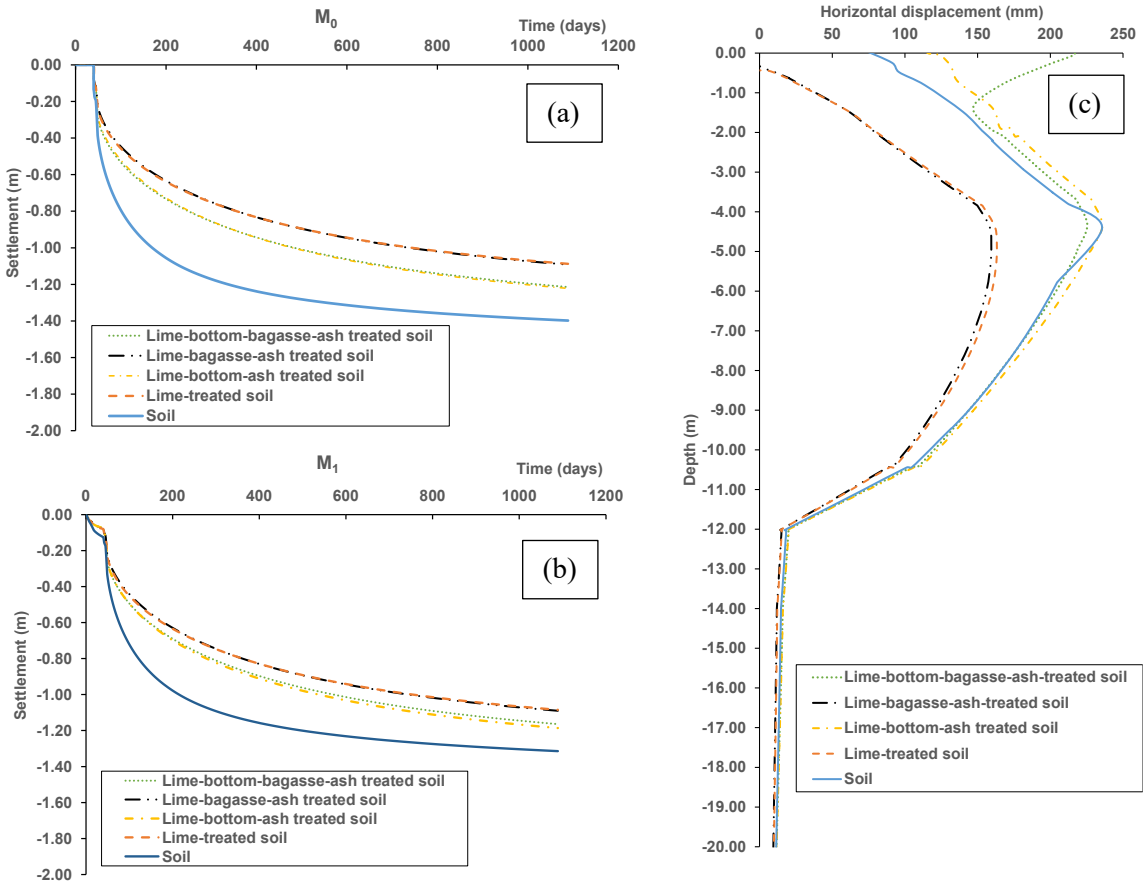


*Figure 8.7 Model 1-Vertical settlement and horizontal displacement of embankment on soft soils with lime-treated soil top layer: (a) settlement of M0 point in embankment at the centre with time, (b) settlement of M1 point under embankment at the centre with time, (c) lateral displacement of embankment toes with depth after 1200 days*

### 8.4.2 *Model 2 - Road embankment with short columns of soil treated with hydrated lime, bottom ash and bagasse ash*

In this model, treated soil columns are distributed in an array of 1.2 m from centre to centre under the working platform, as depicted in Figure 8.8. It can be noted that the alluvium layer was not treated with binder, and the columns stand on transition sandy clay profile, which means they go through only three topsoil layers (alluvium, estuarine silty clay 1 & 2). The phase time for column installation is 7 days, with curing time of 28 days for strength reinforcement. Mesh and water pressure are updated to control deformation parameters with the submergence of column tops, alluvium and embankment under ground-water level. The modelling outputs are illustrated in vertical settlements and horizontal displacement in comparison with different soil materials assigned for installed columns.

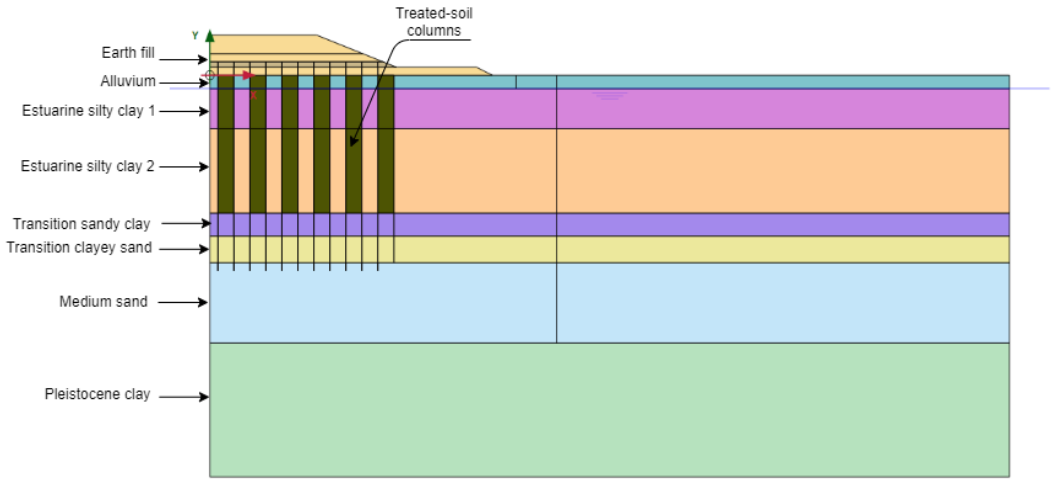


*Figure 8.8 PLAXIS model for soil columns distributed in alluvium and estuarine silty clay layer in Model 2*

Figure 8.9 describes the change of surveyed positions in vertical and horizontal directions, including $M_0$ (point in embankment on its centre), $M_1$ (the point at boundary of alluvium and estuarine silty clay), and vertical line from embankment toe along the side of outermost column. Obviously, the model with soil columns remarkably limited the settlement of embankment and soil layer beneath. In details, lime-treated soil columns reduce the soil settlement from 1.4 m to only 0.27 m. Including secondary binders, such as bottom ash and bagasse ash, further decreased the settlement, but in a marginal range, by only 0.01 m from 0.27 to 0.26. Particularly, all ash involvements gave the same effects on deformation, an identical settling-down amount of 0.26 m at $M_0$, 0.25 m at $M_1$ and 33 mm in horizontal displacement at the depth of 10 m (see Figure 8.9). Thanks to the installation of columns through soft clay layers, the settlement rate at $M_0$ and $M_1$ was improved significantly. The final stabilisation of vertical movement was obtained after around 200 days, which is mostly contributed by compression of transition sandy clay from 10 m to 12 m in depth. This layer is also the culprit of the noticeable peak in lateral displacement since the columns feet tends to directly transfer the pressure of embankment load above to the transition clay below, causing its remarkably compressible. Interestingly, the movement on the top of columns is towards the embankment to balance with displacement at their bottom. Compared to Model 1, Model 2 has greatly improved soil consolidation behaviour by disqualifying the column movement and embankment settlement. However, minor displacements are still observed in the transition sandy clay, which needs to be more investigated. This evaluation is mentioned in the next section for Model 3.

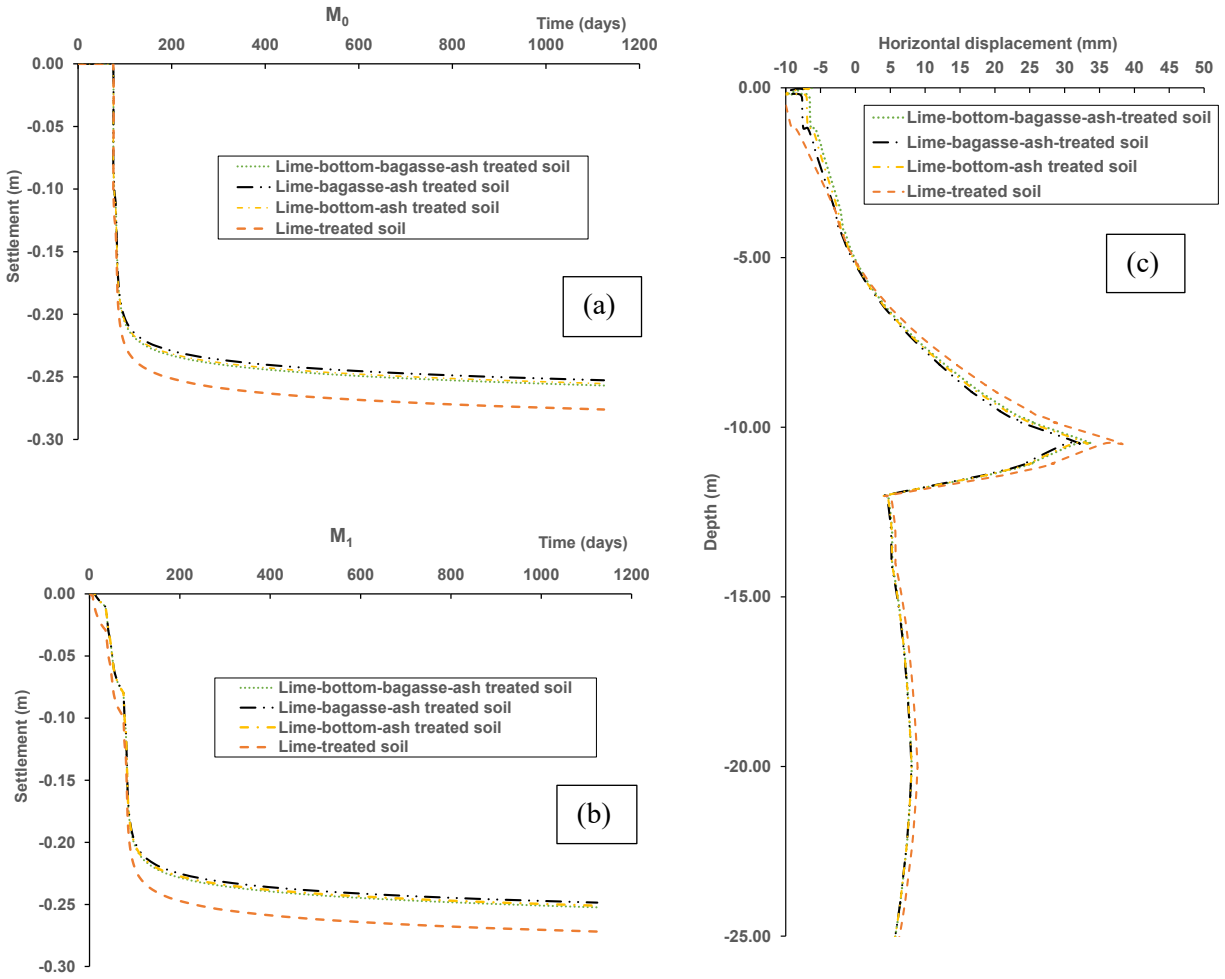


*Figure 8.9 Model 2-Vertical settlement and horizontal displacement of embankment on soft soils with lime-bottom-bagasse-ash treated soil top layer and ash fill: (a) settlement of $M_0$ point in embankment at the centre with time, (b) settlement of $M_1$ point under embankment at the centre with time, (c) lateral displacement of embankment toes with depth after 1200 days*

### 8.4.3 Model 3 - Road pavement with short columns of soil treated with hydrated lime, bottom ash and bagasse ash

In Model 3, the soil columns are anchored to transition sandy clay; thereby it extends the columns length by 2 m in this soil layer. Other configurations are similar to Model 2, including assigned treated soil materials, and outputs for comparison. Figure 8.10 demonstrates the improvement of longer-column installation in the studied soil stratum. It is clear that the settlement is almost disqualified with only around 0.06 m, which is observed for four materials, as shown in Figure 8.10. Furthermore, this value quickly stabilised after 60 days when embankment construction was complete, indicating the settlement counts for compressibility of columns rather than soil profile. As a result, the embankment settlement with bagasse-ash-lime columns is the least since the material has the highest value of Young's modulus (see Table 8.4). A similar pattern is seen for horizontal displacement. However, while the lateral movement at the depth of 10 m was

constrained significantly, there is an obvious slide of column tops for all studied materials, up to about 30 mm. This sliding indicates the rotation of columns to compensate with the small movement of column foot towards the embankment centre. The difference in moving range is also not significant among the variety of treated materials used. Although the movement amount is marginal (around 30 mm), a restriction in this top displacement is necessary to avoid any further column inclination caused by overburden loads on the embankment, especially when road operation commences. In comparison between Model 1 and Model 3, a combination of soil subgrade on the top of columns may help to reduce its lateral displacement. The combining effects are mentioned in Model 4, which is suggested in the next section.

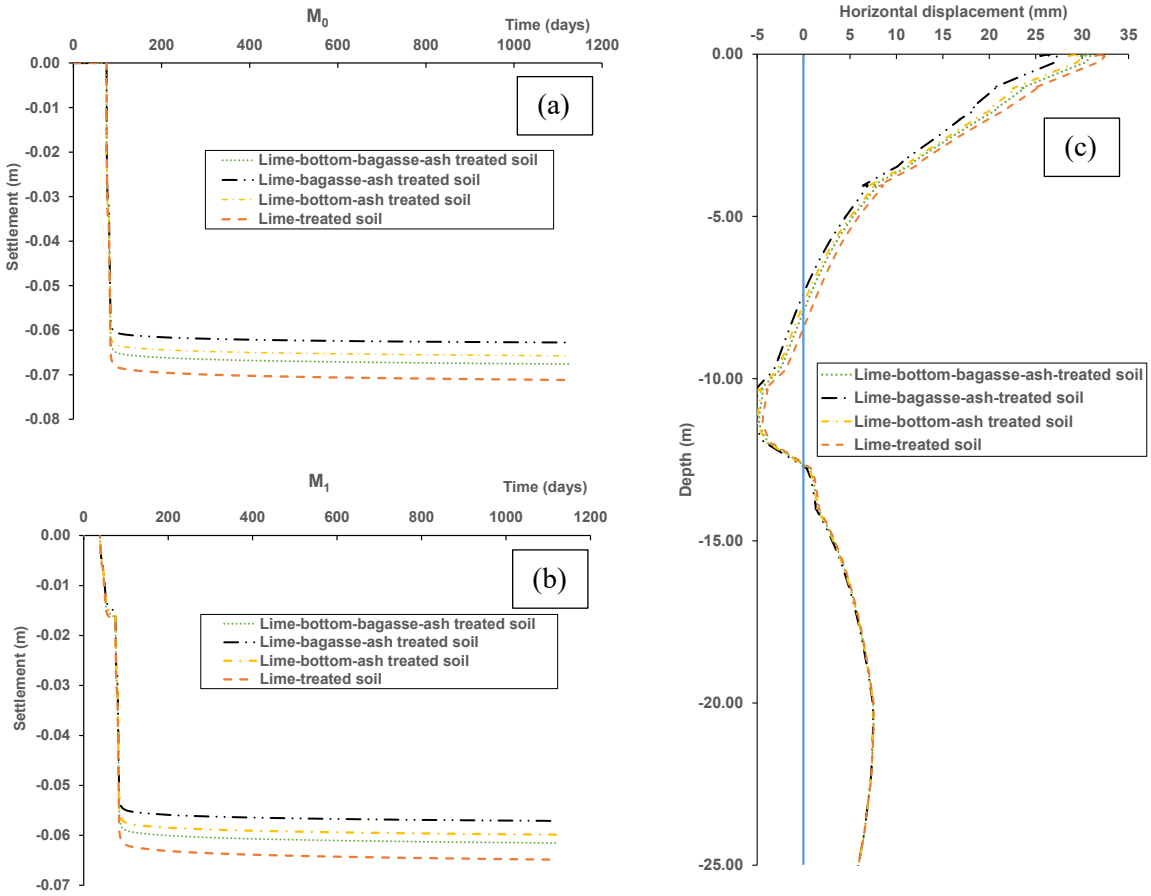


*Figure 8.10 Model 3-Vertical settlement and horizontal displacement of embankment on soft soils with lime-treated soil top layer: (a) settlement of $M_0$ point in the embankment at the centre with time, (b) settlement of $M_1$ point under embankment at the centre with time, (c) lateral displacement of embankment toes with depth after 1200 days*

### 8.4.4 Model 4 - Road embankment with lime-bottom-ash-treated soil top layer and columns

In this model, both treated soil columns and subgrade are adopted in the soil profile as a combination of Model 1 and 3 in a material-by-material manner. It means that if the soil-surface subgrade uses lime as an admixture for stabilisation, the column material will also have lime for

treatment. The same approach is applied to other materials with ash binders. This model, therefore, is called a combining mode, as the summation of single modes, which are mentioned in Model 1-3 (see Figure 8.7). Figure 8.11 depicts the significance of combination in vertical and horizontal displacements. It is apparent that lime-bottom-ash treated soil material caused the largest deformations, which are worse than those in Model 3. In particular, the subgrade settlement ($M_1$) is obviously larger than that at $M_0$, about 0.090 m compared with 0.075 m after 1,100 days. Furthermore, the lime-bottom-ash-soil subgrade also has a detrimental impact on withstanding the side movement, which is shown in Model 1 (refer to Figure 8.7). This is reason why combining column and layer treatment with lime and bottom ash exacerbated the horizontal displacement, from only 30 mm in Model 3 to about 55 mm in Model 4. On the other hand, lime-bagasse-ash-treated soil seems to be the best material with the smallest vertical settlement and horizontal deformation, at 55 mm and 5 mm at the top, respectively. The 3-binder material (i.e., lime, bottom ash and bagasse ash) gains the second position of settlement reduction, followed by the lime-treated soil, but lime-bottom-bagasse-ash treated soil still has a deformation of about 20 mm horizontally. The reason can be associated with the excessive movement of the lime-bottom-bagasse-ash-soil subgrade layer outward embankment centre under the fill loads (see Figure 8.7). Due to the great dependence of horizontal displacement on what material is used to treat the surface soil layer, it is necessary to select the same subgrade treated soil with various column material types to compare. In this case, lime-bagasse-ash treated soil is chosen for the treatment of alluvium layer, while columns vary in different binders added. The combination of different materials in the combing mode forms a new version, named the mixing mode. In the next section, Model 5 deals with this new mode.

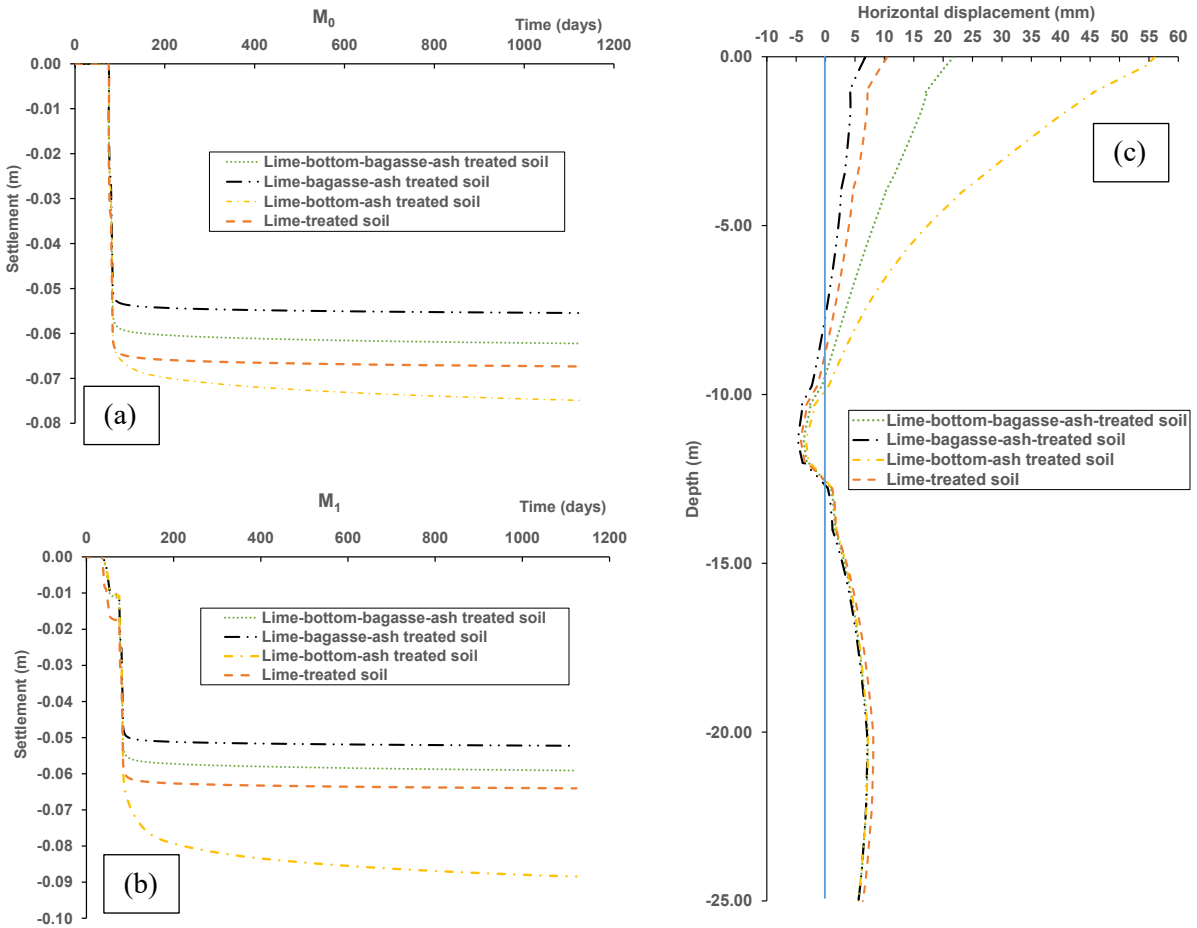


*Figure 8.11 Model 4-Vertical settlement and horizontal displacement of embankment on soft soils with top soil layer and columns treated with hydrated lime, bottom ash and bagasse ash: (a) settlement of $M_0$ point in embankment at the centre with time, (b) settlement of $M_1$ point under embankment at the centre with time, (c) lateral displacement of embankment toes with depth after 1200 days*

### 8.4.5 Model 5 - Road embankment with top layer of lime- bagasse-ash-treated soil and columns made of various treated materials under operation loads

Figure 8.12 depicts the form of settlement with time and deformation along the outermost column without loads from operative activities on the embankment (e.g., the pavement weight and the vehicle axels). As can be seen in Figure 8.12, the lime-bagasse-ash-treated soil subgrade on the topsoil layer could well-restrict the side movement, limited to 5 mm down to the depth of 15 m. Under the depth of 15m, the horizontal displacement of lime-treated soil is separated from others to be over 5 mm, whereas ash-binder-treated materials obtain the lower and identical displacement. Similarly, the lime-treated soil returns to the largest settlement, while ash inclusion to this soil tends to give the same settlement, with around 55 mm at $M_0$ and roughly 50 mm at $M_1$. The settlement stabilisation is also achieved quickly right after the embankment construction, reflecting the even stiffness of entire treatment materials in subgrade and columns. With the mixing mode, all studied materials can now result in the settlement and deformation in a reasonable range, within

70 mm vertically and 5 mm horizontally. Compared to the embankment height and width, these movements can be expressed in ratios of 2.3% (70/3000) and 0.02% (5/28000), which are quite marginal. However, the ratios can be larger when the pavement construction and vehicles are applied on the embankment surface, imposing extra pressure on the ground foundation. Table 8.5 illustrates the properties of pavement materials and applied loading lines from the weight of vehicles through their axels.

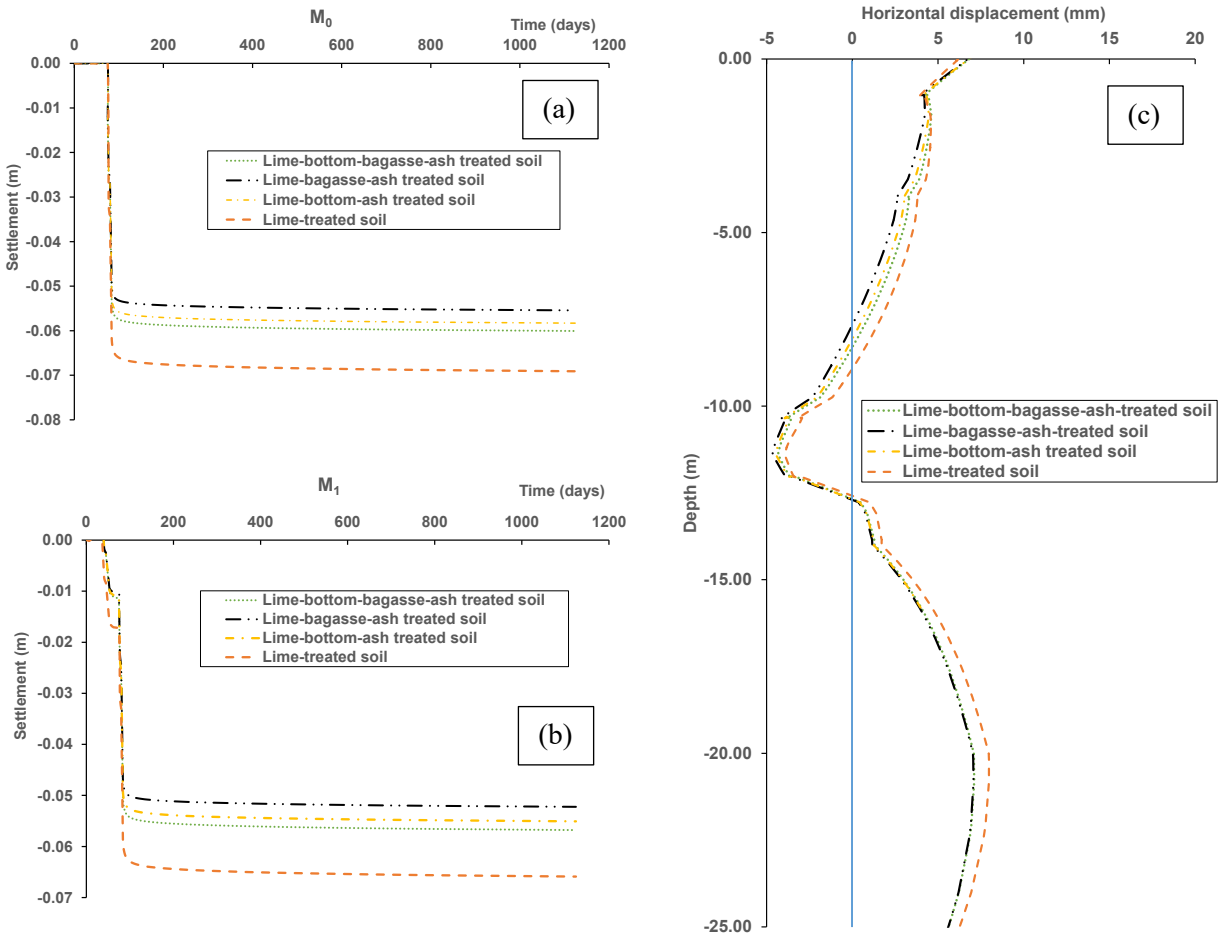


*Figure 8.12 Model 5-Vertical settlement and horizontal displacement of embankment on soft soils with bagasse-ash-lime-treated topsoil layer and soil columns treated with hydrated lime, bottom ash, and bagasse ash (no applied operation loads): (a) settlement of $M_0$ point in the embankment at the centre with time, (b) settlement of $M_1$ point under embankment at the centre with time, (c) lateral displacement of embankment toes with depth after 1200 days*

In the operational condition, there are two pressures possibly applying on the embankment, including pavement and vehicle weights running on the road. While the traffic load is considered to reach a pressure of 20 kN/m$^2$ applied on the embankment, a pavement with asphalt material laying on the embankment surface has a thickness of 350 mm (see Table 8.5). The stiffness of pavement is specified by two parameters, EA for in-plane axial stiffness and EI for flexural rigidity. In the isotropic model, two-direction axial parameters EA1 and EA2 equals to ensure the

same stiffness. The values are claimed in PLAXIS as plate material for pavement, while vehicle load is drawn as loading line positioning on the pavement. The construction and operation are activated in the final stage of phase explore, right after the embankment filling stage is finished.

*Table 8.5. Parameters for pavement and vehicle load on the embankment*

| Parameters | Unit | Value |
|---|---|---|
| Axial stiffness 1 (EA1) | kN/m | 1.12E+11 |
| Axial stiffness 2 (EA2) | kN/m | 1.12E+11 |
| Flexural rigidity (EI) | kN $m^2$/m | 1.12E+09 |
| Asphalt thickness, d | m | 0.35 |
| Poison's ratio (ν) | | 0.3 |
| Vehicle load | kN/$m^2$ | 20 |

Figure 8.13 illustrates the behaviour of ground under embankment with the installation of pavement and over-burden pressure from running load above. As can be seen in the plots of vertical settlements, there is not much difference in movement between treated materials. This differs from Figure 8.12, where ash involvement in soil treatment obviously reduces settlement. In soils included bottom ash, as shown in Figure 8.13, their settlement and displacement are on average between those observed in lime-treated soil and lime-bagasse-ash-soil mixture. The bearing capacity of soil columns treated with various binders is now approximate, and under greater pressures, all of them tend to shift to larger displacement, forming a peak at the depth of 4 m (see Figure 8.13). This is relevant to displacement in soil ground without columns, mentioned in Model 1 (refer to Figure 8.7), but in this mixing mode, the vertical movement is distributed quite even in soil stratum surrounding column system and in soil profile below the columns. From the comparison between materials, it can be included that bagasse ash alone combined with hydrated lime to stabilise soil is enough to build up a strength and bearing capacity to withstand applied pressure and weights from the embankment. Replacing bagasse ash or adding bottom ash in soil columns did not improve the settlement and lateral displacement behaviour of the ground under Ballina embankment. The replacement and addition may be considered in the case of durability since the strength of soil treated with bagasse ash and lime can reduce after a long period of time but quicker than ground treated with both bottom ash and bagasse ash. Therefore, Model 5 with columns treated with lime, bottom ash and bagasse ash can be preferable for the long-term operation of road embankment.

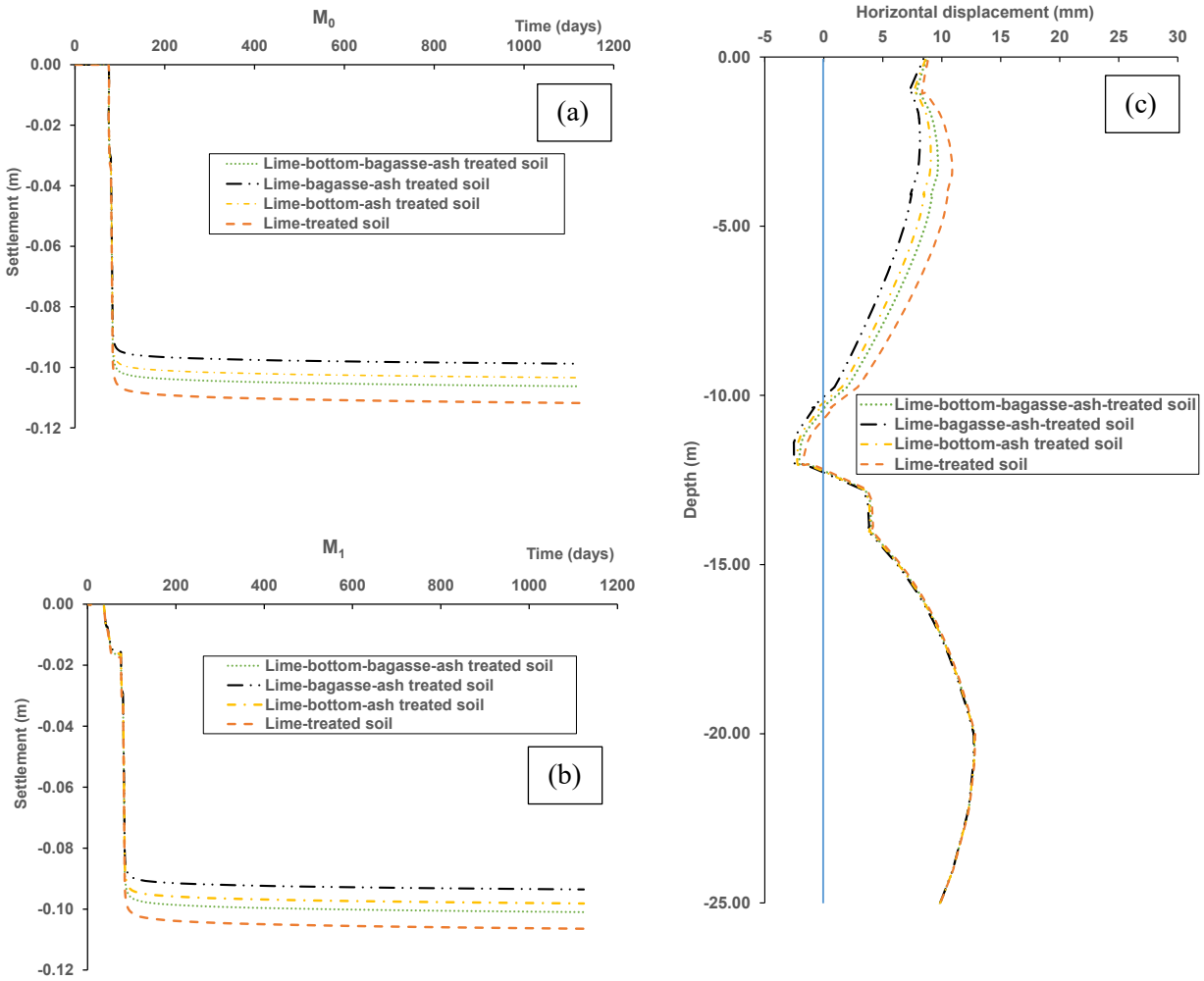


*Figure 8.13 Model 5-Vertical settlement and horizontal displacement of embankment on soft soils with bagasse-ash-lime-treated topsoil layer and soil columns treated with hydrated lime, bottom ash and bagasse ash under operational loading: (a) settlement of $M_0$ point in embankment at the centre with time, (b) settlement of $M_1$ point under the embankment at the centre with time, (c) lateral displacement of embankment toes with depth after 1200 days*

## 8.5 Summary

The numerical modelling simulation presented in this chapter attempted to predict the compressible behaviour of an embankment after ground treatment to constrain its movement. For this purpose, a case study associated with an embankment on soft soil in Ballina Bypass in NSW, Australia, was selected to investigate the effects of soil treatment with hydrated lime and ash binders on ground movements using PLAXIS software. Before this evaluation, soil models were examined to verify their suitability and match with the observed data. This is to ensure that any modification of model by adding or replacing materials can produce reasonable results in the field. Once the validation was satisfied, five models including three modes, namely single, combining and mixing version, were suggested to finally propose a design solution that soil treatment could

facilitate the reduction of the road embankment settlement. The following concluding remarks can be drawn from the findings of the numerical modelling:

- The soft soil creep (SSC) model in estuarine silty clay, divided into two distinct layers, produced a reasonable prediction of vertical settlement and horizontal displacement of ground under the embankment. The transition layer was also divided into separate layers, including transition clayey sand and transition sandy clay incorporating the SSC model. In this simulation, the permeability of entire relevant clay layers was modified to represent dissipation of the clay with drains, which was not activated in this study. As a result, the predicted behaviour of pore water pressure did not fit well with monitored data, particularly the dissipation of pore pressure over the consolidation time. Hence, the settlement and displacement data were considered to compare with the results of models simulating the treated soils.
- Model 1 with surface subgrade of soil treated with hydrated lime or/and bagasse ash resulted in a reasonable decrease of settlement and lateral movement. However, the inclusion of bottom ash in the subgrade increased the horizontal displacement, which was larger than untreated soil deformation. The detrimental effect of bottom ash on this displacement can be attributed to the fact that the ash involvement in soil mixture could reduce the elastic Young's modulus and the cohesion to the level where the treated surface layer could not bear with shear stress; thus, the subgrade might slide.
- Model 2 introduced the presence of soil columns treated with studied binders, including hydrated lime, bottom ash and bagasse ash. The existence of treated soil columns in the topsoil layer and in 2 layers of estuarine clay helped significantly decrease the settlement and lateral deformation.
- Model 3 dealt with modified columns in soil by extending their length deeper to the layer of transition clayey sand. Since the columns in Model 3 stepped on the stiffer layer than clayey soil, the settlement was reduced remarkably to only about 60 mm, which obtained a quick stabilisation right after completion of embankment construction. Furthermore, no peak of lateral displacement was observed at 10 m in depth. However, there was a large displacement at the top of columns in all material investigated.
- Model 4 combined Model 1 and Model 3 with material-by-material selection between the surface subgrade and the treated soil columns, which were both used in Model 4. The results showed that using bagasse ash and lime in two positions produced the lowest settlement and lateral deformation. Bottom-ash-lime-treated soil material caused the worst effect with

the largest lateral movement up to 55 mm at the top of column and the largest settlement after 1,200 days.

- Model 5 considered using bagasse ash and lime for the topsoil layer, while the soil column materials were made of all studied soils untreated and treated with lime and ash. The model outcomes revealed that ash inclusion in soil columns generally has the same effects on ground displacement in two directions. Under pressures from pavement installation and vehicle weights, settlement of embankment foundation tends to be the same in all treated soil materials surveyed. The horizontal displacement appears to have a peak at the depth of 4 m, but the movement along the outermost columns is in an acceptable range within 10 mm. If the strength degradation of treated soil materials is not considered, Model 5 with lime-treated soil without any ash inclusion can be sufficient to give the allowable deformation of embankment. When the durability of soil strength is appreciated, the ash inclusion is welcome in the lime-treated soil with the approximate magnitude of vertical and lateral deformation of the ground under embankment.

# CHAPTER 9

# Conclusions and Recommendations

## 9.1 Conclusions

Thesis conclusions have three main subjects, including hypotheses, electrical conductivity tests for ash-lime-treated soils, and characterisation of soils treated with hydrated lime, bottom ash and bagasse ash. For hypotheses, five main hypotheses are addressed by responding to which statement is supported or not. For electrical conductivity tests, significant conclusions are drawn for soil samples treated with hydrated lime and bottom ash or/and bagasse ash. Finally, the conclusions on the characterisation of treated soils are provided, varying from samples treated with hydrated lime only or with both lime and ash, including bottom ash or/and bagasse ash.

### 9.1.1 Hypotheses

There are three main objectives that the study aims to address, including electrical conductivity (EC) tests, characterisation of soils treated with lime and ashes, and numerical analysis of studied materials for an embankment on treated soils. From three main objectives, five hypotheses were generated and needed to be addressed. The summary of conclusions on these hypotheses is shown in Table 9.1.

*Table 9.1. Summary for responses of five hypotheses*

| No. | Hypotheses | Supported? (Yes/No) |
|---|---|---|
| 1 | *Using electrical conductivity tests helps quickly determine the optimal ratio of bottom ash and bagasse ash to lime in mixtures with expansive soil for its stabilisation.* | Yes |
| 2 | *The mixing content in lime-ash-treated soils based on different dry weights gives different engineering characteristics of mixed samples.* | Yes |
| 3 | *Studied bagasse ash with smaller maximum diameters can enhance the engineering characteristics of lime-bagasse-ash-treated expansive soils.* | No |
| 4 | *There is a degradation in strength modulus of expansive soils treated with hydrated lime, bottom ash and bagasse ash over a long period of time.* | Yes |
| 5 | *Using both ash and lime to stabilise expansive soils can further reduce settlement and lateral displacement of embankment on soft ground.* | Yes |

### 9.1.2 Electrical conductivity tests for ash-lime-treated soils

In this study, electrical conductivity testing was proposed to investigate the lime consumption in the solution of soil, hydrated lime and studied ashes (bottom and bagasse ashes). The conclusions in terms of electrical conductivity tests are drawn into three categories: (1) soils treated with lime and bottom ash, (2) soils treated with lime and bagasse ash, and (3) soils treated with lime, bottom ash and bagasse ash.

#### *9.1.2.1 Soils treated with hydrated lime and bottom ash*

From the studies on EC tests for bottom-ash-lime treated soils, some significant conclusions can be shown as follows:

- Swell-shrinkage potential, presented by free swelling ratio and linear shrinkage, respectively, was correlated with $LC_0$ at the bottom ash content of 15%, where the ash started to react signifcantly with lime. The stage also had a transition of CSH from primary to secondary form since SEM analysis, which indicates a decrease of hydrate fibre from 15% to 25% and an increase of hydrate gels from over 20% to 40% in ash content. Consequently, the linear shrinkage decreased further when the ash was added to soil in the content of more than 25%.
- The changes in *UCS* and *CBR* of soils treated with lime and bottom ash was associated with the bottom ash content of 25% where the ash exceeded hydrated lime to further reduce $LC_0$ from electrical conductivity tests. The *UCS* and *CBR*-value changes of bottom-ash-lime-stabilised soil were linked to the dominance of bottom ash over lime in their reactions. Over 25% ash content, the strength of treated soil decreased because of the abundance of

bottom ash, leading to excess of pozzolan against hydrated lime and reducing *UCS* and *CBR* after 28 days.

#### *9.1.2.2 Soils treated with hydrated lime and bagasse ash*

The significant conclusion can be shown from the tests with *EC* rate for bagasse ash in various maximum sizes of 75, 150 and 425 µm as follows:

- Soil samples with the largest bagasse ash (425 µm) are classified as a non-pozzolanic material, whereas the solutions with bagasse ash in the 75 and 150-µm sizes are the variable pozzolanicity of samples. This was due to the fact that bagasse ash with the small sizes had more amorphous silica than the 425-µm-sized one, which contained a large amount of crystalline quartz and was less reactive to hydrated lime. However, from over 15% content, the conductivity rate started to grow in all studied ashes because of the increasing amount of amorphous silica in suspensions.
- The high *EC* rate of bagasse ash at the smallest size of 75 µm predicted well the high speed of $G_{max}$ evolution. However, the high rate of *EC* did not help improve the values of linear shrinkage and *UCS* since these parameters relied on amount of crystalline silica of bagasse-ash-lime-treated soils. As a result, linear shrinkage of soil treated with lime and 425-µm-bagasse-ash had the highest linear shrinkage and the highest *UCS*, compared to soils treated with lime and finer bagasse ash.

#### *9.1.2.3 Soils treated with hydrated lime, bottom ash and bagasse ash*

The outstanding results from *EC* investigation of the new ash-combined materials (soils treated with hydrated lime and both bottom ash and bagasse ash) can be drawn in the following conclusions:

- The electrical conductivity of aqueous solution of bottom ash and bagasse ash indicated the highest *EC* values from 0% to 30% in the bagasse ash content, whereas the lowest values came from the largest bagasse proportion from 70% to 100%. The 30% bagasse ash was the threshold where the crystalline quartz of bagasse ash partly replaces amorphous silicate of bottom ash, but with a high value of electrical conductivity. In the balance of amorphous and crystalline silicate in the ash compound, the bottom-bagasse ratio of 7 to 3 was optimal contents in combining these two ashes in electrical conductivity tests.
- From the result as 25% optimal ash content in lime-soil mixture and soil-ash mixing ratios through the evaluation of initial loss in conductivity ($LC_0$) with the ash contents, the

suggested percentages of ash-combined material are 17.5% bottom ash, 7.5% bagasse ash, 5% hydrated lime and 75% soil. The optimal bottom-bagasse ratio was determined at 25% in soil-ash-lime mixtures due to the consideration that the amount of amorphous silicate in ash was sufficient to react with lime and compensated the decrease of $LC_0$ caused by the loss of soil elements in the blend.

### 9.1.3 Characterisation of soils treated with hydrated lime, bottom ash and bagasse ash

#### *9.1.3.1 Soils treated with hydrated lime*

The experimental results of soil samples treated with hydrated lime can be summarised as follows:

- Results of pH tests indicate that 5% is the optimal lime content to stabilise the expansive soil. The optimal lime content in soil was confirmed at 5% in the testing results of unconfined compressive strength (UCS) and indirect tensile strength (ITS) tests.
- The inclusion of lime changed the clayey properties of expansive soil and turns the fat clay into elastic silt.
- The linear shrinkage of lime-treated soil was obtained quickly after 7 curing days since no significant shrinkage was observed after 28 days.
- The free-swelling ratio of lime-treated soil was zero if the sample was cured for 28 days, indicating no swelling pressure observed.
- The inclusion of lime in soil improved the bearing capacity significant by increasing *CBR* from 18.7% to 71.9%. However, lime-treated soils were not durable since they experienced a degradation of *CBR* when the samples were soaked in water after 7 days.
- The degradation of strength was also seen in the small-strain shear modulus ($G_{max}$) of lime-treated soil. The $G_{max}$ of lime-soil samples decreased after 56 curing days. The strength downgrade was explained by SEM and EDS analysis, showing the excess formation of calcium silicate hydrate (CSH) and calcium aluminium silicate hydrate (CASH) in the shape of fibre and bars. The hydrate products intertwined in soil structure kept and trapped more water in hydrate gaps, which caused the hydration of soil particles and reduced its strength and modulus.

#### *9.1.3.2 Soils treated with hydrated lime and bottom ash*

The study on bottom-ash-lime-treated soil includes: (1) the changes in their shrinkage-swelling and strength with the various content of bottom ash, and (2) effects of mixing ratio on the strength of treated soils. In summary, the outstanding conclusions can be emphasised as follows:

- The bottom ash content of 15% was the boundary where the free-swelling ratio of ash-lime-treated soil alters from large to lower reduction rate when bottom ash was added to lime-treated soil.
- Linear shrinkage (*LS*) of bottom-ash-lime-soil samples well followed the pattern of $LC_0$ evolution because there were two deflection points in *LS* evolution, including initial decrease, plateau and final decrease. The plateau of *LS* was associated with the transition of micro-structural changes, which showed the replacement of fibre-shaped CASH products by the gluing ones on ash surface. These CASH gels generated the bonding effect in soil structure, which helped to further reduce linear shrinkage of treated soil in the final decrease when ash content was larger than 25%.
- In all mixing ratios investigated, including S-ratio (dry-soil-weight-based ratio), T-ratio (dry-total-weight-based ratio) and SB ratio (dry-soil-and-ash-weight-based ratio), the highest strength was observed in the range of bottom ash from 20% to 25%. With treated soil samples mixed with SB-ratio, the ratio of bottom ash to lime was refined at 25% to 5% in terms of the highest *UCS* and *CBR* values. T-ratio-mixed UCS and CBR samples also had the highest values at the bottom ash content of 25% in soils treated with 5% hydrated lime.
- The $G_{max}$ of soil treated with hydrated lime and bottom ash doubled $G_{max}$ of soil samples with lime only after 56 days for curing. Over a period of time longer than 56 days, both $G_{max}$ of ash-lime-treated and lime-treated samples decreased in the same rate after 1 year of curing.
- However, the bottom-ash-lime-stabilised soil compacted at saturated moisture gained the highest $G_{max}$ after 56 days, which levelled off without degradation over 1 year. The explanation was from the formation of CSH intertwined in a reticular network under the wet condition, which enhanced the shear modulus of treated soils.
- Treated soil compacted at dry moisture contents suffered a loss of shear modulus due to the dehydration of soil layers caused by the excessive formation of CSH in the forms of scattering fibres or sheets with gaps, which held pore water by their affinity capacity.
- In matric suction, soil samples including bottom ash and lime experienced a gradual suction decrease, whereas untreated soil and soil treated with 5% lime had their suction increase steadily over 90 days.
- The high suction of lime-treated soil confirmed the excessive production of CSH fibres, forming an abundance of gaps between CSH products and increasing capillary suction of

lime-treated soil. Meanwhile, the low suction of bottom-ash-lime-stabilised soil was due to the extreme porosity of bottom ash. The inside spaces of bottom ash were opened by the CSH fibres produced on ash surface, resulting in more air-links to these areas, gradually reducing the matric suction with time.

#### *9.1.3.3 Soils treated with hydrated lime and bagasse ash*

The testing results are shown in linear shrinkage, unconfined compressive strength and shear modulus of soils treated with 5% lime and 15% bagasse ash in the sizes of 75, 150 and 425 µm, which reveals the notable conclusions that can be summarised as follows:

- Linear shrinkage (*LS*) of soil treated with 425-µm-sized bagasse ash and hydrated lime was the lowest, compared to sample with 75 and 150-µm ash. The lowest *LS* was due to the benefits of crystalline quartz in 425-µm bagasse ash in reducing the detrimental effects of ettringite on soil structures.
- The same pattern was repeated in UCS results, in which *UCS* of samples with 425-µm-sized-bagasse was highest after 56 curing days. These 56-day *UCS* values for ash in 150-µm and 75-µm size were even smaller than the *UCS* of soil treated with soil. In the same vein, the dominance of crystalline silicate in 425-µm-bagasse-ash-lime-soil samples enhanced their *UCS* due to the high strength of crystalline granular particles, compared to cellular grains in soils with bagasse ash in the size of 75 µm and 150 µm.
- Due to the high content of amorphous silicate, soils treated with lime and 75-µm-size bagasse ash had the highest rate of $G_{max}$, compared to other samples with larger bagasse ash. It was proven by SEM analysis that there was an overwhelming generation of ettringite in 75-µm-ash-treated soil samples while CSH products dominated others.
- However, all ash-lime-treated soil specimens were degraded in $G_{max}$-values after various curing durations. The sample with the smallest ash size suffered the decrease of $G_{max}$ earliest, right after 28 days, followed by the one with 150-µm ash after 42 days, and the soil with largest ash was longest with 56 days before $G_{max}$ degraded. This means that the small size of bagasse ash could accelerate $G_{max}$ in the treated soils, but this also caused a quicker degradation of the shear modulus. This is attributed to the combined detrimental effects of both ettringite and CSH products on the strength of treated soils.

#### *9.1.3.4 Soils treated with hydrated lime, bottom ash and bagasse ash*

The characterisation of soil treated with hydrated lime, bottom ash and bagasse ash is investigated in a wide range of physical, mechanical and micro-structural analysis. For this, the experiments

include liquid limit, linear shrinkage, compaction, swelling-consolidation, UCS, CBR, triaxial shearing parameters, small-strain shearing modulus, matric suction, SEM and EDX tests. The testing findings show the underlying conclusions as follows:

- Soil treated with lime, bottom ash, and bagasse ash had a lower liquid limit than soil with lime bottom ash only and equalled to soil with lime and bagasse ash.
- For compaction, two-ash-lime-stabilised soil had the lowest *OMC* at 24% and the smallest *MDD* at 1.25 ($Mg/m^3$), compared to other treated soils. The significant low of *OMC* indicated the property change of ash-combined mixture towards a coarser material.
- In swelling-consolidation testing, the bottom-bagasse-lime treated sample has a higher swelling ratio than the bottom-lime-treated specimen but less than bagasse-lime stabilised soils. However, the two-ash included material was more compressible than the specimens treated with only bottom ash or bagasse ash. The results indicated that mixing 7.5% bagasse ash in the bottom-ash-lime treated soil slightly increased its free-swelling ratio and compression index, causing lower yield stress of treated soils.
- In the same vein, *UCS* of bottom-bagasse-ash-lime-treated soils was relatively low compared to other ash-lime-treated soil (only 1.75 MPa after 56 days for curing). This is lower than soils treated with lime and bottom ash or bagasse ash but higher than lime-treated soil.
- *CBR* of the two-ash-lime-stabilised sample was lower than *CBR* of soil with lime only after 28 days of curing. However, the *CBR* position changed when the moulds were soaked in water for the next 62 days, revealing the soil with both ashes had soaked *CBR* larger than samples with lime or/and bagasse ash. The sample stabilised with both bottom ash and bagasse ash had the largest deformation for the collapse caused by piston penetration, referring to the ductility of the new ash-combined material.
- In triaxial shearing parameters, the two-ash-lime-treated soil had the same internal friction angle of $45^0$ and zero cohesion of soil with 5% lime and 25% bottom ash. This indicated that 17.5% bottom ash in the suggested material was enough to turn the soil into a coarse sample with sandy behaviours.
- The two-ash-combined material had the highest $G_{max}$ in statistically compacted samples, compared to saturated triaxial samples and OMC-compacted waxed specimens. For dynamically compacted CBR samples, the $G_{max}$ of the new-ash-combined material was lower than the soil with 25% bottom ash and 5% lime, even after soaking in water for 62 days. The high improvement of CBR soil sample with 5% ash and 25% bottom ash suggest

bottom ash as a suitable subgrade admixture, which is more preferable to bagasse ash in soil stabilisation.

- Likewise, the matric suction of the two-ash-lime-soil sample was the highest among other treated samples after 56 curing day. Only the soil containing ashes and lime significantly increased matric suction over 90 days of curing, whereas other samples have slight increases or decreases of suction. The remarkable increase of suction in the ash-combined material was explained by SEM analysis, showing that there was a formation of reticular structures of hydrate products and ettringite between bottom ash and bagasse ash, which increased the micro-suction of treated soils.
- The study on $G_{max}$ evolution and SEM-EDX of waxed samples over 1 year of curing suggested five stages in the development of shear modulus in soils treated with lime and ash: (1) a steady growth in the first days after compaction with CSH and CASH, (2) an acceleration of growth until 28 curing days with CSH and magnesium silicate hydrate (MSH), (3) a levelling-off after 28 days until 56 days with CSH, CASH and ettringite, (4) a collapse after 56 days with an excessive amount of CSH, CASH and ettringite, and (5) a stabilisation after about 1 year of the incubation process.
- $G_{max}$ of soils treated with 5% lime, 17.5% bottom ash, and 7.5% bagasse ash in various sizes (i.e., 75 µm, 150 µm and 425 µm as the maximum particle size of bagasse ash) showed that the modulus of the sample with smallest bagasse ash (75 µm) did not have Stage 3 in its evolution, whereas two-ash-included soils had a longer Stage 3 of $G_{max}$ with larger sizes of bagasse ash. As a result, two-ash-lime-treated soil with 150-µm bagasse ash has Stage 4 starting from the day of 56, while Stage 4 of the soil with 425-µm bagasse ash commenced from the day of 72. In saturated or wet-side-compacted samples with two ashes, the reticular structures of CSH and ettringite in the interfacial transition zone between bagasse ash and bottom ash helped reduce the degradation rate of $G_{max}$ in Stage 4.

### 9.1.4 Numerical analysis on road embankment on soft soil treated with hydrated lime, bottom ash and bagasse ash

The numerical results indicate the significant conclusions as follows:

- Stabilising the top-soil layer (i.e., alluvium) did not help to eliminate the settlement of embankment. However, treating the soil surface with hydrated lime and/or bagasse ash

could deplete the horizontal movement on the surface of the alluvium layer or the working platform of embankment.

- The column installation helped transform embankment loads to the deeper and stiffer soil profile, so the settlement was reduced significantly from 1.1 m to only 0.3 m. In this model, all ash-lime-treated materials resulted in the same settlement and deformation, which were smaller than outputs with lime-treated soils. This indicated the same combined effects of ash and lime on ground reinforcement, regardless of the type of ash used. However, in fully-saturation under water level, the bottom-ash-lime-treated soil columns were recommended because of their durability without any $G_{max}$ degradation after a long curing time.
- Longer soil columns to deeper extend to the layer of transition clayey sand reduce the settlement to about zero while the lateral displacement was limited under 30 mm. However, the largest horizontal deformation of 30 mm occurred on the top ground surface, indicating a sliding movement of the working platform under embankment.
- The modelling results of the same treated soil material for the top layer and columns or the topsoil with the treatment only with hydrated lime and bagasse ash showed that the vertical settlement and horizontal displacement of ground under the embankment were approximate by using any treated-ash-lime soil materials. The effectiveness of constraining the relevant settlement and deformation still existed with the application of pavement and vehicle loads.
- Consequently, the study proposed using bagasse and lime for the topsoil layer, while the soil columns should be treated with bottom ash and lime, and the columns should be extended until the middle of transition soil layer under estuarine silty clay.

## 9.2 Recommendations for future studies

From the findings of the electrical conductivity testing, characterisation of ash-lime-treated soils and numerical analysis, a number of recommendations for future research can be suggested as follows:

- This study proposed employing electrical conductivity (EC) testing for estimating the optimal ratio of ash to lime in their mixture with artificial expansive soil, a combination of bentonite, kaolinite and fine sand. However, natural soils have different chemical compositions; hence the *EC* values can be different from those obtained for the soil samples made in the laboratory. In the future research, it is suggested to quantify the natural

composition of parent soils. For EC experiments on natural soil, the sieving analysis should be conducted to clarify the amount of clay and sand components in the soil. Following Test A, the clay part can firstly be mixed well with water to avoid any clayey clods in its suspension. Meanwhile, the sand components can be mixed thoroughly with ash to pour in the lime-clay solution later.

- Hydrated lime in this study contains an amount of calcite due to carbonation between lime and carbon dioxide in atmosphere. This calcite contamination can reduce the reactivity of lime in soil. Hence, in further studies, the effects of lime impurity on characteristics of soil treated with lime and ash can be investigated.
- Bottom ash is sieved under the unique size of 2.36 mm to constrain the maximum diameter of ash in mixing with soils. Bottom ash with the size over 2.36 mm was not used in the study, and the size effect of bottom ash on the characterisation of bottom-ash-lime-treated soils was not conducted. In future studies, coarse bottom ash can be ground into finer ash to research the size effects of ash on treated soils.
- The studied bagasse ash still contains an amount of graphite as unburnt carbon, determining the typical black colour of ash. Although the study investigates the maximum particle size effects of bagasse ash of 75 µm, 150 µm and 425 µm in diameters on soil stabilisation, *LS* and *UCS* are not improved even with finer ash. It may be due to carbon contamination. In the future investigation, it is recommended that the studied bagasse ash be burnt at a higher temperature to eliminate the possible presence of carbon particles in ash.
- The testing outcomes show the effectiveness of combing bottom ash and bagasse ash in reducing shrinkage and improving small-strain shear modulus ($G_{max}$) in ash-lime-treated soil. Further enhancement is also observed if the material is compacted at the wet side or the saturated condition. However, compared to the bottom-ash-lime-treated soil, the bottom-bagasse-ash-lime-treated soil still suffers a loss of $G_{max}$ over a long period of time. It is suggested that in future research, the bottom ash be mixed with fine and pure bagasse ash (e.g., refined-75-µm ash) and compacted with lime and soil at a moisture content of saturation to investigate their $G_{max}$ stabilisation with time. The durability of suggested samples can be conducted with many cycles of drying and wetting.
- Results from numerical analysis propose the design of ground treatment with hydrated lime, bottom ash and bagasse ash. The analysis assumes that the topsoil layer (i.e., alluvium) treated with studied binders gives the same properties of treated soils in this research. Therefore, the model outcomes may have some discrepancies between numerical

predictions and field behaviour due to the difference between artificial expensive soil and natural ground. However, in comparisons between soils treated with various binders, the study is still validated in the selection of the best combination of lime and ash for plans of soil stabilisation. In future research, the natural soil from the field should be directly employed to test with studied binders and generate more reliable input parameters. Furthermore, the suggestions, established based on numerical modelling outputs, can be adapted in a field embankment onsite to examine the validation and credibility of the proposed models, in which soft ground is treated with hydrated lime, bottom ash and bagasse ash.

**References**


Abhijith, R. P. (2015). Effect of natural Coir fibres on CBR strength of soil subgrade. *International Journal of Scientific and Research Publications*, *5*(4), 1-4.

ABNT NBR 5752. (1992). Determination of Pozzolanic Activity Index with Portland Cement. In *Pozzolans - Pozzolanic Activity* Rio de Janeiro, Brazil: Brazilian Association of Technical Standards.

Abtahi, M., Allaie, H., & Hejazi, M. (2009). An investigative study on chemical soil stabilization. *8th Int cong civ eng, Shiraz, Iran*.

Abu-Hassanein, Z. (1994). Using Electrical Resistivity Techniques as a Quality Control Tool for Compacted Clay Liners. *M. S. Thesis, Department of Civil and Environmental Engineering, University of Wisconsin-Madison.*

Abu-Hassanein, Z. S., Benson, C. H., Wang, X., & Blotz, L. R. (1996). Determining bentonite content in soil-bentonite mixtures using electrical conductivity. *Geotechnical testing journal*, *19*(1), 51-57.

Ajay Goyal, A., Hattori, K., & Ogata, H. (2007). Properties of sugarcane bagasse ash and Its Potential as Cement-Pozzolana Binder. Twelfth International Colloquium on Structural and Geotechnical Engineering, Ain Shams University, Faculty of Engineering, Department of Structural Engineering, Egypt.

Akinwumi, I. (2014). Soil modification by the application of steel slag. *Periodica Polytechnica. Civil Engineering*, *58*(4), 371.

Akinwumi, I., & Aidomojie, O. (2015). Effect of Corncob ash on the geotechnical properties of Lateritic soil stabilized with Portland cement. *International Journal of Geomatics and Geosciences*, *5*(3), 375-392.

Alavéz-Ramírez, R., Montes-Garcia, P., Martínez-Reyes, J., Altamirano-Juárez, D. C., & Gochi-Ponce, Y. (2012). The use of sugarcane bagasse ash and lime to improve the durability and mechanical properties of compacted soil blocks. *Construction and Building Materials*, *34*, 296-305.

Aldaood, A., Bouasker, M., & Al-Mukhtar, M. (2014). Impact of wetting–drying cycles on the microstructure and mechanical properties of lime-stabilized gypseous soils. *Engineering Geology*, *174*, 11-21.

Alhassan, M. (2008). Permeability of lateritic soil treated with lime and rice husk ash. *Assumption University Journal of Thailand*, *12*(2), 115-120.

Ali, M., Arulrajah, A., Disfani, M., & Piratheepan, J. (2011). Suitability of using recycled glass-crushed rock blends for pavement subbase applications. In *Geo-Frontiers 2011: Advances in Geotechnical Engineering* (pp. 1325-1334).

Ali, M., Liu, A., Sou, H., & Chouw, N. (2012). Mechanical and dynamic properties of coconut fibre reinforced concrete. *Construction and Building Materials*, *30*, 814-825.

Amavasai, A., Sivasithamparam, N., Dijkstra, J., & Karstunen, M. (2018). Consistent Class A & C predictions of the Ballina test embankment. *Computers and Geotechnics*, *93*, 75-86.

Amin, N.-u. (2011). Use of bagasse ash in concrete and its impact on the strength and chloride resistivity. *Journal of Materials in Civil Engineering*, *23*(5), 717-720.

Amu, O., Fajobi, A., & Afekhuai, S. (2005). Stabilizing potential of cement and fly ash mixture on expansive clay soil. *Journal of applied sciences*, *5*(9), 1669-1673.

Andrade, L. B., Rocha, J., & Cheriaf, M. (2007). Evaluation of concrete incorporating bottom ash as a natural aggregates replacement. *Waste Management*, *27*(9), 1190-1199.

Anggraini, V., Asadi, A., Farzadnia, N., Jahangirian, H., & Huat, B. B. (2016). Reinforcement benefits of nanomodified coir fiber in lime-treated marine clay. *Journal of Materials in Civil Engineering*, *28*(6), 06016005.

Anupam, A. K., & Kumar, P. (2013). Use of various agricultural and industrial waste materials in road construction. *Procedia-Social and Behavioral Sciences*, *104*, 264-273.

Araei, A. A., Soroush, A., Tabatabaei, S. H., & Ghalandarzadeh, A. (2012). Consolidated undrained behavior of gravelly materials. *Scientia Iranica*, *19*(6), 1391-1410.

Ardejani, F. D., Shokri, B. J., Bagheri, M., & Soleimani, E. (2010). Investigation of pyrite oxidation and acid mine drainage characterization associated with Razi active coal mine and coal washing waste dumps in the Azad shahr–Ramian region, northeast Iran. *Environmental Earth Sciences*, *61*(8), 1547-1560.

Arif, E., Clark, M. W., & Lake, N. (2017). Sugar cane bagasse ash from a high-efficiency co-generation boiler as filler in concrete. *Construction and Building Materials*, *151*, 692-703.

AS 1289.3.2.1. (2009). Methods of testing soils for engineering purposes-Soil classification tests - Determination of the plastic limit of a soil - Standard method. In *Methods of testing soils for engineering purposes*: Australia Standards.

AS 1289.3.4.1. (2008). Soil classification tests - Determination of the linear shrinkage of a soil - Standard method. In *Methods of testing soils for engineering purposes*: Australia Standards.

AS 1289.3.5.1. (2006). Soil classification tests - Determination of the soil particle density of a soil - Standard method. In *Methods of testing soils for engineering purposes*: Australian Standard.

AS 1289.3.6.1. (2009). Soil classification tests - Determination of the particle size distribution of a soil - Standard method of analysis by sieving. In *Methods of testing soils for engineering purposes*: Australian Standards.

AS 1289.3.6.3. (2003). Soil classification tests—Determination of the particle size distribution of a soil—Standard method of fine analysis using a hydrometer. In *Methods of testing soils for engineering purposes*: Australian Standard.

AS 1289.3.9.1. (2015). Soil classification tests - Determination of the cone liquid limit of a soil. In *Methods of testing soils for engineering purposes*: Australia Standards.

AS 1289.5.1.1. (2017). Soil compaction and density tests - Determination of the dry density/moisture content relation of a soil using standard compactive effort. In *Methods of testing soils for engineering purposes*: Australia Standards.

AS 1289.6.1.1. (1998). Soil strength and consolidation tests—Determination of the California Bearing Ratio of a soil—Standard laboratory method for a remoulded specimen. In *Methods of testing soils for engineering purposes*: Australia Standards.

AS 1289.6.4.2. (2016). Soil strength and consolidation tests - Determination of compressive strength of a soil - Compressive strength of a saturated specimen tested in undrained triaxial compression with measurement of pore water pressure. In *Methods of testing soils for engineering purposes*: American Society for Testing and Materials (ASTM).

AS 1289.6.6.1. (1998). Soil strength and consolidation tests—Determination of the one-dimensional consolidation properties of a soil—Standard method. In *Methods of testing soils for engineering purposes*: Australian Standard.

AS 5101.4. (2008). Unconfined compressive strength of compacted materials. In *Methods of testing soils for engineering purposes*: Australia Standards.

Association, A. C. A. (2008). Coal Combustion Product (CCP) production & use survey report. In: ACAA: Aurora, CO.

ASTM-C702. (2018). Standard practice for reducing samples of aggregate to testing size. In: American Society for Testing and Materials (ASTM).

ASTM-D4546. (2014). Standard Test Methods for One-Dimensional Swell or Collapse of Soils. *ASTM International*.

ASTM-D4972. (2019). Standard Test Methods for pH of Soils. In: American Society for Testing and Materials (ASTM).

ASTM D2435. (2020). Standard Test Methods for One-Dimensional Consolidation Properties of Soils Using Incremental Loading. In: American Society for Testing and Materials (ASTM).

ASTM D4186. (2020). Standard Test Method for One-Dimensional Consolidation Properties of Saturated Cohesive Soils Using Controlled-Strain Loading. In: American Society for Testing and Materials (ASTM).

ASTM D4546. (2014). Standard Test Methods for One-Dimensional Swell or Collapse of Soils. In: American Society for Testing and Materials (ASTM).

ASTM D5298. (2016). Standard Test Method for Measurement of Soil Potential (Suction) Using Filter Paper. In: American Society for Testing and Materials (ASTM).

ASTM D6276. (2019). Standard Test Method for using pH to estimate the soil-lime proportion requirement for soil stabilization. In: American Society for Testing and Materials (ASTM).

ASTM Standard. (2007). D2487-Standard practice for classification of soils for engineering purposes (unified soil classification system). In: American Society for Testing and Materials (ASTM).

Azeem, A., & Ati, A. (1992). Erosion and control techniques for slopes of banks and cuttings. Ind geotech conf, Calcutta,

Bade, R., Khan, N. Z., Sahare, J., Ameen, F., & Ahmed, D. (2017). Effect of Wood Shaving Ash on Index Properties of Black Cotton Soil. *International Research Journal of Engineering and Technology (IRJET)*, *4*(02), 38-39.

Bagherpour, I., & Choobbasti, A. J. (2003). Stabilization of fine-grained soils by adding microsilica and lime or microsilica and cement. *Electronic Journal of Geotechnical Engineering*, *8*(B), 1-10.

Bahurudeen, A., Kanraj, D., Dev, V. G., & Santhanam, M. (2015a). Performance evaluation of sugarcane bagasse ash blended cement in concrete. *Cement and Concrete Composites*, *59*, 77-88.

Bahurudeen, A., Marckson, A., Kishore, A., & Santhanam, M. (2014). Development of sugarcane bagasse ash based Portland pozzolana cement and evaluation of compatibility with superplasticizers. *Construction and Building Materials*, *68*, 465-475.

Bahurudeen, A., & Santhanam, M. (2014). Performance evaluation of sugarcane bagasse ash-based cement for durable concrete.

Bahurudeen, A., Wani, K., Basit, M. A., & Santhanam, M. (2015b). Assesment of pozzolanic performance of sugarcane bagasse ash. *Journal of Materials in Civil Engineering*, *28*(2), 04015095.

Barazesh, A., Saba, H., Gharib, M., & Rad, M. Y. (2012). Laboratory Investigation of the Effect of Eggshell powder on Plasticity Index in Clay and Expansive Soils. *European Journal of Experimental Biology*, *2*(6), 2378-2384.

Barroso, T. R. (2011). *Study of pozzolanic activity and use in concrete of the sugar cane bagasse ashes with different physical and chemical properties* Northern Rio de Janeiro State University]. Campos dos Goytacazes, Brazil.

Basha, E. M. A., Hashim, R., & Muntohar, A. S. (2003). Effect of the cementrice husk ash on the plasticity and compaction of soil. *Electronic Journal of Geotechnical Engineering*, *8*(1), 1-8.

Bell, F. (1996). Lime stabilization of clay minerals and soils. *Engineering Geology*, *42*(4), 223-237.

Bergado, D., Anderson, L., Miura, N., & Balasubramaniam, A. (1996). Soft ground improvement in lowland and other environments.

Bernard, E., Lothenbach, B., Cau-Dit-Coumes, C., Chlique, C., Dauzères, A., & Pochard, I. (2018). Magnesium and calcium silicate hydrates, Part I: Investigation of the possible magnesium incorporation in calcium silicate hydrate (CSH) and of the calcium in magnesium silicate hydrate (MSH). *Applied geochemistry*, *89*, 229-242.

Bhuvaneshwari, S., Robinson, R., & Gandhi, S. (2005). Stabilization of expansive soils using fly ash. *Fly Ash India*, *8*, 5.1-5.10.

Bignozzi, M., & Sandrolini, F. (2006). Tyre rubber waste recycling in self-compacting concrete. *Cement and Concrete Research*, *36*(4), 735-739.

Bilba, K., Arsène, M.-A., & Ouensanga, A. (2003). Sugar cane bagasse fibre reinforced cement composites. Part I. Influence of the botanical components of bagasse on the setting of bagasse/cement composite. *Cement and Concrete Composites*, *25*(1), 91-96.

Bolden IV, J. J. (2013). *Innovative uses of Recycled and Waste Materials in Construction Application* North Carolina Agricultural and Technical State University].

Boraste, M. T. H., & Sharma, V. K. (2014). Investigation of Laterite Soil by Waste Glass For Stabilization of Road Embankment.

Bose, B. (2012). Geo engineering properties of expansive soil stabilized with fly ash. *Electronic Journal of Geotechnical Engineering*, *17*, 1339-1353.

Budhu, M. (2008). *SOIL MECHANICS AND FOUNDATIONS, (With CD)*. John Wiley & Sons.

Buhler, R. L., & Cerato, A. B. (2007). Stabilization of Oklahoma expansive soils using lime and class C fly ash. In *Problematic Soils and Rocks and In Situ Characterization* (pp. 1-10).

Bussian, A. (1983). Electrical conductance in a porous medium. *Geophysics*, *48*(9), 1258-1268.

Byiringiro, A. (2014). *Effect of paper mill ash on properties of expansive soils* Stellenbosch: Stellenbosch University].

Cai, Y., Shi, B., Ng, C. W., & Tang, C.-s. (2006). Effect of polypropylene fibre and lime admixture on engineering properties of clayey soil. *Engineering Geology*, *87*(3), 230-240.

Canpolat, F., Yılmaz, K., Köse, M., Sümer, M., & Yurdusev, M. (2004). Use of zeolite, coal bottom ash and fly ash as replacement materials in cement production. *Cement and Concrete Research*, *34*(5), 731-735.

Cao, Y., Shibata, S., & Fukumoto, I. (2006). Mechanical properties of biodegradable composites reinforced with bagasse fibre before and after alkali treatments. *Composites part A: Applied science and Manufacturing*, *37*(3), 423-429.

Castelbaum, D., Olson, M. R., Sale, T. C., & Shackelford, C. D. (2010). Laboratory apparatus and procedures for preparing test specimens of slurry mixed soils. *Geotechnical testing journal*, *34*(1), 18-26.

CEN. (2005). Method of testing cement. Pozzolanicity test for pozzolanic cement. In (Vol. EN 196-5). Belgium, UK: European Committee for Standardization.

Chai, J.-C., Shen, S.-L., Miura, N., & Bergado, D. T. (2001). Simple method of modeling PVD-improved subsoil. *Journal of Geotechnical and Geoenvironmental Engineering*, *127*(11), 965-972.

Chakraborty, S., & Nair, S. (2020). Impact of curing time on moisture-induced damage in lime-treated soils. *International Journal of Pavement Engineering*, *21*(2), 215-227.

Chakraborty, S., Puppala, A. J., & Biswas, N. (2020). Role of Crystalline Silica Admixture in Mitigating Ettringite-Induced Heave in Lime-Treated Sulphate-Rich Soils. *Géotechnique*, 1-49.

Chansoria, A., & Yadav, R. K. (2016). Effect of Quarry Dust on Engineering Properties of Black Cotton Soil. *International Journal*, *2*, 715-718.

Cheah, C. B., & Ramli, M. (2011). The implementation of wood waste ash as a partial cement replacement material in the production of structural grade concrete and mortar: An overview. *Resources, Conservation and Recycling*, *55*(7), 669-685.

Chen, F. H. (2012). *Foundations on expansive soils* (Vol. 12). Elsevier.

Chen, L., & Lin, D.-F. (2009). Stabilization treatment of soft subgrade soil by sewage sludge ash and cement. *Journal of Hazardous Materials*, *162*(1), 321-327.

Chenarboni, H. A., Lajevardi, S. H., MolaAbasi, H., & Zeighami, E. (2021). The effect of zeolite and cement stabilization on the mechanical behavior of expansive soils. *Construction and Building Materials*, *272*, 121630.

Cheriaf, M., Rocha, J. C., & Pera, J. (1999). Pozzolanic properties of pulverized coal combustion bottom ash. *Cement and Concrete Research*, *29*(9), 1387-1391.

Chiang, W.-S., Ferraro, G., Fratini, E., Ridi, F., Yeh, Y.-Q., Jeng, U., Chen, S.-H., & Baglioni, P. (2014). Multiscale structure of calcium-and magnesium-silicate-hydrate gels. *Journal of Materials Chemistry A*, *2*(32), 12991-12998.

Chu, Y., Liu, S., Bate, B., & Xu, L. (2018). Evaluation on expansive performance of the expansive soil using electrical responses. *Journal of Applied Geophysics*, *148*, 265-271.

Chung, S. G., Ryu, C. K., Min, S. C., Lee, J. M., Hong, Y. P., & Odgerel, E. (2012). Geotechnical characterisation of Busan clay. *KSCE Journal of Civil Engineering*, *16*(3), 341-350.

Chusilp, N., Jaturapitakkul, C., & Kiattikomol, K. (2009a). Utilization of bagasse ash as a pozzolanic material in concrete. *Construction and Building Materials*, *23*(11), 3352-3358.

Chusilp, N., Likhitsripaiboon, N., & Jaturapitakkul, C. (2009b). Development of bagasse ash as a pozzolanic material in concrete. *Asian Journal on Energy and Environment*, *10*(3), 149-159.

Cokca, E. (2001). Use of class c fly ashes for the stabilizationof an expansive soil. *Journal of Geotechnical and Geoenvironmental Engineering*, *127*(7), 568-573.

Considine, M. (1984). Soils shrink, trees drink, and houses crack. *ECOS Magazine*, *41*, 13-15.

Consoli, N. C., Prietto, P. D., & Ulbrich, L. A. (1998). Influence of fiber and cement addition on behavior of sandy soil. *Journal of Geotechnical and Geoenvironmental Engineering*, *124*(12), 1211-1214.

Cordeiro, G., Tavares, L., & Toledo Filho, R. (2016). Improved pozzolanic activity of sugar cane bagasse ash by selective grinding and classification. *Cement and Concrete Research*, *89*, 269-275.

Cordeiro, G., Toledo Filho, R., & Fairbairn, E. (2009a). Effect of calcination temperature on the pozzolanic activity of sugar cane bagasse ash. *Construction and Building Materials*, *23*(10), 3301-3303.

Cordeiro, G., Toledo Filho, R., Tavares, L., & Fairbairn, E. (2008). Pozzolanic activity and filler effect of sugar cane bagasse ash in Portland cement and lime mortars. *Cement and Concrete Composites*, *30*(5), 410-418.

Cordeiro, G. C., & Kurtis, K. E. (2017). Effect of mechanical processing on sugar cane bagasse ash pozzolanicity. *Cement and Concrete Research*, *97*, 41-49.

Cordeiro, G. C., Toledo Filho, R. D., Tavares, L. M., & Fairbairn, E. d. M. R. (2009b). Ultrafine grinding of sugar cane bagasse ash for application as pozzolanic admixture in concrete. *Cement and Concrete Research*, *39*(2), 110-115.

Correia, A. G., Winter, M., & Puppala, A. (2016). A review of sustainable approaches in transport infrastructure geotechnics. *Transportation Geotechnics*, *7*, 21-28.

Dahale, P., Nagarnaik, P., & Gajbhiye, A. (2017). Engineering behavior of remolded expansive soil with lime and flyash. *Materials Today: Proceedings*, *4*(9), 10581-10585.

Dang, L. C. (2018). *Enhancing the engineering properties of expansive soil using bagasse ash, bagasse fibre and hydrated lime* [Doctoral thesis, University of Technology Sydney]. Open Publications of UTS Scholars (OPUS).

Dang, L. C., Fatahi, B., & Khabbaz, H. (2016a). Behaviour of Expansive Soils Stabilized with Hydrated Lime and Bagasse Fibres. *Procedia Engineering*, *143*, 658-665.

Dang, L. C., Hasan, H., Fatahi, B., Jones, R., & Khabbaz, H. (2016b). Enhancing the engineering properties of expansive soil using bagasse ash and hydrated lime. *International Journal*, *11*(25), 2447-2454.

Dang, L. C., Hasan, H., Fatahi, B., & Khabbaz, H. (2015). Influence of bagasse ash and hydrated lime on strength and mechanical behaviour of stabilised expansive soil. *GEOQuébec 2015*.

Dang, L. C., Khabbaz, H., & Fatahi, B. (2017). An experimental study on engineering behaviour of lime and bagasse fibre reinforced expansive soils. The 19th International Conference on Soil Mechanics and Geotechnical Engineering (19th ICSMGE), Korea.

Das, B. M., & Sobhan, K. (2013). *Principles of geotechnical engineering*. Cengage Learning.

de Soares, M. M., Garcia, D. C., Figueiredo, R. B., Aguilar, M. T. P., & Cetlin, P. R. (2016). Comparing the pozzolanic behavior of sugar cane bagasse ash to amorphous and crystalline SiO2. *Cement and Concrete Composites*, *71*, 20-25.

De Souza, N. S. L., dos Anjos, M. A. S., de Farias, E. C., de Souza, M. M., Branco, F. G., & Pereira, A. (2020). Evaluation of sugarcane bagasse ash for lightweight aggregates production. *Construction and Building Materials*, 121604.

Deepika, S., Anand, G., Bahurudeen, A., & Santhanam, M. (2017). Construction products with sugarcane bagasse ash binder. *Journal of Materials in Civil Engineering*, *29*(10), 04017189.

Demeyer, A., Nkana, J. V., & Verloo, M. (2001). Characteristics of wood ash and influence on soil properties and nutrient uptake: an overview. *Bioresource technology*, *77*(3), 287-295.

Di Remigio, G., Rocchi, I., & Zania, V. (2021). Scanning Electron Microscopy and clay geomaterials: From sample preparation to fabric orientation quantification. *Applied Clay Science*, *214*, 106249.

Disfani, M., Arulrajah, A., Bo, M., & Hankour, R. (2011). Recycled crushed glass in road work applications. *Waste Management*, *31*(11), 2341-2351.

Disfani, M., Arulrajah, A., Bo, M., & Sivakugan, N. (2012). Environmental risks of using recycled crushed glass in road applications. *Journal of Cleaner Production*, *20*(1), 170-179.

Disfani, M., Arulrajah, A., Suthagaran, V., & Bo, M. (2013). Long-term settlement prediction for wastewater biosolids in road embankments. *Resources, Conservation and Recycling*, *77*, 69-77.

Disfani, M. M., Arul, A., Farshid, M., Bo, M. W., & Narsilio, G. A. (2015). Geotechnical characteristics of stabilised aged biosolids. *Environmental Geotechnics*, *2*(5), 269-279.

Doebelin, N., & Kleeberg, R. (2015). Profex: a graphical user interface for the Rietveld refinement program BGMN. *Journal of applied crystallography*, *48*(5), 1573-1580.

Donatello, S., Tyrer, M., & Cheeseman, C. (2010). Comparison of test methods to assess pozzolanic activity. *Cement and Concrete Composites*, *32*(2), 121-127.

Edil, T. B., Acosta, H. A., & Benson, C. H. (2006). Stabilizing soft fine-grained soils with fly ash. *Journal of Materials in Civil Engineering*, *18*(2), 283-294.

El-Aziz, A., Abo-Hashema, M., & El-Shourbagy, M. (2004). The effect of lime-silica fume stabilizer on engineering properties of clayey subgrade. Engineering Conference of Mansoura University Faculty, Sharm, Egypt.

Ellaby, L. (2010). *The history of soil stabilisation*. Ezine articles. Retrieved 10 June, 2021 from http://ezinearticles.com/?The-History-of-Soil-Stabilisation&id=3917867

Eroglu, H., Acar, H., Ucuncu, O., & Imamoglu, S. (2006). Soil stabilization of forest roads sub-base using lime mud waste from the chemical recovery process in alkaline pulp mill. *Journal of applied sciences*, *6*(5), 1199-1203.

Erzin, Y., & Gunes, N. (2013). The unique relationship between swell percent and swell pressure of compacted clays. *Bulletin of Engineering Geology and the Environment*, *72*(1), 71-80.

Fairbairn, E. M., Americano, B. B., Cordeiro, G. C., Paula, T. P., Toledo Filho, R. D., & Silvoso, M. M. (2010). Cement replacement by sugar cane bagasse ash: CO2 emissions reduction and potential for carbon credits. *Journal of environmental management*, *91*(9), 1864-1871.

Fatahi, B., Fatahi, B., Le, T. M., & Khabbaz, H. (2013). Small-strain properties of soft clay treated with fibre and cement. *Geosynthetics International*, *20*(4), 286-300.

Fatahi, B., & Khabbaz, H. (2013). Influence of fly ash and quicklime addition on behaviour of municipal solid wastes. *Journal of Soils and Sediments*, *13*(7), 1201-1212.

Fatahi, B., & Khabbaz, H. (2015). Influence of Chemical Stabilisation on Permeability of Municipal Solid Wastes. *Geotechnical and Geological Engineering*, *33*(3), 455-466.

Fatahi, B., Khabbaz, H., & Fatahi, B. (2012). Mechanical characteristics of soft clay treated with fibre and cement. *Geosynthetics International*, *19*(3), 252-262.

Feng, S., & Sen, P. (1985). Geometrical model of conductive and dielectric properties of partially saturated rocks. *Journal of Applied Physics*, *58*(8), 3236-3243.

Frı, M., & Rodrı, C. (2008). Effect of incorporating ferroalloy industry wastes as complementary cementing materials on the properties of blended cement matrices. *Cement and Concrete Composites*, *30*(3), 212-219.

Frías, M., Villar-Cociña, E., De Rojas, M. S., & Valencia-Morales, E. (2005). The effect that different pozzolanic activity methods has on the kinetic constants of the pozzolanic reaction in sugar cane straw-clay ash/lime systems: Application of a kinetic–diffusive model. *Cement and Concrete Research*, *35*(11), 2137-2142.

Frías, M., Villar, E., & Savastano, H. (2011). Brazilian sugar cane bagasse ashes from the cogeneration industry as active pozzolans for cement manufacture. *Cement and Concrete Composites*, *33*(4), 490-496.

Fukue, M., Minato, T., Horibe, H., & Taya, N. (1999). The micro-structures of clay given by resistivity measurements. *Engineering Geology*, *54*(1-2), 43-53.

Ganesan, K., Rajagopal, K., & Thangavel, K. (2007). Evaluation of bagasse ash as supplementary cementitious material. *Cement and Concrete Composites*, *29*(6), 515-524.

García, R., de la Villa, R. V., Vegas, I., Frías, M., & de Rojas, M. S. (2008). The pozzolanic properties of paper sludge waste. *Construction and Building Materials*, *22*(7), 1484-1490.

Geetha, S., & Ramamurthy, K. (2011). Properties of sintered low calcium bottom ash aggregate with clay binders. *Construction and Building Materials*, *25*(4), 2002-2013.

Geliga, E. A., & Ismail, D. S. A. (2010). Geotechnical properties of fly ash and its application on soft soil stabilization. *UNIMAS E-Journal of civil engineering*, *1*(2), 1-6.

Ghazali, M., Azhari, C., Abdullah, S., & Omar, M. (2008). Characterisation of natural fibres (sugarcane bagasse) in cement composites. Proceedings of the World Congress on Engineering,

Ghiassian, H., Poorebrahim, G., & Gray, D. H. (2004). Soil reinforcement with recycled carpet wastes. *Waste Management & Research*, *22*(2), 108-114.

Ghobadi, M., Abdilor, Y., & Babazadeh, R. (2014). Stabilization of clay soils using lime and effect of pH variations on shear strength parameters [Article]. *Bulletin of Engineering Geology & the Environment*, *73*(2), 611-619.

Gong, Y., & Chok, Y. H. (2018). Predicted and measured behaviour of a test embankment on Ballina clay. *Computers and Geotechnics*, *93*, 178-190.

Goodarzi, A., & Salimi, M. (2015). Stabilization treatment of a dispersive clayey soil using granulated blast furnace slag and basic oxygen furnace slag. *Applied Clay Science*, *108*, 61-69.

Gourley, C., Newill, D., & Schreiner, H. (2020). Expansive soils: TRL's research strategy. In *Engineering Characteristics of Arid Soils* (pp. 247-260). CRC Press.

Grim, R. E. (1959). Physico-chemical Properties of Soils. *Journal of the Soil Mechanics and Foundations Division, ASCE*, *85*(2), 1-70.

Han, J., & Gabr, M. (2002). Numerical analysis of geosynthetic-reinforced and pile-supported earth platforms over soft soil. *Journal of Geotechnical and Geoenvironmental Engineering*, *128*(1), 44-53.

Hasan, H., Dang, L., Khabbaz, H., Fatahi, B., & Terzaghi, S. (2016a). Remediation of Expansive Soils Using Agricultural Waste Bagasse Ash. *Procedia Engineering*, *143*, 1368-1375.

Hasan, H., Khabbaz, H., & Fatahi, B. (2016b). Expansive Soil Stabilization Using Lime-Bagasse Ash. GeoVancouver, Canana.

Hasan, H. A. (2019). *Adverse effects of expansive soils on road infrastructure and evaluation of chemical remediation techniques* [Doctoral thesis, University of Technology Sydney]. Open Publications of UTS Scholars (OPUS).

He, Y., Zhao, X., Lu, L., Struble, L. J., & Hu, S. (2011). Effect of C/S ratio on morphology and structure of hydrothermally synthesized calcium silicate hydrate. *Journal of Wuhan University of Technology-Mater. Sci. Ed.*, *26*(4), 770-773.

Hejazi, S. M., Sheikhzadeh, M., Abtahi, S. M., & Zadhoush, A. (2012). A simple review of soil reinforcement by using natural and synthetic fibers. *Construction and Building Materials*, *30*, 100-116.

Hernández, J. M., Middendorf, B., Gehrke, M., & Budelmann, H. (1998). Use of wastes of the sugar industry as pozzolana in lime-pozzolana binders: study of the reaction. *Cement and Concrete Research*, *28*(11), 1525-1536.

Hilal, A. A. (2016). Microstructure of concrete. *High Performance Concrete Technology and Applications*, 3-24.

Holtz, R. D., Kovacs, W. D., & Sheahan, T. C. (1981). *An introduction to geotechnical engineering* (Vol. 733). Prentice-Hall Englewood Cliffs.

Hua-dong, M., & Liu, L. (2009). Stability processing technology and application prospect of steel slag [J]. *Steelmaking*, *25*(6), 74.

Huang, W.-H., & Lovell, C. (1990). Bottom ash as embankment material. In *Geotechnics of waste fills—Theory and practice*. ASTM International.

Ikara, I., Kundiri, A., & Mohammed, A. (2015). Effects of Waste Glass (WG) on the Strength Characteristics of Cement Stabilized Expansive Soil. *American Journal of Engineering Research*, *4*(11), 33-41.

Indraratna, B., Baral, P., Rujikiatkamjorn, C., & Perera, D. (2018). Class A and C predictions for Ballina trial embankment with vertical drains using standard test data from industry and large diameter test specimens. *Computers and Geotechnics*, *93*, 232-246.

Jairaj, C., Kumar, M. P., & Raghunandan, M. (2018). Compaction characteristics and strength of BC soil reinforced with untreated and treated coir fibers. *Innovative Infrastructure Solutions*, *3*(1), 21.

Jha, A. K., & Sivapullaiah, P. (2017). Physical and strength development in lime treated gypseous soil with fly ash—Micro-analyses. *Applied Clay Science*, *145*, 17-27.

Jha, A. K., & Sivapullaiah, P. V. (2015). Mechanism of improvement in the strength and volume change behavior of lime stabilized soil [Article]. *Engineering Geology*, *198*, 53-64.

Jones, L. D., & Jefferson, I. (2012). *Expansive soils*. ICE Publishing.

Jorat, M. E., Marto, A., Namazi, E., & Amin, M. (2011). Engineering characteristics of kaolin mixed with various percentages of bottom ash. *Electronic Journal of Geotechnical Engineering*, *16*(2), 841-850.

Juyal, G., Sastry, G., & Mohan Rao, M. (1994). Rehabilitation of a mined area in the Himalayas by geojute & other measures. Proce 5th int conf on geotextiles, Singapore.

Kalkan, E. (2009). Effects of silica fume on the geotechnical properties of fine-grained soils exposed to freeze and thaw. *Cold Regions Science and Technology*, *58*(3), 130-135.

Kalkan, E. (2013). Preparation of scrap tire rubber fiber–silica fume mixtures for modification of clayey soils. *Applied Clay Science*, *80*, 117-125.

Kalkan, E., & Akbulut, S. (2004). The positive effects of silica fume on the permeability, swelling pressure and compressive strength of natural clay liners. *Engineering Geology*, *73*(1-2), 145-156.

Kamei, T., Ahmed, A., & Shibi, T. (2013). The use of recycled bassanite and coal ash to enhance the strength of very soft clay in dry and wet environmental conditions. *Construction & Building Materials*, *38*, 224-235.

Katz, A., & Kovler, K. (2004). Utilization of industrial by-products for the production of controlled low strength materials (CLSM). *Waste Management*, *24*(5), 501-512.

Kaufhold, S., Dohrmann, R., Koch, D., & Houben, G. (2008). The pH of aqueous bentonite suspensions. *Clays and Clay Minerals*, *56*(3), 338-343.

Kawajiri, S., Kawaguchi, T., Yamasaki, S., Nakamura, D., Yamashita, S., & Shibuya, S. (2017). Strength characterisitcs of compacted soil with particular reference to soil structure and anisotropy. *International Journal*, *13*(38), 178-185.

Kayabal, K., & Buluş, G. (2000). The usability of bottom ash as an engineering material when amended with different matrices. *Engineering Geology*, *56*(3-4), 293-303.

Kelly, R., Sloan, S., Pineda, J., Kouretzis, G., & Huang, J. (2018). Outcomes of the Newcastle symposium for the prediction of embankment behaviour on soft soil. *Computers and Geotechnics*, *93*, 9-41.

Khabbaz, H., & Fatahi, B. (2012). Stabilisation of Closed Landfill Sites by Fly Ash Using Deep Mixing Method. In *Grouting and Deep Mixing 2012* (pp. 417-426).

Khan, M. I., & Siddique, R. (2011). Utilization of silica fume in concrete: Review of durability properties. *Resources, Conservation and Recycling*, *57*, 30-35.

Kharade, A. S., Suryavanshi, V. V., Gujar, B. S., & Deshmukh, R. R. (2014). Waste product bagasse ash from sugar industry can be used as stabilizing material for expansive soils. *International Journal of Research in Engineering and Technology*, *3*(3), 506-512.

Khatri, V. N., Dutta, R. K., Venkataraman, G., & Shrivastava, R. (2016). Shear Strength Behaviour of Clay Reinforced with Treated Coir Fibres. *Periodica Polytechnica. Civil Engineering*, *60*(2), 135.

Kibria, G., & Hossain, M. (2012). Investigation of geotechnical parameters affecting electrical resistivity of compacted clays. *Journal of Geotechnical and Geoenvironmental Engineering*, *138*(12), 1520-1529.

Kim, B., & Prezzi, M. (2008). Compaction characteristics and corrosivity of Indiana class-F fly and bottom ash mixtures. *Construction and Building Materials*, *22*(4), 694-702.

Kim, B., Prezzi, M., & Salgado, R. (2005). Geotechnical properties of fly and bottom ash mixtures for use in highway embankments. *Journal of Geotechnical and Geoenvironmental Engineering*, *131*(7), 914-924.

Kim, Y.-T., & Do, T.-H. (2012). Effect of bottom ash particle size on strength development in composite geomaterial. *Engineering Geology*, *139*, 85-91.

Kim, Y., Lee, C., & Park, H. (2011). Experimental study on engineering characteristics of composite geomaterial for recycling dredged soil and bottom ash. *Marine Georesources and Geotechnology*, *29*(1), 1-15.

Kolay, P., & Ramesh, K. (2016). Reduction of expansive index, swelling and compression behavior of kaolinite and bentonite clay with sand and class C fly ash. *Geotechnical and Geological Engineering*, *34*(1), 87-101.

Kolay, P. K., Sii, H. Y., & Taib, S. N. L. (2011). Tropical peat soil stabilization using class F pond ash from coal fired power plant. *International Journal of Civil and Environmental Engineering*, *3*(2), 79-83.

Krishna Reddy, K. (2009). Rutting resistance of pavements on fly ash-lime stabilized expansive subgrade. *International Journal of Geotechnical Engineering*, *3*(1), 147-152.

Krishnan, D. K., Janani, V., Ravichandran, P., Annadurai, R., & Gunturi, M. (2014). Effect of Fly Ash and Phospho Gypsum on Properties of Expansive Soils. *International Journal of Scientific Engineering and Technology*, *3*(5), 592-596.

Kumar, A., & Gupta, D. (2016). Behavior of cement-stabilized fiber-reinforced pond ash, rice husk ash–soil mixtures [Article]. *Geotextiles & Geomembranes*, *44*(3), 466-474.

Kumar, A., Walia, B. S., & Bajaj, A. (2007). Influence of fly ash, lime, and polyester fibers on compaction and strength properties of expansive soil [Article]. *Journal of Materials in Civil Engineering*, *19*(3), 242-248.

Kumar, S., & Vaddu, P. (2004). Time dependent strength and stiffness of PCC bottom ash-bentonite mixtures. *Soil & Sediment Contamination*, *13*(4), 405-413.

Lambe, T. W. (1958a). The engineering behavior of compacted clay. *Journal of the Soil Mechanics and Foundations Division*, *84*(2), 1-35.

Lambe, T. W. (1958b). The structure of compacted clays. *Journal of the Soil Mechanics and Foundations Division*, *84*(2), 1-34.

Lav, A., & Kenny, P. (1996). The use of stabilised fly ash in pavements. National Symposium on the Use of Recycled Materials in Engineering Construction: 1996; Programme & Proceedings, Australia.

Le Blond, J. S., Horwell, C. J., Williamson, B. J., & Oppenheimer, C. (2010). Generation of crystalline silica from sugarcane burning. *Journal of environmental monitoring*, *12*(7), 1459-1470.

Le, T. M. (2015). *Analysing Consolidation Data to Optimise Elastic Visco–plastic Model Parameters for Soft Clay* [Doctoral thesis, University of Technology, Sydney]. Open Publications of UTS Scholars (OPUS).

Le, T. M., Dang, L. C., & Khabbaz, H. (2018). Combined Effect of Bottom Ash and Lime on Behaviour of Expansive Soils. GeoMEast, Egypt.

Le, T. M., Dang, L. C., & Khabbaz, H. (2019). Strength Characteristics of Lime and Bottom Ash Reinforced Expansive Soils. Geo-Congress 2019: Soil Improvement, USA.

Le, T. M., Fatahi, B., Disfani, M., & Khabbaz, H. (2015). Analyzing consolidation data to obtain elastic viscoplastic parameters of clay. *Geomechanics and Engineering*.

Le, T. M., Tang, A. M., & Khabbaz, H. (2021). A modified electrical conductivity test to predict shrinkage-swelling behaviour of expansive soil treated with hydrated lime and bottom ash. *Geotechnique (under review)*.

Lesmes, D. P., & Friedman, S. P. (2005). Relationships between the electrical and hydrogeological properties of rocks and soils. In *Hydrogeophysics* (pp. 87-128). Springer.

Liu, H., Ng, C. W., & Fei, K. (2007). Performance of a geogrid-reinforced and pile-supported highway embankment over soft clay: case study. *Journal of Geotechnical and Geoenvironmental Engineering*, *133*(12), 1483-1493.

López-López, E., Vega-Zamanillo, Á., Calzada-Pérez, M., & Taborga-Sedano, M. (2015). Use of bottom ash from thermal power plant and lime as filler in bituminous mixtures. *Materiales de Construcción*, *65*(318), 051.

Lorenzo, G. A., & Bergado, D. T. (2004). Fundamental parameters of cement-admixed clay—New approach. *Journal of Geotechnical and Geoenvironmental Engineering*, *130*(10), 1042-1050.

Lovell, C., Ke, T.-C., Huang, W.-H., & Lovell, J. (1991). Bottom ash as a highway material. *Transportation Research Record*(1310).

Luxan, M. d., Madruga, F., & Saavedra, J. (1989). Rapid evaluation of pozzolanic activity of natural products by conductivity measurement. *Cement and Concrete Research*, *19*(1), 63-68.

Ma, C., & Eggleton, R. A. (1999). Cation exchange capacity of kaolinite. *Clays and Clay Minerals*, *47*(2), 174-180.

Mackiewicz, S. M., & Ferguson, E. G. (2005). Stabilization of soil with self-cementing coal ashes. *World of Coal Ash (WOCA)*, 1-7.

Maghool, F., Arulrajah, A., Du, Y.-J., Horpibulsuk, S., & Chinkulkijniwat, A. (2017). Environmental impacts of utilizing waste steel slag aggregates as recycled road construction materials. *Clean Technologies and Environmental Policy*, *19*(4), 949-958.

Majizadeh, K., Bokowski, G., & El-Mitiny, R. (1979). Material characteristics of power plant bottom ashes and their performance in bituminous mixtures: A laboratory investigation. Proceedings of the fifth international ash utilization symposium. Morgantown, West Virginia: Department of Energy, USA.

Manikandan, A., & Moganraj, M. (2014). Consolidation and rebound characteristics of expansive soil by using lime and bagasse ash. *International Journal of Research in Engineering and Technology*, *3*(4), 403-411.

Manso, J. M., Ortega-López, V., Polanco, J. A., & Setién, J. (2013). The use of ladle furnace slag in soil stabilization. *Construction and Building Materials*, *40*, 126-134.

McCarter, W., & Tran, D. (1996). Monitoring pozzolanic activity by direct activation with calcium hydroxide. *Construction and Building Materials*, *10*(3), 179-184.

Microscopy Australia. (2020). *Scanning Eletron Microscopy*. Microscopy Australia. Retrieved 10 June, 2021 from https://www.myscope.training/#/SEMlevel_3_1

Miller, G. A., & Azad, S. (2000). Influence of soil type on stabilization with cement kiln dust. *Construction and Building Materials*, *14*(2), 89-97.

Mineral Data Publishing. (2001). Mineral Data Publishing. Retrieved 10 June, 2021 from http://www.handbookofmineralogy.org/pdfs/montmorillonite.pdf

Mirzababaei, M., Miraftab, M., McMahon, P., & Mohamed, M. (2009). Undrained behaviour of clay reinforced with surplus carpet fibres. Second International Symposium on Fiber Recycling, Atlanta, Georgia, USA.

Mitchell, J. K., & Soga, K. (2005). *Fundamentals of soil behavior* (Vol. 3). John Wiley & Sons New York.

Modarres, A., & Nosoudy, Y. M. (2015). Clay stabilization using coal waste and lime—Technical and environmental impacts. *Applied Clay Science*, *116*, 281-288.

Mohammadi, I., Khabbaz, H., & Vessalas, K. (2014). In-depth assessment of Crumb Rubber Concrete (CRC) prepared by water-soaking treatment method for rigid pavements. *Construction and Building Materials*, *71*, 456-471.

Moulton, L. K. (1973). Bottom ash and boiler slag. Proceedings: Third International Ash Utilization Symposium. Sponsored by National Coal Association, Edison Electric Institute, American Public Power Association, National Ash Association, and Bureau of Mines, Pittsburgh, Pa., March 13-14, 1973., USA.

Mu'Azu, M. A. (2007). Influence of compactive effort on Bagasse ash with cement treated lateritic soil. *Leonardo Electronic Journal of Practices and Technologies*, *10*(1), 79-92.

Muthu Kumar, M., & Tamilarasan, V. (2014). Effect of Eggshell Powder in the Index and Engineering Properties of soil. *International Journal of Engineering Trends and Technology*, *11*(7), 319-321.

Nalbantoglu, Z., & Tuncer, E. R. (2001). Compressibility and hydraulic conductivity of a chemically treated expansive clay [Article]. *Canadian Geotechnical Journal*, *38*(1), 154-160.

Negi, C., Yadav, R., & Singhai, A. (2013). Effect of silica fume on engineering properties of black cotton soil. *International Journal of Computational Engineering Research (IJCER)*, 83.

Nelson, J., & Miller, D. J. (1997). *Expansive soils: problems and practice in foundation and pavement engineering*. John Wiley & Sons.

Nelson, J. D., Chao, K. C., Overton, D. D., & Nelson, E. J. (2015). *Foundation engineering for expansive soils*. John Wiley & Sons.

Nguyen, L. D., Fatahi, B., & Khabbaz, H. (2014). A constitutive model for cemented clays capturing cementation degradation. *International Journal of Plasticity*, *56*, 1-18.

Nguyen, T. T. H., Cui, Y.-J., Ferber, V., Herrier, G., Ozturk, T., Plier, F., Puiatti, D., Salager, S., & Tang, A. M. (2019). Effect of freeze-thaw cycles on mechanical strength of lime-treated fine-grained soils. *Transportation Geotechnics*, *21*, 100281.

Niwas, S., Gupta, P. K., & De Lima, O. (2007). Nonlinear electrical conductivity response of shaly-sand reservoir. *Curr. Sci*, *92*(5), 612-617.

NSW Government. (2012). Test method T144 - Hydrated lime for road construction materials (Lime demand test). In: Transport Roads & Martitime Services (NSW Government).

Nyankson, E., Agyei-Tuffour, B., Annan, E., DodooArhin, D., Yaya, A., Brefo, L., Okpoti, E., & Odai, E. (2013). Characteristics of Stabilized Shrink-Swell Deposits using Eggshell Powder. *Global journal of engineering, design and technology*, *2*(3), 1-7.

Oderah, V. (2015). *Shear strength behaviour of sugarcane bagasse reinforced soils* [Master thesis, University of Cape Town].

Okyay, U., & Dias, D. (2010). Use of lime and cement treated soils as pile supported load transfer platform. *Engineering Geology*, *114*(1-2), 34-44.

Olarewaju, A. J., Balogun, M., & Akinlolu, S. (2011). Suitability of eggshell stabilized lateritic soil as subgrade material for road construction. *Electronic Journal of Geotechnical Engineering*, *16*, 899-908.

Oliveira De Paula, M., Ferreira Tinoco, I. d. F., DE SOUZA RODRIGUES, C., SARAZ, O., & ALEXANDER, J. (2010). Sugarcane bagasse ash as a partial-portland-cement-replacement material. *Dyna*, *77*(163), 47-54.

Olufowobi, J., Ogundoju, A., Michael, B., & Aderinlewo, O. (2014). Clay soil stabilization using powdered glass. *Journal of Engineering Science and Technology*, *9*(05), 541-558.

Osinubi, K., Bafyau, V., & Eberemu, A. (2009a). Bagasse ash stabilization of lateritic soil. In *Appropriate technologies for environmental protection in the developing world* (pp. 271-280). Springer.

Osinubi, K., Ijimdiya, T. S., & Nmadu, I. (2009b). Lime stabilization of black cotton soil using bagasse ash as admixture. Advanced Materials Research, Switzerland.

Özkan, Ö., Yüksel, I., & Muratoğlu, Ö. (2007). Strength properties of concrete incorporating coal bottom ash and granulated blast furnace slag. *Waste Management*, *27*(2), 161-167.

Pandian, N., & Krishna, K. (2003). The pozzolanic effect of fly ash on the California bearing ratio behavior of black cotton soil. *Journal of Testing and Evaluation*, *31*(6), 479-485.

Paul, A., Anumol, V., Moideen, F., Jose, J. K., & Abraham, A. (2014). Studies on Improvement of Clayey Soil Using Egg Shell Powder and Quarry Dust. *International Journal of Engineering Research and Applications*, *4*(4), 55-63.

Paya, J., Borrachero, M., Monzo, J., Peris-Mora, E., & Amahjour, F. (2001). Enhanced conductivity measurement techniques for evaluation of fly ash pozzolanic activity. *Cement and Concrete Research*, *31*(1), 41-49.

Payá, J., Monzó, J., Borrachero, M. V., Díaz-Pinzón, L., & Ordonez, L. M. (2002). Sugar-cane bagasse ash (SCBA): studies on its properties for reusing in concrete production. *Journal of Chemical Technology & Biotechnology: International Research in Process, Environmental & Clean Technology*, *77*(3), 321-325.

Payá, J., Monzó, J., Borrachero, M. V., & Peris-Mora, E. (1995). Mechanical treatment of fly ashes. Part I: Physico-chemical characterization of ground fly ashes. *Cement and Concrete Research*, *25*(7), 1469-1479.

Phani Kumar, B., & Sharma, R. S. (2004). Effect of fly ash on engineering properties of expansive soils. *Journal of Geotechnical and Geoenvironmental Engineering*, *130*(7), 764-767.

Phanikumar, B. (1997). A study of swelling characteristics of and granular pile anchor foundation system in expansive soils. *Submitted to JN Technological University, Hyderabad, India*.

Phanikumar, B. (2009). Effect of lime and fly ash on swell, consolidation and shear strength characteristics of expansive clays: a comparative study. *Geomechanics and Geoengineering: An international journal*, *4*(2), 175-181.

Phanikumar, B., Sreedharan, R., & Aniruddh, C. (2015). Swell-compressibility characteristics of lime-blended and cement-blended expansive clays–A comparative study. *Geomechanics and Geoengineering*, *10*(2), 153-162.

Pineda, J., Suwal, L., Kelly, R., Bates, L., & Sloan, S. (2016). Characterisation of Ballina clay. *Géotechnique*, *66*(7), 556-577.

Pliya, P., & Cree, D. (2015). Limestone derived eggshell powder as a replacement in Portland cement mortar. *Construction and Building Materials*, *95*, 1-9.

Poh, H., Ghataora, G. S., & Ghazireh, N. (2006). Soil stabilization using basic oxygen steel slag fines. *Journal of Materials in Civil Engineering*, *18*(2), 229-240.

Prakash, K., & Sridharan, A. (2004). Free swell ratio and clay mineralogy of fine-grained soils. *Geotechnical testing journal*, *27*(2), 220-225.

Prakash, K., & Sridharan, A. (2006). A geotechnical classification system for coal ashes. *Proceedings of the Institution of Civil Engineers-Geotechnical Engineering*, *159*(2), 91-98.

Presti, D. L. (2013). Recycled tyre rubber modified bitumens for road asphalt mixtures: a literature review. *Construction and Building Materials*, *49*, 863-881.

Punthutaecha, K. (2002). Volume change behavior of expansive soils modified with recycled materials. *Ph.D. thesis, University of Texas at Arlington*.

Punthutaecha, K., Puppala, A. J., Vanapalli, S. K., & Inyang, H. (2006). Volume change behaviors of expansive soils stabilized with recycled ashes and fibers. *Journal of Materials in Civil Engineering*, *18*(2), 295-306.

Puppala, A. J., Intharasombat, N., & Vempati, R. K. (2005). Experimental studies on ettringite-induced heaving in soils. *Journal of Geotechnical and Geoenvironmental Engineering*, *131*(3), 325-337.

Puppala, A. J., & Pedarla, A. (2017). Innovative ground improvement techniques for expansive soils. *Innovative Infrastructure Solutions*, *2*(1), 1-15.

Puppala, A. J., Punthutaecha, K., & Vanapalli, S. K. (2006). Soil-water characteristic curves of stabilized expansive soils. *Journal of Geotechnical and Geoenvironmental Engineering*, *132*(6), 736-751.

Radhakrishnan, G., Kumar, M. A., & Raju, G. (2014). Swelling properties of expansive soils treated with chemicals and fly ash. *Am J Eng Res*, *3*(4), 245-250.

Rahman, M. (1987). Effects of cement-rice husk ash mixtures on geotechnical properties of lateritic soils. *Soils and Foundations*, *27*(2), 61-65.

Rahman, M. A. (1986). The potentials of some stabilizers for the use of lateritic soil in construction. *Building and Environment*, *21*(1), 57-61.

Ramesh, H., Nanda, H., & Manoj Krishna, K. (2011). Effect of Soaking on The Strength Behaviour of Shedi Soil Treated With NFA. Procs. of Indian Geotechnical Conference–2011, December 15, India.

Rao, A. N., & Chittaranjan, M. (2011). Applications of agricultural and domestic wastes in geotechnical applications: an overview. *J Environ Res Dev*, *5*(3).

Rezania, M., Nguyen, H., Zanganeh, H., & Taiebat, M. (2018). Numerical analysis of Ballina test embankment on a soft structured clay foundation. *Computers and Geotechnics*, *93*, 61-74.

Richards, B., Peter, P., & Emerson, W. (1983). The effects of vegetation on the swelling and shrinking of soils in Australia. *Geotechnique*, *33*(2), 127-139.

Ríos-Parada, V., Jiménez-Quero, V. G., Valdez-Tamez, P. L., & Montes-García, P. (2017). Characterization and use of an untreated Mexican sugarcane bagasse ash as supplementary material for the preparation of ternary concretes. *Construction and Building Materials*, *157*, 83-95.

Rogbeck, J., & Knutz, Å. (1996). Coal bottom ash as light fill material in construction. *Waste Management*, *16*(1-3), 125-128.

Sabat, A. K. (2012a). Effect of Polypropylene Fiber on Engineering Properties of Rice Husk Ash–Lime Stabilised Expansive Soil. *Electronic Journal of Geotechnical Engineering*, *17*, 651-660.

Sabat, A. K. (2012b). A study on some geotechnical properties of lime stabilised expansive soil–quarry dust mixes. *International Journal of emerging trends in engineering and development*, *1*(2), 42-49.

Sabat, A. K. (2012c). Utilization of bagasse ash and lime sludge for construction of flexible pavements in expansive soil areas. *Electronic Journal of Geo-technical Engineering*, *17*, 1037-1046.

Sabat, A. K., & Bose, B. (2013). Improvement in Geotechnical properties of an Expansive soil using Fly ash-Quarry dust Mixes. *Electronic Journal of Geotechnical Engineering*, *18*, 3487-3500.

Sabat, A. K., & Pati, S. (2014). A review of literature on stabilization of expansive soil using solid wastes. *Electronic Journal of Geotechnical Engineering*, *19*, 6251-6267.

Sabat, A. K., & Pradhan, A. (2014). Fiber reinforced–fly ash stabilized expansive soil mixes as subgrade material in flexible pavement. *Electronic Journal of Geotechnical Engineering*, *19*, 5757-5770.

Sadek, M. S. (1993). *A comparative study of the electrical and hydraulic conductivities of compacted clay*. University of California, Berkeley.

Salahudeen, A., & Ochepo, J. (2015). Effect of Bagasse Ash on Some Engineering Properties of Lateritic Soil. *Jordan Journal of Civil Engineering*, *9*(4).

Santamarina, J. C., Klein, K., & Fam, M. (2001). Soils and Waves: Particulate Materials Behaviour, Characterisation and Process Monitoring. In: Chichester: John Wiley & Sons.

Sarkar, G., Saha, J., & Rokonuzzman, M. (2012). Development of regression equation for optimizing the materials requirements of lime and sand stabilizing adobe based on consistency and linear shrinkage. *International Journal of Applied Science and Engineering Research*, *1*(3), 499-511.

Sarkar, R., Mudgal, A., Bhaskar, S., Gupta, V., & Kurar, R. (2016). A Review on Study on Effect of Various Admixtures on Geotechnical Properties of Expansive Soils. *Indian Journal of Science and Technology*, *9*(44).

Satyanarayana, B. (1966). *Swelling pressure and related mechanical properties of black cotton soils* [PhD thesis, Indian Institute of Science, Bangalore].

Schettino, M. A. S., & Holanda, J. N. F. (2015). Characterization of sugarcane bagasse ash waste for its use in ceramic floor tile. *Procedia Materials Science*, *8*, 190-196.

Seda, J. H., Lee, J. C., & Carraro, J. A. H. (2007). Beneficial use of waste tire rubber for swelling potential mitigation in expansive soils. In *Soil improvement* (pp. 1-9).

Seed, H. B., & Lundgren, R. (1962). Prediction of swelling potential for compacted clays. *Journal of the Soil Mechanics and Foundations Division*, *88*(3), 53-87.

Sensorex. (2021). *Understanding conductivity cell constans*. Sensorex. Retrieved 15 March, 2021 from https://sensorex.com/blog/2017/11/29/conductivity-cell-constants/

Seyyedalipour, S. F., Kebria, D. Y., Malidarreh, N., & Norouznejad, G. (2014). Study of utilization of pulp and paper industry wastes in production of concrete. *International Journal of Engineering Research and Applications*, *4*(1), 115-122.

Sharma, R. S., Phanikumar, B., & Rao, B. V. (2008). Engineering behavior of a remolded expansive clay blended with lime, calcium chloride, and rice-husk ash. *Journal of Materials in Civil Engineering*, *20*(8), 509-515.

Shi, B., Wu, Z., Inyang, H., Chen, J., & Wang, B. (1999). Preparation of soil specimens for SEM analysis using freeze-cut-drying. *Bulletin of Engineering Geology and the Environment*, *58*(1), 1-7.

Shu, X., & Huang, B. (2014). Recycling of waste tire rubber in asphalt and Portland cement concrete: an overview. *Construction and Building Materials*, *67*, 217-224.

Shyam Prakash, K., & Rao, C. H. (2016). Study on Compressive Strength of Quarry Dust as Fine Aggregate in Concrete. *Advances in Civil Engineering*, *2016*.

Siddiki, N., Kim, D., & Salgado, R. (2004). Use of recycled and waste materials in Indiana. *Transportation Research Record: Journal of the Transportation Research Board*(1874), 78-85.

Singh, A. A., & Palsule, S. (2014). Coconut fiber reinforced chemically functionalized high-density polyethylene (CNF/CF-HDPE) composites by Palsule process. *Journal of Composite Materials*, *48*(29), 3673-3684.

Singh, B., Kumar, A., & Sharma, R. K. (2014). Effect of waste materials on strength characteristics of local clay. *International Journal of Civil Engineering Research*, *5*(1), 61-68.

Sivakumar Babu, G., Vasudevan, A., & Sayida, M. (2008). Use of coir fibers for improving the engineering properties of expansive soils. *Journal of Natural Fibers*, *5*(1), 61-75.

Sivapullaiah, P., & Jha, A. K. (2014). Gypsum induced strength behaviour of fly ash-lime stabilized expansive soil. *Geotechnical and Geological Engineering*, *32*(5), 1261-1273.

Sivapullaiah, P. V., Sridharan, A., & Bhaskar Raju, K. V. (2000). Role of amount and type of clay in the lime stabilization of soils [Article]. *Ground Improvement*, *4*(1), 37-45.

Šķēls, P., Bondars, K., Plonis, R., Haritonovs, V., & Paeglītis, A. (2016). Usage of Wood Fly Ash in Stabilization of Unbound Pavement Layers and Soils. Proceedings of 13th Baltic Sea Geotechnical Conference, Lithuania.

Solanki, P., Khoury, N., & Zaman, M. M. (2009). Engineering properties and moisture susceptibility of silty clay stabilized with lime, class C fly ash, and cement kiln dust. *Journal of Materials in Civil Engineering*, *21*(12), 749-757.

Spagnoli, G., & Shimobe, S. (2019). A statistical reappraisal of the relationship between liquid limit and specific surface area, cation exchange capacity and activity of clays. *Journal of Rock Mechanics and Geotechnical Engineering*, *11*(4), 874-881.

Sridharan, A., Rao, A. S., & Sivapullaiah, P. V. (1986). Swelling pressure of clays. *Geotechnical Testing Journal*, *9*(1), 24-33.

Srinivasan, R., & Sathiya, K. (2010). Experimental study on bagasse ash in concrete. *International journal for service learning in engineering*, *5*(2), 60.

Sujjavanidi, S., & Duangchan, A. (2004). Pozzolanic reactivity and water requirement of bagasse ash. Proc. In the 2nd Concrete National Conference, Chiengmai, Thailand.

Tafreshi, S. M., & Norouzi, A. H. (2015). Application of waste rubber to reduce the settlement of road embankment. *Geomechanics and Engineering*, *9*(2), 219-241.

Tang, A.-M., Cui, Y.-J., Trinh, V.-N., Szerman, Y., & Marchadier, G. (2009). Analysis of the railway heave induced by soil swelling at a site in southern France. *Engineering Geology*, *106*(1-2), 68-77.

Tanyu, B., Benson, C., Edil, T., & Kim, W.-H. (2004). Equivalency of crushed rock and three industrial by-products used for working platforms during pavement construction. *Transportation Research Record: Journal of the Transportation Research Board*(1874), 59-69.

Tashima, M. M., Soriano, L., Monzó, J., Borrachero, M., Akasaki, J. L., & Payá, J. (2014). New method to assess the pozzolanic reactivity of mineral admixtures by means of pH and electrical conductivity measurements in lime: pozzolan suspensions. *Materiales de Construcción*, 12.

Tastan, E. O., Edil, T. B., Benson, C. H., & Aydilek, A. H. (2011). Stabilization of organic soils with fly ash. *Journal of Geotechnical and Geoenvironmental Engineering*, *137*(9), 819-833.

Thomas, P., Baker, J., & Zelazny, L. (2000). An expansive soil index for predicting shrink–swell potential. *Soil Science Society of America Journal*, *64*(1), 268-274.

Tombácz, E., & Szekeres, M. (2006). Surface charge heterogeneity of kaolinite in aqueous suspension in comparison with montmorillonite. *Applied Clay Science*, *34*(1-4), 105-124.

Trzciński, J. (2004). Combined SEM and computerized image analysis of clay soils microstructure: technique & application. Advances in geotechnical engineering: The Skempton conference: Proceedings of a three day conference on advances in geotechnical engineering, The Institution of Civil Engineers and held at the Royal Geographical Society, London, UK.

Uzal, B., Turanlı, L., Yücel, H., Göncüoğlu, M., & Çulfaz, A. (2010). Pozzolanic activity of clinoptilolite: a comparative study with silica fume, fly ash and a non-zeolitic natural pozzolan. *Cement and Concrete Research*, *40*(3), 398-404.

Vaníček, I., Jirásko, D., & Vaníček, M. (2016). Added value of transportation geotechnics to the sustainability (design approach). *Procedia Engineering*, *143*, 1417-1424.

Vaníček, I., Jirásko, D., & Vaníček, M. (2017). Transportation and Environmental Geotechnics. *Procedia Engineering*, *189*, 118-125.

Vaníček, I., & Vaníček, M. (2013). Modern earth structures of transport engineering view of sustainable construction. *Procedia Engineering*, *57*, 77-82.

Velázquez, S., Monzó, J., Borrachero, M., & Payá, J. (2014). Assessment of the pozzolanic activity of a spent catalyst by conductivity measurement of aqueous suspensions with calcium hydroxide. *Materials*, *7*(4), 2561-2576.

Vidal, H. (1969). The principle of reinforced earth. *Highway research record*(282).

Villar-Cociña, E., Valencia-Morales, E., Gonzalez-Rodrıguez, R., & Hernandez-Ruız, J. (2003). Kinetics of the pozzolanic reaction between lime and sugar cane straw ash by electrical conductivity measurement: A kinetic–diffusive model. *Cement and Concrete Research*, *33*(4), 517-524.

Viswanadham, B. V. S., Phanikumar, B. R., & Mukherjee, R. V. (2009). Swelling behaviour of a geofiber-reinforced expansive soil. *Geotextiles and Geomembranes*, *27*(1), 73-76.

Wang, L., Bornert, M., Chanchole, S., & Heripre, E. (2013). Experimental investigation of the free swelling of crushed argillite. *Geotechnique Letters*, *3*(2), 89-92.

Wang, Q., Tang, A. M., Cui, Y.-J., Delage, P., & Gatmiri, B. (2012). Experimental study on the swelling behaviour of bentonite/claystone mixture. *Engineering Geology*, *124*, 59-66.

Wang, Y. (2006). Utilization of recycled carpet waste fibers for reinforcement of concrete and soil. *Recycling in textiles*, *238*(7), 213-224.

Wang, Y., Benahmed, N., Cui, Y.-J., & Tang, A. M. (2017a). A novel method for determining the small-strain shear modulus of soil using the bender elements technique. *Canadian Geotechnical Journal*, *54*(2), 280-289.

Wang, Y., Cui, Y.-J., Benahmed, N., Tang, A. M., & Duc, M. (2019). Changes of small strain shear modulus and suction for a lime-treated silt during curing. *Géotechnique*, 1-5.

Wang, Y., Cui, Y.-J., Benahmed, N., Tang, A. M., & Duc, M. (2020a). Changes of small strain shear modulus and suction for a lime-treated silt during curing. *Géotechnique*, *70*(3), 276-280.

Wang, Y., Cui, Y.-J., Tang, A. M., Benahmed, N., & Duc, M. (2017b). Effects of aggregate size on the compressibility and air permeability of lime-treated fine-grained soil. *Engineering Geology*, *228*, 167-172.

Wang, Y., Cui, Y., Tang, A. M., Benahmed, N., Duc, M., & Sun, W. J. (2020b). Shrinkage behaviour of a compacted lime-treated clay. *Geotechnique Letters*, *10*(2), 174-178.

Wang, Y., Duc, M., Cui, Y.-J., Tang, A. M., Benahmed, N., Sun, W. J., & Ye, W. M. (2017c). Aggregate size effect on the development of cementitious compounds in a lime-treated soil during curing. *Applied Clay Science*, *136*, 58-66.

Wilcox, B. S. (1978). Steam: its generation and use. *Thirty-ninth edition, 3rd printing*.

Wild, S., Kinuthia, J., Jones, G., & Higgins, D. (1999). Suppression of swelling associated with ettringite formation in lime stabilized sulphate bearing clay soils by partial substitution of lime with ground granulated blastfurnace slag (GGBS). *Engineering Geology*, *51*(4), 257-277.

Yang, C., & Carter, J. P. (2018). 1-D finite strain consolidation analysis based on isotach plasticity: Class A and Class C predictions of the Ballina embankment. *Computers and Geotechnics*, *93*, 42-60.

Yi, Y., Li, C., & Liu, S. (2014). Alkali-activated ground-granulated blast furnace slag for stabilization of marine soft clay. *Journal of Materials in Civil Engineering*, *27*(4), 04014146.

Yildiz, A., Karstunen, M., & Krenn, H. (2009). Effect of anisotropy and destructuration on behavior of Haarajoki test embankment. *International Journal of Geomechanics*, *9*(4), 153-168.

Yong, R. N., & Warkentin, B. P. (1966). *Introduction to Soil Behaviour*. Macmillan.

Yoo, D. J., Oh, M., Kim, Y. S., & Park, J. (2009). Influences of solution and mixed soil on estimating bentonite content in slurry using electrical conductivity. *Applied Clay Science*, *43*(3), 408-414.

Yoon, G. L., & Park, J. B. (2001). Sensitivity of leachate and fine contents on electrical resistivity variations of sandy soils. *Journal of hazardous materials*, *84*(2-3), 147-161.

Zavatta, R. (1993). The pulp and paper industry. In *Progress in Intercalation Research* (pp. 91-119). Springer.

Zha, F., Liu, S., Du, Y., & Cui, K. (2008). Behavior of expansive soils stabilized with fly ash. *Natural Hazards*, *47*(3), 509-523.

Zhang, Z., Scherer, G. W., & Bauer, A. (2018). Morphology of cementitious material during early hydration. *Cement and Concrete Research*, *107*, 85-100.

Zumrawi, M. M. (2015). Stabilization of Pavement Subgrade by Using Fly Ash Activated by Cement. *American Journal of Civil Engineering and Architecture*, *3*(6), 218-224.